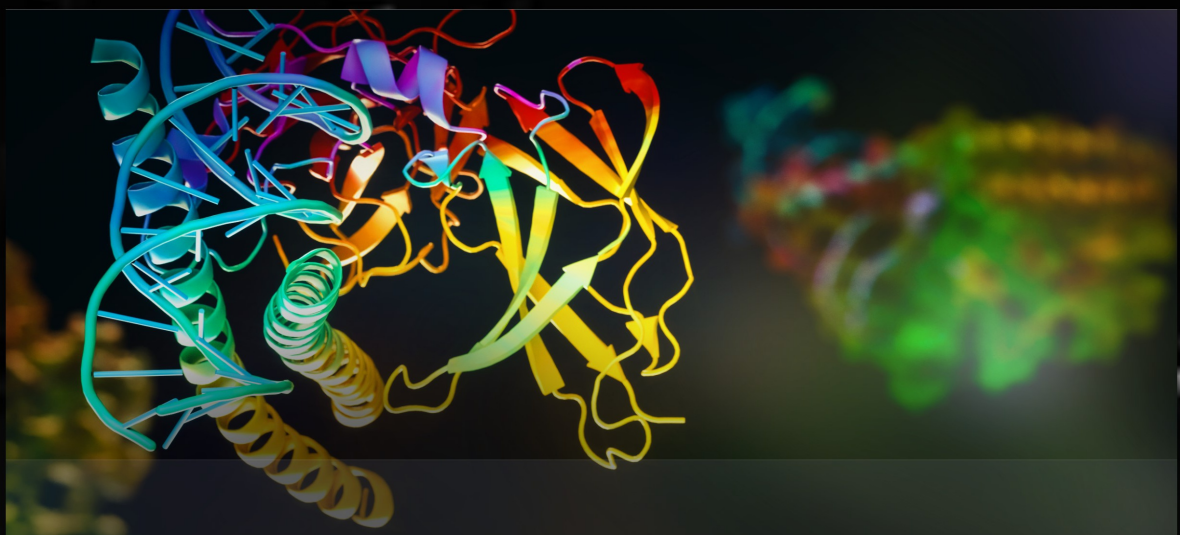
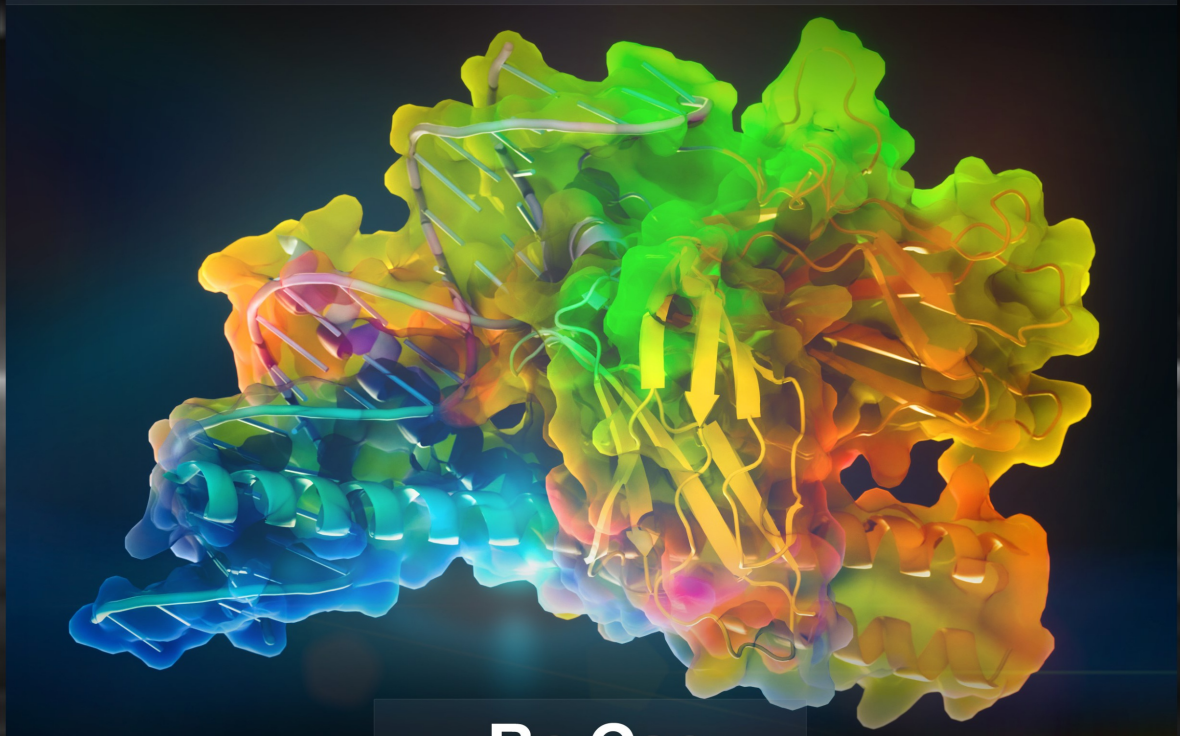


Macrophage–Material Interactions: NFATc1/c-Jun Signaling, Titanium Surface Modifications and Orthopedic Implant Infections



Bo Cao

Macrophage–Material Interactions: NFATc1/c-Jun Signaling, Titanium Surface Modifications and Orthopedic Implant Infections

Bo Cao

Doctoral thesis, Maastricht University—Faculty of Health, Medicine & Life Sciences

Bo Cao, Maastricht, The Netherlands, 2025

Cover design: Bo Cao

Print: ProefschriftMaken

ISBN: 978-94-6534-401-0

Macrophage–Material Interactions: NFATc1/c-Jun Signaling, Titanium Surface Modifications and Orthopedic Implant Infections

DISSERTATION

to obtain the degree of Doctor at Maastricht University,

on the authority of the Rector Magnificus, Prof. Dr. Jan Smits,

in accordance with the decision of the Board of Deans,

to be defended in public on Monday 22 June 2026, at *10.00* hours

by *Bo Cao*

Supervisor:
Dr. Berta Cillero-Pastor, Maastricht University
Prof. Dr. Maarten Honing, Maastricht University

Assessment Committee

Chair:
Prof. dr. Martijn van Griensven (Maastricht University)

Members:
Prof. Dr. Chris Arts (Maastricht University/Eindhoven University of Technology)
Prof. Dr. Ir. Ingrid Dijkgraaf (Maastricht University)
Prof. Dr. Martijn Riool (University Medical Center Regensburg, Germany)
Dr. Bas Zaat (Amsterdam University Medical Center)

Table of Contents

General introduction 6

Chapter 1 - Engineering implant surfaces for preventing orthopaedic infections 13

Chapter 2 - Surface characteristics of titanium modulates macrophage inflammatory response 33

Chapter 3 - Effect of titanium surface roughness on macrophage-bacteria interactions..... 67

Chapter 4 - Application of surface plasmon resonance to elucidate the cooperative DNA binding mechanisms of NFATc1 and c-Jun 109

Chapter 5 - Structure-guided disruption of NFATc1 rewires macrophage polarization to enhance clearance of S. aureus on implant surfaces 131

General Discussion 162

Valorization 167

Summary 171

Samenvatting..... 174

Appendix..... 178

Appendix I-Abbreviations 179

Appendix II-References 183

Appendix III-Supplementary..... 205

Curriculum Vitae..... 322

List of publications..... 324

Acknowledgments 326

General introduction

General introduction

Orthopedic implants have revolutionized the treatment of musculoskeletal disorders by providing essential structural support and restoring function in patients with fractures, joint degeneration, and other orthopedic conditions[1-3]. Predominantly constructed from titanium and its alloys, these implants are valued for their superior mechanical strength, corrosion resistance, and biocompatibility[4]. However, despite these advantages, persistent implant-associated infections remain a significant barrier, impacting clinical outcomes and often requiring complex surgical interventions[5]. When occurring in the early postoperative period, they represent one of the most severe complications in orthopedic surgery[6, 7], increase patient morbidity, healthcare expenditures and high failure rates of implants[8]. The fundamental challenge lies in bacterial colonization on the implant surface, where pathogens can evade host immune defense and establish persistent biofilms[9]. Formed by microbial communities embedded in a protective extracellular polymeric substance (EPS)[10], they offer enhanced resistance to both antibiotics and immune system clearance, complicating the treatment and resolution of infections[11, 12].

1.1. Biofilm formation

Biofilm formation begins with the adsorption of proteins, excreted by the bacteria, on to the biomaterial surface, facilitating adhesion[13-15]. Once they transition to the biofilm state, they undergo phenotypic changes, including decreased metabolic activity and increased tolerance to antimicrobial agents[16-18]. The biofilm matrix not only impedes antibiotic penetration but also restricts immune cell access, further exacerbating the persistence of infection[16, 17, 19]. These adaptive characteristics render biofilm-related infections exceptionally difficult to eradicate, often requiring prolonged antibiotic therapy or surgical debridement[13, 20].

Among the various pathogens implicated in implant infections, *Staphylococcus aureus* (*S. aureus)* stands out due to its ability to adhere to implant surfaces and form elastic biofilms[21, 22]. The virulence of *S. aureus* is attributed to an array of surface adhesins,

toxins, and immune evasion mechanisms, all of which contribute to its persistence and ability for chronic colonization[23]. Its ability to manipulate host immune responses and resist antimicrobial therapies further complicates efforts to eliminate this pathogen[24-26].

Titanium and its alloys are widely used due to their good biocompatibility[27]. And the surface characteristics of these biomaterial influence bacterial adhesion, biofilm formation, and host cell interactions[28],[29]. In more detail, the biomaterial surface roughness has shown to modulate adhesion behavior of both bacterial and host cells[30]. Increased surface roughness can enhance osteoblast attachment and osseointegration but may also create microenvironments ideal for bacterial colonization[31]. This complicates the balance between promoting favorable interactions and minimizing bacterial adhesion[31]. Thus, investigation into the interactions between biofilm and host cells at the interface of infected biomaterials by appropriate models is needed. Lipopolysaccharide (LPS) can recapitulate the early pro-inflammatory cues that typically arise at infection implant sites[32], enabling a controlled and physiologically relevant interaction between the pathogen and the inflamed host microenvironment, which provides a practical *in vitro* infection model for dissecting the processes of host response and bacterial colonization[33].

1.2. Macrophage response

Macrophages comprise a diverse array of subset phenotypes[34], including regulatory macrophages that suppress immune activation[35]. Such an immune response to orthopedic implants is a key determinant of their success[9, 36]. Upon implantation, they serve as the first line of defense, coordinating inflammatory responses influencing tissue integration and infection resolution[37, 38]. At the infected interface, the macrophages predominantly differentiate into a pro-inflammatory M1 phenotype, promoting bacterial clearance, or an anti-inflammatory M2 phenotype, promoting tissue repair and wound healing[39]. This process is strongly influenced by the properties of the biomaterial

surface, as well as the presence of bacterial biofilms[40, 41]. *S. aureus* biofilms, in particular, alter macrophage function, leading to chronic inflammation and impaired tissue healing, ultimately contributing to implant failure[42, 43]. Understanding the molecular mechanisms underlying host-pathogen interactions, at the bio-interface, is essential for the development of advanced implant materials reducing infection risks while promoting immune compatibility[44].

1.3. NFATc1 regulates macrophage differentiation

NFATc1 represents a core DNA transcriptional regulator that integrates extracellular signals to govern macrophage activation and fate decisions[45]. NFATc1 forms the AP-1 complex with c-Jun and c-Fos to coordinate the regulation of macrophage adhesion and inflammatory responses[46]. Compared to other transcription factors, the synergistic DNA binding of NFATc1 and c-Jun constitutes the terminal point for regulating macrophage adhesion and inflammation pathways. Targeting this single terminal point for inhibition offers more precise regulation of macrophages with fewer side effects. Understanding the structure of the AP-1 complex and the dynamics of its formation facilitates the design of more precise and effective inhibitors. Macian et al. systematically defined the binding interfaces, key molecular interactions, and ligand-induced conformational changes within the AP-1 complex[47], however, the kinetics of AP-1 complex formation remain unclear.

1.4. Analytical approaches

In the research of material biology interactions, a variety of analytical techniques are of pivotal importance. Here, both scanning- and transmission electron microscopy (EM) are used to characterize the surface profile and the cell morphology on different titanium surfaces. Fluorescent and spectroscopic techniques allow tracking of phagocytosis events and the identification of surface characteristics. At the molecular scale, gene and protein expression analyses provide opportunities to map how macrophages shift between M1 and M2, connecting surface cues with polarization outcomes. Proteomic profiling further opens the space to discover unexpected signaling pathways and regulatory networks that

respond to topographical differences. Measurements of reactive oxygen species help reveal how activation states unfold during bacterial challenges, linking metabolism with immune behavior[48]. Finally, elucidating the DNA-binding kinetics offer a window into designing drugs that specifically block NFATc1. Together, these analytical approaches form a framework that moves from the physical interface to cellular phenotype and finally to molecular dynamics, enabling a multifaceted understanding of how titanium surface roughness directs macrophage behavior during host-pathogen encounters.

2. Challenges and scientific approach

2.1. Chapter 1: Engineering implant surfaces for preventing orthopaedic infections

Implant infection represents a major clinical challenge due to biofilm-mediated resistance and the complex interplay between biomaterial properties and host immune responses. Understanding how implant surface characteristics influence macrophage behavior is crucial for developing infection-resistant implants. At the same time, targeted immunomodulatory strategies, such as selective disruption of NFATc1 signaling, hold promise for more effective and safer therapies. Chapter 1 serves as a comprehensive overview; it discusses the current knowledge on engineering titanium implant surfaces to modulate macrophage responses and highlights future directions for preventing *S. aureus* infection in orthopedic implants. Subsequent chapters further explore these issues into more detail, focusing on novel interventions aimed at improving patient outcomes in the management of implant-associated infections.

2.2. Chapter 2: Surface characteristics of titanium modulates macrophage inflammatory response

The surface properties of orthopedic implants, particularly the roughness of titanium surfaces, play a crucial role in mediating interactions between the implant and the host immune system[49]. Surface characteristics such as roughness can affect macrophage behavior, which is central to immune responses during infection and inflammation[50]. The balance between M1 and M2 macrophage polarization is essential for resolving

infections and promoting tissue regeneration[51]. This chapter investigates how variations in surface roughness of titanium plates influence macrophage differentiation, adhesion, and polarization, using an LPS-induced model to simulate bacterial infection.

2.3. Chapter 3: Effect of titanium surface roughness on macrophage-bacteria interactions

Titanium's surface roughness profoundly affects macrophage interactions with bacteria and surrounding tissues, crucial for understanding infection mechanisms and guiding the design of implant surfaces that reduce bacterial colonization, enhance immune defense, and improve patient outcomes[52]. Building upon the insights from Chapter 2, this chapter explores the complex interactions between titanium surface roughness, macrophages, and *S. aureus*, a leading cause of orthopedic implant infections. Chapter 3 investigates macrophage responses to *S. aureus* on titanium surfaces of varying roughness, using a RAW264.7 macrophage cell line in an *in vitro* co-culture model to simulate macrophage-bacteria interactions.

2.4. Chapter 4: Application of surface plasmon resonance to elucidate the cooperative DNA binding mechanisms of NFATc1 and c-Jun

Building upon the findings of Chapters 2 and 3, which established that NFATc1-c-Jun signaling is instrumental in modulating macrophage activity and enhancing *S. aureus* clearance in orthopedic implant infections. Selecting NFATc1 as a therapeutic target for developing targeted drugs requires a thorough understanding of its supramolecular structure and the dynamics of its DNA binding. X-ray crystallography[53] and cryo-electron microscopy[54], offer high-resolution snapshots of NFATc1-c-Jun complexes but fail to provide real-time kinetic data[55]. Chapter 4 focuses on elucidating the DNA-binding kinetics of NFATc1 with Surface Plasmon Resonance (SPR).

2.5. Chapter 5: Structure-guided disruption of NFATc1 rewires macrophage polarization to enhance clearance of *S. aureus* on implant surfaces

Conventional strategies, modulating NFATc1 have focused on upstream signaling[56], lacking targeted effects and insufficient molecular binding dynamics[57]. This limitation poses challenges for clinical translation[57]. Building upon the findings from Chapters 2, 3 and 4, Chapter 5 focuses on synthetic peptides targeting the NFATc1/c-Jun complex structure and binding dynamics due to the role of the NFATc1 signaling pathway in macrophage polarization and immune infection responses. Using the model from Chapter 3, Chapter 5 further validated the function of an inhibitory peptide in regulating macrophages[58].

Chapter 1 - Engineering implant surfaces for preventing orthopaedic infections

Based on

Cao B., Cillero-Pastor B., Honing M. Engineering implant surfaces to modulate macrophage responses for preventing Staphylococcus aureus infection. Ready for submission.

Abstract

Implant-associated infections remain a major challenge in orthopedics, largely due to the increasing prevalence of antibiotic resistance, which undermines the efficacy of standard surgical and antibiotic therapies. *Staphylococcus aureus* is the predominant pathogen, adhering to implant surfaces, forming biofilms, and interacting with host immune cells, particularly macrophages, which play a central role in bacterial clearance. In this systematic review, we analyze the cellular and molecular mechanisms underlying implant infection immunity, evaluate current antimicrobial surface modification strategies, and explore novel approaches aimed at overcoming antibiotic resistance. A comprehensive PubMed search over the past 10 years identified 3,167 studies, of which 106 met inclusion criteria for clinical or preclinical evidence on antibiotic resistance, surface engineering, or immune modulation. This review reveals that engineering implant surfaces to enhance macrophage adhesion and activation, coupled with precise regulation of NFATc1 signaling, creates a local microenvironment that strengthens innate immunity. This integrated strategy represents a paradigm shift in orthopedic biomaterial design, transforming implants from passive scaffolds into active immune modulators. Future directions combining hierarchical surface modifications with selective molecular targeting reduce infection-driven revision surgeries, extend implant longevity, and establish new standards for anti-infective implants in clinical orthopedics.

1. Introduction

Orthopedic implants have revolutionized the treatment of orthopedic diseases, restoring mobility and enhancing quality of life for millions of patients worldwide[59]. With the rise in aging populations and the prevalence of musculoskeletal disorders[60], the number of orthopedic implants has been steadily increasing year by year[1] and projections indicate a steep upward trend in the coming decades[61]. In fact, infection remains one of the most serious complications of prosthetic surgery[62], accounting for a significant proportion of implant failures and revision surgeries[63]. Implant infections are not only associated with significant morbidity and healthcare costs, but also pose substantial challenges to both surgeons and patients due to their persistent nature[64]. The clinical intractability of implant infection is largely driven by the dominance of *S. aureus* as the causative pathogen[15]. *S. aureus* possesses an unique combination of virulence factors that enable it to colonize on surfaces of biomaterials, form biofilms, and persist in adverse host environments[13]. Within biofilms, bacteria can evade antibiotics and avoid immune clearance[65]. Moreover, bacteria have the extraordinary ability to both develop antibiotic resistance and evade the host immune response by suppressing phagocytosis and modulating inflammatory signaling[66]. As a result, standard treatment strategies such as systemic antibiotics combined with debridement or revision surgery often fail to achieve complete clearance, leaving patients at risk of recurrent infection[67].

These limitations have prompted a shift in perspective: rather than relying solely on antimicrobial approaches, new strategies aim to harness and direct host immunity as a first line of defense. Among immune cells, macrophages play a key role in determining infection outcomes at the implant interface[49]. Notably, biomaterial-associated infections rarely elicit a uniform macrophage phenotype[68]. M1 and M2 macrophages co-exist at the implant surface, with their proportions shifting dynamically as infection progresses[69]. Early responses are typically skewed toward an M1-dominated pro-inflammatory state that favors pathogen clearance[70], followed by a gradual enrichment of the M2 phenotype that facilitates resolution and integration[70]. These polarization trajectories are not cell-intrinsic, but are critically shaped by the physicochemical

attributes of the biomaterial, including surface roughness, topography, and chemical functionality[71]. Recognition of this immunomodulatory dimension opens avenues for designing next-generation implants that couple osteoconductive with the capacity to direct macrophage fate and, by extension, infection outcomes[52].

When an implant becomes infected, the surface structure of the material also plays an important role in infection treatment[72]. By customizing implant surfaces, this approach holds promise for creating a new generation of orthopedic implants that actively participate in the anti-infection process rather than passively endure microbial colonization. This review systematically examines the cellular and molecular mechanisms underlying implant-associated infections, evaluates current antimicrobial surface strategies, and highlights emerging concepts in immune modulation. By integrating insights from microbiology, immunology, and biomaterials science, we aim to find a way toward developing innovative, immune-informed therapeutic strategies in orthopaedic implant infection.

2. Search strategy and the selection of included studies for this systematic review

The systematic literature search was performed across PubMed. The search keywords used were: "Implant infection," "*Staphylococcus aureus*," "Antibiotic resistance," "Antibacterial surface modification," "Immune modulation," "Macrophage," and "Therapeutic strategies," combined with boolean operators (OR, AND) to develop a search strategy. The search was restricted to studies published within the past 10 years. Studies were considered eligible if they reported clinical or preclinical data on mechanisms of antibiotic resistance in orthopedic implant infections, strategies for surface modification of biomaterials to enhance antibacterial activity, or immune modulation approaches related to implant infections. Publications in English were included when addressing these topics. Exclusion criteria comprised non-English publications, review articles without original experimental or clinical data, and studies lacking quantitative or mechanistic outcomes directly relevant to infection treatment strategies. All results were imported into EndNote 20 to screen the records. Duplicate studies from merging database outputs

were removed (Fig. 1). The remaining 106 full-text articles were included in the systematic review (Tab.S.1).

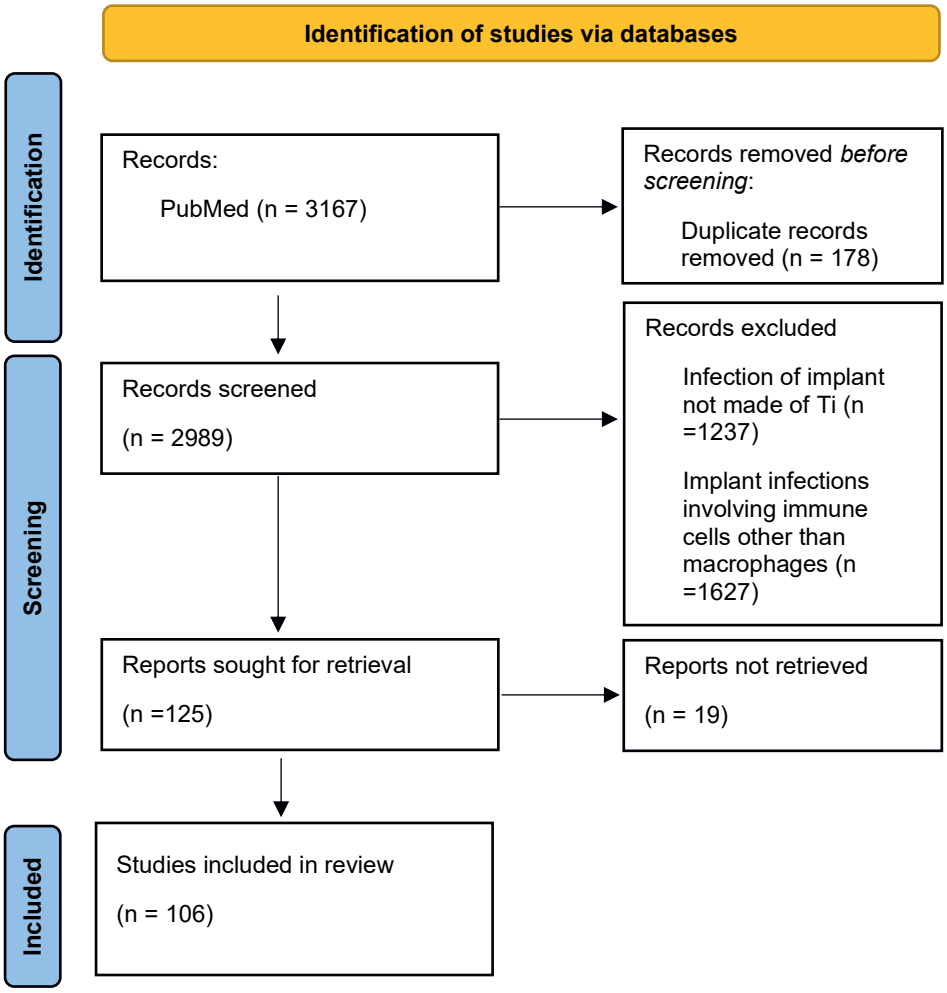


Fig. 1. Eligibility criteria: The flow diagram illustrates the systematic review process, starting with 3167 initial records identified from PubMed databases. After removing 178 duplicates, 2989 records remained for screening. Of these, 2864 were excluded based on infected materials and immune cells. Finally, the remaining 106 full-text articles were assessed for eligibility, and meeting the inclusion criteria, included in the systematic review.

3. Challenges in implant infection

Despite decades of innovation in surgical techniques and significant advances in perioperative care, implant infections remain one of the most challenging complications in orthopedic surgery[3]. Its clinical burden stems from the interplay between bacterial adaptability, the unique environment of biomaterial surfaces, and the limitations of current therapeutic strategies[25]. Unlike acute infections in soft tissues, implant infections are characterized by chronicity, and a high risk of recurrence even after aggressive intervention[73]. A key challenge lies in the biology of *S. aureus*, which is responsible for most of the implant infections in the orthopedic field[42]. Upon adherence to implant surfaces (Fig. 2), *S. aureus* rapidly establishes microcolonies that mature into biofilms[74]. Within this biofilm matrix, bacteria are encased in an extracellular polymeric substance that functions as both a physical and biochemical shield[75]. Biofilms restrict antibiotic penetration, reduce bacterial metabolic activity, and create microenvironments conducive to survival[76]. These dormant subpopulations exhibit profound tolerance to antibiotics, enabling infection to relapse long after the completion of therapy[77].

Beyond biofilm biology, *S. aureus* employs complex immune evasion strategies[78]. It secretes a repertoire of proteins and toxins that impair macrophages recruitment, and block phagocytosis by macrophages[79]. Moreover, these bacteria can survive within host immune cells, exploiting them as a persistent niche by disrupting the cells' bactericidal mechanisms[80]. Such strategies fundamentally undermine host defenses and make eradication particularly challenging.

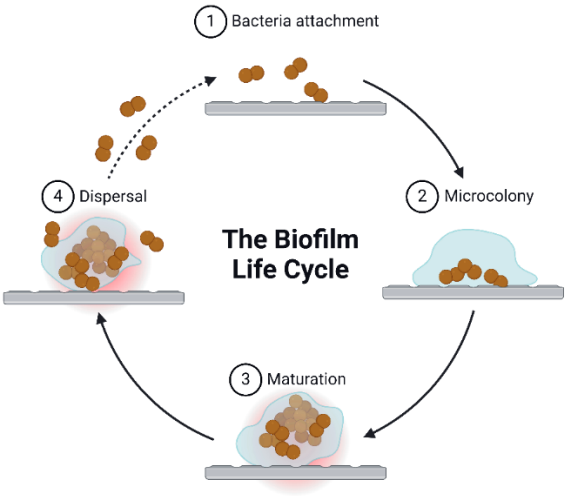


Fig. 2. Schematic overview on bacterial cells attachment to the hip implant and the development of the biofilm architecture through colonization. This figure is created with BioRender.com.

The therapeutic interventions against implant infection is constrained by bacterial defense mechanisms[81]. Prolonged systemic antibiotic regimens often fail to clear the infection, and the global rise in antibiotic resistance further narrows the spectrum of effective drugs [82]. Surgical management, ranging from debridement and implant retention to one- or two-stage revision arthroplasty, remains the standard of care but carries high morbidity, cost, and variable success rates[83]. In elderly or comorbid patients, revision surgery is associated with substantial functional decline and mortality risk[84]. These challenges underscore the urgent need for novel strategies that transcend traditional antimicrobial paradigms.

4. Approaches to the challenge of implant infection

To address this challenge, currently, the new interventions include the use of biofilm-inhibitory peptides[85], phage therapy[85], and the sustained release of antimicrobial ions, such as silver[86] or copper[87], through surface modification of implanted materials

[88]. However, these approaches are often limited by severe side effects, including silver or copper toxicity[89]. Efforts have also focused on physically altering implant surface topography to reduce bacterial adhesion or enhance host immune cell activity[90]. Yet, this strategy also faces inherent trade-offs, smooth surfaces can limit bacterial colonization but concurrently impair immune cell attachment[91], thereby hindering host-mediated clearance[92]. So, effective solutions must simultaneously address dual objectives: preventing excessive *S. aureus* adhesion while maintaining sufficient host immune cell attachment to the implant surface. Addressing this challenge requires a comprehensive understanding of the local microenvironment during infection, including the dynamic interactions among host tissue cells, *S. aureus*, and the implant surface itself.

5. Host cells involved in implant infection

Around infected orthopedic implants, a complex cellular milieu emerges that reflects the interplay between innate and adaptive immunity. Bone-resident cells, and stromal components, among others, are profoundly influenced by the presence of bacterial biofilms [74]. Neutrophils are among the earliest responders in the acute phase, exerting antimicrobial activity through phagocytosis, release of reactive oxygen species and proteolytic enzymes, yet they are frequently unable to penetrate biofilm matrices[93]. Macrophages, derived from circulating monocytes, contribute to pathogen clearance and apoptotic cell removal, but in chronic infection they sustain inflammation through persistent secretion of pro-inflammatory mediators[93]. Dendritic cells, though less abundant, play a pivotal role in antigen presentation, orchestrating the transition from innate to adaptive immune responses[94]. Within the adaptive compartment, $CD4^+$ T helper cells amplify or modulate inflammation[95], $CD8^+$ cytotoxic T lymphocytes directly kill infected host cells[96] and regulatory T cells exert immunosuppressive effects that is co-opted by pathogens to evade clearance[97]. B cells and plasma cells generate antibodies, yet their efficacy is markedly diminished in the biofilm context[98]. Infection also perturbs bone homeostasis: osteoblast activity is suppressed, impairing bone regeneration, while osteoclast activity is enhanced under inflammatory cues, driving bone

resorption and osteolysis[99]. Additional stromal and vascular components further shape the local niche, with fibroblasts contributing to fibrotic encapsulation and endothelial cells promoting angiogenesis under inflammatory conditions[100]. Notably, among the diverse immune populations recruited to the peri-implant environment, macrophages emerge as pivotal cells. They are central to the clearance of *S. aureus* during infection. Following pathogen control, they orchestrate tissue repair by phagocytosing necrotic debris[101].

S. aureus evades immune killing by manipulating macrophage differentiation, and its proactive strategies further complicate the challenge[102]. Factors secreted by the bacterium inhibit phagocytosis, block reactive oxygen species production, and divert macrophages away from the M1 phenotype[103]. Certain *S. aureus* strains can even persist within macrophages, using them as intracellular reservoirs[101]. These adaptive mechanisms directly undermine host defense mechanisms at implant interfaces[74]. This dual role of macrophages underpins the persistence of implant-associated infections and contributes to the remarkable recalcitrance and antibiotic tolerance characteristic of *staphylococcal* biofilm disease[74]. Therefore, when implant infections occur, macrophages represent a highly promising area for research.

6. The role of macrophages in implant infection

Macrophages are not a homogeneous population[74]. Macrophages exist in virtually every organ and display specialized functions tailored to their microenvironment[74]: Kupffer cells in the liver clear pathogens and senescent erythrocytes[104]; alveolar macrophages maintain pulmonary homeostasis[105]; red pulp macrophages are in the spleen recycle iron[106]; microglia regulate synaptic pruning and neurodevelopment [107] and intestinal lamina propria macrophages orchestrate immune tolerance[40]. These populations largely originate from embryonic progenitors and can self-maintain, yet their phenotype and function remain highly plastic in response to local signals[108]. At sites of implant infection, macrophages undergo dynamic polarization along the M1/M2 spectrum[109]. Classically activated M1 macrophages, induced by IFN-γ or LPS, produce pro-inflammatory cytokines and reactive oxygen/nitrogen species[110] whereas

alternatively activated M2 macrophages, producing IL-4, IL-13, IL-10, or TGF-β, support tissue repair, angiogenesis, and immune regulation[41]. M2 macrophages can be further subdivided: M2a (IL-4/IL-13-driven, tissue repair), M2b (immune complex/TLR-induced, immunoregulation), M2c (IL-10/TGF-β-induced, anti-inflammatory and remodeling), and M2d (tumor-associated, pro-angiogenic)[111]. In the context of biomaterial implantation, M1 macrophages often localize to the central lesion to combat pathogens while M2 macrophages accumulate at the periphery to promote repair and matrix remodeling[42]. Their plasticity enables them to integrate signals from the implant surface, surrounding tissues, and pathogens. This results in phenotypes that can either promote bacterial clearance or perpetuate persistent infection[65]. This dual role makes macrophages a critical determinant of the outcome of implant infections.

7. The role of surface properties of implant infection

As mentioned earlier, when an infection occurs, the surface properties of an orthopedic implant is not determined solely by its mechanical performance or integration with bone but also by its ability to engage the host immune system[112]. Classically, Ti surface modification has been pursued to enhance osseointegration[113]. Techniques such as grit blasting, acid etching, and anodization generate micro- and nanoscale features that increase surface area and promote osteoblast adhesion[114]. However, these same modifications also govern how immune cells, especially macrophages, interact with the implant[115]. Increasing evidence shows that the physicochemical characteristics of biomaterial surfaces, particularly those of titanium (Ti) alloy, which is the most widely used orthopedic alloy, profoundly influence macrophage polarization and macrophage adhesion at the tissue–implant interface[116]. A smooth surface tends to limit immune cell engagement, whereas roughened surfaces promote macrophage adhesion and activation[117]. Importantly, the immune response at the interface can dictate infection outcomes[118]. Under the infection, macrophages polarized towards the M1 phenotype exhibit pro-inflammatory activity. Macrophages are characterized by phagocytosis, production of reactive oxygen species (ROS), and secretion of cytokines that enhance

bacterial clearance [119]. By contrast, polarization towards the M2 phenotype fosters tissue repair but can simultaneously create an immunosuppressive niche that permits bacterial persistence [120]. More specifically, the ranges of surface roughness (Ra = 0.51–1.36 μm; Sa = 0.66–2.91 μm) can induce macrophage polarization toward the M2 phenotype[121], which supports tissue repair but compromises infection control. Thus, the balance between M1 and M2 phenotypes, which is strongly influenced by surface architecture, becomes a key determinant of whether an implant resists or succumbs to infection. These findings have given rise to a new paradigm: implants are no longer viewed as passive carriers but as active participants in shaping the host immune response. By engineering customized surface roughness, macrophage behavior can be redirected toward an anti-infective state. This approach to immune modulation through surface engineering offers a powerful complementary strategy to antimicrobial therapies.

8. Signaling pathways of macrophage polarization

Modulating macrophage polarization and function, offers new insights into implant infections. This necessitates further investigation into the signaling pathways regulating macrophages to identify suitable therapeutic targets. The ability of macrophages to differentiate toward bactericidal or reparative phenotypes is governed by complex regulatory networks[65]. Macrophages exhibit remarkable plasticity, adopting distinct functional phenotypes in response to environmental signals[122]. The classically activated M1 phenotype is induced by IFN-γ and microbial products such as lipopolysaccharide (LPS), which converge on key inflammatory signaling pathways[123]. Engagement of TLR4 triggers NF-κB activation, driving robust expression of pro-inflammatory cytokines including TNF-α, IL-6, and IL-1β[124]. In parallel, IFN-γ activates STAT1, reinforcing the transcriptional program associated with antimicrobial defense[125]. Mitogen-activated protein kinase (MAPK) cascades, including p38, JNK, and ERK, further amplify inflammatory signaling, while IRF5 orchestrates the induction of M1-specific gene networks[126]. In contrast, the alternatively activated M2 phenotype arises in response to IL-4, IL-13, and IL-10. M2 macrophage initiate a distinct transcriptional program tailored

for tissue repair, immune regulation, and resolution of inflammation[127]. Central to this program is STAT6, which induces hallmark M2 markers such as Arg1, Fizz1, Ym1, and MRC1/CD206. PPARγ and PPARδ contribute by promoting lipid metabolic reprogramming that stabilizes the M2 phenotype[128]. While IRF4 suppresses M1-associated pathways and facilitates M2 differentiation[51], TGF-β/Smad signaling further enriches the reparative capacity of M2 macrophages, promoting extracellular matrix remodeling and immunosuppression[129]. Interestingly, NFATc1 also exerts influence within the M2 axis, particularly in specialized contexts such as the tumor microenvironment, bone repair, and tissue regeneration, where it facilitates anti-inflammatory programs and remodeling responses[74]. These events highlight NFATc1 as a context-dependent regulator rather than a strict determinant of M1 or M2 identity. By integrating with distinct signaling networks, NFATc1 enables macrophages to dynamically adapt to local microenvironmental cues, thereby fine-tuning immune and tissue responses. This dual capacity underscores the complexity of macrophage polarization and positions NFATc1 as a pivotal node in the bidirectional regulation of inflammation and repair[45].

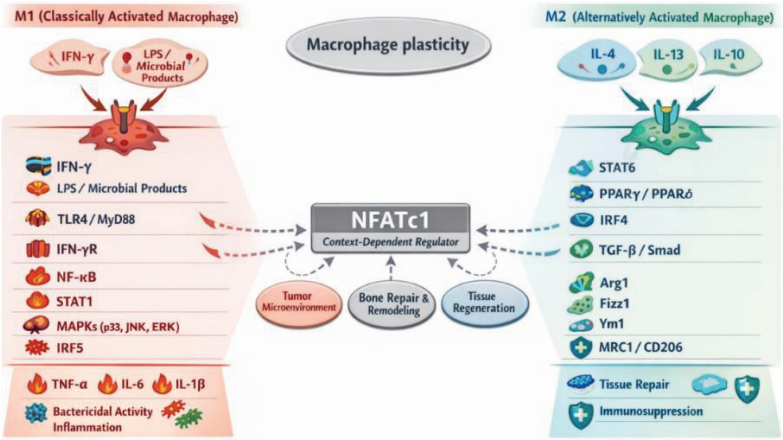


Fig. 3. Signaling pathways of macrophage polarization. This figure is created with Adobe Photoshop.

9. The role of NFATc1 signaling pathway in macrophage polarization

NFATc1 (nuclear factor of activated T cells, cytoplasmic 1) is a member of the NFAT transcription factor family. NFATc1 was originally identified in T lymphocytes as a regulator of activation and cytokine production[130]. NFATc1 integrates calcium signaling through calcineurin to translocate into the nucleus and drive transcriptional programs involved in inflammation, chemotaxis and metabolism[131]. Rather than functioning as a unidirectional determinant of macrophage identity, NFATc1 acts as a dynamic, environment-sensitive switch. NFATc1 coordinates inflammatory and reparative responses depending on extracellular cues[132]. In the context of macrophage polarization, NFATc1 shows a bidirectional role. During acute infection or early inflammation, it cooperates with NF-κB and AP-1 to promote M1-associated genes including IL12, TNF, and NOS2. NFATc1 enhances bactericidal activity through ROS and nitric oxide production[133]. However, in chronic infection or tissue repair, NFATc1 synergizes with IL-4/IL-13 signaling and pathogen-derived factors to activate M2-associated genes such as Arg1, IL10 and Mrc1 (CD206). Thereby, NFATc1 supports immunoregulatory and pro-repair phenotypes[134]. This context-dependent role is particularly evident in implant-associated infections caused by *S. aureus*. In the early phase (8–12 h) after implant contamination, pathogen-associated molecular patterns and damage-associated signals activate Toll-like receptor pathways converging on NFATc1[135]. NFATc1 together with NF-κB drives M1 polarization and pro-inflammatory responses to eliminate planktonic bacteria[136] while in later stages (>12 h), as *S. aureus* biofilms develop, extracellular polysaccharides, surface proteins and metabolic products remodel macrophage signaling through the IL-10/STAT3 pathway [137]. NFATc1 can redirect macrophages toward an M2-like state characterized by expression of Arg1 and IL10[123], but also suppresses bactericidal functions and promotion of immune evasion and biofilm persistence[138]. Therefore, NFATc1 emerges as a potential therapeutic target whose modulation must be stage specific. Its activity should be preserved during early infection to sustain M1-mediated clearance whereas in established biofilm-associated infection selective blockade of NFATc1-driven M2 polarization may restore antimicrobial immunity and improve treatment outcomes.

10. The molecular mechanism of NFATc1 in macrophage polarization

Designing specific inhibitors requires further understanding of the target's structure. Therefore, we need to gain a deeper understanding of the structure of NFATc1. It (Fig. 4) binds to DNA through its Rel homology region (RHR), making both base-specific and backbone contacts, while c-Fos and c-Jun engage the adjacent AP-1 site[139]. Close inspection of its structure revealed extensive protein–DNA interactions by NFAT residues in the RHR-N domain, complemented by contributions from the AP-1 basic regions. In addition, NFAT and AP-1 form a large protein–protein interface, mediated by hydrogen bonds and hydrophobic contacts between NFAT RHR-C and c-Fos–c-Jun helices[140, 141].

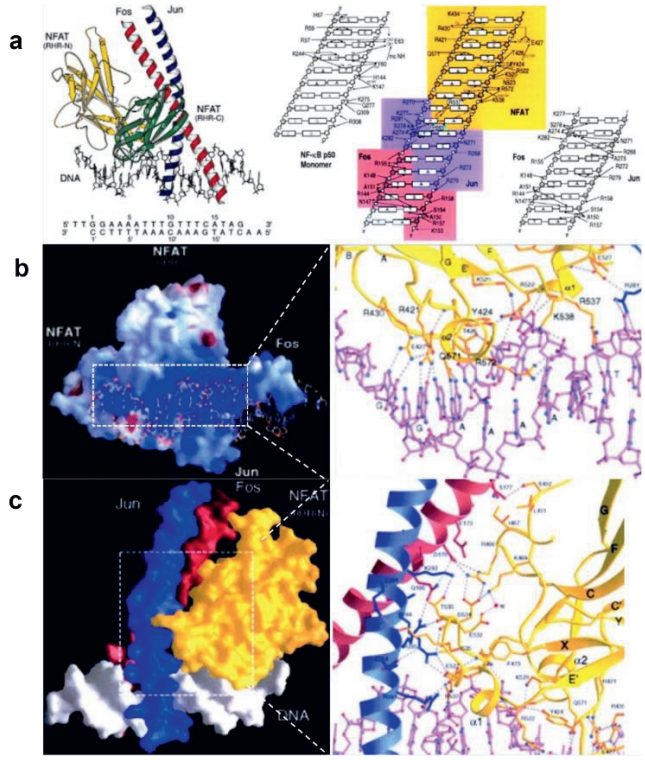


Fig. 4. Structure of the NFAT–AP-1–DNA ternary complex[141]. a, MOLSCRIPT representation of the complex, with NFAT RHR-N (yellow), RHR-C (green), Fos (red), Jun (blue) and DNA (grey/black); schematic at right highlights secondary structures and interacting residues. b, DNA recognition by NFAT and AP-1, showing specific base and backbone contacts mediated by NFAT (R421, Y424, R433) and AP-1 (K358, R537). c, Protein–protein interface between NFAT and AP-1[139, 140]. This figure is created with PyMOL(TM) 3.1.6.1.

11. Compounds that traditionally regulate NFATc1

Conventional strategies to modulate NFATc1 have focused on upstream signaling[56]. Several classes of inhibitors that target NFATc1, a pivotal transcription factor in osteoclast differentiation and tumor-associated bone destruction have been identified[142]. A representative small-molecule inhibitor, NFATc1-IN-1 (A04), can suppress RANKL-induced osteoclast genesis with sub-micromolar potency (IC_{50}: 1.57 μM)[143]. NFATc1-IN-1 (A04) has shown efficacy in both cellular and animal models of bone resorption but clinical data are currently lacking and off-target effects remain to be fully characterized[143]. Nordihydroguaiaretic acid (NDGA), acting through inhibition of calcium signaling, can also directly interfere with NFATc1 activation and attenuate breast cancer–induced osteolysis[144]. However, their poor bioavailability and limited pharmacokinetic data pose challenges for clinical translation[57]. Classical immunosuppressants including cyclosporin A[145] and tacrolimus are calcineurin inhibitors[146] preventing dephosphorylation and nuclear translocation of nFATc1. However their use is associated with nephrotoxicity and hypertension, limiting long-term applicability[146]. More selective strategies have emerged with the development of VIVIT peptides[147]. VIVIT peptides block NFAT protein–protein interactions[147]. Collectively, these pharmacological and natural modulators highlight both the therapeutic potential and mechanistic diversity of NFATc1 inhibition. While underscoring the challenges of toxicity, off-target effects, and pharmacokinetic limitations must be addressed for clinical development[147].

Table. 1. Pharmacological and molecular strategies targeting NFATc1 signaling and their biological implications

Compound / Strategy	Class / Type	Primary Target or Mechanism	Key Properties	Reported Applications	Limitations / Challenges	Ref
NFATc1-IN-1 (A04)	Small-molecule inhibitor	Direct suppression of NFATc1 transcriptional activity downstream of RANKL signaling	Potent inhibition of osteoclast genesis	Inhibition of osteoclast differentiation	Lack of clinical data; off-target effects	[143]
Nordihydroguaiaretic acid (NDGA)	Phenolic compound	Inhibition of calcium signaling, thereby impairing NFATc1 activation	In vivo efficacy in reducing breast cancer–induced osteolysis	Cancer-associated bone destruction	Poor bioavailability	[57,144]
Cyclosporin A	Classical immunosuppressor	Calcineurin inhibition, preventing NFATc1 dephosphorylation and nuclear translocation	Clinically approved; broad NFAT inhibition	Immunosuppression; inhibition of NFAT-dependent pathways	Nephrotoxicity, hypertension, increased infection risk; unsuitable for long-term use	[145,146]
Tacrolimus (FK506)	Classical immunosuppressor	Calcineurin inhibition, blocking NFATc1 activation	High potency; extensive clinical experience	Immunosuppression in transplantation and autoimmune diseases	Severe systemic toxicity	[146]
VIVIT peptide	Engineered peptide inhibitor	Disruption of NFAT–calcineurin protein–protein interaction	High selectivity for NFAT signaling; useful mechanistic probe	Dissection of NFAT-dependent transcriptional programs	Poor in vivo stability	[147]
NFATc1–c-Jun–c-Fos complex disruption	Emerging molecular strategy	Interference with NFATc1-complex	Potential to preserve NFATc1 activity	Selective regulation of macrophage polarization	Peptide stability, and delivery	This work
c-Jun mimetic peptides	Rationally designed peptides	Competitive occupation of NFATc1 binding interfaces	Theoretically enables selective macrophage response modulation	Fine-tuning M1/M2 macrophage polarization	Technical barriers in optimization	This work

Compared to the traditional NFATc1 antagonists, targeting the assembly process of the NFATc1-c-Jun-c-Fos complex offers a novel approach. For instance, c-Jun mimetic peptides designed to competitively occupy the NFATc1 binding domain demonstrate their potential to selectively modulate macrophage responses. Despite remaining challenges in ensuring specificity, stability, and effective delivery, this strategy represents a significant step toward rational immunomodulation. By deciphering the molecular regulatory network of NFATc1 in macrophages, a clearer blueprint for therapeutic interventions is provided. Compared to broad-spectrum inhibition, precisely modulating NFATc1's interaction network may achieve dual objectives: enhancing M1 macrophage-mediated antimicrobial defense while minimizing adverse toxic effects.

12. Integrating surface roughness modification with NFATc1 targeting for implant infection therapy

The integration of material design and molecular targeting strategies have opened multiple translational pathways. One approach involves modifying the surface roughness of titanium to ensure sufficient macrophage adhesion. Another strategy employs peptide therapeutics (c-Jun mimetics) to precisely and dynamically modulate macrophage polarization toward the M1 phenotype. This integration marks a paradigm shift: implants are no longer passive carriers but become active platforms for immune engineering. By combining surface roughness modification with precise molecular regulation, we can design prostheses that not only fuse with host tissues but also establish intrinsic, long-lasting infection defense mechanisms. Such integrated strategies represent the cutting edge of immune orthopedics, promising to reduce infection-related surgical recurrences and redefine the criteria for long-term implant success.

13. Future perspectives

It is important to first build a validated infection model. While a direct co-culture of *S. aureus* with host cells recapitulates aspects of infection complexity, the multitude of bacterial virulence factors complicate interpretation[148]. Simplified models using

bacterial components, such as lipopolysaccharide (LPS), allow controlled analyses. LPS models also can be progressively expanded to mimic more complex infectious microenvironments[149]. Characterizing these systems requires multidimensional approaches, combining (electron) microscopy, molecular assays and proteomics[150]. Omic analyses are powerful for revealing molecular changes in the local microenvironment during infection[151]. Secondly, designing c-Jun-like peptides is also challenging. First, the structure of the protein-DNA complex formed by NFATc1-c-Jun-c-Fos must be precisely determined. Then the binding kinetics must be fully understood. Furthermore, individual differences in patient immune status, comorbidities, and microbiome composition may also influence implant performance. This highlights the potential for personalized, precision-guided strategies. The dual approach of surface-guided immune modulation and NFATc1-targeted molecular intervention has opened new frontiers in the design of orthopedic prostheses. With a deeper understanding of the mechanisms and the maturation of translational technologies, future implants are expected to not only balance mechanical stability and osseointegration but also actively coordinate host immune defenses. Thereby this strategy also redefines the standard for anti-infective biomaterials in clinical orthopedics.

14. Conclusions

Implant infection remains a formidable clinical challenge, primarily due to a combination of bacterial resistance and immune evasion. Surface engineering of titanium implants offers a promising strategy to manipulate host immunity, particularly by modulating macrophage adhesion. NFATc1, a key molecular hub regulating macrophage-mediated antimicrobial responses, provides a potential target for precision immunomodulation, promoting macrophage differentiation into the M1 phenotype. Combining surface topography with targeted molecular intervention may enable the development of next-generation orthopedic implants that not only resist infection but also actively promote tissue integration. This dual approach paves the way for the rational design of

immunomodulatory biomaterials and represents a paradigm shift towards the development of personalized, infection-resistant implants.

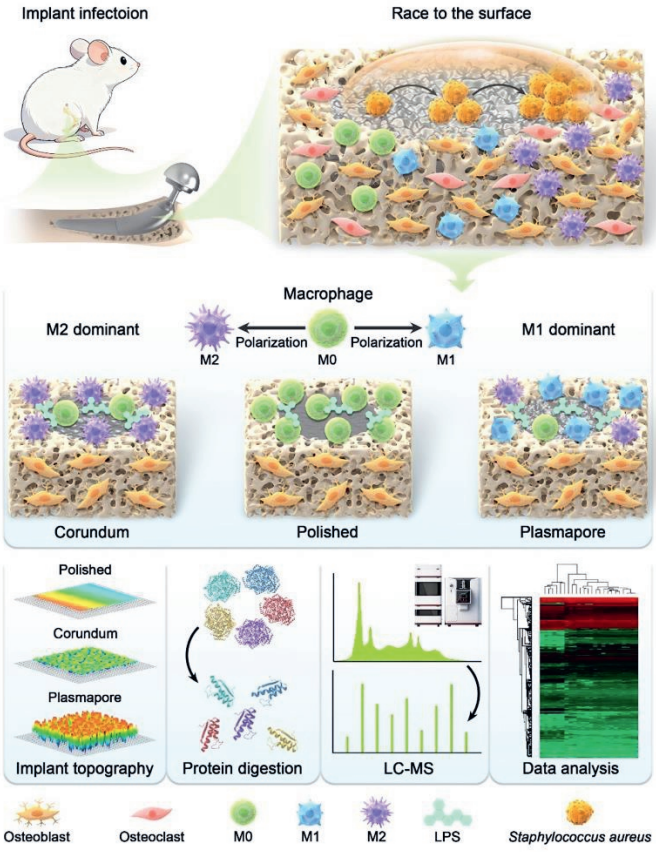
Chapter 2 - Surface characteristics of titanium modulates macrophage inflammatory response

Based on

Cao B., Mohren R., Cillero-Pastor B., Honing M. Surface roughness of titanium implants modulates macrophage inflammatory response. Submitted to Bone & Joint Research.

Abstract

Titanium implant infections remain one of the challenging complications in modern biomedical engineering. Surface properties of biomaterials play a pivotal role in modulating immune response. This study investigates how surface properties of clinically approved titanium implant plates influence macrophage adhesion, activation, and polarization under both homeostatic and inflammatory conditions induced by an *in vitro* LPS-model. The surface structure and chemical composition of polished (polished Ti alloy), corundum (corundum-blasted Ti alloy) and plasmapore (Ti alloy coated with a porous calcium-phosphate layer), were characterized with 3D scanning microscopy SEM coupled with energy-dispersive spectroscopy (EDS) and X-ray diffraction. Macrophages cultured on these surfaces exhibited distinct morphological and molecular responses. Interestingly, in the absence of LPS, only corundum roughness promoted M2-like polarization, suggesting a tissue-reparative phenotype. On the other hand, under LPS stimulation, increasing roughness induced both M1 and M2 polarization, indicating a shift toward a pro-inflammatory state. Proteomic analysis further revealed roughness-dependent changes in protein expression associated with immune signaling and apoptosis. This integrative approach not only enhances our understanding of macrophage-biomaterial interactions but also underscores the potential of tailored biomaterial design in regulating immune reactions for biomedical applications.



Graphical abstract

This figure is created with Adobe Photoshop.

1. Introduction

Titanium (Ti), prized for its biocompatibility and mechanical strength, is extensively used in medical implants such as orthopedic prostheses and dental implants[152]. However, Ti implant infections remain one of the most challenging complications in modern biomedical engineering[153]. Once established, these infections are notoriously difficult to eradicate, often necessitating prolonged antibiotic therapy or surgical intervention[154]. However, in many clinical scenarios, the complete removal of the implant is not feasible, as the device provides essential mechanical or physiological functions to the host[154]. Therefore, understanding and controlling the local immune responses at the implant interface under infectious conditions are of paramount importance[155]. Among various factors influencing the biological infection immune response to biomaterials, surface properties have emerged as an important factor influencing cellular responses, particularly in the context of immune modulation[156].

Upon the Ti implant infection environment, macrophages, as key effector cells of the innate immune system, are central to orchestrating both antibacterial defense and tissue integration processes. Macrophages can adopt diverse phenotypes ranging from pro-inflammatory (M1) to pro-healing (M2), depending on environmental cues and material properties[157]. While previous studies have explored how Ti surfaces characteristics modulates macrophage adhesion and polarization under control conditions[121, 158], little is known about how these surface features influence macrophage behavior during infection[120]. In an infectious microenvironment, macrophages not only adhere to and sense the material surface but also dynamically interact with invading bacteria, balancing between pro-inflammatory and pro-repair phenotypes[159].

Inflammation and infection models provide essential frameworks for dissecting the complex interplay between implant infection and immune activation[160]. Among these, lipopolysaccharide (LPS)–induced inflammation represents one of the most widely employed and mechanistically informative systems[161]. Lipopolysaccharide (LPS), a

major component of the outer membrane of Gram-negative bacteria, acts as a potent agonist of Toll-like receptor 4 (TLR4), triggering a rapid and robust innate immune response[161]. Upon administration, LPS elicits the production of pro-inflammatory cytokines such as TNF-α, IL-1β, and IL-6, leading to systemic inflammatory signaling that closely mimics aspects of bacterial implant infection[162]. This model's strength lies in its reproducibility, temporal precision, and ability to recapitulate key molecular and physiological features of acute inflammation without the confounding variables introduced by pathogens[161]. Hence, the LPS model has become a cornerstone for evaluating anti-inflammatory interventions and elucidating the signaling cascades underlying immune dysregulation[161, 163].

In this study, we provide new insights into how implant surface properties regulate macrophage adhesion and polarization under infectious conditions. Three clinically relevant, approved titanium-based materials were investigated: polished Ti-6Al-4V, corundum-blasted Ti-6Al-4V, and plasma-sprayed Ti-6Al-4V coated with a porous calcium phosphate layer. The effect of surface characteristics both with or without LPS stimulation, on the activation and polarization of macrophages was investigated. Based on an integrated experimental approach, using surface characterization, cell viability assays, gene expression profiling, and proteomic analysis, a deeper insight into the underlying mechanisms by which surface topography and infection mediated conditions influence macrophage adhesion, activation, and polarization is discussed. This work sheds light on an additional facet of surface–immune crosstalk, suggesting possible strategies for designing implant materials that preserve functionality while limiting infection risks.

2. Materials and methods

2.1. Preparation of titanium surfaces

Three types of commercially pure titanium alloy discs (purity > 99.9wt%; diameter 12mm; thickness 1.5mm; Ti-6Al-4V) including highly polished; corundum blasted; and plasmapore coated surfaces (B. Braun, Tuttlingen, Germany). The investigated surfaces

consisted of polished Ti alloy, corundum-blasted Ti alloy, and Ti alloy coated with a porous calcium-phosphate layer. All titanium discs were autoclaved before use.

2.2. Culture of macrophages

Macrophages (RAW264.7 cells, Sigma-Aldrich, USA) were cultured in DMEM medium (Gibco, USA) supplemented with 10% fetal bovine serum (Sigma-Aldrich, USA) and incubated at 37 °C, 5% CO2 in a 95% humidified atmosphere. The cell density was kept at 0.2–1.2 × 106 cells/mL depending on the assay. All discs were put in 24-well non-adherent plates (Greiner-one, Germany) before cell seeding. 5×10^5 monocytes resuspended in 1 mL medium were added to the different surfaces and stimulated with 0, 50, 100, 150, 200, 250, 300 ng/mL LPS (Sigma-Aldrich, USA). Cells were incubated for different time periods until analyses.

2.3. Cell viability: CCK-8

The effect of LPS and Ti disc on macrophage viability was examined using a CCK-8 assay. The UV/VIS absorbance was measured using at 570 nm (Tecan Instruments, Switzerland).

2.4. Surface imaging and morphological analysis

Images of the titanium discs were obtained using a Canon 2000D camera (Canon, Japan) to visually illustrate surface differences. Surface morphology and roughness were further characterized applying scanning electron microscopy (JSM-IT200 InTouchScope™ Scanning Electron Microscope; JEOL, Japan). The material and cells were co-cultured for 24h. The material was washed three times with PBS at 37°C and fixed with glutaraldehyde-osmic acid for 3 h. The fixative was aspirated, and 0.1 mol/L phosphate buffer (pH = 7.2) was added and rinsed for 1 h. The solution was changed four times. The buffer was aspirated and dehydrated by adding ethanol in gradient steps (ethanol concentration 30 % - 50 % - 70 % - 80 % - 90 % - 100 %), with each step remaining for 30 min. Finally, the ethanol was aspirated, a 1:1 mixture of isoamyl acetate and ethanol was added and allowed to soak for 20 minutes with appropriate shaking, then the mixture was aspirated

and pure isoamyl acetate was added and allowed to soak for 20 minutes with appropriate shaking.

The elemental composition of the titanium disc surfaces was analyzed using SEM coupled with energy-dispersive spectroscopy (EDS) and X-ray diffraction (D2 PHASER X-ray Diffractometer; Bruker, Germany). EDS spectra were collected at randomly selected points and averaged across three areas per sample to quantify elemental weight percentages. The EDS analyses were conducted at a landing voltage of 10.0 kV, with a working distance (WD) optimized for imaging, and under high vacuum mode to ensure accurate detection. X-ray diffraction (D2 PHASER X-ray Diffractometer; Bruker, Germany) using Cu Kα radiation (λ=1.5406 Å), 30 kV, 10 mA, coupled 2θ/θ continuous PSD fast scan mode (20–80° 2θ, step 0.02°); data analyzed with Profex 5.6.0. These analyses provided insights into the chemical uniformity of each surface treatment. Surface roughness profiles were determined using a 3D optical surface profiler (OPS-1000 3D Optical Profiler, Komaki, Japan). Measurements were performed in the non-contact mode over a 1 mm² area of each titanium disc. Three replicates were analyzed for each surface type, and the results were averaged to ensure reproducibility.

2.5. Cell adhesion

Macrophage cells were cultured for 2 days. The supernatant was stored for cytokine quantification. Cell monolayers were then washed twice with PBS, immersed in 1 mL MilliQ and went through two freeze and thaw cycles. DNA content was quantified in cell lysates using the Quant-iTTM PicoGreenTM dsDNA Assay Kits and dsDNA reagents (Thermo Fisher, USA) per the manufacturer's protocol.

2.6. Cytokine secretion

The supernatant from all wells was harvested after 24h of incubation. Media were aspirated and transferred to Eppendorf tubes and centrifuged at 400g for 5 min. TNF-α

and IL10 (R&D Systems, USA) ELISA analyses were performed using commercially available kits with a multi-mode spectrophotometer (Tecan Instruments, Switzerland).

2.7. RT-PCR for gene expression analysis

After 24h of culture, wells were washed twice with PBS and total RNA was isolated using the RNeasy Mini Kit (Qiagen, Valencia, CA). RNA quality and quantity were assessed using a Nanodrop ND-1000 Spectrometer (Thermo Scientific, USA). 800 ng of RNA were transcribed to cDNA using SensiFast cDNA Synthesis kit (Meridianbioscience, USA). RT-PCR reactions of GAPDH, INDO, CXCL11, MCR-1, CCL13, TNF-α, IL-10, NFATc1, c-Jun, c-Fos were performed using Fast SYBR Green Master Mix Kit (Meridianbioscience, USA) in an Applied Biosystems PRISM 7500 sequence amplification system with the primers listed in Tab. S1. Each PCR reaction consisted of 1 µL of the cDNA as template, 2 µL (10 pmol) of forward and reverse primers (Tab. S1), 12.5 µL Mastermix, and 9.5 µL RNAase-free water. Thermal cycle conditions consisted of denaturation at 95 °C for 40 s, annealing at 60 °C for 1 min. After 40 cycles, the reaction was completed with a final extension step at 72 °C for 5 min. The expression of target genes was normalized to the relative expression of housekeeping gene GAPDH. Data was calculated using the $2^{-\Delta\Delta Ct}$ method. Representative M1 markers included TNF-α, INDO, and CXCL11, while M2 markers included IL-10, MRC1 (CD206), and CCL13.

2.8. Immunofluorescence characterization of macrophage polarization

To evaluate macrophage polarization states on titanium plates, immunofluorescence staining was performed using markers for M1 (CCR7) and M2 (CD36) phenotypes. Titanium discs with varying roughness were seeded with macrophages and cultured for 24 hrs. After fixation in 4% paraformaldehyde for 15 minutes and permeabilization with 0.3% Triton X-100 in PBS for 10 minutes, samples were blocked with 5% normal goat serum in PBS for 1 hour at room temperature. Primary antibody (Anti-CCR7 antibody, Anti-CD36 antibody) incubation was performed overnight at 4 °C using rabbit monoclonal antibodies diluted in 1% BSA/PBS (Bovine serum albumin/Phosphate buffered saline).

Following PBS washes, samples were incubated for 1 hour at room temperature in the dark with fluorophore-conjugated secondary antibodies (CF™ 568 anti-rabbit IgG, CF™ 488A anti-rabbit IgG). Nuclei were counterstained with DAPI (1 µg/mL), and samples were mounted using antifade medium prior to imaging. Fluorescence images were acquired using a confocal microscope (Zeiss LSM 880) under consistent laser and gain settings across all groups. Quantitative analysis was performed using ImageJ.

2.9. Quantitative assessment of M1/M2 ratio in response to roughness

The macrophage phenotype was assessed based on established surface markers associated with M1 and M2 polarization. CCR7, a chemokine receptor upregulated in classically activated (M1) macrophages[164], and CD36, a scavenger receptor enriched in alternatively activated (M2) macrophages[165], was used as a respective marker[166-168]. To assess the polarization state of macrophages in response to titanium surface roughness, the M1/M2 ratio was redefined based on regions of interest (ROIs), rather than fluorescence intensity. Specifically, individual cells were identified using the DAPI nuclear signal, and ROIs were manually delineated around each cell to ensure accurate cell-based analysis. The number of CCR7-positive ROIs (indicative of M1 polarization) and CD36-positive ROIs (indicative of M2 polarization) were detected using ImageJ. The M1/M2 ratio was calculated by taking the average ratio of CCR7/CD36-positive cells across the population, providing a more cell-specific assessment of polarization. An increase M1/M2 ratio corresponded to a shift toward pro-inflammatory polarization, whereas a lower ratio indicated an M2-dominant, anti-inflammatory state. This quantitative index enabled comparative evaluation of macrophage responses to different titanium surface roughness under both inflammatory and non-inflammatory conditions.

2.10. Label free proteomics

Macrophage cells were seeded and cultured as described above. Then, they were washed four times with 50 mM Ammonium bicarbonate (ABC; Merck). Samples were collected in 5 M Urea, 50 mM Ammonium bicarbonate (ABC) in 1.5 ml Eppendorf tubes. Cell lysis was

performed by three freeze-thaw cycles, (using liquid nitrogen for freezing and sonicating in an ultrasonic bath for thawing). Undissolved particles were removed by centrifugation and proteins in solution were transferred to new tubes. Trypsin-lysC was added to a trypsin: protein ratio of 1:25 and the mixture was incubated overnight at 37 C, adding 20%ACN/10%FA solution, yielding end concentrations of 2%ACN and 1%FA, to stop digestion.

Peptide separation was performed on a Thermo Scientific Ultimate 3000 RSLCnano system equipped with a Thermo Scientific Acclaim PepMap C18 analytical column (15 cm, ID 75 µm, 3 µm). Peptide samples were first desalted on an on-line installed C18 trapping column. After desalting, the peptides were separated with a 30-minute gradient from 4% to 32% Acetonitrile (ACN) with 0.1% FA at a 300 nL/min flow rate. The Thermo Scientific Ultimate 3000 RSLCnano system was coupled to a Q Exactive HF mass spectrometer (Thermo Scientific). The MS was operated in the Data Independent Acquisition (DIA) mode. Thermo Q-Exactive HF was configured to acquire 25 x 24 m/z (400-1000 m/z) precursor isolation window DIA spectra at a resolution of 30,000 using a staggered window pattern. Precursor spectra, mass range 385 – 1015 m/z at 60,000, were interspersed every 25 SEQUEST MS/MS spectra. For protein identification and quantitation, the DIA spectra were analyzed with DIA-NN version 1.8.1. The DIA-NN software was operated in the library-free modus using the *Mus Musculus* (Mouse TaxID 10090_240227) protein database. Cysteine carbamidomethylation was set as fixed modification. RT-dependent cross-run normalization and MaxLFQ normalization. Perseus 2.0.11 software platform was applied for label free comparative analysis.

Adjusted p-values were calculated using the Benjamini–Hochberg procedure to account for false discovery rate (FDR). The protein expression was considered different between conditions at $p \leq 0.05$ (Student's T-test). Principal Component Analysis (PCA) was performed to visualize the variance in proteomic profiles across surface types and LPS treatment conditions. PCA plots were generated using Perseus 2.0.11, with scaling applied

to the data. Functional classification of differentially proteins, Cellular Component analysis and Pathway analysis were carried out using the STRING v.11.5 (https://string-db.org). The proteomics data have been deposited in the PRIDE database via ProteomeXchange(Code: 1-20260423-143013-8014702).

2.11. Statistical analysis

RT-PCR, cell viability and cytokine secretion data are presented as mean ± standard deviation and sample size was 4 (n=4). A one-way ANOVA followed by Tukey post-hoc correction was used for comparison of group means in SPSS (version 21, IBM SPSS statistics, USA6). The Shapiro-Wilk test was employed to assess data normality. A p value of 0.05 was used as a threshold for statistical significance.$*p < 0.05$; $**p < 0.01$; $***p < 0.001$.

3. Results

This study presents the possible correlation between titanium surface characteristics and macrophage polarisation. We evaluated cell viability, adhesion, and morphology across surfaces with different surface profiles. Furthermore, macrophage polarization and proteomic alterations were examined under both basal and LPS-stimulated inflammatory conditions.

3.1. Morphological, roughness profile, and elemental composition of the titanium discs

To characterize the surface properties of three types of commercially available and clinically approved titanium discs, the surface morphology and roughness of polished, corundum, and plasmapore titanium discs were analyzed using 3D scanning microscopy (Fig. 1A), digital imaging (Fig. 1B) and scanning electron microscopy (SEM) (Fig. 1C). Four well accepted surface descriptors reflecting the roughness[169], being mean height (Sa), maximum height (Sz), texture aspect ratio (Str), mean peak curvature (Spc) and developed interfacial area ratio (Sdr), are listed in Tab.1. Hence, the Sa increased significantly between polished (0.69±0.34 µm), corundum (5.51±0.29 µm), and plasmapore

(36.44±1.80 µm). Likewise, the Sz, Str, Spc and Sdr values were well in line with the surface characteristics, supported with images obtained from the microscopy studies (Fig1A, B and C).

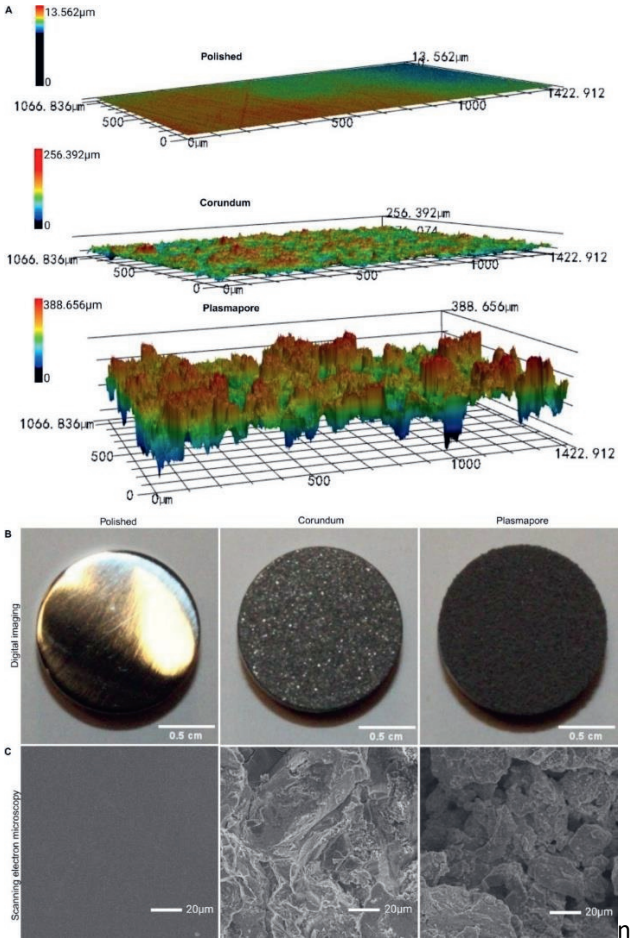


Fig. 1. Surface characterization of polished, corundum and plasmapore titanium discs. (A) 3D surface scanning microscope. Different colors represent the surface elevations; blue is the lowest location, and red is the highest part of the surface. (B) Digital images. (C) Scanning electron microscopy (SEM) images at 20µm.

Tab. 1. Roughness for different discs surfaces. Laser scanning microscopy surface characterization of different titanium discs. (Sa) Arithmetical mean height; (Sz) Maximum height; (Str) Texture aspect ratio; (Spc) arithmetic mean peak curvature;(Sdr) Developed interfacial area ratio.

	Sa(µm)	Sz(µm)	Str	Spc(1/m)	Sdr
Polished	0.69±0.34	344.56±19.49	0.70±0.34	347.04±24.07	0.05±0.01
Corundum	5.51±0.20	73.51±8.39	5.51±0.20	2339.33±143.94	0.39±0.48
Plasmapore	36.44±1.80	7.33±2.82	36.44±1.81	3475.04±2026.87	0.37±0.50

As surface roughness can influence both cell adhesion and viability, it is important to assess compositional differences between samples to understand the effect of topography on macrophage behavior. Therefore, the elemental composition and surface chemistry of the titanium discs were analyzed using SEM-energy dispersive spectroscopy (SEM-EDS) (Tab. 2).

Tab. 2. Elemental composition (SEM-EDS) in weight % as function the different titanium surface disks

	Ti(wt.%)	Al(wt.%)	V(wt.%)	Fe(wt.%)	O(wt.%)	Ca(wt.%)	P(wt.%)
Polished	89.87±0.36	6.48±0.01	3.36±0.11	0.13±0.04	0.16±0.03	0.00	0.00
Corundum	88.80±0.42	6.75±0.30	0.15±0.10	0.15±0.03	3.95±0.03	0.00	0.00
Plasmapore	88.06±0.53	0.20±0.30	0.07±0.10	0.12±0.04	4.97±0.03	3.42±0.05	3.15±0.51

The analysis confirmed the presence of predominately Titanium (Ti) and trace amounts of aluminum (Al), vanadium (V), oxygen (O), Iron (Fe), phosphorus (P) or calcium (Ca), on all surfaces. Aluminum was found in varying amounts which is likely originating from polishing or blasting media, whereas calcium and phosphate residues were mainly detected on the plasmapore discs surface. Titanium was the main element ranging from, 88.87±0.36 wt.% for polished, to 88.80±0.42 wt.% for corundum, and 88.06±0.53 wt.% for plasmapore discs (Fig. 2). The XRD patterns (Fig. 3) of the polished, corundum, and plasmapore surfaces exhibit four prominent diffraction peaks at 35.1°, 38.4°, 40.2°, and 53°, which can be indexed to the (101), (002), and (102) planes of the α-Ti phase, respectively. The sharpness of these peaks indicates that Ti is the predominant element on all sample surfaces. In the polished specimen, an additional peak at 39.2° is attributed

to the formation of a thin TiO_2 oxide film induced by the polishing process. For the corundum surface, diffraction peaks at 25.3°, 43.2°, and 52.4° correspond to the (012), (113), and (006)/(024) planes of Al_2O_3, respectively. Meanwhile, the plasmapore surface exhibits a diffraction peak near 53°, which can be assigned to partially crystallized calcium phosphate (CaP). These findings are consistent with the EDS analysis, confirming that Ti remains the most abundant and constant surface element across all samples. Titanium discs used in this study exhibited comparable elemental compositions, as confirmed by elemental analysis (Tab. 2), allowing assessment of the effects of surface topography on macrophage responses independently of material composition.

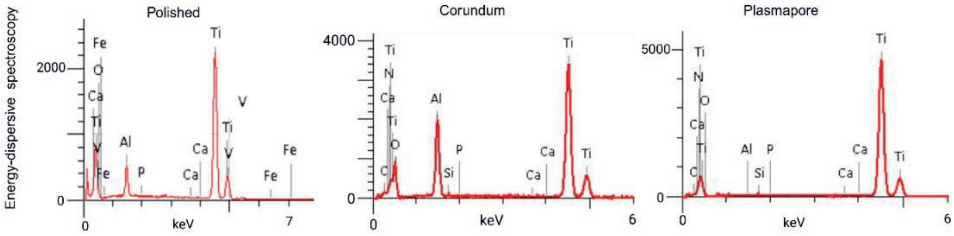


Fig. 2. Energy-dispersive spectroscopy (EDS) spectrum of polished, corundum and plasmapore titanium discs.

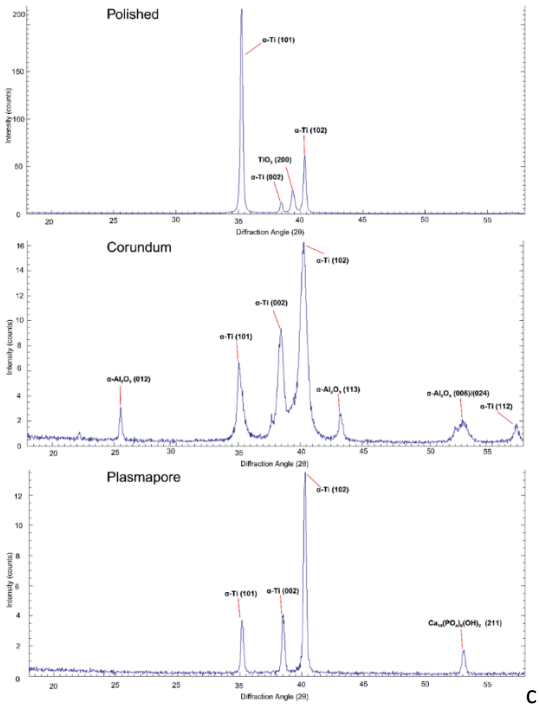


Fig. 3. X-ray diffraction (XRD) patterns of Ti discs. Three surface conditions: polished, corundum, and plasmapore.

3.2. Macrophage viability in response to LPS concentration and titanium surface roughness

Macrophage viability was first assessed following exposure to increasing concentrations of lipopolysaccharide (LPS) (0–300 ng/mL) for 8, 12, and 24 hrs (Fig. S1). A dose- and time-dependent reduction in viability was observed, with 250 ng/mL LPS for 24 h, was selected for subsequent experiments, inducing inflammation while maintaining sufficient cell survival.

The influence of surface roughness on macrophage viability was then assessed using CCK-8 assays (Fig. 4A). Under basal conditions, cell viability remained high (>93%) across all surfaces at all time points. At 24 h, the plasmapore surface exhibited the lowest viability (95.09 ± 0.83%), compared to the polished (98.77 ± 0.98%) and corundum (98.47 ± 0.89%) surfaces. In contrast, under LPS stimulation, viability decreased more substantially on rougher surfaces (Fig. 4B). At 24 h, viability was highest on polished (66.4 ± 1.5%),

intermediate on corundum (61.4 ± 1.1%), and lowest on plasmapore (45.8 ± 1.9%), highlighting the combined effects of surface roughness and inflammatory challenge on macrophage survival.

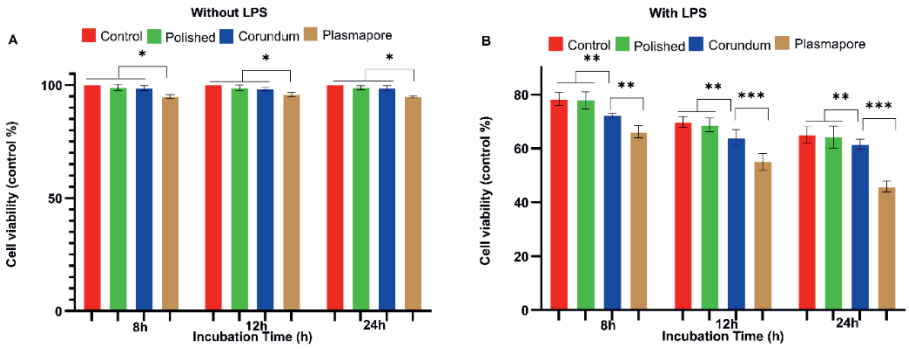


Fig. 4. Macrophage cell viability evaluation by CCK-8 assay. Macrophage cell viability in response to the roughness of Ti discs without LPS (A) and with LPS (B; 250ng/ml). Data show the mean ± SD (control group: cells cultured on 24 wells plate. n=4, *p < 0.05; **p < 0.01; ***p < 0.001).

3.3. Macrophage adhesion and morphology on titanium discs

SEM analysis revealed that surface roughness markedly influenced macrophage morphology (Fig. 5). Under basal conditions, macrophages on polished surfaces were predominantly rounded with limited spreading. Corundum surfaces promoted elongation and extensive adhesion, whereas plasmapore surfaces, despite their higher roughness, displayed reduced spreading and less defined morphology. LPS stimulation enhanced cell spreading across all surfaces, yet corundum surfaces consistently showed superior adherence and morphological integrity, while plasmapore surfaces exhibited lower cell density and compromised structural definition (Fig. 5). Quantification of cell adhesion corroborated these observations (Fig. 6). Corundum surfaces displayed the highest macrophage adhesion (612.23 ± 11.18 ng/mL), followed by plasmapore (575.34 ± 11.01 ng/mL) and polished titanium (485.22 ± 20.54 ng/mL). These results indicate that corundum surface roughness optimizes macrophage adhesion and morphological adaptation under both basal and inflammatory conditions.

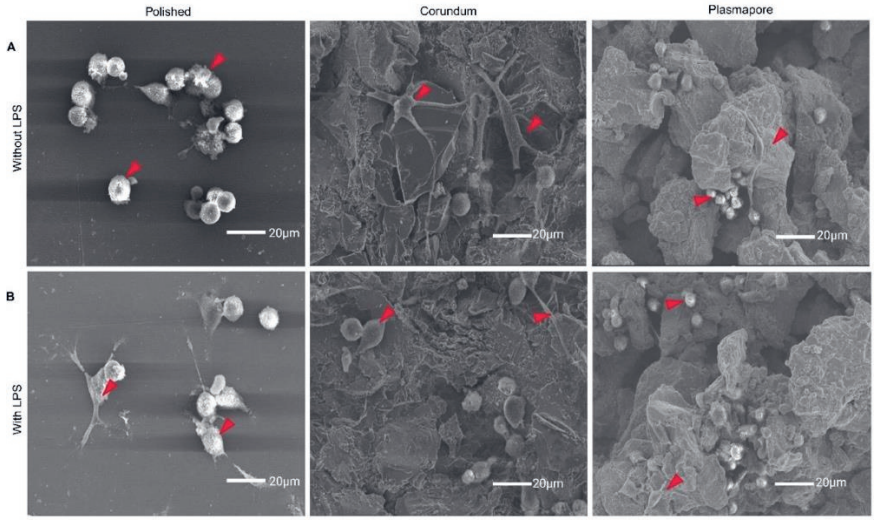


Fig. 5. Morphological characterization of macrophages in interaction with titanium discs (A) before stimulation with LPS and (B) after stimulation with LPS evaluated by SEM imaging. The scale bar shows 20 µm.

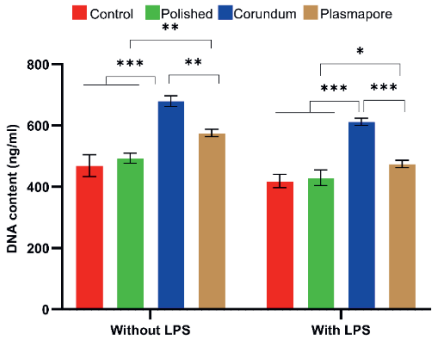


Fig. 6. Macrophage adhesion quantification by Quant-iTTM assay on polished, corundum, and plasmapore Ti discs compared to the control group (24 wells plate) with LPS stimulation or without LPS stimulation. Data show the mean ± SD, one way ANOVA was used to determine statistical significance (n=4, *$p < 0.05$; **$p < 0.01$; ***$p < 0.001$).

3.4. Titanium roughness modulates cytokine secretion

To evaluate the influence of surface roughness on macrophage polarization, the TNF-α and IL-10 secretion was quantified by an ELISA assay. Under basal and LPS-stimulated conditions (Fig. 7) and without LPS stimulation, TNF-α production increased with surface roughness, peaking on plasmapore (35.12 ± 1.26 pg/mL), whereas IL-10 secretion was maximal on corundum surfaces (88.84 ± 6.20 pg/mL), suggesting that moderate roughness favors M2 polarization while excessive roughness enhances basal pro-inflammatory activity. Under LPS stimulation, TNF-α levels escalated substantially, with the highest levels observed on plasmapore (1490.58 ± 48.00 pg/mL). IL-10 secretion remained highest on corundum (145.68 ± 9.95 pg/mL), illustrating that intermediate roughness maintains M2-promoting cues even under inflammatory stress.

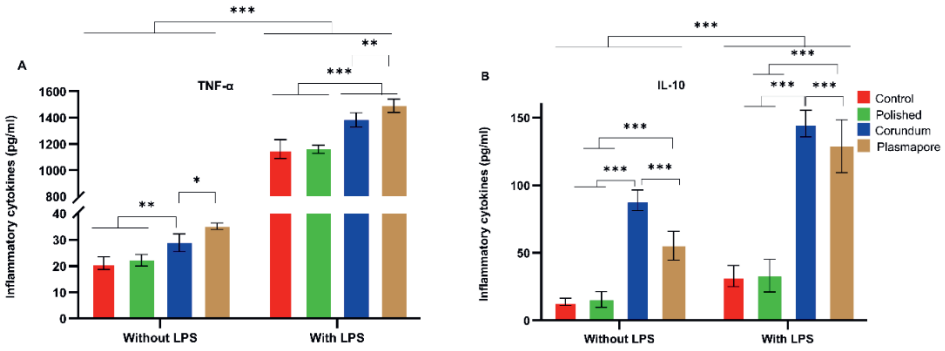


Fig. 7. Quantification of inflammatory cytokines secreted by macrophages cultured on titanium surfaces with LPS stimulation or without LPS stimulation evaluated by ELISA assay. The secretion level of (A) pre-inflammatory cytokine, TNF-α, and (B) anti-inflammatory cytokine, IL-10. Data show the mean ± SD, one way ANOVA was used to determine statistical significance (n=4, *$p < 0.05$; **$p < 0.01$; ***$p < 0.001$).

3.5. Gene expression of inflammatory markers depends on surface roughness

RT-qPCR analysis further characterized macrophage polarization at the transcriptional level (Fig. 8). In the absence of LPS, M1-associated genes increased progressively with roughness, the control group (cells cultured on standard 24-well plates; TNF-α: 0.28 ± 0.11, INDO: 1.54 ± 0.26, CXCL11: 0.94 ± 0.24; $p<0.01$), polished surfaces (TNF-α: 0.28 ± 0.10,

INDO: 1.58 ± 0.54, CXCL11: 1.02 ± 0.32) and corundum surfaces (TNF-α: 0.37 ± 0.06, INDO: 2.39 ± 0.52, CXCL11: 2.47 ± 0.64; $p<0.01$) reaching the highest expression on plasmapore surfaces (TNF-α: 0.49 ± 0.04, INDO: 3.08 ± 0.73, CXCL11: 2.89 ± 0.80: $p<0.01$). Conversely, M2 markers were most upregulated on corundum surfaces group (IL-10: 2.65 ± 0.25, MCR-1: 3.02 ± 0.56, CCL3: 3.19 ± 0.54; $p<0.001$), confirming the preferential induction of reparative phenotypes by moderate roughness. LPS stimulation amplified M1 gene expression across all surfaces, the control group (TNF-α: 60.21 ± 0.71, INDO: 55.18 ± 7.86, CXCL11: 43.75 ± 3.21), polished surfaces (TNF-α: 61.09 ± 1.12, INDO: 53.89 ± 5.17, CXCL11: 44.47 ± 2.40) and corundum surfaces (TNF-α: 68.82 ± 2.05, INDO: 64.46 ± 8.48, CXCL11: 58.84 ± 1.45; $p<0.001$), with plasmapore consistently inducing the highest levels (TNF-α: 74.81 ± 2.88, INDO: 67.09 ± 5.69, CXCL11: 65.36 ± 4.50, $p<0.001$), while corundum surfaces preserved moderate M2-associated gene expression (IL-10: 3.70 ± 0.09, MCR-1: 3.01 ± 0.54, CCL3: 3.62 ± 0.31; $p<0.001$). Transcription factors NFATc1, c-Fos, and c-Jun mirrored these trends, indicating that surface roughness modulates macrophage inflammatory signaling and polarization programs.

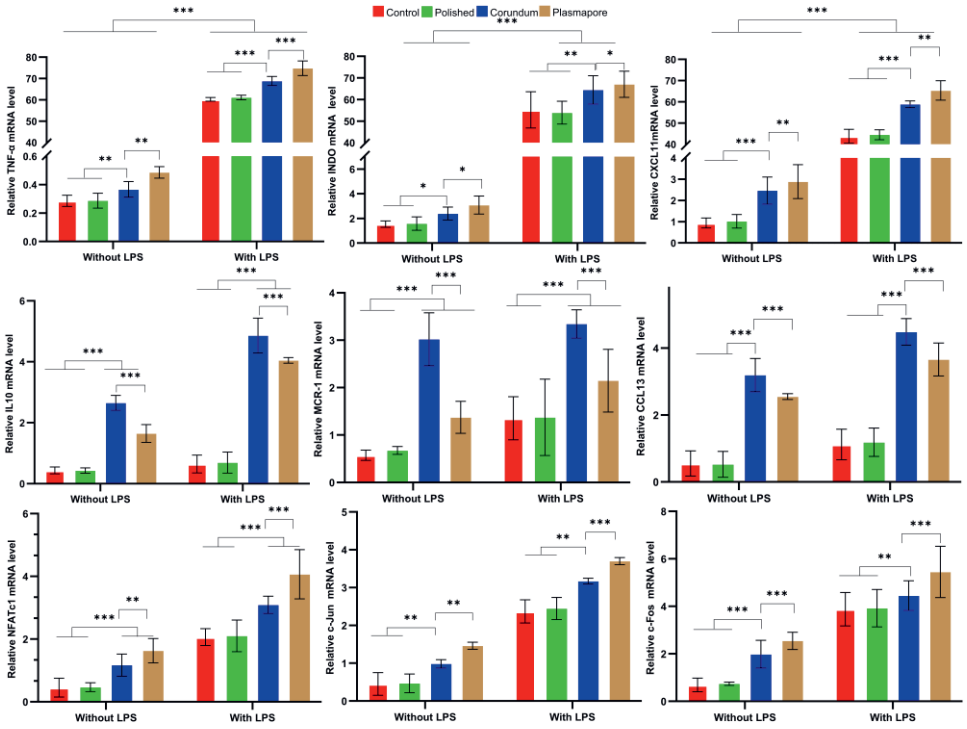


Fig. 8. Relative gene expression of inflammatory markers and immune regulators in macrophages cultured on titanium surfaces with LPS stimulation or without LPS stimulation evaluated by RT-qPCR analysis. The gene expression of (A) pro-inflammatory and M1 macrophage markers (TNF-α, INDO, CXCL11), (B) gene transcription factors (NFATc1, c-Fos, c-Jun), and (C) M2 macrophage markers (IL-10, MCR-1, CCL13). Results are shown as mean ± SD, one way ANOVA was used to determine statistical significance (n=4, *$p < 0.05$; **$p < 0.01$; ***$p < 0.001$).

3.6. Material surface differentially modulates cell marker expression

Differential expression of CCR7 (M1) and CD36 (M2) was observed on titanium surfaces (Fig. 9). Classically activated macrophages (M1) were identified by CCR7 (red fluorescence), while alternatively activated macrophages (M2) were labeled with CD36 (green fluorescence). DAPI staining was used to quantify DNA, indicating that the corundum group promotes cell adhesion. However, the plasmapore group showed fewer adherent cells compared to the polished and corundum groups. This is likely due to the increased

and excessive roughness of the plasmapore surface, which makes cell collection more difficult. Additionally, the fluorescence intensity of CCR7 was consistently higher than that of CD36 across all groups, further confirming that most macrophages were in the M1 state. These findings are consistent with the results obtained from ELISA (Fig. 7) and RT-PCR analyses (Fig. 8). On surfaces with relatively low roughness (polished and corundum), both CCR7 and CD36 fluorescence signals were lower than those observed in the plasmapore group. In contrast, the highly rough plasmapore surface exhibited the lower levels of CD36 and the higher levels of CCR7 signals, suggesting that excessive surface roughness affects both macrophage M1 and M2 differentiation.

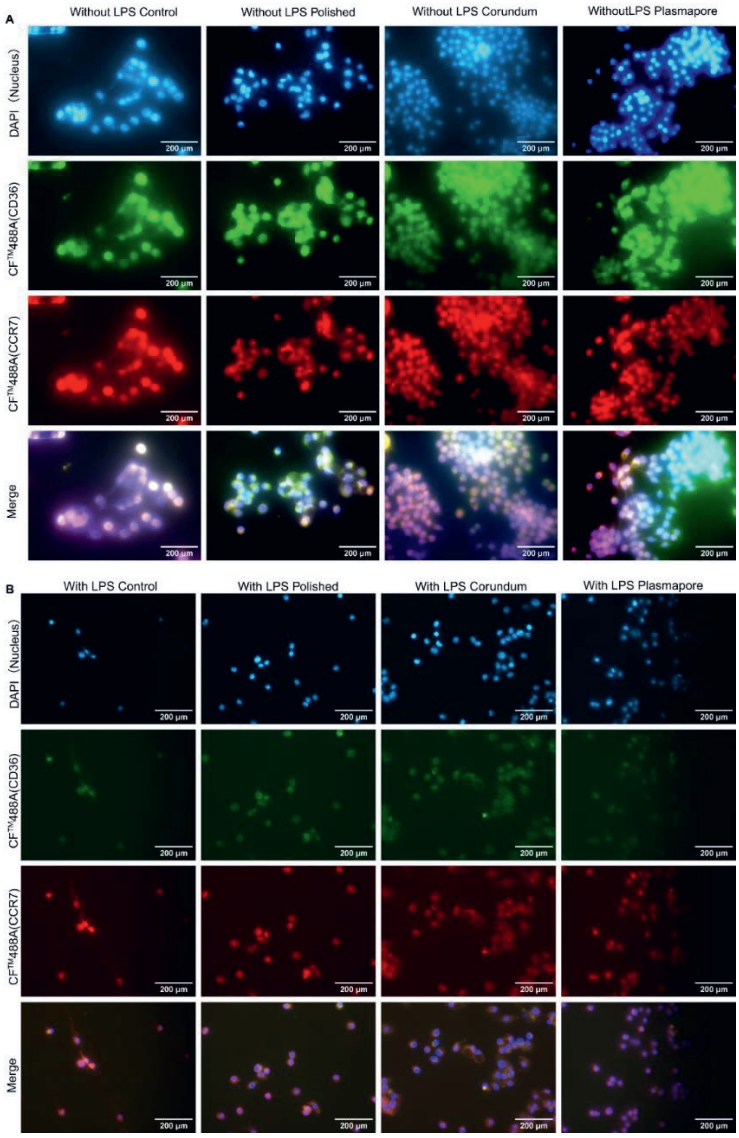


Fig. 9. Immunofluorescence analysis of macrophage polarization on titanium surfaces with different roughness. Macrophages were stimulated without LPS (A) and with LPS (B) cultured on four types of titanium surfaces: Control (24 wells cell plate), polished, corundum, and plasmapore. After 24 h, cells were stained with DAPI (blue, nucleus), anti-CD36 (green, M2 marker, CF™ 488A), and anti-CCR7 (red, M1 marker, CF™ 568). Merged images highlight colocalization of polarization markers with nuclei. The scale bar shows 100 µm.

Quantification of the ratio of CCR7 to CD36 fluorescence intensity (M1/M2 ratio) corroborated these findings (Fig. 10), with corundum surfaces maintaining a more balanced profile, while plasmapore surfaces shifted strongly toward M1, particularly under LPS stimulation. In the absence of LPS stimulation, macrophages exhibited a relatively low M1/M2 ratio across the surface topographies ranging from polished to plasmapore, with a trend toward increased M2 polarization with increasing surface roughness. Notably, the corundum group (0.33 ± 0.16) displayed a significantly lower M1/M2 ratio compared to the control (0.92 ± 0.19), polished (1.01 ± 0.18), and even the plasmapore group (0.33 ± 0.16). The LPS-stimulated control group (cells cultured on 24-well plates) exhibited an M1/M2 ratio of 8.50 ± 0.09. A comparable ratio was observed on polished titanium surfaces (8.62 ± 0.08, $p > 0.05$), indicating no significant difference. In contrast, the corundum surface (8.95 ± 0.12, $p < 0.01$) and plasmapore surface (9.02 ± 0.10, $p < 0.05$) showed a significantly higher M1/M2 ratio. These results suggest that a shift toward M1 polarization with increasing surface roughness, broadly in agreement with ELISA and RT–qPCR data. This trend, together with cell viability data (Fig. 4), suggests that excessive roughness may impair macrophage differentiation by affecting overall cellular function.

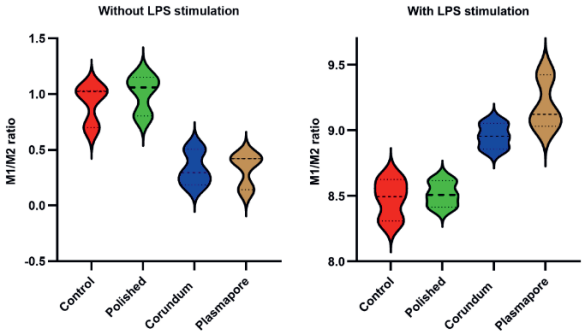


Fig. 10. Quantification of macrophage polarization (M1/M2 ratio) in response to varied roughness. Macrophages were cultured on titanium discs with varying surface roughness in the absence or presence of LPS stimulation. The M1/M2 polarization ratio was determined by quantifying the number of $CCR7^+$ (M1) and $CD36^+$ (M2) positive regions of interest (ROIs) per cell using ImageJ. Data show the mean ± SD (n=4).

3.7. Proteomic profiling and molecular function enrichment in macrophages on titanium surfaces with different roughness

To investigate how surface topography modulates the macrophage proteome under both LPS-stimulated and unstimulated conditions, a classical bottom-up proteomics strategy was employed using liquid chromatography-tandem mass spectrometry (LC-MS/MS). Proteomic analysis identified 1610 (Tab. S2, S3) high-confidence proteins, with differential expression linked to surface roughness.

GO enrichment revealed that corundum surfaces enhanced ATP-dependent and catalytic activity proteins, cytoskeletal elements, mitochondrial components, and immune-related pathways, reflecting a metabolically active, immunocompetent phenotype (Fig. 11). In contrast, plasmapore surfaces showed reduced structural protein enrichment, attenuated immune pathways, and increased stress-response proteins, indicative of an immunosuppressed phenotype (Fig. 11). Compared to the LPS-treated control group, macrophages on polished titanium surfaces showed enrichment of upregulated proteins associated with ATP-dependent activity (57.5%), catalytic activity (25.9%), and molecular adaptor activity (5.3%). Additional upregulated functions included transporter activity (4.3%), binding (2.6%), and molecular transducer activity (2.7%). Downregulated proteins on polished surfaces were mainly involved in molecular function regulator activity (68.6%) and cytoskeletal motor activity (23.4%). Comparing corundum to polished surfaces, upregulated proteins remained enriched for ATP-dependent activity (58.2%) and catalytic activity (27.8%). Downregulated proteins on corundum surfaces showed enrichment in structural molecule activity (28.5%), molecular function regulator activity (45.7%), and antioxidant activity (13.8%). Further comparison between plasmapore and corundum surfaces indicated increased proportions of upregulated proteins linked to catalytic activity (48.7%) and ATP-dependent activity (36.9%) on plasmapore. Downregulated proteins on plasmapore surfaces were predominantly associated with structural molecule activity (58.3%), followed by molecular function regulator activity (16.8%), antioxidant activity (13.8%), and cytoskeletal motor activity (11.1%).

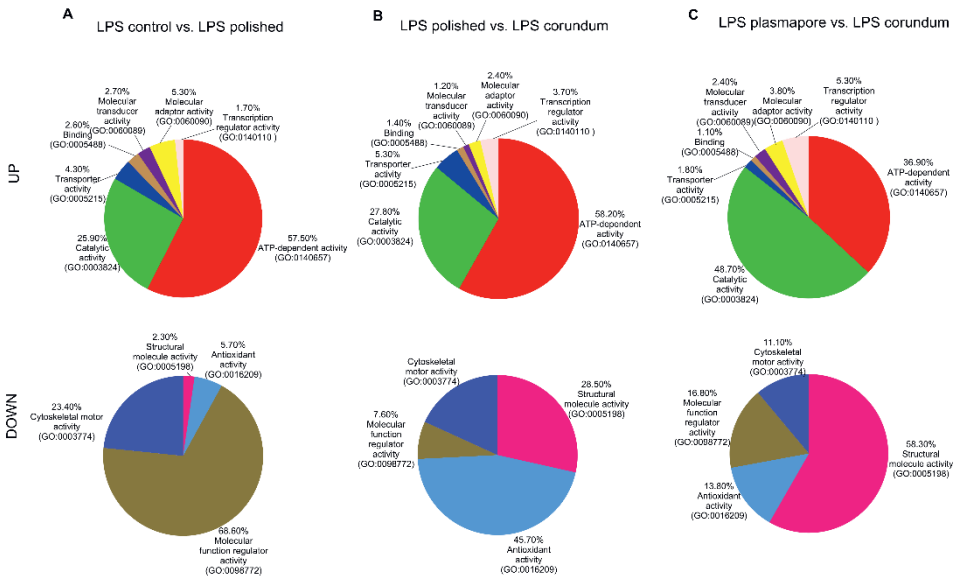


Fig. 11. Pie chart depicting the molecular function classification of differentially regulated proteins in cultured macrophages with LPS stimulation on control compared to polished surface, polished surface compared to corundum discs compared to plasmapore discs. (A) Control compared to polished surface with LPS stimulation, (B) polished surface compared to corundum discs with LPS stimulation, (C) corundum discs compared to plasmapore discs with LPS stimulation.

Cellular component enrichment analysis was conducted to evaluate the impact of titanium surface roughness on macrophages under LPS-stimulated inflammatory conditions. Comparisons were made among control, polished, corundum, and plasmapore surfaces (Fig. 12). Our findings indicate that increasing titanium surface roughness significantly alters the enrichment of specific cellular components in macrophages. These changes suggest that surface topography modulates the inflammatory response by influencing mitochondrial function, cytoskeletal organization, and protein synthesis and processing pathways. Compared to the LPS-treated control group (cells cultured on 24 wells plate with LPS stimulation), macrophages cultured on polished surfaces exhibited moderate enrichment in mitochondrial components,

including mitochondrion, mitochondrial inner membrane, and mitochondrial matrix. Protein synthesis and processing components were also enriched on polished surfaces, such as cytosolic ribosome, spliceosomal complex, proteasome core complex, chaperone complex, rough endoplasmic reticulum, and endomembrane system.

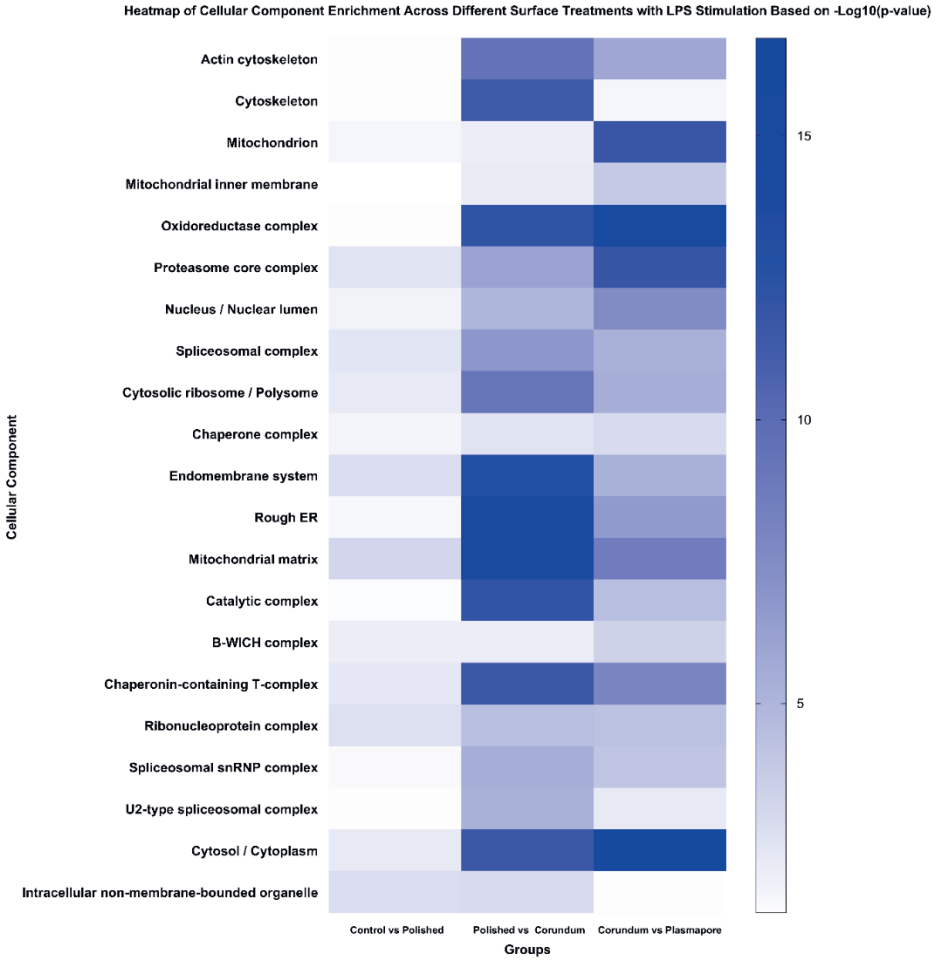


Fig. 12. Heatmap of the enrichment of cellular components (-Log10 fold change) in macrophages stimulated with LPS and cultured on titanium surfaces with varying roughness. The color intensity corresponds to the -Log10 (fold change), where darker colors denote higher statistical significance.

Transitioning from polished to corundum surfaces resulted in increased enrichment across multiple cellular components. Structural elements, including cytoskeleton and actin cytoskeleton, showed marked enrichment. Mitochondrial components increased moderately (mitochondrion, mitochondrial inner membrane, mitochondrial matrix). Components related to oxidative metabolism, such as oxidoreductase complex and catalytic complex, were highly enriched. Protein synthesis and processing components showed further elevation: cytosolic ribosome, spliceosomal complex, proteasome core complex, chaperone complex, rough endoplasmic reticulum, endomembrane system, and chaperonin-containing T-complex. Nuclear components, including nucleus/nuclear lumen and spliceosomal snRNP complex, were also enriched.

Comparisons between corundum and plasmapore surfaces indicated additional changes in enrichment patterns. Mitochondrial components showed increased enrichment (mitochondrion, mitochondrial inner membrane, mitochondrial matrix), along with oxidoreductase complex and proteasome core complex. Structural components decreased relative to corundum (cytoskeleton, actin cytoskeleton). Nuclear and RNA-processing components remained enriched, including nucleus/nuclear lumen, spliceosomal complex, spliceosomal snRNP complex, ribonucleoprotein complex, and U2-type spliceosomal complex. Cytosol/cytoplasm demonstrated the highest enrichment. Endomembrane system, rough endoplasmic reticulum, and chaperonin-containing T-complex maintained elevated enrichment. Intracellular non-membrane-bounded organelles showed mild enrichment in polished versus control and polished versus corundum comparisons but decreased in corundum versus plasmapore. Reactome analysis confirmed that moderate roughness promotes immunometabolic engagement, whereas excessive roughness triggers proteotoxic and biomechanical stress, potentially compromising implant integration under inflammatory conditions (Fig. 13).

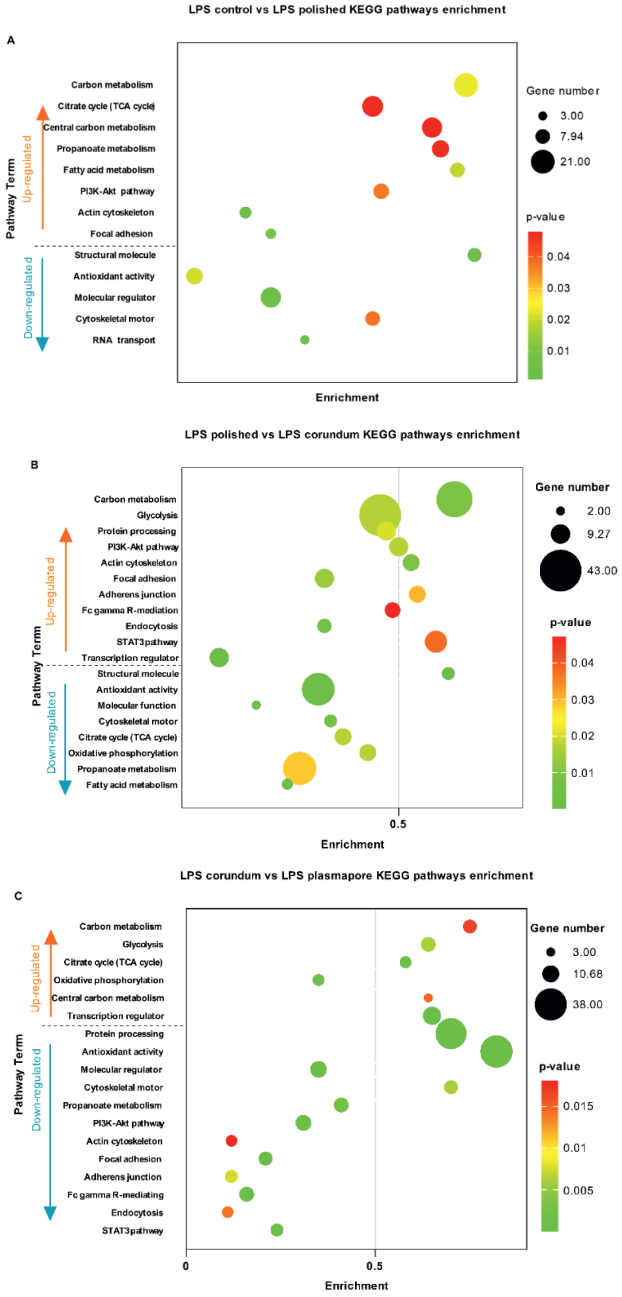


Fig. 13. Enriched reactome pathways associated with proteins differentially expressed in macrophage cells cultured on Ti. Macrophage responses on LPS control vs. LPS polished, LPS polished vs. LPS corundum titanium surfaces and LPS plasmapore vs. LPS corundum titanium surfaces.

Compared to the LPS-stimulated control group (cells cultured on standard 24-well plates), macrophages on polished titanium surfaces showed significant upregulation of innate immune pathways, including Fc epsilon receptor (FCERI) signaling, CD209 (DC-SIGN) signaling, and C-type lectin receptor (CLR) signaling. Metabolic pathways such as the tricarboxylic acid (TCA) cycle, respiratory electron transport, and gluconeogenesis were also enriched. In contrast, pathways involved in cell cycle regulation and protein ubiquitination were downregulated.

Macrophages cultured on corundum surfaces (compared to polished surfaces) exhibited further upregulation of immune-related pathways, including the innate immune system, cytokine signaling, and interferon signaling. Antigen processing and cross-presentation pathways, as well as the endoplasmic reticulum (ER)-phagosome pathway, showed significant enrichment. Metabolic pathways related to mitochondrial function and glycolysis (TCA cycle, glycolysis, and mitochondrial biogenesis) were increased. Some oxidative phosphorylation and mitochondrial translation pathways were downregulated. Additionally, pathways linked to selective autophagy and ER stress were upregulated.

Under LPS stimulation, comparison between corundum and plasmapore surfaces revealed distinct differences in pathway enrichment. FCERI signaling and MAPK activation pathways remained enriched on plasma-treated surfaces; however, interferon signaling, cytokine signaling, and antigen presentation pathways were significantly downregulated relative to corundum. Pathways associated with cellular stress responses, heat shock proteins, and protein folding were upregulated on plasmapore surfaces. Mitochondrial metabolism-related pathways, including the TCA cycle, remained moderately active, supporting the notion that macrophages attempt to meet elevated metabolic demands induced by complex topography, albeit at the cost of inflammatory competence These demonstrate that moderate roughness (corundum) promotes immunometabolic activity and immune engagement, excessive roughness (plasmapore) shifts macrophages toward

a stress-adaptive, metabolically taxed, and immunosuppressed phenotype, potentially undermining implant-tissue integration in inflammatory environments.

4. Discussion

This study examined macrophage responses to titanium surfaces the effect of physico- and chemical properties, both in the absence and presence of LPS stimulation. More specifically, this research focused on the effect of surface roughness and at the presence of polished surface (polished Ti alloy), corundum surface (corundum-blasted Ti alloy) and plasmapore surface (Ti alloy coated with a porous calcium-phosphate layer) on macrophage viability, adhesion, polarization, and immunometabolic programming. Under non-inflammatory conditions, macrophage viability remained consistently high across the three clinically established materials. This is consistent with prior observations by Melo-Fonseca, F., et al., who reported that surface roughness within a certain threshold does not compromise cellular viability. However, at 24 h, macrophages on the plasmapore surface exhibited a modest reduction in viability compared to the corundum surface. This decline is consistent with previous observations that excessively roughness impose mechanical stress on adherent cells [170].

Upon LPS stimulation, the tolerance window narrowed dramatically, with viability dropping to 45.8 ± 1.9% on the plasmapore surface at 24 h whereas corundum maintained robust survival. Excessive roughness may act as a biomechanical stressor that sensitizes macrophages to inflammatory stimuli—a notion further supported by increased expression of stress-responsive transcription factors such as c-Fos and NFATc1. These findings align with prior observations that extreme topographies can disrupt cellular homeostasis and reduce implant biocompatibility and indicate that infection synergizes with topographical stress to trigger macrophage dysfunction, emphasizing the need for balanced roughness in implant design[171].

Surface roughness also governed macrophage adhesion and spreading[172]. Excessively smooth surfaces can impair cell attachment, while overly rough textures may also hinder stable anchorage[173]. DNA quantification and SEM revealed maximal attachment on the corundum surface, which exceeded both polished and plasmapore surfaces under both without and with LPS-stimulation. These observations are consistent with reports by J. Chen et al., which similarly demonstrated optimal macrophage attachment and spreading on moderately rough surfaces, with reduced cell density and poor morphology on excessively rough substrates[174]. This supports the concept of an optimal roughness threshold, where intermediate roughness provides sufficient micro-scale anchorage while avoiding excessive mechanical strain. The improved adhesion on corundum suggests favorable mechanical and biochemical conditions for macrophage engagement, essential for orchestrating subsequent immune and regenerative responses.

Crucially, surface roughness directly modulated macrophage polarization and cytokine secretion [175]. SEM results demonstrate that surface topography not only facilitates M2 polarization under non-inflammatory conditions but can also promote M2-like differentiation even in the presence of an inflammatory stimulus. This also reflected by elevated IL-10 production and upregulation of MCR-1 and CCL3. Excessive roughness acts as a biomechanical stressor capable of activating stress-responsive transcriptional programs. In support of this, we observed progressive upregulation of transcription factors involved in macrophage activation and polarization, c-Fos, NFATc1, and c-Jun, with increasing surface roughness, particularly on the plasmapore surface. These data reveal that increasing topographical complexity drives a progressive shift toward M1 polarization.

Hotchkiss et al. demonstrated that rough titanium surfaces promote macrophage M2 polarization, leading to a more anti-inflammatory environment[176]. Interestingly, corundum surfaces maintained a balanced M1/M2 phenotype even under inflammatory stimulation, suggesting that moderate roughness preserves macrophage plasticity. Immunofluorescence staining confirmed CCR7 (M1-associated)[177] and CD36 (M2-

associated)[178] markers across all surfaces. This is also consistent with previous reports by Jablonski al., which highlighted the overlapping expression of phenotypic markers between M1 and M2 macrophages[179]. We observed that the M1/M2 ratio increased alongside surface roughness, peaking on plasmapore. These are in strong agreement with our SEM observations, ELISA cytokine profiling, and RT-PCR gene expression analyses, reveal that roughness significantly shift toward M1 macrophage polarization. This observation underscores that surface properties are sufficient to bias immune polarization, acting as a mechanotransducive signal. Moderate roughness promotes a functionally balanced macrophage state, while excessive roughness acts as a biomechanical stressor that amplifies inflammation but diminishes viability. Proteomic analysis revealed the molecular basis by which surface roughness governs macrophage function. On the corundum surfaces, proteins involved in ATP-dependent and catalytic activities were upregulated, reflecting elevated metabolic activity. In contrast, proteins downregulated on corundum were enriched in structural, regulatory, and antioxidant functions, suggestive of a macrophage phenotype poised for activation while maintaining redox and structural homeostasis[180]. Enrichment of cytoskeletal and mitochondrial proteins suggests increased mechanotransduction and oxidative metabolism[53, 54]. The activation of proteasome and ER-chaperone networks further indicates an adaptive response to enhanced secretory and metabolic demands[55].

In contrast, macrophages on the plasmapore surfaces exhibited downregulation of structural and motor-related proteins but upregulation of stress-related and protein-folding pathways. This pattern signifies a shift from functional activation to stress adaptation. Pathway enrichment confirmed that corundum surfaces induced immune-related signaling—cytokine, interferon, and antigen presentation pathways—coupled with metabolic programs such as glycolysis and the TCA cycle. Conversely, excessive roughness attenuated pro-inflammatory signaling while activating heat-shock and oxidative stress responses, suggesting cellular exhaustion and compromised immune competence. These findings support the concept that surface roughness acts as a

mechanotransductive regulator, integrating physical cues into immunometabolic and structural reprogramming of macrophages. The interplay between surface characteristics and macrophage behavior provides key insights for biomaterial design. Corundum surface fosters macrophage adhesion, viability, and a balanced immune phenotype—conditions conducive to successful tissue integration. Conversely, plasmapore roughness promotes stress-induced inflammation and cytotoxicity, which may impair osseointegration. These findings suggest that controlling surface topography within an optimal window can fine-tune host immune responses, achieving a balance between necessary inflammatory activation and anti-inflammatory resolution. Such topography-driven immune modulation represents a promising strategy for designing next-generation titanium implants with enhanced immunocompatibility and infection resistance.

Despite its contributions, this study has several limitations. RAW-derived macrophages might exhibit a reduced sensitivity compared to primary macrophages, possibly due to their proliferative nature. The use of human macrophage cells followed by bacterial infection would address some of the limitations of the current study. Moreover, future studies employing co-culture or *in vivo* systems are warranted to elucidate macrophage–material interactions. Under infectious conditions, corundum facilitates macrophage activity, adhesion, and polarization. However, this also poses a challenge: the increased proportion of M2-type macrophages may compromise bacterial clearance at the material interface. Therefore, the use of corundum may require combination strategies involving agents that modulate macrophage polarization to optimize infection control.

5. Conclusion

Surface topography emerges as a key determinant of Ti alloy infection immune compatibility. Moderate Ti alloy with corundum-blasted roughness surfaces preserve macrophage adhesion, viability, and balanced polarization through coordinated metabolic and cytoskeletal activity, whereas extreme Ti alloy roughness with a calcium phosphate coating layer triggers metabolic stress and pro-inflammatory activation. These findings

highlight surface modification as a strategy to modulate immunomodulation in implants infection prevention.

Chapter 3 - Effect of titanium surface roughness on macrophage-bacteria interactions

Based on

Cao B., Cillero-Pastor B., Honing M. Effect of titanium surface roughness on macrophage-bacteria interactions. Submitted to Biofilm.

Abstract

Surface roughness of titanium implants enhances osseointegration but increases susceptibility to *S. aureus* colonization during infection. Macrophages play a key role in bacterial clearance at infected implants. Here, we investigated the impact of titanium surface roughness on macrophage–bacteria interactions. We observed that increased surface roughness alters the balance of macrophage polarization between the M1 and M2 phenotypes. Specifically, during the early phase of infection (within 12 hrs), the proportion of M1 macrophages increases, favoring a pro-inflammatory, bactericidal response. By contrast, at later stages (12–24 hrs), M2 macrophages become more prevalent, accompanied by reduced reactive oxygen species (ROS) generation and a transition towards tissue repair and immune resolution. Proteomic profiling reveals that these phenotypic transitions are mediated through key pathways, including chemokine, HIF and sphingolipid signaling, estrogen response, necrotic and endocytic processes. These findings provide mechanistic insight into how surface topography modulates immune dynamics during implant-associated infection.

1. Introduction

Titanium (Ti) implants are widely used in orthopedic and dental surgery due to their excellent mechanical properties, corrosion resistance, and biocompatibility[181-183]. It is the most widely used material in orthopedic implants, including joint replacements and internal fixation devices[184-186]. Surface modification of titanium can enhance osseointegration and implant stability[113, 187]. Micro- and nanoscale roughening have been extensively employed to enhance implant integration by promoting osteoblast adhesion and bone ingrowth[113, 188, 189]. However, despite their advantages in osseointegration, rough surfaces present a paradox: they also provide a favorable niche for bacterial adhesion and biofilm formation[13], particularly by *S. aureus*, being the most common pathogen associated with implant-related infections[15, 74, 190-192]. These infections remain a leading cause of implant failure, often necessitating revision surgery posing significant clinical and economic burdens[193-195].

Macrophages serve as key regulators of the host response to implanted biomaterials, orchestrating both antimicrobial defense and tissue repair[196, 197]. They are the primary immune cells responsible for bacterial clearance[101, 198]. Upon encountering pathogens, macrophages undergo dynamic phenotypic transitions between classically activated M1 states[199], which mediate inflammation and bacterial killing, and alternatively activated M2 states[200], which support resolution and tissue regeneration[120]. Although the role of macrophages in sterile implant environments has been well studied[201], the role of surface roughness influencing macrophage behavior in the context of bacterial infection remains poorly understood[202]. During implant-associated infections, the impact of surface roughness on the local microenvironment remains unclear[203-205]. Recent studies have suggested that biomaterial surface properties can modulate the function of innate immune cell[52], yet the temporal dynamics of macrophage polarization in response to both topography and infection cues are unclear[52]. Furthermore, the molecular pathways underlying this interaction at the implant–host–pathogen interface are largely unexplored[74].

This study aimed to investigate how Ti surface roughness modulates macrophage–bacteria interactions during both early and late stages of *S. aureus* infection. Through a combination of phenotypic assays, ELISA, RT–PCR, and analyses of macrophage activity, the influence of surface roughness on the regulation of macrophage polarization, adhesion, phagocytosis, and clearance of *S. aureus*, was investigated. Proteomic analysis revealed the key pathways underlying these surface-driven immunological responses. The findings provide new insights into the immunomodulatory role of biomaterial topography under infectious conditions and establish a framework for the rational design of infection-resilient implants via targeted immune modulation.

2. Materials and Methods

2.2. Preparation of titanium discs for cell co-culture

Titanium discs with polished, corundum, and plasmapore surfaces were purchased with 12 mm in diameter and 1.5 mm in thickness (B.Braun, Tuttlingen, Germany). Surface elemental analysis confirmed titanium as the predominant component across all groups (Chapter2). The average surface roughness (Sa) was 0.69 ± 0.34 µm for polished discs, 1.32 ± 0.28 µm for corundum discs, and 36.44 ± 1.80 µm for plasmapore discs. All samples were sterilized by autoclaving at 121 °C for 1520 minutes and stored under aseptic conditions until further use.

2.3. Culture of macrophage cells on titanium discs

Macrophage cells (RAW264.7 cells, Sigma-Aldrich, USA) were cultured in DMEM medium (Gibco, USA) containing 10% fetal bovine serum (FBS, Sigma-Aldrich, USA) in a cell incubator (37 °C, 5% CO2). The cells were added to the surface of the titanium disc with a density of 5×10^5 cells/mL. The culture medium was changed every 48h. Cells in the 24-well plates were labeled as control group.

2.4. Preparation of *GFP-labeled S. aureus*

To construct the *GFP-labeled S. aureus*, 2 µg of GFP plasmid (FigS1, GenScript, UK) was added to *Staphylococcus aureus* (*S. aureus*, Sigma-Aldrich, Germany) cells in a sterile electroporation cuvette (Sigma-Aldrich, Germany). The mixture was incubated for 30 minutes on ice to allow for plasmid uptake. Electroporation was carried out using a pulse electroporator (Eppendorf, Germany) and in a 1 mm cuvette (25 µF, 100 Ω, and 2.2 kV). After transfection was completed, the cells were placed in rescue medium (37 ℃, 1 h). Then 100 µL of *S. aureus* cells was inoculated to the Karamycin agar plate (37 ℃, overnight). Successful transformation was confirmed by fluorescence microscopy, observing GFP expression in the bacterial cells. After overnight incubation single colonies were inoculated in Broth medium (Becton, Dickinson and Company, USA). Following 6h incubation, the bacterial culture was adjusted to a final concentration of 10^4 CFU/mL for use in subsequent co-culture experiments with macrophages.

2.5. Optimization of bacterial concentration for macrophage interaction

Macrophages were cultured in 96-well plate (37°C, 5% CO_2). They were harvested by scraping, counted, and adjusted to 5×10^5 cells/mL. A 100 µL suspension (5×10^4 cells/well) was seeded into a 96-well plate and incubated overnight (37°C, 5% CO_2). *GFP labeled S. aureus* were adjusted to 10^2, 10^4, 10^6, and 10^8 CFU/mL using serial concentrations dilutions in DMEM. The macrophages were washed with sterile PBS to remove non-adherent cells, and 100 µL of *S. aureus* suspension at varying concentrations was added to each well. After incubation (37°C, 5% CO_2, 6, 8, 12, and 24 h), supernatants were aspirated, and the macrophages were washed three times with PBS. To ensure that viable *S. aureus* does not interfere with the detection of macrophage activity, medium containing penicillin (100 U/mL) and streptomycin (100 µg/mL) was added for 1 hour at 37°C. The cells were washed to remove the dead bacteria and antibiotics. The macrophages were detached, centrifuged, resuspended in PBS, and mixed with 0.4% Trypan Blue for viability assessment. Cell viability was measured under a light microscope (ZEISS, Germany) and the percentage of viable cells was calculated.

2.6. Co-culture of macrophages and *GFP-labeled S. aureus* on Ti discs

The macrophages were gently washed with sterile phosphate-buffered saline (PBS) to remove any non-adherent cells. *GFP-labeled S. aureus* (10^4 CFU/mL) was added to each well containing macrophages and titanium discs with different surface roughness: polished, corundum, and plasmapore. The co-culture system was incubated at 37°C in a 5% CO_2 incubator for 6, 12, and 24 hrs to assess macrophage-bacteria interactions at various stages. This setup allowed for the examination of how different titanium surface roughness influences the dynamics of macrophage response to *S. aureus* over time.

2.7. Assessment of macrophage viability on different titanium surfaces

To assess the impact of titanium surface properties on macrophage viability, macrophages were seeded onto titanium discs (polished, corundum, and plasmapore) in 24-well plates at a density of 5×10^4 cells/well. After overnight incubation at 37°C in 5% CO_2 for cell attachment, the medium was replaced with fresh DMEM, and macrophages were cultured for 6, 12, and 24 hrs on the different titanium surfaces. Each condition was performed in triplicate. After incubation (37°C, 5% CO_2, 6, 8, 12, and 24 h), supernatants were aspirated, and macrophages were washed three times with PBS. To ensure that viable *S. aureus* does not interfere with the detection of macrophage activity, medium containing penicillin (100 U/mL) and streptomycin (100 µg/mL) was added for 1 hour at 37°C. Cells were then washed again to remove dead bacteria and antibiotics. Macrophages were detached, centrifuged, resuspended in PBS, and mixed with 0.4% Trypan Blue for viability assessment. Cell viability was measured under a light microscope (ZEISS, Germany) and the percentage of viable cells was calculated.

2.8. SEM and TEM imaging of macrophage morphology

To assess the macrophage morphology on different titanium surfaces, JSM-IT200 inTouchScope scanning electron microscopy (SEM, JEOL Ltd, Japan) and FEI Tecnai G2 Spirit BioTWIN transmission electron microscopy (TEM, Thermo Fisher Scientific, USA) were employed. After co-culture, titanium discs were washed with sterile PBS to remove

non-adherent cells and bacteria. For SEM imaging, the discs were fixed in 2.5% glutaraldehyde in PBS at 4°C overnight, followed by post-fixation in 1% osmium tetroxide for 1 hour. The samples were dehydrated through an ascending series of ethanol concentrations (50%, 70%, 90%, 100%), and critical-point drying was performed to preserve the cell morphology. The dried samples were sputter-coated with gold and examined using a field emission SEM at an accelerating voltage of 5 kV. For TEM imaging, the cells were first scraped from the surface of the titanium discs using a cell scraper, then fixed in the same glutaraldehyde solution and processed through a series of dehydration steps. The samples were embedded in epoxy resin and polymerized at 60°C. Ultra-thin sections (70 nm) were cut using an ultramicrotome and stained with uranyl acetate and lead citrate. The sections were imported in a transmission electron microscope at 80 kV to examine the morphology of macrophage cells on the titanium surfaces.

2.9. Confocal microscopy quantification of *S. aureus* phagocytosis by macrophages

To evaluate the effect of titanium surface roughness on macrophage-mediated phagocytosis of *S. aureus*, macrophages were cultured on polished, corundum, and plasmapore titanium discs. *GFP-labeled S. aureus* was added to the macrophage cultures at a bacterial concentration of 10^4 CFU/mL. The co-cultures were incubated for 6, 12, and 24 hrs at 37°C with 5% CO_2 to allow phagocytosis to occur. After the incubation, macrophages were washed gently with sterile PBS to remove non-adherent bacteria. Cells were fixed with 4% paraformaldehyde for 15 minutes at room temperature, followed by permeabilization with 0.1% Triton X-100 for 10 minutes. To visualize internalized bacteria, macrophages were stained with DAPI (nuclear stain, Sigma, Germany) and Phalloidin–Atto 565 (Atto 565 for actin cytoskeleton stain, Sigma, Germany). Confocal microscopy (Zeiss LSM 800, Germany) was used to capture images of the macrophages, *GFP-labeled S. aureus*. The number of internalized *S. aureus* per macrophage was quantified by analyzing at 20 cells per sample from three independent experiments.

2.10. Quantification of macrophage adhesion on titanium surfaces

Macrophage adhesion was evaluated on different titanium (Ti) surfaces, including polished, corundum, and plasmapore. For adhesion assays, cells were seeded at a density of 1×10^5 cells/well onto the different Ti surfaces or control wells and incubated at 37 °C with 5% CO_2. After cell attachment (4 h), stimulation was performed using *S. aureus* at a multiplicity of infection (MOI) of 10:1. At 8, 12, and 24 h post-stimulation, adherent macrophages were quantified by measuring DNA content using the Quant-iT™ PicoGreen dsDNA assay kit (Thermo Fisher Scientific, USA) according to the manufacturer's instructions. Fluorescence intensity was measured with a microplate reader (excitation/emission: 480/520 nm).

2.11. Fluorescent probe-based ROS quantification in macrophages on different Ti surfaces

The production of reactive oxygen species (ROS) in macrophages was assessed to evaluate the effect of titanium surface roughness on macrophage activation during interaction with *S. aureus*. Macrophages were cultured on polished, corundum, and plasmapore titanium discs as previously described. Following bacterial co-culture with *GFP-labeled S. aureus* for 6, 12, and 24 hrs, the cells were washed gently with sterile PBS to remove non-adherent bacteria. ROS production was quantified using the fluorescent probe 2',7'-dichlorodihydrofluorescein diacetate (H2DCFDA, Invitrogen, USA), a non-fluorescent compound that is converted to fluorescent dichlorofluorescein (DCF) upon oxidation by ROS. Following the co-culture, macrophages were incubated with 10 µM H2DCFDA at 37°C for 30 minutes in the dark. After incubation, cells were washed three times with PBS to remove excess probe and then resuspended in PBS. Fluorescence intensity was measured using a microplate reader at an excitation wavelength of 485 nm and emission wavelength of 530 nm. The levels of ROS were quantified based on the fluorescence intensity, which correlates with the amount of ROS produced within the macrophages. The results were normalized to the number of viable cells determined by the Trypan Blue assay.

2.12. ELISA of pro-inflammatory and anti-inflammatory cytokines

To assess the inflammatory response of macrophages to *S. aureus* on different titanium surfaces, the expression levels of pro-inflammatory and anti-inflammatory cytokines were quantified using an Enzyme-Linked Immunosorbent Assay (ELISA). Cells were cultured on polished, corundum, and plasmapore titanium discs as described previously. After bacterial co-culture for 6, 12, and 24 hrs, the supernatants were collected to measure cytokine release, and the macrophages were lysed for gene expression analysis. The secretion of pro-inflammatory cytokines (TNF-α) and anti-inflammatory cytokines (IL-10) was assessed using commercially available ELISA kits (Thermo Fisher Scientific, USA), following the manufacturer's protocols. Briefly, 100 µL of culture supernatant from each sample was added to the wells of a pre-coated 96-well plate and incubated at room temperature. After incubation, the plates were washed, and antibodies were added, followed by substrate solution. The absorbance was measured at 450 nm using a microplate reader (Tecan Group Ltd, Switzerland). Cytokine concentrations were determined from a standard curve constructed using known cytokine standards.

2.13. Expression of genes associated with inflammation

To assess the response of macrophages to *S. aureus* on different titanium surfaces, total RNA was extracted using the RNeasy Mini Kit (Qiagen, Germany) following the manufacturer's protocol. RNA purity and concentration were measured with a NanoDrop spectrophotometer (Thermo Fisher Scientific, USA). cDNA was synthesized from 1 µg of total RNA using the iScript cDNA Synthesis Kit (Bio-Rad,USA). Gene expression analysis was performed via RT-qPCR using SYBR Green PCR Master Mix (Applied Biosystems, USA) on the ABI 7500 Real-Time PCR System (Thermo Fisher Scientific,USA). The target genes (Table 1) analyzed included oxidative stress response genes (CYBB (NOX2), GPX1, GPX4), macrophage differentiation markers TNF-α, IL-10, NFATC1, RANK, c-Jun, c-Fos, and adhesion-related genes (ITGB2 (CD18), ICAM1 (CD54)). Gene expression levels were normalized to GAPDH and quantified using the $2^{-\Delta\Delta Ct}$ method. The expression profiles of

these genes were compared between different surface roughnesses and bacterial exposure durations.

Tab. 1. Primers used for RT-PCR

Target gene	Forward primer	Reverse primer
GAPDH	GTCTCCTCTGACTTCAACAGCG	ACCACCCTGTTGCTGTAGCCAA
INDO	GCCTGATCTCATAGAGTCTGGC	TGCATCCCAGAACTAGACGTGC
CXCL11	AGCTTGCCTCAATCCTGCATCC	CAGATGCCCTTTTCCAGGACTTC
MCR-1	GGTTTATGGAGCAGGTGGAA	AAACTTGAACGGGAATGCAC
CCL13	GATCTCCTTGCAGAGGCTGAAG	TCTGGACCCACTTCTCCTTTGG
TNF-α	CTCTTCTGCCTGCTGCACTTTG	ATGGGCTACAGGCTTGTCACTC
IL-10	TCTCCGAGATGCCTTCAGCAGA	TCAGACAAGGCTTGGCAACCCA
NFATc1	CACCAAAGTCCTGGAGATCCCA	TTCTTCCTCCCGATGTCCGTCT
c-Jun	CCTTGAAAGCTCAGAACTCGGAG	TGCTGCGTTAGCATGAGTTGGC
c-Fos	GCCTCTCTTACTACCACTCACC	AGATGGCAGTGACCGTGGGAAT
Nfkb1	AGTGCAAAGGAAACGCCAGAAG	GCCAGGGCTTCCGGTACTC
TLR2	ATAAGCTGAAAACACTCCCAGATG	GAAAAGAACCAAGTTGGTC
ICAM1	TGAAGGTGTATGAACTGAGCA	GTGCCCATTATGACTGCGAT

2.14. Label free proteomics

The macrophages were seeded and cultured as described above. Cells were then washed four times with 50 mM ammonium bicarbonate (ABC; Merck) and collected in 5 M urea, 50 mM ABC in 1.5 ml Eppendorf tubes. Cell lysis was achieved by three freeze–thaw cycles, using liquid nitrogen for freezing and sonication in an ultrasonic bath for thawing. Insoluble material was removed by centrifugation, and the resulting supernatant was transferred to new tubes. Proteins were digested overnight at 37 °C with trypsin–LysC at an enzyme-to-protein ratio of 1:25. Digestion was quenched by addition of 20% acetonitrile (ACN)/10% formic acid (FA), yielding final concentrations of 2% ACN and 1% FA.

Peptide separation was achieved using an Ultimate 3000 nano-LC system (Thermo Scientific) equipped with an Acclaim PepMap C18 analytical column (15 cm × 75 µm, 3 µm; Thermo Scientific). Peptide samples were first desalted on an on-line C18 trapping column, followed by separation on the analytical column using a 30-min gradient from 4% to 32% acetonitrile (ACN) with 0.1% formic acid (FA) at a flow rate of 300 nl min^{-1}. The LC system was coupled to a Q Exactive HF mass spectrometer (Thermo Scientific) operated

in data-independent acquisition (DIA) mode. The instrument was configured to acquire 25 × 24 m/z DIA spectra spanning 400–1000 m/z at a resolution of 30,000 with a staggered window pattern. Full MS1 scans (385–1015 m/z) were acquired at a resolution of 60,000 and interspersed every 25 DIA MS/MS scans.

Protein identification and quantification were performed using DIA-NN version 1.8.1(University of Cambridge, UK), employing a Mus Musculus (Mouse TaxID 10090_240227) protein database and cysteine carbamidomethylation as a fixed modification. Data were normalized using RT-dependent cross-run normalization and Maximal Label-Free Quantification (MaxLFQ) normalization. For comparative analysis, Perseus 2.0.11 software (Max Planck Institute of Biochemistry, Germany) was utilized, focusing on label-free quantification. Proteomic profiles of macrophage cells cultured with titanium discs were compared to control groups. Differentially expressed proteins were considered significant at a p-value ≤ 0.05 (Student's test). Differentially expressed proteins were classified based on cellular component analysis and Reactome pathways using the STRING v.11.5 classification system (EMBL Heidelberg, Germany, https://string-db.org).

Adjusted p-values were calculated using the Benjamini–Hochberg procedure to control the false discovery rate (FDR). The protein expression was considered different between conditions at p ≤ 0.05 (Student's T-test). Principal Component Analysis (PCA) was performed to visualize the variance in proteomic profiles across surface types and LPS treatment conditions. PCA plots were generated using the Perseus 2.0.11, with scaling applied to the data. Functional classification of differentially proteins, Cellular Component analysis and Pathways analysis were carried out using the STRING v.11.5 (https://string-db.org) and Reactome Pathway Database (https://reactome.org). The proteomics data have been deposited in the PRIDE database via ProteomeXchange(Code: 1-20260423-143013-4812642).

2.15. Data analysis

RT-PCR, Cell viability and cytokine secretion data are presented as mean ± standard deviation and sample size was 3 (n=3). A one-way ANOVA followed by Tukey post-hoc correction was used for comparison of group means in SPSS (version 21, IBM SPSS statistics, USA6). The Shapiro-Wilk test was employed to assess data normality. A p value of 0.05 was used as a threshold for statistical significance.$*p<0.05$; $**p<0.01$; $***p<0.001$.

3. Results

3.1. Effects of *S. aureus* infection on macrophage viability

To determine an optimal bacterial load for a macrophage infection model (Fig.1), we quantified the effects of *S. aureus* on macrophage viability across a range of concentrations (10^2, 10^4, 10^6, and 10^8 CFU/mL) and incubation periods (6, 8, 12, and 24 h). Viability, measured by CCK-8 assay and normalized to uninfected controls, declined in both a dose- and time-dependent manner. Minimal cytotoxicity was observed at 10^2 and 10^4 CFU/mL, whereas 10^6 and 10^8 CFU/mL markedly impaired viability, particularly after 12 and 24 h. At 24 h, exposure to 10^8 CFU/mL reduced viability to less than 8.66±1.74%, indicating extensive cell death. On this basis, 10^4 CFU/mL was selected for subsequent experiments on titanium discs with varying surface roughness.

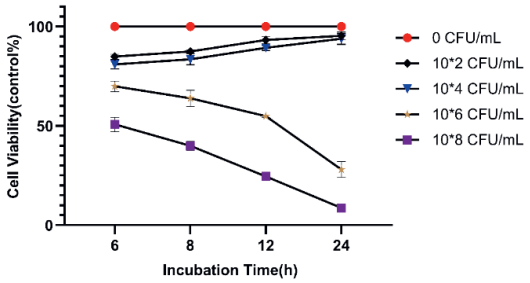


Fig. 1. Effects of *S. aureus* infection on macrophage viability over time. Macrophages were co-cultured with *S. aureus* at different concentrations (10^2, 10^4, 10^6, and 10^8 CFU/mL) and incubated for 6, 8, 12, and 24 hours. Data show the mean ± SD(n=4).

3.2. Macrophage viability on titanium surfaces under *S. aureus* infection

To investigate the effect of different titanium surface roughness on macrophage viability under bacterial infection (10^4 CFU/mL), cell viability was measured using the CCK-8 assay (Fig. 2) at 8 h, 12 h, and 24 h to assess time-dependent changes. As shown in Fig. 2, cell viability decreased over time across all groups, indicating a time-dependent reduction under bacterial challenge. At each time point, the control and polished groups consistently exhibited higher viability compared to corundum and plasmapore surfaces. Specifically, at 8 h, the control group showed a viability of 90.49±4.94%, significantly higher than the plasmapore group (76.31 ± 1.34%) and corundum group (80.12 ± 2.18%). The polished group (88.25 ± 3.21%) also maintained higher viability than plasmapore but was not significantly different from control ($p = 0.124$). At 12 h, the control group remained 82.37 ± 5.02% higher than polished 80.15 ± 4.87% ($p < 0.001$). The corundum 71.46 ± 3.89% is also higher than plasmapore 65.92 ± 2.74%. By 24 h, the viability decrease was more pronounced: control 74.17 ± 6.44%, polished 70.55 ± 4.92% ($p < 0.001$), corundum 63.84 ± 3.21%, and plasmapore 60.75 ± 3.56%. These indicate that surfaces with higher roughness (corundum and plasmapore) promote a higher decrease in macrophage viability over time and under bacterial challenges.

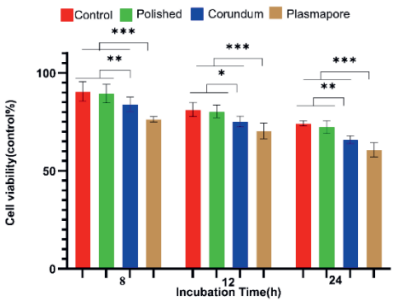


Fig. 2. Cell viability on titanium discs with different surface roughness in the presence of bacterial infection. The effect of different titanium surface roughness on cell viability in the presence of bacterial infection (10^4 CFU/mL). Cell viability was measured using the CCK-8 assay and normalized to 100% for the uninfected well plate group (0 CFU/mL). Measurements were taken at 8h, 12h, and 24h to assess time-dependent changes. Data show the mean ± SD. one way ANOVA was used to determine statistical significance (n=4, *$p < 0.05$; **$p < 0.01$; ***$p < 0.001$).

3.3. Titanium surface morphology differentially regulates macrophage adhesion under *S. aureus* challenge

The DNA content was employed to evaluate the impact of titanium surface morphology on macrophage adhesion under bacterial challenge. Macrophages were cultured on control (24-well plate), polished, corundum, and plasmapore surfaces following *S. aureus* stimulation. As shown in Fig. 3, macrophage adhesion was strongly influenced by the surface roughness. At 8 h, the corundum group exhibited the highest DNA content (662.13 ± 34.75 ng), significantly exceeding that of control (435.62 ± 4.58 ng) and polished surfaces (505.22 ± 36.80 ng). Plasmapore surfaces also promoted adhesion (572.01 ± 58.78 ng), but to a lesser extent than corundum ($p < 0.05$). At 12 h, DNA content decreased across all surfaces, with corundum maintaining the highest level (617.84 ± 91.20 ng), followed by plasmapore (508.49 ± 105.79 ng), control (425.77 ± 69.03 ng) and polished (431.75 ± 63.69 ng). By 24 h, a further decline was observed, with corundum (511.75 ± 94.36 ng) still outperforming other groups. Notably, plasmapore showed reduced adhesion compared to corundum at all time points, particularly at 24 h (435.12 ± 134.81 ng). This showed that excessive surface roughness may hinder macrophage attachment. Overall, the most robust adhesion occurred at 8 h, followed by a time-dependent decline at 12 and 24 h, consistent with decreasing cell viability over time under continuous bacterial challenge.

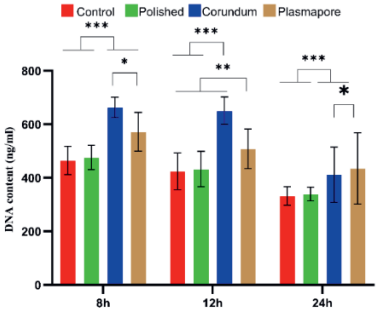


Fig. 3. Quantification of macrophage adhesion on titanium surfaces under *S. aureus* stimulation. Macrophage adhesion was assessed on titanium (Ti) surfaces (polished, corundum, plasmapore) and compared with the control group (24 wells plate) following stimulation with *S. aureus.* DNA content was quantified using the Quant-iT™ assay at 8, 12, and 24 hours. Data show the mean ± SD. one way ANOVA was used to determine statistical significance (n=4, *$p < 0.05$; **$p < 0.01$; ***$p < 0.001$).

3.4. Surface roughness–dependent modulation of macrophage morphology and *S. aureus* infection

To assess macrophage phagocytic capacity at 24 h, SEM experiments were performed to examine cell morphology and interactions with *S. aureus* on titanium surfaces of varying roughness (polished, corundum, and plasmapore) (Fig. 4). Surface characteristics markedly influenced macrophage behavior and *S. aureus*. On polished surfaces, macrophages displayed well-spread, elongated morphologies with extensive filopodia and lamellipodia. Numerous *bacteria* were observed adhered to macrophage membranes (Fig. 4, bottom left, red arrowheads). In contrast, macrophages on corundum surfaces exhibited irregular morphology, pronounced membrane ruffling, and reduced spreading. Fewer bacteria were associated with macrophage surfaces despite a similar overall substrate bacterial burden (Fig. 4, middle panels). On plasmapore surfaces, macrophages showed extensive membrane dynamics, including ruffling and phagocytic cup formation. These indicate that surface roughness strongly influences macrophage–bacteria interactions.

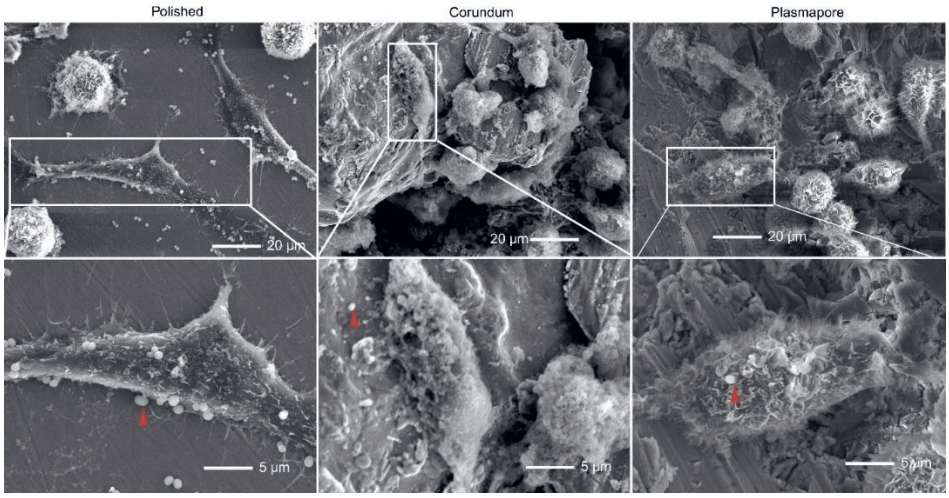


Fig. 4. SEM images of macrophage morphology and *S. aureus* interactions on titanium surfaces. Top panels display low-magnification views showing overall cell distribution and attachment. Insects highlight selected macrophages for detailed visualization. Bottom panels show high-magnification images of macrophages interacting with each surface, with red arrowheads indicating *S. aureus*. Scale bars: 20 µm (top), 5 µm (bottom).

3.5. Nonlinear regulation of macrophage phagocytosis by titanium surface topography

High-resolution confocal fluorescence microscopy was performed to examine whether surface topography affects bacterial internalization. *GFP-labeled S. aureus* (10^4 CFU/mL) within macrophages were cultured on the titanium discs (polished, corundum, or plasmapore surfaces). Intracellular uptake was assessed after 24 h of co-culture. As shown in Fig. 5, confocal imaging revealed clear differences in phagocytic activity across surface conditions. Macrophages on corundum surfaces exhibited the most pronounced reduction in bacterial internalization, displaying fewer intracellular GFP-positive bacteria and a more rounded morphology. By contrast, cells on polished surfaces maintained robust phagocytic uptake, with extensive cytoplasmic GFP signal. Macrophages on plasmapore surfaces, despite irregular morphology and increased cytoplasmic vacuolization, internalized more bacteria than those on corundum, indicating a partial recovery of phagocytic function at higher roughness levels. These demonstrate a nonlinear relationship between titanium surface roughness and macrophage phagocytosis. Corundum roughness markedly impaired bacterial uptake at 24 h, whereas smoother or highly roughness surfaces sustain more efficient internalization.

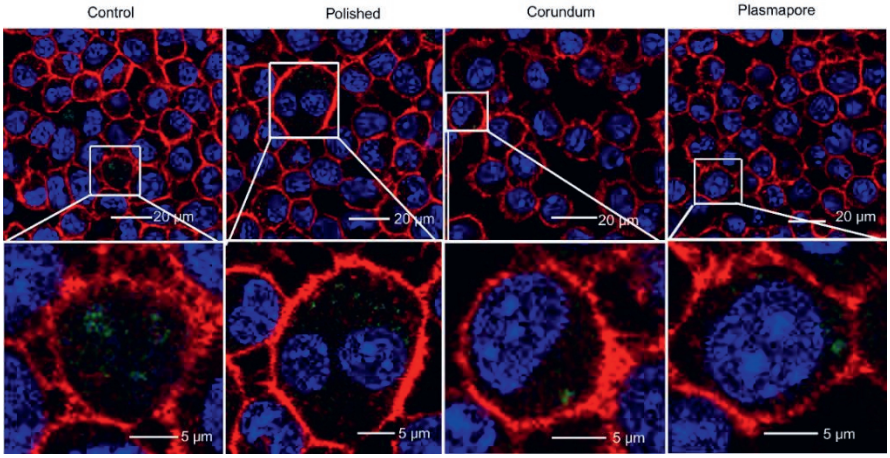


Fig. 5. Confocal images of macrophages cultured on titanium discs with different surface properties: control, polished, corundum, and plasmapore. Cells were incubated with *GFP-expressing S. aureus* (10^4 CFU mL^{-1}). Cell membranes were labeled with phalloidin (red), nuclei with DAPI (blue), and internalized *S. aureus* appear as GFP-positive puncta (green). Insertions show magnified regions highlighting intracellular bacteria. Scale bars: 20 μm (top panels) and 5 μm (bottom panels).

3.6. Surface-dependent remodeling of macrophage subcellular architecture with *S. aureus* infection

Primary macrophages were cultured on Ti discs and exposed to *GFP-labeled S. aureus* (10^4 CFU/mL). Transmission electron microscopy (TEM) was performed 24 h post-infection to further assess subcellular localization and phagocytic capacity (Fig. 6). Macrophages on control surfaces (24-well cell culture plate) displayed a highly active phagocytic phenotype, with extensive filopodia. ER dilation was evident; indicative of enhanced protein synthesis associated with phagocytic stress. Similarly, macrophages adhering to the polished titanium surface exhibited robust phagocytic activity, adopting a flattened morphology with well-developed pseudopodia. The intact endoplasmic reticulum and mitochondrial structures indicated high metabolic activity. In contrast, macrophages on corundum surfaces exhibited markedly impaired phagocytic function. These cells predominantly exhibited a rounded morphology with reduced protrusions. Although the endoplasmic reticulum and mitochondria appeared morphologically intact, the diminished protrusions indicated weakened metabolic and phagocytic activity. Macrophages located on the surface of the plasma pore exhibit significant cytoplasmic vacuolation and larger, fused phagosome structures. Pseudopodial activity remains pronounced, indicating partial restoration of phagocytic capacity at higher roughness levels despite altered subcellular organization. These results show that titanium surface topography exerts a topography-dependent modulation of macrophage phagocytosis. Both corundum and plasmapore surfaces impaired bacterial uptake, and the corundum surface producing the most pronounced functional decline at 24 h.

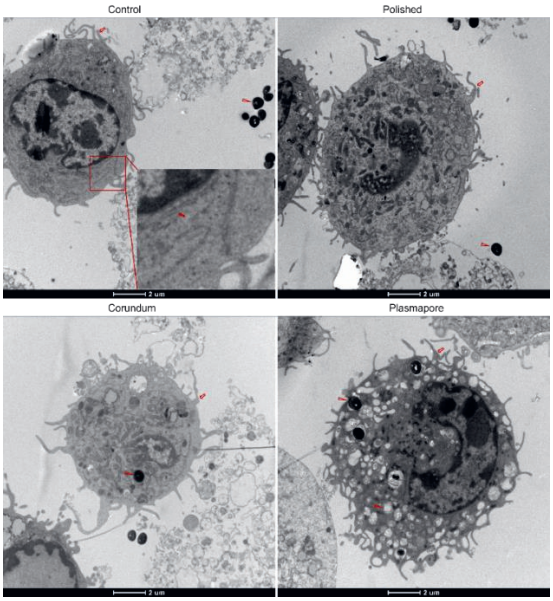


Fig. 6. TEM images of macrophage phagocytosis of *S. aureus* on titanium surfaces with varying roughness. Macrophages were seeded onto titanium discs with different surface topographies, control (cells cultured on 24 well plates), polished, corundum, and plasmapore. *GFP-labeled S. aureus* (10^4 CFU/mL) was added to the cultures and co-incubated for 24 hours. Open red triangles mark *S. aureus*; solid red triangles indicate vacuoles; open arrows point to pseudopodia; and solid arrows denote the endoplasmic reticulum. Scale bars: 2 µm.

3.7. Dynamic regulation of macrophage *S. aureus* uptake across titanium surface roughness

Next to the SEM, Confocal and TEM analyses, the time-dependent effect on phagocytic efficiency was assessed (Fig. 7). Macrophages were cultured on titanium discs with varying surface roughness (polished, corundum, plasmapore) and co-incubated with *GFP-labeled S. aureus* for 8, 12, or 24 hrs. Intracellular bacterial load was quantified by confocal microscopy as GFP intensity normalized to DAPI-labeled nuclei. At 8 h, the phagocytosis efficiency increased with surface roughness, with corundum (1.487 ± 0.096) and plasmapore (1.626 ± 0.101) significantly higher than control (1.143 ± 0.092) and polished (1.172 ± 0.146). Plasmapore induced a higher internalization than corundum, indicating that more complex topographies enhance early-phase bacterial uptake. By 12 h, phagocytic activity peaked on rough surfaces, with corundum (1.863 ± 0.111) and plasmapore (2.062 ± 0.178) significantly exceeding polished (1.239 ± 0.052) and control

(1.176 ± 0.069). Plasmapore remained slightly higher than corundum, reinforcing that early-phase phagocytosis is positively correlated with roughness. After 12 h, the phagocytosis efficiency declined across all groups, with the corundum group showing the most pronounced reduction. At 24 h, control (0.917 ± 0.055) and polished (0.949 ± 0.042) surfaces continued to show decreased uptake compared to earlier time points. Corundum (0.553 ± 0.054) exhibited the largest drop, while plasmapore (0.670 ± 0.057) maintained relatively higher internalization, though still reduced compared to 12 hr. Both corundum and plasmapore remained significantly higher than control and polished surfaces. This indicates that titanium surface roughness modulates macrophage phagocytosis in a time- and topography-dependent manner. Rougher surfaces enhance early bacterial uptake (8–12 h), but prolonged exposure leads to a general decline in phagocytic capacity, with corundum surfaces being most affected. Plasmapore surfaces, despite the decline, sustain higher phagocytic activity than corundum.

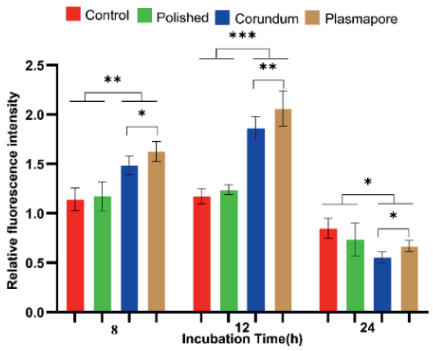


Fig. 7. Macrophage uptake of *S. aureus* quantified by confocal microscopy. Macrophages were co-cultured with GFP-labeled *S. aureus* for 8, 12, and 24 hours, and bacterial uptake was quantified using confocal microscopy. Relative fluorescence intensity, normalized to DAPI-stained macrophage nuclei, was used to assess the phagocytic efficiency. Data show the mean ± SD. one way ANOVA was used to determine statistical significance (n=4, *p < 0.05; **p < 0.01; ***p < 0.001).

3.8. Surface-dependent modulation of macrophage M1–M2 polarization in response to *S. aureus* infection

Immunofluorescence staining (Fig.8) was performed to further assess the effects of titanium surface topography on macrophage polarization under bacterial challenge. Macrophages were co-cultured with *S. aureus* on polished, corundum, and plasmapore titanium surfaces, with nuclear counterstaining (DAPI). At 24 h, macrophages on polished surfaces maintained moderate CCR7 (M1) expression with lower CD36 (M2) levels, consistent with a still predominant M1 phenotype. In contrast, corundum group exhibited minimal CCR7 signal and markedly elevated CD36, reflecting a strong shift toward M2 polarization. Plasmapore surfaces supported a mixed phenotype, with moderate CCR7 and high CD36 expression. Control group (cultured on 24 wells culture plates) displayed low and diffuse staining of both markers, indicative of a relatively quiescent state.

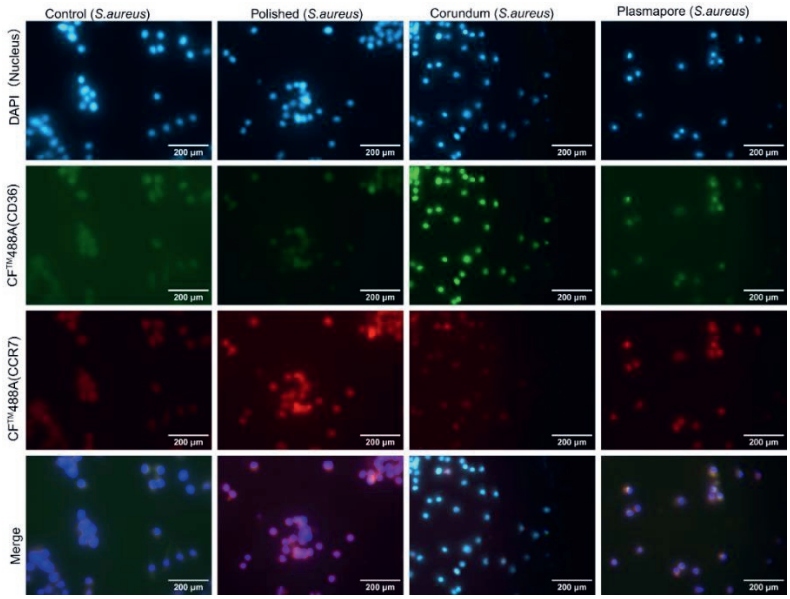


Fig. 8. Immunofluorescence analysis of macrophage polarization on titanium surfaces under *S. aureus* stimulation. Macrophages were cultured for 24 h on four types of Ti surfaces: Control (24 wells plate), polished, corundum, and plasmapore, followed by *S. aureus stimulation*. Cells were stained with DAPI (blue, nuclei), CF™ 488A-conjugated anti-CD36 (green, M2 macrophage marker), and CF™ 568-conjugated anti-CCR7 (red, M1

macrophage marker). Merged images display colocalization of polarization markers with nuclear staining. The scale bar shows 100 µm.

3.9. Early M1 activation followed by late-phase M2 polarization on rough titanium surfaces

ImageJ-assisted immunofluorescence analysis (Fig. 8) was used to quantify the M1/M2 polarization ratio of titanium surface topography on macrophage polarization under *S. aureus* challenge. The M1/M2 polarization ratio was assessed by $CCR7^+$ (M1) and $CD36^+$ (M2) macrophage populations on control, polished, corundum, and plasmapore surfaces at 8, 12, and 24 hrs. At 8 hrs, corundum and plasmapore, exhibited significantly higher M1/M2 ratios (6.19 ± 0.27 and 6.26 ± 0.27) compared to control (2.44 ± 0.36, $p < 0.01$) and polished (4.12 ± 1.68, $p < 0.05$). This shows early M1 polarization and functional activation. At 12 hrs, the M1/M2 ratio decreased noticeably, especially on corundum surfaces (5.32 ± 0.61, $p < 0.05$), suggesting that M1 differentiation was partially suppressed, whereas M2 polarization continued to rise. By 24 hrs, M2-associated phenotypes predominated, with the lowest M1/M2 ratios observed on corundum (0.56 ± 0.19) and plasmapore surfaces (0.65 ± 0.08, $p < 0.01$), while control (1.26 ± 0.30) and polished surfaces (0.90 ± 0.78) maintained relatively higher ratios ($p > 0.05$), indicating a delayed M2 transition. M2 polarization increased over time, reaching its highest value at 24 hrs. Collectively, the early M1 activation is followed by a late-phase M2 response, and corundum surfaces exerting the strongest modulatory effect.

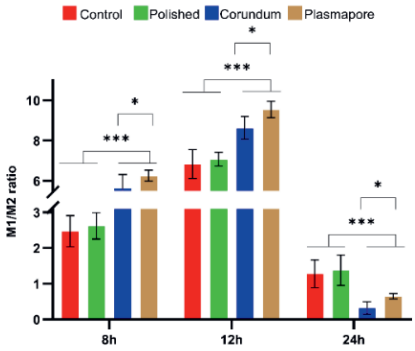


Fig. 9. Quantification of macrophage polarization (M1/M2 ratio) in response to varied roughness. Macrophages were cultured on titanium discs with different surface roughness and with *S. aureus* stimulation evaluated by

ImageJ. The M1/M2 polarization ratio was evaluated by the number of $CCR7^+$ (M1 marker) and $CD36^+$ (M2 marker) regions of interest (ROIs) per cell.

3.10. Time-dependent transcriptional reprogramming of macrophages by titanium surface topography

M1/M2 ratios obtained throughout the experiments, indicated dynamic and, time-dependent modulation of macrophage polarization being exposed to *S. aureus* on titanium surfaces. Next the transcriptional responses were determined in order to asses the influence of surface topography and bacterial challenge on the regulation of the macrophage function (Fig. 10). To this end, the expression of key genes involved in polarization, adhesion, phagocytosis, and inflammatory signaling were assessed by RT–qPCR. Macrophages were cultured on polished, corundum, and plasmapore surfaces following *S. aureus* stimulation. At 12 hrs, M1 genes and functional markers, macrophages on corundum and plasmapore surfaces exhibited significantly elevated expression of M1-associated genes, including TNF-α (corundum 67.04 ± 6.75, plasmapore 76.18 ± 9.73, $p < 0.001$), IDO1 (corundum 65.05 ± 4.93, plasmapore 68.94 ± 7.87, $p < 0.001$), and CXCL11 (corundum 58.92 ± 3.94, plasmapore 65.45 ± 4.60, $p < 0.01$), as well as phagocytosis functional gene TLR2 (corundum 24.94 ± 2.16, plasmapore 28.13 ± 3.50, $p < 0.01$), ROS production functional gene Nfkb1 (corundum 4.60 ± 0.39, plasmapore 4.07 ± 0.37, $p < 0.01$), and adhesion functional gene ICAM1 (corundum 0.94 ± 0.08, plasmapore 0.66 ± 0.17, $p < 0.05$). These indicate that rougher surfaces promote M1 polarization and functional activation, facilitating early bacterial clearance.

Following 12 hrs, M1 gene expression declined markedly, with the corundum group showing the most pronounced reduction, indicating a temporal suppression of pro-inflammatory M1 activity. In contrast, M2-associated genes, including IL-10, MRC1, and CCL13, progressively increased over time, reaching maximum expression at 24 h on corundum (IL-10 6.60 ± 0.14, MRC1 6.35 ± 0.30, CCL13 6.16 ± 0.56) and plasmapore (IL-10 5.95 ± 0.21, $p < 0.001$). This suggested a shift toward anti-inflammatory profiles. Expression of transcription factors involved in macrophage activation (NFATc1, c-Fos, and c-Jun) also increased over time, peaking at 24 hrs on corundum (NFATc1 4.13 ± 1.01, c-Fos 4.47 ± 0.63, c-Jun 3.49 ± 0.20, $p < 0.01$). Notably, despite the upregulation, their

functional impact on promoting M1 activity appears attenuated after 12 h, while M2 polarization dominates. These findings demonstrate that rough titanium surfaces strongly induce M1 polarization and functional activation prior to 12 hrs. After 12 hrs, M1 responses are suppressed (corundum), and M2 markers and transcription factor expression continue to increase, consistent with a temporal shift toward anti-inflammatory functions. Interestingly, plasmapore surfaces, representing the highest roughness, slightly attenuate full M2 polarization, suggesting that excessive topographical complexity may limit late-stage anti-inflammatory responses.

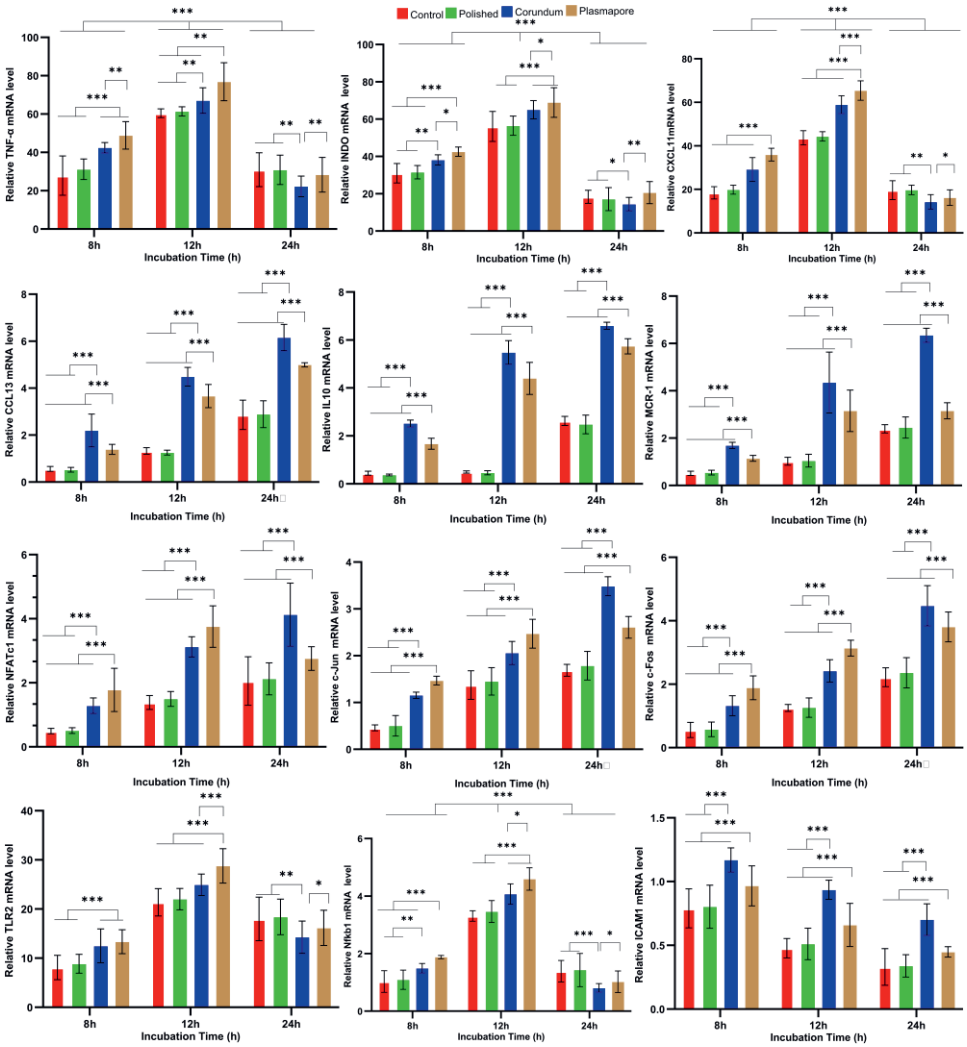


Fig. 10. Relative gene expression profiles of inflammatory and immune-regulatory markers in macrophages stimulated with *S. aureus* on different titanium surfaces. Quantitative RT-PCR analysis of macrophage gene expression after incubation on Ti surfaces (control, polished, corundum, plasmapore) with *S. aureus* stimulation for 8, 12, and 24 hours. (A) Pro-inflammatory and M1 macrophage genes: TNF-α, IDO1, and CXCL11. (B) Transcription factors involved in macrophage activation: NFATc1, c-Fos, and c-Jun. (C) M2 macrophage markers: IL-10, MRC1, and CCL13. (D) Macrophage functional genes: TLR2 (phagocytic function), Nfkb1 (ROS production), and ICAM1 (adhesion). Data normalized to control (24 wells plate without Ti discs) using the $2^{-\Delta\Delta Ct}$ method. Results are shown as mean ± SD, one way ANOVA was used to determine statistical significance (n=4, *$p < 0.05$; **$p < 0.01$; ***$p < 0.001$).

3.11. Time-resolved cytokine responses reveal M1-to-M2 shift on rough titanium surfaces

In a follow-up study, the the time dependent influence of surface roughness on the modulation (M1/M2 ratio) of macrophages was researched. ELISA based assays were used to quantify the secretion of the pro-inflammatory cytokine TNF-α and the anti-inflammatory cytokine IL-10 following *S. aureus* exposure at 8, 12, and 24 hrs (Fig. 11). At 8 hrs, TNF-α levels increased with surface roughness, with plasmapore (688.45 ± 45.17 pg/mL) and corundum (576.86 ± 99.24 pg/mL) significantly higher than control (482.42 ± 37.21 pg/mL) and polished (454.92 ± 57.80 pg/mL). This suggested an early pro-inflammatory response on rougher surfaces. IL-10 levels were also elevated on corundum (88.17 ± 7.33 pg/mL) and plasmapore (55.28 ± 10.73 pg/mL) compared to control (13.55 ± 2.64 pg/mL) and polished (15.58 ± 5.89 pg/mL), indicating early anti-inflammatory signaling. By 12 h, TNF-α secretion reached its peak on rough surfaces, with corundum (1372.46 ± 51.33 pg/mL) and plasmapore (1458.58 ± 90.41 pg/mL) significantly higher than control (1142.50 ± 170.60 pg/mL) and polished (1100.74 ± 84.15 pg/mL, $p < 0.001$). IL-10 levels continued to rise on corundum (145.68 ± 9.95 pg/mL) and plasmapore (128.89 ± 19.62 pg/mL), both significantly elevated over control (17.01 ± 8.24 pg/mL) and polished (16.15 ± 7.87 pg/mL), indicating sustained M1/M2 coexistence. At 24 hrs, TNF-α levels declined sharply, with the corundum group showing the most pronounced decrease (303.13 ± 30.83 pg/mL), while plasmapore (387.25 ± 51.69 pg/mL), polished (494.08 ± 30.89 pg/mL), and control (441.50 ± 6.13 pg/mL) also decreased, though less dramatically. In contrast, IL-10 levels continued to rise, reaching a maximum on corundum (166.35 ± 7.31 pg/mL) and plasmapore (142.89 ± 13.13 pg/mL), while control (54.34 ± 7.12 pg/mL) and polished (51.49 ± 9.41 pg/mL) remained lower ($p < 0.01$). This indicates a sustained anti-inflammatory response on rougher surfaces despite attenuation of TNF-α. These reveal that titanium surface roughness and time interact to regulate macrophage polarization. Before 12 h on rough surfaces display both pro- and anti-inflammatory signaling. TNF-α declines sharply, particularly on corundum, IL-10 remains elevated, suggesting a shift

toward M2 polarization. Notably, plasmapore surfaces induced slightly lower IL-10 compared to corundum, implying that extreme roughness may moderately limit anti-inflammatory signaling.

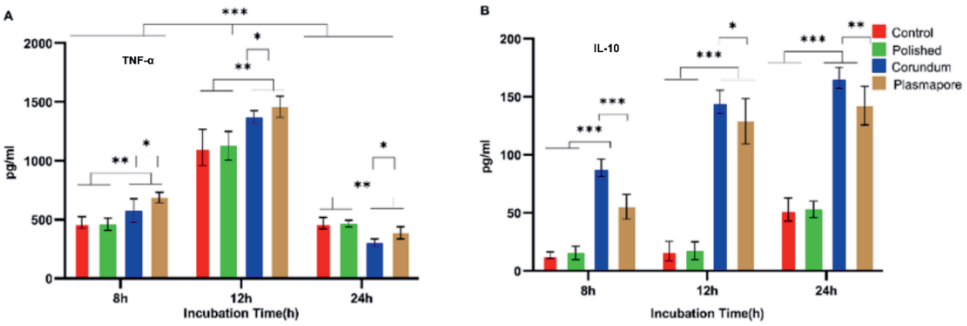


Fig. 11. Quantification of inflammatory cytokines secretion. Macrophages cultured on titanium surfaces with *GFP-labeled S. aureus* for 8, 12, and 24 hours stimulation evaluated by ELISA assay. The secretion level of (a) pro-inflammatory cytokine, and (b) anti-inflammatory cytokine, IL-10. Data show the mean ± SD, one way ANOVA was used to determine statistical significance (n=4, *$p < 0.05$; **$p < 0.01$; ***$p < 0.001$).

3.12. Time-dependent ROS dynamics in macrophages regulated by titanium surface roughness

The DCFH-DA–based fluorescence assay format (Fig. 12) was used to investigate how titanium surface topography and bacterial stimulation jointly influence macrophage reactive oxygen species (ROS) production. Macrophages, cultured on plasmapore and corundum, exhibited elevated ROS levels compared to polished and control groups. The highest levels observed on plasmapore indicated that increased surface roughness enhances oxidative activation. Likewise, and in the absence of *S. aureus*, ROS production increased with roughness over time. At 8 hrs, ROS levels ranged from control (0.28 ± 0.03) to plasmapore (0.41 ± 0.01), while at 24 hrs, levels reached plasmapore (0.57 ± 0.05). Corundum also induced oxidative activity (0.52 ± 0.02), reaching at 24 h. These indicate that surface topography can activate macrophage oxidative pathways in a roughness- and time-dependent manner.

In the presence of *GFP-labeled S. aureus*, ROS dynamics followed a biphasic pattern across all surfaces. ROS levels increased with surface roughness before 12 hrs, peaking sharply at 12 hrs: polished (0.79 ± 0.06, $p < 0.001$), corundum (1.61 ± 0.16, $p < 0.001$), and plasmapore (1.78 ± 0.15, $p < 0.001$). This peak coincided with maximal expression of pro-oxidant genes such as Nfkb1 and TLR2 in RT–qPCR assays and was associated with enhanced M1 polarization, reflected by elevated TNF-α and CXCL11. By 24 hrs, ROS levels markedly declined, particularly on corundum (0.26 ± 0.11), concurrent with increased expression of M2 markers IL-10 and MRC1, suggesting a transition toward redox resolution and anti-inflammatory polarization. These findings support a model in which titanium surface roughness interacts with bacterial stimuli to regulate macrophage oxidative behavior in a time-dependent manner. Rough surfaces initially promoted robust ROS production during M1-skewed activation, followed by a shift toward resolution and redox homeostasis through M2 polarization.

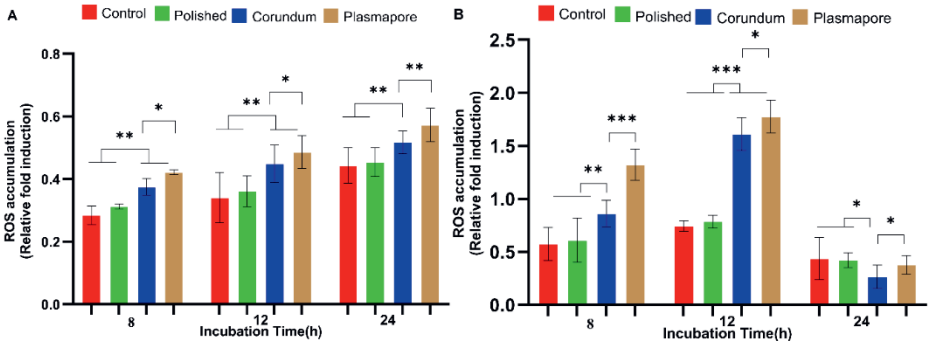


Fig. 12. Reactive oxygen species (ROS) production in macrophages co-cultured without and with GFP-labeled *S. aureus*. The figure displays the ROS production in macrophages cultured on control (24 well plates), polished, corundum, and plasmapore Ti surfaces for 8, 12, and 24 hours. Relative fold induction is normalized to control (macrophage cells cultured on 24 well plates). A: without GFP-labeled *S. aureus*. B: with GFP-labeled *S. aureus*. Data show the mean ± SD. one way ANOVA was used to determine statistical significance (n=4, *$p < 0.05$; **$p < 0.01$; ***$p < 0.001$).

3.13. Proteomic profiling analysis of macrophages on titanium surface with *S. aureus* infection

Titanium surface roughness markedly affects macrophage adhesion, polarization, phagocytic function, and ROS production. In a subsequent study, the underlying molecular mechanisms through unbiased proteomic analysis, was elucidated. A classical bottom-up liquid chromatography-tandem mass spectrometry (LC–MS/MS) workflow was employed to assess macrophage proteomic changes following *S. aureus* stimulation on titanium surfaces with varying surface properties. A total of 1,956 proteins were confidently identified across all samples (FDR < 0.01; Tab. S2), representing a broad spectrum of immune, metabolic, and cytoskeletal regulators.

To investigate the impact of surface modifications on the macrophage response to *S. aureus*, we performed a proteomic profiling followed by principal component analysis (PCA). The first two principal components accounted for 36.38% and 19.97% of the total variance, respectively (Fig. 12). Distinct clustering was observed for each experimental group, indicating condition-specific proteomic signatures. Macrophages exposed to polished surfaces segregated strongly along PC1, while those cultured on plasmapore and corundum surfaces separated along PC2, relative to the control. These findings demonstrate that surface topography profoundly shapes the macrophage proteomic landscape during *S. aureus* challenge, with each modification eliciting a unique response pattern.

Hierarchical clustering and principal component analysis of obtained proteomic profiling data showed that the biological samples derived from the same roughness cluster together and that samples from different surface roughness are different (Fig. 14). Differential expression analysis (adjusted $p < 0.05$) revealed distinct proteomic signatures associated with surface roughness (Tab. S3), encompassing both upregulated and downregulated proteins. These changes implicated pathways related to innate immune activation, phagocytic vesicle maturation, oxidative stress regulation, and macrophage polarization. Notably, proteins involved in actin cytoskeleton remodeling, antigen presentation, and redox homeostasis were differentially expressed in macrophages

cultured on corundum and plasmapore surfaces, consistent with enhanced phagocytic engagement and ROS modulation observed phenotypically.

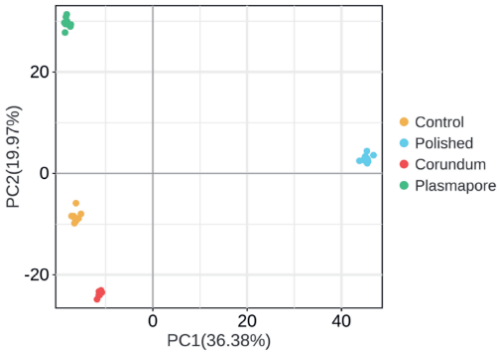


Fig. 13. PCA of macrophage proteomic profiles in response to *S. aureus* under different surface conditions. PCA scores plot of proteomic datasets derived from macrophages challenged with *S. aureus* alone (Control, n = 10, yellow), or in the presence of polished (n = 10, blue), corundum (n = 10, red) or plasmapore (n = 10, green) surfaces. Each point represents an independent replication. PC1 and PC2 explain 36.38% and 19.97% of the total variance, respectively. Distinct clustering indicates that surface modifications markedly alter the macrophage proteomic response to *S. aureus*.

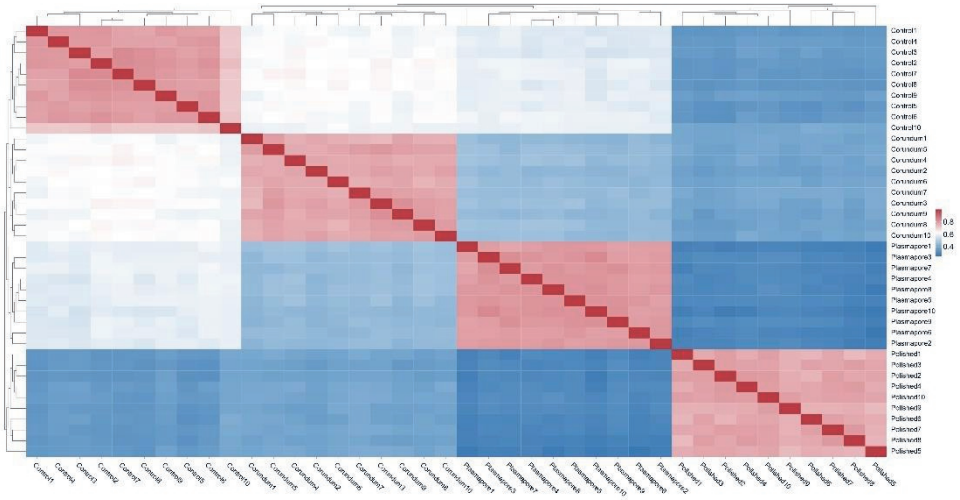


Fig. 14. Proteomic profiling data of macrophages/*S. aureus* (n=10), macrophages /*S. aureus*/polished (n=10), macrophages /*S. aureus*/corundum (n = 10) and macrophages /*S. aureus*/plasmapore (n = 10) illustrated as cluster heatmap of sample-to-sample distances; computed using the Pearson correlation coefficient.

To determine the functional implications of macrophage proteome remodeling on titanium surfaces of varying roughness, we performed Gene Ontology (GO) enrichment analysis at the molecular function level. In *S. aureus*-stimulated macrophages cultured on polished surfaces compared to control (Fig. 15), up-regulated proteins were significantly enriched in S100 protein binding, oxidoreductase activity, and transcription factor binding, highlighting early shifts in redox homeostasis and immune signaling. Concurrently, pathways involved in transcriptional coactivation, SH3 domain binding, and small GTPase interactions were among those down-regulated, indicating reduced cytoskeletal and signal transduction activity.

Comparative analysis between polished and corundum surfaces revealed a transition toward increased expression of proteins with transcription coactivator activity, NAD and ubiquitin ligase binding, reflecting enhanced metabolic and post-translational regulatory processes. In contrast, functions such as chromatin binding, RNA helicase activity, and ATP-dependent transport were suppressed, suggesting dampened nucleic acid remodeling and energy-driven transport under rougher surface conditions. Strikingly, the comparison between corundum versus plasmapore revealed a further shift in macrophage functional programming. Up-regulated proteins were enriched in ubiquitin ligase inhibitor activity, Hsp70/Hsp90 chaperone binding, and protein kinase binding, indicative of elevated protein quality control and stress response. Down-regulated terms included phosphoinositide binding, actin filament binding, and RNA processing-related functions, pointing to attenuated cytoskeletal remodeling and gene regulatory complexity on nano/micro-structured surfaces. These reveal that increasing titanium surface roughness drives progressive remodeling of key molecular functions in macrophages, particularly involving redox control, protein folding, and immune signaling, which underline their divergent inflammatory or healing phenotypes in response to bacterial stimulation[206].

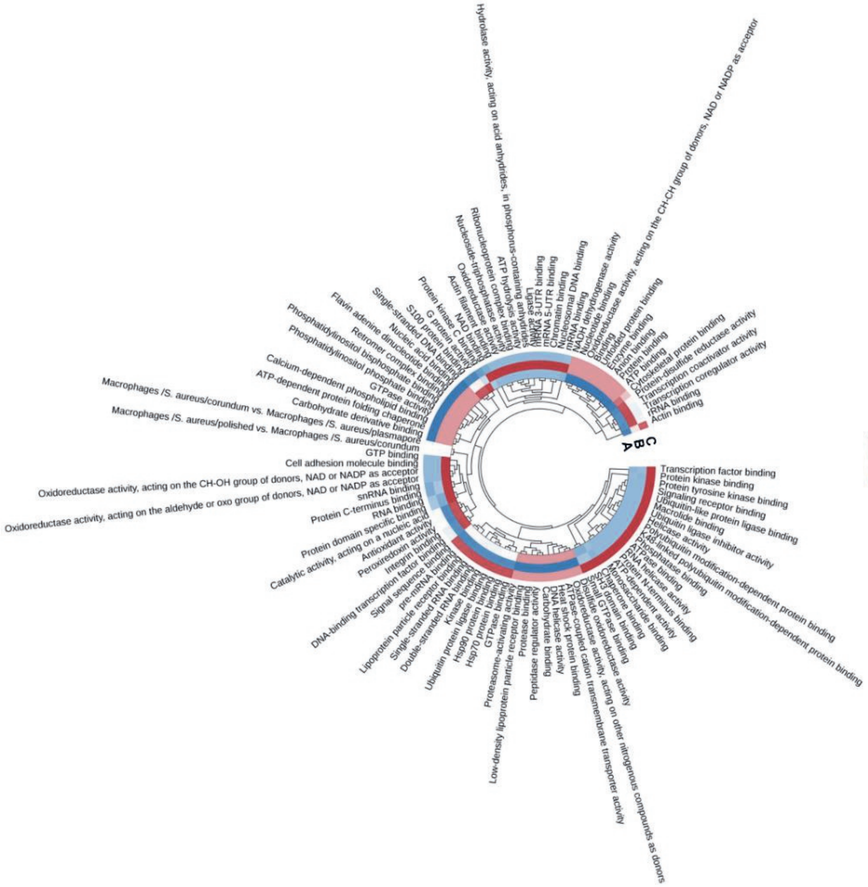


Fig. 15. Gene Ontology molecular function classification of differentially regulated proteins in macrophages stimulated with *S. aureus* and cultured on Ti surfaces. Up- and down-regulated Gene Ontology (GO) molecular function terms were enriched among differentially expressed proteins from macrophages cultured on titanium surfaces with increasing surface roughness under *S. aureus* stimulation. Functional enrichment is shown for three surface comparisons. A: control vs. polished, B: polished vs. corundum, and C: corundum vs. plasmapore. Values indicate enrichment scores.

To determine how the titanium surface roughness influences subcellular localization of macrophage proteins during infection, Gene Ontology (GO) cellular component enrichment was performed across sequential surface comparisons. In the control vs. polished condition, up-regulated proteins were predominantly localized to phagocytic vesicles, lysosomal compartments, and extracellular exosomes, reflecting enhanced vesicle-mediated immune functions and intercellular communication. Notably,

components of the podosome and cortical actin cytoskeleton were enriched, suggesting early cytoskeletal remodeling during macrophage activation.

Transitioning from polished to corundum surfaces, the enrichment shifted toward mitochondrial and nuclear structures. Proteins associated with the mitochondrial respiratory chain complex I, proton-transporting ATP synthase, and respirasome were significantly up-regulated, indicating increased metabolic activity. Simultaneously, nuclear-associated components such as the spliceosome, B-WICH complex, and mRNA stability complexes were enriched, suggesting modulation of RNA processing and transcriptional regulation on rougher surfaces. In the corundum vs. plasmapore comparison, further up-regulation was observed in the cytosol, ribosome, proteasome, and MHC class I peptide loading complex, reflecting activation of antigen presentation and protein turnover pathways. The enrichment of U2-type spliceosomal complex and ribonucleoprotein granules further supports a role for post-transcriptional regulation in shaping macrophage responses. Interestingly, cytoskeletal and lysosomal components showed both up- and down-regulated trends, indicating fine-tuned spatial reorganization depending on surface architecture. These findings reveal that increasing surface roughness modulates the subcellular distribution of macrophage proteins during bacterial challenges, particularly involving vesicle trafficking, mitochondrial energetics, and proteasomal regulation, potentially underpinning the immunomodulatory effects of titanium implant topographies.

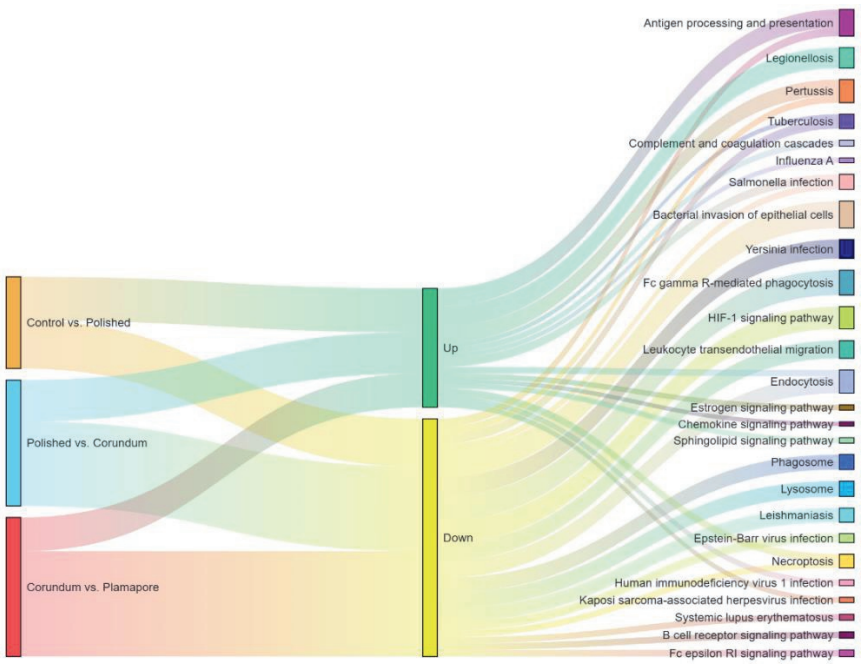
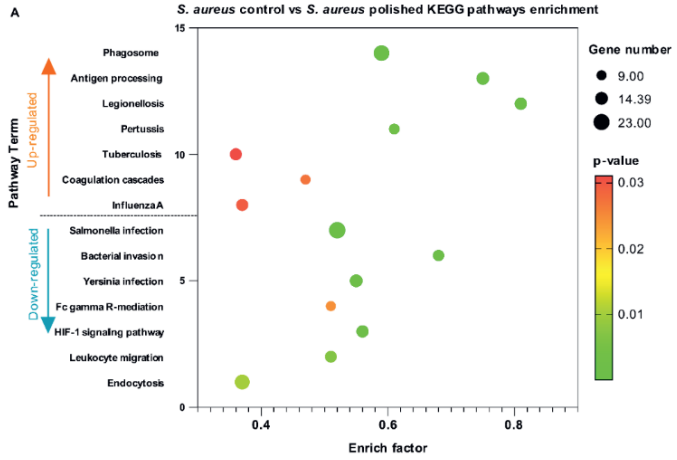
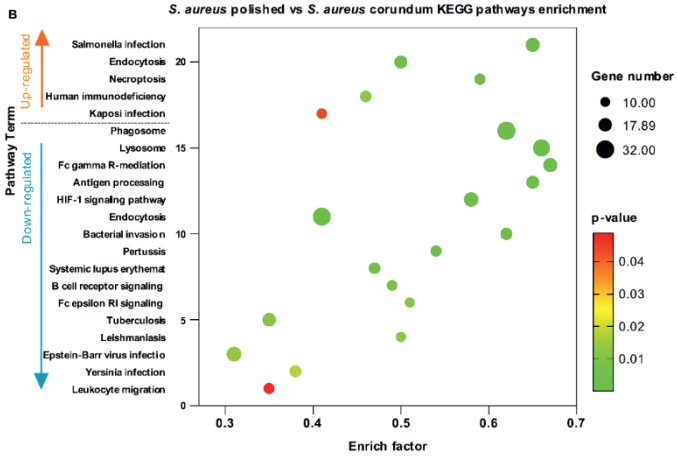


Fig. 16. Cellular component enrichment analysis of differentially regulated proteins in macrophages exposed to *S. aureus* on Ti surfaces with increasing roughness. Alluvial plot shows Gene Ontology (GO) cellular component terms significantly enriched in macrophages cultured on titanium surfaces of increasing roughness under *S. aureus* stimulation. Surface contrasts are indicated on the left, proteins are classified as upregulated (green) or downregulated (yellow) in the center, and functional pathways are shown on the right. Flow width reflects the relative contribution of proteins.

KEGG pathway enrichment analysis was performed to elucidate the impact of titanium surface roughness on macrophage responses under *S. aureus* stimulation. As shown in Fig. 17A, comparison between control and polished surfaces revealed significant enrichment in phagosome, antigen processing, and tuberculosis-related pathways among up-regulated proteins, while down-regulated pathways included leukocyte migration and Fc gamma R-mediated signaling, suggesting a shift in innate immune activation with initial surface refinement. Transitioning from polished to corundum surfaces (Fig. 17B) further amplified immune-related signaling. Notably, pathways related to phagosome, lysosome, and Salmonella infection were enriched among up-regulated targets, while antigen processing, bacterial invasion, and HIF-1 signaling were increasingly down-regulated. This indicated a complex reprogramming of pathogen recognition and intracellular trafficking

machinery on rougher surfaces. In contrast, comparison between corundum and plasmapore surfaces (Fig. 17C) revealed divergent regulation of pathways involved in chemokine signaling, sphingolipid signaling, and estrogen response. Those were up-regulated on corundum, whereas necrotic, endocytic, and HIF-1-mediated processes were suppressed on plasmapore.


A
S. aureus control vs S. aureus polished KEGG pathways enrichment
Pathway Term
Up-regulated
Down-regulated
Phagosome
Antigen processing
Legionellosis
Pertussis
Tuberculosis
Coagulation cascades
Influenza A
Salmonella infection
Bacterial invasion
Yersinia infection
Fc gamma R-mediation
HIF-1 signaling pathway
Leukocyte migration
Endocytosis
Gene number
9.00
14.39
23.00
p-value
0.03
0.02
0.01
Enrich factor


B
S. aureus polished vs S. aureus corundum KEGG pathways enrichment
Pathway Term
Up-regulated
Down-regulated
Salmonella infection
Endocytosis
Necroptosis
Human immunodeficiency
Kaposi infection
Phagosome
Lysosome
Fc gamma R-mediation
Antigen processing
HIF-1 signaling pathway
Endocytosis
Bacterial invasion
Pertussis
Systemic lupus erythemat
B cell receptor signaling
Fc epsilon RI signaling
Tuberculosis
Leishmaniasis
Epstein-Barr virus infectio
Yersinia infection
Leukocyte migration
Gene number
10.00
17.89
32.00
p-value
0.04
0.03
0.02
0.01
Enrich factor

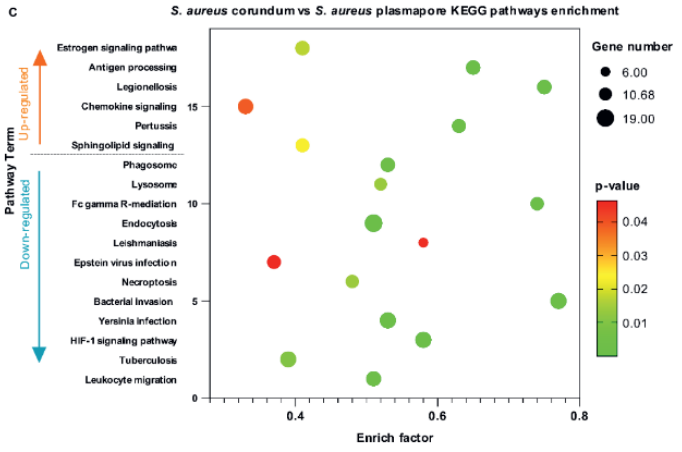

C
S. aureus corundum vs S. aureus plasmapore KEGG pathways enrichment
Pathway Term
Up-regulated
Down-regulated
Estrogen signaling pathwa
Antigen processing
Legionellosis
Chemokine signaling
Pertussis
Sphingolipid signaling
Phagosome
Lysosome
Fc gamma R-mediation
Endocytosis
Leishmaniasis
Epstein virus infection
Necroptosis
Bacterial invasion
Yersinia infection
HIF-1 signaling pathway
Tuberculosis
Leukocyte migration
Gene number
6.00
10.68
19.00
p-value
0.04
0.03
0.02
0.01
Enrich factor

Fig. 17. KEGG pathway enrichment analysis of differentially expressed proteins in macrophages cultured on titanium surfaces of varying roughness under *S. aureus* stimulation. Bubble plots show enriched KEGG pathways associated with differentially expressed proteins in macrophages cultured on Ti surfaces. The x-axis represents the enrichment factor, and the size of the bubbles corresponds to the number of genes enriched in each pathway. Bubble color indicates the statistical significance (p-value), with red representing lower p-values. Pathways are ordered vertically by up-regulated (orange arrow) and down-regulated (blue arrow) enrichment trends.

4. Discussion

This study aimed to elucidate how titanium surface roughness modulates macrophage polarization under *S. aureus* challenge. The main focus of this chapter was on three clinically relevant textures—polished, corundum, and plasmapore type of surfaces. More specifically, the impact of these surfaces on macrophage polarization, adhesion, and reactive oxygen species (ROS) production was investigated. All results revealed that, within the first 12 hrs of infection, the increasing surface roughness promoted M1 polarization and enhanced ROS release. Before 12hrs, corundum surfaces supporting the most robust cell adhesion. However, beyond 12 hrs, macrophages progressively shifted toward an M2 phenotype, a transition most pronounced on corundum. While corundum roughness initially favors bactericidal M1 activity, its prolonged use under infection conditions may facilitate a reparative M2 shift, potentially compromising bacterial clearance.

Surface topography has long been recognized as a determinant of cell viability and function[207]. Consistent with previous reports, macrophage viability across the tested titanium surfaces exhibited only modest variation under basal conditions. However, under bacterial stress, increased roughness imposed an additional metabolic burden, resulting in reduced viability. This suggests that roughness imposes an additional cellular burden, lowering viability under stress conditions, as also reported by Osman, Muataz A., et al.[208].

Macrophage polarization is central to antibacterial immunity. Classically activated M1 macrophages mediate pathogen clearance through pro-inflammatory cytokines and oxidative mechanisms[209], while M2 polarization is largely associated with tissue repair [210]. During infection, an accumulation of M1 macrophages is crucial for pathogen clearance[211], making it essential to understand macrophage polarization under *S. aureus* challenge. In line with previous studies demonstrating a M1/M2 polarization transition during *S. aureus* infection[212, 213], TNF-α levels were lowest at 24 hrs, whereas IL-10 gradually increased, with maximum values on corundum surfaces at 24 hrs. These findings indicate that within the first 12 hrs post-infection, macrophages preferentially polarize toward the M1 phenotype with increasing surface roughness, whereas after 12 hrs, a shift toward M2 polarization occurs, with the highest M2 prevalence observed on corundum surfaces. Immunofluorescence analysis revealed co-expression of M1 and M2 markers (CD36 and CCR7), consistent with the well-documented plasticity of macrophages. Fluorescence intensity of M1 markers increased with surface roughness before 12 hrs but decreased thereafter, whereas M2 marker expression was maximal on corundum surfaces at 24 h, further supporting a temporal switch from M1 to M2 polarization.

To corroborate these observations, RT-PCR analysis of polarization-associated genes showed that M1-related genes (TNF-α, IDO1, CXCL11) were upregulated within the first 12 hrs with increasing roughness, while M2-associated genes (IL-10, MRC1, CCL13) decreased after 12 hrs, particularly on corundum surfaces. Correspondingly, the M1/M2 ratio exhibited a similar temporal trend. These dynamics likely result from the combined effects of *S. aureus* infection and surface roughness. Peng, Kuo-Ti, et al. indicated that *S. aureus* primarily induces M1 polarization before 12 h, shifting to M2 thereafter[214]. Our earlier studies demonstrated that in an LPS-induced infection model, increasing roughness enhanced M1 differentiation, elevating the M1/M2 ratio. However, beyond 12 hrs, the combined influence of *S. aureus* and surface topography promoted M2 polarization, particularly on corundum surfaces. Notably, in the absence of LPS

stimulation, corundum surfaces favored M2 differentiation, and *S. aureus* infection further amplified this effect. These highlight a time-dependent and topography-sensitive modulation of macrophage polarization by *S. aureus*, emphasizing the critical interplay between bacterial challenge and biomaterial surface properties in dictating immune responses.

Effective host defense against implant-associated infection requires not only macrophage polarization but also sufficient adhesion of M1 macrophages to the material surface[69]. In previous studies demonstrated that, in the absence of infection, corundum surfaces supported optimal macrophage attachment. Consistently, Zhang, Yang, et al. reported that moderately rough surfaces favor macrophage adhesion[121]. ICAM1, a key gene associated with macrophage adhesion[215]revealed expression patterns consistent with adhesion trends. Adhesion assays confirmed that corundum surfaces were most conducive to macrophage attachment within the first 12 h, in line with prior LPS-induced infection models. At 24 h, although bacterial adhesion on corundum was lower than on plasmapore surfaces, it remained higher than on polished or control surfaces. These results suggest that moderately rough surfaces promote early macrophage recruitment.

Upon adhesion to infected titanium substrates, macrophages primarily eliminate bacteria via phagocytosis, accompanied by secretion of reactive oxygen species (ROS) to eradicate intracellular *S. aureus*[216]. Surface roughness markedly influenced this process [217]. Consistent with previous findings by Zhang, Xinrui, et al.[218], gene expression revealed that TLR2, indicative of phagocytic function, increased with roughness within 12 hrs, correlating with enhanced bacterial uptake. Beyond 12 h, however, phagocytic activity declined—most notably on corundum surfaces. Quantification of *S. aureus* uptake by confocal microscopy mirrored this biphasic trend. SEM and confocal imaging further confirmed surface-dependent morphological adaptations. On plasmapore surfaces, macrophages displayed extensive membrane remodeling, including ruffling and formation of phagocytic cups. In contrast, corundum-adherent cells exhibited irregular

contours, pronounced ruffling, and reduced spreading, providing an ultrastructural basis for altered adhesion and phagocytic performance. TEM revealed that macrophages on rougher surfaces were predominantly rounded, with fewer protrusions and lower phagosome density, indicative of reduced metabolic and phagocytic activity at the subcellular level. Proteomic profiling supported these observations, showing enrichment of mitochondrial and nuclear components and modulation of metabolic and transcriptional pathways with increasing roughness. On corundum surfaces, proteins associated with transcription coactivator activity, NAD binding, and ubiquitin ligase binding were upregulated, whereas those linked to chromatin binding, RNA helicase activity, and ATP-dependent transport were downregulated.

Upon adhesion to infected titanium substrates, macrophages primarily eliminated bacteria via phagocytosis, accompanied by ROS–mediated killing of intracellular *S. aureus*[219]. Because bacterial clearance is critically dependent on ROS levels[220], insufficient ROS production can facilitate immune evasion, enhance host antibiotic resistance, and potentially promote bacterial dissemination to distal sites [220]. Consistent with this, RT–PCR data revealed that expression of Nfkb1, a gene associated with ROS production[221], increased with surface roughness during the first 12 h, but declined thereafter—most prominently on corundum surfaces. ROS measurements paralleled these transcriptional changes. Consistent with earlier reports linking increased roughness to enhanced early immune activation[117], a transient augmentation of macrophage phagocytic responsiveness on rougher surface was observed, manifested by elevated TLR2 expression and bacterial uptake at early time points. Notably, this response was not sustained: prolonged exposure led to a marked attenuation of phagocytosis, most prominently on highly rough corundum surfaces, revealing a biphasic, time-dependent modulation of macrophage function by surface topography.

Morphological and ultrastructural analyses provide mechanistic context for this functional shift. In agreement with established models of phagocytosis–spreading

coupling, moderately rough plasmapore surfaces promoted membrane ruffling and phagocytic cup formation. By contrast, excessive roughness induced aberrant cytoskeletal remodeling, characterized by irregular cell morphology, exaggerated ruffling, limited spreading, and reduced phagosome abundance, which has also been reported by Roberts RE, Hallett MB[222]. Similar phenotypes have been associated with metabolically constrained or functionally impaired macrophage states in other inflammatory contexts, suggesting that extreme topographical cues may impose physical limits on sustained phagocytic activity.

Proteomic profiling further indicates that these phenotypic changes reflect broader reprogramming of macrophage polarization. Although rougher surfaces enhanced phagosome and lysosome-associated pathways—consistent with early phagocytic activation—key immune programs involved in antigen processing, bacterial invasion, and HIF-1 signaling were concurrently suppressed. In line with early reports[223], on corundum, enrichment of proteins related to transcriptional co-activation, NAD binding, and ubiquitin ligase interactions, together with depletion of chromatin-binding, RNA helicase, and ATP-dependent transport proteins, points to a shift toward metabolic and regulatory adaptation rather than sustained effector function.

Overall, titanium surface roughness exerts a dynamic, time-dependent influence on macrophage–*S. aureus* interactions. While roughened surfaces enhance early bactericidal activity, a subsequent shift toward an anti-inflammatory, tissue-remodeling phenotype may create a permissive niche for bacterial persistence. Mechanistically, this biphasic response involves metabolic reprogramming, transcriptional regulation, and immune signaling, integrating environmental cues from surface topography and bacterial challenge. These findings emphasize the importance of temporally coordinating immune activation and resolution in implant design. Strategies that sustain early M1 activity while modulating M2 transition may enhance bacterial clearance without compromising tissue repair.

Limitations include the in vitro model, which does not fully capture the complex multicellular and biomechanical environment of in vivo implants. Future studies using orthotopic infection models in immunocompetent animals are needed to validate these temporal macrophage dynamics. Additionally, functional validation of candidate proteomic targets (HIF-1α, sphingolipid enzymes) is necessary to confirm causality. Extending investigations to polymicrobial infections and biofilm-resilient strains may provide further insights. These results provide a framework for immuno-informed biomaterial design, where surface topography can be leveraged to modulate macrophage plasticity and host–pathogen dynamics during early infection, ultimately guiding the development of implants that optimize both osteogenesis and immune resilience.

5. Conclusion

This study reveals that titanium surface properties dynamically regulate macrophage behavior during *S. aureus* infection, orchestrating a time-dependent shift from pro-inflammatory clearance to immune resolution. This topography-driven modulation of macrophage polarization, phagocytosis, and bactericidal activity highlights the dualistic role of surface features in mediating both host defense and tissue integration. By uncovering the molecular programs underlying these transitions, a mechanistic basis for designing next-generation biomaterials that align immune activation with infection control is provided.

Chapter 4 - Application of surface plasmon resonance to elucidate the cooperative DNA binding mechanisms of NFATc1 and c-Jun

Based on

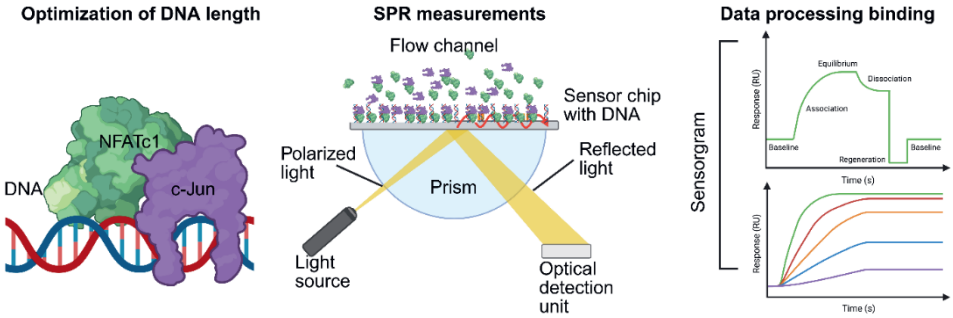
Cao B., Cillero-Pastor B., Honing M. Application of surface plasmon resonance to elucidate the cooperative DNA binding mechanisms of NFATc1 and c-Jun. Biochimica et Biophysica acta. General Subjects 1870.6 (2026): 130924-130924.

Abstract

Background: Transcription factors (TFs) are regulators of gene expression, orchestrating cellular processes such as proliferation, differentiation, and immune response. NFATc1, a member of the NFAT family, is crucial for immune regulation, while c-Jun mediates stress and oncogenic signals. Cooperative binding of these TFs to DNA plays a pivotal role in controlling complex transcriptional networks. However, current methodologies fail to fully capture the dynamic and cooperative nature of these TF-DNA interactions. The problem addressed in this work is the lack of real-time kinetic profiling of the NFATc1 and c-Jun cooperative binding with DNA. Surface plasmon resonance (SPR) was employed in this work to assess the individual and cooperative DNA-binding kinetics of NFATc1 and c-Jun.

Results: Using SPR, the individual and cooperative DNA-binding kinetics of NFATc1 and c-Jun was quantified. NFATc1 binds DNA with a dissociation constant (KD) of (4.11 ± 0.07) × 10^{-7} M, while c-Jun shows a slightly stronger affinity KD = (1.95 ± 0.03) × 10^{-7} M. Not surprisingly, when forming a heterodimeric complex, the NFATc1–c-Jun binding affinity further lowers the KD = (1.63 ± 0.17) × 10^{-7} M, indicating cooperative interaction. More important, kinetic analysis revealed that the association rate (ka) increased more than threefold, from (2.44 ± 0.10) × 10^{5} $M^{-1}s^{-1}$ to (8.29 ± 0.19) × 10^{5} $M^{-1}s^{-1}$, while dissociation kinetics remained dynamic. These results demonstrate that NFATc1 facilitates c-Jun recruitment, enhancing cooperative DNA engagement. Together, the findings highlight the unique ability of SPR to resolve cooperative TF-DNA interactions with high temporal precision, providing insights not attainable through conventional techniques.

Significance: By demonstrating that NFATc1 and c-Jun form a complex with enhanced DNA-binding affinity and accelerated association kinetics, this study provides a mechanistic basis for their synergistic regulation of gene expression. The findings bridge a critical knowledge gap between structural observations and dynamic molecular interactions, offering a framework for modeling transcriptional regulation in immune and oncogenic contexts.



1. Introduction

Transcription factors (TFs) are crucial regulators of gene expression, governing essential cellular processes such as differentiation, proliferation, and apoptosis[224, 225]. Among these, the NFAT family, particularly NFATc1, plays a vital role in immune responses, while c-Jun, part of the AP-1 complex, mediates cellular stress and proliferation signals[225-228]. Cooperative DNA binding between TFs like NFATc1 and c-Jun is a key mechanism in regulating complex gene expression networks, especially in immune and oncogenic contexts[229, 230]. However, the molecular mechanism of this cooperative interaction remains poorly understood, limiting our ability to fully model their regulatory dynamics.

Techniques, such as electrophoretic mobility shift assays (EMSAs) and fluorescence anisotropy, have frequently been used to characterize the DNA-binding kinetics of individual TFs. Yet, they often lack the temporal resolution and precision needed to capture cooperative interactions[231-233]. Structural studies like X-ray crystallography and cryo-electron microscopy provide static snapshots of TF-DNA complexes and are not designed to reveal the kinetic and thermodynamic properties of these interactions in solution[234, 235]. These gaps hinder our understanding of the real time cooperative binding kinetics and thermodynamics to DNA.

Surface Plasmon Resonance (SPR) has gained its position as a valuable tool for studying real-time, label-free biomolecular interactions, enabling precise measurement of binding kinetics and affinity between proteins and DNA[236-238]. However, its potential for studying cooperative TF binding is still rather limited, mainly due to challenges in accurately analyzing multi-protein or multi-site interactions.

This study addresses some of the challenges by developing a SPR-based platform capable of assessing the binding kinetics of multi-protein/DNA interactions. We hypothesize that while NFATc1 and c-Jun bind DNA independently, their heterodimeric complex exhibits enhanced affinity and cooperativity. Here we present our findings, supporting this hypothesis, and addressing the importance, of molecular structural changes upon binding.

2. Experimental methods

2.1. Materials

The SPR (MP-SPR NaviTM 200 OTSO, Finland) was used to study protein-DNA interactions with a peristaltic pump (BioNavis, Finland) to control the flow rate. NFATc1, c-Jun and DNA were purchased from Sigma-Aldrich (Sigma, Netherlands). Biotin-labeled single-stranded DNA was purchased from Sigma. The biotin-avidin Sensors Kit (BioNavis, Finland) encompassed biotinylated chips, regeneration buffer 1 for routine cleaning of the chip and regeneration buffer 2 to remove immobilized proteins and DNA from the chip surface, were applied throughout the study. UV spectrophotometry (Denovix, USA) was applied to assess the concentration and purity of DNA. All other reagents were of analytical grade and used without further purification. The three working buffers used throughout the experiment were: Running buffer (TSB): 50mM Tris–HCl buffer, NaCl 100mM solution, pH 7.4; DNA hybridization buffer (HSM): 10mM Hepes, 50mM NaCl, 10mM MgCl; Protein binding buffer (PBB): 30 mM Tris-Hcl (pH 7.5), 3mM NaOAC, 20mM Nacl, 0.01mg/mL poly-(dIdC), 0.025µm polylysine (pH7.5). In addition, regeneration buffer 1 (10 mM glycine, pH 2.5) was used for chip cleaning, while regeneration buffer 2 (Bionavis formula) was used to regenerate the chip back to its original biotinylated gold state after a series of injections.

2.2. Design and optimization of DNA sequences

To ensure the effective analysis of DNA binding by NFATc1 and c-Jun, the design of specific DNA sequences and optimization of their lengths were performed based on the structural dimensions of the protein-DNA complex. Since NFATc1 interacts with DNA in conjunction with c-Fos, forming a stable NFATc1/c-Jun/c-Fos/DNA complex, we referenced the maximum diameter of this complete complex to refine the DNA sequence design. Compared to the NFATc1/c-Jun complex alone, incorporating c-Fos provides a more physiologically relevant representation of the binding scenario, ensuring that the designed sequences fully accommodate the structural constraints of cooperative binding. The total DNA binding region of the NFATc1/c-Jun/c-Fos/DNA complex was determined to be approximately 22 base pairs (bp), accounting for both the NFAT and AP-1 binding sites along with their necessary spacing. To ensure sufficient spatial availability for NFATc1, c-Jun, and the bound DNA, the structural dimensions of the complex were analyzed. Additionally, a shorter DNA sequence was designed to account for unspecific binding.

A Miniconda3 environment (239) was established to facilitate the use of computational tools, particularly PyMOL(240), for structural analysis. Using PyMOL and custom Python scripting (Text S.1), the maximum diameter of the NFATc1/c-Jun/c-Fos/DNA complex was calculated. It provided essential parameters for the optimization of the DNA sequence length. Based on the structural constrains of the NFATc1/c-Jun/c-Fos/DNA complex, the DNA sequence was extended to ensure ample space for binding while minimizing steric hindrance. Furthermore, a biotin modification was incorporated at the 5’ end of the forward strand was implemented to facilitate the attachment of the DNA to the biotin-functionalized SPR chip. This step ensures stable immobilization during the interaction assays.

2.3. Optimization of DNA hybridization time

Optimal conditions for DNA hybridization were achieved when the single-stranded DNA was dissolved in DNA hybridization buffer (HSM). Single-stranded DNA samples were mixed in equimolar ratios and subjected to heating at 95°C for varying durations: 5 min,

10 min, 20 min, and 45 min. After heating, the samples were allowed to gradually cool to room temperature to promote proper formation of double-stranded DNA. The quality and concentration of annealed DNA were assessed using UV spectrophotometry. Absorbance values at 260 nm were recorded, and the A260/A280 ratio was calculated to evaluate purity. Changes in UV spectra were monitored to confirm the transition from single-stranded to double-stranded DNA.

2.4. Negative-stain EM of reconstituted NFATc1–c-Jun–DNA

NFATc1, c-Jun and DNA were mixed at a 1:1:1 M ratio and overnight incubated at 4 °C to form the NFATc1/c-Jun/DNA complex. The molecular mass of the NFATc1–c-Jun–DNA complex was determined by size-exclusion chromatography coupled to multi-angle light scattering (SEC-MALS) using a Superdex 200 Increase 10/300 GL column (Cytiva, USA) equilibrated in 20 mM HEPES (pH 7.5), 150 mM NaCl, and 1 mM DTT. UV (260/280 nm), MALS, and refractive index signals were recorded and analyzed in ASTRA (Wyatt Technology, USA) using a protein–DNA conjugate model. The peak fractions containing both proteins and DNA were verified by 260/280 nm absorbance and concentrated to 0.1 mg mL^{-1} for EM. For negative staining, freshly purified complex was applied to glow-discharged carbon-coated grids, incubated for 30 - 60s, blotted and stained with 1% uranyl acetate before air-drying. Micrographs were recorded on a 120 kV transmission electron microscope at 120,000× magnification and - 0.5 µm defocus. Images were inspected manually and contrast transfer function (CTF) parameters were estimated with CTFFIND4. Particles were picked using manual and automated approaches in RELION4.0 (MRC Laboratory of Molecular Biology, Cambridge, UK). Iterative 2D classifications yielded reproducible classes with bilobed or elongated features consistent with the NFATc1–c-Jun–DNA complex; a selected subset of particles was used to generate reference 3D averages.

2.5. Surface plasmon resonance system setup

The SPR system was employed to investigate the cooperative DNA binding by NFATc1 and c-Jun. All SPR experiments were carried out at room temperature. For the first 10 min, the system was calibrated using TSB buffer (10mM Tris–HCl buffer, NaCl 100mM solution, pH 7.4) generating a stable baseline signal for 10 min. Flow rate (30μL/min) was controlled using a peristaltic pump. The instrument operating temperature was set to 22 ℃. 250 μL of regeneration buffer1 (10 mM glycine, pH 2.5) was used to clean the chip for 2 min.

2.6. Construction of DNA-chip for surface plasmon resonance measurements

To enable quantitative analysis of NFATc1 and c-Jun DNA binding, a biotin-functionalized sensor chip was constructed with surface-immobilized DNA containing the specific binding sequences for c-Jun and NFATc1. SPR measurements were conducted using a BioNavis 200 SPR system equipped with biotin-functionalized sensor chips. The biotin-functionalized sensor chip was pre-treated with 250 μL of avidin solution (50 μg/mL) for 6.13 min at room temperature to establish a high-affinity avidin binding layer. Excess avidin and unbound material were removed by washing the chip with TBS buffer (10 mM Tris, 150 mM NaCl, pH 7.4). Biotinylated double-stranded DNA, designed to contain the specific binding sequences for c-Jun and NFATc1, was prepared at a concentration of 100 nM in TBS buffer (10 mM Tris, 150 mM NaCl, pH 7.4). The biotinylated DNA was injected over the avidin-functionalized chip surface at a flow rate of 10 μL/min to ensure stable and specific attachment via the biotin-avidin interaction. Following DNA immobilization, unbound DNA was removed by washing the chip with TBS buffer at a flow rate of 20 μL/min for 5 min. Surface stability and DNA immobilization efficiency were verified by monitoring the baseline resonance units (RUs), ensuring consistent and reproducible binding levels.

2.7. Analysis of NFATc1, c-Jun, and NFATc1/c-Jun complex DNA binding kinetics

SPR was applied to quantify the binding kinetics of NFATc1 and c-Jun individually with DNA, as well as the DNA-binding dynamics of their 1:1 complex. Each experiment was

performed in triplicate. NFATc1 and c-Jun proteins were mixed at a 1:1 M ratio in a protein binding buffer (10 mM Hepes, 150 mM NaCl, 1 mM $MgCl_2$, pH 7.4). The mixture was incubated at 4 °C overnight to allow the formation of the NFATc1/c-Jun complex prior to SPR analysis(241). SPR measurements were performed using a BioNavis SPR system. This system has two channels. Both channels were used throughout the experiments. One was used as a measurement/experimental channel to evaluate the binding kinetics. This channel consisted of a biotinylated gold chip with immobilized avidin and immobilized biotinylated-dsDNA. The reference channel included all the components of the experimental channel, except dsDNA. Both channels were exposed to different proteins for DNA-protein binding kinetic evaluation and non-specific binding exclusion. The SPR response was calculated as ΔRU, defined as ΔRU = RUmeasurement – RUreference. Protein samples, including NFATc1, c-Jun, and the NFATc1/c-Jun complex, were prepared in a range of concentrations: 2 nM, 4 nM, 6 nM, 8 nM, 16 nM, 32 nM, and 64 nM. 250 µL of each protein sample was injected sequentially (serial mode, Channel 1) over the DNA-functionalized sensor surface for 6.13 min at a flow rate of 10 µL/min. A post-injection wait time of 5 min was included to ensure equilibrium and facilitate the removal of unbound proteins. Unbound proteins were removed by washing the chip surface with binding buffer at a flow rate of 20 µL/min for 3 min. After each measurement, the sensor surface was regenerated by injecting a low-pH regeneration buffer (10 mM glycine, pH 2.5) to dissociate bound proteins and restore the surface for subsequent measurements.

2.8. Data processing of analysis binding interactions

The SPR-Navi Data Viewer and the TraceDrawer software were applied to analyze the binding kinetics of NFATc1, c-Jun, and the NFATc1/c-Jun complex with DNA, specifically determining the association rate constant (ka), dissociation rate constant (kd), and equilibrium dissociation constant (KD). Raw SPR data were processed using SPR-Navi Data Viewer. Data from Channel L1 (670 nm, biotin-functionalized DNA chip Channel) was used as the experimental detection channel, while Channel L5 (670 nm, biotin-functionalized avidin chip Channel) served as the reference channel to correct non-specific binding and

background noise. Data were exported in purekinetic mode for subsequent analysis. Initial SPR signals were transformed into positive values to facilitate analysis and improve interpretability. Binding kinetics were analyzed using TraceDrawer software. For the NFATc1/c-Jun complex, a fit model (1:1) with two binding sites was applied to account for cooperative interactions with DNA. A global fitting of the dissociation phase was performed to estimate the dissociation rate constant (kd). With kd fixed, the association phase was globally fitted to determine the association rate constant (ka). Both the association and dissociation phases were visually inspected to ensure that the fitted curves closely matched the experimental data. Ka, Kd and KD were presented as mean ± standard deviation and compared using t-tests with SPSS21 (IBM, USA).

3. Results

3.1 Spatial evaluation for NFATc1 and c-Jun DNA binding during SPR detection

To assess whether NFATc1 and c-Jun can effectively bind to specific DNA sequences, computational modeling experiments allowed the evaluation of the spatial constraints of the NFATc1/c-Jun/c-Fos/DNA complex (Fig. 1). Using a Python script (Text S1) within a PyMOL runtime environment configured via Miniconda3 and applying the ConvexHull function(242) function from the scipy.spatial library(243) to construct the dot structure of the NFATc1 complex (Fig. 1A). The calculated maximum diameter of the complex was 94.57 Å (Fig. 1B), indicating the spatial requirements for NFATc1 and c-Jun binding. Based on this, we designed a specific DNA sequence (Fig. 1C) with sufficient length to ensure accessibility of the binding domains while allowing stable attachment to the biotinylated SPR chip. These findings confirm that the designed DNA sequence provides an appropriate spatial framework for NFATc1 and c-Jun interactions.

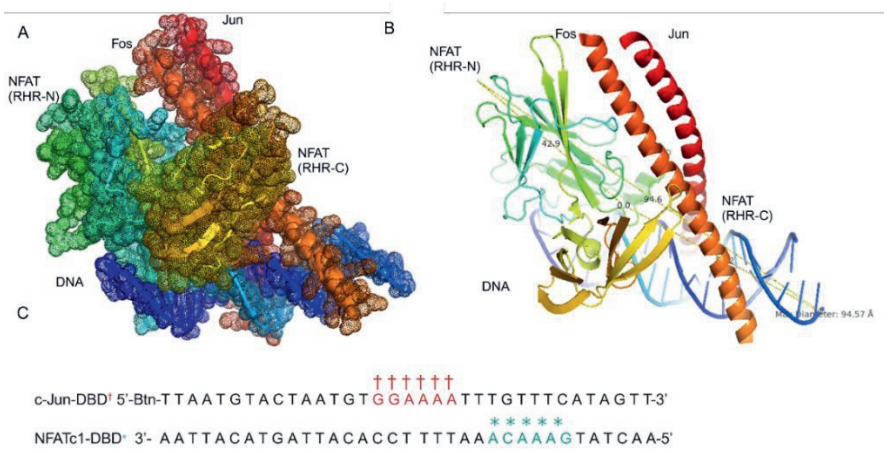


Fig. 1. Spatial Modeling and Dimension of NFATc1/c-Jun/c-Fos/DNA complex (A) Dot structure of the NFATc1/c-Jun/c-Fos/DNA Complex. (B) Cartoon structure of the NFATc1/c-Jun/c-Fos/DNA Complex illustrating the complex diameter. (C) NFATc1 and DNA-specific binding sequences.

3.2. DNA sensor preparation

In optimizing the hybridization conditions for DNA sensor preparation, the kinetics of complementary strand annealing, through the measurement of absorbance at 260 nm as function of time (5, 10, 20, and 30 min) was estimated. As shown in Fig. 2, the absorbance increased over time, indicating progressive formation of double-stranded DNA. At 5 min, the mean absorbance was 26.73 ± 0.11, rising to 27.62 ± 0.07 in 10 min and 29.19 ± 0.07 after 20 min. Next, and more prone after 30 min, the values plateaued (29.25 ± 0.08), suggesting near-complete hybridization. Based on these results, 20 min was determined as the optimal hybridization time for DNA sensor preparation.

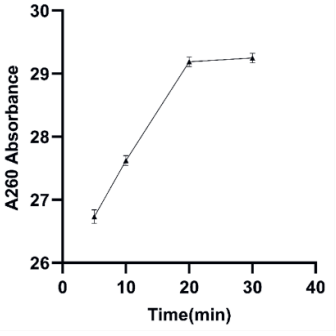


Fig. 2. Kinetics of complementary DNA strand hybridization monitored by UV spectrophotometry.

3.3. Formation and structural characterization of the NFATc1–c-Jun–DNA complex

Reconstitution of NFATc1, c-Jun and dsDNA yielded a stable ternary complex that eluted as a single, symmetric peak on size-exclusion chromatography, consistent with formation of the NFATc1–c-Jun–DNA assembly (Fig 3). The observed molecular mass is consistent with the formation of a stable NFATc1–c-Jun–DNA (240 kDa) assembly. Negative-stain electron microscopy of material from the major SEC fraction (Fig 3A, fraction 17, MW: 240 kDa) revealed well-dispersed particles with a defined NFATc1/c-Jun/DNA architecture (Fig 3A). Individual particles were readily identifiable in raw micrographs, and the characteristic shape was preserved across fields of view (Fig 3B). Particles selected from these micrographs supported the generation of an initial 3D reconstruction (Fig 3C), and a NFATc1/c-Jun/DNA reference map was used to guide model alignment (Fig 3D). The consistent morphology observed throughout the dataset indicates that NFATc1 and c-Jun form a stable complex suitable for SPR analysis.

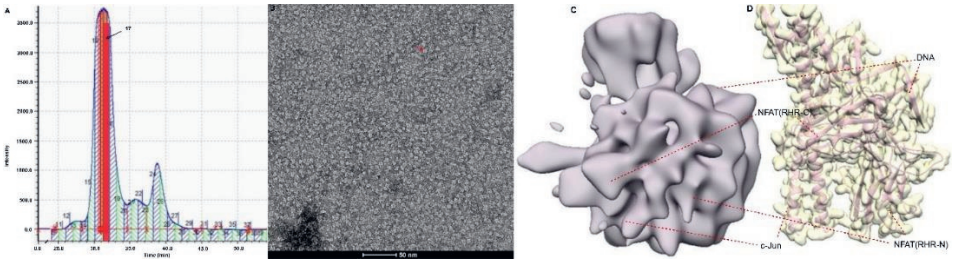


Fig. 3. Negative-stain electron microscopy of the NFATc1–c-Jun complex. (A) SEC profile of the reconstituted NFATc1–c-Jun–DNA with UV absorbance at 260/280 nm. (B) Representative negative-stain micrograph of the NFATc1–c-Jun complex collected from fraction 17 shown in A. (C) Particles selected from the micrograph in Fig.3B were used for 3D reconstruction. (D) Reference model employed during 3D reconstruction. The red arrow indicates the representative (NFATc1–c-Jun) complex. Scale bars: 50 nm.

3.4. Surface plasmon resonance analysis of NFATc1, c-Jun, and NFATc1/c-Jun complex binding to DNA

3.4.1 Sensorgram overview of protein/protein-DNA interaction

To elucidate the DNA-binding mechanisms of NFATc1 and c-Jun, the optimized biotinylated double-stranded DNA (dsDNA) probe was first tested (Fig. 4). The sensorgrams (Fig. 5) revealed the sequential steps of surface immobilization and protein binding, confirming successful functionalization and molecular interactions.

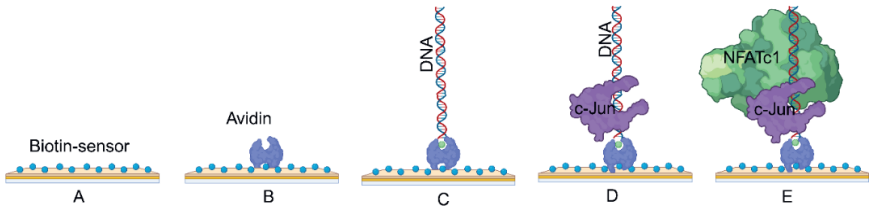


Fig. 4. Schematic diagram for the step-by-step binding of the ligand onto the chip surface. (A) The biotin functionalised gold chip. (B) Avidin binds to biotin functionalised gold chip surface. (C) Biotinlated DNA binds to avidin. (D) c-Jun binds to biotinlated DNA. (E) NFATc1 binds to biotinlated DNA and/or c-Jun.

The SPR experimental workflow included surface regeneration, avidin immobilization, DNA capture, and protein binding. First, the chip surface was cleaned with Regeneration 1 buffer (Block A) to remove residual material. Avidin immobilization (Block B) resulted in a stable increase in response units (RUs), reaching approximately at 69.68±0.03 Deg, confirming the successful attachment of avidin to the chip surface. Followed by the attachment of biotin-labeled dsDNA via avidin-biotin interactions (Block C), leading to an additional increase in RUs, stabilizing at approximately 69.84±0.02 Deg baseline. A single dsDNA molecule generally has a footprint of 10 – 20 nm^2 when densely packed. The observed 0.56 Deg response change suggests a moderate to low density of immobilized DNA, leading to an estimated over average intermolecular spacing of approximately 10 nm(244).

Block D is for DNA-protein interaction analysis, which is elaborated in the following section. The final regeneration step (Block E) successfully removed the bound proteins, restoring the response units to the initial baseline. This complete recovery of baseline RU demonstrates the robustness of the sensor chip, ensuring consistent and reproducible measurements.

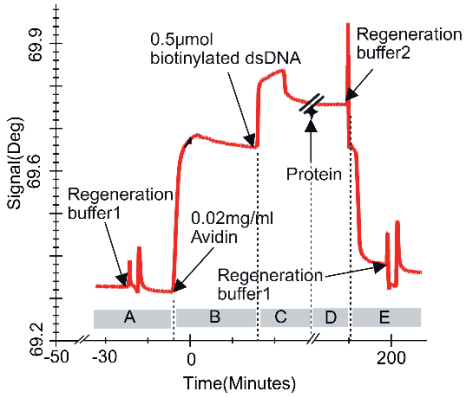


Fig. 5. Sensorgram for protein/protein-DNA interaction analysis experimental procedure. (Block A) Regeneration 1 buffer cleans the chip surface to remove residual material. (Block B) Avidin is immobilized on the surface in buffer. (Block C) Biotin-labeled double-stranded DNA immobilization. (Block D) Various concentrations of protein (2–64nM) are injected. (Block E) Regeneration 2 buffer cleans the surface for reuse. The x-axis represents time (minutes), and the y-axis shows signal response (Deg). Stars indicate the injection of protein.

3.4.2. Binding interactions of NFATc1, c-Jun, and NFATc1/c-Jun complex

The cooperative DNA-binding dynamics of NFATc1 and c-Jun were investigated. To exclude non-specific bindings, experiments included a reference channel running in parallel. This channel included all the components of the experimental channel (Fig. 4), except dsDNA. The measured signals from the experimental channel were deduced from those of the reference channel, allowing for non-specific binding exclusion. In these results, for all conditions, negative signal responses were observed.

NFATc1 binding (Fig. 6A): NFATc1 exhibited a concentration-dependent response across the 2–64 nM range, characterized by both the association and dissociation phases. The initial injection of 2 nM NFATc1 resulted in a signal shift of approximately - 20 mDeg, which

progressively increased with higher concentrations: - 35 mDeg (4 nM), - 50 mDeg (8 nM), - 75 mDeg (16 nM), - 100 mDeg (32 nM), - 125 mDeg (42 nM), - 140 mDeg (52 nM), and - 160 mDeg (64 nM). The negative signal obtained suggest that NFATc1 binding DNA induces conformational changes(245).

Likewise, c-Jun binding (Fig. 6B) was evaluated. Following an initial 2 nM c-Jun interaction, showed a dose-dependent response but with distinct kinetic characteristics. The subsequent c-Jun injections produced stepwise signal reductions: -40 mDeg (4 nM), - 55 mDeg (8 nM), - 80 mDeg (16 nM), - 110 mDeg (32 nM), - 130 mDeg (42 nM), - 150 mDeg (52 nM), and - 170 mDeg (64 nM). Compared to NFATc1, the stronger negative signal observed for c-Jun binding to DNA indicates that c-Jun binding induces larger conformational changes.

The injection of the NFATc1/c-Jun complex (Fig. 6C) resulted in an enhanced binding negative signal compared to individual injections, suggesting the NFATc1/c-Jun complex promotes conformational changes. The 2 nM of the complex resulted in a stronger initial response of -30 mDeg, followed by substantial increases: - 55 mDeg (4 nM), - 75 mDeg (8 nM), - 100 mDeg (16 nM), - 135 mDeg (32 nM), - 160 mDeg (42 nM), - 180 mDeg (52 nM), and - 200 mDeg (64 nM). This indicates that the NFATc1/c-Jun complex undergoes greater conformational upon binding to DNA.

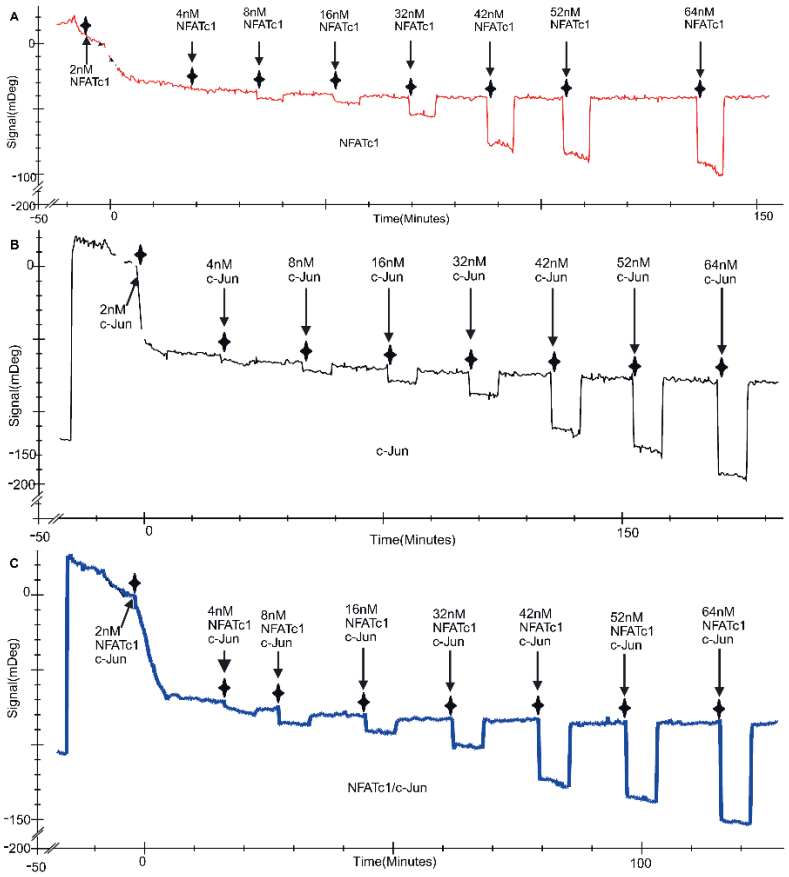


Fig. 6. Sensorgrams of the binding interactions after reference channel subtraction. (A) Binding response of NFATc1 at concentrations ranging from 2 nM to 64 nM, showing stepwise association and dissociation. (B) Binding response of c-Jun, injected at increasing concentrations from 2 nM to 64 nM. (C) Injection of NFATc1/c-Jun complex at increasing concentrations (2–64 nM), demonstrating their interaction and binding kinetics. The x-axis represents time (minutes), and the y-axis shows signal response (mDeg). Stars indicate the injection of respective protein concentrations.

3.4.3. Kinetics of NFATc1 and c-Jun DNA binding

In the follow up data analysis, the binding kinetics of NFATc1, c-Jun, and their interaction, were assessed, using the TraceDrawer software. For all conditions, negative signal responses were observed. The negative signal was inverted to positive response signal to calculate binding kinetics. The experimental data were fitted using a global kinetic model

with two binding sites, reflecting the cooperative interactions between NFATc1 and c-Jun with the DNA target. The dissociation rate constant (kd) was first estimated by globally fitting the dissociation phase, while the association rate constant (ka) was determined by fitting the association phase with kd fixed. The fitted curves closely matched the experimental data, ensuring the accuracy of kinetic parameter estimation. The sensorgrams provided detailed insights into the binding affinities and kinetics of NFATc1 and c-Jun, both individually (Fig. 7).

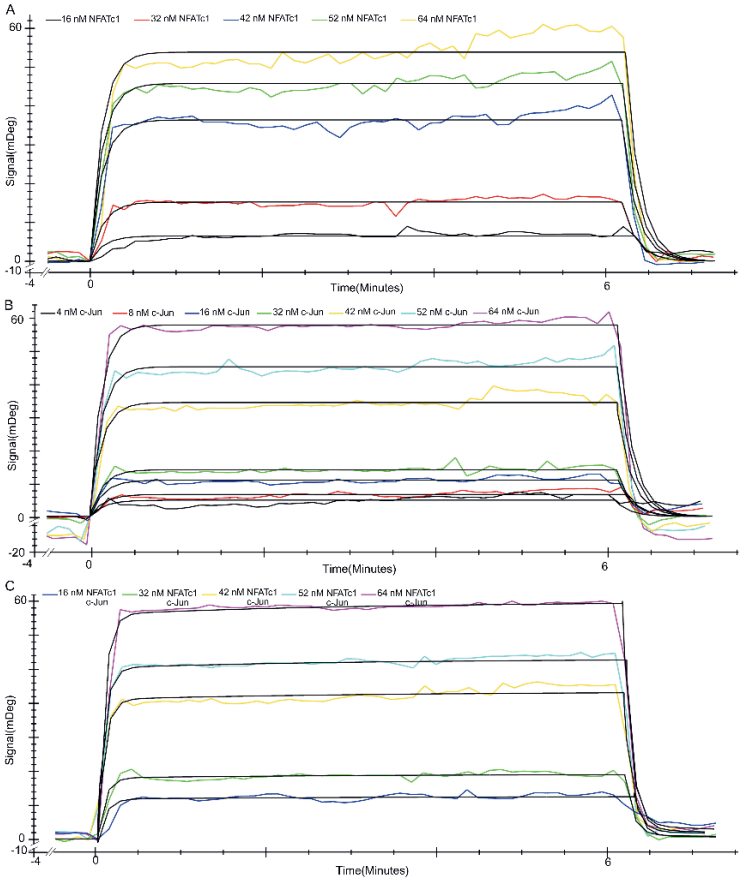


Fig. 7. Association/dissociation analysis of the binding kinetic data. (A) Binding response of NFATc1 at concentrations ranging from 16 to 64 nM. (B) c-Jun binding response at concentrations ranging from 4 to 64 nM. (C) Injection of NFATc1/c-Jun complex from 4 to 64 nM. The x-axis represents time (minutes), and the y-axis shows the signal response (mDeg). The global fitting curves are overlaid on the experimental data to illustrate the kinetic model.

Fig.7A presents the binding response of NFATc1 at increasing concentrations (16–64 nM). The association phase exhibited a rapid increase in signal intensity, reaching a maximum response of approximately 60 mDeg for the highest concentration (64 nM). Dissociation proceeded in a biphasic manner, indicating the presence of both high- and low-affinity interactions. Similarly, c-Jun binding (Fig.7B) was analyzed. A concentration-dependent increase in binding response was observed, reaching a plateau at higher concentrations.

Fig.7C shows the binding interaction of NFATc1/c-Jun complex with dsDNA injected at increasing concentrations. The binding response significantly exceeded the sum of individual NFATc1 and c-Jun interactions. The highest concentration (64 nM) resulted in a binding signal of approximately 65 mDeg, exceeding the responses of NFATc1 or c-Jun separately. Kinetic analysis revealed an increased ka and a reduced kd, further supporting the hypothesis that NFATc1 and c-Jun stabilize each other's DNA binding.

Further analysis (Table 1) confirmed that NFATc1 alone exhibited a lower DNA-binding affinity KD = (4.11 ± 0.07) × 10^{-7} M than c-Jun KD = (1.95 ± 0.03) × 10^{-7} M ($p < 0.01$). However, the NFATc1/c-Jun complex demonstrated a slightly stronger affinity KD = (1.63 ± 0.17) × 10^{-7} M ($p < 0.01$), yet with a significantly increased association rate ka= (8.29 ± 0.19) × 10^{5} $M^{-1}s^{-1}$ ($p < 0.01$) and a slightly elevated dissociation rate kd = (1.45 ± 0.12)×10^{-1} s^{-1} ($p < 0.01$), indicating structural modifications that enhance DNA binding.

Table 1. Kinetic parameters of NFATc1, c-Jun, and their co-binding interactions. This table presents the association rate constant (ka), dissociation rate constant (kd), and equilibrium dissociation constant (KD) were measured for NFATc1, c-Jun, and their complex.

	ka ($(M^{-1}s^{-1})$)	kd (s^{-1})	KD (M)
NFATc1	(2.44 ± 0.10)e5	(1.05 ± 0.02)e-1	(4.11 ± 0.07)e-7
c-Jun	(5.97 ± 0.22)e5	(1.24 ± 0.13)e-1	(1.95 ± 0.03)e-7
NFATc1/c-Jun	(8.29 ± 0.19)e5	(1.45 ± 0.12)e-1	(1.63 ± 0.17)e-7

To investigate the effect of the NFATc1 and c-Jun binding sequence on conformational changes, NFATc1 and c-Jun binding was further investigated through sequential protein addition experiments (Fig. 8). When equilibrium was reached, the response of the red curve (corresponding to DNA pre-incubated with c-Jun before NFATc1 addition) exceeded that of the black curve, in which the order of addition was reversed, indicating that prior c-Jun binding facilitates subsequent conformational changes.

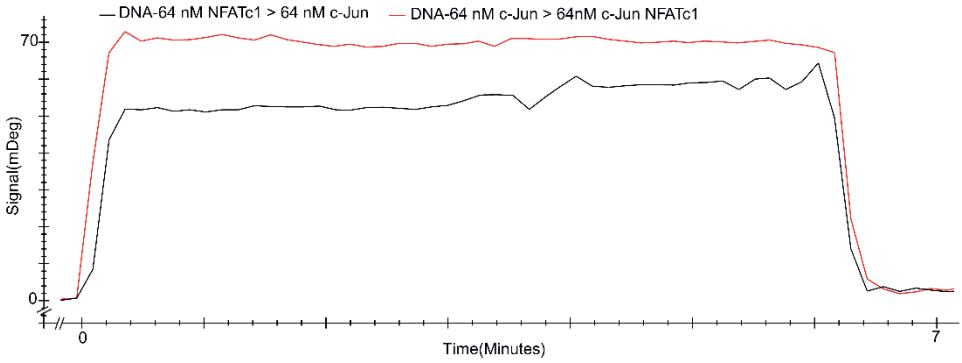


Fig. 8. Analysis of comparing the DNA binding dynamics of NFATc1 and c-Jun under different sequential addition conditions. The black curve represents DNA (64 nM) pre-incubated with NFATc1 (64 nM) before the addition of c-Jun (64 nM), while the red curve shows the reverse order. The x-axis denotes time (minutes), and the y-axis represents the SPR signal response (mDeg).

4. Discussion

TFs are important regulators of gene expression, orchestrating transcriptional control through dynamic and cooperative interactions at regulatory DNA elements(246, 247). These interactions modulate DNA-binding affinity, stability, and turnover rates, ensuring responsiveness to cellular signals. In this study, we applied SPR to investigate the DNA-binding kinetics of NFATc1 and c-Jun, two key TFs involved in immune and developmental gene expression. Our findings reveal that while NFATc1 and c-Jun exhibit independent DNA-binding activity, they also demonstrate cooperative binding, significantly enhancing the association rate constant (ka) while maintaining a dynamic dissociation rate constant (kd). This cooperative mechanism highlights a regulatory system where combinatorial TF

interactions promote recruitment and turnover at target sites, thereby fine-tuning transcriptional output.

Compared to traditional methods such as EMSA and fluorescence anisotropy, SPR offers real-time, high-resolution monitoring of both association and dissociation phases(248), allowing for a more detailed kinetic analysis of TF-DNA interactions. EMSA provides endpoint measurements that lack temporal resolution (249), whereas fluorescence anisotropy offers binding affinity estimates without detailed kinetic parameters(250). On the other hand, SPR enables precise quantification of cooperative binding dynamics(251), capturing transient interactions that are important for transcriptional regulation. Furthermore, to enhance measurement sensitivity and specificity, we developed a biotinylated DNA chip with optimized ligand density, ensuring accurate quantification of cooperative interactions. The observed 0.56 Deg response change suggests a moderate to low density of immobilized DNA, leading to an estimated average intermolecular spacing of approximately 10 nm, which is consistent with previous dual polarization interferometry studies demonstrating quantitative relationships between DNA surface density, probe spacing and hybridization efficiency in biotin–streptavidin-based immobilization systems(252). This methodological advancement not only improves SPR-based TF-DNA studies but also has broader implications for biosensor development and high-throughput TF screening.

Our kinetic measurements provide insights into TF-DNA interactions, complementing and extending previous findings. NFATc1 alone exhibited a ka of (2.44 ± 0.10) × 10^5 $M^{-1}s^{-1}$ and a kd of (1.05 ± 0.02) × 10^{-1} s^{-1}, resulting in a dissociation constant (KD) of (4.11 ± 0.07) × 10^{-7} M, consistent with EMSA values (10^{-8} – 10^{-7} M)(253) while offering improved temporal resolution. In contrast, c-Jun displayed a higher ka (5.97 ± 0.22) × 10^5 $M^{-1}s^{-1}$ and kd (1.24 ± 0.13) × 10^{-1} s^{-1}, leading to a KD of (1.95 ± 0.03) × 10^{-7} M, aligning with fluorescence anisotropy estimates (10^{-7} – 10^{-9} M)(253). Upon cooperative binding, the NFATc1/c-Jun complex exhibited a further increase in ka (8.29 ± 0.19) × 10^5 $M^{-1}s^{-1}$ with a

moderately increased kd ((1.45 ± 0.12) × 10^{-1} s^{-1}), yielding a KD of (1.63 ± 0.17) × 10^{-7} M. These results align with those of Seo, Jungkyun, et al.(254), who reported similar cooperative binding behavior in the AP-1 family, and Li, Ya-Ting, et al.(255), who identified NFATc1 as a critical modulator of dynamic TF recruitment.

We hypothesize that c-Jun binds the composite site with higher affinity KD = (1.95 ± 0.03) × 10^{-7} M than NFATc1 KD = (4.11 ± 0.07) × 10^{-7} M, consistent with their distinct modes of DNA recognition(141). The basic region of the bZIP helix in c-Jun penetrates deeply into the major groove, forming an extensive set of base-specific and electrostatic contacts(141). By contrast, DNA recognition by NFATc1 is distributed across flexible loops of the Rel-homology region, most notably the E′ F loop, which depends on cooperative contacts with both the DNA backbone and AP-1 for full stabilization(141). Under this hypothesis, NFATc1 therefore has lower intrinsic affinity for DNA, reflecting a binding mechanism optimized for assembly of the NFAT–c-Jun–DNA ternary complex rather than for high-affinity binding in isolation(141).

The cooperative binding observed in this study is driven by specific protein-DNA and protein-protein interactions, leading to conformational stabilization of the TF-DNA complex(256-258). X-ray crystallography and cryo-electron microscopy (cryo-EM) experiments can provide insights into the cooperative binding mechanism(259, 260). Structural studies using X-ray crystallography and cryo-electron microscopy have provided static snapshots of NFATc1 and c-Jun bound to DNA but fall short in explaining the kinetic and thermodynamic principles underlying cooperative binding(261). The DNA-binding domain (DBD) of NFATc1 adopts a Rel-like fold, allowing it to recognize NFAT-response elements (NREs), whereas c-Jun, a member of the AP-1 family, interacts with TGAC/GTCA motifs via its basic leucine zipper (bZIP) domain(141). Structural studies of NFAT-AP-1 complexes reveal that NFATc1 and c-Jun interact via their DNA-binding surfaces, forming a composite interface stabilized by hydrogen bonding, van der Waals forces, and electrostatic interactions (262). Key residues such as Arg414 and Lys432 in NFATc1, and

Lys268 and His294 in c-Jun, play critical roles in stabilizing the TF-DNA complex through electrostatic interactions with DNA phosphate groups(141). Additionally, NFATc1 possesses an auxiliary domain that contacts the bZIP domain of c-Jun, inducing a conformational change that increases TF affinity for DNA(263).

Previously reported single-molecule Förster resonance energy transfer (smFRET) studies support this dynamic model, revealing fast association kinetics and moderate dissociation rates in AP-1 family TFs(264). Additionally, hydrogen-deuterium exchange mass spectrometry (HDX-MS) experiments suggest that TF binding induces localized DNA conformational changes, corroborating our hypothesis that NFATc1 facilitates c-Jun recruitment by pre-organizing the DNA-protein interface(265). Those molecular mechanisms align with our SPR-derived kinetic data, demonstrating that cooperative binding accelerates TF association (ka) while preserving a dynamic kd, a feature essential for transcriptional cycling and regulatory plasticity. Our findings contribute to a deeper understanding of TF cooperative binding dynamics and their role in transcriptional regulation.

Future research should extend these findings by exploring additional AP-1 family members and integrating structural techniques to capture real-time conformational changes underlying cooperative TF binding. c-Fos, another AP-1 subunit, may influence NFATc1 interactions; incorporating c-Fos binding assays will refine our understanding of AP-1 heterodimer contributions to cooperative DNA binding. While our in vitro kinetic measurements offer additional insights, further validation in native chromatin environments is essential. Combining SPR with techniques such as single-molecule Förster resonance energy transfer (FRET)(266) or hydrogen-deuterium exchange mass spectrometry (HDX-MS)(267) could provide additional insights into conformational changes during cooperative binding. Our study was conducted in an in vitro system, and future experiments utilizing chromatin immunoprecipitation (ChIP) assays(268) or live-cell

imaging(269) could confirm whether similar cooperative interactions occur in native chromatin environments.

5. Conclusion

A SPR workflow, bridging the gap between static structural studies and modulation, allowing the investigation of multiple protein-DNA interactions, was developed. The obtained data strongly support the NFATc1 and c-Jun cooperatively binding of NFATc1 and c-Jun to DNA, enhancing transcriptional regulation by increasing association kinetics while maintaining dynamic dissociation rates. By integrating SPR kinetic analysis with structural insights, a comprehensive model where NFATc1 facilitates c-Jun recruitment via protein-protein and protein-DNA interactions is presented. As SPR technology continues to advance, higher-resolution kinetic models will further illuminate the molecular mechanisms underlying transcriptional regulation, contributing to a broader understanding of gene expression control.

Chapter 5 - Structure-guided disruption of NFATc1 rewires macrophage polarization to enhance clearance of *S. aureus* on implant surfaces

Based on

Cao B., Cillero-Pastor B., Honing M. Structure-guided disruption of NFATc1 rewires macrophage polarization to enhance clearance of S. aureus on implant surfaces. In preparation.

Abstract

Macrophages play a key role in the clearance of *Staphylococcus aureus* (*S. aureus*) during orthopedic implants infections. However, intermediate surface roughness of implant materials promotes macrophage polarization toward an anti-inflammatory M2 phenotype, which compromises bacterial elimination. NFATc1, a transcription factor that activates gene expression through binding to specific DNA elements, has emerged as a key regulator of macrophage activation and polarization, being a promising target for immunomodulation. In this study, guided by detailed structural and dynamic insights into the NFATc1/c-Jun/DNA complex, a rationally designed peptide, MBB, was tested. The MBB peptide was expected to selectively disrupt the NFATc1–DNA interaction, thereby reprogramming macrophage polarization toward a pro-inflammatory (M1) phenotype. Such a shift will likely enhance bacterial phagocytosis, increase reactive oxygen species (ROS) production, and elevate TNF-α secretion. The findings underscore the potential of structure-guided peptide design to fine-tune macrophage responses for the prevention and treatment of biomaterial-associated infections.

1. Introduction

Orthopedic implants have transformed modern medicine by restoring mobility and quality of life for millions of patients [3, 268, 269]. Titanium surface roughness modification is routinely employed to accelerate osteoblast-driven osseointegration[270, 271]. However, beyond its well-established osteogenic benefits, surface topography also serves as a potent immunoregulatory cue, capable of reprogramming macrophage polarization[40, 152]. Because the local microenvironment, including the physical properties of implant materials, profoundly influences macrophage behavior[49]. Notably, increased surface roughness—frequently employed to enhance osteointegration—has been shown to bias macrophage polarization toward an anti-inflammatory M2 phenotype[52]. While beneficial for tissue healing, this shift can impair antimicrobial defense by limiting the bactericidal activity and cytokine secretion associated with the pro-inflammatory M1 phenotype, thereby compromising *S. aureus* clearance[120].By shaping the host–implant interface in ways that can determine infection outcomes[272].

Implant-associated infections, most commonly caused by *S. aureus*, remain a major clinical challenge[15, 273], often leading to implant failure, repeated surgeries, and long-term antibiotic therapy[274]. The host immune response, particularly the activity of macrophages, plays a critical role in determining the outcome of these infections[101]. As the first line of cellular defense, M1 macrophages are responsible for recognizing and clearing bacterial pathogens at the implant interface[42]. Our previous work described how titanium surface roughness exerts profound immunomodulatory effects on macrophage polarization during *S. aureus* implant infection. It was demonstrated that corundum roughness (Sa:5.51±0.29 µm) supports early M1 polarization within the first 12 h post-infection, enhancing macrophage adhesion, phagocytic uptake of *S. aureus*, and reactive oxygen species (ROS) production. However, after 12 hrs, the same surface induced a shift toward an M2 phenotype, attenuating bactericidal functions and suppressing ROS generation. Mechanistically, it was observed that macrophage polarization was tightly linked to transcription factor activity, particularly NFATc1, within

the DNA-binding complex involving c-Jun and c-Fos. Recent studies have identified the nuclear factor of activated T cells c1 (NFATc1) as a key transcriptional regulator in macrophage activation and polarization[137]. Through binding specific DNA motifs, NFATc1 orchestrates the transcriptional programs that govern macrophage cell function[275]. Although originally characterized in macrophage biology genesis, NFATc1 has now emerged as a potential target for reprogramming macrophage phenotypes in infectious and inflammatory contexts[276]. However, strategies to selectively modulate NFATc1 activity in macrophages remain underexplored.

In this study, the results for a structure-guided peptide, MBB, that selectively disrupts NFATc1–DNA interactions to reprogram macrophage polarization toward a pro-inflammatory M1-like phenotype is reported. Leveraging computational modeling and molecular dynamics simulations of the NFATc1/c-Jun/DNA complex, MBB was specifically engineered to interfere with transcriptional activation pathways central to macrophage functional states. The obtained findings establish a proof-of-concept for structure-based peptide design targeting immune transcriptional regulators and suggest a promising strategy for preventing and treating biomaterial-associated infections.

2. Materials and Experimental methods

2.1. Design of the Maarten-Berta-Bo peptide (MBB)

Based on the structure of c-Jun we designed a c-Jun-like structural peptide called Maarten-Berta-Bo peptide (MBB) for competitive inhibition of the interaction between NFATc1 and c-Jun. The MBB sequence was derived by adding two additional leucine residues in the middle of central region of the c-Jun binding motif. The final peptide sequence was as follows: MRKLRLKLELRILARLEEKVKTLKAQNSELASTANMLREQVAQL. This design is based on the idea that the addition of leucine residues will enhance the stability of the MBB double helix structure, which competes with NFATc1 for binding and thus prevents the formation of the NFATc1/c-Jun/c-Fos/DNA complex, and ultimately prevents NFATc1 from binding to its DNA target. The 3D structure of MBB was predicted using

AlphaFold3[277](https://alphafoldserver.com/) and the model with the highest confidence was selected based on the predicted local distance difference test (pLDDT) score. The peptide sequence was modeled as a monomer, and five independent models were generated with three recycles each. The model with the highest predicted local distance difference test (pLDDT) score was selected, and Amber relaxation was applied to optimize side-chain geometries, ensuring a physically plausible conformation suitable for structural comparison with native c-Jun. Structural comparisons with native c-Jun were performed to validate the peptide design.

2.2. Design of plasmid for MBB expression

A recombinant plasmid was designed for the expression of MBB in *E. coli* based on the amino acid sequence of the Maarten-Berta-Bo peptide (MBB) (MRKLRLKLELRILARLEEKVKTLKAQNSELASTANMLREQVAQL). The MBB sequence was synthesized and optimized for bacterial expression ensuring that the codon usage is *E. coli* host system compatibility. A 6xHis tag was added to the N-terminus of the peptide to facilitate purification by affinity chromatography. The gene encoding MBB was cloned into the pET-28a(+) vector (GenScript, UK) using NcoI and XhoI restriction sites to create a recombinant plasmid[278].

2.3. Cloning and transformation of *E. coli*

The synthetic gene containing MBB sequence was ligated into pET-28a(+) expression vector. The ligation reaction was performed using T4 DNA ligase (Thermo Fisher Scientific, USA) and transformed into *E. coli* (DH5α, Sigma-Aldrich, Germany) for plasmid amplification. Transformants were screened on LB agar (Formedium, UK) plates containing kanamycin (50 µg/mL). Colonies were grown overnight in LB broth containing kanamycin and plasmid DNA was extracted using the QIAprep Spin Miniprep Kit (Formedium, UK). Plasmids were confirmed by sequencing to ensure correct insertion of the MBB gene.

2.4. Bacterial expression of MBB

The recombinant plasmid containing the MBB sequence was transformed into *E. coli* (BL21-DE3, Sigma-Aldrich, Germany). One colony of transformed E. coli was inoculated into 5 mL of LB broth containing kanamycin (50 µg/mL) and incubated overnight at 37°C with shaking (200 rpm). The overnight culture was used to inoculate a larger volume (1 L) of LB medium containing the same kanamycin (50 µg/mL). Cultures grow at 37°C until the OD600 reaches 0.6-0.8. Protein expression is induced by the addition of 1 mM isopropyl-β-D-thiogalactopyranoside (IPTG， Sigma-Aldrich, Germany). Then incubated at 37°C for an additional 6 hrs. The cells were harvested by centrifugation at 4000 rpm for 20 min at 4°C.

2.5. Protein purification

After induction, the bacterial pellet was resuspended in lysis buffer (20 mM Tris-HCl, pH 7.4, 500 mM NaCl, 5 mM imidazole, 1 mM phenylmethylsulfonylfluoride (PMSF)) and sonicated for 10 minutes on ice (30 seconds on, 30 seconds off cycle). The lysates are then cleared by centrifugation at 12,000 rpm for 30 min at 4°C. The supernatant containing the soluble His-tagged MBB peptide was incubated with Ni-NTA agarose resin (Sigma-Aldrich, Germany) for 1 hour at 4°C and then washed with 20 mM Tris-HCl (pH 7.4), 500 mM NaCl, and 30 mM imidazole to remove non-specifically bound proteins. Target proteins were eluted with elution buffer (20 mM Tris-HCl, pH 7.4, 500 mM NaCl, 250 mM imidazole) and analysed by SDS-PAGE to assess purity. The eluted proteins were then dialysed against PBS to remove excess imidazole and concentrated using Amicon Ultra centrifugal filters (Sigma-Aldrich, Germany). The concentration of purified MBB peptides was determined applying Bradford assay (Thermo Fisher Scientific, USA) using BSA as standard. Purified peptides were aliquoted and stored at -80°C for subsequent functional testing.

2.6. Verification of MBB expression and purity

The proper MBB peptide expression was confirmed by SDS-PAGE and Western blot analysis using an anti-His labelled antibody (Thermo Fisher Scientific, USA). After Western blot analysis using Coomassie Brilliant Blue staining and Enhanced Chemiluminescence (ECL) detection, protein bands corresponding to His-tagged MBB peptides were revealed.

2.7. Size-exclusion chromatography (SEC)

Size-exclusion chromatography (SEC) was performed using a Superdex™ 200 Increase 3.2/300 GL column (Cytiva, USA) on a Shimadzu UFLC system to assess the purity and homogeneity of the MBB protein. A total of 20 µL of 0.5 mg/mL MBB was injected onto the column, which was pre-equilibrated with Tis-HCL/NaCl(20 mM Tris-HCl, 500 mM NaCl, pH 7.4). The chromatography was conducted at a flow rate of 0.05 mL/min at a constant temperature of 4 °C. Elution was monitored by UV absorbance at 280 nm. The system pressure remained below 1.8 MPa throughout the run. Chromatograms were analyzed using Shimadzu LabSolutions software, and the area under the curve (AUC) was calculated to estimate the relative abundance of each peak.

2.8. High-resolution mass spectrometry identity and purity of synthetic MBB peptide

The structure of the MBB peptide was assessed by electrospray ionization mass spectrometry (ESI-MS), using a Q Exactive UHMR Hybrid Quadrupole-Orbitrap mass spectrometer (Thermo Fisher Scientific, USA). Samples were prepared in 50% acetonitrile with 0.1% formic acid and introduced by direct infusion at 3 µl min^{-1}. Full-scan spectra were acquired in the positive ion mode (m/z 500–2000).

2.9. Preparation of titanium discs surface

The Titanium discs with a diameter of 12 mm and a and thickness of 1.5 mm (Bbraun, the Netherlands) and a corundum surface, were used throughout the study. They were sterilized by autoclaving at 121°C for 15–20 minutes and stored aseptically until use. The

surface roughness (Sa, average surface roughness) was 5.51±0.29 μm. The titanium content in corundum was 88.80±0.40 wt.%.

2.10. Culture of RAW264.7 cells on titanium discs surface

The macrophage cells (RAW264.7 cells, Sigma-Aldrich, USA) were cultured in DMEM medium (Gibco, USA) which contains 10% fetal bovine serum (FBS, Sigma-Aldrich, USA) in a cell incubator (37 °C, 5% CO2). The cells were added to the surface of the titanium disc with a density of 5×10^5 cells/mL. The culture medium was changed every other day. The cells in the 24-well plates culture wells were labeled as control group.

2.11. Preparation of *GFP-Labeled S. aureus*

To construct the *GFP-labeled S. aureus*, 2 μg of GFP plasmid (GenScript, UK) was added to Staphylococcus aureus (*S.aureus*, Sigma-Aldrich, Germany) cells in a sterile electroporation cuvette (Sigma-Aldrich, Germany). The mixture was incubated for 30 minutes on ice to allow for plasmid uptake. Electroporation was carried out using a pulse electroporator (Eppendorf, Germany) and in a 1 mm cuvette (25 μF, 100 Ω, and 2.0–2.2 kV). After transfection was completed, the cells were placed in rescue medium (37 ℃, 1 h). Then 100 μL of cells were inoculated to the Karamycin agar plate (37 ℃, overnight). Successful transformation was confirmed by fluorescence microscopy, observing GFP expression in the bacterial cells. After overnight incubation single colonies were inoculated in Broth medium (Becton, Dickinson and Company, USA). Following 3-6 incubation, the bacterial culture was adjusted to a final concentration of 10^4 CFU/mL for use in subsequent co-culture experiments with macrophages.

2.12. Cell viability assay

RAW264.7 macrophage cells were seeded in 96-well flat-bottom plates at a density of 1×10^5 cells per well in complete DMEM (10% FBS, 1% penicillin-streptomycin) and allowed to adhere overnight at 37 °C in a humidified incubator with 5% CO_2. The cells were subsequently treated with MBB (0.1–20 μM) diluted in phosphate-buffered saline

(PBS) for 24 h. Vehicle control wells received an equivalent volume of PBS. Following treatment, 10 µL of Cell Counting Kit-8 (CCK-8; Sigma-Aldrich) solution was added to each well, and plates were incubated for an additional 2 h at 37 °C. Absorbance was measured at 450 nm using a microplate reader (Tecan Group Ltd, Switzerland). The cell viability was calculated relative to vehicle-treated controls. Dose–response curves were generated and IC_{50} values determined using nonlinear regression with a four-parameter logistic model (log[inhibitor] vs. response–variable slope) in GraphPad Prism. Confidence intervals (95%) were calculated using profile likelihood estimation.

2.13. Macrophages adhesion and morphology studies

To visualize the effect of MBB on bacterial adhesion and clearance by macrophages, the macrophages were treated with MBB (25 µM) for 24 hrs. Control groups included PBS. After treatment, macrophages were exposed to *S. aureus* at an MOI of 10:1 for 1 hour at 37°C. The cells were then washed three times with PBS to remove unbound bacteria. For transmission electron microscopy (TEM), macrophages were treated and exposed to bacteria as described above. The cells were then fixed with 2.5% glutaraldehyde, followed by 1% osmium tetroxide (Sigma-Aldrich , Germany) post-fixation. The samples were dehydrated through a graded ethanol series and embedded in Epon resin. Thin sections (70 nm) were cut using a Leica Ultracut UC7 ultramicrotome and stained with uranyl acetate and lead citrate. TEM images were acquired using a JEOL JEM-1400 transmission electron microscope. The number of internalized bacteria and the extent of bacterial clearance were quantified from both SEM and TEM images by counting the number of bacteria in contact with or inside macrophages in randomly selected fields. Statistical significance was determined using one-way ANOVA followed by Tukey's post-hoc test, comparing the number of internalized bacteria and the percentage of bacterial clearance across different treatment groups.

2.14. Phagocytosis assay using transmission electron microscopy

To assess the impact of MBB on macrophage phagocytic capacity, RAW 264.7 cells were differentiated into macrophages and treated with MBB (0–100 µM) for 24 h. The cells were then incubated with Staphylococcus aureus (MOI 10:1) for 1 h at 37°C. After washing with PBS, samples were fixed in 2.5% glutaraldehyde in 0.1 M phosphate buffer (pH 7.4) at 4°C, post-fixed with 1% osmium tetroxide, dehydrated, and embedded in epoxy resin. Ultrathin sections (~70 nm) were stained with uranyl acetate and lead citrate and imaged using a JEOL JEM-1400 transmission electron microscope. Quantification of phagocytosed bacteria was performed using ImageJ (NIH). Internalized S. aureus bacteria were identified based on morphology and electron density. The number of bacteria per cell was manually counted in at least 50 cells per condition. The phagocytic index was defined as the total number of internalized bacteria divided by the number of macrophages analyzed. Data were normalized to control values and analyzed using one-way ANOVA followed by Tukey's post-hoc test.

2.15. Macrophage stimulation and cytokine quantification

Macrophages were seeded in 96-well plates at a density of 1×10^5 cells per well and cultured overnight to allow adhesion. *GFP-labeled S. aureus* (1×10^4 CFU/mL) was added to the wells to stimulate the macrophages, with or without the presence of MBB (25 µM) and/or corundum. Cells were incubated at 37 °C with 5% CO_2 for 8, 12, or 24 hrs. At each time point, culture supernatants were collected and centrifuged to remove debris. The concentrations of TNF-α and IL-10 in the supernatants were determined using commercial ELISA kits (Thermo Fisher Scientific, USA) according to the manufacturer's protocols. UV/VIS absorbance was measured at 450 nm using a microplate reader (Tecan Group Ltd, Switzerland). Cytokine concentrations were calculated based on standard curves constructed with recombinant proteins. All experiments were performed independently at least four times (n = 4).

2.16. RT-PCR to detect macrophage differentiation

qPCR was performed using SYBR Green PCR Master Mix (Thermo Fisher Scientific, USA) and gene-specific primers for TNF-α, IL-6 and IL-10. amplification was performed on a CFX96 Touch Real-Time PCR Detection System (Bio-Rad, USA) and the relative expression levels were determined using the ΔΔCt method. Relative expression levels were determined using the ΔΔCt method and normalized to GAPDH. Data were expressed as fold change relative to untreated controls, and statistical significance was analyzed by one-way ANOVA followed by Tukey's post hoc test.

2.17. ROS detection assay

To assess the effect of MBB on intracellular ROS generation, RAW264.7 murine macrophages were seeded in 96-well plates and treated with MBB (0.1–10 μM) for 24 h. Cells were then incubated with 10 μM 2′,7′-dichlorodihydrofluorescein diacetate (DCFH-DA; Sigma-Aldrich) for 30 min at 37°C. Following incubation, cells were washed twice with PBS to remove excess dye. ROS levels were quantified by measuring fluorescence (excitation/emission: 485/535 nm) using a microplate reader (Tecan Group Ltd, Switzerland). Oxidation of DCFH-DA by ROS yields the fluorescent product 2′,7′-dichlorofluorescein (DCF), enabling assessment of ROS accumulation.

2.18. Immunofluorescence staining

Following stimulation, cells were fixed with 4% paraformaldehyde (PFA) in PBS for 15 min at room temperature and permeabilized with 0.1% Triton X-100 in PBS for 10 min. Nonspecific binding was prevented using 5% bovine serum albumin (BSA) in PBS for 1 h at room temperature. The cells were then incubated with directly conjugated primary antibodies against CD36 (M2 macrophage marker; CF™488A, 1:200 dilution; R&D Systems) and CCR7 (M1 macrophage marker; CF™568, 1:200 dilution; Abcam) for 1 h in the dark at room temperature. Nuclei were counterstained with DAPI (1 μg/mL; Thermo Fisher Scientific) for 5 min. After final PBS washes, samples were mounted using anti-fade mounting medium (Vectashield; Vector Laboratories).

2.19. Image acquisition and analysis

Fluorescence imaging was performed using a Zeiss LSM 880 confocal laser scanning microscope (Carl Zeiss) equipped with 405 nm, 488 nm, and 561 nm laser lines for DAPI, CF™488A, and CF™568, respectively. Images were acquired with a 20× objective lens, and laser settings were kept constant across all experimental groups. At least five randomly selected fields per condition were imaged. Image processing and quantification were carried out using ImageJ (NIH), with fluorescence intensity and marker colocalization used to evaluate M1 ($CCR7^+$) and M2 ($CD36^+$) polarization. All experiments were independently repeated at least three times. Image analysis was performed using ImageJ (NIH). Regions of interest (ROIs) positive for CCR7 (M1 marker) and CD36 (M2 marker) were identified, and the number of ROIs per cell were determined. The M1/M2 polarization ratio was calculated for each field as the number of $CCR7^+$ ROIs divided by the number of $CD36^+$ ROIs. At least five random fields were analyzed per condition in three independent experiments.

2.20. Data analysis

RT-PCR, Cell viability and cytokine secretion data are presented as mean ± standard deviation and sample size was 3 (n=3). A one-way ANOVA followed by Tukey post-hoc correction was used for comparison of group means in SPSS (version 21, IBM SPSS statistics, USA6). The Shapiro-Wilk test was employed to assess data normality. Statistical significance was determined using one-way ANOVA followed by Tukey's post hoc test. A p value of 0.05 was used as a threshold for statistical significance.$*p<0.05$; $**p<0.01$; $***p<0.001$.

3. Results

3.1. AlphaFold-based design of MBB peptide

To rationally inhibit the interaction between NFATc1 and c-Jun, we designed MBB peptide based on the structural features of the c-Jun transactivation domain. Guided by structural modeling, two additional leucine residues were inserted into the central helical motif of

c-Jun to enhance α-helical stability and preserve key interaction residues. The predicted 3D conformation of MBB, generated using AlphaFold3, revealed a well-defined α-helix with high confidence scores across most of the peptide (pLDDT >90), suggesting a stable helical fold consistent with native c-Jun. Notably, the N- and C-terminal regions also retained secondary structure integrity, supporting the overall design rationale. Structural alignment with the native c-Jun helix confirmed that MBB closely mimics the binding interface required for interaction with NFATc1. These indicate that MBB function as a competitive inhibitor by mimicking c-Jun structure and disrupting the assembly of the NFATc1/c-Jun/c-Fos/DNA transcriptional complex. The molecular mass of MBB was determined with Peptide 2.0, yielding a calculated molecular mass of 5135.1793 Da.



Fig. 1. Structure-guided design of a MBB peptide. AlphaFold3-predicted 3D structure of the MBB peptide (MBB), a rationally designed peptide intended to mimic the α-helical structure of the c-Jun transactivation domain. The structure shown corresponds to the highest-confidence AlphaFold3 model, color-coded by pLDDT score: dark blue indicates very high confidence (pLDDT >90), and cyan indicates high confidence (90 > pLDDT > 70).

3.2. SEC analysis confirms monodispersity and high purity of MBB

The designed MBB peptide was expressed in *E. coli* and purified via Ni-affinity chromatography, followed by SEC to assess its purity. The resulting chromatogram displayed a single, symmetric peak eluting at 30.1 min. Quantitative integration of the elution profile indicated that the dominant peak accounted for >95% of the total UV signal (AUC), supporting tan acceptable purity of the preparation. No secondary peaks or shoulders were observed within the 20–40 min window, indicating negligible aggregation or degradation. Collectively, we confirm the biochemical homogeneity of MBB. Electrophoretic analysis revealed a single band at approximately 5 kDa for the purified

MBB protein (Fig. 3), which is consistent with its expected molecular weight and in agreement with the results obtained from size-exclusion chromatography.

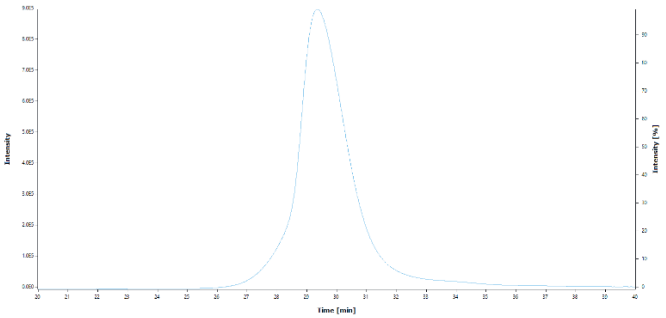


Fig. 2. Size-exclusion chromatographic analysis of purified MBB protein. Size-exclusion chromatography was performed on a Superdex™ 200 Increase 3.2/300 GL column using a Shimadzu UFLC system. UV absorbance at 280 nm was monitored to assess sample purity.

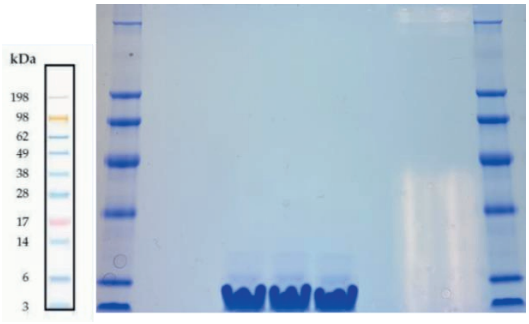


Fig. 3. Electrophoresis analysis of purified MBB protein. The figure shows three replicate samples of purified MBB, with a molecular weight of 5 kDa.

3.3. Orbitrap-MS characterization of the MBB peptide

To confirm the successful synthesis and structural integrity of the MBB, high-resolution mass spectrometry was performed using a Q Exactive UHMR Orbitrap instrument (Fig. 4). The full MS scan revealed a series of multiply charged ion species corresponding to the intact MBB peptide, with charge states ranging from z = 3 to z = 6. The predominant signal was observed at m/z 1027.815 (z = 5), consistent with the theoretical monoisotopic mass

of MBB peptide (5135.1793Da). These data confirm the accurate synthesis and acceptable purity of MBB, enabling functional characterization.

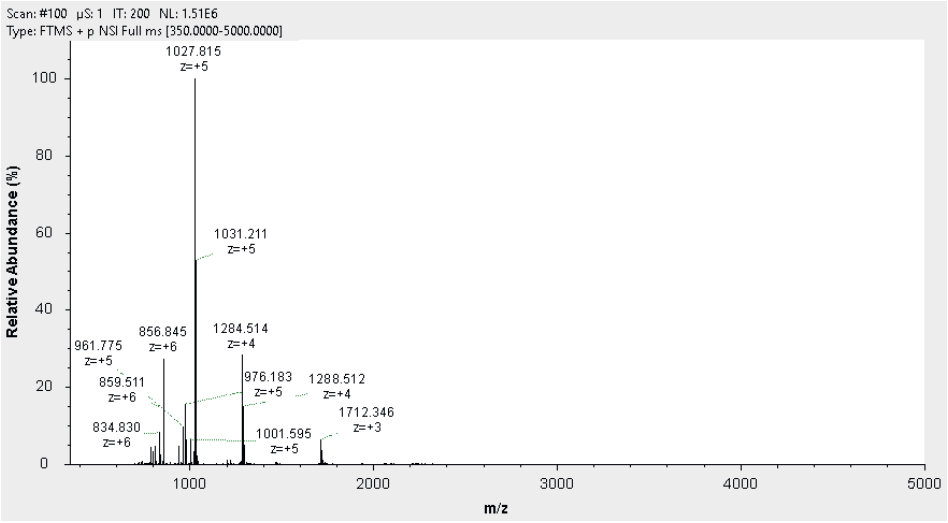


Fig. 4. High-resolution mass spectrum of MBB peptide. Full-scan electrospray ionization (ESI) mass spectrum of the MBB peptide acquired on a Q Exactive UHMR Orbitrap MS system.

3.4. Quantitative assessment of MBB cytotoxicity

To evaluate the cytotoxicity of MBB, macrophage cells were exposed to increasing concentrations of the compound (0–100 µM) for 24 hrs, and viability was assessed using the CCK-8 assay (Fig.5). MBB elicited a dose-dependent decrease in cell viability, with maximal inhibition observed at 20 µM. Nonlinear regression of the dose–response data using a four-parameter logistic model yielded an IC_{50} of 26.14 µM. The fitted curve displayed a steep Hill slope (3.752), consistent with a sharp transition between low- and high-inhibition states. The model showed excellent agreement with the experimental data (R^2 = 0.992), underscoring the robustness of the cytotoxic effect. Based on these results, a concentration of 25 µM was selected for subsequent cellular assays.

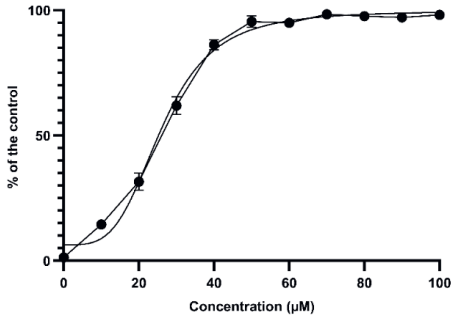


Fig. 5. MBB reduces macrophage cell viability in a dose-dependent manner. Macrophage cells were treated with increasing concentrations of MBB (0–100 μM) for 24 h, followed by Cell Counting Kit-8 (CCK-8) assay to assess cell viability (n = 4). Data show the mean ± SD.

3.5. Effect of MBB on the macrophage cytokine production

An ELISA assay was used to investigate the immunomodulatory effects of MBB on macrophages in response to *S. aureus* infection (Fig. 6). The secretion of the pro-inflammatory cytokine TNF-α and the anti-inflammatory cytokine IL-10 (Fig. 6) was quantified. The macrophages were cultured on titanium surfaces and stimulated with *GFP-labelled S. aureus*, with (25 μM) or without MBB and/or corundum, for 8, 12, and 24 hrs. TNF-α levels increased markedly in response to *S. aureus* (1182.92±65.09pg/mL) and *S. aureus*/corundum (1295.01 ± 131.16 pg/mL), with a maximum at 12 hrs. MBB treatment significantly elevated TNF-α production compared to the control at 8h (377.61 ± 54.63 pg/mL), 12h (824.07 ± 35.05 pg/mL) and 24h (1020.80 ± 102.84 pg/mL). Compared to *S. aureus* group (484.64 ± 25.11 pg/mL), *S. aureus*/MBB caused a pronounced increase TNF-α at 24 h (657.63 ± 42.36 pg/mL). At 24 h, similarly, compared to *S. aureus*/corundum group (451.19 ± 33.87 pg/mL), *S. aureus*/corundum MBB group had significantly enhanced TNF-α (627.83 ± 17.28 pg/mL). Compared to the control, the IL-10 secretion of the S. *aureus*/corundum group increased at 8h (99.31 ± 8.53 pg/mL), 12h (143.02 ± 7.38 pg/mL) and 24h (176.93 ± 10.76 pg/mL). The *S. aureus*/corundum/MBB group significantly reduced IL-10 at 8h (41.31 ± 7.58 pg/mL), 12h (56.18 ± 2.02 pg/mL) and 24h (76.77 ± 8.66 pg/mL). Also compared to *S. aureus* group (54.36 ± 1.88 pg/mL), MBB/*S. aureus*

significantly lowered IL-10 at 24 h (37.85 ± 7.57 pg/mL). These results demonstrate that MBB enhances TNF-α production while suppressing IL-10 secretion.

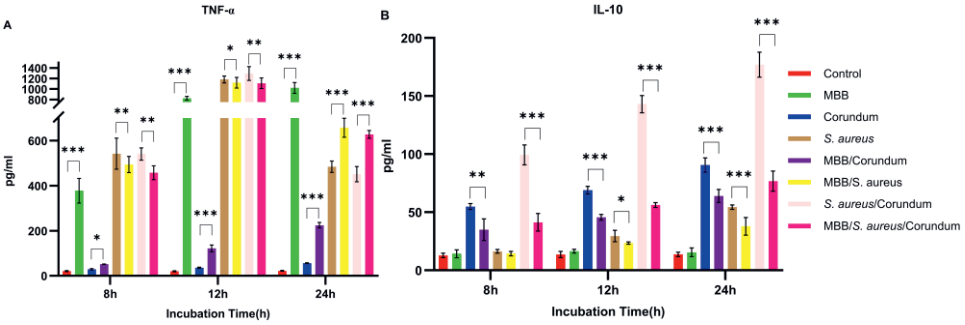


Fig. 6. MBB modulates macrophage inflammatory cytokine secretion in response to *S. aureus* infection. Macrophages were cultured on titanium surfaces and treated with *S. aureus* and/or MBB for 8, 12, or 24 h. Cytokine levels in the supernatants were quantified by ELISA. The secretion level of (a) pro-inflammatory cytokine, TNF-α, and (b) anti-inflammatory cytokine, IL-10 (n = 4). Data show the mean ± SD. one way ANOVA was used to determine statistical significance (n=4, *p < 0.05; **p < 0.01; ***p < 0.001).

3.6. Effects of MBB on the macrophage gene expression

Quantitative RT–PCR analysis revealed expression profiles of inflammatory and immune-regulatory genes. Macrophages were co-cultured with *GFP-labelled S. aureus* under different roughness conditions (Fig. 7). Pro-inflammatory M1 markers, including TNF-α, IDO1, and CXCL11, were markedly upregulated in response to *S. aureus* exposure. Before 12h, TNF-α expression increased (60.30 ± 2.08), declining at 24 h (31.25 ± 9.49). MBB alone moderately elevated TNF-α at 12 h (37.93 ± 4.06) and corundum induced a smaller increase (22.92 ± 1.34). Combined MBB/corundum treatment amplified TNF-α at 12 h (39.97 ± 4.69). In contrast, MBB/*S. aureus*/ corundum resulted in less TNF-α induction (6.39 ± 69.26, p = 0.823).

IDO1 expression followed a similar pattern, with low baseline levels in controls (1.34 ± 0.14) strongly induced by *S. aureus* at 12 h (56.25 ± 8.30) and sustained at 24 h (18.43 ± 3.61). MBB alone modestly increased IDO1 (12 h: 12.71 ± 0.94), and corundum alone caused minor early changes (1.43 ± 0.14). The MBB/corundum combination intermediate induction (15.54 ± 2.96), and MBB/*S. aureus* co-treatment produced a synergistic increase

at 12 h (59.69 ± 4.68). CXCL11 peaked at 12 h in *S. aureus* (56.25 ± 8.30) and MBB/*S. aureus* (59.69 ± 4.68) groups. A moderate upregulation under MBB/corundum (15.54 ± 2.96) and MBB alone (12.71 ± 0.94) was observed.

In contrast, M2 markers were generally low induced. Compared to controls (0.45 ± 0.37), IL-10 was modestly induced by *S. aureus* at 8 h (0.56 ± 0.32), 24 h (2.61 ± 0.03). MBB/corundum surface group elevated IL-10 at 24 h (2.02 ± 0.81). MBB alone showed a small increase at 12 h (1.55 ± 0.23). MBB/S. aureus/ corundum produced IL-10 expression (24 h: 1.05 ± 3.51). CCL13 exhibited low baseline expression at 8 h (0.49 ± 0.30), with the highest induction under corundum at 24 h (5.16 ± 1.34), and moderate increases with MBB/corundum (4.15 ± 1.11) and *S. aureus* (2.79 ± 0.61). MRC1 was minimally expressed across all groups, with slight elevations in corundum at 24 h (3.91 ± 0.92, p = 0.005) and *S. aureus* at 24 h (2.41 ± 0.08). Functional genes linked to macrophage activation were also modulated. TLR2 expressions were downregulated, whereas and ICAM1 were upregulated in *S. aureus*-treated groups, peaking at 24 h.

Collectively, MBB promotes the expression of pro-inflammatory M1 markers (TNF-α, IDO1, CXCL11) and functional genes (Nfkb1, ICAM1), while suppressing M2-associated markers, thereby driving macrophage polarization toward an M1 phenotype. This shift was accompanied by enhanced cell adhesion, increased ROS generation, and augmented bacterial phagocytic capacity.

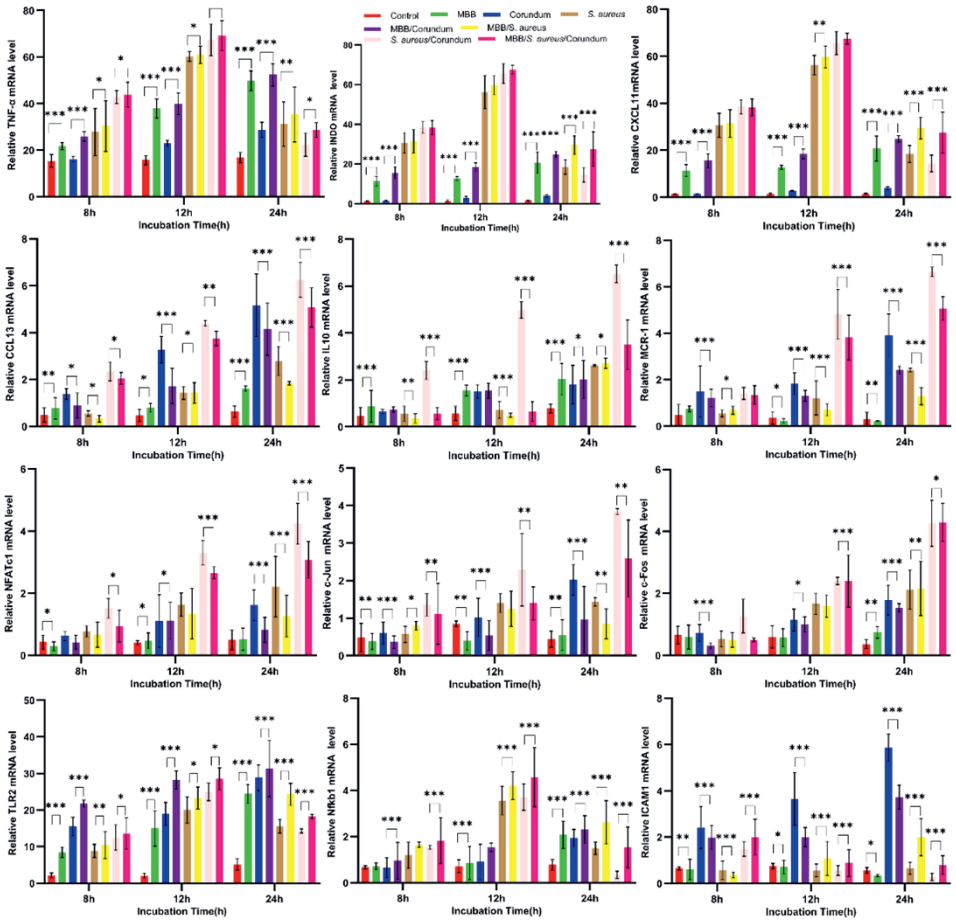


Fig. 7. Expression profiles of inflammatory and immune-regulatory genes in macrophages. Quantitative RT–PCR analysis of pro-inflammatory M1 markers (TNF-α, IDO1, CXCL11), anti-inflammatory M2 markers (IL-10, MRC1, CCL13), and functional genes (TLR2, Nfkb1, ICAM1) in macrophages under different treatment conditions. Data show the mean ± SD. one way ANOVA was used to determine statistical significance (n=4, *$p < 0.05$; **$p < 0.01$; ***$p < 0.001$).

3.7. Immunofluorescence analysis of macrophage

To investigate the effects of MBB, *S. aureus*, and corundum on macrophage polarization, macrophages were cultured on titanium surfaces and assessed for M1 and M2 marker expression after 24 h. Immunofluorescence staining revealed a clear shift toward M1 polarization ($CCR7^+$) in MBB-treated cells across all conditions (Fig. 8) but M2 marker expression ($CD36^+$) was consistently suppressed (Fig. 8). In controls, both M1 and M2 populations were detectable, reflecting a balanced basal state. *S. aureus* or MBB alone

markedly increased CCR7 signal, while CD36 remained low. Corundum alone elicited moderate CD36 expression. The MBB/*S. aureus*/corundum produced the strongest CCR7 staining and minimal CD36, indicating a synergistic promotion of pro-inflammatory M1 polarization. Merged images confirmed clear colocalization of CCR7 with DAPI-stained nuclei. These results demonstrate that MBB robustly drives macrophages toward an M1 phenotype while repressing M2 differentiation.

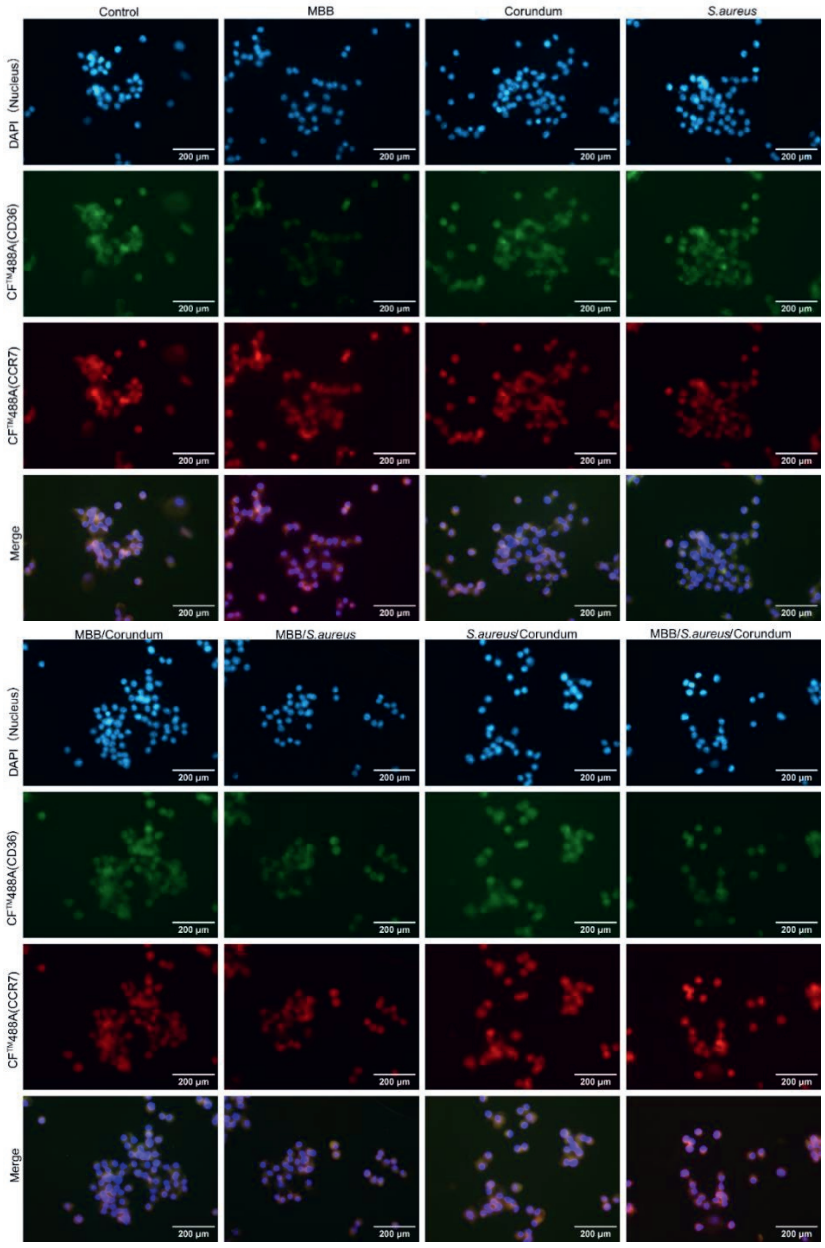


Fig. 8. Immunofluorescence analysis of macrophage polarization on titanium surfaces. Macrophages were cultured for 24 h with MBB, corundum surface, *S. aureus* and combinations. Cells were stained with DAPI (blue, nuclei), CF™ 488A-conjugated anti-CD36 (green, M2 macrophage marker), and CF™ 568-conjugated anti-CCR7 (red, M1 macrophage marker). Merged images display colocalization of polarization markers with nuclear staining. The scale bar shows 200 μm.

3.8. Effects of MBB on the Macrophage M1/M2polarization ratio

To investigate the effects of MBB, *S. aureus*, and corundum on macrophage polarization, macrophages were cultured on titanium surfaces and assessed for M1 ($CCR7^+$) and M2 ($CD36^+$) marker expression after 24 h. Quantitative analysis of M1 ratios ($CCR7^+$/total cells) revealed that MBB significantly enhanced M1 polarization across multiple conditions (Fig. 9). Specifically, the control group exhibited a baseline M1 ratio of 1.28 ± 0.13. Treatment with MBB alone increased the ratio to 2.79 ± 0.61. Corundum alone reduced the M1 ratio to 0.52 ± 0.08, and *S.aureus* alone showed a comparable reduction (0.57 ± 0.19). Corundum/*S. aureus* revealed a synergistic effect of MBB with corundum, elevating the M1 ratio to 4.44 ± 0.63 ($p < 0.001$). But MBB/*S. aureus* induced a modest increase (0.80 ± 0.11). The MBB/*S. aureus*/corundum group resulted in 0.68 ± 0.21, indicating a complex interaction that attenuated M1 induction. *S.aureus*/corundum alone produced the lowest M1 ratio of 0.50 ± 0.09. In parallel, M2 marker expression ($CD36^+$) was consistently suppressed in all MBB-containing conditions, while corundum alone or *S. aureus*/corundum induced M2 expression. Immunofluorescence images confirmed these trends, showing intense CCR7 signal and minimal CD36 staining in MBB groups, particularly in MBB/corundum co-treatment. These indicate that MBB selectively drives macrophages toward a pro-inflammatory M1 phenotype while repressing M2 differentiation, with the strongest effect observed in combination with corundum.

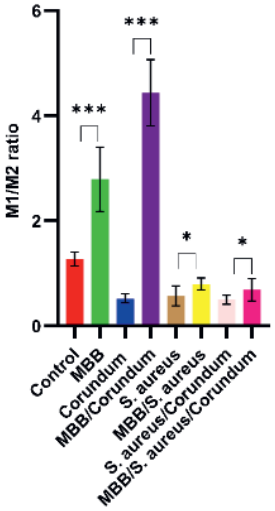


Fig. 9. Quantification of macrophage polarization (M1/M2 ratio). Quantification of macrophage polarization after 24 h of stimulation with MBB, corundum, and *S. aureus*. M1 and M2 macrophages were identified by $CCR7^+$ and $CD36^+$ immunostaining. Data show the mean ± SD. one way ANOVA was used to determine statistical significance (n=4, *$p < 0.05$; **$p < 0.01$; ***$p < 0.001$).

3.9. TEM analysis of co-culture of *S. aureus* and macrophages on the corundum surface

To further investigate the impact of MBB on co-culture of *S. aureus* and macrophages, we performed TEM analysis (Fig.10). Macrophages exposed to MBB alone displayed pronounced phagocytic activity, characterized by increased formation of phagosomes, enrichment of lysosomal compartments, and localized membrane ruffling—features indicative of enhanced bacterial uptake. Nuclear condensation and cytoskeletal rearrangements were also evident, consistent with activation toward a pro-inflammatory M1 phenotype. Treatment with *S. aureus* alone induced moderate phagosome formation and vesicle accumulation, whereas corundum exposure primarily resulted in cytoplasmic disorganization and irregular vacuolization. Co-exposure to MBB and *S. aureus* markedly amplified phagocytic structures, with abundant phagosomes and reinforced cytoskeletal architecture, indicating a synergistic enhancement of bacterial clearance capacity. MBB combined with corundum promoted extensive cytoskeletal remodeling and membrane ruffling. The triple challenge (MBB/*S. aureus*/corundum) elicited both high phagosomal activity and robust adhesion structures, accompanied by moderate cytoplasmic

rarefaction, reflecting an integrated response to simultaneous physical and microbial stimuli. These prove that MBB enhances macrophage bacterial phagocytosis and adhesion, promoting polarization toward an M1-like phenotype. Furthermore, combinatorial physical and microbial challenges remodel macrophage ultrastructure in a manner that supports these functional adaptations.

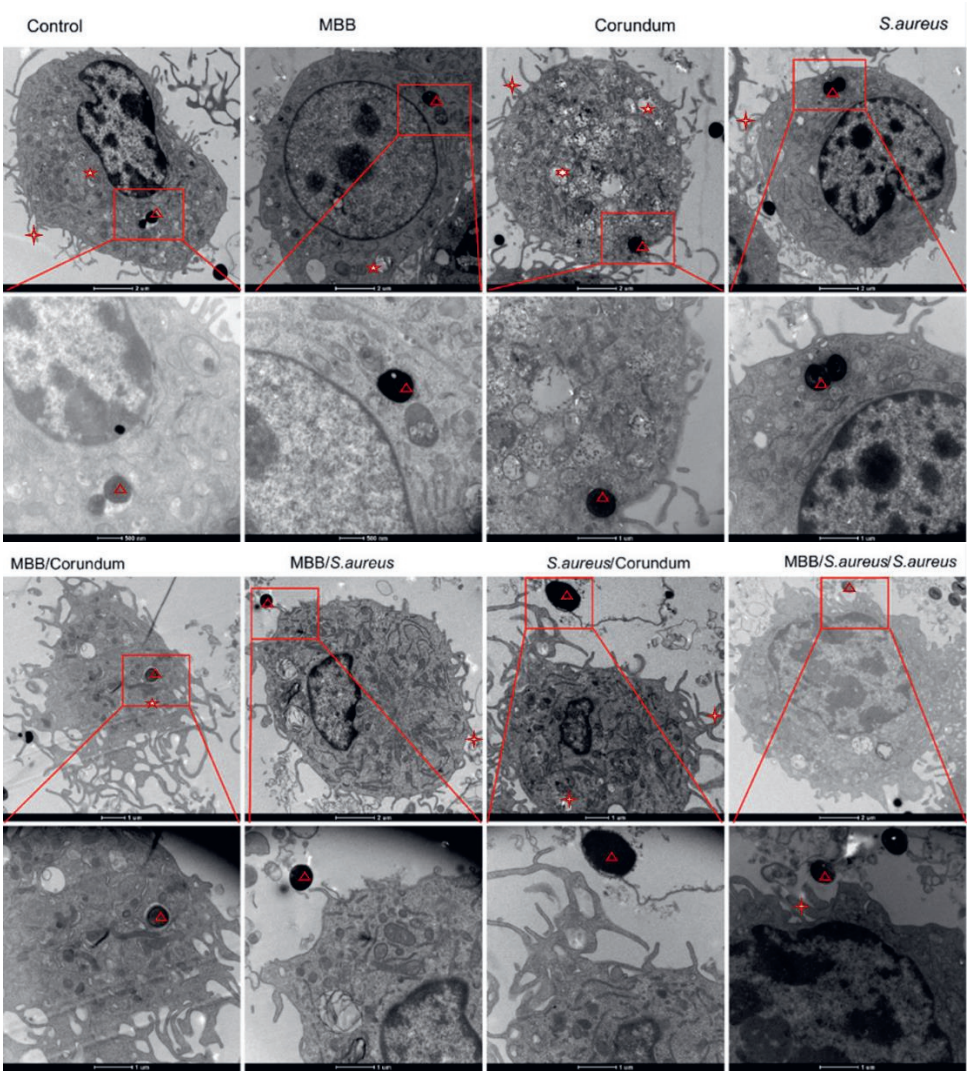


Fig. 10. TEM images of macrophages cultured 24 h with combinations of MBB, corundum, and *S. aureus*. Red triangles indicate *S. aureus*, red squares mark pseudopodia, red stars denote phagosomes, and red hexagrams indicate vacuoles. Top panels show low-magnification overviews (scale bars, 1–2 µm) and bottom panels show higher magnifications (scale bars, 500 nm–1 µm).

3.10. Effects of MBB on macrophage adhesion

Macrophage adhesion was assessed by quantifying DNA content as a proxy for cell attachment (Fig. 11). Compared with uninfected controls (453.7 ± 4.8 ng mL^{-1}), *S. aureus*

infection significantly reduced adhesion (354.8 ± 4.6 ng mL^{-1}, p< 0.05). Corundum surfaces markedly enhanced adhesion under non-infectious conditions (619.6 ± 13.7 ng mL^{-1}, p < 0.01). The highest attachment observed in MBB/corundum-treated macrophages (648.4 ± 15.2 ng mL^{-1}, p < 0.001). MBB alone increased adhesion in both uninfected (475.9 ± 8.7 ng mL^{-1}, p < 0.05) and infected cultures (374.4 ± 8.0 ng mL^{-1}, p < 0.05). In the presence of *S. aureus*, co-treatment with corundum or MBB partially restored attachment. The MBB/*S. aureus*/corundum combination yielded the greatest increase, reaching 547.1 ± 10.5 ng mL^{-1} (p < 0.01), corresponding to a 60% enhancement in adhesion. These indicate that MBB promotes macrophage adhesion and supports M1 polarization, counteracting the adhesion-suppressive effect of bacterial infection and synergizing with corundum to enhance cellular attachment.

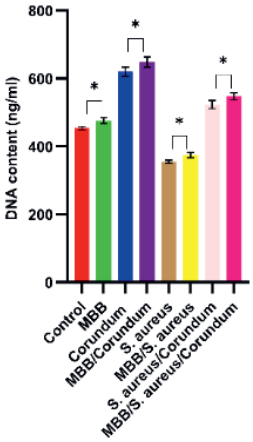


Fig. 11. Quantification of macrophage adhesion. Macrophages were cultured on titanium surfaces and treated with *S. aureus* and/or MBB for 24 h. DNA content, reflecting adherent cell number, was quantified using the Quant-iT™ assay (n = 4). Data show the means ± SD. One way ANOVA was used to determine statistical significance (n=4, *p < 0.05; **p < 0.01; ***p < 0.001).

3.11. Modulation of macrophage ROS responses

To examine the oxidative response of macrophages, intracellular reactive oxygen species (ROS) levels were quantified using the DCFH-DA assay at 8, 12, and 24 h. Macrophages were following co-culture with *GFP-labelled S. aureus* under various treatment conditions (Fig. 12). At 8 h, control group cells exhibited minimal ROS accumulation (0.15 ± 0.03),

whereas MBB alone induced a moderate increase (0.43 ± 0.15). Corundum alone produced a modest response (0.22 ± 0.07), while *S. aureus* markedly enhanced ROS levels (0.62 ± 0.07). Combined MBB/corundum treatment further elevated ROS (0.86 ± 0.04), surpassing either stimulus alone. MBB/*S. aureus* (0.82 ± 0.01), *S. aureus*/corundum (0.76 ± 0.12), and MBB/*S. aureus*/corundum (0.96 ± 0.19) showed slightly attenuated ROS compared with MBB/corundum.

By 12 h, ROS peaked in *S. aureus*-treated macrophages (1.61 ± 0.014). ROS further increased in MBB/corundum (1.67±0.156) and MBB/*S. aureus*/corundum conditions (2.00±0.17). This indicates synergistic oxidative activation. MBB/*S. aureus* (1.77±0.12) and *S. aureus*/corundum (1.78 ± 0.142) maintained ROS levels comparable to MBB/corundum, suggesting bacterial signals sustain oxidative activity. At 24 h, MBB alone induced maximal ROS accumulation (2.39 ± 0.28). Corundum (0.51 ± 0.05) and *S. aureus* alone (0.52 ± 0.14) remained low. MBB/corundum maintained high ROS (2.71 ± 0.13). But MBB/*S. aureus* (0.73 ± 0.13), *S. aureus*/corundum (0.35±0.12), and MBB/*S. aureus*/corundum (0.65±0.21) This showed pronounced attenuation, suggesting that bacterial factors partially dampen MBB- and roughness-induced oxidative stress. MBB potentiates ROS production and promotes M1-like oxidative activation, particularly under high roughness exposure.

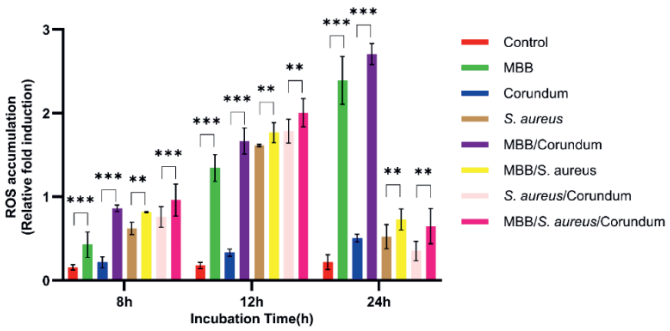


Fig.12. Quantification of macrophages ROS production. Macrophages were co-cultured with *GFP-labelled S. aureus* and treated with MBB (10 μM), Corundum or a combination of both. Intracellular reactive oxygen species (ROS) levels were measured at 8, 12, and 24 hours using the DCFH-DA assay. Data are presented as relative fold induction normalized to untreated control macrophages. Data show the mean ± SD. One way ANOVA was used to determine statistical significance (n=4, *$p < 0.05$; **$p < 0.01$; ***$p < 0.001$).

4. Discussion

The aim of this study was to design a c-Jun–mimetic peptide (MBB) capable of selectively disrupting NFATc1–DNA interactions. When macrophages on corundum surfaces under *S. aureus* challenge, MBB prevented the shift toward an anti-inflammatory M2 phenotype and instead promoting pro-inflammatory M1 polarization. Specifically, at 12 h post-infection, MBB inhibited NFATc1 binding activity, thereby suppressing macrophage polarization toward the anti-inflammatory M2 phenotype. This was accompanied by increased secretion of the pro-inflammatory cytokine TNF-α, reduced production of the anti-inflammatory cytokine IL-10, and enhanced ROS generation. These findings prove that MBB drives macrophages toward a pro-inflammatory M1 state on corundum titanium surfaces (Sa:1.32 ± 0.28 μm; Ti:88.80±0.40 wt.%) under *S. aureus* challenge.

NFATc1 is a pivotal transcription factor governing macrophage polarization [279, 280], whose activity depends on direct binding DNA[281, 282]. Our previous work revealed that NFATc1 alone cannot stably bind DNA, instead requiring the cooperative assistance of c-Jun and c-Fos to form a stable NFATc1/c-Jun/c-Fos/DNA ternary complex. Guided by this structural insight, we engineered MBB, a c-Jun mimetic peptide that occupies the same NFATc1- and DNA-interacting interface as native c-Jun, thereby anchoring firmly to NFATc1. To enhance stability, we introduced paired cysteine residues into the NFATc1–DNA contact region of MBB, enabling intramolecular disulfide bond formation. Upon

binding NFATc1, MBB competitively displaces c-Jun, and—by virtue of its extended "lever arm"—sterically hinders assembly of the NFATc1 complex at this site. Thereby MBB can effectively suppressing NFATc1's transcriptional activity. Guided by these structural insights, we designed a c-Jun–mimetic peptide, termed MBB, using AlphaFold3. The predicted pLDDT score exceeded 90, indicating high model confidence, consistent with prior benchmarks[283]. MBB was expressed in *E. coli*, purified to >95% homogeneity as confirmed by size-exclusion chromatography, and validated via high-resolution mass spectrometry and DNA sequence analysis. Cytotoxicity testing revealed an IC_{50} of 26.14 μM, allowing us to select 25 μM for subsequent functional assays.

MBB competitively inhibited NFATc1–DNA binding. Thereby functionally reprogramed macrophages toward a pro-inflammatory M1 phenotype—an immune state critical for bacterial clearance at infected biomaterial interfaces. M1 macrophages are classically associated with antimicrobial activity[281, 284, 285], whereas M2 macrophages primarily mediate tissue repair[286, 287]. Consistent with this shift, ELISA revealed elevated secretion of TNF-α (M1-associated cytokine[288]) and reduced IL-10 (M2-associated cytokine [289]) in the MBB-treated group. Although neither TNF-α nor IL-10 alone provides definitive discrimination between M1 and M2 states, immunofluorescence analysis further supported this trend: macrophages co-expressing the M1 marker CCR7 [290] (red, CF™ 568) and the M2 marker CD36[291] (green, CF™ 488A) displayed markedly stronger CCR7 fluorescence following MBB treatment. Complementary RT–PCR analysis confirmed upregulation of M1-associated genes (TNF-α, IDO1, CXCL11) alongside suppression of M2-associated transcripts (IL-10, MRC1, CCL13), culminating in a substantially elevated M1/M2 ratio. These results collectively demonstrate that MBB drives macrophage polarization toward a bactericidal phenotype under *S. aureus* challenge.

Following polarization toward an M1 phenotype, an essential next step in bacterial clearance is the firm adhesion of macrophages to the infected implant surface[292].

Without sufficient enrichment of M1 macrophages at the site, effective eradication of pathogens remains unlikely[293]. In our study, RT–PCR analysis revealed significant upregulation of the adhesion-associated gene ICAM1 in the MBB-treated group. Consistently, Quant-iT™ adhesion assays demonstrated a higher number of macrophages attached to corundum-type titanium surfaces following MBB treatment compared with untreated controls. Once adhered, macrophages must phagocytose invading bacteria and subsequently eliminate the internalized pathogens to prevent intracellular bacterial persistence—a known route to immune evasion, antibiotic resistance, and dissemination of infection [294]. Transmission electron microscopy (TEM) of MBB-treated macrophages revealed extensive phagosomal activity, pronounced adhesion structures, and moderate cytoplasmic rarefaction, all indicative of heightened antimicrobial engagement. At the molecular level, TLR2 expression—a key mediator of bacterial recognition[295]—was markedly elevated, suggesting enhanced phagocytic responsiveness. Crucially, intracellular ROS levels, a primary mechanism for killing engulfed bacteria[296], were significantly higher in the MBB group, underscoring the peptide's ability to potentiate bactericidal effector functions. Together, these findings demonstrate that MBB not only reprograms macrophages toward an M1 phenotype but also reinforces the sequential adhesion–phagocytosis–bacterial killing axis essential for controlling implant-associated infections.

Our findings highlight an immunotherapeutic strategy, leveraging structure-guided, transcription factor-targeted peptides, to modulate macrophage polarization in the context of biomaterial-associated infection. This approach offers a versatile complement to existing biomaterial design paradigms, with potential applicability across diverse tissue–material interfaces where immune evasion remains a challenge.

Limitations and future directions include the need for in vivo validation in models of implant-associated infection to evaluate efficacy, pharmacokinetics, and safety. Moreover, as NFATc1 is active in other immune and bone-related cells, strategies for macrophage-specific targeting or local delivery will be essential. We did not assess the

direct binding of the inhibitor to NFATc1, and long-term functional consequences remain unknown, underscoring the importance of comprehensive biochemical validation and longitudinal studies. Additionally, because NFATc1 is active in other immune and bone-related cells, strategies for macrophage-specific targeting or local delivery will be essential. Further studies into the downstream epigenetic and transcriptional programs altered by transient NFATc1 inhibition may provide deeper insight into long-term immune modulation.

5. Conclusion

This study establishes a structure-guided immunomodulatory strategy for enhancing macrophage-mediated clearance of *S. aureus* on orthopedic implant surfaces. By rationally designing the peptide MBB to disrupt NFATc1–DNA interactions, we reprogrammed macrophage polarization toward a pro-inflammatory M1 phenotype, restoring antimicrobial capacity even under surface conditions that typically favor immune suppression. Our findings underscore the critical role of transcriptional regulation in shaping innate immune responses at the biomaterial interface and highlight the potential of peptide-based modulation of immune transcription factors as a therapeutic approach for preventing and treating implant-associated infections. This work provides a framework for the development of precision immunotherapeutics that bridge structural biology, materials science, and host defense.

General Discussion

General Discussion

1. Overview of the thesis

Implant-associated infections remain not only compromising clinical efficacy but also frequently necessitating complex surgical interventions[297]. This thesis explores the molecular mechanisms underlying the polarization of infection-immune macrophages as function of the surface roughness of titanium biomaterials sole or combined with *S. aureus*. In addition, a new targeted immunotherapy strategy to enhance infection resistance, is proposed. Chapter 1 addresses the clinical and biological challenges of implant infections, highlighting the role of bacterial biofilms, modifying material surface properties and the mechanisms of macrophage differentiation on infected surfaces. Chapter 2 investigates how titanium surface characteristics influence macrophage adhesion, polarization and the molecular mechanisms of implant infections. Chapter 3 utilizes this infection model to closely approximate the reality of implant infection. Here, co-cultures of *S. aureus* and macrophages are employed. Based on the NFATc1-mediated macrophage differentiation pathway in infection immunity, as identified in Chapters 2 and 3, Chapter 4 employs SPR to elucidate the cooperative DNA binding mechanisms of NFATc1 and c-Jun, providing molecular insights into macrophage immune regulation. Chapter 5 introduces a rationally designed novel peptide (MBB) that inhibits simultaneous NFATc1/c-Jun/DNA binding and enhances M1 formation and thus macrophage resistance to *S. aureus* infections.

2. Surface characteristics of titanium modulates macrophage inflammatory response

Chapter 2 describes how surface roughness combined with LPS stimulation intensifies macrophage responses, especially under inflammatory conditions. It focused on how titanium surface roughness influences macrophage behavior, particularly under conditions of inflammation induced by LPS. A significant novelty of this research is that surface roughness can simultaneously induce macrophage differentiation into both M1 and M2 types. As the roughness of corundum increases within a certain range, the relative number of M2 cells increases, aligning with previous studies[1] and provides new insights

into how topographical cues from titanium surfaces shape macrophage function at the biointerface. When roughness reaches the level of plasmapore, the ratio of M2 cells decreases. Importantly, pathway enrichment analysis revealed key metabolic and NFATc1 immune pathways influenced by surface roughness. This is also consistent with studies by Zhang, Haiyun et al.[2]and Qian, Xin, et al.[3], suggesting that surface roughness modulates both macrophage polarization and key metabolic pathways that regulate immune responses, including the signaling pathway of NFATc1.

3. Effect of titanium surface roughness on macrophage-bacteria interactions

Chapter 3 builds on these findings while applying a more physiologically relevant infection model using *S. aureus*. This facilitates a deeper understanding of macrophage interactions with titanium surfaces under more complex microbial challenges. Unlike earlier approaches focused on antibiotics or biomaterial coatings[25], this study integrates surface engineering and immune modulation, focusing on how macrophage behavior can be influenced by biomaterial design. This approach could significantly enhance the effectiveness of implants by improving host immune responses while preventing bacterial persistence. A key finding of this chapter is that macrophages differentiate into the M1 phenotype as roughness increases. However, after 12 hrs, the proportion of M2 macrophages increases due to the synergistic effect of *S. aureus* and roughness. This demonstrates the limitations of the model in Chapter 1. This chapter observed increased phagocytosis, elevated ROS production, and an enhanced inflammatory cytokine profile at the corundum group. These suggest that rougher surfaces (Corundum, Sa:5.51±0.29μm) provide a more favorable environment for macrophage activity. Proteomic studies have demonstrated that surface roughness modulates both NFATc1 macrophage polarization signaling pathway and key metabolic pathways that regulate immune responses. The findings offer new strategies for improving the success of titanium implants and combatting biofilm-related infections, by regulating NFATc1. Despite these advances, Chapter 3 identified signaling pathways. One of the pathways is the NFATc1 signaling pathway, as a regulator of macrophage function under infectious conditions and no

further exploration has been undertaken into methods for blocking this NFATc1 target. Finally, given that the structure of NFATc1 has been thoroughly characterized, Chapter 4 will address the binding kinetics of this transcription factor.

4. Application of surface plasmon resonance to elucidate the cooperative DNA binding mechanisms of NFATc1 and c-Jun

Regulation of macrophage immune function by the transcription factor NFATc1 is essential for macrophage clearance of implant-infected *S. aureus* bacteria[134]. Chapter 4 describes the DNA-binding kinetics of NFATc1, using SPR and providing a theoretical foundation for designing macrophage function-regulating peptides. NFATc1 alone exhibited a ka of (2.44±0.10)× 10^5 $M^{-1}s^{-1}$ and a kd of (1.05±0.02)× 10^{-1} s^{-1}, resulting in a dissociation constant (KD) of (4.11±0.07)× 10^{-7} M, consistent with EMSA values (10^{-8}–10^{-7} M) [251] while offering improved temporal resolution. In contrast, c-Jun displayed a higher ka (5.97±0.22)× 10^5 $M^{-1}s^{-1}$ and kd (1.24±0.13)× 10^{-1} s^{-1}, leading to a KD of (1.95±0.03)× 10^{-7} M, aligning with fluorescence anisotropy estimates (10^{-7}–10^{-9} M)[251]. Upon cooperative binding, the NFATc1/c-Jun complex exhibited a further increase in ka (8.29±0.19) × 10^5 $M^{-1}s^{-1}$ with a moderately increased kd (1.45±0.12× 10^{-1} s^{-1}), yielding a KD of (1.63±0.17) × 10^{-7} M. These results align with those of Seo, Jungkyun, et al.[252], who reported similar cooperative binding behavior in the AP-1 family, and Li, Ya-Ting, et al.[253], who identified NFATc1 as a critical modulator of dynamic TF recruitment. This provides a detailed understanding of TF cooperative binding dynamics and provides a molecular dynamics design basis for developing c-Jun analogue peptides that modulate NFATc1. Based on the data and molecular modelling using AlphaFold, a novel inhibitor of the transcription was rationally designed. Chapter 5 presents an first screening of its pharmacological efficacy.

5. Structure-guided disruption of NFATc1 rewires macrophage polarization to enhance clearance of *S. aureus* on implant surfaces

Various strategies exist to modulate macrophage activity, including cytokines, small molecules, and genetic engineering[298]. They, broadly activate innate immune pathways but often cause systemic inflammation and side effects[299]. As mentioned in this chapter a newly designed antimicrobial peptide (MBB) was validated on its antagonistic activity. The experimental data showed that MBB-treated macrophages give rise to a higher M1/M2 ratio and increased bacterial clearance, offering precise immune modulation.

Although this study successfully demonstrated the functional impact of MBB on macrophages and the potential for its incorporation into biomaterial surface modification to control implantation-associated infections, an in-depth pharmacological evaluation is still to be conducted. Structural insights into the interaction of MBB with NFATc1 and c-Fos are yet unknown. Detailed structural analyses of the MBB/NFATc1/c-Fos complex is anticipated to support the deepening of the mechanistic understanding and refine future peptide design.

Valorization

Valorization

This doctoral thesis, "Macrophage–Material Interactions: NFATc1/c-Jun Signaling, Titanium Surface Modifications and Orthopedic Implant Infections," reveals the interactions between titanium implant surfaces, macrophages, and bacterial biofilms, aiming at providing new therapeutic strategies for implant infection control.

1. Academic impact

The presented research advances the fields of biomaterials science, immunology, and implant infection processes by providing new insights into macrophage responses to titanium surface modifications and the cooperative transcriptional regulation of NFATc1 and c-Jun. Mechanistic understanding of the immune response at the infection interface of implant materials is enhanced through the integration of advanced analytical technologies such as SPR, proteomics, confocal microscopy and computational modelling. Key academic contributions include identification of titanium surface roughness as a modulator of macrophage polarization and bacterial interactions during implant infections, bridging the gap between the science of implant biomaterials and immunomodulation of infections; application of SPR to elucidate the mechanism of DNA binding kinetics of NFATc1 and c-Jun, advancing the understanding of synergistic roles of transcription factors in immune responses; and the use of novel peptides as novel immunomodulators.

All together this thesis provides a foundation for follow-up studies investigating immune regulation of implant-based infections, antimicrobial strategies, and transcriptional regulation of immune cells. Most likely, they will provide new fundamental insights supporting the effective design of infection-resistant biomaterials. Hence, the methodologies described can be applied to broader set of studies focusing on immuno engineering of material infection therapies and implant -infected bio interfaces.

2. Industrial impact

The research described has direct implications for the biomedical and orthopedic implant industry, addressing the key challenge of implant-related infections. The findings will most likely help to optimize implant surfaces able to enhance host immune responses, thereby reducing infection-related failure rates and extending the lifespan of implants. Key impacts on industry include advances in biomaterial design and the development of next-generation orthopedic implants with enhanced biocompatibility and resistance to infection. The inhibition of the cooperative interaction of NFACTc1 and c-Jan with DNA, enabling the rational design of MBB like peptides, will act as a basis for a new infection control strategy, particularly when combined with material antibiotic coatings. Next local surgical debridement of infected lesions, and systemic antibiotic treatments to meet the pressing need to combat the urgent need for antibiotic resistance.

From an analytical technology point of view, the use of advanced Surface Plasmon Resonance methodologies, studying complex multi protein interaction kinetics between protein pivotal in the transcription of-DNA interactions, has widen its potential in unrevealing DNA transcription processes.

In summary, by translating these findings into practical applications, this research has the potential to facilitate collaboration between academia and industry to develop innovative infection-fighting biomaterials. This could help improve clinical outcomes for patients with implant infections.

3. Societal impact

Implant infections continue to be a major concern in orthopedics, especially regarding the occurrence of related difficult to treat local infections and inflammation processes. Their steady increase in implant infections threaten the health of patients, posing a significant pressure on medical doctors, and costs control. The progress described in this thesis will

contribute to the effectivity and success of implant surgery, increasing the sustainability of healthcare. Key societal benefits might include improved patient care through the development of implant designs that support immune function and resist bacterial colonization, resulting in fewer complications, faster recovery times and improved quality of life for patients undergoing orthopedic implant surgery.

In addition, reduced reliance on traditional antibiotics through the introduction of an immune-modulating therapy with the introduction of the rationally designed NFATc1/c-Jun antagonists MBB will contribute to the combat against antibiotic resistance. In addition, it will have a significant economic impact on the healthcare system by reducing the incidence of implant infections and the need for revision surgery and the overall healthcare costs by optimizing the allocation of resources in healthcare facilities. Beyond clinical applications, this research contributes to broader societal efforts to integrate bioengineering and immunology to address infectious diseases. By fostering interdisciplinary collaboration and translational research, it paves the way for innovative solutions to improve public health and biomedical technology.

Summary

Summary

This PhD thesis investigates the intricate interplay between titanium alloy surface characteristics, macrophage immune responses and novel therapeutic strategies to enhance the resistance of orthopedic implants to infection. The studies described provide new insights into the role of surface morphology in regulating macrophage function and explores the mechanisms of transcriptional regulation as a potential immunomodulatory target.

Chapter 1 describes the clinical and biological challenges associated with orthopedic implant infections, with particular emphasis on the enduring threat posed by bacterial biofilms and the urgent need for more in-depth host-pathogen-material studies to find a new approach to the treatment of infections in orthopedic implant materials. It also reviews the latest methods employed in infection biology and implantation studies, including advanced imaging, transcriptomics and real-time in vitro infection modelling. It acts as a foundation for the mechanistic exploration of host-pathogen-material interactions.

Chapter 2 investigated the effect of infected titanium surface characteristics on macrophages, revealing that a moderately rough surface promotes macrophage adhesion and polarization towards both M1 and M2 phenotypes. The M1 phenotype is dominant which is critical for early antimicrobial activity, particularly in the context of foreign body-associated infections. Proteomics revealed that key protein and NFATc1 immune pathways are influenced by the titanium disk surface roughness, suggesting that tailored surface engineering may provide a effective approach to the critical early treatment phase of orthopedic implant infections.

Chapter 3 extends this inquiry utilizing a more complex biological scenario, examining macrophage-bacteria interactions on different titanium surfaces. By constructing *GFP*-expressing *S. aureus* strains using electron microscopy, laser confocal, and proteomics

techniques, it was revealed that the combined effects of surface roughness and *S. aureus* co-cultures can significantly reduce macrophage bacterial clearance by inducing macrophage M1 polarization, adhesion, improved phagocytic activity, and reactive oxygen species (ROS) generation. Altering the roughness of orthopedic implant materials opens new frontiers in the design of bio interfaces for anti-infective implants. Proteomics proved that surface roughness modulates both NFATc1 macrophage polarization signaling pathway and key metabolic pathways that regulate immune responses.

Chapter 4 shifts towards molecular processes, describing the cooperative DNA binding kinetics of the transcription factors NFATc1 and c-Jun. Bases on the SPR data, itcan be concluded that although each factor binds DNA independently, their cooperative binding significantly enhances binding kinetics, suggesting a synergistic mechanism of gene regulation. This mechanistic insight provides a conceptual basis for immune-targeted immune interventions that go beyond traditional antimicrobial strategies.

Finally, chapter 5 builds on these observations, introducing a rationally designed peptide, MBB, which structurally mimics c-Jun and selectively inhibits NFATc1/c-Jun DNA co-binding. Functional tests demonstrated that MBB enhanced *S. aureus* phagocytosis and ROS generation by macrophages. This represents a novel class of immunotherapeutic agents for implant infections, as this peptide selectively interferes with NFATc1/c-Jun DNA co-binding and enhances macrophage clearance of the pathogenic bacterium *S. aureus* in the case of implant infections without relying on antibiotics.

Samenvatting

Samenvatting

Dit proefschrift beschrijft in detail de complexe interacties tussen de ruwheid van titaniumoppervlakken, met differentiatie van macrofagen, antimicrobiële activiteit en vorming van een bacteriële biofilm. Met behulp van een geïntegreerde experimentele aanpak, en de toepassing van geavanceerde analytische technieken, zijn nieuwe inzichten in de cellulaire en moleculaire processen onderzocht. In het bijzonder, werd het mechanisme van transcriptieregulatie als potentiële therapeutische middel voor immuno modulatie onderzocht.

Het beschrijft de complexe wisselwerking tussen wijzigingen in de ruwheid van titaniumoppervlakken, immuunreacties van macrofagen, bacteriële biofilm vorming en nieuwe therapeutische strategieën ter verbetering van de infectiebestendigheid van orthopedische implantaten. Deze studie biedt nieuwe inzichten in de rol van oppervlaktemorfologie bij het reguleren van de macrofaagfunctie en onderzoekt de mechanismen van transcriptieregulatie als een potentieel immuno modulerend aangrijpingspunt.

Hoofdstuk 1 beschrijft de klinische en biologische uitdagingen die verbonden zijn aan infecties van orthopedische implantaten, met bijzondere nadruk op de aanhoudende dreiging van bacteriële biofilms en de urgentie voor meer diepgaand onderzoek naar interacties tussen gastheer, pathogeen en materiaal, teneinde nieuwe benaderingen te vinden voor de behandeling van infecties in implantaatmaterialen. Het geeft ook een overzicht van de meest recente methoden binnen infectiebiologie en implantatieonderzoek, waaronder geavanceerde beeldvorming, transcriptomics en real-time *in vitro* infectiemodellering. Daarmee wordt een basis gelegd voor mechanistisch onderzoek naar interacties tussen gastheer, pathogeen en materiaal.

Hoofdstuk 2 onderzocht het effect van geïnfecteerde titaniumoppervlakteruwheid op macrofagen, en toonde aan dat een matig ruw oppervlak de hechting van macrofagen en

hun polarisatie richting zowel M1-achtige als M2-fenotypes bevordert. Het M1-fenotype domineert, wat cruciaal is voor vroege antimicrobiële activiteit, met name in de context van lichaamsvreemd materiaal. Proteomics-analyses onthulden dat zowel metabole als NFATc1-gereguleerde immuun routes worden beïnvloed door oppervlaktestructuur, wat suggereert dat oppervlakte-engineering via het sturen van macrofaagimmuunreacties een nieuwe benadering kan bieden voor de kritieke vroege behandelingsfase van implantaatinfecties.

Hoofdstuk 3 introduceert een complexer biologisch scenario, door interacties tussen macrofagen en bacteriën op titaniumoppervlakken met verschillende topografieën te onderzoeken. Door *GFP-exprimerende S. aureus-stammen* te gebruiken in combinatie met elektronenmicroscopie, laser confocale microscopie en proteomics, werd aangetoond dat de gecombineerde effecten van oppervlaktestructuur en Staphylococcus Aureus de bacteriële klaring door macrofagen aanzienlijk verminderen. door M1-polarisatie, toename van adhesie aan het oppervlak, verbeterde fagocytose en verhoogde productie van reactieve zuurstofsoorten (ROS). De resultaten tonen aan dat het aanpassen van de ruwheid van implantaatmaterialen nieuwe mogelijkheden biedt voor het ontwerp van bio-interfaces. Proteomics toonde ook aan dat de oppervlaktestructuur, zowel de NFATc1-signaleringsroute voor macrofaagpolarisatie als de metabole routes, die immuunreacties reguleren, beïnvloedt.

Hoofdstuk 4 richt zich op de DNA-transcriptie factor NFATc1 een b elangrijke regulator van macrofaagfunctie. Met behulp van SPR werd de coöperatieve DNA-bindingskinetiek van de transcriptiefactoren NFATc1 en c-Jun onderzocht. De resultaten tonen dat hoewel beide factoren onafhankelijk aan DNA binden, hun coöperatieve binding de bindingskinetiek aanzienlijk versterkt, wat wijst op een synergistisch mechanisme van genregulatie. Dit mechanistisch inzicht vormt een conceptuele basis voor immuun-gerichte interventies die verder gaan dan traditionele antimicrobiële strategieën.

Hoofdstuk 5 bouwt direct voort op deze moleculaire bevindingen en introduceert een rationeel ontworpen peptide, MBB, dat structureel lijkt op c-Jun en selectief de NFATc1/c-Jun DNA-co-binding remt. Functionele testen toonden aan dat MBB de fagocytose van *S. aureus* en de ROS-productie door macrofagen verhoogt. Dit vertegenwoordigt een nieuwe klasse immuno therapeutische middelen voor implantaatinfecties, aangezien dit peptide selectief interfereert met NFATc1/c-Jun-co-binding en zo de macrofaagafhankelijke klaring versterkt.

Appendix

Appendix I-Abbreviations

S.aureus	*Staphylococcus aureus*
NFATc1	Nuclear Factor of Activated T-cells, cytoplasmic 1
c-Jun	Cellular Jun
c-Fos	Cellular Fos
CNS	Staphylococcus aureus, coagulase-negative staphylococci
MRSA	Methicillin-susceptible Staphylococcus aureus
CLSM	Confocal laser scanning microscopy
SEM	Scanning electron microscopy
Fn	Fibronectin
Fg	Fibrinogen
VN	Vitronectin
PMN	Polymorphonuclear neutrophils
PRRs	Pattern recognition receptors
TLRs	Toll-like receptors
NLRs	Nod-like receptors
NF-κB	Nuclear factor κB
MAPKs	Mitogen-activated protein kinases
IRFs	Interferon regulatory factors
LPS	Lipopolysaccharide
IFN-γ	Gamma interferon
EDS	Energy-dispersive spectroscopy
3D	Three-Dimensional
Ti	Titanium
ALP	Alkaline phosphatase
OCN	Osteocalcin
BSA	Bovine serum albumin
PBS	Phosphate buffered saline
DAPI	4’,6-diamidino-2-phenylindole
ACN	Acetonitrile
DIA	Data Independent Acquisition
FDR	False discovery rate
PCA	Principal Component Analysis
SEM-EDS	SEM-energy dispersive spectroscopy
Al	Aluminum
C	Carbon
Si	Silicon
P	Phosphorus

Ca	Calcium
ELISA	Enzyme-Linked Immunosorbent Assay
RT-qPCR	Reverse Transcription quantitative Polymerase Chain Reaction
TNF-α	Tumor Necrosis Factor-alpha
INDO	Indoleamine 2,3-dioxygenase
CXCL11	C-X-C motif chemokine ligand 11
IL-10	Interleukin-10
MCR-1	Mannose Receptor C-Type 1
CCL3	C-C motif chemokine ligand 3
CCR7	C-C chemokine receptor type 7
CD36	Cluster of Differentiation 36
LC-MS/MS	Liquid chromatography-tandem mass spectrometry
GO	Gene ontology
FCERI	Fc epsilon receptor
DC-SIGN	CD209
CLR	C-type lectin receptor
TCA	Tricarboxylic acid cycle
ROS	Reactive Oxygen Species
GFP	Green Fluorescent Protein
DMEM	Dulbecco's Modified Eagle Medium
CFU	Colony-Forming Unit
TEM	Transmission Electron Microscopy
H2DCFDA	2’,7’-dichlorodihydrofluorescein diacetate
MaxLFQ	Maximal Label-Free Quantification
CCK-8	Cell Counting Kit-8
KD	Dissociation Constant
Kd	Dissociation Rate Constant
Ka	Association Rate Constant
TFs	Transcription factors
EMSAs	Electrophoretic mobility shift assays
HSM	DNA hybridization buffer
UV	Ultraviolet
SPR	Surface Plasmon Resonance
RUs	Resonance units
bZIP	Basic leucine zipper
smFRET	Single-molecule Förster resonance energy transfer
HDX-MS	Hydrogen-deuterium exchange mass spectrometry

cryo-EM	Cryo-Electron Microscopy
ChIP	Chromatin immunoprecipitation assays
pLDDT	Predicted local distance difference test
MD	Molecular dynamics
PDB	Protein Data Bank
IPTG	Isopropyl-β-D-thiogalactopyranoside
OD600	Optical Density at 600 nm
PMSF	Phenylmethylsulfonylfluoride
Tris-HCl	Tris(hydroxymethyl)aminomethane hydrochloride
SDS-PAGE	Sodium Dodecyl Sulfate–Polyacrylamide Gel Electrophoresis
ECL	Enhanced Chemiluminescence
SEC	Size-exclusion chromatography
AUC	The area under the curve
ESI-MS	Electrospray ionization mass spectrometry
$MgCl_2$	Magnesium chloride
GAPDH	Glyceraldehyde-3-Phosphate Dehydrogenase
MOI	Multiplicity of Infection

Appendix II-References

[1] W. Jin, P.K. Chu, Orthopedic implants, Encyclopedia of biomedical engineering 1(3) (2019) 425-439.

[2] W. Liang, C. Zhou, J. Bai, H. Zhang, B. Jiang, J. Wang, L. Fu, H. Long, X. Huang, J. Zhao, Current advancements in therapeutic approaches in orthopedic surgery: a review of recent trends, Frontiers in Bioengineering and Biotechnology 12 (2024) 1328997.

[3] S. Dixit, S. Gupta, A. Sharma, Surgical Devices for Biomedical Implants, Additive Manufacturing for Biomedical Applications: Recent Trends and Challenges, Springer2024, pp. 195-218.

[4] M. Sarraf, E. Rezvani Ghomi, S. Alipour, S. Ramakrishna, N. Liana Sukiman, A state-of-the-art review of the fabrication and characteristics of titanium and its alloys for biomedical applications, Bio-design and Manufacturing (2021) 1-25.

[5] T.M. Duane, J.M. Huston, M. Collom, A. Beyer, S. Parli, S. Buckman, M. Shapiro, A. McDonald, J. Diaz, J.M. Tessier, Surgical infection society 2020 updated guidelines on the management of complicated skin and soft tissue infections, Surgical infections 22(4) (2021) 383-399.

[6] J.G. Dreyfus, H. Yu, E. Begier, J. Gayle, M.A. Olsen, Incidence and burden of Staphylococcus aureus infection after orthopedic surgeries, Infection Control & Hospital Epidemiology 43(1) (2022) 64-71.

[7] E.C. Rodriguez-Merchan, A.D. Delgado-Martinez, Risk factors for periprosthetic joint infection after primary total knee arthroplasty, Journal of Clinical Medicine 11(20) (2022) 6128.

[8] Y. Xu, T.B. Huang, M.A. Schuetz, P.F. Choong, Mortality, patient-reported outcome measures, and the health economic burden of prosthetic joint infection, EFORT Open Reviews 8(9) (2023) 690-697.

[9] Y. Lu, W.-j. Cai, Z. Ren, P. Han, The role of staphylococcal biofilm on the surface of implants in orthopedic infection, Microorganisms 10(10) (2022) 1909.

[10] K.E. Fish, A.M. Osborn, J. Boxall, Characterising and understanding the impact of microbial biofilms and the extracellular polymeric substance (EPS) matrix in drinking water distribution systems, Environmental science: water research & technology 2(4) (2016) 614-630.

[11] A.G. Abdelhamid, A.E. Yousef, Combating bacterial biofilms: current and emerging antibiofilm strategies for treating persistent infections, Antibiotics 12(6) (2023) 1005.

[12] H.-C. Flemming, E.D. van Hullebusch, B.J. Little, T.R. Neu, P.H. Nielsen, T. Seviour, P. Stoodley, J. Wingender, S. Wuertz, Microbial extracellular polymeric substances in the environment, technology and medicine, Nature Reviews Microbiology 23(2) (2025) 87-105.

[13] A.S. Pugazhendhi, F. Wei, M. Hughes, M. Coathup, Bacterial adhesion, virulence, and biofilm formation, Musculoskeletal Infection, Springer2022, pp. 19-64.

[14] J.G.S. Souza, M.M. Bertolini, R.C. Costa, B.E. Nagay, A. Dongari-Bagtzoglou, V.A.R. Barão, Targeting implant-associated infections: titanium surface loaded with antimicrobial, IScience 24(1) (2021).

[15] G. Pietrocola, D. Campoccia, C. Motta, L. Montanaro, C.R. Arciola, P. Speziale, Colonization and infection of indwelling medical devices by Staphylococcus aureus with an emphasis on orthopedic implants, International journal of molecular sciences 23(11) (2022) 5958.

[16] I.V. Chebotar, M.A. Emelyanova, J.A. Bocharova, N.A. Mayansky, E.E. Kopantseva, V.M. Mikhailovich, The classification of bacterial survival strategies in the presence of antimicrobials, Microbial Pathogenesis 155 (2021) 104901.

[17] P. Shree, C.K. Singh, K.K. Sodhi, J.N. Surya, D.K. Singh, Biofilms: Understanding the structure and contribution towards bacterial resistance in antibiotics, Medicine in Microecology 16 (2023) 100084.

[18] K. Sauer, P. Stoodley, D.M. Goeres, L. Hall-Stoodley, M. Burmølle, P.S. Stewart, T. Bjarnsholt, The biofilm life cycle: expanding the conceptual model of biofilm formation, Nature Reviews Microbiology 20(10) (2022) 608-620.

[19] F. Baquero, J.L. Martinez, V. F. Lanza, J. Rodríguez-Beltrán, J.C. Galán, A. San Millán, R. Cantón, T.M. Coque, Evolutionary pathways and trajectories in antibiotic resistance, Clinical Microbiology Reviews 34(4) (2021) e00050-19.

[20] A. Schulze, F. Mitterer, J.P. Pombo, S. Schild, Biofilms by bacterial human pathogens: Clinical relevance-development, composition and regulation-therapeutical strategies, Microbial Cell 8(2) (2021) 28.

[21] S.W. Lee, K.S. Phillips, H. Gu, M. Kazemzadeh-Narbat, D. Ren, How microbes read the map: Effects of implant topography on bacterial adhesion and biofilm formation, Biomaterials 268 (2021) 120595.

[22] D.A. Mosselhy, M. Assad, T. Sironen, M. Elbahri, Nanotheranostics: a possible solution for drug-resistant Staphylococcus aureus and their biofilms?, Nanomaterials 11(1) (2021) 82.

[23] G.Y. Cheung, J.S. Bae, M. Otto, Pathogenicity and virulence of Staphylococcus aureus, Virulence 12(1) (2021) 547-569.

[24] J. Murugaiyan, P.A. Kumar, G.S. Rao, K. Iskandar, S. Hawser, J.P. Hays, Y. Mohsen, S. Adukkadukkam, W.A. Awuah, R.A.M. Jose, Progress in alternative strategies to combat antimicrobial resistance: focus on antibiotics, Antibiotics 11(2) (2022) 200.

[25] P.P. Kalelkar, M. Riddick, A.J. García, Biomaterial-based antimicrobial therapies for the treatment of bacterial infections, Nature Reviews Materials 7(1) (2022) 39-54.

[26] R.S. Wallis, A. O'Garra, A. Sher, A. Wack, Host-directed immunotherapy of viral and bacterial infections: past, present and future, Nature Reviews Immunology 23(2) (2023) 121-133.

[27] M.A.-H. Gepreel, M. Niinomi, Biocompatibility of Ti-alloys for long-term implantation, Journal of the mechanical behavior of biomedical materials 20 (2013) 407-415.

[28] S. Kligman, Z. Ren, C.-H. Chung, M.A. Perillo, Y.-C. Chang, H. Koo, Z. Zheng, C. Li, The impact of dental implant surface modifications on osseointegration and biofilm formation, Journal of clinical medicine 10(8) (2021) 1641.

[29] P.M. Giraldo Osorno, On targeting host-pathogen interaction to prevent biomaterial-associated infections on titanium implants, 2024.

[30] M. Mu, S. Liu, W. DeFlorio, L. Hao, X. Wang, K.S. Salazar, M. Taylor, A. Castillo, L. Cisneros-Zevallos, J.K. Oh, Influence of surface roughness, nanostructure, and wetting on bacterial adhesion, Langmuir 39(15) (2023) 5426-5439.

[31] Z. Liu, X. Liu, S. Ramakrishna, Surface engineering of biomaterials in orthopedic and dental implants: Strategies to improve osteointegration, bacteriostatic and bactericidal activities, Biotechnology journal 16(7) (2021) 2000116.

[32] Y. Fu, S. Zhang, Q. Yue, Z. An, M. Zhao, C. Zhao, X. Sun, K. Li, B. Li, L. Zhao, The preventative effects of Lactococcus Lactis metabolites against LPS-induced sepsis, Frontiers in Microbiology 15 (2024) 1404652.

[33] M.I. Hofstee, A. Heider, S. Häckel, C. Constant, M. Riool, R.G. Richards, T.F. Moriarty, S.A. Zaat, In vitro 3d staphylococcus aureus abscess communities induce bone marrow cells to expand into myeloid-derived suppressor cells, Pathogens 10(11) (2021) 1446.

[34] S. Gordon, A. Plüddemann, F. Martinez Estrada, Macrophage heterogeneity in tissues: phenotypic diversity and functions, Immunological reviews 262(1) (2014) 36-55.

[35] A.D. Foey, Macrophages—masters of immune activation, suppression and deviation, Immune response activation 276 (2014).

[36] J.O. Abaricia, N. Farzad, T.J. Heath, J. Simmons, L. Morandini, R. Olivares-Navarrete, Control of innate immune response by biomaterial surface topography, energy, and stiffness, Acta Biomaterialia 133 (2021) 58-73.

[37] T. Albrektsson, P. Tengvall, L. Amengual, P. Coli, G. Kotsakis, D. Cochran, Osteoimmune regulation underlies oral implant osseointegration and its perturbation, Frontiers in immunology 13 (2023) 1056914.

[38] A. Mamilos, L. Winter, V.H. Schmitt, F. Barsch, D. Grevenstein, W. Wagner, M. Babel, K. Keller, C. Schmitt, F. Gürtler, Macrophages: from simple phagocyte to an integrative regulatory cell for inflammation and tissue regeneration—a review of the literature, Cells 12(2) (2023) 276.

[39] M. Li, Q. Hou, L. Zhong, Y. Zhao, X. Fu, Macrophage related chronic inflammation in non-healing wounds, Frontiers in Immunology 12 (2021) 681710.

[40] J. Li, X. Jiang, H. Li, M. Gelinsky, Z. Gu, Tailoring materials for modulation of macrophage fate, Advanced Materials 33(12) (2021) 2004172.

[41] A. Miron, C. Giurcaneanu, M.M. Mihai, C. Beiu, V.M. Voiculescu, M.N. Popescu, E. Soare, L.G. Popa, Antimicrobial biomaterials for chronic wound care, Pharmaceutics 15(6) (2023) 1606.

[42] M. Li, J. Yu, G. Guo, H. Shen, Interactions between macrophages and biofilm during Staphylococcus aureus-associated implant infection: difficulties and solutions, Journal of Innate Immunity 15(1) (2023) 499-515.

[43] B.D. Gimza, J.E. Cassat, Mechanisms of antibiotic failure during Staphylococcus aureus osteomyelitis, Frontiers in immunology 12 (2021) 638085.

[44] A. van Belkum, C. Almeida, B. Bardiaux, S.V. Barrass, S.J. Butcher, T. Çaykara, S. Chowdhury, R. Datar, I. Eastwood, A. Goldman, Host-pathogen adhesion as the basis of innovative diagnostics for emerging pathogens, Diagnostics 11(7) (2021) 1259.

[45] A. Yarilina, K. Xu, J. Chen, L.B. Ivashkiv, TNF activates calcium–nuclear factor of activated T cells (NFAT) c1 signaling pathways in human macrophages, Proceedings of the National Academy of Sciences 108(4) (2011) 1573-1578.

[46] H. Khalaf, J. Jass, P.-E. Olsson, Differential cytokine regulation by NF-κB and AP-1 in Jurkat T-cells, BMC immunology 11(1) (2010) 26.

[47] F. Macian, C. López-Rodríguez, A. Rao, Partners in transcription: NFAT and AP-1, Oncogene 20(19) (2001) 2476-2489.

[48] L. Yang, N. Mih, A. Anand, J.H. Park, J. Tan, J.T. Yurkovich, J.M. Monk, C.J. Lloyd, T.E. Sandberg, S.W. Seo, Cellular responses to reactive oxygen species are predicted from molecular mechanisms, Proceedings of the National Academy of Sciences 116(28) (2019) 14368-14373.

[49] M. Pitchai, D. Ipe, S. Tadakamadla, S. Hamlet, Titanium implant surface effects on adherent macrophage phenotype: a systematic review, Materials 15(20) (2022) 7314.

[50] S. Chen, J.A. Jones, Y. Xu, H.-Y. Low, J.M. Anderson, K.W. Leong, Characterization of topographical effects on macrophage behavior in a foreign body response model, Biomaterials 31(13) (2010) 3479-3491.

[51] N. Wang, H. Liang, K. Zen, Molecular mechanisms that influence the macrophage M1–M2 polarization balance, Frontiers in immunology 5 (2014) 614.

[52] F. Batool, H. Özçelik, C. Stutz, P.-Y. Gegout, N. Benkirane-Jessel, C. Petit, O. Huck, Modulation of immune-inflammatory responses through surface modifications of biomaterials to promote bone healing and regeneration, Journal of Tissue Engineering 12 (2021) 20417314211041428.

[53] M. Smyth, J. Martin, x Ray crystallography, Molecular Pathology 53(1) (2000) 8.

[54] J.L. Milne, M.J. Borgnia, A. Bartesaghi, E.E. Tran, L.A. Earl, D.M. Schauder, J. Lengyel, J. Pierson, A. Patwardhan, S. Subramaniam, Cryo-electron microscopy–a primer for the non-microscopist, The FEBS journal 280(1) (2013) 28-45.

[55] K. Moffat, E.E. Lattman, Dynamics and kinetics in structural biology: unravelling function through time-resolved structural analysis, John Wiley & Sons2023.

[56] S. Martinez-Martinez, J.M. Redondo, Inhibitors of the calcineurin/NFAT pathway, Current medicinal chemistry 11(8) (2004) 997-1007.

[57] C.-R. Jan, C.-J. Tseng, Mechanisms of nordihydroguaiaretic acid-induced [Ca2+], increases in MDCK cells, Life Sciences 66(18) (2000) 1753-1762.

[58] V. Atsaves, V. Leventaki, G.Z. Rassidakis, F.X. Claret, AP-1 transcription factors as regulators of immune responses in cancer, Cancers 11(7) (2019) 1037.

[59] A. Neuprez, A.H. Neuprez, J.-F. Kaux, W. Kurth, C. Daniel, T. Thirion, J.-P. Huskin, P. Gillet, O. Bruyère, J.-Y. Reginster, Total joint replacement improves pain, functional quality of life, and health

utilities in patients with late-stage knee and hip osteoarthritis for up to 5 years, Clinical rheumatology 39(3) (2020) 861-871.

[60] R. Fejer, A. Ruhe, What is the prevalence of musculoskeletal problems in the elderly population in developed countries? A systematic critical literature review, Chiropractic & manual therapies 20(1) (2012) 31.

[61] R. Dellink, J. Chateau, E. Lanzi, B. Magné, Long-term economic growth projections in the Shared Socioeconomic Pathways, Global Environmental Change 42 (2017) 200-214.

[62] G. Basile, M. Gallina, A. Passeri, R.M. Gaudio, N. Castelnuovo, P. Ferrante, G.M. Calori, Prosthetic joint infections and legal disputes: a threat to the future of prosthetic orthopedics, Journal of Orthopaedics and Traumatology 22(1) (2021) 44.

[63] S.H. Dougherty, Pathobiology of infection in prosthetic devices, Clinical Infectious Diseases 10(6) (1988) 1102-1117.

[64] A.S. Ooi, D.H. Song, Reducing infection risk in implant-based breast-reconstruction surgery: challenges and solutions, Breast Cancer: Targets and Therapy (2016) 161-172.

[65] A. Almatroudi, Biofilm resilience: Molecular mechanisms driving antibiotic resistance in clinical contexts, Biology 14(2) (2025) 165.

[66] C.-Y. Chiang, I. Uzoma, R.T. Moore, M. Gilbert, A.J. Duplantier, R.G. Panchal, Mitigating the impact of antibacterial drug resistance through host-directed therapies: current progress, outlook, and challenges, MBio 9(1) (2018) 10.1128/mbio. 01932-17.

[67] M.-A. Malahias, A. Gu, E.C. Harris, M. Adriani, A.O. Miller, G.H. Westrich, P.K. Sculco, The role of long-term antibiotic suppression in the management of peri-prosthetic joint infections treated with debridement, antibiotics, and implant retention: a systematic review, The Journal of arthroplasty 35(4) (2020) 1154-1160.

[68] P.M. Kou, J.E. Babensee, Macrophage and dendritic cell phenotypic diversity in the context of biomaterials, Journal of biomedical materials research Part A 96(1) (2011) 239-260.

[69] S. Amin Yavari, S.M. Castenmiller, J.A. van Strijp, M. Croes, Combating implant infections: shifting focus from bacteria to host, Advanced Materials 32(43) (2020) 2002962.

[70] J. Li, L. Zhang, J. Peng, C. Zhao, W. Li, Y. Yu, X. Huang, F. Yang, X. Deng, X. Yang, Mitochondrial metabolic regulation of macrophage polarization in osteomyelitis and other orthopedic disorders: mechanisms and therapeutic opportunities, Frontiers in Cell and Developmental Biology 13 (2025) 1604320.

[71] M. Luo, F. Zhao, H. Cheng, M. Su, Y. Wang, Macrophage polarization: an important role in inflammatory diseases, Frontiers in immunology 15 (2024) 1352946.

[72] D. Losic, Advancing of titanium medical implants by surface engineering: recent progress and challenges, Expert opinion on drug delivery 18(10) (2021) 1355-1378.

[73] L. Branca Vergano, M. Monesi, Bone Infections, Textbook of Emergency General Surgery: Traumatic and Non-traumatic Surgical Emergencies, Springer2023, pp. 1689-1712.

[74] C.R. Arciola, D. Campoccia, L. Montanaro, Implant infections: adhesion, biofilm formation and immune evasion, Nature reviews microbiology 16(7) (2018) 397-409.

[75] P. Di Martino, Extracellular polymeric substances, a key element in understanding biofilm phenotype, AIMS microbiology 4(2) (2018) 274.

[76] E. Roch, J. Ducrocq, N. Jacquier, Recent advances in the understanding, detection and therapeutic targeting of bacterial recalcitrance, BMC microbiology 25(1) (2025) 488.

[77] D. Lebeaux, J.-M. Ghigo, C. Beloin, Biofilm-related infections: bridging the gap between clinical management and fundamental aspects of recalcitrance toward antibiotics, Microbiology and Molecular Biology Reviews 78(3) (2014) 510-543.

[78] B.F. Ricciardi, G. Muthukrishnan, E. Masters, M. Ninomiya, C.C. Lee, E.M. Schwarz, Staphylococcus aureus evasion of host immunity in the setting of prosthetic joint infection: biofilm and beyond, Current reviews in musculoskeletal medicine 11(3) (2018) 389-400.

[79] A. Do Vale, D. Cabanes, S. Sousa, Bacterial toxins as pathogen weapons against phagocytes, Frontiers in microbiology 7 (2016) 42.

[80] A. Thakur, H. Mikkelsen, G. Jungersen, Intracellular pathogens: host immunity and microbial persistence strategies, Journal of immunology research 2019(1) (2019) 1356540.

[81] E. Seebach, K.F. Kubatzky, Chronic implant-related bone infections—can immune modulation be a therapeutic strategy?, Frontiers in immunology 10 (2019) 1724.

[82] R. Laxminarayan, A. Duse, C. Wattal, A.K. Zaidi, H.F. Wertheim, N. Sumpradit, E. Vlieghe, G.L. Hara, I.M. Gould, H. Goossens, Antibiotic resistance—the need for global solutions, The Lancet infectious diseases 13(12) (2013) 1057-1098.

[83] C. Maden, M. Jaibaji, S. Konan, L. Zagra, M. Borella, A. Harvey, A. Volpin, The outcomes of surgical management of failed two-stage revision knee arthroplasty, Acta Bio Medica: Atenei Parmensis 92(3) (2021) e2021197.

[84] L.M. Zhang, M.A. Hornor, T. Robinson, R.A. Rosenthal, C.Y. Ko, M.M. Russell, Evaluation of postoperative functional health status decline among older adults, JAMA surgery 155(10) (2020) 950-958.

[85] M. Gonzalez Moreno, L. Lombardi, M. Di Luca, Antimicrobial peptides for the control of biofilm formation, Current topics in medicinal chemistry 17(17) (2017) 1965-1986.

[86] A.D. Politano, K.T. Campbell, L.H. Rosenberger, R.G. Sawyer, Use of silver in the prevention and treatment of infections: silver review, Surgical infections 14(1) (2013) 8-20.

[87] N. Bisht, N. Dwivedi, P. Kumar, M. Venkatesh, A.K. Yadav, D. Mishra, P. Solanki, N.K. Verma, R. Lakshminarayanan, S. Ramakrishna, Recent advances in copper and copper-derived materials for antimicrobial resistance and infection control, Current Opinion in Biomedical Engineering 24 (2022) 100408.

[88] M. Wang, T. Tang, Surface treatment strategies to combat implant-related infection from the beginning, Journal of orthopaedic translation 17 (2019) 42-54.

[89] I.A. van Hengel, M.W. Tierolf, L.E. Fratila-Apachitei, I. Apachitei, A.A. Zadpoor, Antibacterial titanium implants biofunctionalized by plasma electrolytic oxidation with silver, zinc, and copper: A systematic review, International journal of molecular sciences 22(7) (2021) 3800.

[90] V.A. Barão, R.C. Costa, J.A. Shibli, M. Bertolini, J.G.S. Souza, Emerging titanium surface modifications: The war against polymicrobial infections on dental implants, Brazilian dental journal 33(1) (2022) 1-12.

[91] Y. Luan, H.C. van der Mei, M. Dijk, G.I. Geertsema-Doornbusch, J. Atema-Smit, Y. Ren, H. Chen, H.J. Busscher, Polarization of macrophages, cellular adhesion, and spreading on bacterially contaminated gold nanoparticle-coatings in vitro, ACS Biomaterials Science & Engineering 6(2) (2020) 933-945.

[92] T.J. Foster, Colonization and infection of the human host by staphylococci: adhesion, survival and immune evasion, Veterinary dermatology 20(5-6) (2009) 456-470.

[93] J. Hirschfeld, Dynamic interactions of neutrophils and biofilms, Journal of oral microbiology 6(1) (2014) 26102.

[94] N. Germic, Z. Frangez, S. Yousefi, H.-U. Simon, Regulation of the innate immune system by autophagy: monocytes, macrophages, dendritic cells and antigen presentation, Cell Death & Differentiation 26(4) (2019) 715-727.

[95] L. Cosmi, L. Maggi, V. Santarlasci, F. Liotta, F. Annunziato, T helper cells plasticity in inflammation, Cytometry Part A 85(1) (2014) 36-42.

[96] J. Ruiz, I. Becker, CD8 cytotoxic T cells in cutaneous leishmaniasis, Parasite immunology 29(12) (2007) 671-678.

[97] X. Lai, C. Li, X. Tang, X. Luo, F. Wu, B. Huang, H. Li, Super-enhancers in immune system regulation: mechanisms, pathological reprogramming, and therapeutic opportunities, Frontiers in Immunology 16 (2025) 1652398.

[98] G. Shaghayegh, C. Cooksley, G. Bouras, B.S. Panchatcharam, S. Feizi, S. Javadian, M. Ramezanpour, K.A. Fenix, P.-J. Wormald, A.J. Psaltis, S. aureus biofilm properties correlate with immune B cell subset frequencies and severity of chronic rhinosinusitis, Clinical Immunology 263 (2024) 110221.

[99] T.C. Oliveira, M.S. Gomes, A.C. Gomes, The crossroads between infection and bone loss, Microorganisms 8(11) (2020) 1765.

[100] J. Kreuger, M. Phillipson, Targeting vascular and leukocyte communication in angiogenesis, inflammation and fibrosis, Nature Reviews Drug Discovery 15(2) (2016) 125-142.

[101] G.R. Pidwill, J.F. Gibson, J. Cole, S.A. Renshaw, S.J. Foster, The role of macrophages in Staphylococcus aureus infection, Frontiers in immunology 11 (2021) 620339.

[102] R.S. Flannagan, B. Heit, D.E. Heinrichs, Antimicrobial mechanisms of macrophages and the immune evasion strategies of Staphylococcus aureus, Pathogens 4(4) (2015) 826-868.

[103] G. Weiss, U.E. Schaible, Macrophage defense mechanisms against intracellular bacteria, Immunological reviews 264(1) (2015) 182-203.

[104] T. Li, J. Adams, P. Zhu, T. Zhang, F. Tu, A. Gravitte, X. Zhang, L. Liu, J. Casteel, V. Yakubenko, The role of heme in sepsis induced Kupffer cell PANoptosis and senescence, Cell Death & Disease 16(1) (2025) 284.

[105] F. Hou, K. Xiao, L. Tang, L. Xie, Diversity of macrophages in lung homeostasis and diseases, Frontiers in immunology 12 (2021) 753940.

[106] D. Kurotaki, T. Uede, T. Tamura, Functions and development of red pulp macrophages, Microbiology and immunology 59(2) (2015) 55-62.

[107] A. Mordelt, L.D. de Witte, Microglia-mediated synaptic pruning as a key deficit in neurodevelopmental disorders: Hype or hope?, Current opinion in neurobiology 79 (2023) 102674.

[108] F. Ginhoux, S. Jung, Monocytes and macrophages: developmental pathways and tissue homeostasis, Nature Reviews Immunology 14(6) (2014) 392-404.

[109] B. Liang, H. Wang, D. Wu, Z. Wang, Macrophage M1/M2 polarization dynamically adapts to changes in microenvironment and modulates alveolar bone remodeling after dental implantation, Journal of Leukocyte Biology 110(3) (2021) 433-447.

[110] R. Diez-Orejas, M.J. Feito, M. Cicuendez, L. Casarrubios, J.M. Rojo, M.T. Portolés, Graphene oxide nanosheets increase Candida albicans killing by pro-inflammatory and reparative peritoneal macrophages, Colloids and Surfaces B: Biointerfaces 171 (2018) 250-259.

[111] W. Hu, J. Lin, X. Lian, F. Yu, W. Liu, Y. Wu, X. Fang, X. Liang, W. Hao, M2a and M2b macrophages predominate in kidney tissues and M2 subpopulations were associated with the severity of disease of IgAN patients, Clinical Immunology 205 (2019) 8-15.

[112] K.M. Nuss, B. von Rechenberg, Biocompatibility issues with modern implants in bone-a review for clinical orthopedics, The open orthopaedics journal 2 (2008) 66.

[113] G. Zhu, G. Wang, J.J. Li, Advances in implant surface modifications to improve osseointegration, Materials Advances 2(21) (2021) 6901-6927.

[114] S. Tuikampee, P. Chaijareenont, P. Rungsiyakull, A. Yavirach, Titanium surface modification techniques to enhance osteoblasts and bone formation for dental implants: a narrative review on current advances, Metals 14(5) (2024) 515.

[115] E. Anbarzadeh, B. Mohammadi, Investigation of the Effects of Sandblasting, Acid Etching, and Anodizing Parameters in the SLA+ Anodizing on the Surface Treatment of Titanium Dental Implant Fixtures, Physics of Metals and Metallography 124(13) (2023) 1606-1619.

[116] M. Rahmati, E.A. Silva, J.E. Reseland, C.A. Heyward, H.J. Haugen, Biological responses to physicochemical properties of biomaterial surface, Chemical Society Reviews 49(15) (2020) 5178-5224.

[117] P.R.L. Dabare, A. Bachhuka, J.Y. Quek, L.F. Marsal, J. Hayball, K. Vasilev, Nano-Roughness-Mediated Macrophage Polarization for Desired Host Immune Response, Small Science 3(10) (2023) 2300080.

[118] M. Azuma, Fundamental mechanisms of host immune responses to infection, Journal of periodontal research 41(5) (2006) 361-373.

[119] A. Shapouri-Moghaddam, S. Mohammadian, H. Vazini, M. Taghadosi, S.A. Esmaeili, F. Mardani, B. Seifi, A. Mohammadi, J.T. Afshari, A. Sahebkar, Macrophage plasticity, polarization, and function in health and disease, Journal of cellular physiology 233(9) (2018) 6425-6440.

[120] C.D. Cerdeira, M.R. Brigagão, Targeting macrophage polarization in infectious diseases: M1/M2 functional profiles, immune signaling and microbial virulence factors, Immunological Investigations 53(7) (2024) 1030-1091.

[121] Y. Zhang, X. Cheng, J.A. Jansen, F. Yang, J.J. Van den Beucken, Titanium surfaces characteristics modulate macrophage polarization, Materials Science and Engineering: C 95 (2019) 143-151.

[122] A.A. Tarique, J. Logan, E. Thomas, P.G. Holt, P.D. Sly, E. Fantino, Phenotypic, functional, and plasticity features of classical and alternatively activated human macrophages, American journal of respiratory cell and molecular biology 53(5) (2015) 676-688.

[123] M. Orecchioni, Y. Ghosheh, A.B. Pramod, K. Ley, Macrophage polarization: different gene signatures in M1 (LPS+) vs. classically and M2 (LPS–) vs. alternatively activated macrophages, Frontiers in immunology 10 (2019) 1084.

[124] R. Tewari, S.R. Choudhury, S. Ghosh, V.S. Mehta, E. Sen, Involvement of TNFα-induced TLR4–NF-κB and TLR4–HIF-1α feed-forward loops in the regulation of inflammatory responses in glioma, Journal of molecular medicine 90(1) (2012) 67-80.

[125] C.V. Ramana, M.P. Gil, Y. Han, R.M. Ransohoff, R.D. Schreiber, G.R. Stark, Stat1-independent regulation of gene expression in response to IFN-γ, Proceedings of the National Academy of Sciences 98(12) (2001) 6674-6679.

[126] Q. Yang, Y. Shi, J. He, Z. Chen, The evolving story of macrophages in acute liver failure, Immunology letters 147(1-2) (2012) 1-9.

[127] E.M. O'Brien, K.L. Spiller, Pro-inflammatory polarization primes Macrophages to transition into a distinct M2-like phenotype in response to IL-4, Journal of leukocyte biology 111(5) (2022) 989-1000.

[128] P. Du, Q. Ma, J. Xiong, Y. Wang, F. Yang, F. Jin, Y.-F. Chen, Z.-Z. Shang, Z.-L. Chen, X. Zhou, Corilagin controls post-parasiticide schistosome egg-induced liver fibrosis by inhibiting Stat6 signalling pathway, bioRxiv (2018) 340299.

[129] X. Li, Y. Liu, Y. Tang, Z. Xia, Transformation of macrophages into myofibroblasts in fibrosis-related diseases: emerging biological concepts and potential mechanism, Frontiers in Immunology 15 (2024) 1474688.

[130] F. Macian, NFAT proteins: key regulators of T-cell development and function, Nature Reviews Immunology 5(6) (2005) 472-484.

[131] J. Fric, T. Zelante, A.Y. Wong, A. Mertes, H.-B. Yu, P. Ricciardi-Castagnoli, NFAT control of innate immunity, Blood, The Journal of the American Society of Hematology 120(7) (2012) 1380-1389.

[132] G.R. Casey, Monitoring Cell Signaling Events and Supramolecular Protein Assembly with Peptide-Based Fluorescent Probes, The University of Nebraska-Lincoln, 2019.

[133] S. Colin, G. Chinetti-Gbaguidi, B. Staels, Macrophage phenotypes in atherosclerosis, Immunological reviews 262(1) (2014) 153-166.

[134] S. Chen, A.F. Saeed, Q. Liu, Q. Jiang, H. Xu, G.G. Xiao, L. Rao, Y. Duo, Macrophages in immunoregulation and therapeutics, Signal transduction and targeted therapy 8(1) (2023) 207.

[135] D.R. Emlet, H. Gomez, J.A. Kellum, Pathogen-Associated Molecular Patterns, Damage-Associated Molecular Patterns, and Their Receptors in Acute Kidney Injury, Critical Care Nephrology, Elsevier2019, pp. 121-127. e3.

[136] Y. Wang, H. Liu, J. Zhao, Macrophage polarization induced by probiotic bacteria: a concise review, Probiotics and Antimicrobial Proteins 12(3) (2020) 798-808.

[137] J. Tan, L. Yang, H. Zhao, Y. Ai, L. Ren, F. Zhang, W. Dong, R. Shi, D. Sun, Y. Feng, The role of NFATc1/c-myc/PKM2/IL-10 axis in activating cervical cancer tumor-associated M2 macrophage polarization to promote cervical cancer progression, Experimental Cell Research 413(2) (2022) 113052.

[138] T. Xia, M. Zhang, W. Lei, R. Yang, S. Fu, Z. Fan, Y. Yang, T. Zhang, Advances in the role of STAT3 in macrophage polarization, Frontiers in immunology 14 (2023) 1160719.

[139] V. Ramirez-Carrozzi, T. Kerppola, Asymmetric recognition of nonconsensus AP-1 sites by Fos-Jun and Jun-Jun influences transcriptional cooperativity with NFAT1, Molecular and cellular biology 23(5) (2003) 1737-1749.

[140] J.C. Stroud, L. Chen, Structure of NFAT bound to DNA as a monomer, Journal of molecular biology 334(5) (2003) 1009-1022.

[141] L. Chen, J.M. Glover, P.G. Hogan, A. Rao, S.C. Harrison, Structure of the DNA-binding domains from NFAT, Fos and Jun bound specifically to DNA, Nature 392(6671) (1998) 42-48.

[142] L. Zhou, P. Su, X. Luo, X. Zhong, Q. Liu, Y. Su, C. Zeng, G. Li, Regorafenib Attenuates Osteoclasts Differentiation by Inhibiting the NF-κB, NFAT, ERK, and p38 Signaling Pathways, ACS omega 9(31) (2024) 33574-33593.

[143] C.-L. Chen, C.-C. Lee, F.-L. Liu, T.-C. Chen, A.A.A. Ali, D.-M. Chang, H.-S. Huang, Design, synthesis and SARs of novel salicylanilides as potent inhibitors of RANKL-induced osteoclastogenesis and bone resorption, European journal of medicinal chemistry 117 (2016) 70-84.

[144] Y.-J. Li, A. Kukita, T. Watanabe, T. Takano, P. Qu, K. Sanematsu, Y. Ninomiya, T. Kukita, Nordihydroguaiaretic acid inhibition of NFATc1 suppresses osteoclastogenesis and arthritis bone destruction in rats, Laboratory investigation 92(12) (2012) 1777-1787.

[145] A. Laupacis, P. Keown, R. Ulan, N. McKenzie, C. Stiller, Cyclosporin A: a powerful immunosuppressant, Canadian Medical Association Journal 126(9) (1982) 1041.

[146] M.A. Hooks, Tacrolimus, a new immunosuppressant—a review of the literature, Annals of Pharmacotherapy 28(4) (1994) 501-511.

[147] H. Yu, T.J. van Berkel, E.A. Biessen, Therapeutic potential of VIVIT, a selective peptide inhibitor of nuclear factor of activated T cells, in cardiovascular disorders, Cardiovasc Drug Rev 25(2) (2007) 175-87.

[148] M. Oriano, L. Zorzetto, G. Guagliano, F. Bertoglio, S. van Uden, L. Visai, P. Petrini, The Open Challenge of in vitro Modeling Complex and Multi-Microbial Communities in Three-Dimensional Niches, Front Bioeng Biotechnol 8 (2020) 539319.

[149] T. Bjarnsholt, M. Whiteley, K.P. Rumbaugh, P.S. Stewart, P.O. Jensen, N. Frimodt-Moller, The importance of understanding the infectious microenvironment, Lancet Infect Dis 22(3) (2022) e88-e92.

[150] P. Gupta, N. Rai, A. Verma, V. Gautam, Microscopy based methods for characterization, drug delivery, and understanding the dynamics of nanoparticles, Med Res Rev 44(1) (2024) 138-168.

[151] P.M. Jean Beltran, J.D. Federspiel, X. Sheng, I.M. Cristea, Proteomics and integrative omic approaches for understanding host-pathogen interactions and infectious diseases, Mol Syst Biol 13(3) (2017) 922.

[152] W. Abd-Elaziem, M.A. Darwish, A. Hamada, W.M. Daoush, Titanium-Based alloys and composites for orthopedic implants Applications: A comprehensive review, Materials & Design 241 (2024) 112850.

[153] G.T. El-Bassyouni, S.M. Mouneir, A.M. El-Shamy, Advances in surface modifications of titanium and its alloys: implications for biomedical and pharmaceutical applications, Multiscale and Multidisciplinary Modeling, Experiments and Design 8(5) (2025) 265.

[154] D.R. Long, A. Cifu, S.J. Salipante, R.G. Sawyer, K. Machutta, J.C. Alverdy, Preventing surgical site infections in the era of escalating antibiotic resistance and antibiotic stewardship, JAMA surgery 159(8) (2024) 949-956.

[155] J. Yi, Z. Chen, R. Li, Z. Xu, Y. Song, Q. Fan, J. Wang, W. Chai, Orthopedic Implant Infection Management: Prevention, Barrier Breakthrough, and Immunomodulation, ACS nano 19(30) (2025) 27009-27032.

[156] H. Amani, M. Alipour, E. Shahriari, J.M. Taboas, Immunomodulatory biomaterials: tailoring surface properties to mitigate foreign body reaction and enhance tissue regeneration, Advanced healthcare materials 13(29) (2024) 2401253.

[157] J.-D. Xue, J. Gao, A.-F. Tang, C. Feng, Shaping the immune landscape: Multidimensional environmental stimuli refine macrophage polarization and foster revolutionary approaches in tissue regeneration, Heliyon 10(17) (2024).

[158] C. Chen, Z. Xie, S. Yang, H. Wu, Z. Bi, Q. Zhang, Y. Xiao, Machine learning approach to investigating macrophage polarization on various titanium surface characteristics, Bme Frontiers 6 (2025) 0100.

[159] Q. Du, A. Dickinson, P. Nakuleswaran, S. Maghami, S. Alagoda, A.L. Hook, A.M. Ghaemmaghami, Targeting macrophage polarization for reinstating homeostasis following tissue damage, International Journal of Molecular Sciences 25(13) (2024) 7278.

[160] J.G. Souza, R.C. Costa, A.A. Sampaio, V.L. Abdo, B.E. Nagay, N. Castro, B. Retamal-Valdes, J.A. Shibli, M. Feres, V.A. Barao, Cross-kingdom microbial interactions in dental implant-related infections: is Candida albicans a new villain?, IScience 25(4) (2022).

[161] A. Skrzypczak-Wiercioch, K. Sałat, Lipopolysaccharide-induced model of neuroinflammation: mechanisms of action, research application and future directions for its use, Molecules 27(17) (2022) 5481.

[162] G. Tan, J. Xu, W.M. Chirume, J. Zhang, H. Zhang, X. Hu, Antibacterial and anti-inflammatory coating materials for orthopedic implants: a review, Coatings 11(11) (2021) 1401.

[163] C. Wang, F. Ge, F. Ge, Z. Xu, J. Jiang, Harnessing stem cell therapeutics in LPS-induced animal models: mechanisms, efficacies, and future directions, Stem Cell Research & Therapy 16(1) (2025) 176.

[164] W. Xuan, Q. Qu, B. Zheng, S. Xiong, G.-H. Fan, The chemotaxis of M1 and M2 macrophages is regulated by different chemokines, Journal of Leucocyte Biology 97(1) (2015) 61-69.

[165] R.L. Silverstein, M. Febbraio, CD36, a scavenger receptor involved in immunity, metabolism, angiogenesis, and behavior, Science signaling 2(72) (2009) re3-re3.

[166] A. Mantovani, A. Sica, S. Sozzani, P. Allavena, A. Vecchi, M. Locati, The chemokine system in diverse forms of macrophage activation and polarization, Trends in immunology 25(12) (2004) 677-686.

[167] F.O. Martinez, S. Gordon, The M1 and M2 paradigm of macrophage activation: time for reassessment, F1000prime reports 6 (2014) 13.

[168] G. Chinetti-Gbaguidi, M. Daoudi, M. Rosa, M. Vinod, L. Louvet, C. Copin, M. Fanchon, J. Vanhoutte, B. Derudas, L. Belloy, Human alternative macrophages populate calcified areas of atherosclerotic lesions and display impaired RANKL-induced osteoclastic bone resorption activity, Circulation research 121(1) (2017) 19-30.

[169] D. Yang, J. Tang, F. Xia, W. Zhou, Rough surface characterization parameter set and redundant parameter set for surface modeling and performance research, Materials 15(17) (2022) 5971.

[170] J. W. Nicholson, Titanium alloys for dental implants: A review, Prosthesis 2(2) (2020) 11.

[171] A.G. Harvey, E.W. Hill, A. Bayat, Designing implant surface topography for improved biocompatibility, Expert review of medical devices 10(2) (2013) 257-267.

[172] Z. Huo, W. Yang, J. Harati, A. Nene, F. Borghi, C. Piazzoni, P. Milani, S. Guo, M. Galluzzi, D. Boraschi, Biomechanics of macrophages on disordered surface nanotopography, ACS Applied Materials & Interfaces 16(21) (2024) 27164-27176.

[173] S. Shrivas, H. Samaur, V. Yadav, S.K. Boda, Soft and hard tissue integration around percutaneous bone-anchored titanium prostheses: toward achieving holistic biointegration, ACS Biomaterials Science & Engineering 10(4) (2024) 1966-1987.

[174] J. Chen, S. Mwenifumbo, C. Langhammer, J.P. McGovern, M. Li, A. Beye, W. Soboyejo, Cell/surface interactions and adhesion on Ti-6Al-4V: Effects of surface texture, Journal of Biomedical Materials Research Part B: Applied Biomaterials: An Official Journal of The Society for Biomaterials, The Japanese Society for Biomaterials, and The Australian Society for Biomaterials and the Korean Society for Biomaterials 82(2) (2007) 360-373.

[175] A. Alemifar, K. Burnette, B. Jandres, S. Hurt, H.M. Tse, J.L. Robinson, Electrospun Fiber Surface Roughness Modulates Human Monocyte-Derived Macrophage Phenotype, bioRxiv (2024).

[176] S.M. Hamlet, R.S. Lee, H.J. Moon, M.A. Alfarsi, S. Ivanovski, Hydrophilic titanium surface-induced macrophage modulation promotes pro-osteogenic signalling, Clinical Oral Implants Research 30(11) (2019) 1085-1096.

[177] A. Davoodvandi, R. Sahebnasagh, O. Mardanshah, Z. Asemi, M. Nejati, M.K. Shahrzad, H.R. Mirzaei, H. Mirzaei, Medicinal plants as natural polarizers of macrophages: phytochemicals and pharmacological effects, Current pharmaceutical design 25(30) (2019) 3225-3238.

[178] X. Tang, Q. Chen, M. Guo, Y. Wen, C. Jia, Y. Bu, T. Wang, Y. Zhang, W. Tang, Macrophage EP4 Deficiency Drives Atherosclerosis Progression via CD36-Mediated Lipid Uptake and M1 Polarization, Cells 14(13) (2025) 1021.

[179] K.A. Jablonski, S.A. Amici, L.M. Webb, J.d.D. Ruiz-Rosado, P.G. Popovich, S. Partida-Sanchez, M. Guerau-de-Arellano, Novel markers to delineate murine M1 and M2 macrophages, PloS one 10(12) (2015) e0145342.

[180] S. Liu, J. Liu, Y. Wang, F. Deng, Z. Deng, Oxidative Stress: Signaling Pathways, Biological Functions, and Disease, MedComm 6(7) (2025) e70268.

[181] Y. Kirmanidou, M. Sidira, M.-E. Drosou, V. Bennani, A. Bakopoulou, A. Tsouknidas, N. Michailidis, K. Michalakis, New Ti-alloys and surface modifications to improve the mechanical properties and the biological response to orthopedic and dental implants: A review, BioMed research international 2016(1) (2016) 2908570.

[182] K.O. Babaremu, J. Tien-Chien, P.O. Oladijo, E.T. Akinlabi, Mechanical, corrosion resistance properties and various applications of titanium and its alloys: a review, Revue des Composites et des Matériaux Avancés 32(1) (2022) 11.

[183] R.C. Silva, A. Agrelli, A.N. Andrade, C.L. Mendes-Marques, I.R. Arruda, L.R. Santos, N.F. Vasconcelos, G. Machado, Titanium dental implants: an overview of applied nanobiotechnology to improve biocompatibility and prevent infections, Materials 15(9) (2022) 3150.

[184] C.C. Barber, M. Burnham, O. Ojameruaye, M.D. McKee, A systematic review of the use of titanium versus stainless steel implants for fracture fixation, OTA International 4(3) (2021) e138.

[185] N. Filip, I. Radu, B. Veliceasa, C. Filip, M. Pertea, A. Clim, A.C. Pinzariu, I.C. Drochioi, R.L. Hilitanu, I.L. Serban, Biomaterials in orthopedic devices: current issues and future perspectives, Coatings 12(10) (2022) 1544.

[186] M. Kopec, A. Brodecki, G. Szczęsny, Z.L. Kowalewski, Microstructural analysis of fractured orthopedic implants, Materials 14(9) (2021) 2209.

[187] A. Kurup, P. Dhatrak, N. Khasnis, Surface modification techniques of titanium and titanium alloys for biomedical dental applications: A review, Materials Today: Proceedings 39 (2021) 84-90.

[188] A. Khaskhoussi, L. Calabrese, S. Patané, E. Proverbio, Effect of chemical surface texturing on the superhydrophobic behavior of micro–nano-roughened AA6082 surfaces, Materials 14(23) (2021) 7161.

[189] K. Yu, H. Shi, P. Zhang, Z. Yu, H. Yan, Q. Lu, Micro/nanoengineering of functionalized metal surfaces based on short/ultra-short-pulsed lasers: a review, Journal of Materials Science 59(5) (2024) 1819-1866.

[190] M. Mehdizadeh Allaf, H. Peerhossaini, Cyanobacteria: model microorganisms and beyond, Microorganisms 10(4) (2022) 696.

[191] Y. Kherabi, V. Zeller, Y. Kerroumi, V. Meyssonnier, B. Heym, O. Lidove, S. Marmor, Streptococcal and Staphylococcus aureus prosthetic joint infections: are they really different?, BMC Infectious Diseases 22(1) (2022) 555.

[192] B. Wang, Q. Wang, M. Hamushan, J. Yu, F. Jiang, M. Li, G. Guo, J. Tang, P. Han, H. Shen, Trends in microbiological epidemiology of orthopedic infections: a large retrospective study from 2008 to 2021, BMC Infectious Diseases 23(1) (2023) 567.

[193] K.J. Bozic, A.F. Kamath, K. Ong, E. Lau, S. Kurtz, V. Chan, T.P. Vail, H. Rubash, D.J. Berry, Comparative epidemiology of revision arthroplasty: failed THA poses greater clinical and economic burdens than failed TKA, Clinical Orthopaedics and Related Research® 473(6) (2015) 2131-2138.

[194] P. Sadoghi, A. Koutp, D.P. Prieto, M. Clauss, M.E. Kayaalp, M.T. Hirschmann, The projected economic burden and complications of revision hip and knee arthroplasties: Insights from national registry studies, Knee Surgery, Sports Traumatology, Arthroscopy (2025).

[195] C.F. Ibezim, K.J. Bozic, Revision Burden: Projections in the United States and Worldwide, Revision Total Hip Arthroplasty, Springer2025, pp. 3-12.

[196] R. Whitaker, B. Hernaez-Estrada, R.M. Hernandez, E. Santos-Vizcaino, K.L. Spiller, Immunomodulatory biomaterials for tissue repair, Chemical reviews 121(18) (2021) 11305-11335.

[197] E. Antmen, N.E. Vrana, V. Hasirci, The role of biomaterials and scaffolds in immune responses in regenerative medicine: macrophage phenotype modulation by biomaterial properties and scaffold architectures, Biomaterials science 9(24) (2021) 8090-8110.

[198] P. Sharma, A. Vijaykumar, J.V. Raghavan, S.R. Rananaware, A. Alakesh, J. Bodele, J.U. Rehman, S. Shukla, V. Wagde, S. Nadig, Particle uptake driven phagocytosis in macrophages and neutrophils enhances bacterial clearance, Journal of Controlled Release 343 (2022) 131-141.

[199] T.D. Ricketts, N. Prieto-Dominguez, P.S. Gowda, E. Ubil, Mechanisms of macrophage plasticity in the tumor environment: manipulating activation state to improve outcomes, Frontiers in immunology 12 (2021) 642285.

[200] S. Pérez, S. Rius-Pérez, Macrophage polarization and reprogramming in acute inflammation: a redox perspective, Antioxidants 11(7) (2022) 1394.

[201] Y. Cong, Y. Wang, T. Yuan, Z. Zhang, J. Ge, Q. Meng, Z. Li, S. Sun, Macrophages in aseptic loosening: characteristics, functions, and mechanisms, Frontiers in immunology 14 (2023) 1122057.

[202] N. Grotenhuis, H. Vd Toom, N. Kops, Y. Bayon, E. Deerenberg, I. Mulder, G. Van Osch, J. Lange, Y. Bastiaansen-Jenniskens, In vitro model to study the biomaterial-dependent reaction of macrophages in an inflammatory environment, Journal of British Surgery 101(8) (2014) 983-992.

[203] S.S. Malheiros, B.E. Nagay, M.M. Bertolini, E.D. de Avila, J.A. Shibli, J.G.S. Souza, V.A. Barao, Biomaterial engineering surface to control polymicrobial dental implant-related infections: focusing on disease modulating factors and coatings development, Expert Review of Medical Devices 20(7) (2023) 557-573.

[204] M. Yamada, T. Kimura, N. Nakamura, J. Watanabe, N. Kartikasari, X. He, W. Tiskratok, H. Yoshioka, H. Shinno, H. Egusa, Titanium nanosurface with a biomimetic physical microenvironment to induce endogenous regeneration of the periodontium, ACS applied materials & interfaces 14(24) (2022) 27703-27719.

[205] Y. Yang, T. Zhang, M. Jiang, X. Yin, X. Luo, H. Sun, Effect of the immune responses induced by implants in a integrated three-dimensional micro-nano topography on osseointegration, Journal of Biomedical Materials Research Part A 109(8) (2021) 1429-1440.

[206] B. Brüne, N. Dehne, N. Grossmann, M. Jung, D. Namgaladze, T. Schmid, A. von Knethen, A. Weigert, Redox control of inflammation in macrophages, Antioxidants & redox signaling 19(6) (2013) 595-637.

[207] K. Anselme, M. Bigerelle, Role of materials surface topography on mammalian cell response, International Materials Reviews 56(4) (2011) 243-266.

[208] M.A. Osman, R.A. Alamoush, E. Kushnerev, K.G. Seymour, D.C. Watts, J.M. Yates, Biological response of epithelial and connective tissue cells to titanium surfaces with different ranges of roughness: An in-vitro study, Dental Materials 38(11) (2022) 1777-1788.

[209] M. Benoit, B. Desnues, J.-L. Mege, Macrophage polarization in bacterial infections, The Journal of Immunology 181(6) (2008) 3733-3739.

[210] A. Mantovani, S.K. Biswas, M.R. Galdiero, A. Sica, M. Locati, Macrophage plasticity and polarization in tissue repair and remodelling, The Journal of pathology 229(2) (2013) 176-185.

[211] M. van Lookeren Campagne, C. Wiesmann, E.J. Brown, Macrophage complement receptors and pathogen clearance, Cellular microbiology 9(9) (2007) 2095-2102.

[212] J. Svensson, M.C. Jenmalm, A. Matussek, R. Geffers, G. Berg, J. Ernerudh, Macrophages at the fetal–maternal interface express markers of alternative activation and are induced by M-CSF and IL-10, The Journal of Immunology 187(7) (2011) 3671-3682.

[213] L. Quero, E. Hanser, T. Manigold, A.N. Tiaden, D. Kyburz, TLR2 stimulation impairs anti-inflammatory activity of M2-like macrophages, generating a chimeric M1/M2 phenotype, Arthritis research & therapy 19(1) (2017) 245.

[214] K.-T. Peng, C.-C. Hsieh, T.-Y. Huang, P.-C. Chen, H.-N. Shih, M.S. Lee, P.-J. Chang, Staphylococcus aureus biofilm elicits the expansion, activation and polarization of myeloid-derived suppressor cells in vivo and in vitro, PloS one 12(8) (2017) e0183271.

[215] E.O. Long, ICAM-1: getting a grip on leukocyte adhesion, The Journal of Immunology 186(9) (2011) 5021-5023.

[216] F. Shen, X. Tang, W. Cheng, Y. Wang, C. Wang, X. Shi, Y. An, Q. Zhang, M. Liu, B. Liu, Fosfomycin enhances phagocyte-mediated killing of Staphylococcus aureus by extracellular traps and reactive oxygen species, Scientific reports 6(1) (2016) 19262.

[217] N.H. Hajdamowicz, Hypoxia and Reactive Oxygen Species Modulate the Interaction Between Human Neutrophils and Staphylococcus aureus?, University of Sheffield, 2021.

[218] X. Zhang, C. Yang, T. Xi, J. Zhao, K. Yang, Surface roughness of Cu-bearing stainless steel affects its contact-killing efficiency by mediating the interfacial interaction with bacteria, ACS Applied Materials & Interfaces 13(2) (2021) 2303-2315.

[219] Y. You, X. Yu, J. Jiang, Z. Chen, Y.-X. Zhu, Y. Chen, H. Lin, J. Shi, Bacterial cell wall-specific nanomedicine for the elimination of Staphylococcus aureus and Pseudomonas aeruginosa through electron-mechanical intervention, Nature Communications 16(1) (2025) 2836.

[220] H. Li, X. Zhou, Y. Huang, B. Liao, L. Cheng, B. Ren, Reactive oxygen species in pathogen clearance: the killing mechanisms, the adaption response, and the side effects, Frontiers in microbiology 11 (2021) 622534.

[221] C. Bubici, S. Papa, C. Pham, F. Zazzeroni, G. Franzoso, The NF-kB-mediated control of ROS and JNK signaling, Histology and histopathology (2006).

[222] R.E. Roberts, M.B. Hallett, Neutrophil cell shape change: mechanism and signalling during cell spreading and phagocytosis, International journal of molecular sciences 20(6) (2019) 1383.

[223] M.B. Shrivastava, Regulation of NFATc3 stability by SUMO and E3 ubiquitin-ligases Trim39 and Trim17, Université Montpellier, 2020.

[224] K. Vishnoi, N. Viswakarma, A. Rana, B. Rana, Transcription factors in cancer development and therapy, Cancers 12(8) (2020) 2296.

[225] L.C.P. Dharshini, S. Vishnupriya, K.M. Sakthivel, R.R. Rasmi, Oxidative stress responsive transcription factors in cellular signalling transduction mechanisms, Cellular Signalling 72 (2020) 109670.

[226] S.-H. Im, A. Rao, Activation and deactivation of gene expression by Ca2+/calcineurin-NFAT-mediated signaling, Molecules and cells 18(1) (2004) 1-9.

[227] A.M. Grabiec, P.P. Tak, K.A. Reedquist, Function of histone deacetylase inhibitors in inflammation, Critical Reviews™ in Immunology 31(3) (2011).

[228] J. Cannons, Signal transduction by the T cell costimulatory receptor, 4-1BB, 2001.

[229] Z. Wang, P. Wang, Y. Li, H. Peng, Y. Zhu, N. Mohandas, J. Liu, Interplay between cofactors and transcription factors in hematopoiesis and hematological malignancies, Signal Transduction and Targeted Therapy 6(1) (2021) 24.

[230] P. Rudak, The impacts of psychological stress on innate-like invariant T cell survival, phenotype, and function, The University of Western Ontario (Canada), 2021.

[231] J. Fattori, N. de Carvalho Indolfo, J.C.L. de Oliveira Campos, N.B. Videira, A.V. Bridi, T.R. Doratioto, M. Alex, A.C.M. Figueira, Investigation of Interactions between DNA and Nuclear Receptors: A Review of the Most Used Methods, Nuclear Receptor Research 1(1) (2014) 1-20.

[232] I.N. Lone, High Resolution study of NF-kB-DNA Interactions, Ecole normale supérieure de lyon-ENS LYON, 2013.

[233] P.D. Leitner, I. Vietor, L.A. Huber, T. Valovka, Fluorescent thermal shift-based method for detection of NF-κB binding to double-stranded DNA, Scientific Reports 11(1) (2021) 2331.

[234] M.N. Mivelaz, Dynamic Chromatin Invasion and Remodeling by the Transcription Factor Rap1, EPFL, 2021.

[235] K.E. Hauser, Complementarity in the structure and dynamics of protein-DNA search and recognition: A multiscale modeling study, State University of New York at Stony Brook2016.

[236] J.B. Beusink, Label-free biomolecular interaction sensing on microarrays using surface plasmon resonance imaging, (2009).

[237] J. Arlett, E. Myers, M. Roukes, Comparative advantages of mechanical biosensors, Nature nanotechnology 6(4) (2011) 203-215.

[238] J.S. Shumaker-Parry, Quantitative aspects of SPR spectroscopy and SPR microscopy: Applications in protein binding to immobilized vesicles and dsDNA arrays, University of Washington2002.

[239] D. Hadavi, P. Han, M. Honing, Section 2-Ion mobility spectrometry-tandem mass spectrometry strategies for the on-line monitoring of a continuous microflow reaction, Strategies for molecular structure elucidation in static and dynamic systems 125.

[240] S. Ansari, Prerequisites and Software Installation, Building Computer Vision Applications Using Artificial Neural Networks: With Examples in OpenCV and TensorFlow with Python, Springer2023, pp. 1-13.

[241] W.L. DeLano, Pymol: An open-source molecular graphics tool, CCP4 Newsl. Protein Crystallogr 40(1) (2002) 82-92.

[242] M.C. Hasselluhn, D. Schlösser, L. Versemann, G.E. Schmidt, M. Ulisse, J. Oschwald, Z. Zhang, F. Hamdan, H. Xiao, W. Kopp, An NFATc1/SMAD3/cJUN complex restricted to SMAD4-deficient pancreatic cancer guides rational therapies, Gastroenterology 166(2) (2024) 298-312. e14.

[243] M. Ikehata, S. Siltanen, Numerical method for finding the convex hull of an inclusion in conductivity from boundary measurements, Inverse Problems 16(4) (2000) 1043.

[244] R. Gommers, P. Virtanen, E. Burovski, W. Weckesser, T.E. Oliphant, M. Haberland, D. Cournapeau, T. Reddy, P. Peterson, A. Nelson, scipy/scipy: SciPy 1.9. 0, Zenodo (2022).

[245] T. Mitsis, A. Efthimiadou, F. Bacopoulou, D. Vlachakis, G.P. Chrousos, E. Eliopoulos, Transcription factors and evolution: an integral part of gene expression, World Academy of Sciences Journal 2(1) (2020) 3-8.

[246] L. Song, S.-s.C. Huang, A. Wise, R. Castanon, J.R. Nery, H. Chen, M. Watanabe, J. Thomas, Z. Bar-Joseph, J.R. Ecker, A transcription factor hierarchy defines an environmental stress response network, Science 354(6312) (2016) aag1550.

[247] N. Ravindran, S. Kumar, R. S, M. CA, N. Thirunavookarasu S, S. CK, Recent advances in Surface Plasmon Resonance (SPR) biosensors for food analysis: A review, Critical Reviews in Food Science and Nutrition 63(8) (2023) 1055-1077.

[248] A. Lackner, Y. Qiu, E. Armanus, A.N.K. Macapagal, L. Leonidas, H. Xu, R. McNulty, Measuring Interactions Between Proteins and Small Molecules or Nucleic Acids, Current Protocols 4(7) (2024) e1105.

[249] A. Pepanian, P. Sommerfeld, R. Kasprzyk, T. Kühl, F.A. Binbay, C. Hauser, R. Löser, R. Wodtke, M. Bednarczyk, M. Chrominski, Fluorescence anisotropy assay with guanine nucleotides provides access to functional analysis of Gαi1 proteins, Analytical Chemistry 94(41) (2022) 14410-14418.

[250] W. Abd-Elaziem, M.A. Darwish, A. Hamada, W.M. Daoush, Titanium-Based alloys and composites for orthopedic implants Applications: A comprehensive review, Materials & Design (2024) 112850.

[251] V.R. Ramirez-Carrozzi, T.K. Kerppola, Dynamics of Fos-Jun-NFAT1 complexes, Proceedings of the National Academy of Sciences 98(9) (2001) 4893-4898.

[252] J. Seo, D.D. Koçak, L.C. Bartelt, C.A. Williams, A. Barrera, C.A. Gersbach, T.E. Reddy, AP-1 subunits converge promiscuously at enhancers to potentiate transcription, Genome research 31(4) (2021) 538-550.

[253] Y.-T. Li, Z.-Y. Shen, Y.-s. Ling, M.-Q. Duan, H.-Q. Ye, L.-F. Yang, Y.-G. Mai, Z.-G. Chen, NFATc1 is a Necessary Transcription Factor in Polarisation of T Helper Type 2 Lymphocytes Induced by Thymic Stromal Lymphopoietin, Annals of Clinical & Laboratory Science 49(6) (2019) 722-729.

[254] J. Tsukada, Y. Yoshida, Y. Kominato, P.E. Auron, The CCAAT/enhancer (C/EBP) family of basic-leucine zipper (bZIP) transcription factors is a multifaceted highly-regulated system for gene regulation, Cytokine 54(1) (2011) 6-19.

[255] J. Jain, E. Burgeon, T.M. Badalian, P.G. Hogan, A. Rao, A Similar DNA-binding Motif in NFAT Family Proteins and the Rel Homology Region (∗), Journal of Biological Chemistry 270(8) (1995) 4138-4145.

[256] M. Miller, The importance of being flexible: the case of basic region leucine zipper transcriptional regulators, Current protein and peptide science 10(3) (2009) 244-269.

[257] L. Ling, Divergent chromatin accessibility dynamics promote differentiated enhancer functions and morphological trait evolution, lmu, 2024.

[258] O.V. Bylino, A.N. Ibragimov, Y.V. Shidlovskii, Evolution of regulated transcription, Cells 9(7) (2020) 1675.

[259] J. Kaye, Integrating T cell activation signals to regulate gene expression through cyclosporin-sensitive NFAT, The Journal of Immunology 211(3) (2023) 323-324.

[260] B.R. Peterson, L.J. Sun, G.L. Verdine, A critical arginine residue mediates cooperativity in the contact interface between transcription factors NFAT and AP-1, Proceedings of the National Academy of Sciences 93(24) (1996) 13671-13676.

[261] D.A. Erlanson, M. Chytil, G.L. Verdine, The leucine zipper domain controls the orientation of AP-1 in the NFAT· AP-1· DNA complex, Chemistry & biology 3(12) (1996) 981-991.

[262] W. Chen, W. Lu, P.G. Wolynes, E.A. Komives, Single-molecule conformational dynamics of a transcription factor reveals a continuum of binding modes controlling association and dissociation, Nucleic Acids Research 49(19) (2021) 11211-11223.

[263] D. Resetca, D.J. Wilson, Characterizing rapid, activity-linked conformational transitions in proteins via sub-second hydrogen deuterium exchange mass spectrometry, The FEBS journal 280(22) (2013) 5616-5625.

[264] B. Schuler, W.A. Eaton, Protein folding studied by single-molecule FRET, Current opinion in structural biology 18(1) (2008) 16-26.

[265] Y. Hamuro, S.J. Coales, M.R. Southern, J.F. Nemeth-Cawley, D.D. Stranz, P.R. Griffin, Rapid analysis of protein structure and dynamics by hydrogen/deuterium exchange mass spectrometry, Journal of biomolecular techniques: JBT 14(3) (2003) 171.

[266] P.M. Das, K. Ramachandran, J. vanWert, R. Singal, Chromatin immunoprecipitation assay, Biotechniques 37(6) (2004) 961-969.

[267] O. Gallego, T. Specht, T. Brach, A. Kumar, A.-C. Gavin, M. Kaksonen, Detection and characterization of protein interactions in vivo by a simple live-cell imaging method, PLoS One 8(5) (2013) e62195.

[268] E.H. Ledet, B. Liddle, K. Kradinova, S. Harper, Smart implants in orthopedic surgery, improving patient outcomes: a review, Innovation and entrepreneurship in health (2018) 41-51.

[269] K. Eskandar, Smart orthopedic implants: the future of personalized joint replacement and monitoring, Гений ортопедии 31(3) (2025) 388-398.

[270] S. Kumari, S. Katiyar, Darshna, A. Anand, D. Singh, B.N. Singh, S.P. Mallick, A. Mishra, P. Srivastava, Design strategies for composite matrix and multifunctional polymeric scaffolds with enhanced bioactivity for bone tissue engineering, Frontiers in Chemistry 10 (2022) 1051678.

[271] D. Cai, W. Gao, Z. Li, Y. Zhang, L. Xiao, Y. Xiao, Current development of nano-drug delivery to target macrophages, Biomedicines 10(5) (2022) 1203.

[272] A. Dhall, J.Y. Tan, M.J. Oh, S. Islam, J. Kim, A. Kim, G. Hwang, A dental implant-on-a-chip for 3D modeling of host–material–pathogen interactions and therapeutic testing platforms, Lab on a Chip 22(24) (2022) 4905-4916.

[273] F. Jiang, Y. Chen, J. Yu, F. Zhang, Q. Liu, L. He, H. Musha, J. Du, B. Wang, P. Han, Repurposed Fenoprofen targeting SaeR attenuates Staphylococcus aureus virulence in implant-associated infections, ACS Central Science 9(7) (2023) 1354-1373.

[274] B. Li, T.J. Webster, Bacteria antibiotic resistance: New challenges and opportunities for implant-associated orthopedic infections, Journal of Orthopaedic Research® 36(1) (2018) 22-32.

[275] L. Zhong, Y.-H. Wang, S. Kahlfuss, M. Jishage, M. McDermott, J. Yang, A.Y. Tao, K. Hu, L. Noyer, D. Raphael, STIM1-mediated NFAT signaling synergizes with STAT1 to control T-bet expression and TH1 differentiation, Nature immunology (2025) 1-13.

[276] H. Zheng, Y. Liu, Y. Deng, Y. Li, S. Liu, Y. Yang, Y. Qiu, B. Li, W. Sheng, J. Liu, Recent advances of NFATc1 in rheumatoid arthritis-related bone destruction: mechanisms and potential therapeutic targets, Molecular Medicine 30(1) (2024) 20.

[277] D. Desai, S.V. Kantliwala, J. Vybhavi, R. Ravi, H. Patel, J. Patel, R. RAVI, Review of AlphaFold 3: transformative advances in drug design and therapeutics, Cureus 16(7) (2024).

[278] L. Cocea, Duplication of a region in the multiple cloning site of a plasmid vector to enhance cloning-mediated addition of restriction sites to a DNA fragment, Biotechniques 23(5) (1997) 814-816.

[279] C. Kerneur, C.E. Cano, D. Olive, Major pathways involved in macrophage polarization in cancer, Frontiers in immunology 13 (2022) 1026954.

[280] X. Li, C. Xiao, J. Yuan, X. Chen, Q. Li, F. Shen, Rhein-attenuates LPS-induced acute lung injury via targeting NFATc1/Trem2 axis, Inflammation Research 72(6) (2023) 1237-1255.

[281] Y. Xia, K. Inoue, Y. Du, S.J. Baker, E.P. Reddy, M.B. Greenblatt, B. Zhao, TGFβ reprograms TNF stimulation of macrophages towards a non-canonical pathway driving inflammatory osteoclastogenesis, Nature communications 13(1) (2022) 3920.

[282] K.J. Oestreich, H. Yoon, R. Ahmed, J.M. Boss, NFATc1 regulates PD-1 expression upon T cell activation, The Journal of Immunology 181(7) (2008) 4832-4839.

[283] J. Chae, Z. Wang, I. Gul, J. Ji, Z. Chen, P. Qin, pLDDT-Predictor: High-speed Protein Screening Using Transformer and ESM2, arXiv preprint arXiv:2410.21283 (2024).

[284] K.Y. Lee, M1 and M2 polarization of macrophages: a mini-review, Med Biol Sci Eng 2(1) (2019) 1-5.

[285] F. Menzies, F. Henriquez, J. Alexander, C. Roberts, Sequential expression of macrophage anti-microbial/inflammatory and wound healing markers following innate, alternative and classical activation, Clinical & Experimental Immunology 160(3) (2010) 369-379.

[286] Y. Yu, Z. Yue, M. Xu, M. Zhang, X. Shen, Z. Ma, J. Li, X. Xie, Macrophages play a key role in tissue repair and regeneration, PeerJ 10 (2022) e14053.

[287] Y. Oishi, I. Manabe, Macrophages in inflammation, repair and regeneration, International immunology 30(11) (2018) 511-528.

[288] M.J. Davis, T.M. Tsang, Y. Qiu, J.K. Dayrit, J.B. Freij, G.B. Huffnagle, M.A. Olszewski, Macrophage M1/M2 polarization dynamically adapts to changes in cytokine microenvironments in Cryptococcus neoformans infection, MBio 4(3) (2013) 10.1128/mbio. 00264-13.

[289] S. Mia, A. Warnecke, X.M. Zhang, V. Malmström, R.A. Harris, An optimized protocol for human M2 macrophages using M-CSF and IL-4/IL-10/TGF-β yields a dominant immunosuppressive phenotype, Scandinavian journal of immunology 79(5) (2014) 305-314.

[290] I. Kwiecień, M. Polubiec-Kownacka, D. Dziedzic, D. Wołosz, P. Rzepecki, J. Domagała-Kulawik, CD163 and CCR7 as markers for macrophage polarisation in lung cancer microenvironment, Central European Journal of Immunology 44(4) (2019) 395-402.

[291] M. Qin, L. Wang, F. Li, M. Yang, L. Song, F. Tian, A. Yukht, P.K. Shah, M.E. Rothenberg, B.G. Sharifi, Oxidized LDL activated eosinophil polarize macrophage phenotype from M2 to M1 through activation of CD36 scavenger receptor, Atherosclerosis 263 (2017) 82-91.

[292] S. Sarfraz, Bacterial adhesion on patient-specific implant materials, (2024).

[293] Y.-K. Lin, C.-T. Yeh, K.-T. Kuo, I.-H. Fong, V.K. Yadav, N.G. Kounis, P. Hu, M.-Y. Hung, Apolipoprotein (a)/lipoprotein (a)-induced oxidative-inflammatory α7-nAChR/p38 MAPK/IL-6/RhoA-GTP signaling axis and M1 macrophage polarization modulate inflammation-associated development of coronary artery spasm, Oxidative Medicine and Cellular Longevity 2022(1) (2022) 9964689.

[294] M. J. Worley, Immune evasion and persistence in enteric bacterial pathogens, Gut Microbes 15(1) (2023) 2163839.

[295] M. Naghib, A. Kariminik, M. Kazemi Arababadi, TLR2, as a pathogen recognition receptor, plays critical roles in hepatitis B outcome, Viral Immunology 35(1) (2022) 15-23.

[296] L. Tian, W. Zhou, X. Wu, Z. Hu, L. Qiu, H. Zhang, X. Chen, S. Zhang, Z. Lu, CTLs: killers of intracellular bacteria, Frontiers in Cellular and Infection Microbiology 12 (2022) 967679.

[297] M.C. Tanner, C. Fischer, G. Schmidmaier, P. Haubruck, Evidence-based uncertainty: do implant-related properties of titanium reduce the susceptibility to perioperative infections in clinical fracture management? A systematic review, Infection 49(5) (2021) 813-821.

[298] Y. Niu, Z. Wang, Y. Shi, L. Dong, C. Wang, Modulating macrophage activities to promote endogenous bone regeneration: Biological mechanisms and engineering approaches, Bioactive materials 6(1) (2021) 244-261.

[299] E.J. Mifsud, A.C. Tan, D.C. Jackson, TLR agonists as modulators of the innate immune response and their potential as agents against infectious disease, Frontiers in immunology 5 (2014) 79.

Appendix III-Supplementary material

Chapter 1 - Engineering implant surfaces for preventing orthopaedic infections

Tab. S1. Full reference list (n=106) of studies on implant surfaces, immune responses, and bacterial infections with publication and author country information.

No.	First Author	Full Title	Year	Journal / Publisher	Journal Country	First Author Country
1	Neuprez A	Total joint replacement improves pain, functional quality of life, and health utilities in patients with late-stage knee and hip osteoarthritis for up to 5 years	2020	Clinical Rheumatology (Springer)	Germany	Belgium
2	Fejer R	What is the prevalence of musculoskeletal problems in the elderly population in developed countries? A systematic critical literature review	2012	Chiropractic & Manual Therapies (BMC)	UK	Denmark
3	Jin W	Orthopedic implants	2019	Encyclopedia of Biomedical Engineering (Elsevier)	Netherlands	China
4	Dellink R	Long-term economic growth projections in the Shared Socioeconomic Pathways	2017	Global Environmental Change (Elsevier)	UK	Netherlands
5	Basile G	Prosthetic joint infections and legal disputes: a threat to the future of prosthetic orthopedics	2021	Journal of Orthopaedics and Traumatology (Springer)	Italy	Italy
6	Dougherty SH	Pathobiology of infection in prosthetic devices	1988	Clinical Infectious Diseases (Oxford Academic)	USA	USA
7	Ooi AS	Reducing infection risk in implant-based breast-reconstruction surgery: challenges and solutions	2016	Breast Cancer: Targets and Therapy (Dove Press)	New Zealand	USA
8	Pietrocola G	Colonization and infection of indwelling medical devices by *Staphylococcus aureus* with an emphasis on orthopedic implants	2022	International Journal of Molecular Sciences (MDPI)	Switzerland	Italy
9	Pugazhendhi AS	Bacterial adhesion, virulence, and biofilm formation	2022	Musculoskeletal Infection (Springer Book Chapter)	Switzerland	UK
10	Almatroudi A	Biofilm resilience: molecular mechanisms driving antibiotic resistance in clinical contexts	2025	Biology (MDPI)	Switzerland	Saudi Arabia

No.	First Author	Full Title	Year	Journal / Publisher	Journal Country	First Author Country
11	Chiang C-Y	Mitigating the impact of antibacterial drug resistance through host-directed therapies: current progress, outlook, and challenges	2018	mBio (ASM)	USA	USA
12	Malahias M-A	The role of long-term antibiotic suppression in the management of peri-prosthetic joint infections treated with debridement, antibiotics, and implant retention: a systematic review	2020	Journal of Arthroplasty (Elsevier)	USA	USA
13	Pitchai M	Titanium implant surface effects on adherent macrophage phenotype: a systematic review	2022	Materials (MDPI)	Switzerland	Australia
14	Kou PM	Macrophage and dendritic cell phenotypic diversity in the context of biomaterials	2011	Journal of Biomedical Materials Research Part A (Wiley)	USA	USA
15	Amin Yavari S	Combating implant infections: shifting focus from bacteria to host	2020	Advanced Materials (Wiley)	Germany	Netherlands
16	Li J	Mitochondrial metabolic regulation of macrophage polarization in osteomyelitis and other orthopedic disorders: mechanisms and therapeutic opportunities	2025	Frontiers in Cell and Developmental Biology	Switzerland	China
17	Luo M	Macrophage polarization: an important role in inflammatory diseases	2024	Frontiers in Immunology	Switzerland	China
18	Batool F	Modulation of immune-inflammatory responses through surface modifications of biomaterials to promote bone healing and regeneration	2021	Journal of Tissue Engineering (SAGE)	UK	France
19	Losic D	Advancing of titanium medical implants by surface engineering: recent progress and challenges	2021	Expert Opinion on Drug Delivery	UK	Australia
20	Dixit S	Surgical devices for biomedical implants	2024	Additive Manufacturing for Biomedical Applications (Springer Book)	Switzerland	India

No.	First Author	Full Title	Year	Journal / Publisher	Journal Country	First Author Country
21	Kalelkar PP	Biomaterial-based antimicrobial therapies for the treatment of bacterial infections	2022	Nature Reviews Materials	UK	USA
22	Branca Vergano L	Bone infections	2023	Textbook of Emergency General Surgery (Springer Book)	Switzerland	Italy
23	Li M	Interactions between macrophages and biofilm during *Staphylococcus aureus*-associated implant infection: difficulties and solutions	2023	Journal of Innate Immunity (Karger)	Switzerland	China
24	Arciola CR	Implant infections: adhesion, biofilm formation and immune evasion	2018	Nature Reviews Microbiology	UK	Italy
25	Di Martino P	Extracellular polymeric substances, a key element in understanding biofilm phenotype	2018	AIMS Microbiology	USA	France
No.	First Author	Full Title	Year	Journal / Publisher	Journal Country	First Author Country
26	Roch E	Recent advances in the understanding, detection and therapeutic targeting of bacterial recalcitrance	2025	BMC Microbiology	UK	France
27	Lebeaux D	Biofilm-related infections: bridging the gap between clinical management and fundamental aspects of recalcitrance toward antibiotics	2014	Microbiology and Molecular Biology Reviews (ASM)	USA	France
28	Ricciardi BF	Staphylococcus aureus evasion of host immunity in the setting of prosthetic joint infection: biofilm and beyond	2018	Current Reviews in Musculoskeletal Medicine (Springer)	USA	USA
29	Do Vale A	Bacterial toxins as pathogen weapons against phagocytes	2016	Frontiers in Microbiology	Switzerland	Portugal
30	Thakur A	Intracellular pathogens: host immunity and microbial persistence strategies	2019	Journal of Immunology Research (Hindawi/Wiley)	UK	Denmark
31	Seebach E	Chronic implant-related bone infections—can immune modulation be a therapeutic strategy?	2019	Frontiers in Immunology	Switzerland	Germany

No.	First Author	Full Title	Year	Journal / Publisher	Journal Country	First Author Country
32	Laxminarayan R	Antibiotic resistance—the need for global solutions	2013	The Lancet Infectious Diseases	UK	USA
33	Maden C	The outcomes of surgical management of failed two-stage revision knee arthroplasty	2021	Acta Bio Medica	Italy	UK
34	Zhang LM	Evaluation of postoperative functional health status decline among older adults	2020	JAMA Surgery	USA	USA
35	Gonzalez Moreno M	Antimicrobial peptides for the control of biofilm formation	2017	Current Topics in Medicinal Chemistry	Netherlands	Spain
36	Politano AD	Use of silver in the prevention and treatment of infections: silver review	2013	Surgical Infections	USA	USA
37	Bisht N	Recent advances in copper and copper-derived materials for antimicrobial resistance and infection control	2022	Current Opinion in Biomedical Engineering	Netherlands	India
38	Wang M	Surface treatment strategies to combat implant-related infection from the beginning	2019	Journal of Orthopaedic Translation	Hong Kong	China
39	van Hengel IA	Antibacterial titanium implants biofunctionalized by plasma electrolytic oxidation with silver, zinc, and copper: a systematic review	2021	International Journal of Molecular Sciences (MDPI)	Switzerland	Netherlands
40	Barão VA	Emerging titanium surface modifications: the war against polymicrobial infections on dental implants	2022	Brazilian Dental Journal	Brazil	Brazil
41	Luan Y	Polarization of macrophages, cellular adhesion, and spreading on bacterially contaminated gold nanoparticle-coatings in vitro	2020	ACS Biomaterials Science & Engineering	USA	Netherlands
42	Foster TJ	Colonization and infection of the human host by staphylococci: adhesion, survival and immune evasion	2009	Veterinary Dermatology	UK	Ireland
43	Hirschfeld J	Dynamic interactions of neutrophils and biofilms	2014	Journal of Oral Microbiology	Sweden	Germany
44	Germic N	Regulation of the innate immune system by autophagy: monocytes, macrophages,	2019	Cell Death & Differentiation	UK	Switzerland

No.	First Author	Full Title	Year	Journal / Publisher	Journal Country	First Author Country
		dendritic cells and antigen presentation				
45	Cosmi L	T helper cells plasticity in inflammation	2014	Cytometry Part A (Wiley)	USA	Italy
46	Ruiz J	CD8 cytotoxic T cells in cutaneous leishmaniasis	2007	Parasite Immunology (Wiley)	UK	Spain
47	Lai X	Super-enhancers in immune system regulation: mechanisms, pathological reprogramming, and therapeutic opportunities	2025	Frontiers in Immunology	Switzerland	China
48	Shaghayegh G	Staphylococcus aureus biofilm properties correlate with immune B cell subset frequencies and severity of chronic rhinosinusitis	2024	Clinical Immunology (Elsevier)	USA	Australia
49	Oliveira TC	The crossroads between infection and bone loss	2020	Microorganisms (MDPI)	Switzerland	Portugal
50	Kreuger J	Targeting vascular and leukocyte communication in angiogenesis, inflammation and fibrosis	2016	Nature Reviews Drug Discovery	UK	Sweden
51	Pidwill GR	The role of macrophages in Staphylococcus aureus infection	2021	Frontiers in Immunology	Switzerland	UK
52	Flannagan RS	Antimicrobial mechanisms of macrophages and the immune evasion strategies of Staphylococcus aureus	2015	Pathogens (MDPI)	Switzerland	Canada
53	Weiss G	Macrophage defense mechanisms against intracellular bacteria	2015	Immunological Reviews (Wiley)	Denmark	Austria
54	Li T	The role of heme in sepsis-induced Kupffer cell PANoptosis and senescence	2025	Cell Death & Disease (Springer Nature)	UK	China
55	Hou F	Diversity of macrophages in lung homeostasis and diseases	2021	Frontiers in Immunology	Switzerland	China
56	Kurotaki D	Functions and development of red pulp macrophages	2015	Microbiology and Immunology	Japan	Japan
57	Mordelt A	Microglia-mediated synaptic pruning as a key deficit in neurodevelopmental disorders: hype or hope?	2023	Current Opinion in Neurobiology	UK	Germany
58	Ginhoux F	Monocytes and macrophages: developmental pathways and tissue homeostasis	2014	Nature Reviews Immunology	UK	Singapore

No.	First Author	Full Title	Year	Journal / Publisher	Journal Country	First Author Country
59	Liang B	Macrophage M1/M2 polarization dynamically adapts to changes in microenvironment and modulates alveolar bone remodeling after dental implantation	2021	Journal of Leukocyte Biology	USA	China
60	Diez-Orejas R	Graphene oxide nanosheets increase Candida albicans killing by pro-inflammatory and reparative peritoneal macrophages	2018	Colloids and Surfaces B: Biointerfaces (Elsevier)	Netherlands	Spain
No.	First Author	Full Title	Year	Journal / Publisher	Journal Country	First Author Country
61	Hu W	M2a and M2b macrophages predominate in kidney tissues and M2 subpopulations were associated with the severity of disease of IgAN patients	2019	Clinical Immunology (Elsevier)	Netherlands	China
62	Nuss KM	Biocompatibility issues with modern implants in bone—a review for clinical orthopedics	2008	The Open Orthopaedics Journal	USA	Switzerland
63	Zhu G	Advances in implant surface modifications to improve osseointegration	2021	Materials Advances (RSC)	UK	China
64	Tuikampee S	Titanium surface modification techniques to enhance osteoblasts and bone formation for dental implants: a narrative review on current advances	2024	Metals (MDPI)	Switzerland	Thailand
65	Anbarzadeh E	Investigation of the Effects of Sandblasting, Acid Etching, and Anodizing Parameters in the SLA+ Anodizing on the Surface Treatment of Titanium Dental Implant Fixtures	2023	Physics of Metals and Metallography	Russia	Iran
66	Rahmati M	Biological responses to physicochemical properties of biomaterial surface	2020	Chemical Society Reviews	UK	Norway
67	Dabare PRL	Nano-Roughness-Mediated Macrophage Polarization for Desired Host Immune Response	2023	Small Science	Germany	Australia
68	Azuma M	Fundamental mechanisms of host immune responses to infection	2006	Journal of Periodontal Research	Switzerland	Japan

No.	First Author	Full Title	Year	Journal / Publisher	Journal Country	First Author Country
69	Shapouri-Moghaddam A	Macrophage plasticity, polarization, and function in health and disease	2018	Journal of Cellular Physiology	USA	Iran
70	Cerdeira CD	Targeting macrophage polarization in infectious diseases: M1/M2 functional profiles, immune signaling and microbial virulence factors	2024	Immunological Investigations	UK	Brazil
71	Zhang Y	Titanium surfaces characteristics modulate macrophage polarization	2019	Materials Science and Engineering: C	Netherlands	China
72	Tarique AA	Phenotypic, functional, and plasticity features of classical and alternatively activated human macrophages	2015	American Journal of Respiratory Cell and Molecular Biology	USA	Canada
73	Orecchioni M	Macrophage polarization: different gene signatures in M1 (LPS+) vs. classically and M2 (LPS–) vs. alternatively activated macrophages	2019	Frontiers in Immunology	Switzerland	Italy
74	Tewari R	Involvement of TNFα-induced TLR4–NF-κB and TLR4–HIF-1α feed-forward loops in the regulation of inflammatory responses in glioma	2012	Journal of Molecular Medicine	Germany	India
75	Ramana CV	Stat1-independent regulation of gene expression in response to IFN-γ	2001	Proceedings of the National Academy of Sciences	USA	USA
76	Yang Q	The evolving story of macrophages in acute liver failure	2012	Immunology Letters	Netherlands	China
77	O'Brien EM	Pro-inflammatory polarization primes macrophages to transition into a distinct M2-like phenotype in response to IL-4	2022	Journal of Leukocyte Biology	USA	USA
78	Du P	Corilagin controls post-parasiticide schistosome egg-induced liver fibrosis by inhibiting Stat6 signalling pathway	2018	bioRxiv (preprint)	USA	China
79	Wang N	Molecular mechanisms that influence the macrophage M1–M2 polarization balance	2014	Frontiers in Immunology	Switzerland	China
80	Li X	Transformation of macrophages into myofibroblasts in fibrosis-	2024	Frontiers in Immunology	Switzerland	China

No.	First Author	Full Title	Year	Journal / Publisher	Journal Country	First Author Country
		related diseases: emerging biological concepts and potential mechanism				
81	Yarilina A	TNF activates calcium–nuclear factor of activated T cells (NFAT) c1 signaling pathways in human macrophages	2011	Proceedings of the National Academy of Sciences	USA	USA
82	Macian F	NFAT proteins: key regulators of T-cell development and function	2005	Nature Reviews Immunology	UK	Spain
83	Fric J	NFAT control of innate immunity	2012	Blood	USA	Italy
84	Casey GR	Monitoring Cell Signaling Events and Supramolecular Protein Assembly with Peptide-Based Fluorescent Probes	2019	PhD Thesis, University of Nebraska-Lincoln	USA	USA
85	Colin S	Macrophage phenotypes in atherosclerosis	2014	Immunological Reviews (Wiley)	Denmark	Italy
86	Chen S	Macrophages in immunoregulation and therapeutics	2023	Signal Transduction and Targeted Therapy	UK	China
87	Emlet DR	Pathogen-Associated Molecular Patterns, Damage-Associated Molecular Patterns, and Their Receptors in Acute Kidney Injury	2019	Critical Care Nephrology (Elsevier)	Netherlands	USA
88	Wang Y	Macrophage polarization induced by probiotic bacteria: a concise review	2020	Probiotics and Antimicrobial Proteins	USA	China
89	Tan J	The role of NFATc1/c-myc/PKM2/IL-10 axis in activating cervical cancer tumor-associated M2 macrophage polarization to promote cervical cancer progression	2022	Experimental Cell Research	Netherlands	China
90	Xia T	Advances in the role of STAT3 in macrophage polarization	2023	Frontiers in Immunology	Switzerland	China
91	Ramirez-Carrozzi V	Asymmetric recognition of nonconsensus AP-1 sites by Fos-Jun and Jun-Jun influences transcriptional cooperativity with NFAT1	2003	Molecular and Cellular Biology	USA	USA
92	Stroud JC	Structure of NFAT bound to DNA as a monomer	2003	Journal of Molecular Biology	UK	USA

No.	First Author	Full Title	Year	Journal / Publisher	Journal Country	First Author Country
93	Chen L	Structure of the DNA-binding domains from NFAT, Fos and Jun bound specifically to DNA	1998	Nature	UK	USA
94	Martinez-Martinez S	Inhibitors of the calcineurin/NFAT pathway	2004	Current Medicinal Chemistry	UK	Spain
95	Zhou L	Regorafenib attenuates osteoclast differentiation by inhibiting the NF-κB, NFAT, ERK, and p38 signaling pathways	2024	ACS Omega	USA	China
96	Chen C-L	Design, synthesis and SARs of novel salicylanilides as potent inhibitors of RANKL-induced osteoclastogenesis and bone resorption	2016	European Journal of Medicinal Chemistry	Netherlands	Taiwan
97	Li Y-J	Nordihydroguaiaretic acid inhibition of NFATc1 suppresses osteoclastogenesis and arthritis bone destruction in rats	2012	Laboratory Investigation	USA	Japan
98	Jan C-R	Mechanisms of nordihydroguaiaretic acid-induced [Ca2+] increases in MDCK cells	2000	Life Sciences	Netherlands	Taiwan
99	Laupacis A	Cyclosporin A: a powerful immunosuppressant	1982	Canadian Medical Association Journal	Canada	Canada
100	Hooks MA	Tacrolimus, a new immunosuppressant—a review of the literature	1994	Annals of Pharmacotherapy	USA	USA
101	Yu H	Therapeutic potential of VIVIT, a selective peptide inhibitor of nuclear factor of activated T cells, in cardiovascular disorders	2007	Cardiovascular Drug Review	USA	Netherlands
102	Oriano M	The Open Challenge of in vitro Modeling Complex and Multi-Microbial Communities in Three-Dimensional Niches	2020	Frontiers in Bioengineering and Biotechnology	Switzerland	Italy
103	Günther J	Differentiating Staphylococcus aureus from Escherichia coli mastitis: S. aureus triggers unbalanced immune-dampening and host cell invasion immediately after udder infection	2017	Scientific Reports	UK	Germany

No.	First Author	Full Title	Year	Journal / Publisher	Journal Country	First Author Country
104	Bjarnsholt T	The importance of understanding the infectious microenvironment	2022	Lancet Infectious Diseases	UK	Denmark
105	Gupta P	Microscopy based methods for characterization, drug delivery, and understanding the dynamics of nanoparticles	2024	Med Res Rev	UK	India
106	Jean Beltran PM	Proteomics and integrative omic approaches for understanding host-pathogen interactions and infectious diseases	2017	Molecular Systems Biology	UK	USA

Chapter 2 - Surface roughness of titanium implants modulates macrophage inflammatory response

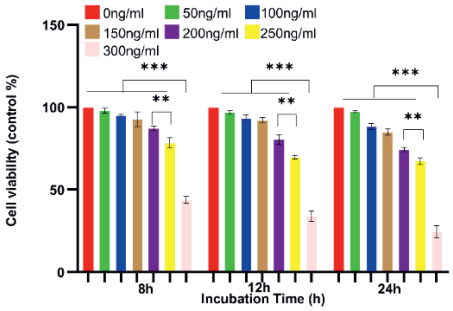


Fig. S1. Macrophage cell viability evaluation by CCK-8 assay. Macrophages were cultured in 96-well plates (control: cells cultured 96-well plates) and treated with a concentration gradient of LPS. Cell viability was assessed using the CCK-8 assay. Data show the mean ± SD, one way ANOVA was used to determine statistical significance (n=4, *p＜0.05; **p＜0.01; ***p＜0.001).

Tab. S1. Primers used for RT-PCR

Target gene	Forward primer	Reverse primer
GAPDH	GTCTCCTCTGACTTCAACAGCG	ACCACCCTGTTGCTGTAGCCAA
INDO	GCCTGATCTCATAGAGTCTGGC	TGCATCCCAGAACTAGACGTGC
CXCL11	AGCTTGCCTCAATCCTGCATCC	CAGATGCCCTTTTCCAGGACTTC
MCR-1	GGTTTATGGAGCAGGTGGAA	AAACTTGAACGGGAATGCAC
CCL13	GATCTCCTTGCAGAGGCTGAAG	TCTGGACCCACTTCTCCTTTGG
TNF-α	CTCTTCTGCCTGCTGCACTTTG	ATGGGCTACAGGCTTGTCACTC
IL-10	TCTCCGAGATGCCTTCAGCAGA	TCAGACAAGGCTTGGCAACCCA
NFATc1	CACCAAAGTCCTGGAGATCCCA	TTCTTCCTCCCGATGTCCGTCT
c-Jun	CCTTGAAAGCTCAGAACTCGGAG	TGCTGCGTTAGCATGAGTTGGC
c-Fos	GCCTCTCTTACTACCACTCACC	AGATGGCAGTGACCGTGGGAAT

Tab. S2. List of differentially abundant proteins identified (DAPs)

	Gene name	Protein name	Changes	p-value	Fold change
Control vs. Polished					
1	Dpysl2	DPYL2	UP	0.01	4.68
2	Itgb1	ITB1	UP	0.00	11.91
3	Anxa1	ANXA1	UP	0.05	2.81
4	Apex1	APEX1	UP	0.01	5.15
5	Pabpc1	PABP1	UP	0.05	2.86
6	Capza1	CAZA1	UP	0.03	3.20
7	Tbca	TBCA	UP	0.05	2.82
8	Atp6v1e1	VATE1	UP	0.00	8.18
9	Stmn1	STMN1	UP	0.04	3.07
10	Atp5f1e	ATP5E	UP	0.04	3.05
11	Timm10	TIM10	UP	0.03	3.46
12	Ppp2ca	PP2AA	UP	0.02	3.89
13	Srsf3	SRSF3	UP	0.02	3.66
14	Srsf3	SRSF3	UP	0.05	2.79
15	Tmpo	LAP2B	UP	0.04	2.91
16	Lasp1	LASP1	UP	0.04	3.12
17	Sh3gl1	SH3G1	UP	0.03	3.32
18	Nomo1	NOMO1	UP	0.03	3.46
19	Ppp2r1a	2AAA	UP	0.03	3.33
20	Mybbp1a	MBB1A	UP	0.04	3.02
21	Mtdh	LYRIC	UP	0.01	5.58
22	Ythdf3	YTHD3	UP	0.00	5.62
23	Cpne1	CPNE1	UP	0.01	4.60
24	Acat2	THIC	UP	0.01	5.58
25	Gnl3	GNL3	UP	0.04	2.94
26	Plcg2	PLCG2	UP	0.00	5.69
27	Prpf8	PRP8	UP	0.00	8.78
28	Tomm34	TOM34	UP	0.03	3.34
29	Akr1a1	AK1A1	UP	0.00	5.91
30	Qki	QKI	UP	0.05	2.87
31	Bag6	BAG6	UP	0.01	4.17
32	Uso1	USO1	UP	0.01	4.15
33	Hnrnpc	HNRPC	UP	0.00	7.34
34	Bin1	BIN1	DOWN	0.05	-2.79
35	Gsto1	GSTO1	DOWN	0.01	-4.64
36	Psmb9	PSB9	DOWN	0.04	-2.97
37	Get3	GET3	DOWN	0.01	-4.11
38	Pik3c2g	P3C2G	DOWN	0.04	-2.95
39	Snx12	SNX12	DOWN	0.00	-6.53
40	Hsd17b12	DHB12	DOWN	0.04	-3.00
41	Gcat	KBL	DOWN	0.02	-4.06
42	H2-D1	HA12	DOWN	0.01	-4.95
43	Pfkl	PFKAL	DOWN	0.05	-2.80
44	Cbx1	CBX1	DOWN	0.01	-4.84
45	Glb1	BGAL	DOWN	0.04	-3.11
46	Map4	MAP4	DOWN	0.04	-3.08
47	Adh5	ADHX	DOWN	0.00	-6.58
48	Dbi	ACBP	DOWN	0.04	-3.02
49	Serpinc1	ANT3	DOWN	0.03	-3.14
50	Rab6a	RAB6A	DOWN	0.00	-5.68
51	Rpl18	RL18	DOWN	0.05	-2.87
52	Hmgcl	HMGCL	DOWN	0.01	-4.33
53	Acsl1	ACSL1	DOWN	0.00	-6.99
54	Septin2	2-Sep	DOWN	0.02	-3.92
55	Nsf	NSF	DOWN	0.03	-3.47
56	Rpl13	RL13	DOWN	0.02	-3.87
57	Ahcy	SAHH	DOWN	0.05	-2.86
58	Lum	LUM	DOWN	0.00	-23.88
59	Ruvbl1	RUVB1	DOWN	0.01	-5.25
60	Eif4a1	IF4A1	DOWN	0.02	-3.82
61	Arl1	ARL1	DOWN	0.02	-3.74
62	Sumo2	SUMO2	DOWN	0.04	-3.11
63	Ppp1ca	PP1A	DOWN	0.02	-3.94
64	Ywhae	1433E	DOWN	0.04	-3.06
65	Rps11	RS11	DOWN	0.02	-3.65
66	Lsm3	LSM3	DOWN	0.02	-4.07
67	Snrpd3	SMD3	DOWN	0.04	-3.02
68	Ran	RAN	DOWN	0.01	-4.49

69	Ywhaq	1433T	DOWN	0.00	-11.35
70	Tuba4a	TBA4A	DOWN	0.03	-3.20
71	Tubb4b	TBB4B	DOWN	0.00	-7.48
72	Rhog	RHOG	DOWN	0.04	-3.05
73	Rps3a	RS3A	DOWN	0.02	-3.59
74	Uba1	UBA1	DOWN	0.03	-3.48
75	Eif5b	IF2P	DOWN	0.03	-3.16
76	Abracl	ABRAL	DOWN	0.05	-2.87
77	Ddx17	DDX17	DOWN	0.04	-2.93
78	Snrpc	RU1C	DOWN	0.01	-4.97
79	Kansl1	KANL1	DOWN	0.00	-6.41
80	Galnt7	GALT7	DOWN	0.00	-8.18
81	Ubap2l	UBP2L	DOWN	0.00	-9.23
82	Psmd11	PSD11	DOWN	0.05	-2.80
83	Ahsa1	AHSA1	DOWN	0.02	-4.05
84	Slc15a3	S15A3	DOWN	0.05	-2.87
85	Asph	ASPH	DOWN	0.02	-3.90
86	Acsl5	ACSL5	DOWN	0.04	-3.05
87	Amdhd2	NAGA	DOWN	0.03	-3.25
88	Ddx39a	DX39A	DOWN	0.03	-3.42
89	Hnrnpu	HNRPU	DOWN	0.01	-4.24
90	Far1	FACR1	DOWN	0.00	-7.99
91	Dpp3	DPP3	DOWN	0.03	-3.18
92	Tomm22	TOM22	DOWN	0.00	-6.24
93	Ppid	PPID	DOWN	0.04	-2.93
94	Nhp2	NHP2	DOWN	0.04	-2.90
95	Tpd52l2	TPD54	DOWN	0.03	-3.15
96	Pgm1	PGM1	DOWN	0.04	-2.89
97	Cyc1	CY1	DOWN	0.04	-2.99
98	U2af1	U2AF1	DOWN	0.02	-3.94
99	Eef1g	EF1G	DOWN	0.01	-4.67
100	Snx5	SNX5	DOWN	0.03	-3.20
101	Ampd2	AMPD2	DOWN	0.03	-3.30
102	Pycr3	P5CR3	DOWN	0.01	-4.22
103	Upf1	RENT1	DOWN	0.01	-5.50
104	Ehd4	EHD4	DOWN	0.04	-3.08
105	Dazap1	DAZP1	DOWN	0.01	-4.38
106	Usp14	UBP14	DOWN	0.04	-2.90
107	Psma6	PSA6	DOWN	0.04	-3.07
108	Psmb3	PSB3	DOWN	0.03	-3.21
109	Sae1	SAE1	DOWN	0.04	-3.13
110	Slc7a5	LAT1	DOWN	0.01	-4.72
Control vs. Plasma					
1	Dld	DLDH	UP	0.05	2.85
2	Aip	AIP	UP	0.04	2.96
3	Epb41l2	E41L2	UP	0.01	4.20
4	Aldoa	ALDOA	UP	0.04	3.04
5	P4hb	PDIA1	UP	0.04	2.97
6	Anxa1	ANXA1	UP	0.01	4.56
7	Cd44	CD44	UP	0.04	3.04
8	H1-1	H11	UP	0.02	4.00
9	Tpi1	TPIS	UP	0.02	3.78
10	Hspa1a	HS71A	UP	0.01	4.69
11	Marcksl1	MRP	UP	0.04	2.91
12	Capza1	CAZA1	UP	0.01	4.64
13	Srprb	SRPRB	UP	0.04	3.03
14	Tbca	TBCA	UP	0.04	2.95
15	Dbt	ODB2	UP	0.04	2.96
16	Rab10	RAB10	UP	0.03	3.39
17	Actr2	ARP2	UP	0.02	3.63
18	Rpl37a	RL37A	UP	0.02	3.93
19	Mtpn	MTPN	UP	0.00	24.51
20	Ybx1	YBOX1	UP	0.02	3.80
21	Hspd1	CH60	UP	0.04	3.07
22	Crip1	CRIP1	UP	0.05	2.85
23	Ppp2ca	PP2AA	UP	0.01	4.66
24	Hint1	HINT1	UP	0.05	2.83
25	Rpl36a	RL36A	UP	0.03	3.23
26	G3bp1	G3BP1	UP	0.04	2.93
27	Tubb5	TBB5	UP	0.05	2.81
28	Lbr	LBR	UP	0.00	11.40
29	Arcn1	COPD	UP	0.02	3.68
30	Tmpo	LAP2B	UP	0.02	3.96

31	Ddx19a	DD19A	UP	0.03	3.21
32	Trim28	TIF1B	UP	0.04	3.10
33	Tfrc	TFR1	UP	0.02	3.86
34	Sh3gl1	SH3G1	UP	0.01	4.55
35	Fkbp3	FKBP3	UP	0.03	3.23
36	Kctd12	KCD12	UP	0.04	2.93
37	Syncrip	HNRPQ	UP	0.02	3.55
38	Mybbp1a	MBB1A	UP	0.03	3.34
39	Cstf2	CSTF2	UP	0.03	3.21
40	Flna	FLNA	UP	0.03	3.33
41	Immt	MIC60	UP	0.05	2.81
42	Gnl3	GNL3	UP	0.05	2.87
43	Plcg2	PLCG2	UP	0.02	3.62
44	Shtn1	SHOT1	UP	0.04	2.92
45	Uhrf1	UHRF1	UP	0.03	3.30
46	Kars1	SYK	UP	0.04	3.05
47	Prpf8	PRP8	UP	0.00	8.91
48	Atp5f1d	ATPD	UP	0.03	3.49
49	Cars1	SYCC	UP	0.03	3.22
50	Tmod3	TMOD3	UP	0.04	2.89
51	Myg1	MYG1	UP	0.05	2.79
52	Mbnl1	MBNL1	UP	0.01	4.73
53	Macroh2a1	H2AY	UP	0.03	3.29
54	Uso1	USO1	UP	0.02	3.70
55	Suclg2	SUCB2	UP	0.03	3.18
56	Itih4	ITIH4	DOWN	0.01	-4.58
57	Prdx1	PRDX1	DOWN	0.02	-3.84
58	Gsto1	GSTO1	DOWN	0.00	-7.31
59	Dhx15	DHX15	DOWN	0.03	-3.25
60	Anp32a	AN32A	DOWN	0.04	-2.96
61	Get3	GET3	DOWN	0.01	-4.46
62	Impa1	IMPA1	DOWN	0.03	-3.19
63	Snx3	SNX3	DOWN	0.03	-3.16
64	Hsd17b12	DHB12	DOWN	0.02	-3.64
65	Wdr1	WDR1	DOWN	0.04	-2.91
66	Dync1i2	DC1I2	DOWN	0.03	-3.27
67	Gcat	KBL	DOWN	0.02	-4.07
68	Mtco2	COX2	DOWN	0.01	-4.55
69	Ldha	LDHA	DOWN	0.02	-3.95
70	S100a4	S10A4	DOWN	0.01	-5.01
71	S100a10	S10AA	DOWN	0.02	-3.64
72	Pgk1	PGK1	DOWN	0.03	-3.45
73	Sod2	SODM	DOWN	0.02	-3.70
74	Eef1a1	EF1A1	DOWN	0.03	-3.30
75	Sub1	TCP4	DOWN	0.02	-3.94
76	Cdk1	CDK1	DOWN	0.04	-2.99
77	Hsp90ab1	HS90B	DOWN	0.03	-3.15
78	Itgb2	ITB2	DOWN	0.03	-3.14
79	Dnmt1	DNMT1	DOWN	0.03	-3.16
80	Mdh1	MDHC	DOWN	0.02	-3.77
81	Rpsa	RSSA	DOWN	0.02	-3.95
82	Rplp0	RLA0	DOWN	0.04	-3.05
83	Nme1	NDKA	DOWN	0.03	-3.17
84	Nme1	NDKA	DOWN	0.04	-2.97
85	Lamp2	LAMP2	DOWN	0.03	-3.23
86	Eno1	ENOA	DOWN	0.04	-3.11
87	Eno2	ENOG	DOWN	0.00	-8.83
88	Ctsd	CATD	DOWN	0.02	-3.55
89	Cox5b	COX5B	DOWN	0.03	-3.44
90	Hspa5	BIP	DOWN	0.01	-4.25
91	Hexb	HEXB	DOWN	0.04	-3.09
92	Tpm1	TPM1	DOWN	0.04	-2.95
93	Cbx1	CBX1	DOWN	0.01	-4.46
94	Glb1	BGAL	DOWN	0.01	-4.93
95	Snrpb	RSMB	DOWN	0.05	-2.86
96	Adh5	ADHX	DOWN	0.04	-3.04
97	Ptpn6	PTN6	DOWN	0.02	-3.70
98	Ahsg	FETUA	DOWN	0.03	-3.18
99	Rab6a	RAB6A	DOWN	0.00	-5.97
100	Nsf	NSF	DOWN	0.01	-4.52
101	Adss2	PURA2	DOWN	0.04	-3.03
102	Pla2g4a	PA24A	DOWN	0.01	-4.43
103	Anxa5	ANXA5	DOWN	0.04	-3.04

104	Cox7a2	CX7A2	DOWN	0.02	-3.66
105	Lum	LUM	DOWN	0.00	-10.02
106	Rab2a	RAB2A	DOWN	0.01	-4.33
107	Rad23b	RD23B	DOWN	0.03	-3.14
108	Arpc4	ARPC4	DOWN	0.01	-4.22
109	Ruvbl1	RUVB1	DOWN	0.04	-3.10
110	Pcbp1	PCBP1	DOWN	0.02	-4.00
111	Sumo2	SUMO2	DOWN	0.00	-7.02
112	Hnrnpk	HNRPK	DOWN	0.02	-3.60
113	Ywhag	1433G	DOWN	0.03	-3.34
114	Rps7	RS7	DOWN	0.04	-2.89
115	Psmc5	PRS8	DOWN	0.03	-3.22
116	Rps23	RS23	DOWN	0.04	-3.01
117	Rps18	RS18	DOWN	0.02	-3.64
118	Rps11	RS11	DOWN	0.02	-3.61
119	Lsm3	LSM3	DOWN	0.01	-4.34
120	Arf6	ARF6	DOWN	0.04	-2.89
121	Ran	RAN	DOWN	0.01	-4.49
122	Rps26	RS26	DOWN	0.04	-3.07
123	Pafah1b1	LIS1	DOWN	0.01	-4.46
124	Ywhaq	1433T	DOWN	0.01	-5.56
125	Tubb4b	TBB4B	DOWN	0.04	-2.89
126	Cct3	TCPG	DOWN	0.03	-3.48
127	Arf5	ARF5	DOWN	0.01	-5.53
128	Mcm2	MCM2	DOWN	0.00	-5.77
129	Mcm6	MCM6	DOWN	0.01	-4.24
130	Rps3a	RS3A	DOWN	0.02	-3.89
131	Ctsc	CATC	DOWN	0.02	-3.60
132	Rplp2	RLA2	DOWN	0.05	-2.87
133	Prdx5	PRDX5	DOWN	0.03	-3.49
134	G6pdx	G6PD1	DOWN	0.03	-3.24
135	Top2a	TOP2A	DOWN	0.03	-3.44
136	Vcp	TERA	DOWN	0.00	-8.12
137	Uba1	UBA1	DOWN	0.02	-3.58
138	Eif5b	IF2P	DOWN	0.00	-5.67
139	Gpsm3	GPSM3	DOWN	0.01	-4.52
140	Pdap1	HAP28	DOWN	0.01	-4.43
141	Ddx17	DDX17	DOWN	0.03	-3.36
142	Serpinb6	SPB6	DOWN	0.01	-4.64
143	Vdac2	VDAC2	DOWN	0.03	-3.38
144	Vdac1	VDAC1	DOWN	0.04	-3.03
145	Hcfc1	HCFC1	DOWN	0.01	-4.52
146	Lcp1	PLSL	DOWN	0.05	-2.79
147	Mcm7	MCM7	DOWN	0.01	-4.38
148	Pcbp2	PCBP2	DOWN	0.02	-3.89
149	Sri	SORCN	DOWN	0.00	-5.62
150	Snrnp200	U520	DOWN	0.04	-2.99
151	Ugt1a7	UD17	DOWN	0.01	-5.54
152	Otub1	OTUB1	DOWN	0.00	-6.15
153	Galnt7	GALT7	DOWN	0.00	-6.67
154	Ahsa1	AHSA1	DOWN	0.02	-3.67
155	Ipo5	IPO5	DOWN	0.01	-4.13
156	Srp68	SRP68	DOWN	0.04	-3.13
157	Slc15a3	S15A3	DOWN	0.05	-2.78
158	Asph	ASPH	DOWN	0.03	-3.19
159	Pgp	PGP	DOWN	0.04	-3.08
160	Gfm1	EFGM	DOWN	0.01	-4.21
161	Ero1a	ERO1A	DOWN	0.02	-3.96
162	Eif3c	EIF3C	DOWN	0.03	-3.19
163	Apobr	APOBR	DOWN	0.05	-2.88
164	Hnrnpu	HNRPU	DOWN	0.02	-3.74
165	Atp5f1c	ATPG	DOWN	0.03	-3.36
166	Slc39a8	S39A8	DOWN	0.03	-3.40
167	Txndc5	TXND5	DOWN	0.05	-2.85
168	Eif3h	EIF3H	DOWN	0.04	-3.01
169	Arrb2	ARRB2	DOWN	0.01	-4.91
170	Smarca5	SMCA5	DOWN	0.05	-2.87
171	Cyrib	CYRIB	DOWN	0.03	-3.26
172	Dars1	SYDC	DOWN	0.01	-4.43
173	Mthfd1	C1TC	DOWN	0.03	-3.38
174	Far1	FACR1	DOWN	0.00	-6.01
175	Actr3	ARP3	DOWN	0.02	-3.60
176	Tmed9	TMED9	DOWN	0.03	-3.17

177	Dpp3	DPP3	DOWN	0.01	-4.41
178	Arhgdia	GDIR1	DOWN	0.05	-2.83
179	Nudcd2	NUDC2	DOWN	0.01	-4.60
180	RTRAF	RTRAF	DOWN	0.03	-3.46
181	Trap1	TRAP1	DOWN	0.00	-50.48
182	Nop10	NOP10	DOWN	0.03	-3.39
183	Rpl11	RL11	DOWN	0.02	-3.93
184	Blvra	BIEA	DOWN	0.04	-2.89
185	Uqcrc1	QCR1	DOWN	0.01	-4.79
186	Ube2v1	UB2V1	DOWN	0.01	-5.13
187	Pgm1	PGM1	DOWN	0.03	-3.18
188	Cyc1	CY1	DOWN	0.01	-4.45
189	Cndp2	CNDP2	DOWN	0.01	-5.33
190	Rpl34	RL34	DOWN	0.01	-4.12
191	Dlst	ODO2	DOWN	0.04	-2.97
192	Itpa	ITPA	DOWN	0.02	-4.01
193	Uqcrc2	QCR2	DOWN	0.03	-3.23
194	Ehd4	EHD4	DOWN	0.05	-2.87
195	Usp14	UBP14	DOWN	0.00	-7.28
196	Cnpy2	CNPY2	DOWN	0.04	-3.05
197	Comp	COMP	DOWN	0.04	-3.03
198	Psmb2	PSB2	DOWN	0.04	-3.03
199	Psma1	PSA1	DOWN	0.02	-3.96
200	Snx1	SNX1	DOWN	0.05	-2.88
201	Tagln2	TAGL2	DOWN	0.04	-3.07
202	Psmd13	PSD13	DOWN	0.02	-3.81
203	Lipa	LICH	DOWN	0.00	-7.05
204	Ddx39b	DX39B	DOWN	0.01	-4.55
205	Clic1	CLIC1	DOWN	0.02	-3.72
206	Strap	STRAP	DOWN	0.04	-3.08
Control vs. Corundum					
1	Prdx6	PRDX6	UP	0.01	4.51
2	Ppt1	PPT1	UP	0.01	4.27
3	Itgb1	ITB1	UP	0.00	10.86
4	Ncl	NUCL	UP	0.03	3.34
5	Ppia	PPIA	UP	0.02	3.64
6	Gc	VTDB	UP	0.04	2.91
7	H2ax	H2AX	UP	0.05	2.85
8	Eci1	ECI1	UP	0.05	2.88
9	Capzb	CAPZB	UP	0.04	2.95
10	Rab1A;	RAB1A	UP	0.03	3.47
11	Cyb5a	CYB5	UP	0.01	4.43
12	Pdcd5	PDCD5	UP	0.03	3.41
13	Cycs	CYC	UP	0.03	3.41
14	Ybx1	YBOX1	UP	0.04	2.93
15	Pfn1	PROF1	UP	0.03	3.26
16	Ctps1	PYRG1	UP	0.04	3.07
17	Cct7	TCPH	UP	0.04	2.97
18	Samhd1	SAMH1	UP	0.00	7.34
19	Tmpo	LAP2B	UP	0.00	6.15
20	Ptpn18	PTN18	UP	0.00	8.31
21	Mapre1	MARE1	UP	0.02	3.76
22	Snrpa	SNRPA	UP	0.00	6.82
23	Trim28	TIF1B	UP	0.02	3.73
24	Iars2	SYIM	UP	0.02	3.93
25	Nceh1	NCEH1	UP	0.05	2.83
26	Ythdf3	YTHD3	UP	0.01	5.43
27	Acat2	THIC	UP	0.00	13.79
28	Dnm1l	DNM1L	UP	0.05	2.85
29	Acot7	BACH	UP	0.03	3.23
30	Prpf8	PRP8	UP	0.01	4.36
31	Tbcb	TBCB	UP	0.04	3.00
32	Ebna1bp2	EBP2	UP	0.01	4.65
33	Mrpl12	RM12	UP	0.04	2.95
34	Iah1	IAH1	UP	0.03	3.17
35	Uchl3	UCHL3	UP	0.03	3.26
36	Mbnl1	MBNL1	UP	0.02	3.53
37	Stap1	STAP1	UP	0.05	2.84
38	Gsto1	GSTO1	DOWN	0.00	-3.16
39	Impa1	IMPA1	DOWN	0.01	-0.54
40	Vamp8	VAMP8	DOWN	0.03	-1.26
41	Snx12	SNX12	DOWN	0.00	-1.83
42	Gcat	KBL	DOWN	0.01	-1.34

43	Ptprc	PTPRC	DOWN	0.02	-0.76
44	Hsp90b1	ENPL	DOWN	0.01	-0.32
45	Eif4a1	IF4A1	DOWN	0.02	-1.70
46	Sub1	TCP4	DOWN	0.04	-2.35
47	Itgb2	ITB2	DOWN	0.03	-1.07
48	Umps	UMPS	DOWN	0.04	-0.23
49	Lamp2	LAMP2	DOWN	0.03	-1.07
50	Ap2a1	AP2A1	DOWN	0.01	-2.09
51	Tpm1	TPM1	DOWN	0.03	-1.49
52	Cd72	CD72	DOWN	0.02	-1.16
53	Pnp	PNPH	DOWN	0.01	-2.20
54	Pcmt1	PIMT	DOWN	0.02	-1.69
55	Glb1	BGAL	DOWN	0.03	-1.85
56	Capg	CAPG	DOWN	0.01	-0.14
57	Atxn10	ATX10	DOWN	0.03	-0.62
58	Dbi	ACBP	DOWN	0.02	-2.29
59	Serpinc1	ANT3	DOWN	0.02	-0.53
60	Rab6a	RAB6A	DOWN	0.04	-2.35
61	Lig1	DNLI1	DOWN	0.03	-0.94
62	Stat1	STAT1	DOWN	0.04	-1.03
63	Nsf	NSF	DOWN	0.04	-1.43
64	Adss2	PURA2	DOWN	0.03	-0.56
65	Lum	LUM	DOWN	0.00	-4.06
66	Jak1;Jak2	JAK1	DOWN	0.04	-1.61
67	Rpl10a	RL10A	DOWN	0.05	-1.13
68	Ruvbl1	RUVB1	DOWN	0.02	-1.25
69	Eif4a1	IF4A1	DOWN	0.03	-1.71
70	Rpl26	RL26	DOWN	0.01	-0.86
71	Magoh	MGN2	DOWN	0.05	-2.75
72	Snrpg	RUXG	DOWN	0.01	-0.91
73	Lsm6	LSM6	DOWN	0.01	-0.83
74	Snrpd2	SMD2	DOWN	0.03	-1.20
75	Ran	RAN	DOWN	0.05	-0.15
76	Mapk1	MK01	DOWN	0.03	-1.41
77	Tubb4b	TBB4B	DOWN	0.05	-0.75
78	Idh3g	IDHG1	DOWN	0.05	-1.93
79	Rhog	RHOG	DOWN	0.01	-0.47
80	Mcm2	MCM2	DOWN	0.00	-2.95
81	Top2a	TOP2A	DOWN	0.01	-0.94
82	Top1	TOP1	DOWN	0.04	-1.72
83	Pzp	PZP	DOWN	0.03	-0.52
84	Bcl2l1	B2CL1	DOWN	0.04	-2.29
85	Sri	SORCN	DOWN	0.00	-0.73
86	Galnt7	GALT7	DOWN	0.00	-1.71
87	Ipo5	IPO5	DOWN	0.00	-1.45
88	Asph	ASPH	DOWN	0.02	-1.65
89	Pgp	PGP	DOWN	0.04	-2.64
90	Eif3b	EIF3B	DOWN	0.05	-1.54
91	Tma7	TMA7	DOWN	0.04	-1.35
92	Eif3l	EIF3L	DOWN	0.02	-1.70
93	Ddx39a	DX39A	DOWN	0.04	-0.42
94	Sfpq	SFPQ	DOWN	0.03	-0.85
95	Txndc5	TXND5	DOWN	0.03	-1.13
96	Mpst	THTM	DOWN	0.04	-0.53
97	Dpp3	DPP3	DOWN	0.04	-1.00
98	Clint1	EPN4	DOWN	0.03	-0.91
99	Sec61b	SC61B	DOWN	0.02	-0.84
100	Ppid	PPID	DOWN	0.01	-1.05
101	Smc3	SMC3	DOWN	0.00	-2.16
102	Chtop	CHTOP	DOWN	0.00	-1.70
103	Tmed10	TMEDA	DOWN	0.01	-2.21
104	Rpl34	RL34	DOWN	0.04	-1.11
105	Dlst	ODO2	DOWN	0.03	-2.65
106	Itpa	ITPA	DOWN	0.04	-1.63
107	Eef1g	EF1G	DOWN	0.04	-0.56
108	Gsdmd	GSDMD	DOWN	0.05	-0.76
109	Snx5	SNX5	DOWN	0.01	-0.51
110	Upf1	RENT1	DOWN	0.01	-1.47
111	Dazap1	DAZP1	DOWN	0.00	-0.90
112	Psma6	PSA6	DOWN	0.01	-3.31
113	Comp	COMP	DOWN	0.03	-1.85
114	Psmb3	PSB3	DOWN	0.00	-2.04
115	Myo1c	MYO1C	DOWN	0.04	-0.82

116	Psmd13	PSD13	DOWN	0.03	-1.82
117	Slc7a5	LAT1	DOWN	0.01	-0.75
118	Atp6v1c1	VATC1	DOWN	0.00	-1.65
Polished vs. Plasma					
1	Lamp1	LAMP1	UP	0.04	2.95
2	Lyn	LYN	UP	0.02	3.58
3	Map2k1	MP2K1	UP	0.04	3.07
4	Ppp2ca	PP2AA	UP	0.04	3.08
5	Hdgfl2	HDGR2	UP	0.02	3.55
6	Skap2	SKAP2	UP	0.01	4.27
7	Dpysl2	DPYL2	DOWN	0.01	-4.22
8	Dnmt1	DNMT1	DOWN	0.02	-3.90
9	Eno2	ENOG	DOWN	0.00	-6.50
10	Ndufs6	NDUS6	DOWN	0.04	-3.00
11	Rab10	RAB10	DOWN	0.04	-3.11
12	Ube2d2	UB2D2	DOWN	0.02	-3.87
13	Mapre1	MARE1	DOWN	0.05	-2.82
14	Dpp3	DPP3	DOWN	0.05	-2.88
15	Ndufab1	ACPM	DOWN	0.04	-2.96
16	Pfkp	PFKAP	DOWN	0.03	-3.16
Polished vs. Corundum					
1	F2	THRB	UP	0.05	2.83
2	Hmgcl	HMGCL	UP	0.05	2.80
3	Phb1	PHB1	UP	0.04	2.92
4	Mat2a	METK2	UP	0.04	3.04
5	Ptpn18	PTN18	UP	0.02	3.58
6	Nfatc1	NFATC1	UP	0.01	5.00
7	Dnm1l	DNM1L	UP	0.03	3.29
8	Ebna1bp2	EBP2	UP	0.03	3.32
9	Hnrnpf	HNRPF	UP	0.02	3.98
10	Hnrnph1	HNRH1	DOWN	0.04	-3.03
11	Lig1	DNLI1	DOWN	0.00	-6.94
12	Ppid	PPID	DOWN	0.03	-3.46
13	Atp6v1g1	VATG1	DOWN	0.05	-2.87
14	Plin3	PLIN3	DOWN	0.05	-2.84
15	Dazap1	DAZP1	DOWN	0.00	-5.84
16	Ruvbl2	RUVB2	DOWN	0.03	-3.36
17	Psma5	PSA5	DOWN	0.05	-2.78
Plasma vs. Corundum					
1	Rap1gds1	GDS1	UP	0.04	2.95
2	Gcat	KBL	UP	0.03	3.20
3	Lig1	DNLI1	UP	0.01	5.26
4	Nfatc1	NFATc1	UP	0.02	3.78
5	Pygb	PYGB	UP	0.04	3.12
6	Mpst	THTM	UP	0.04	3.10
7	Fam136a	F136A	UP	0.05	2.79
8	Hexa	HEXA	DOWN	0.01	-4.44
9	Ranbp1	RANG	DOWN	0.03	-3.37
10	Rab1A	RAB1A	DOWN	0.04	-3.01
11	Ywhab	1433B	DOWN	0.00	-7.83
12	Rps14	RS14	DOWN	0.04	-2.88
13	Ran	RAN	DOWN	0.04	-3.11
14	Mapre1	MARE1	DOWN	0.01	-5.50
15	Nudcd2	NUDC2	DOWN	0.02	-3.74
16	Cyb5r3	NB5R3	DOWN	0.05	-2.84
17	Hnrnpf	HNRPF	DOWN	0.05	-2.86
Control vs. LPS Control					
1	Itih4	ITIH4	UP	0.00	3.46
2	Osbpl8	OSBL8	UP	0.01	2.76
3	Gls	GLSK	UP	0.03	2.36
4	Atp2b1	AT2B1	UP	0.00	4.78
5	Hk2	HXK2	UP	0.04	2.18
6	Capn2	CAN2	UP	0.04	2.17
7	Hsd17b10	HCD2	UP	0.01	2.90
8	Prdx4	PRDX4	UP	0.00	3.79
9	Prdx1	PRDX1	UP	0.00	4.57
10	Diaph1	DIAP1	UP	0.00	3.37
11	Eef2	EF2	UP	0.00	3.51
12	Degs1	DEGS1	UP	0.00	5.12
13	Gsto1	GSTO1	UP	0.04	2.15
14	Dhx15	DHX15	UP	0.00	3.77
15	Anp32a	AN32A	UP	0.01	3.01
16	Psmd14	PSDE	UP	0.00	3.38

17	Ap1b1	AP1B1	UP	0.03	2.37
18	C1qbp	C1QBP	UP	0.01	2.87
19	Hnrnph2	HNRH2	UP	0.01	3.09
20	Hnrnph1	HNRH1	UP	0.00	3.42
21	Bcat2	BCAT2	UP	0.01	3.00
22	Timm44	TIM44	UP	0.00	3.90
23	Calu	CALU	UP	0.00	3.12
24	Irak1	IRAK1	UP	0.01	2.99
25	Septin7	SEPTIN7	UP	0.01	2.91
26	Atp2a2	AT2A2	UP	0.00	4.75
27	Psmb5	PSB5	UP	0.00	5.74
28	Aif1	AIF1	UP	0.00	4.37
29	Pgam2	PGAM2	UP	0.00	3.60
30	Vamp8	VAMP8	UP	0.01	3.08
31	Psma3	PSA3	UP	0.00	4.42
32	Snx3	SNX3	UP	0.01	2.72
33	Hsd17b12	DHB12	UP	0.01	2.72
34	Pfdn2	PFD2	UP	0.01	2.70
35	Wdr1	WDR1	UP	0.01	3.10
36	Creg1	CREG1	UP	0.04	2.20
37	Clpp	CLPP	UP	0.00	3.55
38	Nfatc1	NFAC1	UP	0.00	14.72
39	Cpd	CBPD	UP	0.00	10.30
40	Rbm3	RBM3	UP	0.00	4.29
41	Dhfr	DYR	UP	0.01	2.98
42	B2m	B2MG	UP	0.02	2.52
43	Hba	HBA	UP	0.00	3.24
44	Aldoa	ALDOA	UP	0.01	2.70
45	Jun	JUN	UP	0.00	20.49
46	Myl1	MYL1	UP	0.00	3.85
47	Ldha	LDHA	UP	0.01	2.86
48	Hsp90aa1	HS90A	UP	0.02	2.62
49	Aprt	APT	UP	0.01	3.09
50	Hsp90b1	ENPL	UP	0.00	5.42
51	Hsp90b1	ENPL	UP	0.01	2.72
52	Gnai2	GNAI2	UP	0.04	2.13
53	Lyz1	LYZ1	UP	0.03	2.27
54	Pgk1	PGK1	UP	0.00	3.41
55	Pgk1	PGK1	UP	0.01	2.98
56	Sod2	SODM	UP	0.00	7.15
57	Eef1a1	EF1A1	UP	0.00	3.39
58	Eef1a1	EF1A1	UP	0.00	3.20
59	Ctsb	CATB	UP	0.00	3.72
60	Eif4a1	IF4A1	UP	0.00	3.82
61	Eif4a1	IF4A1	UP	0.00	3.59
62	Gstm1	GSTM1	UP	0.01	3.00
63	Cd14	CD14	UP	0.00	5.92
64	Sub1	TCP4	UP	0.02	2.43
65	Fn1	FINC	UP	0.03	2.35
66	Hsp90ab1	HS90B	UP	0.00	4.45
67	Itga5	ITA5	UP	0.00	5.44
68	Tcp1	TCPA	UP	0.02	2.51
69	Pfkl	PFKAL	UP	0.04	2.13
70	Mdh1	MDHC	UP	0.04	2.16
71	Rpsa	RSSA	UP	0.01	2.93
72	Calr	CALR	UP	0.00	3.72
73	Lmna	LMNA	UP	0.01	3.12
74	Rplp0	RLA0	UP	0.00	3.39
75	Nme1	NDKA	UP	0.00	4.94
76	Nme1	NDKA	UP	0.00	3.92
77	Ass1	ASSY	UP	0.00	3.32
78	Gapdh	G3P	UP	0.03	2.34
79	Eno1	ENOA	UP	0.01	2.96
80	Hk1	HXK1	UP	0.02	2.45
81	Lyz1	LYZ1	UP	0.02	2.51
82	Mthfd2	MTDC	UP	0.02	2.55
83	Bsg	BASI	UP	0.00	6.42
84	Cox5b	COX5B	UP	0.02	2.51
85	Hspa5	BIP	UP	0.00	3.61
86	Hexb	HEXB	UP	0.00	4.18
87	Prdx3	PRDX3	UP	0.00	5.17
88	Vim	VIME	UP	0.00	3.84
89	Fcer1g	FCERG	UP	0.00	3.22

90	Plg	PLMN	UP	0.00	3.30
91	Cst3	CYTC	UP	0.02	2.60
92	Cd72	CD72	UP	0.00	4.08
93	Cbx3	CBX3	UP	0.00	4.41
94	Cbx1	CBX1	UP	0.01	3.03
95	Cbx3	CBX3	UP	0.01	2.64
96	Pnp	PNPH	UP	0.00	3.24
97	Pcmt1	PIMT	UP	0.00	3.62
98	Cat	CATA	UP	0.01	2.80
99	Bcat1	BCAT1	UP	0.00	3.36
100	Impdh2	IMDH2	UP	0.00	3.57
101	Glud1	DHE3	UP	0.00	4.26
102	Psmd7	PSMD7	UP	0.01	3.07
103	Marcks	MARCS	UP	0.00	7.33
104	Pdia3	PDIA3	UP	0.01	2.79
105	Vav1	VAV	UP	0.00	3.92
106	Nap1l1	NP1L1	UP	0.03	2.36
107	Atxn10	ATX10	UP	0.00	7.28
108	Mug1	MUG1	UP	0.01	2.96
109	Ptpn6	PTN6	UP	0.01	2.95
110	Hexa	HEXA	UP	0.00	3.53
111	Nedd8	NEDD8	UP	0.00	4.93
112	Ahsg	FETUA	UP	0.02	2.42
113	Msr1	MSRE	UP	0.02	2.57
114	Dbi	ACBP	UP	0.01	2.68
115	Serpinc1	ANT3	UP	0.00	3.49
116	Wars1	SYWC	UP	0.00	3.27
117	Rab6a	RAB6A	UP	0.02	2.42
118	Canx	CALX	UP	0.00	4.52
119	Prdx1	PRDX1	UP	0.00	11.15
120	Rpl12	RL12	UP	0.00	3.71
121	Por	NCPR	UP	0.03	2.38
122	Acsl1	ACSL1	UP	0.00	3.99
123	Csk	CSK	UP	0.01	2.73
124	Eci1	ECI1	UP	0.01	2.99
125	Septin2	SEPTIN2	UP	0.00	3.23
126	Stat1	STAT1	UP	0.00	4.17
127	Cct8	TCPQ	UP	0.00	4.10
128	Akr1b1	ALDR	UP	0.00	3.56
129	Akr1b8	ALD2	UP	0.00	4.39
130	Vps4b	VPS4B	UP	0.01	2.66
131	Tes	TES	UP	0.00	4.00
132	Pla2g4a	PA24A	UP	0.01	2.88
133	Aldh2	ALDH2	UP	0.02	2.42
134	Aldh3a1	AL3A1	UP	0.00	3.30
135	Anxa5	ANXA5	UP	0.00	3.60
136	Slc25a4	ADT1	UP	0.04	2.18
137	Clec10a	CLC10	UP	0.00	3.69
138	Hnrnpa1	ROA1	UP	0.00	4.23
139	Hcls1	HCLS1	UP	0.00	4.09
140	Mcm5	MCM5	UP	0.03	2.31
141	Srp9	SRP09	UP	0.01	3.09
142	Ahcy	SAHH	UP	0.00	3.77
143	Atp6v1a	VATA	UP	0.00	4.44
144	Pa2g4	PA2G4	UP	0.00	4.16
145	Rpl9	RL9	UP	0.00	3.95
146	Hdgf	HDGF	UP	0.00	3.19
147	Atp6v0d1	VA0D1	UP	0.01	2.80
148	Slc25a5	ADT2	UP	0.01	2.97
149	Kpna2	IMA1	UP	0.00	3.54
150	Jak1	JAK1	UP	0.00	3.89
151	Pkm	KPYM	UP	0.00	3.58
152	Rpl10a	RL10A	UP	0.00	3.53
153	Rab2a	RAB2A	UP	0.00	3.27
154	Idh2	IDHP	UP	0.01	3.03
155	Rad23b	RD23B	UP	0.01	2.74
156	Psmc4	PRS6B	UP	0.00	3.88
157	Adsl	PUR8	UP	0.00	3.78
158	Adprh	ADPRH	UP	0.00	3.39
159	Acod1	IRG1	UP	0.00	20.09
160	Arpp19	ARP19	UP	0.00	3.20
161	Atp5f1b	ATPB	UP	0.00	6.33
162	Eef1d	EF1D	UP	0.00	4.87

163	Tm9sf2	TM9S2	UP	0.02	2.61
164	Eef2	EF2	UP	0.00	5.02
165	Arpc4	ARPC4	UP	0.00	3.60
166	Pcbp1	PCBP1	UP	0.00	3.47
167	Actb	ACTB	UP	0.00	4.02
168	Cdc42	CDC42	UP	0.02	2.47
169	Eif4a1	IF4A1	UP	0.00	3.46
170	Rps20	RS20	UP	0.00	3.26
171	Ube2n	UBE2N	UP	0.01	2.73
172	Arf1;Arf3	ARF1	UP	0.04	2.21
173	Abce1	ABCE1	UP	0.00	3.20
174	Magoh	MGN2	UP	0.00	3.58
175	Sec61a1	S61A1	UP	0.00	3.35
176	Sumo2	SUMO2	UP	0.01	2.77
177	Hnrnpk	HNRPK	UP	0.04	2.13
178	Ywhag	YWHG	UP	0.00	3.76
179	Ywhab	YWHAB	UP	0.02	2.54
180	Ppp1ca	PP1A	UP	0.00	3.70
181	Ppp1ca	PP1A	UP	0.00	3.67
182	Psmc1	PRS4	UP	0.01	2.91
183	Psmc5	PRS8	UP	0.00	3.61
184	Ywhae	1433E	UP	0.01	2.80
185	Snrpe	RUXE	UP	0.00	6.17
186	Snrpg	RUXG	UP	0.00	3.41
187	Lsm3	LSM3	UP	0.01	2.67
188	Snrpd3	SMD3	UP	0.02	2.61
189	Psmc6	PRS10	UP	0.00	3.39
190	Atp6v1b2	VATB2	UP	0.01	3.06
191	Rps15	RS15	UP	0.01	2.84
192	Rps26	RS26	UP	0.03	2.38
193	Rps28	RS28	UP	0.00	3.65
194	Gnb1	GBB1	UP	0.01	3.00
195	Rpl30	RL30	UP	0.00	3.21
196	Rps3	RS3	UP	0.00	3.46
197	Tra2b	TRA2B	UP	0.00	3.86
198	Pafah1b1	LIS1	UP	0.01	2.76
199	Hspa8	HSP7C	UP	0.00	4.34
200	Tpt1	TCTP	UP	0.02	2.57
201	Dnaja1	DNJA1	UP	0.04	2.16
202	Hspd1	CH60	UP	0.00	3.97
203	Eif4e	IF4E	UP	0.00	5.30
204	Mapk1	MK01	UP	0.00	4.32
205	Mapk1	MK01	UP	0.00	3.77
206	Ywhaz	YWHAZ	UP	0.01	2.75
207	Ywhab	YWHAB	UP	0.00	4.05
208	Sumo1	SUMO1	UP	0.02	2.49
209	Dynll1	DYL1	UP	0.00	3.58
210	Rps17	RS17	UP	0.02	2.53
211	Ube2i	UBC9	UP	0.01	3.03
212	Phb1	PHB1	UP	0.00	5.45
213	Csnk2b	CSK2B	UP	0.01	3.02
214	Rpl22	RL22	UP	0.00	3.26
215	Actc1	ACTC	UP	0.00	3.61
216	Rack1	RACK1	UP	0.01	2.70
217	Ywhaq	1433T	UP	0.03	2.35
218	Tuba4a	TBA4A	UP	0.00	7.16
219	Tuba1c	TBA1C	UP	0.00	3.26
220	Tubb4b	TBB4B	UP	0.01	2.74
221	Tubb4b	TBB5	UP	0.02	2.48
222	Tuba1c	TBA1C	UP	0.02	2.52
223	Idh3g	IDHG1	UP	0.00	3.59
224	Ctps1	PYRG1	UP	0.00	3.46
225	Cct2	TCPB	UP	0.00	4.15
226	Cct4	TCPD	UP	0.00	6.58
227	Cct5	TCPE	UP	0.00	5.33
228	Cct6a	TCPZ	UP	0.00	3.79
229	Cct3	TCPG	UP	0.00	3.31
230	Nucb2	NUCB2	UP	0.00	3.19
231	Eloc	ELOC	UP	0.02	2.52
232	Arf5	ARF5	UP	0.03	2.27
233	Erh	ERH	UP	0.00	4.05
234	Rhog	RHOG	UP	0.04	2.19
235	Serpinf1	PEDF	UP	0.01	2.87

236	Mcm2	MCM2	UP	0.01	2.64
237	Mcm6	MCM6	UP	0.00	3.69
238	Csrp1	CSRP1	UP	0.05	2.12
239	Anxa11	ANX11	UP	0.01	2.88
240	Smarcc1	SMRC1	UP	0.00	3.45
241	Fh	FUMH	UP	0.00	3.45
242	Ctsc	CATC	UP	0.00	3.49
243	Anp32e	AN32E	UP	0.02	2.41
244	Rplp2	RLA2	UP	0.00	3.31
245	Prdx5	PRDX5	UP	0.00	7.73
246	G6pdx	G6PD1	UP	0.01	2.78
247	Apoa1	APOA1	UP	0.00	3.28
248	Uba1	UBA1	UP	0.04	2.16
249	Nucb1	NUCB1	UP	0.00	3.84
250	Atp5f1a	ATPA	UP	0.00	5.23
251	Pfdn6	PFD6	UP	0.01	2.88
252	Anxa7	ANXA7	UP	0.01	2.80
253	Bax	BAX	UP	0.02	2.62
254	Fbln1	FBLN1	UP	0.00	3.51
255	Ssrp1	SSRP1	UP	0.03	2.35
256	Nsun2	NSUN2	UP	0.01	3.10
257	Ppp1r7	PP1R7	UP	0.01	2.86
258	Skap2	SKAP2	UP	0.00	4.05
259	Abracl	ABRAL	UP	0.00	3.30
260	Arap1	ARAP1	UP	0.00	4.17
261	Cdv3	CDV3	UP	0.00	3.17
262	Ddx17	DDX17	UP	0.02	2.61
263	Ddx46	DDX46	UP	0.03	2.27
264	Ogdh	ODO1	UP	0.00	4.75
265	Grb2	GRB2	UP	0.00	3.25
266	Csnk2a1	CSK21	UP	0.01	2.83
267	Serpinb6	SPB6	UP	0.03	2.32
268	Vdac2	VDAC2	UP	0.00	3.82
269	Vdac1	VDAC1	UP	0.00	3.22
270	Rbbp4	RBBP4	UP	0.04	2.16
271	Rbbp7	RBBP7	UP	0.01	2.99
272	Rbbp7	RBBP7	UP	0.01	2.94
273	Asns	ASNS	UP	0.02	2.61
274	Hars1	HARS1	UP	0.01	2.94
275	Prdx2	PRDX2	UP	0.00	3.18
276	Clns1a	ICLN	UP	0.05	2.10
277	Hcfc1	HCFC1	UP	0.03	2.38
278	Hspa4	HSP74	UP	0.00	5.05
279	Cct6b	TCPW	UP	0.00	3.54
280	Cyba	CY24A	UP	0.00	3.66
281	Alcam	CD166	UP	0.05	2.12
282	Glg1	GSLG1	UP	0.00	3.64
283	Ewsr1	EWS	UP	0.00	4.36
284	Gdi2	GDIB	UP	0.00	3.31
285	Arhgdib	GDIR2	UP	0.00	3.88
286	Hsph1	HS105	UP	0.02	2.54
287	A2m	A2MG	UP	0.01	2.86
288	Mcm7	MCM7	UP	0.01	2.64
289	Pcbp2	PCBP2	UP	0.01	2.88
290	Pon3	PON3	UP	0.01	2.72
291	Srsf2	SRSF2	UP	0.04	2.19
292	Ssr4	SSRD	UP	0.00	3.99
293	Rpa2	RFA2	UP	0.00	3.24
294	Shh	SHH	UP	0.03	2.30
295	Snrpc	RU1C	UP	0.01	2.93
296	Snrnp70	RU17	UP	0.02	2.58
297	Eif4g2	IF4G2	UP	0.00	4.59
298	Sqstm1	SQSTM	UP	0.00	3.63
299	Bcl2l1	B2CL1	UP	0.01	2.81
300	Hspe1	CH10	UP	0.00	4.10
301	Cltc	CLH1	UP	0.01	3.10
302	Ahcyl1	SAHH2	UP	0.01	2.71
303	Mars1	SYMC	UP	0.04	2.16
304	Nop58	NOP58	UP	0.00	4.27
305	A2m	A2MG	UP	0.01	2.98
306	Cpsf6	CPSF6	UP	0.00	4.39
307	Eif4g1	IF4G1	UP	0.01	2.79
308	Sri	SORCN	UP	0.01	2.74

309	Ppp2r2a	2ABA	UP	0.00	3.19
310	Snrnp200	U520	UP	0.01	2.82
311	Abcf1	ABCF1	UP	0.00	4.63
312	Xpo1	XPO1	UP	0.02	2.62
313	Oxsr1	OXSR1	UP	0.04	2.20
314	Lrpprc	LPPRC	UP	0.01	2.90
315	Srsf1	SRSF1	UP	0.04	2.16
316	Jpt2	JUPI2	UP	0.02	2.59
317	Camk2d	KCC2D	UP	0.05	2.07
318	Kctd12	KCD12	UP	0.00	4.84
319	Mlec	MLEC	UP	0.00	3.66
320	Ugt1a7	UD17	UP	0.01	2.89
321	Lsm8	LSM8	UP	0.00	5.35
322	Nap1l4	NP1L4	UP	0.01	3.11
323	Mtch2	MTCH2	UP	0.04	2.24
324	Luc7l	LC7L2	UP	0.00	3.65
325	Dek	DEK	UP	0.05	2.08
326	Kansl1	KANL1	UP	0.01	3.11
327	Fnbp1	FNBP1	UP	0.02	2.43
328	Wnk4	WNK4	UP	0.00	3.51
329	Septin9	SEPTI N9	UP	0.01	3.11
330	Mogs	MOGS	UP	0.01	3.09
331	Ubap2l	UBP2L	UP	0.00	3.33
332	Grwd1	GRWD1	UP	0.00	4.99
333	Tufm	EFTU	UP	0.00	5.73
334	Tnpo1	TNPO1	UP	0.00	3.19
335	Actbl2	ACTBL	UP	0.00	4.52
336	Hnrnpa3	ROA3	UP	0.01	2.75
337	Psmd11	PSD11	UP	0.03	2.26
338	Tm9sf4	TM9S4	UP	0.00	3.83
339	Cfap69	CFA69	UP	0.00	7.09
340	Cstf2	CSTF2	UP	0.00	3.19
341	Ahsa1	AHSA1	UP	0.02	2.42
342	Ipo5	IPO5	UP	0.00	4.44
343	Eea1	EEA1	UP	0.00	4.66
344	Dlat	ODP2	UP	0.01	3.08
345	Lars1	SYLC	UP	0.00	3.24
346	Slc15a3	S15A3	UP	0.00	4.88
347	Srrm2	SRRM2	UP	0.00	6.08
348	Larp4	LARP4	UP	0.01	2.81
349	Etf1	ERF1	UP	0.00	3.58
350	Myef2	MYEF2	UP	0.01	3.12
351	Abi1	ABI1	UP	0.00	3.36
352	Smco1	SMCO1	UP	0.01	2.98
353	Lonp1	LONM	UP	0.01	2.70
354	Pygb	PYGB	UP	0.00	3.66
355	Gpr84	GPR84	UP	0.01	2.87
356	Eif3b	EIF3B	UP	0.01	3.08
357	Acsl5	ACSL5	UP	0.00	4.22
358	Amdhd2	NAGA	UP	0.02	2.47
359	Gfm1	EFGM	UP	0.00	5.02
360	Coq9	COQ9	UP	0.00	7.97
361	Shtn1	SHOT1	UP	0.00	8.33
362	Ddx18	DDX18	UP	0.00	3.62
363	Eif3l	EIF3L	UP	0.00	3.55
364	Aimp2	AIMP2	UP	0.04	2.23
365	Eif3c	EIF3C	UP	0.00	3.81
366	Uqcr10	QCR9	UP	0.01	2.93
367	Apbb1ip	AB1IP	UP	0.00	3.22
368	Arl6ip5	PRAF3	UP	0.00	3.88
369	Cth	CGL	UP	0.00	4.18
370	Myh9	MYH9	UP	0.03	2.38
371	Adpgk	ADPGK	UP	0.00	3.86
372	Psmd2	PSMD2	UP	0.00	4.09
373	Atp1a1	AT1A1	UP	0.01	2.72
374	Ddx39a	DX39A	UP	0.01	2.97
375	Rcc1	RCC1	UP	0.01	2.93
376	Sfpq	SFPQ	UP	0.05	2.09
377	Eif4a3	IF4A3	UP	0.01	2.91
378	Ddx1	DDX1	UP	0.01	2.89
379	Sh3bgrl3	SH3L3	UP	0.00	7.32
380	Slc39a8	S39A8	UP	0.00	3.31
381	Txndc5	TXND5	UP	0.00	4.22

382	Fubp1	FUBP1	UP	0.00	3.46
383	Arrb2	ARRB2	UP	0.01	2.98
384	Twf1	TWF1	UP	0.00	3.19
385	Grhpr	GRHPR	UP	0.00	3.70
386	Ugp2	UGPA	UP	0.02	2.58
387	Snx18	SNX18	UP	0.05	2.11
388	Scpep1	RISC	UP	0.00	3.56
389	Tardbp	TADBP	UP	0.00	3.86
390	Hnrnpll	HNRLL	UP	0.01	2.66
391	Sf3b3	SF3B3	UP	0.00	3.57
392	Dars1	SYDC	UP	0.01	2.89
393	Mthfd1	C1TC	UP	0.01	2.83
394	Rfc4	RFC4	UP	0.01	2.84
395	Nans	SIAS	UP	0.00	3.92
396	Mpst	THTM	UP	0.01	2.95
397	Actr3	ARP3	UP	0.01	2.81
398	Tmed9	TMED9	UP	0.03	2.31
399	Aco2	ACON	UP	0.01	3.04
400	Clint1	EPN4	UP	0.00	4.45
401	Dhrs1	DHRS1	UP	0.01	2.76
402	St13	F10A1	UP	0.03	2.28
403	Grpel1	GRPE1	UP	0.01	2.83
404	Nasp	NASP	UP	0.02	2.55
405	Srrt	SRRT	UP	0.00	3.25
406	Arhgdia	GDIR1	UP	0.00	3.24
407	Tomm22	TOM22	UP	0.00	3.40
408	Mydgf	MYDGF	UP	0.00	7.17
409	Nudcd2	NUDC2	UP	0.00	3.57
410	RTRAF	RTRAF	UP	0.00	3.28
411	Trap1	TRAP1	UP	0.01	2.93
412	Atp5pb	AT5F1	UP	0.00	3.43
413	Sec61b	SC61B	UP	0.01	2.86
414	Ifitm3	IFM3	UP	0.00	3.18
415	Ppid	PPID	UP	0.01	2.90
416	Slc25a11	M2OM	UP	0.01	3.08
417	Fam136a	F136A	UP	0.00	3.49
418	Nhp2	NHP2	UP	0.00	3.92
419	Ranbp3	RANB3	UP	0.00	3.86
420	Arpc2	ARPC2	UP	0.01	2.80
421	Atic	PUR9	UP	0.01	2.83
422	Snx1	SNX1	UP	0.02	2.48
423	Rbm8a	RBM8A	UP	0.00	4.50
424	Cnih4	CNIH4	UP	0.01	2.70
425	Tmed5	TMED5	UP	0.00	3.44
426	Manf	MANF	UP	0.00	4.08
427	Cacybp	CYBP	UP	0.00	4.70
428	Ssr1	SSRA	UP	0.03	2.31
429	Blvra	BIEA	UP	0.03	2.32
430	Uqcrc1	QCR1	UP	0.00	4.44
431	Shmt2	GLYM	UP	0.01	2.72
432	Cs	CISY	UP	0.00	4.26
433	Tomm70	TOM70	UP	0.01	2.64
434	Ube2v1	UB2V1	UP	0.00	3.77
435	;Ube2v2	UB2V2	UP	0.01	2.88
436	Pbdc1	PBDC1	UP	0.00	3.89
437	Prpsap1	KPRA	UP	0.02	2.62
438	Cyc1	CY1	UP	0.00	3.36
439	Tars1	SYTC	UP	0.03	2.39
440	Ppil1	PPIL1	UP	0.01	3.06
441	Cndp2	CNDP2	UP	0.00	4.07
442	Tmed10	TMEDA	UP	0.00	3.49
443	Chordc1	CHRD1	UP	0.00	3.87
444	Dlst	ODO2	UP	0.00	4.55
445	Atp5f1d	ATPD	UP	0.02	2.62
446	Sf3a3	SF3A3	UP	0.01	3.10
447	Rpl22l1	RL22L	UP	0.03	2.26
448	Timm50	TIM50	UP	0.01	2.97
449	Itpa	ITPA	UP	0.03	2.37
450	Chmp4b	CHM4B	UP	0.00	4.69
451	Eef1g	EF1G	UP	0.00	4.94
452	Bola1	BOLA1	UP	0.00	3.92
453	Psmd12	PSD12	UP	0.01	3.08
454	Gatm	GATM	UP	0.01	2.96

455	Dcps	DCPS	UP	0.02	2.53
456	Uqcrc2	QCR2	UP	0.00	3.75
457	Pelp1	PELP1	UP	0.00	3.25
458	Ap2b1	AP2B1	UP	0.01	2.83
459	Srpra	SRPRA	UP	0.00	5.48
460	Pgam1	PGAM1	UP	0.00	4.09
461	Ampd2	AMPD2	UP	0.00	3.44
462	Eif3k	EIF3K	UP	0.00	3.69
463	Pycr3	P5CR3	UP	0.02	2.46
464	Pgd	6PGD	UP	0.04	2.20
465	Ssr3	SSRG	UP	0.00	3.62
466	Paics	PUR6	UP	0.02	2.61
467	Ethe1	ETHE1	UP	0.01	2.78
468	Akr1e2	AKCL2	UP	0.00	3.65
469	Etfb	ETFB	UP	0.04	2.24
470	Pik3ap1	BCAP	UP	0.01	2.83
471	Vps35	VPS35	UP	0.02	2.44
472	Set	SET	UP	0.01	2.68
473	Ranbp2	RBP2	UP	0.00	3.54
474	Plek	PLEK	UP	0.01	2.93
475	Ide	IDE	UP	0.04	2.16
476	Prmt1	ANM1	UP	0.00	3.23
477	Copb1	COPB	UP	0.01	3.02
478	Dazap1	DAZP1	UP	0.00	3.46
479	Wdr12	WDR12	UP	0.00	5.82
480	Hyou1	HYOU1	UP	0.02	2.51
481	Arpc3	ARPC3	UP	0.00	3.23
482	Stap1	STAP1	UP	0.00	3.64
483	Usp14	UBP14	UP	0.00	4.15
484	Glrx	GLRX1	UP	0.01	2.86
485	Rhoa	RHOA	UP	0.00	3.17
486	Psma6	PSA6	UP	0.01	3.00
487	Tlr2	TLR2	UP	0.00	5.76
488	Prep	PPCE	UP	0.00	3.76
489	Ptk2b	FAK2	UP	0.05	2.12
490	Lsm4	LSM4	UP	0.01	2.82
491	Slc25a13	CMC2	UP	0.01	3.02
492	Vapa	VAPA	UP	0.00	3.34
493	Vps29	VPS29	UP	0.00	3.95
494	Esd	ESTD	UP	0.00	11.37
495	Dstn	DEST	UP	0.00	3.79
496	Sec11a	SC11A	UP	0.00	3.29
497	Tmed2	TMED2	UP	0.03	2.37
498	Prpf40a	PR40A	UP	0.00	4.01
499	Psmb3	PSB3	UP	0.00	3.36
500	Psmb2	PSB2	UP	0.01	3.00
501	Psma1	PSA1	UP	0.05	2.12
502	Sae1	SAE1	UP	0.00	3.19
503	Timm23	TIM23	UP	0.02	2.61
504	Skp1	SKP1	UP	0.01	2.87
505	Pfdn5	PFD5	UP	0.03	2.37
506	Coro1b	COR1B	UP	0.00	3.42
507	Uchl5	UCHL5	UP	0.00	3.31
508	Ctsz	CATZ	UP	0.00	4.14
509	Asah1	ASAH1	UP	0.03	2.38
510	Bub3	BUB3	UP	0.00	3.54
511	Tagln2	TAGL2	UP	0.00	3.14
512	Psmd13	PSD13	UP	0.00	3.95
513	Eif2s3x	IF2G	UP	0.01	2.69
514	Bpnt1	BPNT1	UP	0.00	4.57
515	Aifm1	AIFM1	UP	0.00	3.99
516	Atp6v1c1	VATC1	UP	0.01	2.84
517	Ddx39b	DX39B	UP	0.02	2.48
518	Clic1	CLIC1	UP	0.01	2.68
519	Strap	STRAP	UP	0.00	5.43
520	Sucla2	SUCB1	UP	0.04	2.16
521	Psma5	PSA5	UP	0.02	2.55
522	Dnpep	DNPEP	UP	0.01	2.95
523	Mpeg1	MPEG1	DOWN	0.01	-2.94
524	Sh3pxd2b	SPD2B	DOWN	0.00	-4.42
525	Plxnb2	PLXB2	DOWN	0.00	-5.91
526	H2ac11	H2A1B	DOWN	0.00	-6.50
527	Mki67	KI67	DOWN	0.00	-6.12

528	Nolc1	NOLC1	DOWN	0.04	-2.16
529	Myo1e	MYO1E	DOWN	0.05	-2.10
530	Numa1	NUMA1	DOWN	0.00	-4.37
531	Arfip1	ARFP1	DOWN	0.04	-2.20
532	Dpysl2	DPYL2	DOWN	0.00	-8.60
533	Alyref	THOC4	DOWN	0.00	-6.85
534	Tcof1	TCOF	DOWN	0.03	-2.37
535	Aip	AIP	DOWN	0.02	-2.58
536	Srsf5	SRSF5	DOWN	0.00	-3.67
537	Fkbp8	FKBP8	DOWN	0.00	-3.42
538	Hnrnph1	HNRH1	DOWN	0.02	-2.50
539	Psmb10	PSB10	DOWN	0.00	-3.47
540	Banf1	BAF	DOWN	0.00	-6.73
541	Eef1b	EF1B	DOWN	0.00	-3.35
542	Nmt1	NMT1	DOWN	0.00	-4.07
543	Epb41l2	E41L2	DOWN	0.00	-4.34
544	Ctss	CATS	DOWN	0.00	-6.15
545	Stx7	STX7	DOWN	0.00	-5.52
546	Capns1	CPNS1	DOWN	0.01	-2.70
547	Ppt1	PPT1	DOWN	0.00	-3.40
548	Tpp1	TPP1	DOWN	0.03	-2.32
549	Coro1a	COR1A	DOWN	0.02	-2.46
550	H2-D1	HA12	DOWN	0.00	-3.31
551	Hbb-b1	HBB1	DOWN	0.02	-2.53
552	Iap	IGEB	DOWN	0.00	-6.75
553	Cd74	HG2A	DOWN	0.00	-4.43
554	Aldoc	ALDOC	DOWN	0.00	-5.19
555	Aldoa	ALDOA	DOWN	0.00	-3.59
556	Got2	AATM	DOWN	0.00	-6.51
557	Itgam	ITAM	DOWN	0.00	-4.03
558	Alb	ALBU	DOWN	0.01	-3.06
559	Pdia4	PDIA4	DOWN	0.00	-3.13
560	Fcgr2	FCGR2	DOWN	0.00	-3.57
561	Lyz2	LYZ2	DOWN	0.00	-5.39
562	Itgb1	ITB1	DOWN	0.00	-3.44
563	Csf1r	CSF1R	DOWN	0.01	-2.89
564	H2az1	H2AV	DOWN	0.01	-2.89
565	Anxa1	ANXA1	DOWN	0.03	-2.27
566	Txn	THIO	DOWN	0.00	-4.18
567	Tcea1	TCEA1	DOWN	0.00	-3.68
568	H2bc14	H2B1C	DOWN	0.03	-2.35
569	H1-0	H10	DOWN	0.04	-2.21
570	Parp1	PARP1	DOWN	0.03	-2.34
571	Cfp	PROP	DOWN	0.01	-2.99
572	Rpl7a	RL7A	DOWN	0.00	-8.63
573	Cd5	CD5	DOWN	0.03	-2.28
574	Dnmt1	DNMT1	DOWN	0.00	-6.30
575	Rpl27a	RL27A	DOWN	0.00	-10.11
576	Rps16	RS16	DOWN	0.00	-5.94
577	Hmox1	HMOX1	DOWN	0.02	-2.53
578	Cd44	CD44	DOWN	0.00	-4.48
579	H1-2	H12	DOWN	0.00	-3.99
580	H1-2	H12	DOWN	0.02	-2.47
581	H1-1	H11	DOWN	0.03	-2.36
582	H1-2	H12	DOWN	0.00	-7.08
583	H1-3	H13	DOWN	0.01	-2.80
584	H1-4	H14	DOWN	0.00	-5.86
585	H1-3	H13	DOWN	0.00	-5.77
586	Lgals1	LEG1	DOWN	0.00	-3.68
587	Hspa1l	BIP	DOWN	0.01	-2.87
588	Ptbp1	PTBP1	DOWN	0.01	-2.91
589	Tpi1	TPIS	DOWN	0.00	-3.91
590	Slc2a1	GTR1	DOWN	0.00	-4.56
591	Hspa1a	HS71A	DOWN	0.01	-3.05
592	Cfl1	COF1	DOWN	0.01	-2.75
593	Rpl13a	RL13A	DOWN	0.00	-4.84
594	Cox4i1	COX41	DOWN	0.00	-4.85
595	Lsp1	LSP1	DOWN	0.00	-8.87
596	Eif3a	EIF3A	DOWN	0.02	-2.53
597	Rps2	RS2	DOWN	0.00	-8.16
598	Tln1	TLN1	DOWN	0.00	-5.48
599	Ezr	EZRI	DOWN	0.03	-2.25
600	Ptma	PTMA	DOWN	0.01	-2.99

601	U2af2	U2AF2	DOWN	0.01	-2.76
602	Sars1	SYSC	DOWN	0.00	-3.16
603	Rpl3	RL3	DOWN	0.00	-10.28
604	H2ax	H2AX	DOWN	0.00	-6.38
605	Apex1	APEX1	DOWN	0.01	-2.64
606	Grn	GRN	DOWN	0.03	-2.35
607	Prkcd	KPCD	DOWN	0.02	-2.51
608	Pabpc1	PABP1	DOWN	0.00	-3.29
609	Alox5ap	AL5AP	DOWN	0.04	-2.22
610	Fkbp4	FKBP4	DOWN	0.01	-2.82
611	Hmgb2	HMGB2	DOWN	0.00	-3.94
612	Hmgb1	HMGB1	DOWN	0.01	-2.85
613	C5ar1	C5AR1	DOWN	0.00	-6.70
614	Cd68	CD68	DOWN	0.00	-4.86
615	Ssb	LA	DOWN	0.00	-3.95
616	Mif	MIF	DOWN	0.02	-2.55
617	Rpl18	RL18	DOWN	0.00	-11.02
618	Dnm2	DYN2	DOWN	0.02	-2.53
619	Cap1	CAP1	DOWN	0.00	-3.91
620	Rpl28	RL28	DOWN	0.00	-7.18
621	H1-4	H14	DOWN	0.00	-10.51
622	H1-5	H15	DOWN	0.01	-2.89
623	H1-1	H11	DOWN	0.00	-7.03
624	H1-5	H15	DOWN	0.00	-9.81
625	Rpl6	RL6	DOWN	0.00	-22.64
626	Rplp1	RLA1	DOWN	0.00	-3.68
627	Rpl13	RL13	DOWN	0.00	-11.00
628	Rpl36	RL36	DOWN	0.00	-10.58
629	Tbca	TBCA	DOWN	0.04	-2.17
630	Lmna	LMNA	DOWN	0.00	-3.29
631	Arsb	ARSB	DOWN	0.02	-2.60
632	Rab7a	RAB7A	DOWN	0.00	-4.86
633	Pitpna	PIPNA	DOWN	0.00	-4.56
634	Cnbp	CNBP	DOWN	0.00	-3.42
635	Stmn1	STMN1	DOWN	0.00	-4.03
636	Stmn2	STMN2	DOWN	0.00	-5.87
637	Rab8a	RAB8A	DOWN	0.01	-2.65
638	Lrpap1	AMRP	DOWN	0.02	-2.56
639	Cox6b1	CX6B1	DOWN	0.00	-4.03
640	Actn4	ACTN4	DOWN	0.00	-5.49
641	Rab10	RAB10	DOWN	0.03	-2.39
642	Rab10	RAB10	DOWN	0.00	-3.62
643	Ube2m	UBC12	DOWN	0.00	-3.62
644	Rpl26	RL26	DOWN	0.00	-4.02
645	Rpl37a	RL37A	DOWN	0.02	-2.56
646	Ywhab	YWHAB	DOWN	0.00	-3.76
647	Ywhag	YWHAG	DOWN	0.00	-3.98
648	Rps8	RS8	DOWN	0.02	-2.57
649	Rps14	RS14	DOWN	0.00	-3.97
650	Rps29	RS29	DOWN	0.00	-3.64
651	Rpl18a	RL18A	DOWN	0.00	-3.21
652	Rpl23a	RL23A	DOWN	0.00	-6.41
653	Rps6	RS6	DOWN	0.00	-8.02
654	Rab1A	RAB1A	DOWN	0.00	-3.38
655	Rpl23	RL23	DOWN	0.01	-2.64
656	Rps24	RS24	DOWN	0.02	-2.47
657	Gnb1	GBB1	DOWN	0.01	-3.12
658	Gnb2	GBB2	DOWN	0.01	-3.10
659	Cycs	CYC	DOWN	0.04	-2.14
660	Rpl31	RL31	DOWN	0.00	-4.06
661	Rpl8	RL8	DOWN	0.00	-17.77
662	Pfn1	PROF1	DOWN	0.00	-4.88
663	Rac1	RAC1	DOWN	0.00	-3.21
664	Crip1	CRIP1	DOWN	0.00	-6.35
665	Rps12	RS12	DOWN	0.00	-3.37
666	Tubb4b	TBB4B	DOWN	0.04	-2.14
667	Hint1	HINT1	DOWN	0.04	-2.15
668	Elavl1	ELAV1	DOWN	0.00	-3.49
669	Slc9a3r1	NHRF1	DOWN	0.00	-4.09
670	Rpl36a	RL36A	DOWN	0.00	-7.44
671	Rpl19	RL19	DOWN	0.00	-12.88
672	Srsf3	SRSF3	DOWN	0.02	-2.61
673	Atp5pf	ATP5J	DOWN	0.02	-2.52

674	Sirpa	SHPS1	DOWN	0.04	-2.14
675	Fxyd5	FXYD5	DOWN	0.00	-3.53
676	Tubb5	TBB5	DOWN	0.01	-2.68
677	Hnrnpul2	HNRL2	DOWN	0.03	-2.39
678	Fabp5	FABP5	DOWN	0.01	-2.72
679	Lgals3bp	LG3BP	DOWN	0.00	-6.09
680	Hp1bp3	HP1B3	DOWN	0.00	-5.09
681	Uap1l1	UAP1L	DOWN	0.00	-3.74
682	Khsrp	FUBP2	DOWN	0.02	-2.54
683	Lbr	LBR	DOWN	0.00	-4.53
684	Eif3j1	EI3JA	DOWN	0.02	-2.51
685	Niban1	NIBA1	DOWN	0.00	-3.31
686	Ddx17	DDX17	DOWN	0.00	-5.33
687	Arcn1	COPD	DOWN	0.02	-2.60
688	Hnrnpd	HNRPD	DOWN	0.00	-3.85
689	Arhgef2	ARHG2	DOWN	0.00	-3.59
690	Tmpo	LAP2B	DOWN	0.00	-4.70
691	Tmpo	LAP2A	DOWN	0.00	-9.14
692	Cdc37	CDC37	DOWN	0.00	-3.51
693	Arhgef1	ARHG1	DOWN	0.05	-2.09
694	Lcp1	PLSL	DOWN	0.01	-3.02
695	Pls3	PLST	DOWN	0.00	-8.95
696	Hspa4	HS105	DOWN	0.02	-2.61
697	Ddx19a	DD19A	DOWN	0.04	-2.20
698	Itih3	ITIH3	DOWN	0.03	-2.37
699	Cd47	CD47	DOWN	0.00	-4.13
700	Lasp1	LASP1	DOWN	0.03	-2.38
701	Snrpa	SNRPA	DOWN	0.03	-2.37
702	Trim28	TIF1B	DOWN	0.01	-2.91
703	Tfrc	TFR1	DOWN	0.03	-2.40
704	Tpd52	TPD52	DOWN	0.01	-2.67
705	Dbnl	DBNL	DOWN	0.00	-3.16
706	Sh3gl1	SH3G1	DOWN	0.00	-3.76
707	Ostf1	OSTF1	DOWN	0.00	-3.91
708	Ndrg1	NDRG1	DOWN	0.00	-9.91
709	Fkbp3	FKBP3	DOWN	0.02	-2.42
710	Zyx	ZYX	DOWN	0.00	-4.93
711	Raly	RALY	DOWN	0.00	-4.23
712	Spr	SPRE	DOWN	0.00	-4.10
713	Btf3	BTF3	DOWN	0.00	-3.71
714	Tpp2	TPP2	DOWN	0.02	-2.53
715	Vcl	VINC	DOWN	0.00	-3.81
716	Cltb	CLCB	DOWN	0.00	-3.26
717	Uggt1	UGGG1	DOWN	0.00	-3.83
718	Nes	NEST	DOWN	0.00	-5.75
719	Rab35	RAB35	DOWN	0.02	-2.44
720	Rpl10	RL10	DOWN	0.01	-2.84
721	Rpl35	RL35	DOWN	0.03	-2.27
722	Cyfip1	CYFP1	DOWN	0.00	-5.33
723	Syncrip	HNRPQ	DOWN	0.00	-4.12
724	Rragc	RRAGC	DOWN	0.03	-2.28
725	Dnph1	DNPH1	DOWN	0.01	-2.85
726	Mtdh	LYRIC	DOWN	0.00	-4.88
727	Pld4	PLD4	DOWN	0.00	-3.47
728	Pck2	PCKGM	DOWN	0.02	-2.49
729	Echs1	ECHM	DOWN	0.00	-3.59
730	Ganab	GANAB	DOWN	0.03	-2.29
731	Nup93	NUP93	DOWN	0.01	-3.07
732	Srsf7	SRSF7	DOWN	0.03	-2.25
733	Nceh1	NCEH1	DOWN	0.00	-4.04
734	Hadha	ECHA	DOWN	0.01	-2.87
735	Rpl24	RL24	DOWN	0.00	-6.66
736	Sp110	SP110	DOWN	0.00	-3.60
737	Rsl1d1	RL1D1	DOWN	0.01	-2.76
738	Gemin5	GEMI5	DOWN	0.01	-2.68
739	Ythdf3	YTHD3	DOWN	0.01	-2.73
740	Agps	ADAS	DOWN	0.03	-2.32
741	Ncaph	CND2	DOWN	0.04	-2.14
742	Acat2	THIC	DOWN	0.00	-6.80
743	Prpf31	PRP31	DOWN	0.01	-2.87
744	Macroh2a1	H2AW	DOWN	0.01	-2.90
745	Eprs1	SYEP	DOWN	0.05	-2.08
746	Hist1h2bp	H2B1P	DOWN	0.02	-2.42

747	Gnl3	GNL3	DOWN	0.00	-3.58
748	Plcg2	PLCG2	DOWN	0.02	-2.62
749	Pak2	PAK2	DOWN	0.03	-2.40
750	Hmgcs1	HMCS1	DOWN	0.02	-2.46
751	Plekho2	PKHO2	DOWN	0.00	-4.06
752	Fermt3	URP2	DOWN	0.02	-2.50
753	Colgalt1	GT251	DOWN	0.01	-2.76
754	Matr3	MATR3	DOWN	0.02	-2.43
755	Hnrnpl	HNRPL	DOWN	0.03	-2.31
756	Ubqln1	UBQL1	DOWN	0.00	-3.38
757	Ubxn4	UBXN4	DOWN	0.03	-2.40
758	Uhrf1	UHRF1	DOWN	0.00	-3.95
759	Ccdc115	CC115	DOWN	0.00	-3.94
760	Rpe	RPE	DOWN	0.00	-4.18
761	Arl8a	ARL8A	DOWN	0.03	-2.32
762	Hnrnpu	HNRPU	DOWN	0.00	-9.61
763	Amot	AMOT	DOWN	0.01	-2.64
764	Acot7	BACH	DOWN	0.03	-2.31
765	Ndufs1	NDUS1	DOWN	0.00	-9.44
766	Rbmxl1	RMXL1	DOWN	0.03	-2.34
767	Lrp1	LRP1	DOWN	0.00	-7.49
768	Supt16h	SP16H	DOWN	0.00	-3.96
769	Acaa1a	THIKA	DOWN	0.00	-7.38
770	Tf	TRFE	DOWN	0.00	-5.58
771	Nop2	NOP2	DOWN	0.01	-2.96
772	Thumpd1	THUM1	DOWN	0.01	-2.84
773	Rap1b	RAP1B	DOWN	0.01	-3.06
774	Acy1	ACY1	DOWN	0.00	-3.81
775	Psat1	SERC	DOWN	0.04	-2.22
776	Dctn2	DCTN2	DOWN	0.00	-3.46
777	Abhd12	ABD12	DOWN	0.00	-3.50
778	Dpy30	DPY30	DOWN	0.03	-2.38
779	Kars1	SYK	DOWN	0.01	-2.84
780	Lpxn	LPXN	DOWN	0.00	-4.37
781	Sf3b1	SF3B1	DOWN	0.05	-2.09
782	Rrbp1	RRBP1	DOWN	0.00	-10.27
783	Igf2bp3	IF2B3	DOWN	0.02	-2.63
784	Cox6c	COX6C	DOWN	0.00	-4.09
785	Rpl17	RL17	DOWN	0.00	-6.07
786	Glo1	LGUL	DOWN	0.00	-5.81
787	Arpc5	ARPC5	DOWN	0.00	-4.42
788	Dut	DUT	DOWN	0.01	-2.77
789	Pgls	6PGL	DOWN	0.00	-3.14
790	Vps25	VPS25	DOWN	0.01	-3.06
791	Ndufb4	NDUB4	DOWN	0.01	-2.88
792	Nudt21	CPSF5	DOWN	0.01	-2.77
793	Cotl1	COTL1	DOWN	0.01	-2.84
794	Glrx3	GLRX3	DOWN	0.01	-3.08
795	Rps21	RS21	DOWN	0.01	-3.12
796	Txndc12	TXD12	DOWN	0.00	-4.17
797	Rpl14	RL14	DOWN	0.00	-3.14
798	Mrps14	RT14	DOWN	0.04	-2.25
799	Snw1	SNW1	DOWN	0.01	-2.84
800	Rprd1b	RPR1B	DOWN	0.02	-2.44
801	Smc1a	SMC1A	DOWN	0.00	-4.58
802	Snx2	SNX2	DOWN	0.00	-6.28
803	Pfdn1	PFD1	DOWN	0.03	-2.36
804	Sugt1	SGT1	DOWN	0.00	-4.21
805	Hnrnpa0	ROA0	DOWN	0.00	-4.90
806	Tecr	TECR	DOWN	0.00	-3.45
807	Chtop	CHTOP	DOWN	0.00	-3.61
808	Rpl15	RL15	DOWN	0.00	-7.83
809	Cmss1	CMS1	DOWN	0.02	-2.45
810	Rps19	RS19	DOWN	0.04	-2.18
811	Sarnp	SARNP	DOWN	0.01	-2.95
812	Atp6v1f	VATF	DOWN	0.00	-3.23
813	Rpl34	RL34	DOWN	0.00	-8.03
814	Sec23b	SC23B	DOWN	0.00	-3.81
815	Dusp3	DUS3	DOWN	0.00	-4.61
816	Ppa1	IPYR	DOWN	0.02	-2.53
817	Arpc5l	ARP5L	DOWN	0.00	-3.63
818	Rpl4	RL4	DOWN	0.00	-9.07
819	Ebna1bp2	EBP2	DOWN	0.02	-2.61

820	Napa	SNAA	DOWN	0.01	-2.96
821	Iah1	IAH1	DOWN	0.01	-3.09
822	Plin3	PLIN3	DOWN	0.00	-4.08
823	Xrn2	XRN2	DOWN	0.00	-3.54
824	Eif3f	EIF3F	DOWN	0.01	-2.96
825	Ndufa8	NDUA8	DOWN	0.00	-4.09
826	Atp5pd	ATP5H	DOWN	0.02	-2.48
827	Pycard	ASC	DOWN	0.02	-2.49
828	Cars1	SYCC	DOWN	0.00	-4.64
829	Cse1l	XPO2	DOWN	0.00	-3.36
830	Inpp5d	SHIP1	DOWN	0.00	-3.53
831	Rtn3	RTN3	DOWN	0.02	-2.58
832	Dkc1	DKC1	DOWN	0.00	-3.27
833	Cwc15	CWC15	DOWN	0.04	-2.22
834	Rpl38	RL38	DOWN	0.00	-4.39
835	Uchl3	UCHL3	DOWN	0.01	-2.76
836	Iqgap1	IQGA1	DOWN	0.02	-2.61
837	Mbnl1	MBNL1	DOWN	0.00	-3.74
838	Hmgn5	HMGN5	DOWN	0.02	-2.49
839	Copg1	COPG1	DOWN	0.00	-3.77
840	Plec	PLEC	DOWN	0.00	-3.20
841	Vapb	VAPB	DOWN	0.01	-2.78
842	Macroh2a1	H2AY	DOWN	0.00	-7.06
843	Ak2	KAD2	DOWN	0.00	-4.14
844	Ak3	KAD3	DOWN	0.02	-2.46
845	Pfkp	PFKAP	DOWN	0.00	-3.54
846	Eif4h	IF4H	DOWN	0.02	-2.42
847	Coro1c	COR1C	DOWN	0.00	-3.26
848	Timm9	TIM9	DOWN	0.00	-4.52
849	Vnn1	VNN1	DOWN	0.00	-3.80
850	Vars1	SYVC	DOWN	0.00	-3.44
851	Deaf1	DEAF1	DOWN	0.00	-3.26
852	Suclg2	SUCB2	DOWN	0.00	-3.28
853	Actl6a	ACL6A	DOWN	0.00	-4.38
LPS Control vs. LPS Polished					
1	Psmb5	PSB5	UP	0.00	7.07
2	Emc8	EMC8	UP	0.04	3.06
3	Ppt1	PPT1	UP	0.02	3.72
4	S100a6	S10A6	UP	0.04	2.95
5	Anxa6	ANXA6	UP	0.04	2.93
6	Ldhb	LDHB	UP	0.04	3.04
7	Cbx3	CBX3	UP	0.02	3.60
8	Impdh2	IMDH2	UP	0.04	2.97
9	Lyn	LYN	UP	0.03	3.29
10	Marcksl1	MRP	UP	0.04	2.90
11	Fkbp4	FKBP4	UP	0.01	4.53
12	Serpinc1	ANT3	UP	0.02	3.90
13	Wars1	SYWC	UP	0.05	2.78
14	Canx	CALX	UP	0.02	3.56
15	Ndufs6	NDUS6	UP	0.01	4.48
16	Serpinf1	PEDF	UP	0.00	5.73
17	Nop58	NOP58	UP	0.05	2.80
18	Psmd11	PSD11	UP	0.04	3.00
19	Iars1	SYIC	UP	0.04	2.97
20	Rap2c	RAP2C	UP	0.03	3.27
21	Cpne1	CPNE1	UP	0.03	3.42
22	Arl8a	ARL8A	UP	0.04	3.00
23	Dars1	SYDC	UP	0.01	4.50
24	Ndufs5	NDUS5	UP	0.01	5.03
25	Itpa	ITPA	UP	0.02	3.75
26	Pgam1	PGAM1	UP	0.05	2.85
27	Ipo7	IPO7	UP	0.01	5.00
28	Scly	SCLY	UP	0.00	21.94
29	Vps29	VPS29	UP	0.03	3.19
30	Cad	PYR1	DOWN	0.03	-3.20
31	Tpr	TPR	DOWN	0.01	-4.99
32	Psmb1	PSB1	DOWN	0.03	-3.32
33	Fkbp8	FKBP8	DOWN	0.04	-3.10
34	Cops6	CSN6	DOWN	0.00	-7.68
35	H1-2	H12	DOWN	0.03	-3.14
36	Ass1	ASSY	DOWN	0.04	-3.04
37	Eno1	ENOA	DOWN	0.01	-4.13
38	Eno3	ENOB	DOWN	0.00	-7.48

39	Eif3a	EIF3A	DOWN	0.03	-3.34
40	Atxn10	ATX10	DOWN	0.02	-3.79
41	Alox5ap	AL5AP	DOWN	0.03	-3.19
42	Hmgb1	HMGB1	DOWN	0.01	-4.93
43	Rpl18	RL18	DOWN	0.03	-3.39
44	Rpl13	RL13	DOWN	0.01	-4.11
45	Idh2	IDHP	DOWN	0.00	-5.63
46	Adprh	ADPRH	DOWN	0.01	-4.20
47	Rpl18a	RL18A	DOWN	0.02	-3.69
48	Tubb4b	TBB4B	DOWN	0.01	-4.27
49	Erh	ERH	DOWN	0.02	-3.92
50	G3bp1	G3BP1	DOWN	0.00	-6.40
51	Myl12b	ML12B	DOWN	0.05	-2.81
52	Ttll12	TTL12	DOWN	0.01	-4.93
53	Hspe1	CH10	DOWN	0.04	-3.01
54	Cand1	CAND1	DOWN	0.03	-3.28
55	Eif2a	EIF2A	DOWN	0.05	-2.84
56	Pak2	PAK2	DOWN	0.05	-2.86
57	Hdlbp	VIGLN	DOWN	0.02	-4.03
58	Rpe	RPE	DOWN	0.01	-4.37
59	Ciapin1	CPIN1	DOWN	0.00	-6.04
60	Smarca5	SMCA5	DOWN	0.04	-3.08
61	Rfc4	RFC4	DOWN	0.04	-2.96
62	Mpst	THTM	DOWN	0.01	-4.16
63	Vwa5a	VMA5A	DOWN	0.03	-3.34
64	Etfa	ETFA	DOWN	0.03	-3.20
65	Grpel1	GRPE1	DOWN	0.04	-3.00
66	Atp6v1g1	VATG1	DOWN	0.01	-4.09
67	Sugt1	SGT1	DOWN	0.04	-2.93
68	Uqcrc1	QCR1	DOWN	0.02	-4.05
69	Gatd3	GAL3A	DOWN	0.02	-3.70
70	Akap8	AKAP8	DOWN	0.04	-3.12
71	Myo1c	MYO1C	DOWN	0.03	-3.42
72	Gk2	GLPK2	DOWN	0.03	-3.25
73	Eif2s3x	IF2G	DOWN	0.04	-3.05
LPS Control vs. LPS Plasma					
1	Itih4	ITIH4	UP	0.00	7.63
2	Rbm25	RBM25	UP	0.05	2.81
3	Rpl21	RL21	UP	0.03	3.14
4	Psmb9	PSB9	UP	0.01	4.92
5	C1qbp	C1QBP	UP	0.01	5.31
6	Nudc	NUDC	UP	0.02	3.64
7	Lsm2	LSM2	UP	0.02	3.72
8	Get3	GET3	UP	0.05	2.80
9	Pgrmc1	PGRC1	UP	0.02	3.87
10	Psmb5	PSB5	UP	0.00	7.21
11	Dhx9	DHX9	UP	0.04	3.13
12	Eef1b	EF1B	UP	0.03	3.34
13	Psma3	PSA3	UP	0.02	3.69
14	Creg1	CREG1	UP	0.02	4.09
15	Cpd	CBPD	UP	0.01	5.22
16	Rbm3	RBM3	UP	0.01	4.77
17	Hbb-b1	HBB1	UP	0.05	2.82
18	Ldha	LDHA	UP	0.02	3.59
19	Gpi	G6PI	UP	0.02	3.63
20	Anxa2	ANXA2	UP	0.01	4.89
21	Hsp90aa1	HS90A	UP	0.04	2.94
22	Sod1	SODC	UP	0.00	7.75
23	P4hb	PDIA1	UP	0.00	6.42
24	H2az1	H2AV	UP	0.02	3.70
25	Calm1	CALM1	UP	0.03	3.43
26	Ctsb	CATB	UP	0.01	5.27
27	Fn1	FINC	UP	0.00	9.08
28	Hsp90ab1	HS90B	UP	0.00	8.33
29	S100a6	S10A6	UP	0.01	4.50
30	Mdh1	MDHC	UP	0.02	3.91
31	Anxa6	ANXA6	UP	0.03	3.37
32	Nme1	NDKA	UP	0.04	3.00
33	Ldhb	LDHB	UP	0.05	2.85
34	Hspa1l	BIP	UP	0.02	4.08
35	Hmga1	HMGA1	UP	0.00	9.22
36	Eno1	ENOA 1	UP	0.01	5.18
37	Eno2	ENOA2	UP	0.00	8.99

38	Ppia	PPIA	UP	0.01	4.88
39	Hspa5	BIP	UP	0.01	4.37
40	Tmsb4x	TYB4	UP	0.05	2.79
41	Prdx3	PRDX3	UP	0.00	7.09
42	Fcer1g	FCERG	UP	0.00	8.41
43	Plg	PLMN	UP	0.04	3.03
44	Cbx3	CBX3	UP	0.00	7.26
45	Cbx5	CBX35	UP	0.00	18.91
46	Impdh2	IMDH2	UP	0.00	5.73
47	M6pr	MPRD	UP	0.02	3.74
48	Lyn	LYN	UP	0.00	13.61
49	Adh5	ADHX	UP	0.03	3.14
50	Marcksl1	MRP	UP	0.02	3.73
51	Prkcd	KPCD	UP	0.02	3.73
52	Ptpn6	PTN6	UP	0.01	5.27
53	Nedd8	NEDD8	UP	0.01	4.71
54	Serpinc1	ANT3	UP	0.01	5.34
55	Ranbp1	RANG	UP	0.00	5.85
56	Mif	MIF	UP	0.00	7.00
57	Acsl1	ACSL1	UP	0.04	2.88
58	Srprb	SRPRB	UP	0.02	3.58
59	Alox5	LOX5	UP	0.04	3.06
60	Mcm4	MCM4	UP	0.02	3.53
61	Arsb	ARSB	UP	0.04	3.13
62	Atp6v1a	VATA	UP	0.03	3.15
63	Pa2g4	PA2G4	UP	0.00	10.63
64	Rpl9	RL9	UP	0.04	3.04
65	Pkm	KPYM	UP	0.01	5.07
66	Rpl10a	RL10A	UP	0.05	2.79
67	Acod1	IRG1	UP	0.02	4.05
68	Arpc4	ARPC4	UP	0.01	4.26
69	Arf1	ARF1	UP	0.02	3.51
70	Rps13	RS13	UP	0.00	9.83
71	Snrpd2	SMD2	UP	0.01	5.44
72	Arf6	ARF6	UP	0.02	3.67
73	H4c1	H4	UP	0.02	3.83
74	Rps3	RS3	UP	0.01	4.57
75	Ybx1	YBOX1	UP	0.01	5.45
76	Rps27a	RS27A	UP	0.02	3.66
77	Hspd1	CH60	UP	0.01	5.01
78	Hmgb1	HMGB1	UP	0.00	5.77
79	Rps10	RS10	UP	0.02	3.93
80	Actc1	ACTC	UP	0.03	3.21
81	Tuba4a	TBA4A	UP	0.04	3.11
82	Idh3g	IDHG1	UP	0.05	2.81
83	Naca	NACAM	UP	0.00	6.61
84	Cct4	TCPD	UP	0.00	9.88
85	Atp1b3	AT1B3	UP	0.00	6.05
86	Anxa11	ANX11	UP	0.03	3.22
87	G6pdx	G6PD1	UP	0.01	4.88
88	Nme2	NDKB	UP	0.03	3.40
89	Ckb	KCRB	UP	0.01	4.14
90	Rac2	RAC2	UP	0.00	24.65
91	Eif5b	IF2P	UP	0.00	7.14
92	Atp5me	ATP5I	UP	0.00	11.77
93	Eif3j1	EI3JA	UP	0.03	3.45
94	Pdap1	HAP28	UP	0.02	3.71
95	Edc4	EDC4	UP	0.04	2.92
96	Ppp1r7	PP1R7	UP	0.01	4.38
97	Naa10	NAA10	UP	0.01	4.14
98	Lrrfip1	LRRF1	UP	0.00	5.72
99	Abracl	ABRAL	UP	0.04	2.90
100	Arhgef1	ARHG1	UP	0.00	7.53
101	Ewsr1	EWS	UP	0.04	2.94
102	Srsf2	SRSF2	UP	0.03	3.48
103	Snrpa	SNRPA	UP	0.01	4.37
104	Ndufa4	NDUA4	UP	0.00	12.46
105	Cstb	CYTB	UP	0.02	3.66
106	A2m	A2MG	UP	0.00	9.43
107	Snx6	SNX6	UP	0.02	3.89
108	Oxsr1	OXSR1	UP	0.00	6.79
109	Jpt2	JUPI2	UP	0.05	2.84
110	Lsm8	LSM8	UP	0.01	4.94

111	Rps9	RS9	UP	0.02	3.96
112	Rps27	RS27	UP	0.01	4.65
113	Nap1l4	NP1L4	UP	0.00	21.02
114	Luc7l2	LC7L2	UP	0.03	3.27
115	Gatd1	GALD1	UP	0.00	10.74
116	Hnrnpa3	ROA3	UP	0.02	3.62
117	Psmd11	PSD11	UP	0.00	6.11
118	Samm50	SAM50	UP	0.04	2.97
119	Bola2	BOLA2	UP	0.03	3.40
120	Pck2	PCKGM	UP	0.05	2.88
121	Cfap69	CFA69	UP	0.01	5.48
122	Ahsa1	AHSA1	UP	0.02	3.53
123	Nceh1	NCEH1	UP	0.01	5.13
124	Qars1	SYQ	UP	0.03	3.31
125	Rcn2	RCN2	UP	0.00	8.44
126	Trnt1	TRNT1	UP	0.01	4.81
127	Dnm1l	DNM1L	UP	0.00	6.82
128	Eif3l	EIF3L	UP	0.03	3.39
129	Uqcr10	QCR9	UP	0.01	4.09
130	Myh9	MYH9	UP	0.02	3.56
131	Ddx39a	DX39A	UP	0.00	9.05
132	Arl8a	ARL8A	UP	0.00	7.28
133	Acot7	BACH	UP	0.01	5.08
134	Rab14	RAB14	UP	0.02	3.51
135	Slc39a8	S39A8	UP	0.00	6.14
136	Basp1	BASP1	UP	0.04	3.04
137	Rpn1	RPN1	UP	0.01	4.39
138	Dars1	SYDC	UP	0.01	5.11
139	Cers2	CERS2	UP	0.03	3.14
140	Nans	SIAS	UP	0.03	3.47
141	Gps1	CSN1	UP	0.02	3.81
142	Ndufs5	NDUS5	UP	0.01	5.27
143	Npm3	NPM3	UP	0.00	7.22
144	Nudt21	CPSF5	UP	0.02	3.66
145	Ifitm3	IFM3	UP	0.02	3.63
146	Cyb5b	CYB5B	UP	0.01	4.24
147	Hypk	HYPK	UP	0.00	9.98
148	Chchd3	MIC19	UP	0.01	5.22
149	Rprd1b	RPR1B	UP	0.04	3.11
150	Hnrnpa0	ROA0	UP	0.03	3.37
151	Ssr1	SSRA	UP	0.01	4.61
152	Serbp1	PAIRB	UP	0.01	4.98
153	Tmed10	TMEDA	UP	0.03	3.47
154	Dlst	ODO2	UP	0.03	3.16
155	Atp5f1d	ATPD	UP	0.02	3.93
156	Serpinb12	SPB12	UP	0.01	5.24
157	Rpl4	RL4	UP	0.01	4.61
158	Rpn2	RPN2	UP	0.03	3.35
159	Pgam1	PGAM1	UP	0.00	5.84
160	Paics	PUR6	UP	0.00	6.38
161	Aldh6a1	MMSA	UP	0.03	3.42
162	Mesd	MESD	UP	0.01	4.18
163	Prmt1	ANM1	UP	0.02	3.77
164	Copb1	COPB	UP	0.04	2.88
165	Ybx3	YBOX3	UP	0.03	3.20
166	Mbnl1	MBNL1	UP	0.03	3.27
167	Rhoa	RHOA	UP	0.00	6.94
168	Vapa	VAPA	UP	0.03	3.20
169	Vps29	VPS29	UP	0.00	8.46
170	Tmed2	TMED2	UP	0.04	2.91
171	Plp2	PLP2	UP	0.00	5.65
172	Uchl5	UCHL5	UP	0.00	10.20
173	Ctsz	CATZ	UP	0.02	3.97
174	Lipa	LICH	UP	0.02	3.69
175	Atp6v1c1	VATC1	UP	0.02	3.91
176	Cad	PYR1	DOWN	0.02	-4.07
177	Gls	GLSK	DOWN	0.01	-4.82
178	Nolc1	NOLC1	DOWN	0.04	-3.01
179	Bin1	BIN1	DOWN	0.03	-3.32
180	Sec22b	SC22B	DOWN	0.00	-11.11
181	Clta	CLCA	DOWN	0.03	-3.17
182	Dld	DLDH	DOWN	0.00	-7.98
183	Prkcsh	GLU2B	DOWN	0.02	-4.01

184	Atox1	ATOX1	DOWN	0.02	-3.73
185	Degs1	DEGS1	DOWN	0.02	-3.70
186	Gsto1	GSTO1	DOWN	0.03	-3.23
187	Atp5if1	ATIF1	DOWN	0.01	-4.43
188	Srsf5	SRSF5	DOWN	0.00	-5.70
189	Anp32a	AN32A	DOWN	0.00	-13.68
190	Fkbp8	FKBP8	DOWN	0.03	-3.42
191	Anxa3	ANXA3	DOWN	0.00	-9.44
192	Hnrnph1	HNRH1	DOWN	0.00	-9.89
193	Eif6	IF6	DOWN	0.04	-3.07
194	Snx12	SNX12	DOWN	0.02	-3.56
195	Hsd17b12	DHB12	DOWN	0.00	-6.76
196	Wdr1	WDR1	DOWN	0.04	-2.96
197	Dhcr7	DHCR7	DOWN	0.00	-7.80
198	Gcat	KBL	DOWN	0.01	-4.41
199	Coro1a	COR1A	DOWN	0.00	-8.60
200	Mtco2	COX2	DOWN	0.01	-4.28
201	C4b	CO4B	DOWN	0.01	-5.05
202	B2m	B2MG	DOWN	0.02	-3.77
203	H2-D1	HA11	DOWN	0.01	-4.24
204	Iap	IGEB	DOWN	0.00	-6.87
205	Aldoc	ALDOC	DOWN	0.04	-3.11
206	Got1	AATC	DOWN	0.03	-3.42
207	Itgam	ITAM	DOWN	0.04	-2.91
208	Pdia4	PDIA4	DOWN	0.03	-3.33
209	Lyz1	LYZ1	DOWN	0.00	-5.90
210	Pgk1	PGK1	DOWN	0.04	-3.12
211	Eef1a1	EF1A1	DOWN	0.01	-5.23
212	Cd14	CD14	DOWN	0.02	-3.62
213	Slc3a2	4F2	DOWN	0.03	-3.35
214	Itga5	ITA5	DOWN	0.02	-3.89
215	Itgb2	ITB2	DOWN	0.01	-4.71
216	Tcp1	TCPA	DOWN	0.03	-3.27
217	Rps16	RS16	DOWN	0.01	-4.44
218	Bpgm	PMGE	DOWN	0.01	-4.59
219	H1-2	H12	DOWN	0.03	-3.26
220	H1-1	H11	DOWN	0.02	-3.59
221	H1-3	H13	DOWN	0.01	-5.43
222	H1-2	H12	DOWN	0.03	-3.28
223	Gapdh	G3P	DOWN	0.03	-3.34
224	Eno1	ENOA	DOWN	0.05	-2.82
225	Fasn	FAS	DOWN	0.01	-4.94
226	Cox4i1	COX41	DOWN	0.04	-2.95
227	Tpm1	TPM1	DOWN	0.02	-3.73
228	Eno3	ENOB	DOWN	0.01	-4.58
229	Pcmt1	PIMT	DOWN	0.01	-4.32
230	Lta4h	LKHA4	DOWN	0.00	-9.63
231	Tln1	TLN1	DOWN	0.00	-10.74
232	Msn	MOES	DOWN	0.00	-7.87
233	Glud1	DHE3	DOWN	0.02	-3.67
234	Psmd7	PSMD7	DOWN	0.00	-13.19
235	Snrpb	RSMB	DOWN	0.00	-7.03
236	Msr1	MSRE	DOWN	0.01	-5.12
237	Alox5ap	AL5AP	DOWN	0.01	-4.97
238	Hmgb1	HMGB1	DOWN	0.01	-5.22
239	C5ar1	C5AR1	DOWN	0.03	-3.42
240	Lig1	DNLI1	DOWN	0.04	-2.95
241	Hspa9	GRP75	DOWN	0.02	-3.65
242	Dnm2	DYN2	DOWN	0.03	-3.44
243	Fen1	FEN1	DOWN	0.02	-3.63
244	Septin2	SEPTIN2	DOWN	0.03	-3.23
245	Stat1	STAT1	DOWN	0.03	-3.34
246	Fkbp2	FKBP2	DOWN	0.00	-6.71
247	Aldh2	ALDH2	DOWN	0.01	-4.37
248	Capza1	CAZA1	DOWN	0.01	-5.24
249	Rplp1	RLA1	DOWN	0.01	-4.56
250	Rpl13	RL13	DOWN	0.01	-5.25
251	Tbca	TBCA	DOWN	0.04	-3.07
252	Hdgf	HDGF	DOWN	0.01	-5.53
253	Lum	LUM	DOWN	0.04	-2.88
254	Pitpna	PIPNA	DOWN	0.04	-3.07
255	Idh2	IDHP	DOWN	0.00	-10.45
256	Rad23b	RD23B	DOWN	0.05	-2.81

257	Atp5mf	ATPK	DOWN	0.00	-8.96
258	Usp5	UBP5	DOWN	0.01	-4.43
259	Erp29	ERP29	DOWN	0.01	-5.22
260	Eef1d	EF1D	DOWN	0.00	-6.57
261	Eif5	IF5	DOWN	0.02	-4.04
262	Sf3b6	SF3B6	DOWN	0.02	-3.69
263	Pcbp1	PCBP1	DOWN	0.04	-3.06
264	Actr1a	ACTY	DOWN	0.01	-5.58
265	Psme3	PSME3	DOWN	0.04	-3.07
266	Hnrnpk	HNRPK	DOWN	0.01	-4.50
267	Ywhab	1433B	DOWN	0.02	-3.67
268	Timm13	TIM13	DOWN	0.01	-4.75
269	Psmc5	PRS8	DOWN	0.00	-7.16
270	Rps14	RS14	DOWN	0.02	-3.85
271	Rps18	RS18	DOWN	0.02	-3.58
272	Rps29	RS29	DOWN	0.04	-3.01
273	Snrpe	RUXE	DOWN	0.04	-2.99
274	Snrpg	RUXG	DOWN	0.02	-3.96
275	Rpl18a	RL18A	DOWN	0.00	-9.71
276	Rps15	RS15	DOWN	0.01	-4.23
277	Rps24	RS24	DOWN	0.01	-4.48
278	Rpl8	RL8	DOWN	0.00	-10.51
279	Pfn1	PROF1	DOWN	0.01	-4.42
280	Rac2	RAC2	DOWN	0.03	-3.25
281	Dnaja1	DNJA1	DOWN	0.04	-3.00
282	Ppp1cc	PP1G	DOWN	0.03	-3.21
283	Rps12	RS12	DOWN	0.03	-3.49
284	Tubb4b	TBB4B	DOWN	0.01	-4.72
285	Tubb6	TBB6	DOWN	0.02	-3.57
286	Hnrnph2	HNRH2	DOWN	0.02	-4.08
287	Cct3	TCPG	DOWN	0.03	-3.33
288	Renbp	RENBP	DOWN	0.01	-5.15
289	Phf5a	PHF5A	DOWN	0.00	-5.69
290	Rhog	RHOG	DOWN	0.02	-3.82
291	Rpl19	RL19	DOWN	0.04	-3.00
292	Srsf3	SRSF3	DOWN	0.03	-3.25
293	Anxa4	ANXA4	DOWN	0.01	-4.21
294	Bop1	BOP1	DOWN	0.02	-3.64
295	Rps5	RS5	DOWN	0.01	-4.73
296	Ctsc	CATC	DOWN	0.04	-3.01
297	G3bp1	G3BP1	DOWN	0.03	-3.15
298	Uba1	UBA1	DOWN	0.02	-3.79
299	Pfdn6	PFD6	DOWN	0.05	-2.78
300	Lgals3bp	LG3BP	DOWN	0.00	-6.19
301	Bax	BAX	DOWN	0.04	-3.12
302	Prrc2c	PRC2C	DOWN	0.05	-2.84
303	Uap1l1	UAP1L	DOWN	0.00	-12.73
304	Khsrp	FUBP2	DOWN	0.01	-4.11
305	Puf60	PUF60	DOWN	0.01	-4.26
306	Cdv3	CDV3	DOWN	0.01	-4.81
307	Ddx17	DDX17	DOWN	0.01	-4.45
308	Ctc1	CTC1	DOWN	0.04	-2.94
309	Hnrnpd	HNRPD	DOWN	0.00	-5.80
310	Caprin1	CAPR1	DOWN	0.01	-4.50
311	Eif1a	IF1AX	DOWN	0.04	-3.01
312	Hars1	HARS1	DOWN	0.04	-3.02
313	Cybb	CY24B	DOWN	0.00	-7.86
314	Mapre1	MARE1	DOWN	0.05	-2.78
315	Clns1a	ICLN	DOWN	0.00	-7.06
316	Hcfc1	HCFC1	DOWN	0.01	-4.26
317	Glg1	GSLG1	DOWN	0.04	-2.93
318	Ddx5	DDX5	DOWN	0.01	-5.52
319	Kif5b	KINH	DOWN	0.05	-2.82
320	Lasp1	LASP1	DOWN	0.04	-2.99
321	Pzp	PZP	DOWN	0.04	-2.93
322	Shh	SHH	DOWN	0.00	-8.96
323	Tpd52	TPD52	DOWN	0.00	-9.69
324	Sh3gl1	SH3G1	DOWN	0.01	-4.31
325	Eif4g2	IF4G2	DOWN	0.00	-5.84
326	Zyx	ZYX	DOWN	0.01	-5.43
327	Sf1	SF01	DOWN	0.00	-5.75
328	Bcl2l1	B2CL1	DOWN	0.00	-6.99
329	Hspe1	CH10	DOWN	0.04	-3.00

330	Tpp2	TPP2	DOWN	0.01	-4.21
331	Gk	GLPK	DOWN	0.00	-7.12
332	Cdc5l	CDC5L	DOWN	0.04	-3.00
333	Nomo1	NOMO1	DOWN	0.03	-3.24
334	Snrnp200	U520	DOWN	0.05	-2.87
335	Uggt1	UGGG1	DOWN	0.00	-6.19
336	Pcnp	PCNP	DOWN	0.02	-3.54
337	Chd4	CHD4	DOWN	0.04	-3.12
338	Camk2d	KCC2D	DOWN	0.02	-3.97
339	Cand1	CAND1	DOWN	0.00	-9.19
340	Ugt1a7	UD17	DOWN	0.01	-4.77
341	Atp5mk	ATPMK	DOWN	0.04	-2.89
342	Snd1	SND1	DOWN	0.02	-3.54
343	Mogs	MOGS	DOWN	0.03	-3.30
344	Flnb	FLNB	DOWN	0.01	-5.16
345	Eif4b	IF4B	DOWN	0.00	-10.62
346	Nup93	NUP93	DOWN	0.03	-3.17
347	Srsf7	SRSF7	DOWN	0.02	-3.84
348	Srp68	SRP68	DOWN	0.02	-3.54
349	Slc25a24	SCMC1	DOWN	0.00	-5.68
350	Dlat	ODP2	DOWN	0.04	-3.02
351	Lars1	SYLC	DOWN	0.02	-4.00
352	Srrm2	SRRM2	DOWN	0.01	-4.96
353	Sec62	SEC62	DOWN	0.04	-2.99
354	Qdpr	DHPR	DOWN	0.02	-3.69
355	Gemin5	GEMI5	DOWN	0.02	-3.86
356	Agps	ADAS	DOWN	0.03	-3.47
357	Septin11	SEPTIN11	DOWN	0.01	-4.82
358	Macroh2a2	H2AW	DOWN	0.01	-4.54
359	Macroh2a1	H2AW	DOWN	0.00	-7.17
360	Pgp	PGP	DOWN	0.01	-5.36
361	Ubqln1	UBQL1	DOWN	0.05	-2.84
362	Hdlbp	VIGLN	DOWN	0.02	-3.63
363	Atp1a1	AT1A1	DOWN	0.00	-12.41
364	Rpe	RPE	DOWN	0.00	-7.33
365	Rpa1	RFA1	DOWN	0.03	-3.22
366	Sfpq	SFPQ	DOWN	0.00	-7.42
367	Nono	NONO	DOWN	0.02	-3.62
368	Ciapin1	CPIN1	DOWN	0.02	-3.62
369	Ndufs1	NDUS1	DOWN	0.01	-4.52
370	Grhpr	GRHPR	DOWN	0.00	-5.70
371	Smarca5	SMCA5	DOWN	0.00	-6.42
372	Acaa1a	THIKA	DOWN	0.00	-9.10
373	Mthfd1	C1TC	DOWN	0.04	-2.99
374	Blvrb	BLVRB	DOWN	0.01	-4.44
375	Sf3b5	SF3B5	DOWN	0.03	-3.29
376	Psmd6	PSMD6	DOWN	0.00	-10.06
377	Vwa5a	VMA5A	DOWN	0.00	-8.09
378	Etfa	ETFA	DOWN	0.00	-7.97
379	Grpel1	GRPE1	DOWN	0.00	-14.83
380	Abhd12	ABD12	DOWN	0.05	-2.86
381	Park7	PARK7	DOWN	0.01	-4.64
382	Nasp	NASP	DOWN	0.02	-3.52
383	Prpf8	PRP8	DOWN	0.03	-3.21
384	Arpc5	ARPC5	DOWN	0.04	-3.11
385	Dut	DUT	DOWN	0.01	-5.17
386	RTRAF	RTRAF	DOWN	0.02	-3.90
387	Rps21	RS21	DOWN	0.01	-4.34
388	Atp6v1g1	VATG1	DOWN	0.00	-9.35
389	Snw1	SNW1	DOWN	0.03	-3.38
390	Atic	PUR9	DOWN	0.00	-6.39
391	Snx2	SNX2	DOWN	0.02	-3.57
392	Snx1	SNX1	DOWN	0.05	-2.82
393	Pin4	PIN4	DOWN	0.01	-4.12
394	Tomm34	TOM34	DOWN	0.02	-4.08
395	Uqcrc1	QCR1	DOWN	0.05	-2.83
396	Nsfl1c	NSF1C	DOWN	0.01	-5.07
397	Gars1	GARS	DOWN	0.01	-5.26
398	Rpl15	RL15	DOWN	0.00	-6.47
399	Shmt2	GLYM	DOWN	0.00	-5.98
400	Tsfm	EFTS	DOWN	0.01	-4.32
401	Cmss1	CMS1	DOWN	0.01	-5.55
402	Cs	CISY	DOWN	0.01	-4.51

403	Srsf9	SRSF9	DOWN	0.04	-2.91
404	Pbdc1	PBDC1	DOWN	0.05	-2.80
405	Hnrnpm	HNRPM	DOWN	0.05	-2.80
406	Pgm1	PGM1	DOWN	0.03	-3.20
407	Oxct1	SCOT1	DOWN	0.01	-4.67
408	Snu13	NH2L1	DOWN	0.02	-3.57
409	Gatd3	GAL3A	DOWN	0.02	-3.88
410	Cndp2	CNDP2	DOWN	0.02	-3.81
411	Sf3a3	SF3A3	DOWN	0.01	-4.15
412	Prps1	PRPS1	DOWN	0.03	-3.33
413	U2af1	U2AF1	DOWN	0.01	-4.25
414	Chmp4b	CHM4B	DOWN	0.01	-5.03
415	Snx5	SNX5	DOWN	0.01	-4.34
416	Atp5po	ATPO	DOWN	0.01	-4.43
417	Plin3	PLIN3	DOWN	0.00	-9.53
418	Ampd2	AMPD2	DOWN	0.01	-4.17
419	Pycr3	P5CR3	DOWN	0.05	-2.80
420	Ethe1	ETHE1	DOWN	0.00	-6.16
421	Akr1e2	AKCL2	DOWN	0.01	-5.17
422	Ehd4	EHD4	DOWN	0.02	-4.02
423	Dazap1	DAZP1	DOWN	0.01	-4.19
424	Fmnl1	FMNL1	DOWN	0.00	-6.11
425	Acsl4	ACSL4	DOWN	0.03	-3.42
426	Prep	PPCE	DOWN	0.01	-4.64
427	Plec	PLEC	DOWN	0.03	-3.18
428	Eif3i	EIF3I	DOWN	0.02	-3.76
429	Ptges3	TEBP	DOWN	0.01	-4.95
430	Tapbp	TPSN	DOWN	0.00	-9.31
431	Ruvbl2	RUVB2	DOWN	0.00	-6.03
432	Ak2	KAD2	DOWN	0.03	-3.36
433	Gk2	GLPK2	DOWN	0.00	-7.58
434	Pdcd6ip	PDC6I	DOWN	0.02	-4.02
435	Pfkp	PFKAP	DOWN	0.04	-2.93
436	Eif4h	IF4H	DOWN	0.00	-9.58
437	Coro1b	COR1B	DOWN	0.04	-3.07
438	Suclg1	SUCA	DOWN	0.02	-3.82
439	Timm8a1	TIM8A	DOWN	0.02	-3.75
440	Atp6v0a1	VPP1	DOWN	0.04	-3.04
441	Ddx39b	DX39B	DOWN	0.05	-2.79
442	Clic1	CLIC1	DOWN	0.00	-17.53
443	Sucla2	SUCB1	DOWN	0.00	-12.01
444	Dnpep	DNPEP	DOWN	0.01	-5.29
LPS Control vs. LPS Corundum					
1	Rbm25	RBM25	UP	0.03	3.14
2	Hk2	HXK2	UP	0.05	2.87
3	C1qbp	C1QBP	UP	0.03	3.21
4	Nudc	NUDC	UP	0.01	5.39
5	Lsm2	LSM2	UP	0.00	11.01
6	Get3	GET3	UP	0.04	2.95
7	Pgrmc1	PGRC1	UP	0.00	19.23
8	Dhx9	DHX9	UP	0.01	5.13
9	Ncf2	NCF2	UP	0.05	2.79
10	Eef1b	EF1B	UP	0.01	4.60
11	Psma3	PSA3	UP	0.01	4.23
12	Creg1	CREG1	UP	0.01	4.61
13	Cpd	CBPD	UP	0.02	4.03
14	Hbb-b1	HBB1	UP	0.03	3.22
15	H3-3a	H31	UP	0.04	3.01
16	Jun	JUN	UP	0.01	4.88
17	Gpi	G6PI	UP	0.01	4.92
18	Fcgr2	FCGR2	UP	0.01	4.56
19	Sod1	SODC	UP	0.04	2.99
20	Ncl	NUCL	UP	0.02	3.56
21	H2az1	H2AV	UP	0.00	5.94
22	Ctsb	CATB	UP	0.00	6.63
23	Hsp90ab1	HS90B	UP	0.01	5.17
24	Cfp	PROP	UP	0.01	5.51
25	Gsn	GELS	UP	0.01	5.29
26	S100a6	S10A6	UP	0.01	4.48
27	Anxa6	ANXA6	UP	0.02	3.97
28	Rplp0	RLA0	UP	0.03	3.27
29	Nme1	NDKA	UP	0.04	2.91
30	Ldhb	LDHB	UP	0.04	2.97

31	Eno1	ENOA	UP	0.01	4.48
32	Ppia	PPIA	UP	0.02	3.85
33	Prdx3	PRDX3	UP	0.02	3.99
34	Fcer1g	FCERG	UP	0.01	4.35
35	Tpm3	TPM3	UP	0.02	3.75
36	Cbx3	CBX3	UP	0.04	2.95
37	Impdh2	IMDH2	UP	0.00	6.99
38	M6pr	MPRD	UP	0.01	4.82
39	Mug1	MUG1	UP	0.00	6.67
40	Ptpn6	PTN6	UP	0.02	3.70
41	Nedd8	NEDD8	UP	0.01	5.34
42	Fkbp4	FKBP4	UP	0.00	13.36
43	Aimp1	AIMP1	UP	0.00	6.14
44	Serpinc1	ANT3	UP	0.00	6.37
45	Ranbp1	RANG	UP	0.01	4.74
46	Canx	CALX	UP	0.01	4.09
47	Rpl12	RL12	UP	0.04	2.97
48	Alox5	LOX5	UP	0.02	3.85
49	Hcls1	HCLS1	UP	0.04	3.09
50	Mcm4	MCM4	UP	0.03	3.16
51	Arsb	ARSB	UP	0.02	3.63
52	Atp6v1a	VATA	UP	0.03	3.20
53	Pa2g4	PA2G4	UP	0.00	6.96
54	Pkm	KPYM	UP	0.01	4.84
55	Acod1	IRG1	UP	0.03	3.24
56	Ctbp2	CTBP2	UP	0.05	2.85
57	Arf1	ARF1	UP	0.02	4.08
58	Rpl27	RL27	UP	0.02	3.65
59	Rps7	RS7	UP	0.00	6.89
60	Rps13	RS13	UP	0.01	5.20
61	Arf6	ARF6	UP	0.01	4.92
62	Rpl30	RL30	UP	0.04	2.96
63	Rps3	RS3	UP	0.05	2.82
64	Ybx1	YBOX1	UP	0.03	3.31
65	Rps27a	RS27A	UP	0.01	4.91
66	Hspd1	CH60	UP	0.01	4.35
67	Hmgb1	HMGB1	UP	0.00	5.65
68	Rps10	RS10	UP	0.01	4.17
69	Tuba1c	TBA1C	UP	0.03	3.20
70	Hint1	HINT1	UP	0.00	6.30
71	Idh3g	IDHG1	UP	0.01	4.54
72	Cct4	TCPD	UP	0.02	3.99
73	Arf5	ARF5	UP	0.01	4.21
74	Csrp1	CSRP1	UP	0.01	4.59
75	Ckb	KCRB	UP	0.00	5.93
76	Rac2	RAC2	UP	0.00	5.84
77	Eif5b	IF2P	UP	0.00	6.44
78	Atp5me	ATP5I	UP	0.05	2.78
79	Ncf1	NCF1	UP	0.02	3.61
80	Ppp1r7	PP1R7	UP	0.01	5.41
81	Abracl	ABRAL	UP	0.04	2.91
82	Vdac1	VDAC1	UP	0.02	3.83
83	Rbbp7	RBBP7	UP	0.00	6.80
84	Srsf2	SRSF2	UP	0.01	4.24
85	Swap70	SWP70	UP	0.03	3.41
86	Snx6	SNX6	UP	0.02	3.89
87	Oxsr1	OXSR1	UP	0.00	5.78
88	Lsm8	LSM8	UP	0.00	11.79
89	Nap1l4	NP1L4	UP	0.00	12.59
90	Luc7l2	LC7L2	UP	0.03	3.47
91	Hnrnpa3	ROA3	UP	0.03	3.28
92	Psmd11	PSD11	UP	0.00	8.56
93	Bola2	BOLA2	UP	0.01	4.99
94	Ahsa1	AHSA1	UP	0.05	2.82
95	Immt	MIC60	UP	0.03	3.26
96	Trnt1	TRNT1	UP	0.02	3.86
97	Ddx39a	DX39A	UP	0.01	5.45
98	Arl8a	ARL8A	UP	0.01	4.10
99	Slc25a3	MPCP	UP	0.01	5.47
100	Slc39a8	S39A8	UP	0.01	4.63
101	Rpn1	RPN1	UP	0.03	3.24
102	Dars1	SYDC	UP	0.01	4.18
103	Nans	SIAS	UP	0.01	4.83

104	Ndufs5	NDUS5	UP	0.01	4.46
105	Ifitm3	IFM3	UP	0.01	4.24
106	Ndufab1	ACPM	UP	0.03	3.49
107	Hypk	HYPK	UP	0.00	8.18
108	Pfdn1	PFD1	UP	0.01	5.35
109	Serpinb12	SPB12	UP	0.01	5.47
110	Rpl22l1	RL22L	UP	0.03	3.42
111	Rpl4	RL4	UP	0.00	5.85
112	Cnpy3	CNPY3	UP	0.01	4.18
113	Pgam1	PGAM1	UP	0.03	3.25
114	Paics	PUR6	UP	0.01	4.40
115	Mesd	MESD	UP	0.01	4.14
116	Rpl38	RL38	UP	0.03	3.16
117	Scly	SCLY	UP	0.03	3.48
118	Rhoa	RHOA	UP	0.04	3.00
119	Dstn	DEST	UP	0.04	3.01
120	Psmb2	PSB2	UP	0.02	3.81
121	Plp2	PLP2	UP	0.03	3.43
122	Lipa	LICH	UP	0.02	3.52
123	Tpr	TPR	DOWN	0.05	-2.86
124	Bin1	BIN1	DOWN	0.02	-4.03
125	Dld	DLDH	DOWN	0.05	-2.84
126	Gsto1	GSTO1	DOWN	0.02	-3.58
127	Anp32a	AN32A	DOWN	0.00	-10.86
128	Anxa3	ANXA3	DOWN	0.02	-3.51
129	Hnrnph1	HNRH1	DOWN	0.00	-5.62
130	Pgam2	PGAM2	DOWN	0.01	-4.36
131	Hsd17b12	DHB12	DOWN	0.00	-7.80
132	Pfdn2	PFD2	DOWN	0.01	-4.80
133	Cops4	CSN4	DOWN	0.03	-3.24
134	Nfatc1	NFAC1	DOWN	0.03	-3.29
135	Gcat	KBL	DOWN	0.04	-3.12
136	Coro1a	COR1A	DOWN	0.02	-3.66
137	B2m	B2MG	DOWN	0.00	-6.14
138	Aldoc	ALDOC	DOWN	0.02	-3.59
139	Lyz1	LYZ1	DOWN	0.03	-3.30
140	Anxa1	ANXA1	DOWN	0.02	-3.62
141	Itga5	ITA5	DOWN	0.01	-4.90
142	H1-2	H12	DOWN	0.02	-3.50
143	Eno3	ENOB	DOWN	0.01	-5.14
144	Pcmt1	PIMT	DOWN	0.02	-3.68
145	Lta4h	LKHA4	DOWN	0.02	-3.66
146	Ezr	EZRI	DOWN	0.04	-3.11
147	Psmd7	PSMD7	DOWN	0.02	-3.61
148	Snrpb	RSMB	DOWN	0.00	-5.76
149	Nap1l1	NP1L1	DOWN	0.01	-4.55
150	Grn	GRN	DOWN	0.04	-3.06
151	Hmgb1	HMGB1	DOWN	0.04	-3.09
152	C5ar1	C5AR1	DOWN	0.01	-4.12
153	Cap1	CAP1	DOWN	0.00	-5.66
154	Aldh2	ALDH2	DOWN	0.03	-3.16
155	Capza1	CAZA1	DOWN	0.03	-3.15
156	S100a11	S10AB	DOWN	0.00	-6.05
157	Rab2a	RAB2A	DOWN	0.00	-7.51
158	Idh2	IDHP	DOWN	0.00	-20.36
159	Rad23b	RD23B	DOWN	0.01	-4.42
160	Atp5mf	ATPK	DOWN	0.03	-3.39
161	Usp5	UBP5	DOWN	0.02	-3.91
162	Actn4	ACTN4	DOWN	0.02	-3.60
163	Pcbp1	PCBP1	DOWN	0.01	-4.66
164	Rab8b	RAB8B	DOWN	0.01	-5.21
165	Actr1a	ACTY	DOWN	0.04	-3.01
166	Psme3	PSME3	DOWN	0.03	-3.21
167	Hnrnpk	HNRPK	DOWN	0.04	-2.98
168	Ywhab	YWHAB	DOWN	0.04	-2.92
169	Timm13	TIM13	DOWN	0.01	-4.55
170	Rps14	RS14	DOWN	0.02	-3.53
171	Rpl18a	RL18A	DOWN	0.03	-3.45
172	Gnb2	GBB2	DOWN	0.01	-4.57
173	Rpl8	RL8	DOWN	0.00	-6.22
174	Vamp3	VAMP3	DOWN	0.01	-5.15
175	Tpt1	TCTP	DOWN	0.00	-6.29
176	Ywhaz	1433Z	DOWN	0.01	-4.82

177	Phf5a	PHF5A	DOWN	0.00	-16.00
178	Rpl19	RL19	DOWN	0.03	-3.22
179	Mcm2	MCM2	DOWN	0.00	-5.60
180	Anxa4	ANXA4	DOWN	0.04	-3.03
181	Pfdn6	PFD6	DOWN	0.03	-3.31
182	Bax	BAX	DOWN	0.03	-3.29
183	Myl12b	ML12B	DOWN	0.04	-3.05
184	Uap1l1	UAP1L	DOWN	0.01	-4.29
185	Ttll12	TTL12	DOWN	0.03	-3.17
186	Puf60	PUF60	DOWN	0.04	-2.95
187	Cdv3	CDV3	DOWN	0.05	-2.87
188	Eif1a	IF1AX	DOWN	0.04	-3.06
189	Mapre1	MARE1	DOWN	0.03	-3.25
190	Clns1a	ICLN	DOWN	0.03	-3.44
191	Hsph1	HS105	DOWN	0.02	-3.91
192	Pzp	PZP	DOWN	0.00	-7.32
193	Trim28	TIF1B	DOWN	0.03	-3.15
194	Tpd52	TPD52	DOWN	0.01	-4.59
195	Sf1	SF01	DOWN	0.01	-4.68
196	Bcl2l1	B2CL1	DOWN	0.04	-2.96
197	Hspe1	CH10	DOWN	0.04	-2.98
198	Tpp2	TPP2	DOWN	0.02	-3.76
199	Gk	GLPK	DOWN	0.05	-2.88
200	Snrnp200	U520	DOWN	0.01	-4.61
201	Abcf1	ABCF1	DOWN	0.02	-3.82
202	Camk2d	KCC2D	DOWN	0.04	-2.90
203	Cand1	CAND1	DOWN	0.00	-5.73
204	Atxn2l	ATX2L	DOWN	0.02	-4.06
205	Naa15	NAA15	DOWN	0.05	-2.84
206	Eif4b	IF4B	DOWN	0.03	-3.44
207	Slc25a24	SCMC1	DOWN	0.01	-4.23
208	Lars1	SYLC	DOWN	0.05	-2.78
209	Slc15a3	S15A3	DOWN	0.03	-3.28
210	Srrm2	SRRM2	DOWN	0.02	-3.60
211	Septin11	SEPTIN2	DOWN	0.01	-4.42
212	Macroh2a2	H2AW	DOWN	0.04	-3.12
213	Macroh2a1	H2AW2	DOWN	0.01	-4.81
214	Shtn1	SHOT1	DOWN	0.02	-3.91
215	Hdlbp	VIGLN	DOWN	0.05	-2.86
216	Rpe	RPE	DOWN	0.01	-5.30
217	Ciapin1	CPIN1	DOWN	0.01	-4.11
218	Acly	ACLY	DOWN	0.03	-3.16
219	Ndufs1	NDUS1	DOWN	0.02	-3.89
220	Smarca5	SMCA5	DOWN	0.03	-3.15
221	Sf3b3	SF3B3	DOWN	0.02	-3.87
222	Mthfd1	C1TC	DOWN	0.02	-3.78
223	Pdia6	PDIA6	DOWN	0.00	-8.22
224	Mpst	THTM	DOWN	0.01	-5.27
225	Vwa5a	VMA5A	DOWN	0.00	-7.22
226	Tmed9	TMED9	DOWN	0.01	-4.30
227	Dnajb11	DJB11	DOWN	0.02	-3.95
228	Gmpr2	GMPR2	DOWN	0.01	-4.77
229	Etfa	ETFA	DOWN	0.03	-3.19
230	Grpel1	GRPE1	DOWN	0.02	-3.73
231	Srrt	SRRT	DOWN	0.05	-2.82
232	Atp5mg	ATP5L	DOWN	0.03	-3.30
233	Dut	DUT	DOWN	0.03	-3.17
234	Ywhab	1433B	DOWN	0.01	-4.34
235	Atp6v1g1	VATG1	DOWN	0.01	-4.55
236	Sugt1	SGT1	DOWN	0.04	-3.05
237	Mrps22	RT22	DOWN	0.00	-6.10
238	Uqcrc1	QCR1	DOWN	0.04	-2.95
239	Gars1	GARS	DOWN	0.02	-3.75
240	Rpl15	RL15	DOWN	0.03	-3.27
241	Ube2v1	UB2V1	DOWN	0.04	-3.11
242	Gatd3	GAL3A	DOWN	0.04	-3.11
243	Acp1	PPAC	DOWN	0.04	-2.97
244	Prps1	PRPS1	DOWN	0.02	-3.75
245	Chmp5	CHMP5	DOWN	0.03	-3.41
246	Plin3	PLIN3	DOWN	0.02	-3.72
247	Ampd2	AMPD2	DOWN	0.05	-2.81
248	Ethe1	ETHE1	DOWN	0.04	-2.89
249	Akr1e2	AKCL2	DOWN	0.00	-10.23

250	Etfb	ETFB	DOWN	0.00	-6.37
251	Upf1	RENT1	DOWN	0.00	-6.59
252	Cwc15	CWC15	DOWN	0.05	-2.81
253	Dync1h1	DYHC1	DOWN	0.00	-6.71
254	Dazap1	DAZP1	DOWN	0.00	-5.76
255	Sh3bgrl	SH3L1	DOWN	0.01	-4.16
256	Acsl4	ACSL4	DOWN	0.00	-6.58
257	Plec	PLEC	DOWN	0.02	-3.57
258	Ptges3	TEBP	DOWN	0.04	-2.91
259	Tapbp	TPSN	DOWN	0.01	-4.59
260	Myo1c	MYO1C	DOWN	0.03	-3.46
261	Ak2	KAD2	DOWN	0.02	-3.82
262	Timm23	TIM23	DOWN	0.02	-4.07
263	Gk2	GLPK2	DOWN	0.02	-3.59
264	Eif4h	IF4H	DOWN	0.03	-3.18
265	Pacsin2	PACN2	DOWN	0.05	-2.79
266	Eif2s3x	IF2G	DOWN	0.01	-4.25
267	Sucla2	SUCB1	DOWN	0.00	-6.05
268	Sart1	SNUT1	DOWN	0.04	-2.89
LPS Polished vs. LPS Plasma					
1	Osbpl8	OSBL8	UP	0.03	3.14
2	Psmb5	PSB5	UP	0.02	3.99
3	Cops6	CSN6	UP	0.00	5.82
4	Creg1	CREG1	UP	0.02	3.65
5	Ldha	LDHA	UP	0.03	3.27
6	Gpi	G6PI	UP	0.04	2.98
7	Hsp90ab1	HS90B	UP	0.02	3.85
8	Hmga1	HMGA1	UP	0.02	3.63
9	Cbx3	CBX3	UP	0.00	22.05
10	M6pr	MPRD	UP	0.02	3.58
11	Nap1l1	NP1L1	UP	0.03	3.42
12	Oat	OAT	UP	0.01	4.91
13	Rpl12	RL12	UP	0.03	3.17
14	Mcm4	MCM4	UP	0.03	3.44
15	Pa2g4	PA2G4	UP	0.04	2.96
16	Pkm	KPYM	UP	0.04	3.10
17	Acod1	IRG1	UP	0.00	8.14
18	Atp6v1d	VATD	UP	0.02	3.55
19	Snrpd2	SMD2	UP	0.01	4.33
20	Hspd1	CH60	UP	0.02	4.00
21	Hmgb1	HMGB1	UP	0.05	2.80
22	Cct4	TCPD	UP	0.00	6.05
23	Erh	ERH	UP	0.01	4.14
24	Atp5f1a	ATPA	UP	0.03	3.26
25	Rac2	RAC2	UP	0.00	5.99
26	Ttll12	TTL12	UP	0.02	3.77
27	Eif3j1	EI3JA	UP	0.03	3.20
28	Arhgef2	ARHG2	UP	0.04	3.09
29	Rbbp4	RBBP4	UP	0.05	2.82
30	Arhgef1	ARHG1	UP	0.04	3.02
31	Cstb	CYTB	UP	0.05	2.84
32	Snx6	SNX6	UP	0.05	2.82
33	Gatd1	GALD1	UP	0.01	5.07
34	Nceh1	NCEH1	UP	0.03	3.39
35	Gspt1	ERF3A	UP	0.02	3.66
36	Sgpl1	SGPL1	UP	0.01	4.20
37	Rab14	RAB14	UP	0.04	2.99
38	Abcf2	ABCF2	UP	0.04	3.12
39	Npm3	NPM3	UP	0.00	6.27
40	Ifitm3	IFM3	UP	0.03	3.20
41	Cyb5b	CYB5B	UP	0.01	5.02
42	Chchd3	MIC19	UP	0.01	4.86
43	Mesd	MESD	UP	0.04	2.91
44	Mbnl1	MBNL1	UP	0.04	2.99
45	Rhoa	RHOA	UP	0.01	4.94
46	Vps29	VPS29	UP	0.00	8.30
47	Uchl5	UCHL5	UP	0.01	5.52
48	Prkcsh	GLU2B	DOWN	0.01	-4.57
49	Anp32a	AN32A	DOWN	0.05	-2.83
50	Slk	SLK	DOWN	0.05	-2.81
51	Ppt1	PPT1	DOWN	0.02	-3.72
52	Itgb1	ITB1	DOWN	0.04	-3.01
53	Anxa1	ANXA1	DOWN	0.03	-3.28

54	Eef1a1	EF1A1	DOWN	0.01	-4.35
55	Txn	THIO	DOWN	0.03	-3.22
56	Glud1	DHE3	DOWN	0.01	-4.60
57	Psmd7	PSMD7	DOWN	0.01	-4.95
58	Dnm2	DYN2	DOWN	0.01	-4.35
59	Csk	CSK	DOWN	0.04	-2.95
60	Rpl13	RL13	DOWN	0.04	-3.06
61	Ndufs6	NDUS6	DOWN	0.02	-3.76
62	Idh2	IDHP	DOWN	0.04	-2.92
63	Atp5mf	ATPK	DOWN	0.01	-5.30
64	Hnrnpk	HNRPK	DOWN	0.01	-5.39
65	Rps18	RS18	DOWN	0.03	-3.28
66	Snrpg	RUXG	DOWN	0.01	-5.12
67	Ybx1	YBOX1	DOWN	0.04	-3.13
68	Ppp1cc	PP1G	DOWN	0.05	-2.78
69	Phb1	PHB1	DOWN	0.03	-3.14
70	Csnk2b	CSK2B	DOWN	0.01	-4.91
71	Hnrnph2	HNRH2	DOWN	0.01	-4.26
72	Renbp	RENBP	DOWN	0.01	-5.13
73	Serpinf1	PEDF	DOWN	0.04	-3.02
74	Ctsc	CATC	DOWN	0.01	-4.95
75	Prrc2c	PRC2C	DOWN	0.04	-2.95
76	Hnrnpd	HNRPD	DOWN	0.04	-3.04
77	Eif1a	IF1AX	DOWN	0.03	-3.23
78	Hars1	HARS1	DOWN	0.03	-3.19
79	Vcl	VINC	DOWN	0.04	-2.96
80	Gart	PUR2	DOWN	0.05	-2.79
81	Uggt1	UGGG1	DOWN	0.04	-3.06
82	Pcnp	PCNP	DOWN	0.03	-3.26
83	Cand1	CAND1	DOWN	0.00	-6.10
84	Atp5mk	ATPMK	DOWN	0.05	-2.79
85	Wasf2	WASF2	DOWN	0.04	-3.12
86	Echs1	ECHM	DOWN	0.04	-3.07
87	Sec62	SEC62	DOWN	0.02	-3.99
88	Macroh2a2	H2AW	DOWN	0.03	-3.47
89	Pgp	PGP	DOWN	0.04	-2.93
90	Acat1	THIL	DOWN	0.02	-3.70
91	Psmd2	PSMD2	DOWN	0.04	-3.08
92	Grhpr	GRHPR	DOWN	0.02	-3.79
93	Smarca5	SMCA5	DOWN	0.04	-2.94
94	Acaa1a	THIKA	DOWN	0.02	-3.88
95	Tf	TRFE	DOWN	0.04	-2.98
96	Psmd6	PSMD6	DOWN	0.00	-8.61
97	Grpel1	GRPE1	DOWN	0.01	-4.13
98	Prpf8	PRP8	DOWN	0.02	-3.73
99	Dut	DUT	DOWN	0.00	-8.22
100	Sdhb	SDHB	DOWN	0.02	-3.77
101	Snx1	SNX1	DOWN	0.03	-3.26
102	Cyc1	CY1	DOWN	0.05	-2.78
103	Ppil1	PPIL1	DOWN	0.04	-3.01
104	Sf3a3	SF3A3	DOWN	0.02	-3.76
105	Prps1	PRPS1	DOWN	0.02	-3.50
106	Napa	SNAA	DOWN	0.00	-5.99
107	Ampd2	AMPD2	DOWN	0.01	-5.21
108	Ndufa9	NDUA9	DOWN	0.02	-3.63
109	Ethe1	ETHE1	DOWN	0.03	-3.23
110	Nif3l1	NIF3L	DOWN	0.02	-3.63
111	Nit2	NIT2	DOWN	0.01	-4.42
112	Dazap1	DAZP1	DOWN	0.05	-2.82
113	Ddx21	DDX21	DOWN	0.00	-7.37
114	Prep	PPCE	DOWN	0.01	-5.24
115	Sucla2	SUCB1	DOWN	0.00	-10.50
LPS Polished vs. LPS Corundum					
1	Tpr	TPR	UP	0.04	3.04
2	Hk2	HXK2	UP	0.02	3.94
3	Bcat2	BCAT2	UP	0.05	2.81
4	Dhx9	DHX9	UP	0.04	2.97
5	Psma3	PSA3	UP	0.05	2.84
6	Cops6	CSN6	UP	0.00	10.06
7	Creg1	CREG1	UP	0.02	4.06
8	Jun	JUN	UP	0.00	5.62
9	Gpi	G6PI	UP	0.03	3.19
10	Fcgr2	FCGR2	UP	0.01	4.21

11	M6pr	MPRD	UP	0.01	4.79
12	Rpl12	RL12	UP	0.02	4.02
13	Pkm	KPYM	UP	0.03	3.34
14	Acod1	IRG1	UP	0.01	4.47
15	Atp6v1d	VATD	UP	0.01	4.68
16	Rps23	RS23	UP	0.05	2.80
17	Rab1A	RAB1A	UP	0.05	2.86
18	Rpl30	RL30	UP	0.02	3.65
19	Hspd1	CH60	UP	0.03	3.16
20	Cct4	TCPD	UP	0.04	2.92
21	Csrp1	CSRP1	UP	0.02	4.03
22	Fh	FUMH	UP	0.01	4.93
23	Atp5f1a	ATPA	UP	0.01	4.89
24	Rac2	RAC2	UP	0.03	3.28
25	Vdac1	VDAC1	UP	0.02	3.61
26	Rbbp4	RBBP4	UP	0.03	3.14
27	Cct6b	TCPW	UP	0.02	3.91
28	Nfatc1	NFATC1	UP	0.02	4.02
29	Swap70	SWP70	UP	0.05	2.85
30	Snx6	SNX6	UP	0.03	3.17
31	Lsm8	LSM8	UP	0.02	3.90
32	Actbl2	ACTBL	UP	0.03	3.22
33	Bola2	BOLA2	UP	0.04	3.13
34	Mob1a	MOB1A	UP	0.04	3.04
35	Sgpl1	SGPL1	UP	0.04	2.89
36	Prpf19	PRP19	UP	0.05	2.84
37	Abcf2	ABCF2	UP	0.03	3.14
38	Ifitm3	IFM3	UP	0.02	3.54
39	Rpl22l1	RL22L	UP	0.03	3.29
40	Gatm	GATM	UP	0.04	3.00
41	Rhoa	RHOA	UP	0.04	2.92
42	Psma6	PSA6	UP	0.05	2.84
43	Dstn	DEST	UP	0.02	3.74
44	Rap1gds1	GDS1	DOWN	0.03	-3.38
45	Eef2	EF2	DOWN	0.04	-2.93
46	Anp32a	AN32A	DOWN	0.05	-2.81
47	Nfatc1	NFAC1	DOWN	0.03	-3.19
48	Anxa1	ANXA1	DOWN	0.01	-4.54
49	Ezr	EZRI	DOWN	0.05	-2.87
50	Glud1	DHE3	DOWN	0.05	-2.81
51	C5ar1	C5AR1	DOWN	0.00	-7.45
52	Csk	CSK	DOWN	0.00	-5.82
53	Idh2	IDHP	DOWN	0.05	-2.88
54	Hnrnpk	HNRPK	DOWN	0.02	-3.53
55	Snrpf	RUXF	DOWN	0.03	-3.16
56	Rps26	RS26	DOWN	0.02	-3.68
57	Tpt1	TCTP	DOWN	0.02	-3.97
58	Csnk2b	CSK2B	DOWN	0.00	-8.13
59	Cct5	TCPE	DOWN	0.01	-4.49
60	Rpl19	RL19	DOWN	0.04	-2.97
61	Serpinf1	PEDF	DOWN	0.04	-3.07
62	Mcm2	MCM2	DOWN	0.04	-2.92
63	Eif1a	IF1AX	DOWN	0.03	-3.17
64	Hsph1	HS105	DOWN	0.04	-3.10
65	Cand1	CAND1	DOWN	0.04	-3.00
66	Sec62	SEC62	DOWN	0.02	-3.51
67	Pitrm1	PREP	DOWN	0.03	-3.27
68	Tor1aip1	TOIP1	DOWN	0.00	-7.51
69	Mthfd1	C1TC	DOWN	0.03	-3.49
70	Pdia6	PDIA6	DOWN	0.01	-5.18
71	Dnajb11	DJB11	DOWN	0.03	-3.48
72	Dut	DUT	DOWN	0.01	-4.09
73	Sdhb	SDHB	DOWN	0.02	-3.57
74	Prps1	PRPS1	DOWN	0.02	-3.59
75	Etfb	ETFB	DOWN	0.02	-3.87
76	Dync1h1	DYHC1	DOWN	0.02	-3.94
77	Nit2	NIT2	DOWN	0.01	-4.47
78	Stk3	STK3	DOWN	0.02	-3.73
79	Eif2s3x	IF2G	DOWN	0.03	-3.20
80	Sucla2	SUCB1	DOWN	0.01	-5.09
81	Sart1	SNUT1	DOWN	0.04	-3.06
LPS Plasma vs. LPS Corundum					
1	Irak1	IRAK1	UP	0.04	3.04

2	Lin7a	LIN7A	UP	0.04	3.10
3	Sod1	SODC	UP	0.03	3.26
4	Fn1	FINC	UP	0.01	4.57
5	Mdh1	MDHC	UP	0.03	3.24
6	Hspa1l	HS71L	UP	0.03	3.41
7	Lyn	LYN	UP	0.01	4.36
8	Cct8	TCPQ	UP	0.03	3.46
9	Rab8b	RAB8B	UP	0.02	3.87
10	Ube2n	UBE2N	UP	0.02	3.53
11	Rpl23a	RL23A	UP	0.04	2.91
12	Phf5a	PHF5A	UP	0.00	7.44
13	Mcm2	MCM2	UP	0.03	3.34
14	Nfatc1	NFATC1	UP	0.01	4.60
15	Cbx5	CBX5	UP	0.01	4.14
16	Pzp	PZP	UP	0.04	2.92
17	Ndufa4	NDUA4	UP	0.01	4.19
18	Gatd1	GALD1	UP	0.02	3.98
19	Nceh1	NCEH1	UP	0.04	2.94
20	Smco1	SMCO1	UP	0.02	3.52
21	Dnajb11	DJB11	UP	0.02	3.90
22	Gmpr2	GMPR2	UP	0.05	2.82
23	Hypk	HYPK	UP	0.03	3.43
24	Slc25a11	M2OM	UP	0.04	2.98
25	Atp5f1d	ATPD	UP	0.02	3.58
26	Bola1	BOLA1	UP	0.04	3.13
27	Hyou1	HYOU1	UP	0.05	2.82
28	Sart1	SNUT1	UP	0.03	3.18
29	Sec22b	SC22B	DOWN	0.01	-4.38
30	Bcat2	BCAT2	DOWN	0.02	-3.73
31	Eif6	IF6	DOWN	0.03	-3.33
32	Jun	JUN	DOWN	0.05	-2.78
33	Pdia4	PDIA4	DOWN	0.04	-2.92
34	Glb1	BGAL	DOWN	0.03	-3.39
35	Lta4h	LKHA4	DOWN	0.00	-9.06
36	Rps2	RS2	DOWN	0.04	-2.88
37	Psmd7	PSMD7	DOWN	0.02	-3.92
38	Fen1	FEN1	DOWN	0.04	-2.97
39	Capza2	CAZA2	DOWN	0.03	-3.42
40	Kpna2	IMA1	DOWN	0.04	-2.92
41	Rps18	RS18	DOWN	0.03	-3.30
42	Snrpg	RUXG	DOWN	0.04	-2.94
43	Snrpd3	SMD3	DOWN	0.01	-4.36
44	Rps4x	RS4X	DOWN	0.01	-4.93
45	Rps6	RS6	DOWN	0.05	-2.81
46	Ran	RAN	DOWN	0.04	-3.03
47	Rps24	RS24	DOWN	0.04	-2.88
48	Rpl8	RL8	DOWN	0.01	-4.31
49	Pfn1	PROF1	DOWN	0.01	-4.72
50	Rac1	RAC1	DOWN	0.04	-2.93
51	Dnaja1	DNJA1	DOWN	0.00	-9.87
52	Ppp2ca	PP2AA	DOWN	0.04	-3.09
53	Fh	FUMH	DOWN	0.02	-3.69
54	Cybb	CY24B	DOWN	0.00	-6.31
55	Clns1a	ICLN	DOWN	0.04	-2.90
56	Cct6b	TCPW	DOWN	0.04	-2.92
57	Tpd52	TPD52	DOWN	0.04	-3.03
58	Bcl2l1	B2CL1	DOWN	0.04	-3.08
59	Atp5mk	ATPMK	DOWN	0.00	-6.72
60	Nap1l4	NP1L4	DOWN	0.04	-3.13
61	Bola2	BOLA2	DOWN	0.04	-3.03
62	Macroh2a1	H2AW	DOWN	0.01	-5.08
63	Atp1a1	AT1A1	DOWN	0.00	-5.86
64	Slc25a3	MPCP	DOWN	0.05	-2.85
65	Smarca5	SMCA5	DOWN	0.04	-2.92
66	Etfa	ETFA	DOWN	0.04	-2.99
67	Pin4	PIN4	DOWN	0.04	-2.89
68	Rpl15	RL15	DOWN	0.01	-4.93
69	Tsfm	EFTS	DOWN	0.04	-3.08
70	Cs	CISY	DOWN	0.03	-3.37
71	Oxct1	SCOT1	DOWN	0.04	-3.03
72	Cndp2	CNDP2	DOWN	0.04	-3.03
73	U2af1	U2AF1	DOWN	0.00	-7.29
74	Plin3	PLIN3	DOWN	0.00	-6.28

75	Rpl38	RL38	DOWN	0.02	-3.58
76	Hnrnpf	HNRPF	DOWN	0.01	-5.43

Tab. S3 Differentially expressed proteins of macrophages cultured on titanium plates with varying surface roughness LPS stimulation.

	LPS Control vs. LPS Polished	LPS Polished vs. LPS Corundum	LPS Plasma vs. LPS Corundum
Up	29	43	28
Down	44	38	48
Total	73	81	76

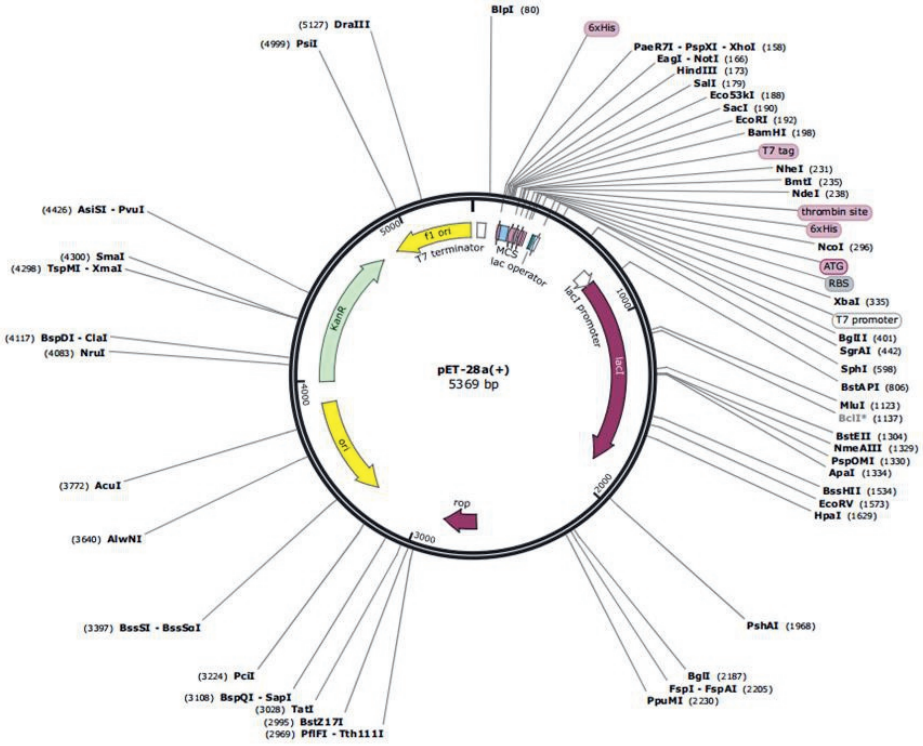


Fig. S1 Plasmid map of pET-28a(+) (5369 bp). Circular map illustrates the genetic elements and restriction enzyme recognition sites of the pET-28a(+) expression vector. T7 promoter for high-level expression in *E. coli* under IPTG induction. Green: filtered sites; Blus: checked sites; Red: kept sites. Kanamycin resistance gene (KanR) for antibiotic selection in bacteria. Rop gene and ColE1 origin (ori) for plasmid replication and stability in *E. col*

Tab. S1. Differentially expressed proteins of macrophages cultured on titanium plates with varying surface roughness with *S. aureus* stimulation.

	Polished vs Corundum	Polished vs Plasmapore	Corundum vs Plasmapore
Up	871	507	937
Down	793	1204	610
Total	1664	1711	1547

Tab.S2. List of differentially abundant proteins (DAPs) identified in Groups

	Gene name	Protein name	Changes	p-value(log 10)	Fold change(log2)
Control vs. Polished					
1	Mpeg1	MPEG1	UP	-9.79	1.06
2	Myh10	MYH10	UP	-12.08	1.63
3	Itih4	ITIH4	UP	-15.37	1.93
4	Tomm5	TOM5	UP	-4.27	1.77
5	Plxnb2	PLXB2	UP	-2.02	0.32
6	Adgrg4	AGRG4	UP	-11.60	2.38
7	Osbpl8	OSBL8	UP	-6.80	0.81
8	H2ac11	H2A1B	UP	-19.12	1.90
9	Hmcn1	HMCN1	UP	-8.97	1.79
10	Bin1;Bin2	BIN1	UP	-6.97	1.45
11	Gcn1	GCN1	UP	-1.26	0.31
12	Sbf2	MTMRD	UP	-5.04	1.23
13	Map3k19	M3K19	UP	-10.89	0.60
14	Kif23	KIF23	UP	-5.49	2.05
15	Rap1gds1	GDS1	UP	-3.07	0.79
16	Adgb	ADGB	UP	-0.97	1.10
17	Hk1	HXK1	UP	-4.24	1.01
18	Bin1	BIN1	UP	-4.91	1.61
19	Dpysl2	DPYL2	UP	-5.33	0.18
20	Emd	EMD	UP	-3.06	0.44
21	Alyref	THOC4	UP	-7.01	0.54
22	Myh11	MYH11	UP	-3.57	1.10
23	Myh10	MYH10	UP	-15.41	1.15
24	Arg2	ARGI2	UP	-14.52	3.77
25	Prkcsh	GLU2B	UP	-8.86	0.73
26	Prdx4	PRDX4	UP	-15.54	1.45
27	Prdx1	PRDX1	UP	-10.43	1.36
28	Eftud2	U5S1	UP	-1.56	0.18
29	Eef2	EF2	UP	-22.72	2.01
30	Degs1	DEGS1	UP	-3.12	0.62
31	Hdac1	HDAC1	UP	-1.60	0.60
32	Gsto1	GSTO1	UP	-5.95	2.52
33	Man2b1	MA2B1	UP	-2.38	1.36
34	Rpl21	RL21	UP	-2.60	0.27
35	Gclm	GSH0	UP	-2.70	0.35
36	Grcc10	C10	UP	-2.44	0.81
37	Phb2	PHB2	UP	-17.08	1.17
38	Dhx15	DHX15	UP	-12.18	1.01
39	Anp32a	AN32A	UP	-11.40	0.81
40	Ppef2	PPE2	UP	-3.24	1.14
41	Psmb9	PSB9	UP	-4.65	1.33
42	Psmd14	PSDE	UP	-5.07	2.73
43	Anxa3	ANXA3	UP	-3.41	0.27
44	Ap1b1	AP1B1	UP	-4.84	1.35
45	Myadm	MYADM	UP	-7.67	2.87
46	Nudc	NUDC	UP	-5.47	0.57
47	Hnrnph1	HNRH1	UP	-0.92	0.15
48	Hnrnph2	HNRH1	UP	-4.58	0.30
49	Hnrnpf	HNRH1	UP	-17.14	2.10
50	Hnrnpf&1	HNRH1	UP	-5.53	0.98
51	Api5	API5	UP	-1.96	0.19
52	Timm44	TIM44	UP	-6.72	1.22
53	Ddost	OST48	UP	-11.41	1.23
54	Man2b2	MA2B2	UP	-9.96	1.77
55	Banf1	BAF	UP	-5.34	0.60
56	Sap18	SAP18	UP	-1.67	0.59
57	Septin7	45907	UP	-4.29	0.30
58	Eif6	IF6	UP	-16.26	0.82
59	Rpl35a	RL35A	UP	-6.74	0.80
60	Atp2a2	AT2A2	UP	-9.33	1.28
61	Dhx9	DHX9	UP	-8.78	0.84
62	Pik3c2g	P3C2G	UP	-18.34	2.36
63	Eif3d	EIF3D	UP	-2.57	0.52
64	Pgam2	PGAM2	UP	-20.16	2.23
65	Pgam1	PGAM1	UP	-15.87	1.76

66	Ctss	CATS	UP	-6.74	0.93
67	Vamp8	VAMP8	UP	-4.74	0.62
68	Psma3	PSA3	UP	-8.70	1.57
69	Snx3	SNX3	UP	-5.08	0.30
70	Snx12;Snx3	SNX12	UP	-9.61	0.86
71	Snx12	SNX12	UP	-3.20	0.35
72	Smpd2	NSMA	UP	-3.33	0.99
73	Wdr1	WDR1	UP	-11.28	0.53
74	Dhcr7	DHCR7	UP	-2.59	1.09
75	Capns1	CPNS1	UP	-0.97	0.46
76	Dnmt3a	DNM3A	UP	-0.90	0.33
77	Ppt1	PPT1	UP	-11.89	0.48
78	Cops4	CSN4	UP	-8.86	1.89
79	Hnrnpa2b1	ROA2	UP	-14.23	0.58
80	Hnrnpa1	ROA1	UP	-1.98	0.54
81	Creg1	CREG1	UP	-6.80	1.50
82	Idh1	IDHC	UP	-5.93	0.50
83	Lgmn	LGMN	UP	-9.12	1.96
84	Afm	AFAM	UP	-12.08	2.42
85	Coro1a	COR1A	UP	-17.14	1.03
86	Dhfr	DYR	UP	-4.58	0.39
87	Mtco2	COX2	UP	-13.16	2.96
88	Hprt1	HPRT	UP	-12.36	0.89
89	C3	CO3	UP	-14.41	1.59
90	C4b	CO4B	UP	-4.23	1.77
91	B2m	B2MG	UP	-15.25	1.55
92	H2-L	HA1L	UP	-4.30	1.84
93	H2-D1	HA11	UP	-3.65	1.13
94	H2-L	HA1L	UP	-3.30	0.48
95	Hba	HBA	UP	-18.53	1.71
96	Hbb-b2	HBB2	UP	-14.40	1.79
97	Hbb-y	HBB1	UP	-11.74	1.10
98	H3-3a	H31	UP	-20.80	2.04
99	Iap	IGEB	UP	-4.94	0.36
100	Gfap	GFAP	UP	-6.97	0.82
101	Gfap	GFAP	UP	-7.50	0.88
102	Aldoa	ALDOA	UP	-12.92	0.42
103	Got1	AATC	UP	-7.38	0.77
104	Got2	AATM	UP	-2.59	0.18
105	Itgam	ITAM	UP	-2.91	0.22
106	Myl1	MYL1	UP	-7.99	2.18
107	Ldha	LDHA	UP	-13.74	1.00
108	C9	CO9	UP	-18.91	1.99
109	Ctsl	CATL1	UP	-12.73	1.67
110	Ptprc	PTPRC	UP	-14.81	1.00
111	S100a4	S10A4	UP	-17.40	1.29
112	Anxa2	ANXA2	UP	-17.76	1.33
113	Alb	ALBU	UP	-19.53	1.59
114	Hsp90aa1	HS90A	UP	-16.27	0.84
115	Aprt	APT	UP	-12.01	0.71
116	Fcgr2	FCGR2	UP	-2.51	0.38
117	Hsp90b1	ENPL	UP	-19.40	0.81
118	Hsp90b1	ENPL	UP	-17.95	1.69
119	S100a10	S10AA	UP	-0.83	0.12
120	Sod1	SODC	UP	-6.21	0.26
121	Mdh2	MDHM	UP	-14.80	0.58
122	Gnai2	GNAI2	UP	-13.91	1.50
123	Lyz2	LYZ2	UP	-9.68	0.68
124	Lyz1	LYZ1	UP	-8.03	1.36
125	Pgk1	PGK1	UP	-13.46	0.54
126	Itgb1	ITB1	UP	-12.36	1.20
127	P4hb	PDIA1	UP	-9.62	0.25
128	Ncl	NUCL	UP	-9.30	0.21
129	Sod2	SODM	UP	-14.21	0.65
130	Calm1	CALM1	UP	-12.55	1.12
131	Anxa1	ANXA1	UP	-8.99	0.21
132	Eef1a1	EF1A1	UP	-16.79	0.98
133	Eef1a2	EF1A1	UP	-18.12	1.16
134	Ctsb	CATB	UP	-20.11	1.48
135	Eif4a2	IF4A1	UP	-16.71	1.56
136	Eif4a3	IF4A3	UP	-11.83	0.97
137	Cd14	CD14	UP	-12.56	1.10
138	Slc3a2	4F2	UP	-9.85	0.68

139	H2bc14	H2B1B	UP	-6.63	0.35
140	H1-0	H10	UP	-10.35	1.26
141	Spp1	OSTP	UP	-0.84	0.30
142	Fn1	FINC	UP	-0.89	0.29
143	Lamp1	LAMP1	UP	-1.92	0.42
144	Hsp90ab1	HS90B	UP	-14.33	0.68
145	Tcp1	TCPA	UP	-8.59	0.47
146	App	A4	UP	-6.05	1.34
147	Pfkl;Pfkp	PFKAL	UP	-12.19	2.76
148	Cox5a	COX5A	UP	-10.20	0.40
149	Gsn	GELS	UP	-15.04	0.66
150	Dnmt1	DNMT1	UP	-3.19	0.44
151	S100a6	S10A6	UP	-11.98	1.92
152	Rps16	RS16	UP	-2.71	0.14
153	Rpl7	RL7	UP	-7.60	0.34
154	Mdh1	MDHC	UP	-7.06	0.34
155	Rpsa	RSSA	UP	-11.21	0.64
156	Calr	CALR	UP	-9.02	0.39
157	Psmd3	PSMD3	UP	-4.31	0.28
158	Lmnb1	LMNB1	UP	-13.13	0.81
159	Lmna	LMNA	UP	-12.94	1.19
160	Anxa6	ANXA6	UP	-12.97	1.37
161	Rplp0	RLA0	UP	-12.09	0.75
162	Hmox1	HMOX1	UP	-1.61	0.70
163	Bpgm	PMGE	UP	-16.53	2.15
164	Nme1	NDKA	UP	-3.79	0.36
165	Nme1	NDKA	UP	-17.53	1.09
166	Ass1	ASSY	UP	-10.22	1.41
167	Hspa1l	HS71L	UP	-12.13	1.52
168	Hspa1l	HS71L	UP	-16.77	1.64
169	Hspa1l	HS71L	UP	-5.71	1.57
170	Ctsa	PPGB	UP	-14.49	1.13
171	Gapdh	G3P	UP	-16.80	1.04
172	Lamp2	LAMP2	UP	-16.40	1.40
173	Hmga1	HMGA1	UP	-2.37	0.98
174	Hspa2	HSP72	UP	-16.65	1.27
175	Eno1	ENOA	UP	-13.87	1.34
176	Eno3	ENOA	UP	-7.04	0.72
177	Eno1&3	ENOA	UP	-6.41	2.53
178	Ptbp1	PTBP1	UP	-6.13	0.36
179	Hk1	HXK1	UP	-7.08	0.78
180	Ppia	PPIA	UP	-10.42	0.24
181	Slc2a1	GTR1	UP	-6.75	2.04
182	Pcna	PCNA	UP	-9.68	0.37
183	Ctsd	CATD	UP	-8.93	0.23
184	Cfl1;Dstn	COF1	UP	-5.27	0.80
185	Cox5b	COX5B	UP	-3.11	0.77
186	Cox4i1	COX41	UP	-6.89	0.43
187	Hspa5	BIP	UP	-18.47	0.75
188	Hexb	HEXB	UP	-11.52	1.39
189	Prdx3	PRDX3	UP	-14.07	1.02
190	Vim	VIME	UP	-25.54	1.41
191	Fcer1g	FCERG	UP	-14.77	1.10
192	Plg	PLMN	UP	-4.50	2.99
193	Tpm1	TPM1	UP	-14.39	1.32
194	Akr1b7	ALD1	UP	-7.10	1.03
195	Cst3	CYTC	UP	-7.15	2.63
196	Gc	VTDB	UP	-8.63	2.62
197	Cd72	CD72	UP	-6.38	1.15
198	Mfge8	MFGM	UP	-2.48	0.47
199	Ap1g1	AP1G1	UP	-5.95	1.33
200	Eif3a	EIF3A	UP	-1.26	0.10
201	Cbx3	CBX3	UP	-1.59	0.11
202	Cbx5	CBX5	UP	-2.73	1.65
203	Cat	CATA	UP	-8.08	0.57
204	Ppib	PPIB	UP	-12.92	1.27
205	Lta4h	LKHA4	UP	-1.80	0.72
206	Impdh2	IMDH2	UP	-1.02	0.11
207	Impdh1	IMDH2	UP	-1.58	0.15
208	Acp2	PPAL	UP	-2.29	0.55
209	M6pr	MPRD	UP	-8.73	0.83
210	Lyn	LYN	UP	-8.42	2.03
211	Ezr	EZRI	UP	-11.43	0.69

212	Msn	MOES	UP	-17.56	0.76
213	Msn	MOES	UP	-20.13	2.31
214	Ptma	PTMA	UP	-10.48	0.62
215	Glud1	DHE3	UP	-14.27	0.71
216	Psmd7	PSMD7	UP	-9.17	0.72
217	Sars1	SYSC	UP	-5.91	0.49
218	Marcks	MARCS	UP	-1.53	0.38
219	Snrpb	RSMB	UP	-15.30	1.40
220	Plaa	PLAP	UP	-0.82	0.28
221	Pdia3	PDIA3	UP	-11.38	0.28
222	Vav1	VAV	UP	-6.10	0.58
223	Cebpb	CEBPB	UP	-1.35	0.68
224	Atxn10	ATX10	UP	-5.55	1.89
225	Mug1	MUG1	UP	-20.71	2.57
226	Grn	GRN	UP	-14.30	1.80
227	Ptpn6	PTN6	UP	-6.16	0.40
228	Hexa	HEXA	UP	-8.81	1.38
229	Ahsg	FETUA	UP	-12.85	2.01
230	Msr1	MSRE	UP	-8.34	1.35
231	Alox5ap	AL5AP	UP	-19.13	1.57
232	Rbpj	SUH	UP	-4.17	1.31
233	Dbi	ACBP	UP	-5.30	1.57
234	Map2k1	MP2K1	UP	-10.72	1.42
235	Cd68	CD68	UP	-11.81	0.66
236	Scp2	SCP2	UP	-3.11	0.20
237	Drg1	DRG1	UP	-1.19	0.64
238	Serpinc1	ANT3	UP	-14.16	1.77
239	Ranbp1	RANG	UP	-4.50	0.35
240	Mif	MIF	UP	-2.85	0.21
241	Rab6a	RAB6A	UP	-3.94	1.81
242	Ppard	PPARD	UP	-11.78	2.54
243	Pdha1	ODPA	UP	-4.83	1.37
244	Fbl	FBRL	UP	-5.56	0.54
245	Canx	CALX	UP	-18.77	1.30
246	Prdx1	PRDX1	UP	-16.23	0.77
247	Hmgcl	HMGCL	UP	-3.21	0.39
248	Hspa9	GRP75	UP	-5.96	0.24
249	Dnm1	DYN1	UP	-2.68	0.37
250	Cap1	CAP1	UP	-3.76	0.12
251	Tkt	TKT	UP	-2.54	0.11
252	Rpl28	RL28	UP	-10.10	1.21
253	Acsl1	ACSL1	UP	-4.75	1.45
254	Acsl5	ACSL5	UP	-1.87	0.51
255	Cd86	CD86	UP	-4.61	0.92
256	Cct8	TCPQ	UP	-11.98	0.46
257	H1-3	H13	UP	-13.30	2.57
258	Akr1b1	ALDR	UP	-20.97	1.36
259	Akr1b8	ALD2	UP	-2.88	0.38
260	Fkbp2	FKBP2	UP	-5.55	0.57
261	Rab11b	RB11B	UP	-2.38	0.30
262	Stt3a	STT3A	UP	-7.47	1.67
263	Pla2g4a	PA24A	UP	-1.58	0.14
264	Aldh2	ALDH2	UP	-10.31	0.64
265	Capza2	CAZA1	UP	-5.78	0.36
266	Capza2	CAZA2	UP	-11.38	1.22
267	Capzb	CAPZB	UP	-15.05	1.20
268	Srprb	SRPRB	UP	-4.28	0.34
269	Mtx1	MTX1	UP	-1.59	0.47
270	Rpl13	RL13	UP	-2.44	0.15
271	Anxa5	ANXA5	UP	-22.10	1.63
272	Lmna	LMNA	UP	-23.84	1.34
273	Pcnt	PCNT	UP	-8.31	0.85
274	Cox7a2	CX7A2	UP	-14.28	3.20
275	Slc25a4	ADT1	UP	-11.63	0.91
276	Slc25a4	ADT1	UP	-16.15	0.58
277	Hnrnpa1	ROA1	UP	-18.48	0.78
278	Mcm5	MCM5	UP	-3.44	0.64
279	Srp9	SRP09	UP	-4.57	0.80
280	Impdh1	IMDH1	UP	-3.71	1.29
281	Ahcy	SAHH	UP	-14.01	0.96
282	Arsb	ARSB	UP	-7.77	0.48
283	Atp6v1a	VATA	UP	-12.35	0.78
284	Atp6v1e1	VATE1	UP	-7.19	0.51

285	S100a11	S10AB	UP	-7.07	0.66
286	Pa2g4	PA2G4	UP	-6.90	0.60
287	Rpl9	RL9	UP	-6.29	0.51
288	Hsd17b4	DHB4	UP	-2.60	0.54
289	Slc25a5	ADT2	UP	-14.16	1.23
290	Slc1a5	AAAT	UP	-1.36	0.76
291	Kpna2	IMA1	UP	-9.18	1.11
292	Pkm	KPYM	UP	-14.49	0.65
293	Rpl10a	RL10A	UP	-4.01	0.42
294	Pitpna	PIPNA	UP	-8.19	1.17
295	Rab2a	RAB2A	UP	-1.63	0.25
296	Idh2	IDHP	UP	-9.74	0.76
297	Msh6	MSH6	UP	-6.88	2.69
298	Rad23b	RD23B	UP	-8.85	0.93
299	Psmc4	PRS6B	UP	-1.21	0.33
300	Adsl	PUR8	UP	-3.02	1.40
301	Acod1	IRG1	UP	-12.50	1.82
302	Rab10	RAB10	UP	-5.21	2.54
303	Rab1A	RAB8B	UP	-4.17	1.10
304	Lrpap1	AMRP	UP	-2.78	0.09
305	Atp5mf	ATPK	UP	-15.59	1.44
306	Atp5f1b	ATPB	UP	-18.42	1.31
307	Exosc10	EXOSX	UP	-18.13	2.00
308	Atp6v1d	VATD	UP	-1.71	0.52
309	Eef1d	EF1D	UP	-13.83	1.08
310	Actn1	ACTN1	UP	-7.42	0.46
311	Tm9sf2	TM9S2	UP	-8.66	2.17
312	Idi1	IDI1	UP	-1.31	0.65
313	Eef2	EF2	UP	-16.45	1.03
314	Bcl2l13	B2L13	UP	-0.94	0.82
315	Rin3	RIN3	UP	-5.59	1.71
316	Arpc4	ARPC4	UP	-17.50	1.08
317	Eif3e	EIF3E	UP	-8.02	1.67
318	Pcbp1	PCBP1	UP	-14.18	0.82
319	Pcbp1;Pcbp2	PCBP1	UP	-13.97	1.00
320	Actb;Actg1	ACTB ;ACTG	UP	-8.99	0.47
321	Cdc42	CDC42	UP	-8.44	0.41
322	Rac1	RAC1	UP	-11.41	0.87
323	Ensa	ENSA	UP	-1.72	0.81
324	Eif4a1	IF4A1	UP	-10.38	1.14
325	Rps20	RS20	UP	-17.92	1.00
326	Rab10	RAB10	UP	-7.17	1.69
327	Rab8b	RAB8B	UP	-1.98	0.38
328	Ube2n	UBE2N	UP	-1.80	0.33
329	Arf1;Arf3	ARF1 ;ARF3	UP	-7.57	2.91
330	Rpl26	RL26	UP	-9.46	0.75
331	Psme3	PSME3	UP	-6.54	2.15
332	Magoh;Magohb	MGN2 ;MGN	UP	-9.13	1.47
333	Rpl27	RL27	UP	-6.15	0.30
334	Rpl37a	RL37A	UP	-8.79	1.30
335	Sec61a1	S61A1	UP	-6.48	2.15
336	Arf4	ARF4	UP	-8.60	2.48
337	Arf4;Arf5	ARF4 ;ARF5	UP	-7.44	2.49
338	Sumo2	SUMO2	UP	-2.28	0.12
339	Hnrnpk	HNRPK	UP	-16.61	1.21
340	Ywhag	1433G	UP	-15.05	1.62
341	Ywhag;Ywhah	1433F ;1433G	UP	-13.36	3.40
342	Timm8b	TIM8B	UP	-6.10	1.51
343	Rps7	RS7	UP	-2.32	0.09
344	Ppp1ca	PP1A	UP	-3.03	0.32
345	Ppp1cc	PP1G	UP	-5.66	1.82
346	Psmc1	PRS4	UP	-1.55	0.38
347	Psmc5	PRS8	UP	-7.61	1.02
348	Rps15a	RS15A	UP	-14.81	1.23
349	Ywhae	1433E	UP	-12.03	0.89
350	Rps14	RS14	UP	-9.92	0.68
351	Rps23	RS23	UP	-3.46	0.36
352	Rps18	RS18	UP	-8.68	0.43
353	Rps29	RS29	UP	-6.73	0.62
354	Rps11	RS11	UP	-10.77	0.62
355	Snrpf	RUXF	UP	-12.38	2.44
356	Snrpg	RUXG	UP	-17.20	1.67
357	Lsm3	LSM3	UP	-5.03	1.21

358	Lsm6	LSM6	UP	-7.33	1.62
359	Snrpd1	SMD1	UP	-1.07	0.67
360	Snrpd2	SMD2	UP	-12.14	2.22
361	Snrpd3	SMD3	UP	-14.50	2.03
362	Psmc6	PRS10	UP	-3.95	0.17
363	Eef1a2	EF1A2	UP	-7.05	2.57
364	Rps4x	RS4X	UP	-15.60	0.78
365	Rpl18a	RL18A	UP	-6.25	0.68
366	Rps6	RS6	UP	-7.84	0.39
367	H4c1	H4	UP	-13.13	1.37
368	Atp6v1b2	VATB2	UP	-3.33	0.15
369	Rab1A	RAB1A	UP	-6.76	0.55
370	Ran	RAN	UP	-11.50	0.86
371	Rap1a	RAP1A	UP	-2.66	0.37
372	Rps15	RS15	UP	-3.05	0.65
373	Rps26	RS26	UP	-14.06	1.98
374	Rps28	RS28	UP	-3.38	0.28
375	Gnb1	GBB1	UP	-6.91	1.01
376	Gnb1;Gnb2	GBB1 ;GBB2	UP	-16.03	2.33
377	Gnb2	GBB2	UP	-9.65	0.86
378	Rpl30	RL30	UP	-12.05	0.64
379	Rpl31	RL31	UP	-13.06	0.65
380	Rps3	RS3	UP	-19.16	1.19
381	Rpl8	RL8	UP	-12.74	0.65
382	Ybx1	YBOX1	UP	-9.38	0.84
383	Rps27a;Uba52	RL40 ;RS27A	UP	-22.78	1.91
384	Tra2b	TRA2B	UP	-4.50	0.98
385	Rac1	RAC1	UP	-2.91	0.69
386	Rac1;Rac2	RAC1 ;RAC2	UP	-11.08	0.52
387	Hspa8	HSP7C	UP	-14.86	0.66
388	Tpt1	TCTP	UP	-10.52	1.56
389	Dnaja1	DNJA1	UP	-3.69	1.03
390	Eif4e	IF4E	UP	-5.58	0.78
391	Mapk1	MK01	UP	-7.05	0.61
392	Mapk1;Mapk3	MK01 ;MK03	UP	-4.82	1.27
393	Ppp1cc	PP1G	UP	-7.84	1.29
394	Ywhaz	1433Z	UP	-16.01	1.07
395	Ywhab	1433B	UP	-5.74	2.15
396	Dynll1;Dynll2	DYL1 ;DYL2	UP	-1.26	0.30
397	Rps17	RS17	UP	-9.76	0.98
398	Ube2i	UBC9	UP	-12.59	0.85
399	Rps10	RS10	UP	-2.88	0.35
400	Phb1	PHB1	UP	-9.55	0.50
401	Rpl22	RL22	UP	-10.13	1.14
402	Acta1;Actc1	ACTC ;ACTS	UP	-16.07	2.33
403	Rack1	RACK1	UP	-19.55	1.21
404	Ywhaq	1433T	UP	-6.91	1.22
405	Tuba4a	TBA4A	UP	-12.41	0.81
406	Tuba1c&c	TBA1C	UP	-6.18	0.43
407	Tuba1c;Tuba4a	TBA1C	UP	-11.22	1.96
408	Tuba8	TBA8	UP	-13.77	0.93
409	Tubb4b	TBB4B	UP	-19.16	1.55
410	Tubb2a;Tubb6	TBB6	UP	-16.40	2.68
411	Tubb5;Tubb6	TBB5 ;TBB6	UP	-10.28	0.68
412	Tubb2a&5	TBB2B ;TBB5	UP	-14.40	1.66
413	Tubb5	TBB2A ;TBB2B	UP	-15.62	2.57
414	Tubb2b	TBB5 ;TBB6	UP	-5.27	2.28
415	Tubb3;Tubb4b;Tubb5	TBB3 ;TBB4B	UP	-16.13	1.97
416	Tubb4b;Tubb6	TBB4B ;TBB6	UP	-0.85	1.02
417	Ywhah	1433F	UP	-7.26	0.63
418	Kpnb1	IMB1	UP	-4.41	0.21
419	Elavl1	ELAV1	UP	-6.20	0.27
420	Idh3g	IDHG1	UP	-12.18	1.10
421	Naca	NACAM	UP	-17.71	1.00
422	Casp3	CASP3	UP	-10.16	4.35
423	Cct7	TCPH	UP	-8.89	0.72
424	Cct2	TCPB	UP	-6.85	0.25
425	Cct4	TCPD	UP	-12.44	0.55
426	Cct6a	TCPZ	UP	-6.37	0.35
427	Cct3	TCPG	UP	-16.94	1.12
428	Wnk1	WNK1	UP	-3.90	0.26
429	Arf5	ARF5	UP	-9.01	1.26
430	Erh	ERH	UP	-1.07	0.79

431	Ap2m1	AP2M1	UP	-13.46	1.79
432	Rhog	RHOG	UP	-3.04	0.26
433	Srsf3	SRSF3	UP	-10.20	0.59
434	Srsf3;Srsf7	SRSF3 ;SRSF7	UP	-1.68	0.85
435	Serpinf1	PEDF	UP	-16.22	3.70
436	Mcm2	MCM2	UP	-8.32	1.05
437	Mcm6	MCM6	UP	-13.88	1.28
438	Atp1b3	AT1B3	UP	-7.69	2.00
439	Anxa4	ANXA4	UP	-10.90	1.14
440	Sirpa	SHPS1	UP	-5.83	1.50
441	Fh	FUMH	UP	-5.97	0.34
442	Fxyd5	FXYD5	UP	-7.79	0.95
443	Ctsc	CATC	UP	-12.11	1.28
444	Anp32e	AN32E	UP	-12.60	1.40
445	G3bp1	G3BP1	UP	-11.24	0.85
446	Rbbp6	RBBP6	UP	-10.06	2.42
447	Tubb2a;Tubb2b	TBB2A ;TBB2B	UP	-8.46	1.86
448	Tubb3;Tubb5	TBB2A ;TBB2B	UP	-12.55	1.80
449	Uqcrh	QCR6	UP	-1.30	0.17
450	G6pdx	G6PD1	UP	-18.16	1.08
451	Apoa1	APOA1	UP	-18.64	1.56
452	Hnrnpul2	HNRL2	UP	-1.06	0.11
453	Top2a	TOP2A	UP	-10.55	1.12
454	Vcp	TERA	UP	-14.33	0.77
455	Uba1	UBA1	UP	-10.95	0.94
456	C1qc	C1QC	UP	-8.24	1.72
457	Nucb1	NUCB1	UP	-9.69	0.94
458	Atp5f1a	ATPA	UP	-13.57	0.61
459	Ckb	KCRB	UP	-13.21	0.79
460	Top1	TOP1	UP	-0.99	0.25
461	Anxa7	ANXA7	UP	-6.36	1.73
462	Acads	ACADS	UP	-8.03	1.78
463	Ambp	AMBP	UP	-18.16	1.75
464	Pros1	PROS	UP	-3.02	1.03
465	Fbln1	FBLN1	UP	-13.05	1.47
466	Ncf1	NCF1	UP	-1.39	0.36
467	Nsun2	NSUN2	UP	-2.57	0.71
468	Myl12b	ML12B	UP	-1.05	0.46
469	Gmps	GUAA	UP	-5.00	0.42
470	Mat2a	METK2	UP	-6.05	0.54
471	Prrc2c	PRC2C	UP	-1.16	0.42
472	Hk3	HXK3	UP	-2.08	0.64
473	Srsf6	SRSF6	UP	-7.47	0.34
474	Esyt1	ESYT1	UP	-0.88	0.40
475	Pdap1	HAP28	UP	-2.34	1.28
476	Mylk2;Mylk3	MYLK2 ;MYLK3	UP	-11.59	1.23
477	Sf3b2	SF3B2	UP	-11.10	0.92
478	Smu1	SMU1	UP	-7.29	1.20
479	Arglu1	ARGL1	UP	-2.77	1.36
480	Skap2	SKAP2	UP	-4.13	0.54
481	Ttbk2	TTBK2	UP	-5.69	2.41
482	Abracl	ABRAL	UP	-6.12	1.57
483	Ddx17;Ddx5	DDX17 ;DDX5	UP	-15.57	1.17
484	Srrm1	SRRM1	UP	-1.59	0.55
485	Thrap3	TR150	UP	-7.19	1.03
486	Mypn	MYPN	UP	-17.78	2.08
487	Rilp	RILP	UP	-3.64	2.44
488	Ogdh	ODO1	UP	-1.69	0.28
489	Myl6	MYL6	UP	-11.72	0.66
490	Grb2	GRB2	UP	-16.43	1.22
491	Psmb6	PSB6	UP	-17.50	1.69
492	Csnk2a1	CSK21	UP	-4.89	1.65
493	Serpinb6	SPB6	UP	-10.09	1.13
494	Stip1	STIP1	UP	-9.07	0.46
495	Vdac2	VDAC2	UP	-10.95	0.76
496	Vdac1	VDAC1	UP	-9.37	0.74
497	Rbbp4;Rbbp7	RBBP4 ;RBBP7	UP	-5.86	0.49
498	Tmpo	LAP2A	UP	-1.15	0.88
499	Hars1	HARS1	UP	-1.44	0.39
500	Mapre1	MARE1	UP	-3.54	0.17
501	Prdx2	PRDX2	UP	-10.97	0.95
502	Pafah1b2	PA1B2	UP	-3.25	0.98
503	Psap	SAP	UP	-18.53	1.37

504	Lcp1	PLSL	UP	-13.78	0.40
505	Lcp1;Pls3	PLSL ;PLST	UP	-13.33	1.30
506	Soat1	SOAT1	UP	-6.99	0.76
507	Hspa4	HSP74	UP	-13.69	0.46
508	Bcap31	BAP31	UP	-1.73	0.60
509	Glg1	GSLG1	UP	-10.97	1.17
510	Ewsr1	EWS	UP	-2.96	0.85
511	Fxr1	FXR1	UP	-1.53	0.37
512	Gdi2	GDIB	UP	-2.89	0.18
513	Arhgdib	GDIR2	UP	-11.61	1.29
514	Ddx5	DDX5	UP	-13.03	0.68
515	Itih2	ITIH2	UP	-19.99	1.65
516	Itih3	ITIH3	UP	-17.15	1.83
517	Lasp1	LASP1	UP	-2.08	0.13
518	Pzp	PZP	UP	-12.91	1.48
519	A2m;Pzp	A2MG ;PZP	UP	-7.97	1.59
520	Myh10;Myh9	MYH10 ;MYH9	UP	-4.37	0.41
521	Mcm7	MCM7	UP	-9.33	1.01
522	Pcbp2	PCBP2	UP	-11.41	0.67
523	Srsf2	SRSF2	UP	-15.49	1.11
524	Ssr4	SSRD	UP	-15.08	1.97
525	Shh	SHH	UP	-19.84	2.37
526	Tsn	TSN	UP	-8.70	1.40
527	Tfrc	TFR1	UP	-1.07	0.37
528	Snrnp70	RU17	UP	-12.08	1.38
529	Eif4g2	IF4G2	UP	-8.16	1.41
530	Raly	RALY	UP	-6.51	0.34
531	Lilrb4a	LRB4A	UP	-7.10	1.55
532	Stxbp2	STXB2	UP	-0.94	0.34
533	Sqstm1	SQSTM	UP	-5.29	0.49
534	Hspe1	CH10	UP	-2.07	0.10
535	Atp1a1;Atp1a2	AT1A1 ATP4A	UP	-14.74	1.93
536	Atp1a1;Atp4a	AT1A1 ;ATP4A	UP	-15.29	2.74
537	H2ac20	H2A2A	UP	-8.14	0.68
538	Cltc	CLH1	UP	-14.91	0.60
539	Ahcyl2	SAHH3	UP	-1.19	0.50
540	A2m	A2MG	UP	-17.37	1.92
541	Nomo1	NOMO1	UP	-2.43	0.30
542	Tpm4	TPM4	UP	-3.88	0.23
543	U2surp	SR140	UP	-1.36	1.47
544	Sri	SORCN	UP	-9.89	2.17
545	Rrp12	RRP12	UP	-10.74	2.56
546	Fkbp15	FKB15	UP	-1.98	0.56
547	Txlna	TXLNA	UP	-1.83	0.37
548	Pigs	PIGS	UP	-4.62	1.50
549	Srsf1	SRSF1	UP	-10.80	0.80
550	Stoml3	STML3	UP	-5.19	3.02
551	Camk2d	KCC2D	UP	-7.01	2.37
552	Atp1a1;Atp1a2	AT1A1 ;AT1A2	UP	-12.48	0.67
553	Kctd12	KCD12	UP	-4.07	0.58
554	Wdr43	WDR43	UP	-6.12	0.79
555	Ugt1a7	UD17	UP	-8.29	0.92
556	Lsm8	LSM8	UP	-4.83	1.35
557	Rps9	RS9	UP	-18.85	1.38
558	Rps27;Rps27l	RS27L ;RS27	UP	-16.22	1.42
559	Rpl10	RL10	UP	-10.81	0.99
560	Rpl35	RL35	UP	-6.91	0.61
561	Eif2s1	IF2A	UP	-10.17	1.04
562	Snd1	SND1	UP	-12.35	0.67
563	Mtch2	MTCH2	UP	-3.38	0.82
564	Luc7l;Luc7l2	LC7L2 ;LUC7L	UP	-10.29	1.20
565	Spag7	SPAG7	UP	-1.28	0.38
566	Eml2	EMAL2	UP	-2.58	1.38
567	Mybbp1a	MBB1A	UP	-12.10	1.26
568	Septin9	45909	UP	-5.77	0.98
569	Naa15	NAA15	UP	-4.06	0.68
570	Hydin	HYDIN	UP	-3.87	0.93
571	Mtdh	LYRIC	UP	-2.42	0.24
572	Tufm	EFTU	UP	-8.08	0.42
573	Tnpo1	TNPO1	UP	-3.52	0.94
574	Actbl2	ACTBL	UP	-15.80	1.25
575	Hnrnpa3	ROA3	UP	-14.52	0.84
576	Pld4	PLD4	UP	-3.55	0.91

577	Psmd11	PSD11	UP	-6.61	0.51
578	Eif4b	IF4B	UP	-2.43	0.17
579	Samm50	SAM50	UP	-0.95	0.48
580	Pck2	PCKGM	UP	-7.19	0.89
581	Tm9sf4	TM9S4	UP	-10.78	2.97
582	Wasf2	WASF2	UP	-6.75	0.57
583	Slc25a12	S2512	UP	-0.84	0.39
584	Clic6	CLIC6	UP	-1.71	1.61
585	Ganab	GANAB	UP	-8.30	0.68
586	Iars2	SYIM	UP	-0.86	0.30
587	Cstf2	CSTF2	UP	-4.45	0.42
588	Psmd5	PSMD5	UP	-1.03	0.72
589	Ahsa1	AHSA1	UP	-11.19	1.33
590	Rcc2	RCC2	UP	-4.67	0.34
591	Ipo5	IPO5	UP	-1.78	0.29
592	Srsf7	SRSF7	UP	-10.73	0.87
593	Arid5b	ARI5B	UP	-6.67	2.35
594	Slc25a24	SCMC1	UP	-6.40	0.95
595	Lars1	SYLC	UP	-10.25	0.90
596	Ckap4	CKAP4	UP	-5.84	1.08
597	Qars1	SYQ	UP	-1.33	0.83
598	Cibar1	CBAR1	UP	-2.31	0.60
599	Mob1a	MOB1A	UP	-1.99	0.57
600	Slc15a3	S15A3	UP	-6.12	1.82
601	Cnpy4	CNPY4	UP	-1.78	0.57
602	Hus1	HUS1	UP	-4.99	1.36
603	Flna	FLNA	UP	-5.83	0.17
604	Flna;Flnc	FLNA ;FLNC	UP	-10.92	2.25
605	Sec62	SEC62	UP	-2.61	0.65
606	Etf1	ERF1	UP	-9.39	0.92
607	Gemin5	GEMI5	UP	-11.36	1.47
608	Vps13c	VP13C	UP	-3.66	0.95
609	Ppp4r4	PP4R4	UP	-18.89	2.00
610	Rae1	RAE1L	UP	-3.12	1.44
611	Rassf4	RASF4	UP	-1.65	0.77
612	Pabpn1	PABP2	UP	-4.58	1.56
613	Smco1	SMCO1	UP	-7.78	1.44
614	Pgp	PGP	UP	-6.58	0.99
615	Gnl3	GNL3	UP	-1.45	0.56
616	Copa	COPA	UP	-3.54	0.31
617	Gpr84	GPR84	UP	-11.96	1.43
618	Eif3b	EIF3B	UP	-5.55	0.55
619	Acsl5	ACSL5	UP	-1.58	0.92
620	Slc25a1	TXTP	UP	-0.86	0.29
621	Gfm1	EFGM	UP	-10.74	1.67
622	Fermt3	URP2	UP	-3.53	0.68
623	Nckap1l	NCKPL	UP	-7.09	1.36
624	Brox	BROX	UP	-11.50	1.55
625	Ddx18	DDX18	UP	-0.87	0.26
626	Eif3l	EIF3L	UP	-2.62	0.56
627	Aimp2	AIMP2	UP	-6.42	1.28
628	Gspt1	ERF3A	UP	-4.61	0.56
629	Hnrnpl	HNRPL	UP	-7.26	0.50
630	Sgpl1	SGPL1	UP	-5.99	2.22
631	Ero1a	ERO1A	UP	-10.45	0.91
632	Eif3c	EIF3C	UP	-1.70	0.15
633	Apobr	APOBR	UP	-4.00	1.46
634	Rnpep	AMPB	UP	-5.61	0.73
635	Myh9	MYH9	UP	-15.36	0.50
636	Adpgk	ADPGK	UP	-5.51	1.65
637	Psmd2	PSMD2	UP	-2.81	0.28
638	Hnrnpul1	HNRL1	UP	-1.24	0.64
639	Atp1a1	AT1A1	UP	-0.84	0.07
640	Ddx39a	DX39A	UP	-14.51	1.14
641	Zng1	ZNG1	UP	-2.87	0.52
642	Slc25a3	S25A3	UP	-16.99	1.59
643	Rbm39	RBM39	UP	-13.82	2.00
644	Amot	AMOT	UP	-8.09	2.07
645	Gatad2b	P66B	UP	-3.41	0.84
646	Sfpq	SFPQ	UP	-4.64	0.24
647	Nono;Sfpq	NONO ;SFPQ	UP	-11.35	1.42
648	Tram1	TRAM1	UP	-0.89	0.40
649	Rab14	RAB14	UP	-3.31	0.33

650	Ck054	CK054	UP	-1.16	0.51
651	Acly	ACLY	UP	-9.38	0.77
652	Eif4a3	IF4A3	UP	-12.60	3.06
653	Rnh1	RINI	UP	-3.89	0.18
654	Atp5f1c	ATPG	UP	-7.88	1.08
655	Sh3bgrl3	SH3L3	UP	-14.09	1.55
656	Slc39a8	S39A8	UP	-14.88	1.91
657	Txndc5	TXND5	UP	-8.36	0.91
658	Rpn1	RPN1	UP	-11.16	0.48
659	Twf1	TWF1	UP	-7.85	0.80
660	Dnajc3	DNJC3	UP	-1.29	0.62
661	Ugp2	UGPA	UP	-11.32	1.82
662	Snx18	SNX18	UP	-4.37	1.51
663	Mia2	MIA2	UP	-4.86	1.43
664	Scpep1	RISC	UP	-2.46	0.46
665	Fdps	FPPS	UP	-12.38	0.91
666	Tardbp	TADBP	UP	-14.40	1.63
667	Hnrnpll	HNRLL	UP	-1.07	0.34
668	Tf	TRFE	UP	-13.43	1.35
669	Sf3b3	SF3B3	UP	-5.81	0.63
670	Cyrib	CYRIB	UP	-5.82	0.64
671	Tor1aip1	TOIP1	UP	-7.02	0.58
672	Dars1	SYDC	UP	-14.11	1.12
673	Mthfd1	C1TC	UP	-2.32	0.22
674	Pcyt2	PCY2	UP	-3.48	1.34
675	Mtarc2	45718	UP	-2.76	0.97
676	Pdia6	PDIA6	UP	-7.79	0.52
677	Trim59	TRI59	UP	-12.11	2.48
678	Blvrb	BLVRB	UP	-11.48	0.89
679	Sf3b5	SF3B5	UP	-12.62	2.78
680	Dhrs7b	DRS7B	UP	-2.64	0.78
681	Rfc4	RFC4	UP	-1.41	0.86
682	Mpst	THTM	UP	-2.73	0.47
683	Psip1	PSIP1	UP	-5.80	0.69
684	Sfxn1	SFXN1	UP	-2.21	0.33
685	Acy1	ACY1	UP	-2.70	0.32
686	Lims1	LIMS1	UP	-2.55	0.89
687	Hadhb	ECHB	UP	-3.87	1.90
688	Actr3	ARP3	UP	-15.68	0.83
689	Nono	NONO	UP	-9.76	0.84
690	Psat1	SERC	UP	-2.44	0.18
691	Hagh	GLO2	UP	-4.77	0.39
692	Vwa5a	VMA5A	UP	-3.97	0.32
693	Tmed9	TMED9	UP	-8.20	2.90
694	Aco2	ACON	UP	-17.29	0.52
695	Lactb2	LACB2	UP	-3.49	0.73
696	Dhrs1	DHRS1	UP	-4.44	0.59
697	Gmpr2	GMPR2	UP	-3.43	0.76
698	Eif2s2	IF2B	UP	-9.47	1.08
699	Ndufa10	NDUAA	UP	-3.48	0.87
700	Gps1	CSN1	UP	-3.19	1.13
701	Abhd12	ABD12	UP	-5.37	0.52
702	Gtpbp4	GTPB4	UP	-4.87	1.22
703	Pard3	PARD3	UP	-4.57	1.62
704	Rtn4	RTN4	UP	-2.65	0.29
705	Arhgdia	GDIR1	UP	-14.46	1.08
706	Prpf8	PRP8	UP	-8.80	0.93
707	Npm3	NPM3	UP	-2.13	0.23
708	Tomm22	TOM22	UP	-8.30	1.81
709	Mtap	MTAP	UP	-7.63	0.44
710	Chmp1b2	CH1B2	UP	-1.91	0.26
711	Cotl1	COTL1	UP	-11.16	0.49
712	Trap1	TRAP1	UP	-1.18	0.75
713	Atp5pb	AT5F1	UP	-1.83	0.52
714	Sec61b	SC61B	UP	-5.10	0.47
715	Ywhab	1433B	UP	-14.03	1.61
716	Arl8b	ARL8B	UP	-8.44	0.87
717	Ifitm3	IFM3	UP	-16.57	2.43
718	Cyb5b	CYB5B	UP	-9.51	1.16
719	Ppid	PPID	UP	-0.95	0.09
720	Rpl14	RL14	UP	-1.11	0.10
721	Slc25a11	M2OM	UP	-6.51	1.90
722	Chchd3	MIC19	UP	-1.53	0.14

723	Arpc2	ARPC2	UP	-17.80	1.58
724	Atic	PUR9	UP	-8.42	0.43
725	Snx1;Snx2	SNX1 ;SNX2	UP	-1.23	0.82
726	Pfdn1	PFD1	UP	-2.42	0.38
727	Rbm8a	RBM8A	UP	-11.51	2.86
728	Tmed5	TMED5	UP	-5.68	1.85
729	Manf	MANF	UP	-1.20	0.13
730	Cacybp	CYBP	UP	-13.43	1.18
731	Ssr1	SSRA	UP	-11.70	2.87
732	Chtop	CHTOP	UP	-2.62	0.63
733	Blvra	BIEA	UP	-6.33	0.48
734	Creld2	CREL2	UP	-3.33	1.33
735	Tomm34	TOM34	UP	-2.83	0.33
736	Spcs2	SPCS2	UP	-5.28	0.60
737	Uqcrc1	QCR1	UP	-11.93	0.82
738	Gars1	GARS	UP	-3.13	0.24
739	Shmt2	GLYM	UP	-15.30	0.76
740	Cs	CISY	UP	-18.82	1.57
741	Ube2v1	UB2V1	UP	-8.64	2.19
742	Srsf9	SRSF9	UP	-1.33	0.26
743	Pbdc1	PBDC1	UP	-1.81	0.77
744	Lman1	LMAN1	UP	-0.89	0.56
745	Pgm1	PGM1	UP	-4.56	0.58
746	Oxct1	SCOT1	UP	-9.39	0.78
747	Prpsap1	KPRA	UP	-5.26	1.50
748	Cyc1	CY1	UP	-4.31	0.44
749	Tars1	SYTC	UP	-4.62	0.60
750	Lsm12	LSM12	UP	-2.02	0.33
751	Ciao2b	CIA2B	UP	-1.34	0.62
752	Tmed10	TMEDA	UP	-3.91	0.61
753	Rab1b	RAB1B	UP	-2.18	0.62
754	Chchd2	CHCH2	UP	-5.04	1.50
755	Bcas2	SPF27	UP	-6.11	0.51
756	Dlst	ODO2	UP	-8.49	0.98
757	Atp5f1d	ATPD	UP	-13.50	0.89
758	Sf3a3	SF3A3	UP	-4.91	0.76
759	Ppil6	PPIL6	UP	-5.24	1.75
760	Idh3a	IDH3A	UP	-7.45	0.60
761	Fam162a	F162A	UP	-2.15	1.23
762	Nop56	NOP56	UP	-3.29	0.23
763	Prps1	PRPS1	UP	-0.95	0.25
764	Serpinb12	SPB12	UP	-10.50	1.80
765	Rpl22l1	RL22L	UP	-12.10	1.11
766	Timm50	TIM50	UP	-4.27	1.37
767	U2af1	U2AF1	UP	-1.35	1.25
768	Eef1g	EF1G	UP	-15.35	0.88
769	Rexo2	ORN	UP	-1.33	0.25
770	Bola1	BOLA1	UP	-4.96	0.85
771	Snx5	SNX5	UP	-6.44	0.52
772	Psmd12	PSD12	UP	-4.99	0.53
773	Efhd2	EFHD2	UP	-12.52	1.22
774	Tnfaip8l2	TP8L2	UP	-2.42	0.88
775	Tmem160	TM160	UP	-2.11	0.67
776	Atp5po	ATPO	UP	-9.91	0.65
777	Uqcrc2	QCR2	UP	-9.99	0.55
778	Ap2b1	AP2B1	UP	-3.76	0.82
779	Rpn2	RPN2	UP	-0.98	0.60
780	Lman2	LMAN2	UP	-4.87	2.63
781	Pgam1	PGAM1	UP	-11.35	0.91
782	Xrn2	XRN2	UP	-1.81	0.23
783	Tmem43	TMM43	UP	-15.66	2.48
784	Eif3k	EIF3K	UP	-7.88	1.20
785	Pgd	6PGD	UP	-4.79	0.18
786	Paics	PUR6	UP	-0.91	0.37
787	Ethe1	ETHE1	UP	-6.91	0.52
788	Cyb5r3	NB5R3	UP	-12.94	1.46
789	Akr1e2	AKCL2	UP	-13.63	1.22
790	Vps35	VPS35	UP	-8.28	1.97
791	Ehd4	EHD4	UP	-2.47	0.24
792	Set	SET	UP	-9.11	0.51
793	Mesd	MESD	UP	-4.39	0.80
794	Cse1l	XPO2	UP	-4.97	0.50
795	Scamp2	SCAM2	UP	-2.99	0.64

796	Anp32b	AN32B	UP	-11.36	0.97
797	Brd4	BRD4	UP	-5.22	1.36
798	Rnf114	RN114	UP	-3.70	0.71
799	Jph3	JPH3	UP	-1.82	0.51
800	Plek	PLEK	UP	-10.68	2.21
801	Ide	IDE	UP	-9.13	1.93
802	Gtf2ird1	GT2D1	UP	-9.91	2.56
803	Prmt1	ANM1	UP	-11.18	1.18
804	Dazap1	DAZP1	UP	-4.66	0.63
805	Akr1a1	AK1A1	UP	-6.38	0.65
806	Rpl38	RL38	UP	-11.01	0.81
807	Sh3bgrl	SH3L1	UP	-1.94	0.43
808	Ybx3	YBOX3	UP	-1.24	0.14
809	Tmod2	TMOD2	UP	-12.03	1.58
810	Hyou1	HYOU1	UP	-12.93	0.97
811	Adrm1	ADRM1	UP	-2.92	0.16
812	Aldh9a1	AL9A1	UP	-7.67	0.43
813	Arpc3	ARPC3	UP	-5.50	0.30
814	Usp14	UBP14	UP	-15.52	0.96
815	Edf1	EDF1	UP	-4.58	1.42
816	Txnrd1	TRXR1	UP	-3.75	0.58
817	Rhoa	RHOA	UP	-13.70	3.14
818	Acsl4	ACSL4	UP	-1.81	0.22
819	Psma6	PSA6	UP	-12.73	1.41
820	Prep	PPCE	UP	-5.52	1.29
821	Lsm4	LSM4	UP	-6.25	1.85
822	Copg2	COPG2	UP	-4.94	1.60
823	Plec	PLEC	UP	-15.15	0.44
824	Ehd1;Ehd3	EHD1 ;EHD3	UP	-1.25	0.30
825	Vapa;Vapb	VAPA ;VAPB	UP	-8.60	2.54
826	Clic4	CLIC4	UP	-2.97	0.18
827	Qki	QKI	UP	-1.92	0.26
828	Vps29	VPS29	UP	-5.62	0.99
829	Fhl3	FHL3	UP	-1.25	0.32
830	Comp	COMP	UP	-7.63	3.16
831	Esd	ESTD	UP	-13.14	0.82
832	Dstn	DEST	UP	-1.69	0.38
833	Sec11a	SC11A	UP	-2.81	1.34
834	Tmed2	TMED2	UP	-12.36	2.10
835	Srsf10	SRS10	UP	-0.98	0.33
836	Sqor	SQOR	UP	-5.74	0.52
837	Psma4	PSA4	UP	-10.03	1.20
838	Psmb3	PSB3	UP	-6.39	1.62
839	Psmb2	PSB2	UP	-8.35	1.04
840	Psma1	PSA1	UP	-6.58	0.31
841	Plp2	PLP2	UP	-8.87	2.65
842	Ak3	KAD3	UP	-4.61	0.62
843	Skp1	SKP1	UP	-2.97	1.40
844	Slc37a2	G6PT3	UP	-3.73	0.72
845	Stub1	CHIP	UP	-4.28	1.52
846	Uchl5	UCHL5	UP	-5.97	1.77
847	Ctsz	CATZ	UP	-18.63	1.46
848	Fam50a	FA50A	UP	-1.52	0.48
849	Arpc1b	ARC1B	UP	-12.94	0.83
850	Asah1	ASAH1	UP	-5.31	2.22
851	Vapa	VAPA	UP	-5.13	2.00
852	Timm8a1	TIM8A	UP	-2.43	0.16
853	Bub3	BUB3	UP	-4.75	1.02
854	Tagln2	TAGL2	UP	-16.19	1.25
855	Ehd1	EHD1	UP	-6.80	0.52
856	Npc2	NPC2	UP	-8.97	1.86
857	Lipa	LICH	UP	-6.58	1.40
858	Bpnt1	BPNT1	UP	-3.62	0.80
859	Aldh18a1	P5CS	UP	-10.42	1.11
860	Slc7a5	LAT1	UP	-2.82	0.85
861	Sumo3	SUMO3	UP	-1.08	0.35
862	Uba2	SAE2	UP	-4.46	0.40
863	Ddx39b	DX39B	UP	-2.32	0.32
864	Clic1	CLIC1	UP	-20.33	1.01
865	Vars1	SYVC	UP	-6.20	0.71
866	Deaf1	DEAF1	UP	-10.71	1.81
867	Hnrnpc	HNRPC	UP	-8.82	0.44
868	Psma7	PSA7	UP	-11.81	0.69

869	Psma5	PSA5	UP	-6.99	0.50
870	Hnrnpf	HNRPF	UP	-11.23	0.93
871	Sart1	SNUT1	UP	-1.20	1.66
872	Cul4b	CUL4B	DOWN	-1.40	-0.62
873	Sh3pxd2b	SPD2B	DOWN	-6.62	-0.78
874	Ddi2	DDI2	DOWN	-4.70	-2.41
875	Map7d1	MA7D1	DOWN	-6.70	-1.48
876	Cntrl	CNTRL	DOWN	-14.45	-3.50
877	Tpx2	TPX2	DOWN	-4.38	-0.90
878	Ppig	PPIG	DOWN	-4.94	-1.06
879	Ttn	TITIN	DOWN	-7.83	-1.83
880	H2ac11	H2A1B	DOWN	-10.73	-1.29
881	Safb	SAFB1	DOWN	-2.81	-0.38
882	Safb;Safb2	SAFB1 ;SAFB2	DOWN	-11.13	-1.21
883	Gls	GLSK	DOWN	-5.30	-2.11
884	Mki67	KI67	DOWN	-5.41	-0.87
885	Irf2bp2	I2BP2	DOWN	-9.69	-2.35
886	Rnf213	RN213	DOWN	-8.70	-2.46
887	Myo1e	MYO1E	DOWN	-2.21	-0.46
888	Myo1e;Myo1f	MYO1E	DOWN	-3.31	-1.63
889	Numa1	NUMA1	DOWN	-7.56	-0.61
890	Tpr	TPR	DOWN	-7.01	-0.63
891	QNG1	QNG1	DOWN	-3.55	-1.98
892	Hk2	HXK2	DOWN	-5.43	-0.65
893	Capn2	CAN2	DOWN	-8.34	-0.66
894	Clta	CLCA	DOWN	-2.07	-0.24
895	Dld	DLDH	DOWN	-9.14	-0.59
896	Hsd17b10	HCD2	DOWN	-7.87	-2.16
897	Tcof1	TCOF	DOWN	-6.68	-0.92
898	Dctn1	DCTN1	DOWN	-6.23	-1.54
899	Diaph1	DIAP1	DOWN	-3.82	-1.61
900	Aip	AIP	DOWN	-1.17	-0.58
901	Atox1	ATOX1	DOWN	-16.59	-1.08
902	Psmd4	PSMD4	DOWN	-9.65	-1.12
903	Exoc7	EXOC7	DOWN	-13.61	-3.66
904	Purb	PURB	DOWN	-8.67	-0.88
905	Srsf5	SRSF5	DOWN	-4.48	-0.37
906	Srsf4Srsf6	SRSF4SRSF6	DOWN	-6.91	-0.73
907	Kpna4	IMA3	DOWN	-1.11	-0.79
908	Kpna3;Kpna4	IMA3 ;IMA4	DOWN	-1.09	-0.25
909	Anp32a	AN32A	DOWN	-7.04	-0.78
910	Fkbp8	FKBP8	DOWN	-6.31	-0.84
911	Fyb1	FYB1	DOWN	-6.83	-0.64
912	Ap1b1;Ap2b1	AP1B1 ;AP2B1	DOWN	-6.24	-0.98
913	C1qbp	C1QBP	DOWN	-11.02	-1.33
914	Pnn	PININ	DOWN	-4.13	-0.42
915	Calu	CALU	DOWN	-4.46	-0.45
916	Psmb10	PSB10	DOWN	-10.43	-0.80
917	Hmgb3	HMGB3	DOWN	-9.77	-2.51
918	Pgrmc1	PGRC1	DOWN	-9.44	-1.09
919	Impa1	IMPA1	DOWN	-6.94	-0.72
920	Copb2	COPB2	DOWN	-8.38	-0.67
921	Stk10	STK10	DOWN	-2.06	-0.54
922	Aif1	AIF1	DOWN	-2.89	-0.38
923	Eef1b	EF1B	DOWN	-25.40	-2.26
924	Eef1b;Eef1d	EF1B ;EF1D	DOWN	-17.58	-2.55
925	Nmt1	NMT1	DOWN	-8.37	-1.05
926	Epb41l2	E41L2	DOWN	-1.02	-0.14
927	Hsd17b12	DHB12	DOWN	-1.47	-0.17
928	Psmc3	PRS6A	DOWN	-2.67	-0.40
929	Ctbp1	CTBP1	DOWN	-0.86	-0.51
930	Lin7c	LIN7C	DOWN	-3.29	-1.89
931	Yme1l1	YMEL1	DOWN	-15.04	-3.90
932	Cope	COPE	DOWN	-3.28	-1.10
933	Mt2	MT2	DOWN	-13.01	-1.24
934	Mt1	MT1	DOWN	-15.21	-1.33
935	Mtatp8	ATP8	DOWN	-9.15	-3.72
936	Ada	ADA	DOWN	-3.33	-1.69
937	Cd74	HG2A	DOWN	-7.65	-0.87
938	Aldoc	ALDOC	DOWN	-11.28	-0.66
939	Aldoa;Aldoc	ALDOA ;ALDOC	DOWN	-22.27	-2.04
940	Gpi	G6PI	DOWN	-5.73	-0.29
941	Pdia4	PDIA4	DOWN	-16.38	-0.99

942	Kras;Nras	RASK ;RASN	DOWN	-6.74	-0.86
943	Polr2a	RPB1	DOWN	-6.05	-1.17
944	Pgk1	PGK1	DOWN	-5.37	-0.18
945	Junb	JUNB	DOWN	-11.59	-1.88
946	H2az1;H2az2	H2AV ;H2AZ	DOWN	-13.62	-0.95
947	Pet117	PT117	DOWN	-7.60	-2.36
948	Ndufb1	NDUB1	DOWN	-6.29	-1.31
949	Eif4a2	IF4A2	DOWN	-6.97	-4.93
950	Txn	THIO	DOWN	-3.55	-0.43
951	Gstm1	GSTM1	DOWN	-2.09	-0.52
952	Tcea1	TCEA1	DOWN	-7.56	-0.96
953	H2bc14;Hist2h2bb	H2B1M ;H2B2B	DOWN	-19.97	-3.66
954	Cxcl2	CXCL2	DOWN	-8.65	-2.19
955	Parp1	PARP1	DOWN	-3.44	-0.72
956	Gpx1	GPX1	DOWN	-12.91	-2.77
957	Itga5	ITA5	DOWN	-3.01	-0.41
958	Itgb2	ITB2	DOWN	-4.35	-0.14
959	Oas1a	OAS1A	DOWN	-11.71	-3.22
960	Gusb	BGLR	DOWN	-8.54	-3.06
961	Cd5	CD5	DOWN	-10.41	-1.06
962	Umps	UMPS	DOWN	-2.42	-0.33
963	Icam1	ICAM1	DOWN	-6.92	-2.75
964	Rpl27a	RL27A	DOWN	-13.88	-1.16
965	Srp54	SRP54	DOWN	-3.84	-0.97
966	Glul	GLNA	DOWN	-8.13	-1.47
967	Cd44	CD44	DOWN	-8.63	-0.64
968	Spn	LEUK	DOWN	-1.90	-1.19
969	H1-2	H12	DOWN	-6.17	-1.28
970	H1-1;H1-2;H1-4	H11 ;H12 ;H14	DOWN	-12.55	-3.79
971	H1-3&14	H13 ;H14	DOWN	-10.84	-1.57
972	H1-2;H1-3;H1-4;H1-5	H12 ;H13	DOWN	-21.41	-2.08
973	H1-2;H1-3;H1-4	H12 ;H13 ;H14	DOWN	-18.17	-1.16
974	H1-2;H1-3	H12 ;H13	DOWN	-9.96	-0.53
975	Lgals1	LEG1	DOWN	-7.69	-0.55
976	Lgals3	LEG3	DOWN	-6.83	-0.34
977	Srp14	SRP14	DOWN	-4.39	-1.49
978	Hspa1l;Hspa2	BIP ;HS71L	DOWN	-8.21	-0.44
979	Hspa9	GRP75	DOWN	-1.46	-0.22
980	Eno1	ENOA	DOWN	-9.29	-0.24
981	Eno2	ENOG	DOWN	-1.00	-0.35
982	Eno2;Eno3	ENOB ;ENOG	DOWN	-9.64	-2.26
983	Tpi1	TPIS	DOWN	-19.03	-1.07
984	Rps6ka3	KS6A3	DOWN	-5.01	-0.81
985	Cfl1	COF1	DOWN	-17.45	-0.81
986	Fasn	FAS	DOWN	-4.35	-0.19
987	Rpl13a	RL13A	DOWN	-14.36	-1.06
988	Lsp1	LSP1	DOWN	-12.59	-0.82
989	Tmsb4x	TYB4	DOWN	-14.76	-0.96
990	Tpm3	TPM3	DOWN	-10.58	-0.97
991	Tpm3;Tpm4	TPM3 ;TPM4	DOWN	-3.09	-0.99
992	Akr1b7	ALD1	DOWN	-2.29	-1.53
993	Eno3	ENOB	DOWN	-5.19	-1.40
994	Lmnb2	LMNB2	DOWN	-4.53	-1.23
995	Rarb	RARB	DOWN	-10.54	-2.91
996	Hmbs	HEM3	DOWN	-5.25	-1.83
997	Pnp	PNPH	DOWN	-1.94	-0.48
998	Pcmt1	PIMT	DOWN	-5.49	-2.97
999	Capg	CAPG	DOWN	-13.51	-0.71
1000	Mcm3	MCM3	DOWN	-1.68	-0.23
1001	Rps2	RS2	DOWN	-10.53	-0.42
1002	Tln1	TLN1	DOWN	-19.78	-0.74
1003	Ezr	EZRI	DOWN	-4.20	-0.22
1004	Rdx	RADI	DOWN	-8.36	-1.08
1005	U2af2	U2AF2	DOWN	-13.78	-1.34
1006	Map4	MAP4	DOWN	-8.13	-1.02
1007	Gna13	GNA13	DOWN	-14.91	-3.25
1008	Rpl3	RL3	DOWN	-1.96	-0.12
1009	H2ax	H2AX	DOWN	-8.77	-0.34
1010	Apex1	APEX1	DOWN	-4.97	-1.76
1011	Adh5	ADHX	DOWN	-9.63	-0.61
1012	Nap1l1	NP1L1	DOWN	-5.46	-0.85
1013	Nap1l1;Nap1l4	NP1L1 ;NP1L4	DOWN	-3.21	-0.16
1014	Prkcd	KPCD	DOWN	-8.95	-0.81

1015	Pabpc1	PABP1	DOWN	-3.71	-0.09
1016	Hmgb2	HMGB2	DOWN	-21.00	-1.32
1017	Hmgb1;Hmgb2	HMGB1 ;HMGB2	DOWN	-2.33	-0.19
1018	C5ar1	C5AR1	DOWN	-2.53	-0.67
1019	Aimp1	AIMP1	DOWN	-6.28	-0.63
1020	Map2k1	MP2K1	DOWN	-6.69	-1.17
1021	Ssb	LA	DOWN	-5.00	-0.27
1022	Cd81	CD81	DOWN	-5.25	-0.91
1023	Rpl12	RL12	DOWN	-3.20	-0.25
1024	Rpl18	RL18	DOWN	-1.26	-0.10
1025	Lig1	DNLI1	DOWN	-7.97	-1.46
1026	Dnm2	DYN2	DOWN	-4.78	-1.04
1027	Csk	CSK	DOWN	-1.63	-0.92
1028	Eci1	ECI1	DOWN	-2.98	-0.15
1029	Cox6a1	CX6A1	DOWN	-6.00	-1.35
1030	Msh2	MSH2	DOWN	-7.80	-1.82
1031	H1-1;H1-3	H11 ;H13	DOWN	-8.27	-1.34
1032	H1-3;H1-4;H1-5	H13 ;H14 ;H15	DOWN	-13.46	-1.17
1033	H1-1	H11	DOWN	-14.31	-1.38
1034	H1-5	H15	DOWN	-14.09	-0.80
1035	Acadm	ACADM	DOWN	-5.01	-0.64
1036	Rangap1	RAGP1	DOWN	-3.05	-0.30
1037	Nsf	NSF	DOWN	-2.43	-0.31
1038	Vps4b	VPS4B	DOWN	-2.73	-0.82
1039	Adss2	PURA2	DOWN	-0.97	-0.08
1040	Tes	TES	DOWN	-1.97	-0.55
1041	Gsr	GSHR	DOWN	-13.21	-1.20
1042	Rpl6	RL6	DOWN	-16.64	-1.48
1043	Rpl29	RL29	DOWN	-13.59	-1.96
1044	Crkl	CRKL	DOWN	-5.70	-1.65
1045	Rplp1	RLA1	DOWN	-15.10	-1.43
1046	Rpl5	RL5	DOWN	-11.89	-0.88
1047	Eif1	EIF1	DOWN	-7.97	-1.98
1048	Tbca	TBCA	DOWN	-11.59	-1.80
1049	Alox5	LOX5	DOWN	-7.03	-2.86
1050	Clec10a	CLC10	DOWN	-2.39	-0.42
1051	Hnrnpa1;Hnrnpa3	ROA1 ;ROA3	DOWN	-12.41	-1.46
1052	Hcls1	HCLS1	DOWN	-8.42	-0.36
1053	Mcm4	MCM4	DOWN	-5.15	-1.26
1054	Cast	ICAL	DOWN	-8.34	-2.37
1055	Rab7a	RAB7A	DOWN	-3.82	-0.33
1056	Gla	AGAL	DOWN	-8.07	-1.08
1057	Dynlt1	DYLT1	DOWN	-1.88	-0.57
1058	Hdgf	HDGF	DOWN	-3.43	-0.21
1059	Ndufs6	NDUS6	DOWN	-8.34	-1.57
1060	Dbt	ODB2	DOWN	-1.08	-0.35
1061	Cnbp	CNBP	DOWN	-15.43	-0.98
1062	Dnajc2	DNJC2	DOWN	-7.00	-1.74
1063	Stmn1	STMN1	DOWN	-1.39	-0.07
1064	Stmn1;Stmn2	STMN1 ;STMN2	DOWN	-14.99	-1.25
1065	Ddx6	DDX6	DOWN	-1.09	-0.20
1066	Sh3bp1	3BP1	DOWN	-13.44	-3.37
1067	Rab8a	RAB8A	DOWN	-1.84	-0.59
1068	Rab10	RAB10	DOWN	-6.54	-2.40
1069	Gfer	ALR	DOWN	-9.13	-1.49
1070	Acyp1	ACYP1	DOWN	-10.84	-3.06
1071	Atp5f1e	ATP5E	DOWN	-2.07	-0.81
1072	Cox6b1	CX6B1	DOWN	-9.66	-0.46
1073	Cyb5a	CYB5	DOWN	-2.31	-0.25
1074	Usp5	UBP5	DOWN	-4.12	-0.51
1075	Ctbp2	CTBP2	DOWN	-4.59	-1.42
1076	Fus	FUS	DOWN	-6.60	-0.50
1077	Erp29	ERP29	DOWN	-10.53	-0.95
1078	Actn4	ACTN4	DOWN	-5.87	-0.35
1079	Snrpa1	RU2A	DOWN	-2.28	-0.29
1080	Ptpa	PTPA	DOWN	-16.30	-3.86
1081	Tpm1	TPM1	DOWN	-8.85	-1.62
1082	Ruvbl1	RUVB1	DOWN	-3.71	-0.29
1083	Nploc4	NPL4	DOWN	-7.65	-2.15
1084	Acta1	ACTB	DOWN	-1.11	-0.05
1085	Actr2	ARP2	DOWN	-8.60	-0.71
1086	Actr1a;Actr1b	ACTY ;ACTZ	DOWN	-10.00	-0.59
1087	Abce1	ABCE1	DOWN	-12.37	-1.74

1088	Vbp1	PFD3	DOWN	-4.53	-0.76
1089	Copz1	COPZ1	DOWN	-3.66	-1.38
1090	Sumo2	SUMO2	DOWN	-3.33	-0.59
1091	Ufm1	UFM1	DOWN	-10.24	-1.26
1092	Nutf2	NTF2	DOWN	-13.61	-1.88
1093	Ywhab	1433B	DOWN	-5.39	-0.46
1094	Ywhah	1433G	DOWN	-11.83	-2.46
1095	Timm10	TIM10	DOWN	-1.60	-0.51
1096	Timm13	TIM13	DOWN	-7.42	-0.47
1097	Rps8	RS8	DOWN	-14.01	-1.37
1098	Rps13	RS13	DOWN	-6.66	-0.31
1099	Dynlrb1	DLRB1	DOWN	-1.44	-0.15
1100	Rpl23a	RL23A	DOWN	-12.26	-0.63
1101	Mtpn	MTPN	DOWN	-1.57	-0.55
1102	Rpl23	RL23	DOWN	-8.53	-0.41
1103	Rps25	RS25	DOWN	-6.17	-0.28
1104	Fau	RS30	DOWN	-19.19	-1.20
1105	Elob	ELOB	DOWN	-1.57	-0.55
1106	Rpl39	RL39	DOWN	-13.73	-3.43
1107	Cycs	CYC	DOWN	-1.87	-0.22
1108	Rpl32	RL32	DOWN	-12.01	-0.82
1109	Ybx1;Ybx3	YBOX1 ;YBOX3	DOWN	-8.25	-0.62
1110	Rps27a	RS27A	DOWN	-12.66	-1.56
1111	Uba52	RL40	DOWN	-9.73	-2.92
1112	Pafah1b1	LIS1	DOWN	-14.82	-2.17
1113	Sumo1	SUMO1	DOWN	-1.15	-0.45
1114	Dynll1	DYL1	DOWN	-11.20	-2.57
1115	Crip1	CRIP1	DOWN	-11.15	-0.96
1116	Rps12	RS12	DOWN	-17.46	-1.36
1117	Ppp2ca	PP2AA	DOWN	-6.76	-0.74
1118	Ube2l3	UB2L3	DOWN	-1.49	-0.11
1119	Tuba1c	TBA1C	DOWN	-10.72	-0.78
1120	Tuba1c;Tuba8	TBA1C ;TBA8	DOWN	-10.76	-1.55
1121	Psmb7	PSB7	DOWN	-2.11	-0.41
1122	Lxn	LXN	DOWN	-7.04	-1.89
1123	Pkn1	PKN1	DOWN	-3.05	-1.15
1124	Mpp1	EM55	DOWN	-6.12	-0.88
1125	Tial1	TIAR	DOWN	-4.59	-2.13
1126	Hnrnph2	HNRH2	DOWN	-1.67	-0.51
1127	Hint1	HINT1	DOWN	-3.20	-0.28
1128	Nherf1	NHRF1	DOWN	-6.24	-1.15
1129	Vasp	VASP	DOWN	-7.13	-0.59
1130	Gaa	LYAG	DOWN	-1.11	-0.43
1131	Tgfbi	BGH3	DOWN	-13.50	-3.41
1132	Phf5a	PHF5A	DOWN	-11.62	-0.80
1133	Rpl36a	RL36A	DOWN	-11.61	-0.70
1134	Cbx1	CBX1	DOWN	-2.97	-1.13
1135	Eloc	ELOC	DOWN	-3.25	-0.91
1136	Rpl19	RL19	DOWN	-15.67	-1.25
1137	Csrp1	CSRP1	DOWN	-4.43	-1.32
1138	Ncf4	NCF4	DOWN	-3.17	-0.45
1139	Psme1	PSME1	DOWN	-11.74	-1.41
1140	Psme1;Psme2	PSME1 ;PSME2	DOWN	-16.62	-2.48
1141	Psme2	PSME2	DOWN	-2.17	-0.63
1142	G3bp2	G3BP2	DOWN	-8.20	-2.15
1143	Atp5pf	ATP5J	DOWN	-9.24	-0.81
1144	Bop1	BOP1	DOWN	-7.69	-0.92
1145	Rps5	RS5	DOWN	-9.22	-0.50
1146	Gclc	GSH1	DOWN	-8.06	-1.72
1147	Smarcc1	SMRC1	DOWN	-1.26	-0.25
1148	Smn1	SMN	DOWN	-13.84	-1.36
1149	Dab2	DAB2	DOWN	-7.89	-0.47
1150	Tubb5	TBB5	DOWN	-1.39	-0.11
1151	Yy1;Yy2	TYY1 ;TYY2	DOWN	-1.63	-0.64
1152	Nme2	NDKB	DOWN	-2.32	-0.12
1153	Pfdn6	PFD6	DOWN	-8.06	-0.91
1154	Rac2	RAC2	DOWN	-3.54	-0.31
1155	Fabp5	FABP5	DOWN	-21.61	-2.55
1156	Larp7	LARP7	DOWN	-5.30	-2.37
1157	Cab39	CAB39	DOWN	-1.95	-0.30
1158	Atp5me	ATP5I	DOWN	-3.57	-0.58
1159	Bax	BAX	DOWN	-11.63	-1.28
1160	Lyar	LYAR	DOWN	-0.93	-0.66

1161	Ssrp1	SSRP1	DOWN	-4.38	-0.41
1162	Zc3h18	ZCH18	DOWN	-6.29	-1.51
1163	Rbm15	RBM15	DOWN	-4.66	-1.48
1164	Pepd	PEPD	DOWN	-5.38	-1.50
1165	Osbp	OSBP1	DOWN	-8.71	-2.53
1166	Arhgap45	HMHA1	DOWN	-6.40	-1.38
1167	Abraxas2	ABRX2	DOWN	-4.94	-1.11
1168	Hp1bp3	HP1B3	DOWN	-14.30	-3.24
1169	Zc3h15	ZC3HF	DOWN	-2.95	-1.62
1170	Usp39	UBP39	DOWN	-10.65	-2.55
1171	Uap1l1	UAP1L	DOWN	-7.09	-0.48
1172	Srsf4;Srsf6	SRSF4 ;SRSF6	DOWN	-4.92	-1.25
1173	Psmd1	PSMD1	DOWN	-3.46	-0.27
1174	Khsrp	FUBP2	DOWN	-9.85	-0.39
1175	Fubp1;Khsrp	FUBP1 ;FUBP2	DOWN	-3.33	-0.94
1176	Ddb1	DDB1	DOWN	-2.25	-0.90
1177	Gpsm3	GPSM3	DOWN	-0.93	-0.16
1178	Lbr	LBR	DOWN	-1.06	-0.10
1179	Puf60	PUF60	DOWN	-11.15	-0.91
1180	Eif3j1;Eif3j2	EI3JA ;EI3JB	DOWN	-15.28	-1.32
1181	Arhgap17	RHG17	DOWN	-9.12	-1.98
1182	Edc4	EDC4	DOWN	-5.88	-1.71
1183	Hdgfl2	HDGR2	DOWN	-6.83	-1.27
1184	Niban1	NIBA1	DOWN	-8.57	-1.10
1185	Lrrfip1	LRRF1	DOWN	-3.99	-0.38
1186	Dnah12	DYH12	DOWN	-1.03	-0.64
1187	Ccdc88b	CC88B	DOWN	-11.68	-2.66
1188	Cdv3	CDV3	DOWN	-12.19	-1.48
1189	Lrrc47	LRC47	DOWN	-2.48	-0.73
1190	Ddx46	DDX46	DOWN	-9.09	-2.30
1191	Aldh16a1	A16A1	DOWN	-0.91	-0.53
1192	Spag9	JIP4	DOWN	-0.97	-0.45
1193	Nufip2	NUFP2	DOWN	-5.38	-1.19
1194	Pfas	PUR4	DOWN	-1.61	-0.16
1195	Cluh	CLU	DOWN	-9.99	-2.79
1196	Utp20	UTP20	DOWN	-11.78	-1.61
1197	Arcn1	COPD	DOWN	-9.45	-1.08
1198	Nfatc2	NFAC2	DOWN	-1.99	-0.78
1199	Irag2	IRAG2	DOWN	-0.95	-0.39
1200	Hnrnpd	HNRPD	DOWN	-14.52	-1.01
1201	Hnrnpd;Hnrnpdl	HNRDL	DOWN	-16.38	-1.58
1202	Khdrbs1	KHDR1	DOWN	-6.79	-0.59
1203	Gas7	GAS7	DOWN	-6.40	-1.65
1204	Caprin1	CAPR1	DOWN	-1.41	-0.32
1205	Reep5	REEP5	DOWN	-3.29	-0.98
1206	Eif1a;Eif1ax	IF1AX	DOWN	-9.66	-0.90
1207	Arhgef2	ARHG2	DOWN	-3.81	-0.75
1208	Rbbp4	RBBP4	DOWN	-2.96	-1.36
1209	Rbbp7	RBBP7	DOWN	-2.22	-0.48
1210	Asns	ASNS	DOWN	-5.58	-0.87
1211	Tmpo	LAP2B	DOWN	-4.42	-0.58
1212	Tmpo	LAP2A ;LAP2B	DOWN	-3.09	-0.32
1213	Pak3	PAK3	DOWN	-11.74	-3.19
1214	Ppm1g	PPM1G	DOWN	-1.78	-0.53
1215	Cdc37	CDC37	DOWN	-3.97	-0.35
1216	Cybb	CY24B	DOWN	-4.60	-2.12
1217	Ptpn18	PTN18	DOWN	-0.98	-0.30
1218	Ctcf	CTCF	DOWN	-12.51	-2.09
1219	Hcfc1	HCFC1	DOWN	-4.48	-0.38
1220	Arhgef1	ARHG1	DOWN	-4.15	-0.79
1221	Sntb2	SNTB2	DOWN	-6.57	-2.38
1222	Hspa4;Hsph1	HS105 ;HSP74	DOWN	-0.93	-0.15
1223	Hadh	HCDH	DOWN	-5.18	-1.00
1224	Znf638	ZN638	DOWN	-7.10	-1.76
1225	Ddx19a	DD19A	DOWN	-8.68	-1.29
1226	Pea15	PEA15	DOWN	-5.32	-0.38
1227	Ddx3x	DDX3X	DOWN	-2.12	-0.20
1228	Sf3a2	SF3A2	DOWN	-4.72	-1.32
1229	Trim28	TIF1B	DOWN	-2.01	-0.17
1230	Tpd52	TPD52	DOWN	-16.06	-1.32
1231	Dbnl	DBNL	DOWN	-9.82	-0.75
1232	Sh3gl1	SH3G1	DOWN	-2.06	-0.21
1233	Ostf1	OSTF1	DOWN	-4.15	-0.38

1234	Ndufa4	NDUA4	DOWN	-11.11	-0.54
1235	Cstb	CYTB	DOWN	-4.17	-0.57
1236	Ndrg1	NDRG1	DOWN	-5.46	-0.34
1237	Fkbp3	FKBP3	DOWN	-12.66	-1.49
1238	Vat1	VAT1	DOWN	-2.32	-2.35
1239	Zyx	ZYX	DOWN	-9.69	-1.03
1240	Mapk3	MK03	DOWN	-2.28	-0.66
1241	Spr	SPRE	DOWN	-9.15	-1.07
1242	Btf3	BTF3	DOWN	-9.57	-1.15
1243	Sf1	SF01	DOWN	-12.17	-0.84
1244	Ly6e	LY6E	DOWN	-5.22	-1.40
1245	Fkbp5	FKBP5	DOWN	-2.67	-0.66
1246	Atp7a	ATP7A	DOWN	-4.77	-1.20
1247	H2bc3	H2B1B ;H2B1P	DOWN	-19.17	-2.94
1248	Srm	SPEE	DOWN	-3.58	-0.97
1249	Vcl	VINC	DOWN	-3.13	-0.90
1250	Gart	PUR2	DOWN	-12.83	-0.65
1251	Mars1	SYMC	DOWN	-6.04	-1.08
1252	Prex1	PREX1	DOWN	-5.43	-2.20
1253	Myof	MYOF	DOWN	-4.40	-1.36
1254	Macf1	K0754 ;MACF1	DOWN	-4.05	-0.75
1255	Pds5a	PDS5A	DOWN	-5.76	-1.30
1256	Swap70	SWP70	DOWN	-5.39	-0.71
1257	Cep170	CE170	DOWN	-3.34	-0.65
1258	Cdc5l	CDC5L	DOWN	-13.64	-1.19
1259	FAM120A	F120A	DOWN	-4.82	-1.41
1260	Nop58	NOP58	DOWN	-2.88	-0.32
1261	Brme1	BRME1	DOWN	-17.60	-6.57
1262	Cltb	CLCB	DOWN	-11.53	-1.50
1263	Dnajc8	DNJC8	DOWN	-1.25	-0.41
1264	Zc3h11a	ZC11A	DOWN	-5.46	-1.70
1265	Eif4g1	IF4G1	DOWN	-2.14	-0.22
1266	Smchd1	SMHD1	DOWN	-8.00	-2.95
1267	Uggt1	UGGG1	DOWN	-0.91	-0.29
1268	Pcnp	PCNP	DOWN	-1.63	-0.59
1269	Snx6	SNX6	DOWN	-0.96	-0.62
1270	Oxsr1	OXSR1	DOWN	-11.21	-2.70
1271	Lrpprc	LPPRC	DOWN	-1.38	-0.35
1272	Ecpas	ECM29	DOWN	-0.84	-0.69
1273	Chd4	CHD4	DOWN	-16.83	-1.97
1274	Nup98	NUP98	DOWN	-3.56	-1.10
1275	Jpt2	JUPI2	DOWN	-6.21	-0.70
1276	Washc2	WASC2	DOWN	-4.98	-1.13
1277	Cand1	CAND1	DOWN	-7.12	-0.59
1278	Rps27	RS27	DOWN	-3.95	-0.39
1279	Rps27l	RS27L	DOWN	-3.73	-1.64
1280	Tmsb10	TYB10	DOWN	-11.16	-3.09
1281	Ppp2r1a	2AAA	DOWN	-6.36	-0.40
1282	Atp5mk	ATPMK	DOWN	-1.42	-0.94
1283	Apool	MIC27	DOWN	-4.58	-0.53
1284	Nap1l4	NP1L4	DOWN	-2.02	-0.35
1285	Picalm	PICAL	DOWN	-5.61	-0.62
1286	Syncrip	HNRPQ	DOWN	-10.79	-0.61
1287	Dek	DEK	DOWN	-11.19	-1.07
1288	Sh3d21	SH321	DOWN	-16.52	-2.66
1289	Cyld	CYLD	DOWN	-2.07	-0.75
1290	Fnbp1	FNBP1	DOWN	-2.96	-0.71
1291	Usp8	UBP8	DOWN	-2.67	-0.98
1292	Vac14	VAC14	DOWN	-2.24	-0.64
1293	Ubap2l	UBP2L	DOWN	-4.00	-0.69
1294	Flnb	FLNB	DOWN	-8.81	-1.71
1295	Flna;Flnb	FLNA ;FLNB	DOWN	-8.59	-1.30
1296	Flna	FLNA	DOWN	-6.16	-1.69
1297	Rraga	RRAGA	DOWN	-4.04	-0.77
1298	Nucks1	NUCKS	DOWN	-2.81	-0.63
1299	Glrx5	GLRX5	DOWN	-2.40	-0.81
1300	Safb2	SAFB2	DOWN	-5.60	-1.17
1301	Poldip3	PDIP3	DOWN	-2.27	-0.87
1302	Bola2	BOLA2	DOWN	-7.16	-0.57
1303	Echs1	ECHM	DOWN	-3.66	-1.16
1304	Tbl1xr1	TBL1R	DOWN	-1.95	-0.61
1305	Psmf1	PSMF1	DOWN	-1.97	-0.57
1306	Sgta	SGTA	DOWN	-13.90	-1.57

1307	Eif2a	EIF2A	DOWN	-3.59	-0.31
1308	Eea1	EEA1	DOWN	-0.86	-0.20
1309	Nceh1	NCEH1	DOWN	-0.83	-0.64
1310	Srp68	SRP68	DOWN	-2.56	-0.90
1311	Acbd3	GCP60	DOWN	-0.92	-0.66
1312	Hadha	ECHA	DOWN	-0.87	-0.15
1313	Rpl24	RL24	DOWN	-15.95	-1.49
1314	Elmo1	ELMO1	DOWN	-1.42	-0.56
1315	Ppp1r18	PPR18	DOWN	-6.42	-0.78
1316	Cc2d1b	C2D1B	DOWN	-2.73	-1.10
1317	Asph	ASPH	DOWN	-3.16	-1.33
1318	Iars1	SYIC	DOWN	-13.82	-0.85
1319	Qdpr	DHPR	DOWN	-10.49	-3.00
1320	Sp110	SP110	DOWN	-7.58	-1.03
1321	Rsl1d1	RL1D1	DOWN	-17.15	-1.90
1322	Nob1	NOB1	DOWN	-5.04	-1.27
1323	Lpcat2	PCAT2	DOWN	-2.28	-0.32
1324	Map1s	MAP1S	DOWN	-1.34	-0.54
1325	Farsa	SYFA	DOWN	-7.85	-0.97
1326	Asrgl1	ASGL1	DOWN	-11.01	-2.59
1327	Ncaph	CND2	DOWN	-1.62	-0.40
1328	Cpne1	CPNE1	DOWN	-5.39	-1.32
1329	Mbnl1;Mbnl2	MBNL1 ;MBNL2	DOWN	-7.13	-0.93
1330	Septin11	45911	DOWN	-8.74	-1.26
1331	Septin11;Septin6	SEP11 ;SEPT6	DOWN	-13.47	-2.26
1332	Immt	MIC60	DOWN	-6.64	-0.22
1333	Acat2	THIC	DOWN	-8.88	-0.93
1334	Txnl1	TXNL1	DOWN	-4.02	-0.24
1335	Pus7l	PUS7L	DOWN	-3.17	-2.06
1336	Slc38a2	S38A2	DOWN	-5.79	-1.20
1337	Smc4	SMC4	DOWN	-3.49	-0.56
1338	Smc2	SMC2	DOWN	-3.18	-1.25
1339	Tcerg1	TCRG1	DOWN	-2.02	-0.87
1340	Hist1h2bp	H2B1P	DOWN	-13.87	-2.51
1341	Slain2	SLAI2	DOWN	-5.95	-0.97
1342	Pdlim5	PDLI5	DOWN	-8.78	-1.57
1343	Pygb	PYGB	DOWN	-0.84	-0.36
1344	Plcg2	PLCG2	DOWN	-8.73	-1.72
1345	Ppat	PUR1	DOWN	-7.05	-1.31
1346	Pak2	PAK2	DOWN	-12.20	-1.07
1347	Mrgprx1	MRGX1	DOWN	-13.93	-3.96
1348	Afg3l2	AFG32	DOWN	-2.86	-1.16
1349	Rbm17	SPF45	DOWN	-1.96	-0.51
1350	Bclaf1	BCLF1	DOWN	-7.46	-1.11
1351	Gmds	GMDS	DOWN	-4.79	-0.90
1352	Plekho2	PKHO2	DOWN	-10.42	-1.24
1353	Wipf1	WIPF1	DOWN	-10.11	-2.50
1354	Ppp1r11	PP1RB	DOWN	-7.52	-2.11
1355	Dnm1l	DNM1L	DOWN	-7.41	-1.71
1356	Lrrc25	LRC25	DOWN	-3.81	-0.96
1357	Colgalt1	GT251	DOWN	-3.44	-0.50
1358	Sdha	SDHA	DOWN	-1.28	-0.20
1359	Otud6b	OTU6B	DOWN	-12.32	-1.62
1360	Agfg1	AGFG1	DOWN	-0.99	-0.63
1361	Shtn1	SHOT1	DOWN	-10.56	-1.20
1362	Matr3	MATR3	DOWN	-4.81	-0.67
1363	Babam2	BABA2	DOWN	-11.86	-3.14
1364	Arhgef6;Arhgef7	ARHG6 ;ARHG7	DOWN	-3.94	-0.68
1365	Naxe	NNRE	DOWN	-1.49	-0.42
1366	Sf3a1	SF3A1	DOWN	-1.61	-0.30
1367	Acat1	THIL	DOWN	-4.36	-0.33
1368	Tprkb	TPRKB	DOWN	-3.58	-1.05
1369	Mbnl3	MBNL3	DOWN	-8.56	-1.26
1370	Blmh	BLMH	DOWN	-3.99	-0.73
1371	Gtf2f2	T2FB	DOWN	-7.49	-1.72
1372	Uqcr10	QCR9	DOWN	-0.83	-0.39
1373	Nudcd3	NUDC3	DOWN	-8.01	-0.98
1374	Dync1li1	DC1L1	DOWN	-4.80	-2.18
1375	Mtss1	MTSS1	DOWN	-5.56	-2.21
1376	Dnttip2	TDIF2	DOWN	-1.20	-0.58
1377	Ptrh2	PTH2	DOWN	-6.29	-1.39
1378	Ubqln1	UBQL1	DOWN	-7.09	-1.94
1379	Micos13	MIC13	DOWN	-9.11	-2.23

1380	Nup85	NUP85	DOWN	-2.84	-2.89
1381	Mavs	MAVS	DOWN	-3.23	-0.56
1382	Cth	CGL	DOWN	-9.93	-1.88
1383	Washc1	WASH1	DOWN	-10.85	-2.04
1384	Hdlbp	VIGLN	DOWN	-0.81	-0.08
1385	Ptgr2	PTGR2	DOWN	-1.17	-0.76
1386	Mrps23	RT23	DOWN	-11.56	-2.64
1387	Pdcd10	PDC10	DOWN	-5.52	-1.27
1388	Srsf4	SRSF4	DOWN	-6.52	-1.05
1389	Ccdc115	CC115	DOWN	-10.72	-1.39
1390	Rpe	RPE	DOWN	-7.24	-1.91
1391	Hnrnpu	HNRPU	DOWN	-2.28	-0.13
1392	Flnc	FLNC	DOWN	-1.12	-1.38
1393	Oas3	OAS3	DOWN	-9.58	-2.14
1394	Ciapin1	CPIN1	DOWN	-12.21	-0.97
1395	Acot7	BACH	DOWN	-9.93	-1.35
1396	Ndufs1	NDUS1	DOWN	-0.81	-0.13
1397	Nifk	MK67I	DOWN	-6.94	-1.96
1398	Pqbp1	PQBP1	DOWN	-4.56	-1.34
1399	Rbmxl1	RMXL1	DOWN	-0.91	-0.05
1400	Chchd6	MIC25	DOWN	-5.27	-1.18
1401	Ddx1	DDX1	DOWN	-9.97	-1.41
1402	Ubap2	UBAP2	DOWN	-2.70	-0.73
1403	Rbms1	RBMS1	DOWN	-5.45	-1.59
1404	Fubp1	FUBP1	DOWN	-10.88	-0.96
1405	Dnajc9	DNJC9	DOWN	-6.28	-1.96
1406	Yars1	SYYC	DOWN	-7.91	-0.80
1407	Cisd1	CISD1	DOWN	-4.68	-1.04
1408	Trex1	TREX1	DOWN	-4.66	-1.25
1409	Dap	DAP1	DOWN	-0.99	-0.39
1410	Dus3l	DUS3L	DOWN	-9.13	-1.81
1411	Basp1	BASP1	DOWN	-9.42	-0.41
1412	Arrb2	ARRB2	DOWN	-2.35	-0.80
1413	Lrrc49	LRC49	DOWN	-8.32	-2.00
1414	Rrp1b	RRP1B	DOWN	-3.09	-1.88
1415	Prpf6	PRP6	DOWN	-6.58	-1.97
1416	Ptgr1	PTGR1	DOWN	-1.53	-0.75
1417	Ndufv1	NDUV1	DOWN	-2.91	-0.93
1418	Ttc1	TTC1	DOWN	-6.89	-1.84
1419	Grhpr	GRHPR	DOWN	-5.62	-1.52
1420	Smarca5	SMCA5	DOWN	-2.04	-0.45
1421	Lrp1	LRP1	DOWN	-6.46	-0.38
1422	Supt16h	SP16H	DOWN	-6.28	-0.86
1423	Rab31	RAB31	DOWN	-5.20	-1.84
1424	Lrch4	LRCH4	DOWN	-9.96	-1.33
1425	Acaa1a	THIKA	DOWN	-7.52	-0.89
1426	Ddx27	DDX27	DOWN	-13.44	-2.43
1427	Far1	FACR1	DOWN	-4.24	-1.10
1428	Nop2	NOP2	DOWN	-10.32	-0.91
1429	Glyr1	GLYR1	DOWN	-15.75	-1.95
1430	Pycr2	P5CR2	DOWN	-11.44	-1.18
1431	Lrrc59	LRC59	DOWN	-13.10	-0.57
1432	Prkx	PRKX	DOWN	-5.59	-0.86
1433	Prpf3	PRPF3	DOWN	-4.15	-0.86
1434	Cers2	CERS2	DOWN	-1.16	-0.40
1435	Taldo1	TALDO	DOWN	-8.29	-0.44
1436	Hnrnpab	ROAA	DOWN	-9.32	-0.37
1437	Thumpd1	THUM1	DOWN	-7.49	-1.87
1438	Stoml2	STML2	DOWN	-4.83	-1.42
1439	Mvd	MVD1	DOWN	-12.97	-3.54
1440	Psmd6	PSMD6	DOWN	-7.76	-0.63
1441	Rap1b	RAP1B	DOWN	-4.96	-0.90
1442	Pls3	PLST	DOWN	-1.49	-0.23
1443	Stk24	STK24	DOWN	-12.04	-2.59
1444	Dctn2	DCTN2	DOWN	-9.51	-0.95
1445	Cmas	NEUA	DOWN	-3.93	-1.02
1446	Dpp3	DPP3	DOWN	-3.46	-0.94
1447	Clint1	EPN4	DOWN	-3.11	-0.55
1448	Prpf19	PRP19	DOWN	-5.40	-0.32
1449	Nampt	NAMPT	DOWN	-8.01	-0.56
1450	Vmp1	VMP1	DOWN	-12.33	-1.40
1451	Triobp	TARA	DOWN	-5.61	-3.05
1452	Hibadh	3HIDH	DOWN	-5.78	-1.15

1453	St13	F10A1	DOWN	-3.86	-0.21
1454	Dhrs4	DHRS4	DOWN	-1.83	-0.86
1455	Mat2b	MAT2B	DOWN	-6.54	-2.22
1456	Etfa	ETFA	DOWN	-10.28	-0.43
1457	Rtcb	RTCB	DOWN	-0.96	-0.28
1458	Cttnbp2nl	CT2NL	DOWN	-6.15	-1.11
1459	Grpel1	GRPE1	DOWN	-6.75	-0.76
1460	Ndufs5	NDUS5	DOWN	-4.60	-1.45
1461	Rnps1	RNPS1	DOWN	-9.08	-0.88
1462	Nasp	NASP	DOWN	-4.96	-0.44
1463	Kars1	SYK	DOWN	-1.27	-0.41
1464	Srrt	SRRT	DOWN	-4.80	-0.30
1465	Adar	DSRAD	DOWN	-13.90	-2.72
1466	Klb	KLOTB	DOWN	-2.12	-0.71
1467	Lpxn	LPXN	DOWN	-8.55	-1.23
1468	Mrps18b	RT18B	DOWN	-4.24	-1.82
1469	Mrps5	RT05	DOWN	-7.90	-1.24
1470	Ubqln4	UBQL4	DOWN	-7.05	-1.38
1471	Ogfr	OGFR	DOWN	-5.15	-1.59
1472	Rrbp1	RRBP1	DOWN	-8.22	-0.59
1473	Igf2bp3	IF2B3	DOWN	-9.10	-1.02
1474	Cox6c	COX6C	DOWN	-8.33	-1.24
1475	Atp5mg	ATP5L	DOWN	-10.16	-0.84
1476	Rpl17	RL17	DOWN	-5.07	-0.21
1477	Mydgf	MYDGF	DOWN	-0.97	-0.18
1478	Glo1	LGUL	DOWN	-3.29	-0.27
1479	Glod4	GLOD4	DOWN	-3.89	-1.32
1480	Arpc5	ARPC5	DOWN	-13.67	-1.58
1481	Ssr2	SSRB	DOWN	-3.61	-0.67
1482	Atg3	ATG3	DOWN	-6.28	-1.24
1483	Lap3	AMPL	DOWN	-3.47	-0.89
1484	Dut	DUT	DOWN	-5.55	-0.47
1485	Ndufc2	NDUC2	DOWN	-7.60	-1.70
1486	Pgls	6PGL	DOWN	-9.45	-1.12
1487	Uqcrq	QCR8	DOWN	-4.50	-1.36
1488	Ndufa2	NDUA2	DOWN	-7.99	-1.97
1489	Sdhb	SDHB	DOWN	-1.50	-0.32
1490	Cisd2	CISD2	DOWN	-4.79	-1.43
1491	Sar1b	SAR1B	DOWN	-10.77	-2.09
1492	Rgs10	RGS10	DOWN	-4.25	-0.88
1493	RTRAF	RTRAF	DOWN	-2.58	-0.39
1494	Nudt21	CPSF5	DOWN	-11.84	-3.22
1495	Gmfb	GMFB	DOWN	-2.45	-0.57
1496	Denr	DENR	DOWN	-5.10	-1.63
1497	Txndc17	TXD17	DOWN	-20.48	-1.83
1498	Glrx3	GLRX3	DOWN	-7.11	-0.84
1499	Mrpl41	RM41	DOWN	-7.93	-1.34
1500	Acot13	ACO13	DOWN	-6.26	-1.29
1501	Txndc12	TXD12	DOWN	-4.70	-1.61
1502	Kgd4	KGD4	DOWN	-6.35	-1.56
1503	Ndufb3	NDUB3	DOWN	-6.75	-1.40
1504	Atp6v1g1	VATG1	DOWN	-11.31	-1.62
1505	Uqcrfs1	UCRI	DOWN	-4.36	-0.60
1506	Carhsp1	CHSP1	DOWN	-6.35	-0.73
1507	Fam136a	F136A	DOWN	-7.04	-2.35
1508	Nhp2	NHP2	DOWN	-7.65	-0.91
1509	Snw1	SNW1	DOWN	-5.58	-0.48
1510	Rprd1b	RPR1B	DOWN	-13.82	-1.56
1511	Ranbp3	RANB3	DOWN	-4.59	-0.85
1512	Smc1a	SMC1A	DOWN	-2.30	-0.85
1513	Raver1	RAVR1	DOWN	-12.38	-2.04
1514	Tubb2b	TBB2B	DOWN	-1.82	-0.53
1515	Snx2	SNX2	DOWN	-10.99	-0.77
1516	Ctnnbl1	CTBL1	DOWN	-5.10	-1.77
1517	Pin4	PIN4	DOWN	-4.02	-0.45
1518	Napg	SNAG	DOWN	-4.84	-0.67
1519	Ist1	IST1	DOWN	-1.37	-0.57
1520	Sugt1	SGT1	DOWN	-7.01	-0.99
1521	Hnrnpa0	ROA0	DOWN	-11.83	-0.76
1522	Rpl11	RL11	DOWN	-15.66	-0.74
1523	Ndufs4	NDUS4	DOWN	-2.15	-0.72
1524	Tecr	TECR	DOWN	-2.41	-0.10
1525	Serbp1	SERB1	DOWN	-8.24	-0.79

1526	Gar1	GAR1	DOWN	-11.19	-3.51
1527	Gins3	PSF3	DOWN	-5.65	-1.43
1528	Luc7l	LUC7L	DOWN	-1.09	-0.40
1529	Tpd52l2	TPD54	DOWN	-3.09	-0.87
1530	Ola1	OLA1	DOWN	-11.73	-1.34
1531	Rpl15	RL15	DOWN	-6.88	-0.61
1532	Tsfm	EFTS	DOWN	-9.26	-0.93
1533	Mtrex	MTREX	DOWN	-5.20	-1.84
1534	Rps19	RS19	DOWN	-5.01	-0.16
1535	Ccdc47	CCD47	DOWN	-0.85	-0.28
1536	Pdhb	ODPB	DOWN	-2.93	-0.24
1537	Rars1	SYRC	DOWN	-1.57	-0.17
1538	Ptms	PTMS	DOWN	-3.57	-0.49
1539	Ddx56	DDX56	DOWN	-8.79	-2.25
1540	Snu13	NH2L1	DOWN	-11.99	-0.78
1541	Znf706	ZN706	DOWN	-6.95	-1.80
1542	Gatd3	GAL3A	DOWN	-2.96	-0.91
1543	Tbcb	TBCB	DOWN	-5.32	-1.79
1544	Necap2	NECP2	DOWN	-13.99	-3.69
1545	Sarnp	SARNP	DOWN	-9.05	-0.83
1546	Lamtor5	LTOR5	DOWN	-1.24	-0.40
1547	Erp44	ERP44	DOWN	-3.80	-0.96
1548	Rpl34	RL34	DOWN	-1.71	-0.18
1549	Coro7	CORO7	DOWN	-3.37	-0.77
1550	Acp1	PPAC	DOWN	-2.16	-0.40
1551		CX049	DOWN	-2.33	-1.59
1552	Gcc1	GCC1	DOWN	-8.74	-2.08
1553	Ndufv2	NDUV2	DOWN	-6.44	-1.88
1554	Trir	TRIR	DOWN	-9.79	-1.34
1555	Dusp3	DUS3	DOWN	-7.72	-1.27
1556	Ppa1	IPYR	DOWN	-1.51	-0.24
1557	Uqcrb	QCR7	DOWN	-1.96	-0.71
1558	Itpa	ITPA	DOWN	-8.25	-1.45
1559	Arpc5l	ARP5L	DOWN	-14.17	-2.78
1560	Chmp4b	CHM4B	DOWN	-1.79	-0.16
1561	Rpl4	RL4	DOWN	-8.78	-0.63
1562	Ebna1bp2	EBP2	DOWN	-10.86	-3.18
1563	Exosc1	EXOS1	DOWN	-5.54	-0.94
1564	Dcps	DCPS	DOWN	-1.70	-0.20
1565	Cnpy3	CNPY3	DOWN	-9.11	-2.54
1566	Napa	SNAA	DOWN	-3.28	-0.69
1567	Mrpl12	RM12	DOWN	-8.02	-0.53
1568	Alg5	ALG5	DOWN	-3.60	-1.35
1569	Prkar1a	KAP0	DOWN	-5.39	-0.45
1570	Ftsj3	SPB1	DOWN	-8.77	-1.94
1571	Plin3	PLIN3	DOWN	-2.86	-0.40
1572	Srpra	SRPRA	DOWN	-7.71	-1.75
1573	Acadsb	ACDSB	DOWN	-3.79	-1.19
1574	Cmpk1	KCY	DOWN	-1.95	-0.51
1575	Akap8	AKAP8	DOWN	-5.95	-1.24
1576	Ampd2	AMPD2	DOWN	-2.65	-1.86
1577	Pycr3	P5CR3	DOWN	-3.16	-0.77
1578	Pak1ip1	PK1IP	DOWN	-7.73	-2.09
1579	Ssr3	SSRG	DOWN	-1.28	-0.22
1580	Trmt112	TR112	DOWN	-2.29	-1.60
1581	Ndufa8	NDUA8	DOWN	-5.60	-1.07
1582	Ciao2a	CIA2A	DOWN	-4.08	-1.31
1583	Ppp1r2	IPP2	DOWN	-10.38	-2.18
1584	Mecr	MECR	DOWN	-3.10	-1.46
1585	Etfb	ETFB	DOWN	-3.14	-0.12
1586	Emc7	EMC7	DOWN	-2.17	-0.75
1587	Pycard	ASC	DOWN	-5.93	-0.55
1588	Upf1	RENT1	DOWN	-2.64	-0.87
1589	Hsd17b11	DHB11	DOWN	-1.43	-0.51
1590	Pes1	PESC	DOWN	-18.17	-3.49
1591	Mvp	MVP	DOWN	-8.28	-0.54
1592	Mycbp	MYCBP	DOWN	-14.53	-2.03
1593	Stx12	STX12	DOWN	-4.34	-1.52
1594	Cars1	SYCC	DOWN	-3.31	-0.47
1595	Lima1	LIMA1	DOWN	-2.27	-0.88
1596	Ranbp2	RBP2	DOWN	-4.32	-0.81
1597	Sdf2l1	SDF2L	DOWN	-0.97	-0.37
1598	Gtf2i	GTF2I	DOWN	-2.46	-1.33

1599	Tm9sf3	TM9S3	DOWN	-7.78	-2.12
1600	Tmod3	TMOD3	DOWN	-4.00	-0.46
1601	Cwc15	CWC15	DOWN	-4.15	-0.96
1602	Isyna1	INO1	DOWN	-3.57	-1.64
1603	Nit2	NIT2	DOWN	-7.43	-2.08
1604	Copb1	COPB	DOWN	-8.63	-1.47
1605	Nup50	NUP50	DOWN	-10.66	-3.07
1606	Ddx21	DDX21	DOWN	-12.45	-0.92
1607	Ralb	RALB	DOWN	-1.60	-0.76
1608	Acin1	ACINU	DOWN	-5.97	-1.07
1609	Sh3glb1	SHLB1	DOWN	-6.49	-0.51
1610	Myg1	MYG1	DOWN	-6.51	-1.28
1611	Uchl3	UCHL3	DOWN	-11.98	-3.43
1612	Ap3m1	AP3M1	DOWN	-5.69	-1.47
1613	Iqgap1	IQGA1	DOWN	-6.11	-0.26
1614	Nudt5	NUDT5	DOWN	-13.91	-0.76
1615	Hmgn5	HMGN5	DOWN	-10.60	-2.85
1616	Sart3	SART3	DOWN	-4.08	-1.03
1617	Cd2ap	CD2AP	DOWN	-8.24	-1.93
1618	Git2	GIT2	DOWN	-5.55	-1.62
1619	Nt5c	NT5C	DOWN	-8.23	-0.95
1620	Znf207	ZN207	DOWN	-7.09	-1.07
1621	Glrx	GLRX1	DOWN	-4.80	-0.57
1622	Pin1	PIN1	DOWN	-2.87	-0.51
1623	Ptk2b	FAK2	DOWN	-12.53	-0.98
1624	Vapb	VAPB	DOWN	-7.69	-0.37
1625	Dnajc7	DNJC7	DOWN	-5.54	-2.64
1626	Eif3i	EIF3I	DOWN	-7.11	-0.77
1627	Copg1	COPG1	DOWN	-10.52	-1.64
1628	Ripk3	RIPK3	DOWN	-4.35	-1.33
1629	Macroh2a1	H2AY	DOWN	-5.98	-1.17
1630	Zranb2	ZRAB2	DOWN	-0.95	-0.91
1631	Gyg1	GLYG	DOWN	-3.62	-0.28
1632	Ptges3	TEBP	DOWN	-4.10	-0.31
1633	Mta2	MTA2	DOWN	-12.62	-2.93
1634	Nsdhl	NSDHL	DOWN	-5.32	-0.82
1635	Sae1	SAE1	DOWN	-12.30	-0.77
1636	Septin6	45906	DOWN	-8.55	-1.66
1637	Tapbp	TPSN	DOWN	-10.60	-0.68
1638	Myo1c	MYO1C	DOWN	-5.62	-0.70
1639	Ak2	KAD2	DOWN	-11.37	-0.95
1640	Pfdn5	PFD5	DOWN	-3.00	-1.35
1641	Pdcd6ip	PDC6I	DOWN	-6.48	-0.30
1642	Ccs	CCS	DOWN	-5.38	-1.27
1643	Farsb	SYFB	DOWN	-6.12	-0.21
1644	Eif4h	IF4H	DOWN	-6.19	-0.90
1645	Rfc2	RFC2	DOWN	-6.31	-2.65
1646	Coro1b	COR1B	DOWN	-5.01	-0.31
1647	Coro1c	COR1C	DOWN	-6.11	-0.46
1648	Suclg1	SUCA	DOWN	-5.51	-0.46
1649	Snx1	SNX1	DOWN	-6.45	-0.79
1650	Timm9	TIM9	DOWN	-5.35	-1.39
1651	Apip	MTNB	DOWN	-8.75	-1.66
1652	Celf2	CELF2	DOWN	-6.06	-2.65
1653	Bcl10	BCL10	DOWN	-6.10	-1.47
1654	Eif2s3x	IF2G	DOWN	-4.07	-0.30
1655	Twf2	TWF2	DOWN	-11.39	-2.84
1656	Aifm1	AIFM1	DOWN	-2.94	-0.76
1657	Ilf3	ILF3	DOWN	-16.83	-3.35
1658	Uso1	USO1	DOWN	-6.12	-1.08
1659	Strap	STRAP	DOWN	-5.46	-0.37
1660	Baz1b	BAZ1B	DOWN	-9.68	-2.24
1661	Pmm2	PMM2	DOWN	-2.92	-1.24
1662	Actl6a	ACL6A	DOWN	-3.74	-0.95
1663	Unc119	U119A	DOWN	-7.63	-1.65
1664	Plpbp	PLPHP	DOWN	-9.30	-1.21
Polished vs. Corundum				#NUM!	
1	Cul4b	CUL4B	UP	-1.33	0.63
2	Ddi2	DDI2	UP	-1.99	1.26
3	Cntrl	CNTRL	UP	-14.32	3.34
4	Ppig	PPIG	UP	-5.40	1.04
5	Ttn	TITIN	UP	-7.02	1.15
6	H2ac11	H2A1B	UP	-14.33	2.04

7	Safb;Safb2	SAFB1 ;SAFB2	UP	-15.08	1.24
8	Gls	GLSK	UP	-4.22	1.27
9	Irf2bp2	I2BP2	UP	-6.80	1.62
10	Rnf213	RN213	UP	-4.98	1.64
11	Myo1e	MYO1E	UP	-1.08	0.51
12	Myo1e;Myo1f	MYO1E ;MYO1F	UP	-6.04	0.75
13	Tpr	TPR	UP	-1.69	0.16
14	QNG1	QNG1	UP	-2.97	1.77
15	Capn2	CAN2	UP	-2.63	0.25
16	Myh11;Myh9	MYH11 ;MYH9	UP	-2.55	0.15
17	Hsd17b10	HCD2	UP	-10.76	2.06
18	Dctn1	DCTN1	UP	-9.17	1.85
19	Diaph1	DIAP1	UP	-3.17	1.48
20	Atox1	ATOX1	UP	-15.52	0.75
21	Psmd4	PSMD4	UP	-2.99	0.29
22	Exoc7	EXOC7	UP	-12.70	3.52
23	Kpna3;Kpna4	IMA3 ;IMA4	UP	-1.07	0.54
24	Anp32a	AN32A	UP	-5.76	0.70
25	Fkbp8	FKBP8	UP	-8.27	0.65
26	Fyb1	FYB1	UP	-2.10	0.18
27	Ap1b1;Ap2b1	AP1B1 ;AP2B1	UP	-7.32	1.32
28	C1qbp	C1QBP	UP	-12.62	1.34
29	Calu	CALU	UP	-2.39	0.18
30	Hmgb3	HMGB3	UP	-8.40	2.25
31	Get3	GET3	UP	-1.43	0.48
32	Slk;Stk10	SLK ;STK10	UP	-0.88	0.25
33	Pgrmc1	PGRC1	UP	-9.24	0.74
34	Impa1	IMPA1	UP	-5.34	0.32
35	Copb2	COPB2	UP	-5.72	0.45
36	Atp2a2;Atp2a3	AT2A2 ;AT2A3	UP	-5.22	0.28
37	Eef1b	EF1B	UP	-22.75	1.15
38	Eef1b;Eef1d	EF1B ;EF1D	UP	-13.04	1.90
39	Nmt1	NMT1	UP	-3.59	0.53
40	Hsd17b12	DHB12	UP	-1.72	0.15
41	Psmc3	PRS6A	UP	-1.60	0.28
42	Lin7c	LIN7C	UP	-1.40	1.18
43	Yme1l1	YMEL1	UP	-9.47	3.18
44	Cope	COPE	UP	-3.37	0.75
45	Mt2	MT2	UP	-5.44	0.41
46	Mtatp8	ATP8	UP	-8.81	1.05
47	Ada	ADA	UP	-1.06	0.95
48	Aldoa;Aldoc	ALDOA ;ALDOC	UP	-16.26	0.88
49	Gpi	G6PI	UP	-7.22	0.37
50	Hsp90aa1	HS90A	UP	-5.15	0.14
51	Pdia4	PDIA4	UP	-17.12	0.86
52	H2az1;H2az2	H2AV ;H2AZ	UP	-12.65	0.90
53	Eif4a2	IF4A2	UP	-3.40	3.33
54	Txn	THIO	UP	-4.59	0.52
55	H2bc14;Hist2h2bb	H2B1M ;H2B2B	UP	-18.77	3.64
56	Cxcl2	CXCL2	UP	-13.84	2.08
57	Parp1	PARP1	UP	-5.26	0.63
58	Itgb2	ITB2	UP	-0.96	0.04
59	Oas1a	OAS1A	UP	-18.17	3.16
60	Gusb	BGLR	UP	-14.25	3.03
61	Rpl7a	RL7A	UP	-2.01	0.11
62	Icam1	ICAM1	UP	-3.58	1.49
63	Rpl27a	RL27A	UP	-13.71	0.97
64	Srp54	SRP54	UP	-4.04	0.96
65	Spn	LEUK	UP	-1.97	1.12
66	H1-2	H12	UP	-10.06	1.00
67	H1-1	H11	UP	-12.80	3.33
68	H1-3;H1-4	H13 ;H14	UP	-10.52	1.32
69	H1-5	H12	UP	-23.70	2.75
70	H1-2	H12	UP	-17.94	1.28
71	H1-2;H1-3	H12 ;H13	UP	-1.65	0.12
72	Lgals1	LEG1	UP	-6.04	0.33
73	Lgals3	LEG3	UP	-4.07	0.16
74	Hspa1l	HSP7C	UP	-10.79	0.55
75	Eno1	ENOA	UP	-8.65	0.23
76	Eno2	ENOG	UP	-1.02	0.48
77	Tpi1	TPIS	UP	-17.46	0.67
78	Rps6ka3	KS6A3	UP	-7.58	0.69
79	Cfl1	COF1	UP	-17.21	0.68

80	Rpl13a	RL13A	UP	-15.14	1.12
81	Tmsb4x	TYB4	UP	-17.34	1.29
82	Tpm3;Tpm4	TPM3 ;TPM4	UP	-2.24	0.81
83	Akr1b7	ALD1	UP	-8.79	2.15
84	Eno3	ENOB	UP	-6.09	1.13
85	Rarb	RARB	UP	-6.16	1.94
86	Hmbs	HEM3	UP	-7.21	1.78
87	Pnp	PNPH	UP	-1.99	0.36
88	Pcmt1	PIMT	UP	-2.07	0.27
89	Rps2	RS2	UP	-5.13	0.14
90	Tln1	TLN1	UP	-12.73	0.29
91	Ezr	EZRI	UP	-5.62	0.20
92	Rdx	RADI	UP	-10.57	0.95
93	U2af2	U2AF2	UP	-15.30	1.14
94	Map4	MAP4	UP	-10.25	0.86
95	Gna13	GNA13	UP	-14.81	1.68
96	Rpl3	RL3	UP	-2.12	0.13
97	Apex1	APEX1	UP	-6.91	1.09
98	Adh5	ADHX	UP	-7.61	0.36
99	Nap1l1	NP1L1	UP	-5.81	0.86
100	Pabpc1	PABP1	UP	-3.29	0.07
101	Hmgb2	HMGB2	UP	-16.33	1.23
102	C5ar1	C5AR1	UP	-3.64	0.76
103	Aimp1	AIMP1	UP	-2.60	0.24
104	Map2k1	MP2K1	UP	-4.38	2.15
105	Usp15;Usp4	UBP15 ;UBP4	UP	-0.99	0.23
106	Cd81	CD81	UP	-1.91	0.48
107	Lig1	DNLI1	UP	-9.73	1.21
108	Dnm2	DYN2	UP	-5.71	1.70
109	Septin2	45902	UP	-2.81	0.19
110	Msh2	MSH2	UP	-5.74	1.38
111	H1-1;H1-3;H1-4;H1-5	H11 ;H13 ;H14 ;H15	UP	-5.68	0.58
112	H1-1	H11	UP	-10.29	0.58
113	H1-5	H15	UP	-9.51	0.47
114	Acadm	ACADM	UP	-2.21	0.21
115	Vps4b	VPS4B	UP	-3.01	0.68
116	Gsr	GSHR	UP	-9.34	0.80
117	Rpl6	RL6	UP	-14.58	1.19
118	Rpl29	RL29	UP	-11.62	1.30
119	Crkl	CRKL	UP	-6.60	1.48
120	Rplp1	RLA1	UP	-1.45	0.14
121	Rpl5	RL5	UP	-15.10	1.04
122	Eif1	EIF1	UP	-1.13	0.76
123	Alox5	LOX5	UP	-1.14	0.55
124	Hnrnpa1;Hnrnpa3	ROA1 ;ROA3	UP	-17.55	1.78
125	Cast	ICAL	UP	-10.44	2.22
126	Rab7a	RAB7A	UP	-1.21	0.11
127	Gla	AGAL	UP	-4.63	0.95
128	Hdgf	HDGF	UP	-7.68	0.38
129	Hdgf	HDGF	UP	-0.79	0.43
130	Ndufs6	NDUS6	UP	-2.96	0.65
131	Stmn1;Stmn2	STMN1 ;STMN2	UP	-14.99	0.90
132	Ddx6	DDX6	UP	-3.38	0.45
133	Sh3bp1	3BP1	UP	-4.70	1.65
134	Rab8a	RAB8A	UP	-1.80	0.48
135	Rab10	RAB10	UP	-10.87	2.85
136	Acyp1	ACYP1	UP	-10.90	2.57
137	Atp5mpl	ATP68	UP	-2.67	0.66
138	Atp5f1e	ATP5E	UP	-3.81	1.40
139	Usp5	UBP5	UP	-1.04	0.17
140	Ctbp2	CTBP2	UP	-4.79	1.45
141	Fus	FUS	UP	-8.25	0.70
142	Erp29	ERP29	UP	-10.45	0.73
143	Actn4	ACTN4	UP	-9.16	0.59
144	Snrpa1	RU2A	UP	-6.83	0.52
145	Ptpa	PTPA	UP	-6.23	2.95
146	Nploc4	NPL4	UP	-5.24	0.83
147	Actr2	ARP2	UP	-7.27	0.47
148	Actr1a;Actr1b	ACTY ;ACTZ	UP	-5.03	0.36
149	Abce1	ABCE1	UP	-10.45	1.59
150	Copz1	COPZ1	UP	-4.14	0.98
151	Sumo2	SUMO2	UP	-6.13	0.65
152	Ufm1	UFM1	UP	-5.78	1.65

153	Nutf2	NTF2	UP	-6.24	2.74
154	Ywhab	1433B	UP	-7.65	1.64
155	Timm13	TIM13	UP	-11.32	0.50
156	Rps8	RS8	UP	-13.58	1.06
157	Rps13	RS13	UP	-6.83	0.36
158	Rpl23a	RL23A	UP	-13.69	0.71
159	Mtpn	MTPN	UP	-0.78	0.31
160	Rpl23	RL23	UP	-8.76	0.31
161	Fau	RS30	UP	-13.95	0.56
162	Elob	ELOB	UP	-3.43	0.46
163	Rpl39	RL39	UP	-9.95	2.07
164	Cycs	CYC	UP	-4.80	0.50
165	Rpl32	RL32	UP	-8.16	0.49
166	Ybx1	YBOX1	UP	-4.30	0.74
167	Pfn1	PROF1	UP	-2.25	0.12
168	Rps27a	RS27A	UP	-10.56	0.91
169	Uba52	RL40	UP	-11.17	2.75
170	Pafah1b1	LIS1	UP	-9.09	2.02
171	Hmgb1	HMGB1	UP	-2.83	0.18
172	Dynll1	DYL1	UP	-9.30	2.77
173	Rps12	RS12	UP	-17.82	1.40
174	Ppp2ca	PP2AA	UP	-7.30	0.79
175	Ube2l3	UB2L3	UP	-5.01	0.27
176	Tuba1c	TBA1C	UP	-10.34	0.64
177	Tuba1c	TBA1C	UP	-4.58	2.03
178	Psmb7	PSB7	UP	-3.09	0.63
179	Lxn	LXN	UP	-6.56	1.56
180	Tial1	TIAR	UP	-1.07	0.30
181	Nherf1	NHRF1	UP	-6.41	0.75
182	Tgfbi	BGH3	UP	-7.23	2.78
183	Cbx1	CBX1	UP	-8.75	1.61
184	Eloc	ELOC	UP	-2.28	0.69
185	Rpl19	RL19	UP	-12.96	0.78
186	Csrp1	CSRP1	UP	-1.16	0.23
187	Rps3a	RS3A	UP	-4.28	0.17
188	Psme1	PSME1	UP	-13.43	1.40
189	Psme1;Psme2	PSME1 ;PSME2	UP	-14.38	2.85
190	Psme2	PSME2	UP	-3.07	0.84
191	G3bp2	G3BP2	UP	-11.93	2.18
192	Atp5pf	ATP5J	UP	-7.03	0.94
193	Gclc	GSH1	UP	-0.81	0.13
194	Dab2	DAB2	UP	-6.28	0.34
195	Rplp2	RLA2	UP	-6.07	0.19
196	Nme2	NDKB	UP	-6.58	0.29
197	Pfdn6	PFD6	UP	-9.07	1.10
198	Fabp5	FABP5	UP	-17.79	2.13
199	Larp7	LARP7	UP	-1.76	1.04
200	Cab39	CAB39	UP	-6.89	1.57
201	Bax	BAX	UP	-5.33	0.43
202	Lyar	LYAR	UP	-1.18	0.48
203	Ssrp1	SSRP1	UP	-0.98	0.48
204	Zc3h18	ZCH18	UP	-7.14	1.32
205	Rbm15	RBM15	UP	-1.75	0.64
206	Pepd	PEPD	UP	-6.54	1.17
207	Osbp	OSBP1	UP	-6.13	1.52
208	Arhgap45	HMHA1	UP	-3.19	0.75
209	Abraxas2	ABRX2	UP	-7.08	1.24
210	Hp1bp3	HP1B3	UP	-7.91	2.71
211	Srsf4;Srsf6	SRSF4 ;SRSF6	UP	-6.56	1.06
212	Psmd1	PSMD1	UP	-4.53	0.46
213	Fubp1;Khsrp	FUBP1 ;FUBP2	UP	-4.10	0.55
214	Puf60	PUF60	UP	-7.36	0.65
215	Eif3j1;Eif3j2	EI3JA ;EI3JB	UP	-11.87	0.87
216	Edc4	EDC4	UP	-5.35	1.07
217	Hdgfl2	HDGR2	UP	-2.98	0.49
218	Lrrfip1	LRRF1	UP	-4.75	0.47
219	Ddx46	DDX46	UP	-3.79	1.58
220	Aldh16a1	A16A1	UP	-4.36	1.08
221	Cluh	CLU	UP	-14.45	1.29
222	Utp20	UTP20	UP	-8.69	1.42
223	Arcn1	COPD	UP	-11.64	0.93
224	Nfatc2	NFAC2	UP	-2.51	0.90
225	Hnrnpd	HNRPD	UP	-11.96	0.53

226	Hnrnpd;Hnrnpdl	HNRDL ;HNRPD	UP	-16.09	1.30
227	Gas7	GAS7	UP	-2.32	0.71
228	Eif1a;Eif1ax	IF1AX ;IF1A	UP	-6.01	0.26
229	Rbbp7	RBBP7	UP	-3.23	0.76
230	Asns	ASNS	UP	-5.48	0.90
231	Tmpo	LAP2B	UP	-4.28	0.48
232	Tmpo	LAP2A ;LAP2B	UP	-2.30	0.17
233	Pak3	PAK3	UP	-7.53	2.95
234	Cdc37	CDC37	UP	-1.93	0.22
235	Cybb	CY24B	UP	-5.35	1.68
236	Ctcf	CTCF	UP	-2.19	0.81
237	Hcfc1	HCFC1	UP	-6.90	0.44
238	Sntb2	SNTB2	UP	-1.12	0.94
239	Hadh	HCDH	UP	-1.60	1.09
240	Znf638	ZN638	UP	-5.56	1.24
241	Pea15	PEA15	UP	-7.58	0.54
242	Rhoa;Rhoc	RHOA ;RHOC	UP	-2.66	0.47
243	Ddx3x	DDX3X	UP	-2.39	0.20
244	Sf3a2	SF3A2	UP	-2.31	0.66
245	Tpd52	TPD52	UP	-12.39	0.85
246	Ndufa4	NDUA4	UP	-14.97	0.73
247	Fkbp3	FKBP3	UP	-11.71	1.04
248	Vat1	VAT1	UP	-2.90	0.78
249	Spr	SPRE	UP	-8.27	0.69
250	Btf3	BTF3	UP	-5.16	0.45
251	Sf1	SF01	UP	-3.47	0.31
252	Ly6e	LY6E	UP	-10.66	2.79
253	Fkbp5	FKBP5	UP	-1.05	0.28
254	Sord	DHSO	UP	-1.02	0.84
255	H2bc3;Hist1h2bp	H2B1B ;H2B1P	UP	-19.32	3.65
256	Gart	PUR2	UP	-8.15	0.44
257	Mars1	SYMC	UP	-3.80	1.00
258	Prex1	PREX1	UP	-6.01	1.48
259	Pds5a	PDS5A	UP	-4.10	0.87
260	Swap70	SWP70	UP	-7.36	0.75
261	FAM120A	F120A	UP	-7.53	1.10
262	Nop58	NOP58	UP	-6.51	0.39
263	Cltb	CLCB	UP	-15.71	1.08
264	Cpsf6	CPSF6	UP	-5.89	0.91
265	Dnajc8	DNJC8	UP	-5.82	0.79
266	Zc3h11a	ZC11A	UP	-1.05	0.22
267	Abcf1	ABCF1	UP	-2.99	0.33
268	Smchd1	SMHD1	UP	-14.14	3.19
269	Uggt1	UGGG1	UP	-0.90	0.30
270	Snx6	SNX6	UP	-2.71	0.72
271	Chd4	CHD4	UP	-1.13	0.11
272	Nup98	NUP98	UP	-2.07	0.67
273	Jpt2	JUPI2	UP	-2.63	0.31
274	Washc2	WASC2	UP	-6.78	0.55
275	Rps27	RS27	UP	-7.27	0.48
276	Tmsb10	TYB10	UP	-9.47	3.04
277	Ppp2r1a	2AAA	UP	-10.27	0.63
278	Atp5mk	ATPMK	UP	-1.68	0.88
279	Nap1l4	NP1L4	UP	-0.85	0.13
280	Picalm	PICAL	UP	-2.87	0.33
281	Syncrip	HNRPQ	UP	-4.89	0.19
282	Dek	DEK	UP	-6.16	0.58
283	Sh3d21	SH321	UP	-8.84	3.43
284	Cyld	CYLD	UP	-1.51	0.29
285	Fnbp1	FNBP1	UP	-2.86	0.95
286	Vac14	VAC14	UP	-2.05	0.51
287	Ubap2l	UBP2L	UP	-2.68	0.35
288	Flnb	FLNB	UP	-5.04	0.57
289	Flna;Flnb	FLNA ;FLNB	UP	-5.44	1.08
290	Flnc	FLNC	UP	-12.85	1.71
291	Rraga	RRAGA	UP	-2.52	0.85
292	Nucks1	NUCKS	UP	-4.38	1.07
293	Echs1	ECHM	UP	-3.52	0.45
294	Tbl1xr1	TBL1R	UP	-1.26	0.29
295	Eea1	EEA1	UP	-1.71	0.29
296	Acbd3	GCP60	UP	-3.37	1.38
297	Hadha	ECHA	UP	-3.22	0.39
298	Rpl24	RL24	UP	-18.18	1.51

299	Asph	ASPH	UP	-3.86	0.94
300	Iars1	SYIC	UP	-4.96	0.31
301	Qdpr	DHPR	UP	-3.87	2.06
302	Sp110	SP110	UP	-3.08	0.48
303	Rsl1d1	RL1D1	UP	-18.25	2.21
304	Nob1	NOB1	UP	-1.29	0.35
305	Lpcat2	PCAT2	UP	-3.16	0.30
306	Septin11	45911	UP	-10.44	1.64
307	Septin11;Septin6	SEP11 ;SEPT6	UP	-9.76	2.26
308	Acat2	THIC	UP	-3.51	0.20
309	Pus7l	PUS7L	UP	-2.77	1.82
310	Slc38a2	S38A2	UP	-7.19	1.48
311	Tcerg1	TCRG1	UP	-3.86	1.09
312	Pdlim5	PDLI5	UP	-5.86	1.38
313	Plcg2	PLCG2	UP	-4.43	1.37
314	Ppat	PUR1	UP	-3.93	0.94
315	Pak2	PAK2	UP	-11.21	0.63
316	Afg3l2	AFG32	UP	-5.14	1.02
317	Bclaf1	BCLF1	UP	-6.12	0.38
318	Plekho2	PKHO2	UP	-5.37	0.61
319	Wipf1	WIPF1	UP	-0.79	0.14
320	Ppp1r11	PP1RB	UP	-3.95	0.42
321	Dnm1l	DNM1L	UP	-5.09	1.09
322	Lrrc25	LRC25	UP	-1.03	0.40
323	Otud6b	OTU6B	UP	-5.17	1.24
324	Agfg1	AGFG1	UP	-0.86	0.54
325	Babam2	BABA2	UP	-9.94	2.19
326	Tprkb	TPRKB	UP	-0.77	0.22
327	Mbnl3	MBNL3	UP	-2.62	0.27
328	Blmh	BLMH	UP	-2.22	0.58
329	Gtf2f2	T2FB	UP	-4.70	0.76
330	Nudcd3	NUDC3	UP	-1.06	0.18
331	Dync1li1	DC1L1	UP	-6.22	2.21
332	Ptrh2	PTH2	UP	-7.14	1.24
333	Micos13	MIC13	UP	-9.74	1.88
334	Tmx1	TMX1	UP	-1.55	0.77
335	Mavs	MAVS	UP	-1.40	0.41
336	Ubxn4	UBXN4	UP	-3.42	1.13
337	Washc1	WASH1	UP	-7.45	1.75
338	Mrps23	RT23	UP	-11.14	1.87
339	Rpa1	RFA1	UP	-2.14	0.39
340	Flnc	FLNC	UP	-2.15	2.34
341	Oas3	OAS3	UP	-8.48	1.02
342	Ciapin1	CPIN1	UP	-11.23	0.61
343	Acot7	BACH	UP	-10.63	1.28
344	Nifk	MK67I	UP	-2.01	0.25
345	Rbmxl1	RMXL1	UP	-8.45	0.35
346	Ddx1	DDX1	UP	-10.89	1.44
347	Rbms1	RBMS1	UP	-6.07	1.23
348	Fubp1	FUBP1	UP	-4.72	0.27
349	Dnajc9	DNJC9	UP	-9.40	1.51
350	Yars1	SYYC	UP	-0.86	0.13
351	Cisd1	CISD1	UP	-4.42	0.94
352	Trex1	TREX1	UP	-5.30	1.15
353	Dap	DAP1	UP	-2.04	0.53
354	Basp1	BASP1	UP	-12.10	0.52
355	Lrrc49	LRC49	UP	-7.64	1.49
356	Rrp1b	RRP1B	UP	-1.43	1.33
357	Prpf6	PRP6	UP	-1.98	0.72
358	Ndufv1	NDUV1	UP	-4.00	1.21
359	Ttc1	TTC1	UP	-0.97	0.20
360	Grhpr	GRHPR	UP	-1.24	0.46
361	Supt16h	SP16H	UP	-3.54	0.53
362	Rab31	RAB31	UP	-2.72	1.12
363	Lrch4	LRCH4	UP	-2.63	0.69
364	Etfdh	ETFD	UP	-0.91	0.22
365	Acaa1a	THIKA	UP	-7.44	0.72
366	Far1	FACR1	UP	-4.63	1.22
367	Nop2	NOP2	UP	-3.71	0.75
368	Glyr1	GLYR1	UP	-7.70	1.57
369	Pycr2	P5CR2	UP	-4.60	0.27
370	Lrrc59	LRC59	UP	-7.64	0.31
371	Prkx	PRKX	UP	-5.09	0.86

372	Prpf3	PRPF3	UP	-3.17	0.79
373	Taldo1	TALDO	UP	-6.04	0.29
374	Hnrnpab	ROAA	UP	-3.86	0.11
375	Thumpd1	THUM1	UP	-4.18	0.75
376	Stoml2	STML2	UP	-6.17	1.37
377	Mvd	MVD1	UP	-11.81	3.01
378	Psmd6	PSMD6	UP	-1.09	0.18
379	Stk24	STK24	UP	-5.21	2.11
380	Cmas	NEUA	UP	-1.52	0.38
381	Dpp3	DPP3	UP	-1.90	0.59
382	Clint1	EPN4	UP	-7.10	0.78
383	Prpf19	PRP19	UP	-9.18	0.49
384	Vmp1	VMP1	UP	-7.19	1.35
385	Triobp	TARA	UP	-3.73	2.43
386	Hibadh	3HIDH	UP	-5.45	1.24
387	Etfa	ETFA	UP	-10.41	0.33
388	Cttnbp2nl	CT2NL	UP	-4.81	0.99
389	Grpel1	GRPE1	UP	-3.53	0.39
390	Ndufs5	NDUS5	UP	-8.16	1.01
391	Rnps1	RNPS1	UP	-9.68	0.82
392	Nasp	NASP	UP	-0.91	0.09
393	Srrt	SRRT	UP	-3.63	0.22
394	Adar	DSRAD	UP	-12.55	1.26
395	Lpxn	LPXN	UP	-6.52	0.48
396	Rrbp1	RRBP1	UP	-2.25	0.11
397	Igf2bp3	IF2B3	UP	-8.43	1.06
398	Cox6c	COX6C	UP	-1.77	0.30
399	Atp5mg	ATP5L	UP	-7.99	0.71
400	Rpl17	RL17	UP	-8.89	0.41
401	Arpc5	ARPC5	UP	-14.94	1.03
402	Atg3	ATG3	UP	-3.61	0.53
403	Ndufc2	NDUC2	UP	-5.78	1.35
404	Cisd2	CISD2	UP	-5.22	0.58
405	Sar1b	SAR1B	UP	-7.34	1.48
406	Rgs10	RGS10	UP	-5.09	0.75
407	Nudt21	CPSF5	UP	-7.66	2.63
408	Denr	DENR	UP	-5.36	1.23
409	Txndc17	TXD17	UP	-17.14	1.55
410	Glrx3	GLRX3	UP	-8.16	1.06
411	Mrpl41	RM41	UP	-2.28	0.69
412	Acot13	ACO13	UP	-4.43	1.01
413	Kgd4	KGD4	UP	-5.70	1.32
414	Ndufb3	NDUB3	UP	-9.67	1.81
415	Atp6v1g1	VATG1	UP	-8.33	1.12
416	Nhp2	NHP2	UP	-1.63	0.27
417	Rprd1b	RPR1B	UP	-5.67	0.46
418	Ranbp3	RANB3	UP	-5.88	0.65
419	Raver1	RAVR1	UP	-6.13	2.29
420	Ctnnbl1	CTBL1	UP	-5.47	1.21
421	Napg	SNAG	UP	-1.86	0.43
422	Ist1	IST1	UP	-1.55	0.62
423	Sugt1	SGT1	UP	-5.24	0.45
424	Rpl11	RL11	UP	-10.90	0.45
425	Ndufs4	NDUS4	UP	-5.87	1.71
426	Tecr	TECR	UP	-3.74	0.18
427	Serbp1	SERB1	UP	-7.95	0.75
428	Gar1	GAR1	UP	-12.98	3.28
429	Luc7l	LUC7L	UP	-1.71	0.21
430	Tpd52l2	TPD54	UP	-3.37	0.81
431	Ola1	OLA1	UP	-3.09	1.47
432	Tsfm	EFTS	UP	-3.43	0.45
433	Mtrex	MTREX	UP	-4.40	1.30
434	Ccdc47	CCD47	UP	-0.99	0.32
435	Ptms	PTMS	UP	-7.73	0.77
436	Dynll2	DYL2	UP	-3.63	1.21
437	Ddx56	DDX56	UP	-12.07	1.38
438	Snu13	NH2L1	UP	-4.23	0.25
439	Tbcb	TBCB	UP	-5.10	1.32
440	Necap2	NECP2	UP	-8.97	0.91
441	Sarnp	SARNP	UP	-0.87	0.06
442		CX049	UP	-1.70	1.36
443	Gcc1	GCC1	UP	-4.79	0.88
444	Ndufv2	NDUV2	UP	-3.98	0.79

445	Dusp3	DUS3	UP	-1.50	0.29
446	Itpa	ITPA	UP	-1.47	0.67
447	Rpl4	RL4	UP	-8.40	0.57
448	Psmd12	PSD12	UP	-0.86	0.39
449	Ebna1bp2	EBP2	UP	-7.43	3.19
450	Exosc1	EXOS1	UP	-5.36	0.84
451	Dcps	DCPS	UP	-1.17	0.65
452	Cnpy3	CNPY3	UP	-10.99	1.27
453	Napa	SNAA	UP	-3.39	1.09
454	Mrpl12	RM12	UP	-4.83	0.27
455	Alg5	ALG5	UP	-2.86	1.04
456	Ftsj3	SPB1	UP	-2.30	0.91
457	Srpra	SRPRA	UP	-7.03	1.36
458	Acadsb	ACDSB	UP	-1.91	0.46
459	Cmpk1	KCY	UP	-1.14	0.34
460	Akap8	AKAP8	UP	-4.36	0.76
461	Ampd2	AMPD2	UP	-0.98	0.12
462	Pak1ip1	PK1IP	UP	-5.96	1.59
463	Eif3f	EIF3F	UP	-2.08	0.44
464	Ndufa8	NDUA8	UP	-10.98	1.93
465	Ppp1r2	IPP2	UP	-9.71	1.53
466	Pes1	PESC	UP	-5.41	2.61
467	Mycbp	MYCBP	UP	-9.35	2.04
468	Gtf2i	GTF2I	UP	-4.91	2.01
469	Tm9sf3	TM9S3	UP	-6.46	1.78
470	Cwc15	CWC15	UP	-1.50	0.76
471	Isyna1	INO1	UP	-3.72	2.45
472	Nit2	NIT2	UP	-3.92	1.22
473	Copb1	COPB	UP	-7.16	0.89
474	Nup50	NUP50	UP	-10.61	2.82
475	Ddx21	DDX21	UP	-11.48	0.92
476	Acin1	ACINU	UP	-6.93	0.97
477	Uchl3	UCHL3	UP	-11.08	3.16
478	Ap3m1	AP3M1	UP	-8.12	1.21
479	Iqgap1	IQGA1	UP	-7.45	0.32
480	Hmgn5	HMGN5	UP	-9.07	2.55
481	Arpc3	ARPC3	UP	-5.69	0.30
482	Ptk2b	FAK2	UP	-11.20	0.77
483	Vapb	VAPB	UP	-7.27	0.33
484	Dnajc7	DNJC7	UP	-6.11	2.43
485	Eif3i	EIF3I	UP	-3.49	0.39
486	Copg1	COPG1	UP	-2.16	0.80
487	Ripk3	RIPK3	UP	-1.39	0.57
488	Macroh2a1	H2AY	UP	-4.83	0.81
489	Mta2	MTA2	UP	-13.33	2.86
490	Sae1	SAE1	UP	-16.23	0.96
491	Septin6	45906	UP	-5.31	1.57
492	Tapbp	TPSN	UP	-2.07	0.20
493	Pfdn5	PFD5	UP	-4.36	1.63
494	Pdcd6ip	PDC6I	UP	-4.62	0.22
495	Ccs	CCS	UP	-0.90	0.31
496	Rfc2	RFC2	UP	-15.04	2.20
497	Snx1	SNX1	UP	-4.11	0.49
498	Apip	MTNB	UP	-7.72	1.26
499	Bcl10	BCL10	UP	-5.80	1.10
500	Eif2s3x	IF2G	UP	-5.32	0.40
501	Tjp2	ZO2	UP	-2.59	0.47
502	Aifm1	AIFM1	UP	-1.30	0.42
503	Ilf3	ILF3	UP	-7.94	2.58
504	Strap	STRAP	UP	-7.68	0.36
505	Baz1b	BAZ1B	UP	-8.66	1.77
506	Pmm2	PMM2	UP	-3.93	1.70
507	Actl6a	ACL6A	UP	-2.78	0.55
508	Mpeg1	MPEG1	DOWN	-8.78	-0.86
509	Sh3pxd2b	SPD2B	DOWN	-8.41	-0.75
510	Map7d1	MA7D1	DOWN	-5.22	-0.42
511	Tpx2	TPX2	DOWN	-3.00	-0.55
512	Myh10	MYH10	DOWN	-13.80	-1.95
513	Itih4	ITIH4	DOWN	-13.70	-1.27
514	Tomm5	TOM5	DOWN	-3.81	-1.77
515	Cad	PYR1	DOWN	-4.83	-1.40
516	Plxnb2	PLXB2	DOWN	-3.67	-0.51
517	Adgrg4	AGRG4	DOWN	-10.72	-2.08

518	Osbpl8	OSBL8	DOWN	-9.79	-0.83
519	H2ac11	H2A1B	DOWN	-15.44	-1.34
520	Hmcn1	HMCN1	DOWN	-11.75	-1.62
521	Safb	SAFB1	DOWN	-6.82	-0.37
522	Bin2	BIN2	DOWN	-9.50	-1.26
523	Bin1;Bin2	BIN1 ;BIN2	DOWN	-10.55	-2.42
524	Mki67	KI67	DOWN	-1.00	-0.15
525	Sbf2	MTMRD	DOWN	-6.60	-1.18
526	Map3k19	M3K19	DOWN	-16.82	-1.25
527	Nolc1	NOLC1	DOWN	-8.92	-0.43
528	Kif23	KIF23	DOWN	-4.75	-1.77
529	Numa1	NUMA1	DOWN	-7.16	-0.32
530	Rap1gds1	GDS1	DOWN	-8.70	-1.13
531	Rnpepl1	RNPL1	DOWN	-1.22	-0.77
532	Hk2	HXK2	DOWN	-2.27	-0.36
533	Hk1;Hk2	HXK1 ;HXK2	DOWN	-3.41	-0.84
534	Bin1	BIN1	DOWN	-4.77	-1.52
535	Sec22b	SC22B	DOWN	-2.15	-0.70
536	Dpysl2	DPYL2	DOWN	-18.36	-0.97
537	Emd	EMD	DOWN	-1.46	-0.28
538	Alyref	THOC4	DOWN	-14.97	-0.99
539	Clta	CLCA	DOWN	-2.31	-0.20
540	Myh11	MYH11	DOWN	-2.93	-0.92
541	Myh10	MYH10	DOWN	-11.69	-0.68
542	Arg2	ARGI2	DOWN	-13.27	-3.23
543	Prdx6	PRDX6	DOWN	-2.57	-0.32
544	Dld	DLDH	DOWN	-3.24	-0.17
545	Prkcsh	GLU2B	DOWN	-11.46	-0.89
546	Prdx4	PRDX4	DOWN	-17.47	-1.50
547	Prdx1;Prdx4	PRDX1 ;PRDX4	DOWN	-12.90	-1.14
548	Eftud2	U5S1	DOWN	-3.16	-0.30
549	Eef2;Eftud2	EF2 ;U5S1	DOWN	-22.13	-1.88
550	Degs1	DEGS1	DOWN	-3.18	-0.64
551	Gsto1	GSTO1	DOWN	-5.73	-2.45
552	Man2b1	MA2B1	DOWN	-8.65	-2.61
553	Rpl21	RL21	DOWN	-2.85	-0.27
554	Gclm	GSH0	DOWN	-3.20	-0.33
555	Grcc10	C10	DOWN	-1.27	-0.85
556	Phb2	PHB2	DOWN	-16.38	-1.20
557	Dhx15	DHX15	DOWN	-11.80	-0.82
558	Purb	PURB	DOWN	-3.45	-0.17
559	Srsf5	SRSF5	DOWN	-6.79	-0.45
560	Srsf4	SRSF4	DOWN	-15.18	-1.14
561	Kpna4	IMA3	DOWN	-5.29	-1.19
562	Kpna3	IMA4	DOWN	-2.60	-0.72
563	Anp32a;Anp32b	AN32A ;AN32B	DOWN	-10.62	-0.85
564	Ppef2	PPE2	DOWN	-2.60	-0.83
565	Psmb9	PSB9 ;PSB9_MUSMB	DOWN	-5.51	-1.39
566	Psmd14	PSDE	DOWN	-4.00	-2.70
567	Scamp3	SCAM3	DOWN	-9.85	-0.76
568	Anxa3	ANXA3	DOWN	-5.38	-0.37
569	Ap1b1	AP1B1	DOWN	-5.28	-1.09
570	Neu1	NEUR1	DOWN	-5.21	-1.45
571	Myadm	MYADM	DOWN	-6.65	-2.58
572	Nudc	NUDC	DOWN	-4.71	-0.49
573	Pnn	PININ	DOWN	-8.97	-0.81
574	Hnrnph1	HNRH1	DOWN	-7.68	-0.79
575	Hnrnph1;Hnrnph2	HNRH1 ;HNRH2	DOWN	-8.08	-0.48
576	Hnrnph2	HNRH2 ;HNRPF	DOWN	-16.14	-1.78
577	Hnrnpf;Hnrnph1	HNRH1 ;HNRPF	DOWN	-3.40	-0.56
578	Api5	API5	DOWN	-1.18	-0.15
579	Bcat2	BCAT2	DOWN	-5.30	-0.46
580	Timm44	TIM44	DOWN	-9.01	-1.76
581	Psmb10	PSB10	DOWN	-15.06	-1.03
582	Ddost	OST48	DOWN	-11.53	-1.33
583	Man2b2	MA2B2	DOWN	-7.90	-1.38
584	Banf1	BAF	DOWN	-11.03	-1.29
585	Slk	SLK	DOWN	-2.99	-0.56
586	Stk10	STK10	DOWN	-7.14	-0.62
587	Sap18	SAP18	DOWN	-1.40	-0.48
588	Septin7	45907	DOWN	-0.82	-0.11
589	Eif6	IF6	DOWN	-20.95	-1.29
590	Rpl35a	RL35A	DOWN	-10.49	-1.28

591	Atp2a2	AT2A2	DOWN	-9.22	-1.22
592	Dhx9	DHX9	DOWN	-10.80	-1.08
593	Ncf2	NCF2	DOWN	-4.49	-0.21
594	Pik3c2g	P3C2G	DOWN	-17.37	-1.77
595	Pip4k2a	PI42A	DOWN	-16.04	-1.54
596	Eif3d	EIF3D	DOWN	-2.85	-0.57
597	Pgam2	PGAM2	DOWN	-18.89	-1.96
598	Pgam1;Pgam2	PGAM1 ;PGAM2	DOWN	-16.20	-1.61
599	Epb41l2	E41L2	DOWN	-6.05	-0.59
600	Ctss	CATS	DOWN	-5.42	-0.75
601	Vamp8	VAMP8	DOWN	-8.44	-0.79
602	Psma3	PSA3	DOWN	-8.26	-1.45
603	Stx7	STX7	DOWN	-6.98	-0.56
604	Sfn	1433S	DOWN	-5.53	-0.56
605	Sfn	1433B	DOWN	-2.91	-0.36
606	Snx3	SNX3	DOWN	-12.52	-0.75
607	Snx12;Snx3	SNX12 ;SNX3	DOWN	-10.32	-0.96
608	Snx12	SNX12	DOWN	-8.22	-0.55
609	Sp3	SP3	DOWN	-1.60	-0.56
610	Smpd2	NSMA	DOWN	-3.08	-0.83
611	Pfdn2	PFD2	DOWN	-1.04	-0.15
612	Cfdp1	CFDP1	DOWN	-2.13	-0.47
613	Wdr1	WDR1	DOWN	-14.22	-0.74
614	Dhcr7	DHCR7	DOWN	-0.86	-0.48
615	Dync1i2	DC1I2	DOWN	-9.03	-1.21
616	Dnmt3a	DNM3A	DOWN	-4.88	-0.85
617	Ppt1	PPT1	DOWN	-13.81	-0.72
618	Cops4	CSN4	DOWN	-6.54	-2.07
619	Hnrnpa2b1	ROA2	DOWN	-14.94	-0.64
620	Creg1	CREG1	DOWN	-1.92	-0.72
621	Idh1	IDHC	DOWN	-7.94	-0.79
622	Lgmn	LGMN	DOWN	-4.68	-1.40
623	Afm	AFAM	DOWN	-11.34	-1.85
624	Coro1a	COR1A	DOWN	-17.21	-1.04
625	Coro1a;Coro1b	COR1A ;COR1B	DOWN	-24.87	-5.07
626	Dhfr	DYR	DOWN	-5.58	-0.41
627	Mtco2	COX2	DOWN	-11.06	-2.28
628	Hprt1	HPRT	DOWN	-9.91	-0.58
629	C3	CO3	DOWN	-13.15	-1.39
630	C4b	CO4B	DOWN	-2.89	-1.29
631	B2m	B2MG	DOWN	-15.37	-1.47
632	H2-L	HA1L	DOWN	-6.93	-2.87
633	H2-D1;H2-L	HA11 ;HA1L	DOWN	-4.98	-1.41
634	H2-D1;H2-L	HA11 ;HA12 ;HA1L	DOWN	-0.77	-0.16
635	H2-D1	HA12	DOWN	-10.41	-1.15
636	Hba	HBA	DOWN	-18.60	-1.49
637	Hbb-b1;Hbb-b2	HBB1 ;HBB2	DOWN	-14.59	-1.98
638	Hbb-b1	HBB1	DOWN	-9.91	-0.77
639	H3-3a;H3-5;H3c1;H3c2	H31	DOWN	-20.16	-1.76
640	Mt1	MT1	DOWN	-5.55	-0.29
641	Iap	IGEB	DOWN	-12.79	-0.77
642	Gfap	GFAP	DOWN	-10.37	-1.23
643	Gfap;Vim	GFAP ;VIME	DOWN	-10.51	-1.12
644	Cd74	HG2A	DOWN	-3.19	-0.25
645	Aldoc	ALDOC	DOWN	-11.35	-0.58
646	Aldoa	ALDOA	DOWN	-16.57	-0.45
647	Got1	AATC	DOWN	-5.68	-0.55
648	Itgam	ITAM	DOWN	-15.17	-1.14
649	Myl1;Myl3	MYL1 ;MYL3	DOWN	-6.84	-1.84
650	Ldha	LDHA	DOWN	-11.98	-0.81
651	C9	CO9	DOWN	-13.25	-1.34
652	Ctsl	CATL1	DOWN	-9.55	-1.33
653	Ptprc	PTPRC	DOWN	-14.70	-1.21
654	S100a4	S10A4	DOWN	-16.66	-1.09
655	Anxa2	ANXA2	DOWN	-17.58	-1.27
656	Alb	ALBU	DOWN	-16.81	-1.06
657	Hsp90aa1;Hsp90ab1	HS90A ;HS90B	DOWN	-15.28	-0.73
658	Aprt	APT	DOWN	-13.23	-0.70
659	Fcgr2	FCGR2	DOWN	-3.29	-0.47
660	Hsp90b1	ENPL	DOWN	-19.71	-0.80
661	Hsp90ab1;Hsp90b1	ENPL ;HS90B	DOWN	-18.56	-1.49
662	S100a10	S10AA	DOWN	-1.88	-0.20
663	Sod1	SODC	DOWN	-15.02	-0.66

664	Mdh2	MDHM	DOWN	-15.23	-0.66
665	Kras;Nras	RASK ;RASN	DOWN	-1.14	-0.20
666	Gnai2	GNAI2	DOWN	-14.66	-1.59
667	Lyz2	LYZ2	DOWN	-12.65	-0.86
668	Lyz1;Lyz2	LYZ1 ;LYZ2	DOWN	-10.47	-1.61
669	Pgk1;Pgk2	PGK1 ;PGK2	DOWN	-9.22	-0.42
670	Itgb1	ITB1	DOWN	-12.30	-1.15
671	P4hb	PDIA1	DOWN	-5.89	-0.12
672	Ncl	NUCL	DOWN	-5.96	-0.13
673	Pgk1	PGK1	DOWN	-1.12	-0.04
674	Junb	JUNB	DOWN	-15.21	-1.69
675	Sod2	SODM	DOWN	-10.53	-0.43
676	Pet117	PT117	DOWN	-15.32	-1.19
677	Ndufb1	NDUB1	DOWN	-2.40	-0.43
678	Ifi204	IFI4	DOWN	-1.07	-0.41
679	Calm1;Calm2;Calm3	CALM1	DOWN	-12.76	-0.91
680	Anxa1	ANXA1	DOWN	-8.11	-0.26
681	Eef1a1	EF1A1	DOWN	-15.20	-0.78
682	Eef1a1;Eef1a2	EF1A1 ;EF1A2	DOWN	-17.23	-0.97
683	Ctsb	CATB	DOWN	-17.99	-1.15
684	Eif4a1;Eif4a2	IF4A1 ;IF4A2	DOWN	-16.66	-1.47
685	Eif4a1;Eif4a2;Eif4a3	IF4A1	DOWN	-12.31	-1.45
686	Tcea1	TCEA1	DOWN	-9.23	-0.56
687	Cd14	CD14	DOWN	-12.62	-0.98
688	Slc3a2	4F2	DOWN	-11.87	-0.74
689	H2bc14	H2B1M	DOWN	-13.41	-4.98
690	H2bc14;H2bc3	H2B1B	DOWN	-13.30	-0.56
691	H1-0	H10	DOWN	-10.47	-1.32
692	Spp1	OSTP	DOWN	-2.03	-0.60
693	Sub1	TCP4	DOWN	-5.16	-2.08
694	Lamp1	LAMP1	DOWN	-5.48	-0.97
695	Cdk1	CDK1	DOWN	-0.88	-0.34
696	Hsp90ab1	HS90B	DOWN	-15.19	-0.58
697	Cfp	PROP	DOWN	-1.80	-0.69
698	Tcp1	TCPA	DOWN	-8.08	-0.40
699	App	A4	DOWN	-9.18	-1.84
700	Pfkl;Pfkp	PFKAL ;PFKAP	DOWN	-11.43	-2.58
701	Cox5a	COX5A	DOWN	-17.04	-1.11
702	Gsn	GELS	DOWN	-15.89	-0.75
703	Cd5	CD5	DOWN	-9.83	-0.69
704	Dnmt1	DNMT1	DOWN	-5.48	-0.76
705	S100a6	S10A6	DOWN	-12.19	-2.13
706	Rps16	RS16	DOWN	-8.11	-0.38
707	Rpl7	RL7	DOWN	-5.96	-0.22
708	Mdh1	MDHC	DOWN	-6.57	-0.34
709	Rpsa	RSSA	DOWN	-13.21	-0.77
710	Calr	CALR	DOWN	-7.08	-0.26
711	Psmd3	PSMD3	DOWN	-5.51	-0.32
712	Lmnb1	LMNB1	DOWN	-13.94	-1.03
713	Lmnb1;Lmnb2	LMNB1 ;LMNB2	DOWN	-15.02	-1.99
714	Lmna	LMNA	DOWN	-21.70	-1.68
715	Anxa6	ANXA6	DOWN	-15.10	-1.50
716	Rplp0	RLA0	DOWN	-12.22	-0.69
717	Hmox1	HMOX1	DOWN	-2.92	-0.74
718	Glul	GLNA	DOWN	-10.65	-0.99
719	Bpgm	PMGE	DOWN	-14.71	-1.76
720	Cd44	CD44	DOWN	-1.86	-0.12
721	Nme1	NDKA	DOWN	-7.53	-0.47
722	Nme1;Nme2	NDKA ;NDKB	DOWN	-18.55	-1.09
723	Srp14	SRP14	DOWN	-4.53	-0.45
724	Ass1	ASSY	DOWN	-9.39	-1.28
725	Hspa1l	HS71L	DOWN	-9.94	-1.14
726	Hspa1	HS71L	DOWN	-16.63	-1.51
727	Hspa1l;Hspa8	HS71L ;HSP7C	DOWN	-2.40	-0.80
728	Ctsa	PPGB	DOWN	-19.13	-1.22
729	Gapdh	G3P	DOWN	-16.55	-0.86
730	Lamp2	LAMP2	DOWN	-13.72	-1.16
731	Hmga1	HMGA1	DOWN	-3.50	-1.25
732	Hspa2	HSP72	DOWN	-1.87	-2.38
733	Hspa9	HSP7C	DOWN	-3.42	-0.51
734	Hspa2;Hspa8	HSP72 ;HSP7C	DOWN	-18.28	-1.28
735	Eno1;Eno2	ENOA ;ENOG	DOWN	-13.48	-1.16
736	Eno1	ENOA	DOWN	-6.24	-0.49

737	Eno2;Eno3	ENOB ;ENOG	DOWN	-14.93	-1.65
738	Ptbp1	PTBP1	DOWN	-5.30	-0.24
739	Ap2a1	AP2A1	DOWN	-0.97	-0.65
740	Hk1	HXK1	DOWN	-7.48	-0.83
741	Ppia	PPIA	DOWN	-16.40	-0.60
742	Slc2a1	GTR1	DOWN	-6.43	-1.85
743	Pcna	PCNA	DOWN	-11.06	-0.50
744	Cox5b	COX5B	DOWN	-1.82	-0.50
745	Cox4i1	COX41	DOWN	-5.46	-0.28
746	Lsp1	LSP1	DOWN	-4.49	-0.19
747	Hspa5	BIP	DOWN	-18.54	-0.67
748	Hexb	HEXB	DOWN	-10.91	-1.30
749	Prdx3	PRDX3	DOWN	-13.32	-0.84
750	Vim	VIME	DOWN	-25.70	-1.38
751	Fcer1g	FCERG	DOWN	-16.93	-1.44
752	Plg	PLMN	DOWN	-4.09	-2.76
753	Tpm3	TPM3	DOWN	-1.93	-0.20
754	Tpm1;Tpm3	TPM1 ;TPM3	DOWN	-15.95	-1.46
755	Akr1b7;Akr1b8	ALD1 ;ALD2	DOWN	-10.06	-1.15
756	Cst3	CYTC	DOWN	-6.89	-2.49
757	Gc	VTDB	DOWN	-6.97	-2.11
758	Lmnb2	LMNB2	DOWN	-7.12	-0.63
759	Cd72	CD72	DOWN	-10.90	-1.89
760	Mfge8	MFGM	DOWN	-1.18	-0.37
761	Ap1g1	AP1G1	DOWN	-6.35	-1.28
762	Eif3a	EIF3A	DOWN	-9.60	-0.63
763	Cbx3	CBX3	DOWN	-10.49	-0.54
764	Cbx3;Cbx5	CBX3 ;CBX5	DOWN	-3.46	-1.98
765	Glb1	BGAL	DOWN	-4.68	-0.62
766	Cat	CATA	DOWN	-12.93	-0.72
767	Ppib	PPIB	DOWN	-10.55	-0.94
768	Capg	CAPG	DOWN	-14.05	-0.68
769	Lta4h	LKHA4	DOWN	-5.28	-1.58
770	Impdh2	IMDH2	DOWN	-6.56	-0.43
771	Impdh1;Impdh2	IMDH1 ;IMDH2	DOWN	-4.03	-0.33
772	Acp2	PPAL	DOWN	-8.96	-1.14
773	M6pr	MPRD	DOWN	-8.44	-0.78
774	Mcm3	MCM3	DOWN	-7.37	-0.73
775	Lyn	LYN	DOWN	-9.07	-2.30
776	Ezr;Msn;Rdx	EZRI ;MOES ;RADI	DOWN	-8.91	-0.45
777	Msn	MOES	DOWN	-16.76	-0.64
778	Msn;Rdx	MOES ;RADI	DOWN	-19.73	-2.12
779	Ptma	PTMA	DOWN	-6.64	-0.38
780	Glud1	DHE3	DOWN	-12.22	-0.58
781	Psmd7	PSMD7	DOWN	-7.88	-0.75
782	Sars1	SYSC	DOWN	-9.93	-0.74
783	Marcks	MARCS	DOWN	-6.17	-0.62
784	Fkbp1a	FKB1A	DOWN	-3.81	-0.63
785	Snrpb;Snrpn	RSMB ;RSMN	DOWN	-17.18	-1.38
786	Plaa	PLAP	DOWN	-1.04	-0.39
787	H2ax	H2AX	DOWN	-14.73	-0.91
788	Pdia3	PDIA3	DOWN	-13.86	-0.39
789	Vav1	VAV	DOWN	-9.96	-0.99
790	Cebpb	CEBPB	DOWN	-8.55	-2.18
791	Psmb8	PSB8	DOWN	-1.19	-0.39
792	Nap1l1;Nap1l4	NP1L1 ;NP1L4	DOWN	-11.94	-0.42
793	Atxn10	ATX10	DOWN	-4.93	-1.71
794	Mug1	MUG1	DOWN	-19.04	-2.08
795	Grn	GRN	DOWN	-17.63	-1.55
796	Ptpn6	PTN6	DOWN	-7.58	-0.53
797	Hexa	HEXA	DOWN	-9.06	-1.35
798	Ahsg	FETUA	DOWN	-16.49	-1.87
799	Oat	OAT	DOWN	-1.94	-0.15
800	Msr1	MSRE	DOWN	-7.51	-1.32
801	Alox5ap	AL5AP	DOWN	-17.92	-1.57
802	Fkbp4	FKBP4	DOWN	-11.72	-0.41
803	Hmgb1;Hmgb2	HMGB1 ;HMGB2	DOWN	-2.78	-0.16
804	Rbpj	SUH	DOWN	-1.49	-0.56
805	Dbi	ACBP	DOWN	-4.50	-1.33
806	Map2k1;Map2k2	MP2K1 ;MP2K2	DOWN	-14.85	-1.52
807	Cd68	CD68	DOWN	-13.81	-0.69
808	Scp2	SCP2	DOWN	-1.85	-0.15
809	Ssb	LA	DOWN	-1.10	-0.09

810	Serpinc1	ANT3	DOWN	-12.94	-1.41
811	Wars1	SYWC	DOWN	-1.30	-0.13
812	Ranbp1	RANG	DOWN	-7.85	-0.60
813	Mif	MIF	DOWN	-15.34	-0.97
814	Rab5c	RAB5C	DOWN	-1.86	-0.42
815	Rab6a	RAB6A	DOWN	-6.13	-2.14
816	Ppard	PPARD	DOWN	-10.37	-2.18
817	Pdha1	ODPA	DOWN	-2.45	-0.67
818	Fbl	FBRL	DOWN	-6.64	-0.66
819	Canx	CALX	DOWN	-17.80	-1.15
820	Prdx1	PRDX1	DOWN	-17.59	-0.90
821	Rpl18	RL18	DOWN	-4.24	-0.25
822	Gnl1	GNL1	DOWN	-9.28	-1.93
823	Hmgcl	HMGCL	DOWN	-7.87	-0.81
824	Hspa9	GRP75	DOWN	-10.51	-0.46
825	Dnm1;Dnm2	DYN1 ;DYN2	DOWN	-11.27	-1.00
826	Dnm2;Dnm3	DYN2 ;DYN3	DOWN	-9.31	-1.41
827	Fen1	FEN1	DOWN	-2.91	-0.40
828	Tkt	TKT	DOWN	-14.50	-0.56
829	Rpl28	RL28	DOWN	-11.45	-1.28
830	Acsl1	ACSL1	DOWN	-4.59	-1.40
831	Acsl1;Acsl5	ACSL1 ;ACSL5	DOWN	-1.44	-0.44
832	Csk	CSK	DOWN	-2.89	-0.46
833	Cd86	CD86	DOWN	-9.91	-1.73
834	Cct8	TCPQ	DOWN	-11.55	-0.46
835	Cox6a1	CX6A1	DOWN	-6.70	-0.82
836	H1-4	H14	DOWN	-7.61	-0.84
837	H1-3	H13	DOWN	-10.86	-2.17
838	Akr1b1	ALDR	DOWN	-21.40	-1.32
839	Akr1b8	ALD2	DOWN	-4.33	-0.50
840	Fkbp2	FKBP2	DOWN	-8.59	-1.07
841	Rangap1	RAGP1	DOWN	-1.97	-0.21
842	Nsf	NSF	DOWN	-3.25	-0.44
843	Psmc2	PRS7	DOWN	-1.08	-0.22
844	Rab11b	RB11B	DOWN	-1.30	-0.18
845	Adss2	PURA2	DOWN	-6.48	-0.24
846	Stt3a	STT3A	DOWN	-6.25	-1.47
847	Pla2g4a	PA24A	DOWN	-11.90	-0.77
848	Aldh2	ALDH2	DOWN	-11.64	-0.78
849	Capza1;Capza2	CAZA1 ;CAZA2	DOWN	-16.23	-1.05
850	Capza2	CAZA2	DOWN	-11.11	-1.21
851	Capzb	CAPZB	DOWN	-15.29	-1.21
852	Srprb	SRPRB	DOWN	-1.18	-0.13
853	Mtx1	MTX1	DOWN	-1.84	-0.47
854	Rpl13	RL13	DOWN	-12.27	-0.55
855	Rpl36	RL36	DOWN	-2.17	-0.39
856	Anxa5	ANXA5	DOWN	-22.72	-1.46
857	Tbca	TBCA	DOWN	-1.80	-0.18
858	Lmna	LMNA	DOWN	-24.01	-1.33
859	Pcnt	PCNT	DOWN	-13.52	-1.40
860	Cox7a2	CX7A2	DOWN	-12.96	-2.70
861	Slc25a4	ADT1	DOWN	-12.63	-1.00
862	Slc25a4;Slc25a5	ADT1 ;ADT2	DOWN	-14.95	-0.55
863	Clec10a	CLC10	DOWN	-5.71	-1.03
864	Hnrnpa1	ROA1	DOWN	-17.46	-0.89
865	Mcm4	MCM4	DOWN	-5.50	-0.34
866	Mcm5	MCM5	DOWN	-3.93	-0.72
867	Psma2	PSA2	DOWN	-0.80	-0.18
868	Srp9	SRP09	DOWN	-1.30	-0.42
869	Impdh1	IMDH1	DOWN	-2.18	-1.05
870	Ahcy	SAHH	DOWN	-13.43	-0.88
871	Arsb	ARSB	DOWN	-15.28	-1.13
872	Atp6v1a	VATA	DOWN	-15.57	-0.96
873	Atp6v1e1	VATE1	DOWN	-10.40	-1.10
874	S100a11	S10AB	DOWN	-5.01	-0.50
875	Pa2g4	PA2G4	DOWN	-8.99	-0.68
876	Acadl	ACADL	DOWN	-1.95	-0.24
877	Rpl9	RL9	DOWN	-6.68	-0.50
878	Hsd17b4	DHB4	DOWN	-4.36	-0.91
879	Atp6v0d1	VA0D1	DOWN	-0.95	-0.66
880	Slc25a5	ADT2	DOWN	-11.54	-0.88
881	Slc1a5	AAAT	DOWN	-4.10	-1.28
882	Kpna2	IMA1	DOWN	-8.39	-1.77

883	Pkm	KPYM	DOWN	-14.46	-0.61
884	Rpl10a	RL10A	DOWN	-3.95	-0.40
885	Dbt	ODB2	DOWN	-6.73	-1.25
886	Hccs	CCHL	DOWN	-6.32	-2.34
887	Pitpna	PIPNA	DOWN	-9.08	-1.40
888	Rab2a	RAB2A	DOWN	-2.03	-0.30
889	Cnbp	CNBP	DOWN	-9.75	-0.41
890	Idh2	IDHP	DOWN	-9.53	-0.74
891	Msh6	MSH6	DOWN	-11.32	-3.04
892	Rad23b	RD23B	DOWN	-7.66	-0.89
893	Psmc4	PRS6B	DOWN	-3.51	-0.71
894	Adsl	PUR8	DOWN	-2.98	-1.33
895	Acod1	IRG1	DOWN	-13.24	-1.87
896	Rab10	RAB10	DOWN	-2.86	-1.24
897	Rab8b	RAB8B	DOWN	-4.76	-1.03
898	Lrpap1	AMRP	DOWN	-5.93	-0.17
899	Stmn2	STMN2	DOWN	-4.04	-3.44
900	Atp5mf	ATPK	DOWN	-15.69	-1.47
901	Gfer	ALR	DOWN	-9.16	-0.85
902	Cox6b1	CX6B1	DOWN	-4.37	-0.16
903	Cyb5a	CYB5	DOWN	-3.88	-0.28
904	Atp5f1b	ATPB	DOWN	-17.16	-1.04
905	Pdcd5	PDCD5	DOWN	-1.44	-0.31
906	Exosc10	EXOSX	DOWN	-17.58	-1.97
907	Atp6v1d	VATD	DOWN	-4.97	-0.77
908	Eef1d	EF1D	DOWN	-13.96	-1.03
909	Actn1;Actn4	ACTN1 ;ACTN4	DOWN	-12.62	-0.78
910	Tm9sf2	TM9S2	DOWN	-8.15	-2.00
911	Eef2	EF2	DOWN	-15.87	-0.88
912	Tpm1	TPM1	DOWN	-8.07	-0.80
913	Bcl2l13	B2L13	DOWN	-3.96	-2.07
914	Eif5	IF5	DOWN	-5.34	-0.53
915	Rin3	RIN3	DOWN	-6.13	-1.88
916	Arpc4	ARPC4	DOWN	-17.84	-1.05
917	Eif3e	EIF3E	DOWN	-7.91	-1.68
918	Pcbp1	PCBP1	DOWN	-16.79	-0.94
919	Pcbp1	PCBP1	DOWN	-11.87	-0.90
920	Actb	ACTB	DOWN	-10.29	-0.49
921	Acta1	ACTB	DOWN	-10.45	-0.35
922	Cdc42	CDC42	DOWN	-10.43	-0.53
923	Cdc42	CDC42	DOWN	-9.07	-0.64
924	Eif4a1	IF4A1	DOWN	-11.47	-1.30
925	Rps20	RS20	DOWN	-17.13	-0.98
926	Rab10	RAB10	DOWN	-7.06	-1.81
927	Rab8b	RAB8B	DOWN	-5.82	-0.82
928	Ube2d3	UB2D3	DOWN	-2.90	-0.56
929	Ube2m	UBC12	DOWN	-3.88	-0.47
930	Ube2n	UBE2N	DOWN	-3.16	-0.53
931	Arf1;Arf3	ARF1 ;ARF3	DOWN	-5.23	-2.29
932	Rpl26	RL26	DOWN	-7.03	-0.46
933	Psme3	PSME3	DOWN	-2.74	-1.71
934	Magoh;Magohb	MGN2 ;MGN	DOWN	-8.53	-1.54
935	Rpl27	RL27	DOWN	-1.42	-0.12
936	Rpl37a	RL37A	DOWN	-10.85	-1.65
937	Sec61a1	S61A1	DOWN	-6.60	-2.29
938	Arf4	ARF4	DOWN	-8.37	-2.47
939	Arf4;Arf5	ARF4 ;ARF5	DOWN	-6.30	-2.06
940	Vbp1	PFD3	DOWN	-5.42	-0.34
941	Hnrnpk	HNRPK	DOWN	-16.09	-1.03
942	Ywhag	1433G	DOWN	-13.27	-1.30
943	Ywhaz	1433Z	DOWN	-13.44	-0.99
944	Ywhah	1433G	DOWN	-12.36	-2.67
945	Timm8b	TIM8B	DOWN	-6.78	-1.55
946	Ppp1ca	PP1A	DOWN	-7.59	-0.58
947	Ppp1cc	PP1G	DOWN	-5.76	-1.87
948	Psmc1	PRS4	DOWN	-2.67	-0.58
949	Psmc5	PRS8	DOWN	-7.53	-1.04
950	Rps15a	RS15A	DOWN	-13.42	-0.93
951	Ywhae	1433E	DOWN	-11.47	-0.86
952	Rps14	RS14	DOWN	-19.46	-1.33
953	Rps23	RS23	DOWN	-2.76	-0.28
954	Rps18	RS18	DOWN	-11.87	-0.67
955	Rps29	RS29	DOWN	-16.28	-1.75

956	Rps11	RS11	DOWN	-12.17	-0.83
957	Snrpf	RUXF	DOWN	-7.97	-1.39
958	Snrpg	RUXG	DOWN	-18.30	-1.62
959	Lsm3	LSM3	DOWN	-7.68	-1.34
960	Lsm6	LSM6	DOWN	-7.42	-1.66
961	Snrpd1	SMD1	DOWN	-2.55	-0.98
962	Snrpd2	SMD2	DOWN	-11.92	-2.05
963	Snrpd3	SMD3	DOWN	-12.58	-1.50
964	Psmc6	PRS10	DOWN	-5.39	-0.20
965	Dynlrb1	DLRB1	DOWN	-5.02	-0.36
966	Eef1a2	EF1A2	DOWN	-5.86	-2.03
967	Rps4x	RS4X	DOWN	-18.99	-1.07
968	Rpl18a	RL18A	DOWN	-11.88	-0.77
969	Rps6	RS6	DOWN	-7.13	-0.31
970	H4c1	H4	DOWN	-12.60	-1.16
971	Atp6v1b2	VATB2	DOWN	-13.41	-0.83
972	Rab1A	RAB1A	DOWN	-1.77	-0.21
973	Ran	RAN	DOWN	-11.64	-0.78
974	Rap1a;Rap1b	RAP1A ;RAP1B	DOWN	-8.50	-1.20
975	Rps15	RS15	DOWN	-1.02	-0.29
976	Rps25	RS25	DOWN	-4.97	-0.23
977	Rps26	RS26	DOWN	-15.57	-2.03
978	Rps28	RS28	DOWN	-9.97	-0.60
979	Gnb1	GBB1	DOWN	-12.39	-1.91
980	Gnb1;Gnb2	GBB1 ;GBB2	DOWN	-15.29	-2.11
981	Gnb2	GBB2	DOWN	-12.75	-1.18
982	Rpl30	RL30	DOWN	-12.29	-0.69
983	Rpl31	RL31	DOWN	-17.19	-1.00
984	Rps3	RS3	DOWN	-21.95	-1.12
985	Rpl8	RL8	DOWN	-17.21	-1.08
986	Ybx1	YBOX1	DOWN	-11.52	-1.23
987	Rps27a;Uba52	RL40 ;RS27A	DOWN	-22.27	-1.50
988	Tra2b	TRA2B	DOWN	-6.46	-1.35
989	Rac1	RAC1	DOWN	-2.91	-0.55
990	Rac1;Rac2	RAC1 ;RAC2	DOWN	-15.83	-0.86
991	Hspa8	HSP7C	DOWN	-14.11	-0.54
992	Tpt1	TCTP	DOWN	-9.00	-1.14
993	Dnaja1	DNJA1	DOWN	-3.77	-0.77
994	Hspd1	CH60	DOWN	-7.15	-0.22
995	Eif4e	IF4E	DOWN	-2.62	-0.38
996	Mapk1	MK01	DOWN	-13.71	-1.36
997	Mapk1;Mapk3	MK01 ;MK03	DOWN	-1.07	-0.62
998	Ppp1cc	PP1G	DOWN	-11.10	-1.58
999	Ywhaz	1433Z	DOWN	-15.65	-1.01
1000	Ywhab;Ywhaq;Ywhaz	1433B ;1433T ;1433Z	DOWN	-4.46	-1.69
1001	Sumo1	SUMO1	DOWN	-2.97	-0.47
1002	Dynll1;Dynll2	DYL1 ;DYL2	DOWN	-2.67	-0.47
1003	Gng2	GBG2	DOWN	-0.94	-0.14
1004	Eif5a	IF5A1	DOWN	-2.52	-0.26
1005	Crip1	CRIP1	DOWN	-9.98	-0.34
1006	Rps17	RS17	DOWN	-10.50	-1.10
1007	Ube2i	UBC9	DOWN	-10.43	-0.79
1008	Rps10	RS10	DOWN	-1.04	-0.18
1009	Phb1	PHB1	DOWN	-13.68	-0.79
1010	Rpl22	RL22	DOWN	-14.05	-1.16
1011	Acta1;Actc1	ACTC ;ACTS	DOWN	-17.40	-1.60
1012	Rack1	RACK1	DOWN	-19.91	-1.02
1013	Ywhaq	1433T	DOWN	-5.74	-0.96
1014	Tuba4a	TBA4A	DOWN	-16.53	-0.89
1015	Tuba1c;Tuba4a	TBA1C ;TBA4A	DOWN	-8.63	-0.65
1016	Tuba8;Tubal3	TBA8 ;TBAL3	DOWN	-9.58	-1.55
1017	Tuba4a;Tuba8	TBA4A ;TBA8	DOWN	-14.45	-0.70
1018	Tubb4b	TBB4B	DOWN	-18.67	-1.44
1019	Tubb4b;Tubb5	TBB4B ;TBB5	DOWN	-1.74	-0.38
1020	Tubb2a	TBB2A	DOWN	-14.57	-1.93
1021	Tubb3;Tubb4b	TBB3 ;TBB4B	DOWN	-14.04	-0.74
1022	Tubb4b;Tubb5	TBB4B ;TBB5	DOWN	-12.79	-1.45
1023	Tubb2a	TBB2A	DOWN	-11.95	-1.59
1024	Tubb4b;Tubb5	TBB4B ;TBB5	DOWN	-3.74	-1.68
1025	Tubb5	TBB5	DOWN	-16.27	-1.49
1026	Tubb4b;Tubb6	TBB4B ;TBB6	DOWN	-0.81	-0.98
1027	Ywhah	1433F	DOWN	-4.52	-0.46
1028	Kpnb1	IMB1	DOWN	-11.85	-0.62

1029	Pkn1	PKN1	DOWN	-11.10	-0.99
1030	Mpp1	EM55	DOWN	-6.43	-0.81
1031	Hnrnph2	HNRH2	DOWN	-6.86	-1.80
1032	Hint1	HINT1	DOWN	-1.83	-0.10
1033	Elavl1	ELAV1	DOWN	-8.23	-0.42
1034	Idh3g	IDHG1	DOWN	-11.21	-1.15
1035	Vasp	VASP	DOWN	-9.05	-0.75
1036	Naca	NACAM	DOWN	-18.94	-1.03
1037	Casp3	CASP3	DOWN	-10.61	-4.61
1038	Gaa	LYAG	DOWN	-1.77	-0.55
1039	Cct7	TCPH	DOWN	-9.81	-0.74
1040	Cct2	TCPB	DOWN	-5.55	-0.18
1041	Cct4	TCPD	DOWN	-11.91	-0.58
1042	Cct5	TCPE	DOWN	-2.97	-0.24
1043	Cct6a	TCPZ	DOWN	-10.09	-0.61
1044	Cct3	TCPG	DOWN	-16.82	-1.02
1045	Renbp	RENBP	DOWN	-8.53	-1.33
1046	Wnk1	WNK1	DOWN	-16.63	-1.37
1047	Arf5	ARF5	DOWN	-6.21	-0.80
1048	Erh	ERH	DOWN	-1.70	-1.10
1049	Ap2m1	AP2M1	DOWN	-11.37	-1.33
1050	Rhog	RHOG	DOWN	-8.71	-0.72
1051	Srsf3	SRSF3	DOWN	-12.74	-0.74
1052	Srsf3;Srsf7	SRSF3 ;SRSF7	DOWN	-1.30	-0.70
1053	Serpinf1	PEDF	DOWN	-11.71	-2.62
1054	Mcm2	MCM2	DOWN	-10.40	-1.32
1055	Mcm6	MCM6	DOWN	-15.55	-1.44
1056	Atp1b3	AT1B3	DOWN	-7.12	-1.90
1057	Anxa4	ANXA4	DOWN	-12.46	-1.46
1058	Rps5	RS5	DOWN	-7.87	-0.42
1059	Smarcc1	SMRC1	DOWN	-0.84	-0.16
1060	Sirpa	SHPS1	DOWN	-7.88	-1.97
1061	Smn1	SMN	DOWN	-20.26	-1.48
1062	Fh	FUMH	DOWN	-13.28	-0.57
1063	Ctsc	CATC	DOWN	-11.94	-1.19
1064	Anp32e	AN32E	DOWN	-12.02	-1.18
1065	G3bp1	G3BP1	DOWN	-12.12	-1.01
1066	Rbbp6	RBBP6	DOWN	-11.99	-2.45
1067	Tubb5	TBB5	DOWN	-3.53	-0.22
1068	Tubb5	TBB2A	DOWN	-5.12	-1.02
1069	ubb5	TBB2A	DOWN	-8.94	-1.10
1070	Uqcrh	QCR6	DOWN	-11.14	-1.00
1071	Prdx5	PRDX5	DOWN	-3.84	-0.24
1072	Xdh	XDH	DOWN	-2.36	-0.46
1073	G6pdx	G6PD1	DOWN	-19.65	-1.00
1074	Apoa1	APOA1	DOWN	-18.02	-1.39
1075	Hnrnpul2	HNRL2	DOWN	-3.68	-0.32
1076	Top2a	TOP2A	DOWN	-12.28	-0.87
1077	Vcp	TERA	DOWN	-17.12	-0.90
1078	Uba1	UBA1	DOWN	-13.19	-1.06
1079	C1qc	C1QC	DOWN	-7.71	-1.59
1080	Nucb1	NUCB1	DOWN	-16.05	-1.67
1081	Atp5f1a	ATPA	DOWN	-15.14	-0.63
1082	Ckb	KCRB	DOWN	-12.86	-0.73
1083	Top1	TOP1	DOWN	-4.00	-0.35
1084	Rac2	RAC2	DOWN	-5.89	-0.36
1085	Atp5me	ATP5I	DOWN	-13.61	-1.44
1086	Anxa7	ANXA7	DOWN	-6.31	-1.76
1087	Acads	ACADS	DOWN	-12.58	-1.57
1088	Ambp	AMBP	DOWN	-18.93	-1.26
1089	Lgals3bp	LG3BP	DOWN	-0.91	-0.21
1090	Cbfb	PEBB	DOWN	-6.95	-2.35
1091	Pros1	PROS	DOWN	-7.39	-1.11
1092	Fbln1	FBLN1	DOWN	-11.92	-1.26
1093	Ncf1	NCF1	DOWN	-4.89	-0.96
1094	Npepps	PSA	DOWN	-5.48	-1.97
1095	Nsun2	NSUN2	DOWN	-3.25	-0.79
1096	Myl12b	ML12B	DOWN	-1.69	-0.65
1097	Gmps	GUAA	DOWN	-9.55	-0.70
1098	Mat2a	METK2	DOWN	-8.68	-0.77
1099	Usp39	UBP39	DOWN	-8.82	-0.98
1100	Prrc2c	PRC2C	DOWN	-6.35	-0.78
1101	Hk3	HXK3	DOWN	-3.50	-0.97

1102	Uap1l1	UAP1L	DOWN	-10.60	-0.79
1103	Srsf6	SRSF6	DOWN	-19.01	-1.44
1104	Khsrp	FUBP2	DOWN	-9.55	-0.39
1105	Ddb1	DDB1	DOWN	-2.06	-0.21
1106	Gpsm3	GPSM3	DOWN	-7.62	-0.83
1107	Esyt1	ESYT1	DOWN	-3.48	-0.87
1108	Lbr	LBR	DOWN	-7.78	-0.56
1109	Pdap1	HAP28	DOWN	-1.26	-1.11
1110	Arhgap17	RHG17	DOWN	-3.75	-0.30
1111	Mylk2	MYLK2	DOWN	-10.80	-1.15
1112	Sf3b2	SF3B2	DOWN	-10.60	-0.99
1113	Smu1	SMU1	DOWN	-7.81	-1.35
1114	Arglu1	ARGL1	DOWN	-1.11	-0.81
1115	Ppp1r7	PP1R7	DOWN	-3.31	-0.38
1116	Skap2	SKAP2	DOWN	-5.62	-0.61
1117	Ttbk2	TTBK2	DOWN	-4.35	-1.86
1118	Rcsd1	CPZIP	DOWN	-4.41	-1.02
1119	Mthfd1l	C1TM	DOWN	-5.96	-0.40
1120	Abracl	ABRAL	DOWN	-6.50	-1.61
1121	Cdv3	CDV3	DOWN	-8.30	-0.61
1122	Ddx17	DDX17	DOWN	-10.22	-0.69
1123	Ddx17;Ddx5	DDX17 ;DDX5	DOWN	-14.96	-1.15
1124	Lrrc47	LRC47	DOWN	-2.28	-0.38
1125	Thrap3	TR150	DOWN	-13.95	-1.88
1126	Spag9	JIP4	DOWN	-2.15	-0.40
1127	Mypn	MYPN	DOWN	-13.95	-1.70
1128	Nufip2	NUFP2	DOWN	-1.46	-0.91
1129	Rilp	RILP	DOWN	-2.67	-2.04
1130	Pfas	PUR4	DOWN	-3.42	-0.25
1131	Ogdh	ODO1	DOWN	-2.66	-0.40
1132	Myl6	MYL6	DOWN	-13.25	-0.76
1133	Grb2	GRB2	DOWN	-16.93	-1.35
1134	Irag2	IRAG2	DOWN	-10.34	-1.20
1135	Ppp5c	PPP5	DOWN	-4.22	-0.96
1136	Psmb6	PSB6	DOWN	-21.20	-2.19
1137	Samhd1	SAMH1	DOWN	-1.78	-0.41
1138	Csnk2a1	CSK21	DOWN	-5.87	-1.97
1139	Khdrbs1	KHDR1	DOWN	-5.94	-0.41
1140	Serpinb6	SPB6	DOWN	-10.62	-0.95
1141	Stip1	STIP1	DOWN	-9.71	-0.49
1142	Vdac2	VDAC2	DOWN	-12.35	-0.89
1143	Vdac1	VDAC1	DOWN	-10.93	-0.76
1144	Rbbp4;Rbbp7	RBBP4 ;RBBP7	DOWN	-8.67	-0.61
1145	Tmpo	LAP2A	DOWN	-6.15	-1.10
1146	Hars1	HARS1	DOWN	-2.97	-0.67
1147	Ppm1g	PPM1G	DOWN	-2.51	-0.72
1148	Ptpn18	PTN18	DOWN	-10.20	-1.22
1149	Mapre1	MARE1	DOWN	-8.55	-0.60
1150	Prdx2	PRDX2	DOWN	-13.12	-0.89
1151	Pafah1b2	PA1B2	DOWN	-9.38	-1.09
1152	Psap	SAP	DOWN	-17.74	-1.23
1153	Arhgef1	ARHG1	DOWN	-4.08	-0.41
1154	Lcp1	PLSL	DOWN	-9.20	-0.21
1155	Lcp1;Pls3	PLSL ;PLST	DOWN	-11.79	-1.09
1156	Soat1	SOAT1	DOWN	-6.02	-0.65
1157	Hspa4	HSP74	DOWN	-13.87	-0.49
1158	Hspa4;Hsph1	HS105 ;HSP74	DOWN	-8.80	-0.76
1159	Glg1	GSLG1	DOWN	-8.45	-0.90
1160	Ewsr1	EWS	DOWN	-1.68	-0.52
1161	Fxr1	FXR1	DOWN	-2.08	-0.42
1162	Gdi2	GDIB	DOWN	-3.59	-0.24
1163	Arhgdib	GDIR2	DOWN	-12.18	-1.29
1164	Ddx5	DDX5	DOWN	-14.69	-0.72
1165	Cbx5	CBX5	DOWN	-7.37	-0.86
1166	Itih2	ITIH2	DOWN	-18.35	-1.36
1167	Itih3	ITIH3	DOWN	-14.41	-1.32
1168	Kif5b	KINH	DOWN	-2.72	-0.37
1169	Lasp1	LASP1	DOWN	-8.22	-0.37
1170	Pzp	PZP	DOWN	-13.34	-1.33
1171	A2m;Pzp	A2MG ;PZP	DOWN	-12.59	-1.62
1172	Mcm7	MCM7	DOWN	-12.71	-1.47
1173	Pcbp2	PCBP2	DOWN	-12.26	-0.71
1174	Srsf2	SRSF2	DOWN	-16.41	-1.18

1175	Rhoc	RHOC	DOWN	-5.31	-1.79
1176	Ssr4	SSRD	DOWN	-13.30	-1.69
1177	Shh	SHH	DOWN	-18.49	-2.01
1178	Snrpc	RU1C	DOWN	-7.61	-1.22
1179	Tsn	TSN	DOWN	-8.63	-1.23
1180	Tfrc	TFR1	DOWN	-1.86	-0.55
1181	Snrnp70	RU17	DOWN	-14.06	-1.56
1182	Zpr1	ZPR1	DOWN	-2.47	-1.83
1183	Dbnl	DBNL	DOWN	-12.52	-0.62
1184	Sh3gl1	SH3G1	DOWN	-10.32	-0.74
1185	Ostf1	OSTF1	DOWN	-5.92	-0.35
1186	Ndrg1	NDRG1	DOWN	-12.50	-0.52
1187	Eif4g2	IF4G2	DOWN	-11.04	-1.73
1188	Mapk3	MK03	DOWN	-5.28	-0.72
1189	Raly	RALY	DOWN	-12.15	-0.65
1190	Btf3;Btf3l4	BT3L4 ;BTF3	DOWN	-12.35	-3.57
1191	Lilrb4a	LRB4A	DOWN	-6.47	-1.51
1192	Stxbp2	STXB2	DOWN	-2.44	-0.61
1193	Sqstm1	SQSTM	DOWN	-6.28	-0.58
1194	Bcl2l1	B2CL1	DOWN	-2.28	-0.91
1195	Hspe1	CH10	DOWN	-9.23	-0.45
1196	Atp1a2;Atp4a	AT1A2 ;ATP4A	DOWN	-16.75	-1.85
1197	Atp1a1;Atp4a	AT1A1 ;ATP4A	DOWN	-12.64	-1.95
1198	H2bc3	H2B1B	DOWN	-17.47	-4.24
1199	Tpp2	TPP2	DOWN	-6.28	-0.44
1200	Gpd2	GPDM	DOWN	-0.84	-0.33
1201	H2ac20;Hist2h2aa1	H2A2A ;H2A2C	DOWN	-15.21	-1.12
1202	Hist2h2bb	H2B2B	DOWN	-20.70	-5.79
1203	Srm	SPEE	DOWN	-3.21	-0.55
1204	Vcl	VINC	DOWN	-6.41	-0.91
1205	Cltc	CLH1	DOWN	-18.86	-0.94
1206	Ahcyl2	SAHH3	DOWN	-1.09	-0.48
1207	Macf1	K0754 ;MACF1	DOWN	-4.32	-0.84
1208	Cep170	CE170	DOWN	-4.18	-0.32
1209	A2m	A2MG	DOWN	-18.99	-1.57
1210	Nomo1	NOMO1	DOWN	-8.65	-1.01
1211	Tpm4	TPM4	DOWN	-10.77	-0.65
1212	U2surp	SR140	DOWN	-1.47	-1.17
1213	Eif4g1	IF4G1	DOWN	-3.24	-0.35
1214	Sri	SORCN	DOWN	-5.69	-2.19
1215	Xpnpep1	XPP1	DOWN	-2.22	-0.53
1216	Ppp2r2a	2ABA	DOWN	-2.90	-0.86
1217	Snrnp200	U520	DOWN	-6.98	-0.50
1218	Rrp12	RRP12	DOWN	-7.56	-1.71
1219	Xpo1	XPO1	DOWN	-1.00	-0.61
1220	Nes	NEST	DOWN	-12.36	-0.64
1221	Pcnp	PCNP	DOWN	-4.65	-0.44
1222	Fkbp15	FKB15	DOWN	-10.49	-2.67
1223	Txlna	TXLNA	DOWN	-2.62	-0.39
1224	Pigs	PIGS	DOWN	-5.62	-1.58
1225	Srsf1	SRSF1	DOWN	-13.29	-1.04
1226	Stoml3	STML3	DOWN	-5.14	-2.99
1227	Naa50	NAA50	DOWN	-4.07	-0.48
1228	Camk2d	KCC2D	DOWN	-6.92	-2.39
1229	Atp1a1;Atp1a2	AT1A1 ;AT1A2	DOWN	-12.00	-0.59
1230	Kctd12	KCD12	DOWN	-11.24	-1.50
1231	Wdr43	WDR43	DOWN	-4.47	-0.61
1232	Ugt1a7	UD17	DOWN	-7.70	-0.81
1233	Lsm8	LSM8	DOWN	-4.89	-1.39
1234	Rps9	RS9	DOWN	-18.83	-1.34
1235	Rps27;Rps27l	RS27L ;RS27	DOWN	-21.73	-1.89
1236	Rpl10	RL10	DOWN	-11.41	-1.02
1237	Rpl35	RL35	DOWN	-12.68	-0.75
1238	Eif2s1	IF2A	DOWN	-11.01	-1.15
1239	Apool	MIC27	DOWN	-8.46	-0.89
1240	Snd1	SND1	DOWN	-15.96	-1.04
1241	Mtch1	MTCH1	DOWN	-5.88	-1.73
1242	Mtch2	MTCH2	DOWN	-5.94	-1.15
1243	Cyfip1	CYFP1	DOWN	-8.61	-0.92
1244	Shq1	SHQ1	DOWN	-1.81	-0.34
1245	Luc7l;Luc7l2	LC7L2 ;LUC7L	DOWN	-11.62	-1.43
1246	Spag7	SPAG7	DOWN	-9.98	-1.87
1247	Eml2	EMAL2	DOWN	-1.83	-1.35

1248	Mybbp1a	MBB1A	DOWN	-11.06	-1.10
1249	Septin9	45909	DOWN	-1.97	-0.51
1250	Naa15	NAA15	DOWN	-3.20	-0.56
1251	Mogs	MOGS	DOWN	-10.11	-1.35
1252	Dnph1	DNPH1	DOWN	-6.11	-0.86
1253	Hydin	HYDIN	DOWN	-5.33	-0.80
1254	Mtdh	LYRIC	DOWN	-13.56	-1.11
1255	Glrx5	GLRX5	DOWN	-14.07	-1.81
1256	Safb2	SAFB2	DOWN	-2.16	-0.68
1257	Gns	GNS	DOWN	-6.69	-0.58
1258	Tufm	EFTU	DOWN	-11.57	-0.63
1259	Tnpo1	TNPO1	DOWN	-4.78	-1.15
1260	Actbl2	ACTBL	DOWN	-13.85	-0.88
1261	Hnrnpa3	ROA3	DOWN	-14.93	-0.80
1262	Pld4	PLD4	DOWN	-3.22	-0.82
1263	Psmd11	PSD11	DOWN	-7.61	-0.59
1264	Eif4b	IF4B	DOWN	-9.53	-0.63
1265	Samm50	SAM50	DOWN	-4.47	-0.89
1266	Aars1	SYAC	DOWN	-1.53	-0.29
1267	Bola2	BOLA2	DOWN	-13.22	-0.59
1268	Smndc1	SPF30	DOWN	-4.33	-1.83
1269	Pck2	PCKGM	DOWN	-10.23	-1.32
1270	Tm9sf4	TM9S4	DOWN	-5.89	-2.48
1271	Wasf2	WASF2	DOWN	-15.12	-1.14
1272	Slc25a12	S2512	DOWN	-2.04	-0.65
1273	Clic6	CLIC6	DOWN	-0.99	-0.98
1274	Ptbp3	PTBP3	DOWN	-8.61	-0.71
1275	Ganab	GANAB	DOWN	-9.18	-0.96
1276	Iars2	SYIM	DOWN	-1.80	-0.53
1277	Cstf2	CSTF2	DOWN	-8.10	-0.69
1278	Nup93	NUP93	DOWN	-2.98	-0.72
1279	Psmd5	PSMD5	DOWN	-7.82	-2.27
1280	Ahsa1	AHSA1	DOWN	-14.10	-1.90
1281	Rcc2	RCC2	DOWN	-8.16	-0.59
1282	Ipo5	IPO5	DOWN	-7.47	-0.78
1283	Srsf7	SRSF7	DOWN	-7.34	-0.49
1284	Arid5b	ARI5B	DOWN	-5.86	-2.05
1285	Srp68	SRP68	DOWN	-1.80	-0.23
1286	Slc25a24	SCMC1	DOWN	-2.07	-0.69
1287	Dlat	ODP2	DOWN	-10.87	-0.73
1288	Lars1	SYLC	DOWN	-12.59	-1.16
1289	Ckap4	CKAP4	DOWN	-8.36	-1.46
1290	Qars1	SYQ	DOWN	-4.03	-1.95
1291	Cibar1	CBAR1	DOWN	-1.26	-0.45
1292	Nars1	SYNC	DOWN	-2.23	-0.41
1293	Metap1	MAP11	DOWN	-5.11	-0.59
1294	Elmo1	ELMO1	DOWN	-1.60	-0.48
1295	Slc15a3	S15A3	DOWN	-9.55	-2.11
1296	Ppp1r18	PPR18	DOWN	-6.47	-0.57
1297	Cnpy4	CNPY4	DOWN	-10.82	-1.94
1298	Hus1	HUS1	DOWN	-6.05	-1.04
1299	Srrm2	SRRM2	DOWN	-12.33	-0.60
1300	Flna	FLNA	DOWN	-8.44	-0.26
1301	Flna;Flnc	FLNA ;FLNC	DOWN	-10.62	-2.08
1302	Sec62	SEC62	DOWN	-8.79	-1.09
1303	Atp6v1h	VATH	DOWN	-1.62	-1.03
1304	Acaa2	THIM	DOWN	-2.16	-0.67
1305	Etf1	ERF1	DOWN	-8.42	-0.69
1306	Gemin5	GEMI5	DOWN	-11.70	-0.93
1307	Vps13c	VP13C	DOWN	-13.40	-1.41
1308	Taok3	TAOK3	DOWN	-2.50	-0.42
1309	Map1s	MAP1S	DOWN	-9.49	-1.16
1310	Asrgl1	ASGL1	DOWN	-14.76	-3.11
1311	Ppp4r4	PP4R4	DOWN	-19.70	-1.89
1312	Cpne1	CPNE1	DOWN	-17.48	-1.58
1313	Rbm14	RBM14	DOWN	-10.18	-0.76
1314	Rae1	RAE1L	DOWN	-7.35	-2.69
1315	Myef2	MYEF2	DOWN	-9.59	-0.82
1316	Immt	MIC60	DOWN	-1.08	-0.06
1317	Rassf4	RASF4	DOWN	-1.55	-0.68
1318	Abi1	ABI1	DOWN	-5.00	-1.99
1319	Pabpn1	PABP2	DOWN	-5.43	-1.75
1320	Txnl1	TXNL1	DOWN	-3.78	-0.23

1321	Smco1	SMCO1	DOWN	-5.72	-1.18
1322	Smc2	SMC2	DOWN	-11.78	-0.95
1323	Eprs1	SYEP	DOWN	-2.00	-0.13
1324	Lonp1	LONM	DOWN	-5.04	-0.33
1325	H2bc12	H2B1K	DOWN	-18.73	-7.86
1326	Hist1h2bp	H2B1P	DOWN	-12.06	-0.70
1327	Pgp	PGP	DOWN	-9.86	-1.43
1328	Slain2	SLAI2	DOWN	-4.02	-0.43
1329	Copa	COPA	DOWN	-6.65	-0.61
1330	Gpr84	GPR84	DOWN	-12.79	-1.68
1331	Mrgprx1	MRGX1	DOWN	-3.19	-0.16
1332	Trip10	CIP4	DOWN	-4.13	-1.91
1333	Eif3b	EIF3B	DOWN	-7.68	-0.81
1334	Acsl5	ACSL5	DOWN	-1.04	-0.85
1335	Slc25a1	TXTP	DOWN	-2.62	-0.88
1336	Gmds	GMDS	DOWN	-7.06	-0.96
1337	Gfm1	EFGM	DOWN	-9.57	-1.43
1338	Pdxk	PDXK	DOWN	-13.69	-0.86
1339	Cmc2	COXM2	DOWN	-6.27	-1.46
1340	Fermt3	URP2	DOWN	-2.58	-0.54
1341	Spats2	SPAS2	DOWN	-4.14	-0.90
1342	Nckap1l	NCKPL	DOWN	-2.11	-0.67
1343	Colgalt1	GT251	DOWN	-5.37	-0.83
1344	Brox	BROX	DOWN	-11.52	-1.37
1345	Shtn1	SHOT1	DOWN	-0.81	-0.08
1346	Matr3	MATR3	DOWN	-2.60	-0.34
1347	Sf3a1	SF3A1	DOWN	-7.52	-0.42
1348	Eif3l	EIF3L	DOWN	-1.55	-0.41
1349	Aimp2	AIMP2	DOWN	-5.89	-1.16
1350	Gspt1	ERF3A	DOWN	-5.24	-0.61
1351	Hnrnpl	HNRPL	DOWN	-7.02	-0.43
1352	Sgpl1	SGPL1	DOWN	-6.17	-2.17
1353	Klhl36	KLH36	DOWN	-2.55	-0.67
1354	Ero1a	ERO1A	DOWN	-11.26	-0.85
1355	Eif3c	EIF3C	DOWN	-6.78	-0.35
1356	Mtss1	MTSS1	DOWN	-15.26	-0.80
1357	Spart	SPART	DOWN	-5.01	-0.91
1358	Ubqln1	UBQL1	DOWN	-9.15	-0.85
1359	Apobr	APOBR	DOWN	-5.66	-2.00
1360	Cth	CGL	DOWN	-7.06	-0.67
1361	Rnpep	AMPB	DOWN	-5.04	-0.67
1362	Myh9	MYH9	DOWN	-15.80	-0.57
1363	Hdlbp	VIGLN	DOWN	-2.15	-0.15
1364	Adpgk	ADPGK	DOWN	-6.68	-1.95
1365	Psmd2	PSMD2	DOWN	-9.16	-0.64
1366	Atp1a1	AT1A1	DOWN	-5.01	-0.27
1367	Ptgr2	PTGR2	DOWN	-5.84	-2.28
1368	Ddx39a;Ddx39b	DX39A ;DX39B	DOWN	-12.96	-0.99
1369	Rcc1	RCC1	DOWN	-5.61	-0.66
1370	Pdcd10	PDC10	DOWN	-10.73	-1.11
1371	Srsf4	SRSF4	DOWN	-8.28	-0.73
1372	Ccdc115	CC115	DOWN	-5.85	-0.41
1373	Rpe	RPE	DOWN	-2.04	-0.40
1374	Zng1	ZNG1	DOWN	-1.29	-0.49
1375	Hnrnpu	HNRPU	DOWN	-5.68	-0.23
1376	Slc25a3	S25A3	DOWN	-14.97	-1.62
1377	Rbm39	RBM39	DOWN	-15.31	-2.15
1378	Amot	AMOT	DOWN	-3.89	-0.80
1379	Gatad2b	P66B	DOWN	-8.39	-1.64
1380	Sfpq	SFPQ	DOWN	-10.58	-0.66
1381	Nono;Sfpq	NONO ;SFPQ	DOWN	-17.27	-1.97
1382	Tram1	TRAM1	DOWN	-1.66	-0.62
1383	Rab14	RAB14	DOWN	-0.96	-0.16
1384	Sfxn3	SFXN3	DOWN	-5.83	-2.31
1385	Acly	ACLY	DOWN	-9.16	-0.86
1386	Eif4a3	IF4A3	DOWN	-13.74	-3.34
1387	Ndufs1	NDUS1	DOWN	-6.35	-0.56
1388	Rnh1	RINI	DOWN	-8.84	-0.34
1389	Pqbp1	PQBP1	DOWN	-10.74	-0.77
1390	Chchd6	MIC25	DOWN	-4.83	-1.03
1391	Atp5f1c	ATPG	DOWN	-9.91	-1.26
1392	Brk1	BRK1	DOWN	-10.85	-2.55
1393	Sh3bgrl3	SH3L3	DOWN	-14.17	-1.53

1394	Slc39a8	S39A8	DOWN	-22.46	-1.89
1395	Csde1	CSDE1	DOWN	-3.35	-0.34
1396	Txndc5	TXND5	DOWN	-10.36	-0.81
1397	Hkdc1	HKDC1	DOWN	-12.29	-2.00
1398	Eif3h	EIF3H	DOWN	-2.18	-0.18
1399	Dus3l	DUS3L	DOWN	-3.85	-0.56
1400	Arrb2	ARRB2	DOWN	-3.98	-0.58
1401	Rpn1	RPN1	DOWN	-14.94	-0.64
1402	Twf1	TWF1	DOWN	-5.78	-0.57
1403	Dnajc3	DNJC3	DOWN	-2.27	-1.06
1404	Ugp2	UGPA	DOWN	-9.38	-1.46
1405	Snx18	SNX18	DOWN	-3.60	-1.28
1406	Dst	DYST	DOWN	-1.92	-1.06
1407	Mia2	MIA2	DOWN	-6.58	-1.53
1408	Lrp1	LRP1	DOWN	-4.89	-0.29
1409	Scpep1	RISC	DOWN	-2.07	-0.40
1410	Fdps	FPPS	DOWN	-12.73	-0.93
1411	Tardbp	TADBP	DOWN	-14.28	-1.61
1412	Tf	TRFE	DOWN	-14.60	-1.07
1413	Sf3b3	SF3B3	DOWN	-5.21	-0.57
1414	Cyrib	CYRIB	DOWN	-7.26	-0.75
1415	Tor1aip1	TOIP1	DOWN	-11.82	-1.16
1416	Dars1	SYDC	DOWN	-14.95	-1.31
1417	Mthfd1	C1TC	DOWN	-3.26	-0.17
1418	Pcyt2	PCY2	DOWN	-3.25	-1.60
1419	Mtarc2	45718	DOWN	-11.48	-1.91
1420	Pdia6	PDIA6	DOWN	-8.11	-0.45
1421	Ubxn1	UBXN1	DOWN	-12.56	-1.38
1422	Trim59	TRI59	DOWN	-9.00	-1.58
1423	Blvrb	BLVRB	DOWN	-15.17	-1.41
1424	Sf3b5	SF3B5	DOWN	-11.78	-2.44
1425	Cers2	CERS2	DOWN	-11.87	-1.98
1426	Dhrs7b	DRS7B	DOWN	-7.76	-1.23
1427	Rfc4	RFC4	DOWN	-2.06	-1.04
1428	Mpst	THTM	DOWN	-17.59	-1.28
1429	Psip1	PSIP1	DOWN	-8.15	-0.83
1430	Sfxn1	SFXN1	DOWN	-5.10	-0.61
1431	Hadhb	ECHB	DOWN	-5.08	-2.44
1432	Actr3	ARP3	DOWN	-14.97	-0.75
1433	Nono	NONO	DOWN	-9.67	-0.90
1434	Psat1	SERC	DOWN	-4.54	-0.30
1435	Hagh	GLO2	DOWN	-15.50	-1.76
1436	Vwa5a	VMA5A	DOWN	-4.51	-0.70
1437	Tmed9	TMED9	DOWN	-6.54	-2.68
1438	Aco2	ACON	DOWN	-19.84	-0.78
1439	Dhrs1	DHRS1	DOWN	-7.53	-0.90
1440	Gmpr2	GMPR2	DOWN	-4.24	-0.96
1441	Eif2s2	IF2B	DOWN	-9.05	-1.10
1442	St13	F10A1	DOWN	-3.38	-0.17
1443	Mat2b	MAT2B	DOWN	-2.58	-0.23
1444	Ndufa10	NDUAA	DOWN	-1.40	-0.47
1445	Gps1	CSN1	DOWN	-2.11	-0.78
1446	Abcf2	ABCF2	DOWN	-7.87	-0.92
1447	Abhd12	ABD12	DOWN	-6.93	-0.67
1448	Gtpbp4	GTPB4	DOWN	-6.09	-1.08
1449	Mrps18b	RT18B	DOWN	-1.95	-0.78
1450	Mrps5	RT05	DOWN	-9.47	-0.83
1451	Ubqln4	UBQL4	DOWN	-6.87	-0.65
1452	Sf3b1	SF3B1	DOWN	-2.09	-0.34
1453	Pard3	PARD3	DOWN	-4.16	-1.50
1454	Rtn4	RTN4	DOWN	-8.75	-0.55
1455	Ogfr	OGFR	DOWN	-5.58	-0.51
1456	Arhgdia	GDIR1	DOWN	-15.82	-1.12
1457	Prpf8	PRP8	DOWN	-11.50	-1.31
1458	Npm3	NPM3	DOWN	-9.95	-0.82
1459	Tomm22	TOM22	DOWN	-7.84	-1.67
1460	Mydgf	MYDGF	DOWN	-4.77	-0.40
1461	Ssr2	SSRB	DOWN	-16.61	-1.78
1462	Lamtor1	LTOR1	DOWN	-3.79	-0.90
1463	Nudcd2	NUDC2	DOWN	-3.87	-0.62
1464	Pgls	6PGL	DOWN	-9.74	-0.82
1465	Mtap	MTAP	DOWN	-12.22	-0.83
1466	Uqcrq	QCR8	DOWN	-9.60	-0.70

1467	Ndufa2	NDUA2	DOWN	-1.15	-0.48
1468	Ntpcr	NTPCR	DOWN	-6.37	-1.24
1469	Chmp1b2	CH1B2	DOWN	-13.89	-1.06
1470	Gmfb	GMFB	DOWN	-10.41	-1.47
1471	Cotl1	COTL1	DOWN	-6.06	-0.27
1472	Trap1	TRAP1	DOWN	-3.91	-1.83
1473	Atp5pb	AT5F1	DOWN	-1.97	-0.56
1474	Rps21	RS21	DOWN	-2.07	-0.18
1475	Ppp6c	PPP6	DOWN	-8.62	-1.44
1476	Sec61b	SC61B	DOWN	-1.84	-0.21
1477	Txndc12	TXD12	DOWN	-2.99	-0.37
1478	Ywhab	1433B	DOWN	-18.98	-1.61
1479	Arl8b	ARL8B	DOWN	-7.46	-0.79
1480	Ifitm3	IFM3	DOWN	-16.01	-1.83
1481	Cyb5b	CYB5B	DOWN	-12.45	-1.46
1482	Ufc1	UFC1	DOWN	-2.01	-0.61
1483	Ppid	PPID	DOWN	-1.63	-0.18
1484	Hypk	HYPK	DOWN	-2.58	-0.60
1485	Rpl14	RL14	DOWN	-4.13	-0.23
1486	Slc25a11	M2OM	DOWN	-5.99	-1.75
1487	Uqcrfs1	UCRI	DOWN	-8.53	-0.79
1488	Carhsp1	CHSP1	DOWN	-1.90	-0.32
1489	Fam136a	F136A	DOWN	-0.92	-0.18
1490	Chchd3	MIC19	DOWN	-8.80	-0.65
1491	Snw1	SNW1	DOWN	-1.36	-0.19
1492	Smc1a	SMC1A	DOWN	-8.71	-0.66
1493	Arpc2	ARPC2	DOWN	-19.78	-1.47
1494	Smc3	SMC3	DOWN	-9.14	-0.98
1495	Tubb2b	TBB2B	DOWN	-5.63	-1.19
1496	Atic	PUR9	DOWN	-12.31	-0.54
1497	Snx2	SNX2	DOWN	-2.80	-0.15
1498	Pfdn1	PFD1	DOWN	-9.42	-1.08
1499	Pin4	PIN4	DOWN	-11.22	-1.15
1500	Rbm8a	RBM8A	DOWN	-10.93	-2.52
1501	Hnrnpa0	ROA0	DOWN	-7.97	-0.43
1502	Tmed5	TMED5	DOWN	-5.40	-1.80
1503	Cacybp	CYBP	DOWN	-11.82	-0.92
1504	Mrps28	RT28	DOWN	-13.97	-1.08
1505	Ssr1	SSRA	DOWN	-5.26	-2.44
1506	Chtop	CHTOP	DOWN	-4.73	-0.97
1507	Blvra	BIEA	DOWN	-7.84	-0.69
1508	Gins3	PSF3	DOWN	-9.91	-0.51
1509	Zcchc8	ZCHC8	DOWN	-6.15	-1.08
1510	Tomm34	TOM34	DOWN	-8.73	-0.90
1511	Spcs2	SPCS2	DOWN	-9.31	-1.17
1512	Uqcrc1	QCR1	DOWN	-16.37	-1.24
1513	Nsfl1c	NSF1C	DOWN	-4.46	-0.35
1514	Gars1	GARS	DOWN	-5.09	-0.29
1515	Rpl15	RL15	DOWN	-2.64	-0.16
1516	Shmt2	GLYM	DOWN	-15.76	-0.99
1517	Cs	CISY	DOWN	-18.11	-1.48
1518	Tomm70	TOM70	DOWN	-2.04	-0.38
1519	Rps19	RS19	DOWN	-9.15	-0.38
1520	Ube2v1	UB2V1	DOWN	-7.65	-1.87
1521	Pdhb	ODPB	DOWN	-0.96	-0.10
1522	Srsf9	SRSF9	DOWN	-4.75	-0.85
1523	Pbdc1	PBDC1	DOWN	-2.09	-0.86
1524	Hnrnpm	HNRPM	DOWN	-7.24	-0.35
1525	Lman1	LMAN1	DOWN	-4.23	-1.55
1526	Pgm1	PGM1	DOWN	-6.32	-0.86
1527	Oxct1	SCOT1	DOWN	-9.18	-0.73
1528	Prpsap1	KPRA	DOWN	-6.03	-1.71
1529	Cyc1	CY1	DOWN	-8.74	-0.59
1530	Tars1	SYTC	DOWN	-5.41	-0.70
1531	Lsm12	LSM12	DOWN	-12.72	-1.56
1532	Znf706	ZN706	DOWN	-6.67	-0.36
1533	Gatd3	GAL3A	DOWN	-13.83	-2.07
1534	Ciao2b	CIA2B	DOWN	-5.27	-1.80
1535	Cndp2	CNDP2	DOWN	-1.39	-0.15
1536	Vps28	VPS28	DOWN	-3.18	-0.67
1537	Tmed10	TMEDA	DOWN	-7.93	-0.60
1538	Rab1b	RAB1B	DOWN	-0.99	-0.34
1539	Chchd2	CHCH2	DOWN	-2.23	-1.48

1540	Chordc1	CHRD1	DOWN	-1.56	-0.38
1541	Rpl34	RL34	DOWN	-5.76	-0.53
1542	Bcas2	SPF27	DOWN	-11.96	-1.25
1543	Dlst	ODO2	DOWN	-14.65	-1.17
1544	Acp1	PPAC	DOWN	-1.37	-0.25
1545	Atp5f1d	ATPD	DOWN	-16.93	-1.22
1546	Sf3a3	SF3A3	DOWN	-1.21	-0.40
1547	Sec23b	SC23B	DOWN	-1.93	-0.99
1548	Ppil6	PPIL6	DOWN	-6.40	-1.66
1549	Idh3a	IDH3A	DOWN	-10.44	-0.76
1550	Nop56	NOP56	DOWN	-4.99	-0.33
1551	Lhpp	LHPP	DOWN	-5.09	-1.91
1552	Serpinb12	SPB12	DOWN	-10.96	-1.42
1553	Rpl22l1	RL22L	DOWN	-13.21	-1.26
1554	Rpl37	RL37	DOWN	-2.41	-0.60
1555	Timm50	TIM50	DOWN	-3.99	-1.29
1556	Arpc5l	ARP5L	DOWN	-5.57	-0.42
1557	Chmp4b	CHM4B	DOWN	-6.24	-0.40
1558	Eef1g	EF1G	DOWN	-15.32	-0.96
1559	Rexo2	ORN	DOWN	-12.19	-1.58
1560	Bola1	BOLA1	DOWN	-6.93	-1.25
1561	Gsdmd	GSDMD	DOWN	-4.51	-0.52
1562	Slirp	SLIRP	DOWN	-0.90	-0.60
1563	Snx5	SNX5	DOWN	-6.08	-0.51
1564	Efhd2	EFHD2	DOWN	-15.47	-1.69
1565	Tnfaip8l2	TP8L2	DOWN	-2.93	-0.97
1566	Atg7	ATG7	DOWN	-6.48	-0.98
1567	Tmem160	TM160	DOWN	-8.42	-1.56
1568	Gatm	GATM	DOWN	-1.64	-0.29
1569	Atp5po	ATPO	DOWN	-10.61	-0.79
1570	Uqcrc2	QCR2	DOWN	-11.34	-0.65
1571	Prkar1a	KAP0	DOWN	-5.63	-0.66
1572	Ap2b1	AP2B1	DOWN	-1.02	-0.28
1573	Lman2	LMAN2	DOWN	-8.00	-3.04
1574	Pgam1	PGAM1	DOWN	-12.14	-1.00
1575	Xrn2	XRN2	DOWN	-15.17	-1.43
1576	Tmem43	TMM43	DOWN	-12.12	-1.98
1577	Eif3k	EIF3K	DOWN	-5.71	-0.82
1578	Pycr3	P5CR3	DOWN	-5.93	-0.70
1579	Pgd	6PGD	DOWN	-9.30	-0.29
1580	Trmt112	TR112	DOWN	-4.84	-0.75
1581	Ciao2a	CIA2A	DOWN	-5.59	-0.60
1582	Paics	PUR6	DOWN	-1.68	-0.55
1583	Ethe1	ETHE1	DOWN	-17.80	-1.65
1584	Cyb5r3	NB5R3	DOWN	-18.29	-1.59
1585	Akr1e2	AKCL2	DOWN	-19.96	-1.73
1586	Etfb	ETFB	DOWN	-7.84	-0.38
1587	Atp5pd	ATP5H	DOWN	-4.29	-0.15
1588	Emc7	EMC7	DOWN	-14.96	-1.14
1589	Pycard	ASC	DOWN	-4.57	-0.33
1590	Pik3ap1	BCAP	DOWN	-0.86	-0.18
1591	Vps35	VPS35	DOWN	-5.89	-1.47
1592	Ehd4	EHD4	DOWN	-7.13	-0.60
1593	Set	SET	DOWN	-5.87	-0.38
1594	Stx12	STX12	DOWN	-2.43	-0.39
1595	Mesd	MESD	DOWN	-5.95	-1.07
1596	Cse1l	XPO2	DOWN	-4.81	-0.50
1597	Scamp2	SCAM2	DOWN	-6.44	-1.10
1598	Inpp5d	SHIP1	DOWN	-1.61	-0.28
1599	Sdf2l1	SDF2L	DOWN	-2.01	-0.30
1600	Anp32b	AN32B	DOWN	-9.17	-0.94
1601	Brd4	BRD4	DOWN	-1.89	-0.79
1602	Dkc1	DKC1	DOWN	-12.04	-1.23
1603	Rnf114	RN114	DOWN	-9.08	-1.47
1604	Jph3	JPH3	DOWN	-3.46	-1.10
1605	Tmod3	TMOD3	DOWN	-2.99	-0.17
1606	Plek	PLEK	DOWN	-10.66	-1.39
1607	Ide	IDE	DOWN	-3.60	-1.60
1608	Dync1h1	DYHC1	DOWN	-3.27	-0.23
1609	Stk3	STK3	DOWN	-4.77	-0.73
1610	Gtf2ird1	GT2D1	DOWN	-9.28	-2.24
1611	Naip6	BIR1F	DOWN	-0.90	-0.49
1612	Prmt1	ANM1	DOWN	-8.76	-0.80

1613	Dazap1	DAZP1	DOWN	-14.68	-1.68
1614	Akr1a1	AK1A1	DOWN	-7.98	-0.48
1615	Flii	FLII	DOWN	-5.98	-0.85
1616	Rpl38	RL38	DOWN	-14.87	-0.97
1617	Sh3bgrl	SH3L1	DOWN	-2.25	-0.40
1618	Sh3glb1	SHLB1	DOWN	-1.52	-0.18
1619	Myg1	MYG1	DOWN	-4.86	-0.42
1620	Ybx3	YBOX3	DOWN	-1.34	-0.21
1621	Mrpl39	RM39	DOWN	-2.19	-0.74
1622	Tmod2	TMOD2	DOWN	-13.08	-1.68
1623	Hyou1	HYOU1	DOWN	-15.93	-0.84
1624	Adrm1	ADRM1	DOWN	-20.43	-1.57
1625	Fmnl1	FMNL1	DOWN	-2.97	-0.21
1626	Sart3	SART3	DOWN	-13.93	-1.17
1627	Aldh9a1	AL9A1	DOWN	-12.32	-0.79
1628	Cd2ap	CD2AP	DOWN	-2.14	-0.20
1629	Git2	GIT2	DOWN	-6.24	-1.09
1630	Nt5c	NT5C	DOWN	-4.66	-0.38
1631	Stap1	STAP1	DOWN	-1.55	-0.16
1632	Usp14	UBP14	DOWN	-14.07	-0.65
1633	Znf207	ZN207	DOWN	-3.91	-0.19
1634	Edf1	EDF1	DOWN	-4.07	-1.06
1635	Txnrd1	TRXR1	DOWN	-3.54	-0.55
1636	Rhoa	RHOA	DOWN	-9.78	-2.04
1637	Acsl4	ACSL4	DOWN	-5.56	-0.43
1638	Psma6	PSA6	DOWN	-10.22	-1.12
1639	Prep	PPCE	DOWN	-4.43	-1.12
1640	Pin1	PIN1	DOWN	-3.94	-0.41
1641	Lsm4	LSM4	DOWN	-6.78	-2.02
1642	Copg2	COPG2	DOWN	-10.92	-1.66
1643	Plec	PLEC	DOWN	-20.13	-0.74
1644	Cnpy2	CNPY2	DOWN	-13.00	-0.95
1645	Slc25a13	S2513	DOWN	-0.86	-0.12
1646	Ehd1;Ehd3	EHD1 ;EHD3	DOWN	-2.11	-0.37
1647	Vapa;Vapb	VAPA ;VAPB	DOWN	-8.21	-2.31
1648	Clic4	CLIC4	DOWN	-6.16	-0.34
1649	Rdh11	RDH11	DOWN	-8.99	-0.79
1650	Qki	QKI	DOWN	-11.04	-0.85
1651	Vps29	VPS29	DOWN	-2.76	-1.39
1652	Slc25a10	DIC	DOWN	-1.00	-0.53
1653	Fhl3	FHL3	DOWN	-2.46	-0.51
1654	Gyg1	GLYG	DOWN	-10.32	-0.58
1655	Comp	COMP	DOWN	-7.96	-3.38
1656	Esd	ESTD	DOWN	-14.70	-0.78
1657	Dstn	DEST	DOWN	-7.27	-0.98
1658	Sec11a	SC11A	DOWN	-2.37	-1.13
1659	Tmed2	TMED2	DOWN	-8.04	-1.19
1660	Srsf10	SRS10	DOWN	-3.21	-0.77
1661	Acot9	ACOT9	DOWN	-1.61	-0.52
1662	Sqor	SQOR	DOWN	-6.91	-0.56
1663	Psma4	PSA4	DOWN	-7.08	-0.82
1664	Psmb3	PSB3	DOWN	-3.29	-1.13
1665	Psmb2	PSB2	DOWN	-12.10	-1.56
1666	Psma1	PSA1	DOWN	-7.93	-0.47
1667	Plp2	PLP2	DOWN	-9.25	-2.47
1668	Myo1c	MYO1C	DOWN	-7.58	-0.78
1669	Ruvbl2	RUVB2	DOWN	-2.70	-0.50
1670	Ak3	KAD3	DOWN	-11.77	-1.44
1671	Skp1	SKP1	DOWN	-3.35	-1.41
1672	Pfkp	PFKAP	DOWN	-1.77	-0.15
1673	Stub1	CHIP	DOWN	-8.41	-2.30
1674	Eif4h	IF4H	DOWN	-4.95	-0.59
1675	Coro1b	COR1B	DOWN	-12.19	-1.75
1676	Suclg1	SUCA	DOWN	-1.10	-0.12
1677	Uchl5	UCHL5	DOWN	-5.23	-1.42
1678	Ctsz	CATZ	DOWN	-17.94	-1.29
1679	Fam50a	FA50A	DOWN	-2.22	-0.50
1680	Arpc1b	ARC1B	DOWN	-13.17	-0.78
1681	Asah1	ASAH1	DOWN	-4.85	-2.02
1682	Vapa	VAPA	DOWN	-1.97	-0.83
1683	Timm9	TIM9	DOWN	-1.44	-0.44
1684	Timm8a1	TIM8A	DOWN	-12.63	-0.88
1685	Bub3	BUB3	DOWN	-5.25	-1.12

1686	Tagln2	TAGL2	DOWN	-15.16	-1.08
1687	Psmd13	PSD13	DOWN	-9.64	-0.93
1688	Ehd1	EHD1	DOWN	-10.05	-0.83
1689	Npc2	NPC2	DOWN	-8.30	-1.58
1690	Lipa	LICH	DOWN	-5.15	-1.12
1691	Twf2	TWF2	DOWN	-13.38	-1.70
1692	Bpnt1	BPNT1	DOWN	-3.06	-0.67
1693	Aldh18a1	P5CS	DOWN	-12.35	-0.89
1694	Slc7a5	LAT1	DOWN	-2.24	-0.77
1695	Sumo3	SUMO3	DOWN	-1.78	-0.44
1696	Uba2	SAE2	DOWN	-11.98	-1.09
1697	Atp6v1c1	VATC1	DOWN	-8.29	-0.69
1698	Ddx39b	DX39B	DOWN	-2.03	-0.33
1699	Ndufa7	NDUA7	DOWN	-2.80	-0.58
1700	Clic1	CLIC1	DOWN	-18.06	-0.93
1701	Vars1	SYVC	DOWN	-7.96	-0.84
1702	Deaf1	DEAF1	DOWN	-15.16	-1.68
1703	Uso1	USO1	DOWN	-1.02	-0.16
1704	Hnrnpc	HNRPC	DOWN	-5.38	-0.26
1705	Suclg2	SUCB2	DOWN	-2.91	-0.36
1706	Crlf3	CRLF3	DOWN	-5.42	-1.89
1707	Psma7	PSA7	DOWN	-9.74	-0.53
1708	Psma5	PSA5	DOWN	-14.19	-1.28
1709	Hnrnpf	HNRPF	DOWN	-12.50	-0.92
1710	Plpbp	PLPHP	DOWN	-6.33	-0.49
1711	Sart1	SNUT1	DOWN	-0.89	-0.96
Corundum vs. Plasmapore					
1	Mpeg1	MPEG1	UP	-3.47	0.24
2	Sh3pxd2b	SPD2B	UP	-6.46	1.59
3	Tpx2	TPX2	UP	-6.84	1.36
4	Myh10	MYH10	UP	-7.54	0.50
5	Itih4	ITIH4	UP	-12.19	0.82
6	Cad	PYR1	UP	-8.19	2.16
7	Adgrg4	AGRG4	UP	-15.13	1.06
8	Osbpl8	OSBL8	UP	-3.75	0.37
9	H2ac11	H2A1B	UP	-14.17	0.83
10	Hmcn1	HMCN1	UP	-10.61	1.04
11	Safb	SAFB1	UP	-6.22	2.12
12	Bin2	BIN2	UP	-4.61	0.35
13	Bin1;Bin2	BIN1 ;BIN2	UP	-7.39	1.55
14	Sbf2	MTMRD	UP	-5.39	0.93
15	Map3k19	M3K19	UP	-17.54	1.36
16	Nolc1	NOLC1	UP	-12.19	1.00
17	Numa1	NUMA1	UP	-13.79	1.29
18	Tpr	TPR	UP	-1.75	0.46
19	QNG1	QNG1	UP	-1.17	0.59
20	Rnpepl1	RNPL1	UP	-2.89	0.81
21	Hk2	HXK2	UP	-3.90	0.59
22	Sec22b	SC22B	UP	-1.33	0.75
23	Dpysl2	DPYL2	UP	-15.38	0.62
24	Emd	EMD	UP	-4.58	1.22
25	Alyref	THOC4	UP	-14.94	1.03
26	Clta	CLCA	UP	-9.49	0.68
27	Arg2	ARGI2	UP	-6.85	2.41
28	Dld	DLDH	UP	-9.30	0.45
29	Tcof1	TCOF	UP	-4.42	0.39
30	Prkcsh	GLU2B	UP	-10.44	0.45
31	Prdx4	PRDX4	UP	-9.16	0.49
32	Prdx1;Prdx4	PRDX1 ;PRDX4	UP	-4.70	0.30
33	Eef2;Eftud2	EF2 ;U5S1	UP	-10.96	0.39
34	Aip	AIP	UP	-8.14	1.63
35	Atox1	ATOX1	UP	-6.93	0.20
36	Degs1	DEGS1	UP	-4.10	0.39
37	Man2b1	MA2B1	UP	-7.92	0.73
38	Rpl21	RL21	UP	-1.51	0.14
39	Gclm	GSH0	UP	-12.94	1.24
40	Phb2	PHB2	UP	-9.05	0.45
41	Atp5if1	ATIF1	UP	-10.91	0.87
42	Psmd4	PSMD4	UP	-3.36	0.34
43	Purb	PURB	UP	-8.32	0.57
44	Srsf5	SRSF5	UP	-2.16	0.17
45	Srsf4	SRSF4	UP	-3.18	1.42
46	Kpna4	IMA3	UP	-10.11	2.00

47	Anp32a;Anp32b	AN32A ;AN32B	UP	-10.41	0.71
48	Fkbp8	FKBP8	UP	-2.66	0.57
49	Neu1	NEUR1	UP	-5.30	1.47
50	Pnn	PININ	UP	-7.37	1.72
51	Hnrnph1	HNRH1	UP	-7.33	0.59
52	Hnrnpf	HNRH1	UP	-8.58	0.75
53	Calu	CALU	UP	-1.79	0.11
54	Psmb10	PSB10	UP	-15.38	1.37
55	Ddost	OST48	UP	-2.08	0.19
56	Man2b2	MA2B2	UP	-3.44	0.81
57	Stk10	STK10	UP	-3.70	0.79
58	Eif6	IF6	UP	-5.76	0.18
59	Rpl35a	RL35A	UP	-6.33	0.73
60	Dhx9	DHX9	UP	-11.04	0.64
61	Ncf2	NCF2	UP	-8.72	0.78
62	Pip4k2a	PI42A	UP	-4.50	2.03
63	Aif1	AIF1	UP	-1.54	0.76
64	Pgam2	PGAM2	UP	-15.00	0.90
65	Pgam1	PGAM1	UP	-14.87	1.04
66	Eef1b	EF1B	UP	-19.65	1.47
67	Eef1b;Eef1d	EF1B ;EF1D	UP	-9.91	1.44
68	Epb41l2	E41L2	UP	-6.59	0.73
69	Ctss	CATS	UP	-1.06	0.09
70	Vamp8	VAMP8	UP	-2.17	0.22
71	Psma3	PSA3	UP	-1.25	0.12
72	Stx7	STX7	UP	-8.67	0.58
73	Wdr1	WDR1	UP	-8.71	0.32
74	Dync1i2	DC1I2	UP	-8.63	0.89
75	Ppt1	PPT1	UP	-8.34	0.37
76	Hnrnpa2b1	ROA2	UP	-12.93	0.54
77	Psmc3	PRS6A	UP	-1.49	0.31
78	Idh1	IDHC	UP	-4.19	0.36
79	Lgmn	LGMN	UP	-2.46	0.81
80	Afm	AFAM	UP	-10.05	0.98
81	Mtco2	COX2	UP	-9.16	1.86
82	C3	CO3	UP	-11.75	0.68
83	C4b	CO4B	UP	-4.85	1.16
84	B2m	B2MG	UP	-3.94	0.20
85	H2-L	HA1L	UP	-13.52	1.29
86	H2-D1;H2-L	HA11 ;HA1L	UP	-3.17	0.54
87	H2-D1	HA12	UP	-14.26	1.31
88	Hba	HBA	UP	-10.52	0.43
89	Hbb-b1	HBB1	UP	-11.91	0.88
90	Mt2	MT2	UP	-11.80	1.48
91	Mt1	MT1	UP	-13.83	1.66
92	Mtatp8	ATP8	UP	-16.99	2.61
93	Iap	IGEB	UP	-12.29	0.71
94	Gfap;Vim	GFAP ;VIME	UP	-2.57	0.20
95	Cd74	HG2A	UP	-1.63	0.31
96	Aldoc	ALDOC	UP	-10.97	1.32
97	Aldoa;Aldoc	ALDOA ;ALDOC	UP	-14.47	1.35
98	Aldoa	ALDOA	UP	-22.67	0.88
99	Itgam	ITAM	UP	-4.63	0.43
100	Myl1;Myl3	MYL1 ;MYL3	UP	-14.92	1.22
101	Ldha	LDHA	UP	-11.02	0.42
102	C9	CO9	UP	-8.64	0.82
103	Gpi	G6PI	UP	-2.71	0.11
104	Alb	ALBU	UP	-15.07	0.77
105	Hsp90aa1	HS90A	UP	-4.72	0.16
106	Hsp90aa1;Hsp90ab1	HS90A ;HS90B	UP	-11.72	0.43
107	Pdia4	PDIA4	UP	-7.70	0.18
108	Hsp90b1	ENPL	UP	-12.39	0.26
109	Hsp90ab1;Hsp90b1	ENPL ;HS90B	UP	-12.91	0.59
110	Sod1	SODC	UP	-17.67	0.73
111	Kras;Nras	RASK ;RASN	UP	-9.17	2.27
112	Gnai2	GNAI2	UP	-15.34	0.71
113	Polr2a	RPB1	UP	-5.17	0.85
114	Lyz2	LYZ2	UP	-2.74	0.13
115	Lyz1;Lyz2	LYZ1 ;LYZ2	UP	-8.59	0.91
116	Pgk1;Pgk2	PGK1 ;PGK2	UP	-12.57	0.61
117	Itgb1	ITB1	UP	-6.25	0.44
118	P4hb	PDIA1	UP	-17.48	0.56
119	Ncl	NUCL	UP	-14.14	0.38

120	Pgk1	PGK1	UP	-21.43	1.14
121	Junb	JUNB	UP	-11.33	2.55
122	H2az1;H2az2	H2AV ;H2AZ	UP	-4.75	0.26
123	Pet117	PT117	UP	-11.14	2.40
124	Ifi204	IFI4	UP	-6.78	0.43
125	Eef1a1	EF1A1	UP	-17.02	0.83
126	Eef1a1;Eef1a2	EF1A1 ;EF1A2	UP	-9.74	0.29
127	Ctsb	CATB	UP	-5.86	0.13
128	Eif4a1;Eif4a2Eif4a3	IF4A1 ;IF4A2IF4A3	UP	-7.59	0.42
129	Txn	THIO	UP	-9.88	0.91
130	Tcea1	TCEA1	UP	-13.25	0.62
131	Cd14	CD14	UP	-10.72	1.11
132	H2bc14	H2B1B	UP	-7.90	0.58
133	H2bc14	H2B1M	UP	-19.94	0.86
134	Fn1	FINC	UP	-4.70	1.07
135	Gpx1	GPX1	UP	-3.58	0.96
136	Hsp90ab1	HS90B	UP	-11.68	2.01
137	Itga5	ITA5	UP	-13.30	0.36
138	Tcp1	TCPA	UP	-5.55	0.70
139	App	A4	UP	-6.50	0.24
140	Cox5a	COX5A	UP	-8.03	1.66
141	Cd5	CD5	UP	-17.70	1.88
142	Umps	UMPS	UP	-9.72	0.86
143	Icam1	ICAM1	UP	-5.15	0.72
144	Calr	CALR	UP	-3.43	1.62
145	Lmnb1	LMNB1	UP	-8.88	0.31
146	Lmnb1;Lmnb2	LMNB1 ;LMNB2	UP	-9.03	0.55
147	Lmna	LMNA	UP	-7.90	2.80
148	Anxa6	ANXA6	UP	-17.17	1.40
149	Glul	GLNA	UP	-4.70	0.22
150	Bpgm	PMGE	UP	-11.73	2.27
151	Cd44	CD44	UP	-10.72	0.81
152	Nme1	NDKA	UP	-15.58	1.48
153	Nme1;Nme2	NDKA ;NDKB	UP	-7.12	0.40
154	H1-2;H1-3;H1-4;H1-5	H12 ;H13 ;H14 ;H15	UP	-13.24	0.69
155	H1-2;H1-3;H1-4	H12 ;H13 ;H14	UP	-11.14	1.05
156	H1-2;H1-3	H12 ;H13	UP	-13.40	0.95
157	Lgals1	LEG1	UP	-2.42	0.19
158	Lgals3	LEG3	UP	-4.31	0.12
159	Srp14	SRP14	UP	-10.43	0.55
160	Hspa1l	HS71L	UP	-8.64	2.43
161	Hspa1	BIP	UP	-7.05	0.49
162	Hspa2;Hspa8	HSP72 ;HSP7C	UP	-8.25	0.29
163	Ctsa	PPGB	UP	-12.74	0.44
164	Gapdh	G3P	UP	-17.13	0.81
165	Lamp2	LAMP2	UP	-16.27	0.90
166	Hspa2;Hspa8	HSP72 ;HSP7C	UP	-7.55	0.43
167	Eno1	ENOA	UP	-12.62	0.41
168	Eno1;Eno2	ENOA ;ENOG	UP	-12.67	0.36
169	Eno2;Eno3	ENOB ;ENOG	UP	-4.71	0.42
170	Ap2a1	AP2A1	UP	-11.45	3.23
171	Ppia	PPIA	UP	-9.03	2.27
172	Tpi1	TPIS	UP	-19.66	1.32
173	Slc2a1	GTR1	UP	-22.03	0.99
174	Pcna	PCNA	UP	-4.54	1.13
175	Ctsd	CATD	UP	-13.19	0.74
176	Cox4i1	COX41	UP	-14.11	0.63
177	Lsp1	LSP1	UP	-7.36	0.51
178	Hspa5	BIP	UP	-11.39	0.77
179	Hexb	HEXB	UP	-15.88	0.33
180	Prdx3	PRDX3	UP	-5.61	0.31
181	Vim	VIME	UP	-6.04	0.29
182	Fcer1g	FCERG	UP	-24.40	0.91
183	Plg	PLMN	UP	-14.10	0.42
184	Tpm3	TPM3	UP	-5.32	0.48
185	Tpm1;Tpm3	TPM1 ;TPM3	UP	-14.60	1.79
186	Tpm4	TPM4	UP	-14.88	0.80
187	Gc	VTDB	UP	-8.58	0.66
188	Cd72	CD72	UP	-6.71	1.57
189	Rarb	RARB	UP	-1.29	0.23
190	Eif3a	EIF3A	UP	-1.73	0.83
191	Cbx3	CBX3	UP	-10.55	0.94
192	Cbx3;Cbx5	CBX3 ;CBX5	UP	-7.28	0.31

193	Pcmt1	PIMT	UP	-6.18	2.05
194	Cat	CATA	UP	-9.87	2.88
195	Capg	CAPG	UP	-10.55	0.39
196	Lta4h	LKHA4	UP	-21.06	1.68
197	Impdh2	IMDH2	UP	-11.32	1.73
198	Impdh1;Impdh2	IMDH1 ;IMDH2	UP	-8.05	0.38
199	Rps2	RS2	UP	-8.30	0.73
200	Lyn	LYN	UP	-5.81	0.21
201	Tln1	TLN1	UP	-4.77	0.82
202	Ezr	EZRI	UP	-12.48	0.33
203	Msn	MOES	UP	-3.26	0.19
204	Msn;Rdx	MOES ;RADI	UP	-11.24	0.29
205	U2af2	U2AF2	UP	-5.95	0.31
206	Sars1	SYSC	UP	-2.93	0.16
207	Fkbp1a	FKB1A	UP	-4.38	0.27
208	Snrpb;Snrpn	RSMB ;RSMN	UP	-9.35	0.56
209	Gna13	GNA13	UP	-12.82	0.90
210	H2ax	H2AX	UP	-15.76	2.80
211	Pdia3	PDIA3	UP	-17.26	1.49
212	Cebpb	CEBPB	UP	-19.29	0.70
213	Apex1	APEX1	UP	-10.74	2.18
214	Nap1l1	NP1L1	UP	-4.78	0.80
215	Nap1l1;Nap1l4	NP1L1 ;NP1L4	UP	-1.32	0.13
216	Mug1	MUG1	UP	-14.29	1.69
217	Grn	GRN	UP	-14.67	1.03
218	Prkcd	KPCD	UP	-12.65	0.57
219	Pabpc1	PABP1	UP	-2.75	1.09
220	Hexa	HEXA	UP	-14.75	0.39
221	Nedd8	NEDD8	UP	-1.67	0.11
222	Ahsg	FETUA	UP	-1.02	0.43
223	Oat	OAT	UP	-12.49	1.06
224	Alox5ap	AL5AP	UP	-1.94	0.12
225	Fkbp4	FKBP4	UP	-0.94	0.06
226	Hmgb2	HMGB2	UP	-13.90	0.63
227	Hmgb1;Hmgb2	HMGB1 ;HMGB2	UP	-9.91	0.54
228	Aimp1	AIMP1	UP	-18.56	1.93
229	Cd68	CD68	UP	-1.43	0.08
230	Scp2	SCP2	UP	-7.70	1.07
231	Serpinc1	ANT3	UP	-9.43	1.31
232	Wars1	SYWC	UP	-10.75	1.11
233	Ranbp1	RANG	UP	-12.79	1.25
234	Mif	MIF	UP	-13.23	0.72
235	Rab21	RAB21	UP	-21.14	2.08
236	Ppard	PPARD	UP	-2.73	1.06
237	Prdx1	PRDX1	UP	-0.99	0.27
238	Rpl18	RL18	UP	-15.78	0.57
239	Gnl1	GNL1	UP	-1.26	0.07
240	Hspa9	GRP75	UP	-6.81	1.54
241	Dnm2;Dnm3	DYN2 ;DYN3	UP	-11.68	0.37
242	Tkt	TKT	UP	-4.55	1.92
243	Csk	CSK	UP	-13.05	0.42
244	Cd86	CD86	UP	-1.39	0.16
245	Septin2	45902	UP	-4.33	0.69
246	Cox6a1	CX6A1	UP	-4.99	0.26
247	H1-3;H1-4;H1-5	H13 ;H14 ;H15	UP	-6.72	1.51
248	H1-1	H11	UP	-10.49	2.03
249	H1-5	H15	UP	-10.81	1.54
250	Akr1b1	ALDR	UP	-3.94	0.18
251	Akr1b8	ALD2	UP	-3.74	0.10
252	Fkbp2	FKBP2	UP	-5.73	0.27
253	Rangap1	RAGP1	UP	-4.49	0.78
254	Nsf	NSF	UP	-6.78	0.63
255	Psmc2	PRS7	UP	-3.34	0.37
256	Adss2	PURA2	UP	-2.54	0.19
257	Stt3a	STT3A	UP	-8.89	0.54
258	Tes	TES	UP	-3.63	0.86
259	Aldh2	ALDH2	UP	-6.09	0.55
260	Capza1;Capza2	CAZA1 ;CAZA2	UP	-8.82	0.31
261	Capzb	CAPZB	UP	-5.00	1.37
262	Srprb	SRPRB	UP	-7.11	0.45
263	Rpl29	RL29	UP	-6.05	0.53
264	Rplp1	RLA1	UP	-8.75	0.97
265	Rpl13	RL13	UP	-18.39	2.04

266	Rpl36	RL36	UP	-16.19	1.03
267	Eif1	EIF1	UP	-11.83	1.33
268	Anxa5	ANXA5	UP	-1.39	1.02
269	Tbca	TBCA	UP	-3.00	0.06
270	Lmna	LMNA	UP	-4.12	1.93
271	Alox5	LOX5	UP	-7.36	0.14
272	Hnrnpa1	ROA1	UP	-3.74	0.42
273	Hcls1	HCLS1	UP	-14.50	0.67
274	Mcm4	MCM4	UP	-9.91	0.60
275	Psma2	PSA2	UP	-6.86	2.90
276	Srp9	SRP09	UP	-1.37	0.32
277	Arsb	ARSB	UP	-2.36	0.77
278	Acadl	ACADL	UP	-12.83	0.67
279	Rpl9	RL9	UP	-5.82	0.34
280	Dynlt1	DYLT1	UP	-2.52	0.16
281	Hdgf	HDGF	UP	-2.98	0.81
282	Kpna2	IMA1	UP	-2.02	0.14
283	Pkm	KPYM	UP	-1.36	0.33
284	Ndufs6	NDUS6	UP	-17.83	0.69
285	Rpl10a	RL10A	UP	-1.11	0.85
286	Dbt	ODB2	UP	-14.62	0.62
287	Hccs	CCHL	UP	-10.94	1.49
288	Pitpna	PIPNA	UP	-5.58	1.59
289	Cnbp	CNBP	UP	-1.42	0.22
290	Dnajc2	DNJC2	UP	-18.31	1.51
291	Stmn1;Stmn2	STMN1 ;STMN2	UP	-1.22	0.85
292	Msh6	MSH6	UP	-8.62	0.60
293	Rad23b	RD23B	UP	-3.38	0.73
294	Acod1	IRG1	UP	-3.72	0.45
295	Sh3bp1	3BP1	UP	-8.98	0.83
296	Lrpap1	AMRP	UP	-3.06	1.36
297	Stmn2	STMN2	UP	-11.62	0.63
298	Atp5mf	ATPK	UP	-1.80	2.29
299	Gfer	ALR	UP	-2.28	0.11
300	Atp5f1e	ATP5E	UP	-10.40	1.86
301	Cox6b1	CX6B1	UP	-2.04	0.58
302	Cyb5a	CYB5	UP	-13.50	0.77
303	Atp5f1b	ATPB	UP	-4.59	0.67
304	Pdcd5	PDCD5	UP	-17.09	0.77
305	Exosc10	EXOSX	UP	-1.18	0.21
306	Erp29	ERP29	UP	-13.85	0.99
307	Eef1d	EF1D	UP	-7.78	0.50
308	Eef2	EF2	UP	-10.99	0.57
309	Tpm1	TPM1	UP	-13.10	0.40
310	Eif5	IF5	UP	-7.68	1.91
311	Rin3	RIN3	UP	-2.75	0.69
312	Arpc4	ARPC4	UP	-7.57	2.02
313	Eif3e	EIF3E	UP	-10.00	0.31
314	Nploc4	NPL4	UP	-8.32	0.73
315	Actb;Actg1	ACTB ;ACTG	UP	-3.65	0.87
316	Actc1;Actg1	ACTG ;ACTS	UP	-8.20	0.41
317	Cdc42	CDC42	UP	-19.60	1.22
318	Rps20	RS20	UP	-5.18	0.22
319	Rab8b	RAB8B	UP	-14.89	0.72
320	Actr2	ARP2	UP	-7.20	0.39
321	Rpl37a	RL37A	UP	-10.19	0.56
322	Arf4	ARF4	UP	-5.23	0.28
323	Arf4;Arf5	ARF4 ;ARF5	UP	-1.11	0.44
324	Vbp1	PFD3	UP	-12.10	1.26
325	Copz1	COPZ1	UP	-8.17	2.29
326	Sumo2;Sumo3	SUMO2 ;SUMO3	UP	-0.96	0.39
327	Ywhab	1433B	UP	-0.97	0.10
328	Ywhag;Ywhah	1433F ;1433G	UP	-13.63	2.58
329	Ywhah	1433G	UP	-10.91	1.05
330	Timm10	TIM10	UP	-1.75	0.60
331	Timm13	TIM13	UP	-3.49	1.17
332	Timm8b	TIM8B	UP	-6.96	0.40
333	Rps7	RS7	UP	-3.48	0.88
334	Ppp1ca	PP1A	UP	-1.43	0.06
335	Rps15a	RS15A	UP	-4.81	0.27
336	Rps14	RS14	UP	-7.02	0.28
337	Rps23	RS23	UP	-11.00	0.70
338	Rps18	RS18	UP	-3.71	0.16

339	Rps29	RS29	UP	-12.93	0.80
340	Rps13	RS13	UP	-17.43	2.16
341	Snrpf	RUXF	UP	-0.98	0.08
342	Snrpg	RUXG	UP	-5.06	0.89
343	Lsm6	LSM6	UP	-1.66	0.08
344	Snrpd3	SMD3	UP	-4.20	0.98
345	Dynlrb1	DLRB1	UP	-7.61	0.54
346	Eef1a2	EF1A2	UP	-7.29	2.49
347	Rps4x	RS4X	UP	-12.24	2.10
348	Rpl23a	RL23A	UP	-19.81	0.73
349	Rps6	RS6	UP	-8.79	0.50
350	Atp6v1b2	VATB2	UP	-0.98	0.09
351	Rpl23	RL23	UP	-12.81	0.63
352	Rap1a;Rap1b	RAP1A ;RAP1B	UP	-10.86	0.31
353	Rps15	RS15	UP	-2.39	0.33
354	Rps24	RS24	UP	-10.07	0.90
355	Rps25	RS25	UP	-6.95	1.39
356	Rps28	RS28	UP	-10.41	0.84
357	Fau	RS30	UP	-17.69	1.66
358	Elob	ELOB	UP	-16.48	0.99
359	Gnb1	GBB1	UP	-3.41	0.78
360	Rpl30	RL30	UP	-8.04	1.53
361	Rpl39	RL39	UP	-9.89	0.43
362	Rpl31	RL31	UP	-4.35	1.09
363	Rps3	RS3	UP	-16.15	1.02
364	Rpl32	RL32	UP	-5.12	0.10
365	Rpl8	RL8	UP	-9.75	0.92
366	Ybx1	YBOX1	UP	-14.62	0.64
367	Pfn1	PROF1	UP	-5.67	0.46
368	Rps27a	RS27A	UP	-7.30	0.24
369	Rac1;Rac2	RAC1 ;RAC2	UP	-11.81	1.67
370	Hspa8	HSP7C	UP	-14.23	0.65
371	Dnaja1	DNJA1	UP	-18.86	0.66
372	Hspd1	CH60	UP	-1.32	0.46
373	Mapk1	MK01	UP	-16.61	0.53
374	Ywhab;Ywhaq;Ywhaz	1433B ;1433T ;1433Z	UP	-12.38	0.89
375	Sumo1	SUMO1	UP	-13.92	1.39
376	Dynll1;Dynll2	DYL1 ;DYL2	UP	-6.63	0.49
377	Gng2	GBG2	UP	-2.02	0.29
378	Eif5a	IF5A1	UP	-5.75	0.86
379	Crip1	CRIP1	UP	-12.20	0.93
380	Phb1	PHB1	UP	-18.77	1.83
381	Acta1;Actc1	ACTC ;ACTS	UP	-6.92	0.21
382	Tuba1c;Tuba4a	TBA1C ;TBA4A	UP	-15.18	1.25
383	Tubal3	TBAL3	UP	-1.35	0.19
384	Tubb4b	TBB4B	UP	-9.17	0.61
385	Tubb4b;Tubb5	TBB4B ;TBB5	UP	-13.89	0.73
386	Tubb2a	TBB2A	UP	-11.14	2.49
387	Tubb5	TBB5	UP	-12.81	0.49
388	Tubb5	TBB5	UP	-11.22	0.81
389	Tubb3	TBB3	UP	-9.94	1.38
390	Tubb4b;Tubb6	TBB4B ;TBB6	UP	-15.41	1.00
391	Tuba1c;Tuba8	TBA1C ;TBA8	UP	-4.90	2.62
392	Kpnb1	IMB1	UP	-1.04	0.85
393	Psmb7	PSB7	UP	-14.83	0.61
394	Pkn1	PKN1	UP	-1.97	0.32
395	Mpp1	EM55	UP	-10.43	2.09
396	Pebp1	PEBP1	UP	-6.39	1.45
397	Tial1	TIAR	UP	-7.91	0.65
398	Hnrnph2	HNRH2	UP	-4.40	1.73
399	Hint1	HINT1	UP	-5.08	1.61
400	Elavl1	ELAV1	UP	-4.68	0.85
401	Vasp	VASP	UP	-7.11	0.38
402	Naca	NACAM	UP	-11.14	1.02
403	Gaa	LYAG	UP	-5.69	0.20
404	Cct7	TCPH	UP	-1.03	0.21
405	Cct2	TCPB	UP	-6.23	0.26
406	Cct5	TCPE	UP	-2.91	0.14
407	Cct6a	TCPZ	UP	-3.98	0.14
408	Cct3	TCPG	UP	-5.02	0.17
409	Wnk1	WNK1	UP	-5.77	0.10
410	Phf5a	PHF5A	UP	-5.40	2.31
411	Rpl36a	RL36A	UP	-10.64	1.57

412	Rhog	RHOG	UP	-7.16	0.68
413	Rpl19	RL19	UP	-7.12	0.37
414	Srsf3	SRSF3	UP	-11.09	0.72
415	Serpinf1	PEDF	UP	-13.35	0.72
416	Csrp1	CSRP1	UP	-3.23	0.99
417	Rps3a	RS3A	UP	-0.93	0.21
418	Bop1	BOP1	UP	-12.52	0.48
419	Rps5	RS5	UP	-11.38	1.12
420	Gclc	GSH1	UP	-16.47	1.09
421	Smarcc1	SMRC1	UP	-6.55	1.17
422	Sirpa	SHPS1	UP	-3.91	1.27
423	Fh	FUMH	UP	-1.17	0.27
424	Fxyd5	FXYD5	UP	-6.34	0.22
425	G3bp1	G3BP1	UP	-1.34	0.72
426	Rbbp6	RBBP6	UP	-12.02	0.87
427	Tubb5	TBB5	UP	-7.86	0.62
428	Tubb2a	TBB2A	UP	-9.89	0.44
429	Tubb5	TBB5	UP	-14.12	1.16
430	Uqcrh	QCR6	UP	-1.01	0.80
431	Apoa1	APOA1	UP	-9.17	0.75
432	Nme2	NDKB	UP	-15.17	0.72
433	Vcp	TERA	UP	-3.84	0.20
434	C1qc	C1QC	UP	-12.40	0.30
435	Nucb1	NUCB1	UP	-8.38	1.85
436	Atp5f1a	ATPA	UP	-5.96	0.28
437	Ckb	KCRB	UP	-19.22	0.59
438	Rac2	RAC2	UP	-17.40	0.78
439	Larp7	LARP7	UP	-5.11	0.29
440	Atp5me	ATP5I	UP	-2.17	0.77
441	Acads	ACADS	UP	-9.66	1.97
442	Ambp	AMBP	UP	-3.30	0.32
443	Lgals3bp	LG3BP	UP	-14.93	0.70
444	Bax	BAX	UP	-6.07	0.97
445	Cbfb	PEBB	UP	-5.33	2.36
446	Pros1	PROS	UP	-10.79	2.49
447	Fbln1	FBLN1	UP	-3.72	0.58
448	Npepps	PSA	UP	-16.23	1.10
449	Nsun2	NSUN2	UP	-9.77	2.13
450	Myl12b	ML12B	UP	-2.54	0.22
451	Gmps	GUAA	UP	-7.00	0.34
452	Mat2a	METK2	UP	-6.27	0.47
453	Usp39	UBP39	UP	-6.71	0.29
454	Prrc2c	PRC2C	UP	-12.54	1.32
455	Uap1l1	UAP1L	UP	-10.44	2.20
456	Srsf6	SRSF6	UP	-17.88	1.47
457	Psmd1	PSMD1	UP	-15.78	1.10
458	Khsrp	FUBP2	UP	-9.12	1.03
459	Fubp1;Khsrp	FUBP1 ;FUBP2	UP	-17.65	1.05
460	Lbr	LBR	UP	-2.38	0.68
461	Eif3j1;Eif3j2	EI3JA ;EI3JB	UP	-2.89	0.23
462	Arhgap17	RHG17	UP	-8.72	0.95
463	Mylk2	MYLK2	UP	-7.17	1.53
464	Smu1	SMU1	UP	-12.05	1.02
465	Ttbk2	TTBK2	UP	-3.05	0.83
466	Niban1	NIBA1	UP	-7.55	2.74
467	Rcsd1	CPZIP	UP	-9.34	0.55
468	Mthfd1l	C1TM	UP	-3.86	0.58
469	Abracl	ABRAL	UP	-2.71	0.20
470	Ccdc88b	CC88B	UP	-2.19	1.41
471	Cdv3	CDV3	UP	-10.10	1.93
472	Ddx17	DDX17	UP	-17.00	1.94
473	Lrrc47	LRC47	UP	-3.72	0.45
474	Thrap3	TR150	UP	-9.44	1.80
475	Mypn	MYPN	UP	-5.89	0.49
476	Nufip2	NUFP2	UP	-3.14	0.27
477	Rilp	RILP	UP	-3.40	1.83
478	Pfas	PUR4	UP	-4.34	2.72
479	Cluh	CLU	UP	-2.60	0.18
480	Grb2	GRB2	UP	-4.49	0.99
481	Irag2	IRAG2	UP	-2.94	0.21
482	Hnrnpd	HNRPD	UP	-6.72	0.69
483	Hnrnpd;Hnrnpdl	HNRDL ;HNRPD	UP	-1.81	0.12
484	Ppp5c	PPP5	UP	-13.67	1.34

485	Psmb6	PSB6	UP	-1.84	0.74
486	Csnk2a1	CSK21	UP	-6.02	0.44
487	Khdrbs1	KHDR1	UP	-4.63	0.60
488	Stip1	STIP1	UP	-8.55	1.10
489	Eif1a;Eif1ax	IF1AX ;IF1A	UP	-8.91	0.34
490	Arhgef2	ARHG2	UP	-14.29	0.92
491	Rbbp4	RBBP4	UP	-4.23	0.86
492	Rbbp4;Rbbp7	RBBP4 ;RBBP7	UP	-5.73	1.34
493	Asns	ASNS	UP	-7.77	0.56
494	Tmpo	LAP2A	UP	-2.45	0.22
495	Hars1	HARS1	UP	-1.54	0.72
496	Ppm1g	PPM1G	UP	-1.92	0.15
497	Cdc37	CDC37	UP	-3.76	0.57
498	Ptpn18	PTN18	UP	-5.15	0.66
499	Ctcf	CTCF	UP	-9.62	1.48
500	Mapre1	MARE1	UP	-1.70	0.81
501	Prdx2	PRDX2	UP	-2.01	0.26
502	Psap	SAP	UP	-6.76	0.33
503	Arhgef1	ARHG1	UP	-12.26	0.41
504	Sntb2	SNTB2	UP	-13.72	1.23
505	Hspa4;Hsph1	HS105 ;HSP74	UP	-1.43	1.04
506	Ewsr1	EWS	UP	-9.69	0.96
507	Arhgdib	GDIR2	UP	-2.42	0.26
508	Ddx19a	DD19A	UP	-10.50	0.59
509	Ddx5	DDX5	UP	-7.70	0.90
510	Cbx5	CBX5	UP	-10.58	0.38
511	Itih2	ITIH2	UP	-5.64	0.68
512	Itih3	ITIH3	UP	-15.46	0.75
513	Lasp1	LASP1	UP	-14.81	0.90
514	Pzp	PZP	UP	-5.51	0.29
515	A2m;Pzp	A2MG ;PZP	UP	-11.77	0.73
516	Mcm7	MCM7	UP	-8.02	0.78
517	Npm1	NPM	UP	-10.75	0.62
518	Pon3	PON3	UP	-7.53	0.26
519	Rhoc	RHOC	UP	-2.13	0.27
520	Ssr4	SSRD	UP	-6.53	0.89
521	Shh	SHH	UP	-1.37	0.10
522	Snrpc	RU1C	UP	-13.88	1.06
523	Tfrc	TFR1	UP	-9.64	2.04
524	Snrnp70	RU17	UP	-4.90	0.45
525	Zpr1	ZPR1	UP	-6.94	0.47
526	Tpd52	TPD52	UP	-2.72	2.04
527	Dbnl	DBNL	UP	-9.76	0.51
528	Sh3gl1	SH3G1	UP	-8.87	0.65
529	Ostf1	OSTF1	UP	-6.58	2.72
530	Ndrg1	NDRG1	UP	-7.35	0.43
531	Fkbp3	FKBP3	UP	-12.55	0.85
532	Vat1	VAT1	UP	-2.30	1.35
533	Zyx	ZYX	UP	-1.61	0.95
534	Mapk3	MK03	UP	-11.72	0.92
535	Raly	RALY	UP	-6.91	0.64
536	Spr	SPRE	UP	-2.25	0.33
537	Btf3	BTF3	UP	-2.35	0.34
538	Btf3;Btf3l4	BT3L4 ;BTF3	UP	-5.11	1.53
539	Fkbp5	FKBP5	UP	-11.29	2.94
540	Atp7a	ATP7A	UP	-9.95	1.69
541	Hspe1	CH10	UP	-4.74	0.74
542	Atp1a1;Atp4a	AT1A1 ;ATP4A	UP	-14.10	0.76
543	H2bc3	H2B1B	UP	-4.68	0.87
544	H2bc3;Hist1h2bp	H2B1B ;H2B1P	UP	-13.51	3.52
545	Tpp2	TPP2	UP	-3.38	0.62
546	H2ac20;Hist2h2aa1	H2A2A ;H2A2C	UP	-5.13	0.32
547	Gart	PUR2	UP	-6.92	0.37
548	Myof	MYOF	UP	-1.14	0.09
549	Macf1	K0754 ;MACF1	UP	-7.09	0.92
550	Cep170	CE170	UP	-3.57	1.06
551	Cdc5l	CDC5L	UP	-1.11	0.39
552	Nop58	NOP58	UP	-5.16	0.93
553	Brme1	BRME1	UP	-7.14	0.69
554	A2m	A2MG	UP	-17.66	2.88
555	Cltb	CLCB	UP	-17.81	1.03
556	Zc3h11a	ZC11A	UP	-4.07	1.54
557	Eif4g1	IF4G1	UP	-8.12	1.95

558	Ppp2r2a	2ABA	UP	-4.71	0.31
559	Uggt1	UGGG1	UP	-2.26	0.81
560	Nes	NEST	UP	-2.38	0.27
561	Fkbp15	FKB15	UP	-12.69	0.73
562	Oxsr1	OXSR1	UP	-14.33	1.79
563	Srsf1	SRSF1	UP	-1.55	1.53
564	Chd4	CHD4	UP	-2.88	0.22
565	Naa50	NAA50	UP	-6.83	2.09
566	Kctd12	KCD12	UP	-2.77	0.31
567	Cand1	CAND1	UP	-4.80	0.46
568	Rps27;Rps27l	RS27L ;RS27	UP	-5.30	0.47
569	Rpl10	RL10	UP	-21.10	2.14
570	Eif2s1	IF2A	UP	-6.39	0.63
571	Tmsb10	TYB10	UP	-1.77	0.21
572	Apool	MIC27	UP	-3.28	1.22
573	Snd1	SND1	UP	-9.28	2.53
574	Mtch1	MTCH1	UP	-12.36	0.41
575	Mtch2	MTCH2	UP	-4.30	1.10
576	Cyfip1	CYFP1	UP	-3.16	0.27
577	Syncrip	HNRPQ	UP	-5.00	0.43
578	Luc7l;Luc7l2	LC7L2 ;LUC7L	UP	-10.31	0.43
579	Spag7	SPAG7	UP	-9.57	0.61
580	Atxn2l	ATX2L	UP	-3.24	0.87
581	Sh3d21	SH321	UP	-5.72	1.61
582	Dnph1	DNPH1	UP	-4.10	1.74
583	Hydin	HYDIN	UP	-8.22	1.12
584	Mtdh	LYRIC	UP	-1.20	0.42
585	Flnb	FLNB	UP	-15.08	1.27
586	Glrx5	GLRX5	UP	-3.18	0.62
587	Safb2	SAFB2	UP	-11.19	2.45
588	Tufm	EFTU	UP	-6.06	1.93
589	Actbl2	ACTBL	UP	-4.40	0.18
590	Hnrnpa3	ROA3	UP	-13.26	0.66
591	Pld4	PLD4	UP	-7.40	0.31
592	Poldip3	PDIP3	UP	-3.67	0.22
593	Eif4b	IF4B	UP	-5.14	0.69
594	Bola2	BOLA2	UP	-12.62	0.87
595	Smndc1	SPF30	UP	-8.07	1.40
596	Pck2	PCKGM	UP	-4.83	1.48
597	Wasf2	WASF2	UP	-3.38	0.38
598	Ptbp3	PTBP3	UP	-1.27	0.09
599	Cstf2	CSTF2	UP	-1.30	0.12
600	Sgta	SGTA	UP	-3.50	2.02
601	Eif2a	EIF2A	UP	-4.84	1.58
602	Psmd5	PSMD5	UP	-4.26	0.34
603	Ahsa1	AHSA1	UP	-3.83	1.99
604	Ipo5	IPO5	UP	-7.01	0.92
605	Eea1	EEA1	UP	-6.83	0.84
606	Srsf7	SRSF7	UP	-1.10	0.33
607	Arid5b	ARI5B	UP	-2.66	0.49
608	Srp68	SRP68	UP	-4.66	1.81
609	Dlat	ODP2	UP	-2.20	0.89
610	Qars1	SYQ	UP	-8.36	0.77
611	Metap1	MAP11	UP	-7.05	0.70
612	Rpl24	RL24	UP	-3.96	1.55
613	Elmo1	ELMO1	UP	-9.24	0.75
614	Slc15a3	S15A3	UP	-0.97	0.47
615	Ppp1r18	PPR18	UP	-4.57	1.24
616	Cnpy4	CNPY4	UP	-8.94	1.32
617	Cc2d1b	C2D1B	UP	-8.80	1.08
618	Srrm2	SRRM2	UP	-2.80	1.16
619	Flna	FLNA	UP	-11.00	0.53
620	Iars1	SYIC	UP	-14.48	0.29
621	Sp110	SP110	UP	-3.27	0.29
622	Nob1	NOB1	UP	-4.55	0.60
623	Gemin5	GEMI5	UP	-3.09	1.05
624	Map1s	MAP1S	UP	-7.70	0.44
625	Asrgl1	ASGL1	UP	-5.75	1.08
626	Mbnl1;Mbnl2	MBNL1 ;MBNL2	UP	-6.28	3.84
627	Rbm14	RBM14	UP	-11.02	2.87
628	Rae1	RAE1L	UP	-11.92	0.90
629	Myef2	MYEF2	UP	-4.69	1.82
630	Immt	MIC60	UP	-5.36	0.53

631	Abi1	ABI1	UP	-10.62	0.49
632	Pabpn1	PABP2	UP	-3.50	1.57
633	Txnl1	TXNL1	UP	-5.17	0.91
634	Smc2	SMC2	UP	-2.07	0.34
635	Eprs1	SYEP	UP	-5.33	1.75
636	Lonp1	LONM	UP	-4.69	0.14
637	Hist1h2bp	H2B1P	UP	-2.57	0.17
638	Pgp	PGP	UP	-13.96	3.42
639	Slain2	SLAI2	UP	-4.21	0.23
640	Copa	COPA	UP	-3.79	1.28
641	Plcg2	PLCG2	UP	-4.23	0.23
642	Gpr84	GPR84	UP	-1.39	0.73
643	Pak2	PAK2	UP	-11.44	0.92
644	Mrgprx1	MRGX1	UP	-7.22	0.42
645	Trip10	CIP4	UP	-13.18	3.73
646	Eif3b	EIF3B	UP	-7.89	2.02
647	Bclaf1	BCLF1	UP	-6.83	0.52
648	Gmds	GMDS	UP	-7.48	1.10
649	Cmc2	COXM2	UP	-8.16	0.64
650	Wipf1	WIPF1	UP	-12.61	2.47
651	Ppp1r11	PP1RB	UP	-7.07	1.61
652	Spats2	SPAS2	UP	-5.65	1.21
653	Colgalt1	GT251	UP	-4.59	1.09
654	Shtn1	SHOT1	UP	-7.21	1.07
655	Matr3	MATR3	UP	-5.68	0.85
656	Babam2	BABA2	UP	-4.81	0.50
657	Arhgef6;Arhgef7	ARHG6 ;ARHG7	UP	-2.28	0.67
658	Sf3a1	SF3A1	UP	-4.43	1.46
659	Acat1	THIL	UP	-6.98	0.53
660	Tprkb	TPRKB	UP	-4.48	0.21
661	Mbnl3	MBNL3	UP	-1.65	0.40
662	Aimp2	AIMP2	UP	-0.96	0.40
663	Ero1a	ERO1A	UP	-2.15	0.21
664	Nudcd3	NUDC3	UP	-1.97	0.14
665	Mtss1	MTSS1	UP	-4.82	0.69
666	Spart	SPART	UP	-15.11	2.66
667	Ubqln1	UBQL1	UP	-6.41	1.27
668	Myh9	MYH9	UP	-9.94	3.02
669	Adpgk	ADPGK	UP	-5.39	0.12
670	Atp1a1	AT1A1	UP	-6.50	1.04
671	Ptgr2	PTGR2	UP	-4.29	0.19
672	Ddx39a;Ddx39b	DX39A ;DX39B	UP	-4.62	2.32
673	Pdcd10	PDC10	UP	-5.13	0.23
674	Srsf4	SRSF4	UP	-7.41	2.50
675	Ccdc115	CC115	UP	-11.39	1.01
676	Rpe	RPE	UP	-13.47	1.50
677	Hnrnpu	HNRPU	UP	-3.54	0.31
678	Amot	AMOT	UP	-9.88	0.30
679	Gatad2b	P66B	UP	-1.31	0.27
680	Oas3	OAS3	UP	-2.38	0.62
681	Sfpq	SFPQ	UP	-1.70	0.45
682	Nono;Sfpq	NONO ;SFPQ	UP	-14.58	1.03
683	Ciapin1	CPIN1	UP	-13.64	1.01
684	Sfxn3	SFXN3	UP	-5.88	0.44
685	Eif4a3	IF4A3	UP	-9.99	2.38
686	Nifk	MK67I	UP	-3.26	0.38
687	Pqbp1	PQBP1	UP	-3.58	1.34
688	Chchd6	MIC25	UP	-11.06	4.03
689	Atp5f1c	ATPG	UP	-8.28	1.59
690	Ddx1	DDX1	UP	-1.04	0.20
691	Brk1	BRK1	UP	-1.09	0.25
692	Sh3bgrl3	SH3L3	UP	-5.71	1.70
693	Ubap2	UBAP2	UP	-11.71	0.73
694	Slc39a8	S39A8	UP	-2.83	1.01
695	Txndc5	TXND5	UP	-15.08	0.70
696	Hkdc1	HKDC1	UP	-3.94	0.26
697	Fubp1	FUBP1	UP	-8.54	1.79
698	Dus3l	DUS3L	UP	-11.18	0.80
699	Ttc1	TTC1	UP	-8.84	2.11
700	Grhpr	GRHPR	UP	-9.09	2.22
701	Lrp1	LRP1	UP	-1.36	0.52
702	Tf	TRFE	UP	-7.33	0.49
703	Ddx27	DDX27	UP	-9.48	0.69

704	Tor1aip1	TOIP1	UP	-3.75	1.71
705	Dars1	SYDC	UP	-5.03	0.42
706	Tubb6	TBB6	UP	-7.51	0.36
707	Lrrc59	LRC59	UP	-1.66	0.10
708	Ubxn1	UBXN1	UP	-14.43	0.80
709	Trim59	TRI59	UP	-11.87	1.00
710	Blvrb	BLVRB	UP	-1.92	0.54
711	Sf3b5	SF3B5	UP	-10.77	0.72
712	Cers2	CERS2	UP	-14.22	2.28
713	Taldo1	TALDO	UP	-8.72	1.67
714	Hnrnpab	ROAA	UP	-9.59	0.46
715	Thumpd1	THUM1	UP	-12.97	0.81
716	Dhrs7b	DRS7B	UP	-3.68	0.96
717	Rfc4	RFC4	UP	-5.38	0.80
718	Mpst	THTM	UP	-2.17	0.73
719	Psip1	PSIP1	UP	-9.79	0.78
720	Acy1	ACY1	UP	-1.65	0.18
721	Nono	NONO	UP	-2.42	0.88
722	Hagh	GLO2	UP	-2.33	0.25
723	Stk24	STK24	UP	-6.56	0.98
724	Dctn2	DCTN2	UP	-0.90	0.59
725	Nampt	NAMPT	UP	-7.24	1.20
726	Dhrs1	DHRS1	UP	-6.72	0.60
727	St13	F10A1	UP	-0.93	0.40
728	Mat2b	MAT2B	UP	-8.67	0.51
729	Abcf2	ABCF2	UP	-11.22	2.28
730	Rtcb	RTCB	UP	-10.86	2.14
731	Grpel1	GRPE1	UP	-1.55	0.95
732	Dpy30	DPY30	UP	-4.44	0.51
733	Park7	PARK7	UP	-4.10	1.02
734	Rnps1	RNPS1	UP	-4.97	0.24
735	Nasp	NASP	UP	-4.98	0.38
736	Gtpbp4	GTPB4	UP	-3.24	0.24
737	Kars1	SYK	UP	-1.22	0.26
738	Adar	DSRAD	UP	-3.95	0.26
739	Lpxn	LPXN	UP	-5.64	0.94
740	Mrps18b	RT18B	UP	-3.85	0.44
741	Mrps5	RT05	UP	-9.92	1.37
742	Ubqln4	UBQL4	UP	-9.13	1.88
743	Pard3	PARD3	UP	-10.58	1.97
744	Ogfr	OGFR	UP	-7.31	2.11
745	Rrbp1	RRBP1	UP	-10.29	2.51
746	Arhgdia	GDIR1	UP	-6.37	0.31
747	Prpf8	PRP8	UP	-4.99	0.20
748	Npm3	NPM3	UP	-4.22	0.29
749	Cox6c	COX6C	UP	-11.91	1.50
750	Rpl17	RL17	UP	-5.23	0.90
751	Mydgf	MYDGF	UP	-1.51	0.10
752	Glo1	LGUL	UP	-4.43	0.38
753	Glod4	GLOD4	UP	-3.64	0.52
754	Arpc5	ARPC5	UP	-1.73	0.84
755	Ssr2	SSRB	UP	-1.62	0.12
756	Atg3	ATG3	UP	-14.63	2.80
757	Dut	DUT	UP	-1.43	0.34
758	Pgls	6PGL	UP	-4.48	0.47
759	Mtap	MTAP	UP	-14.00	1.18
760	Uqcrq	QCR8	UP	-2.16	0.22
761	Ndufa2	NDUA2	UP	-12.10	3.02
762	Chmp1b2	CH1B2	UP	-6.78	1.91
763	Gmfb	GMFB	UP	-8.84	1.26
764	Cotl1	COTL1	UP	-6.66	1.67
765	Trap1	TRAP1	UP	-13.89	0.61
766	Atp5pb	AT5F1	UP	-1.70	0.86
767	Rps21	RS21	UP	-1.45	0.52
768	Ppp6c	PPP6	UP	-7.01	0.97
769	Txndc12	TXD12	UP	-8.06	1.47
770	Ifitm3	IFM3	UP	-8.02	2.45
771	Ppid	PPID	UP	-18.81	1.55
772	Hypk	HYPK	UP	-3.59	0.37
773	Atp6v1g1	VATG1	UP	-2.35	0.40
774	Rpl14	RL14	UP	-6.63	0.75
775	Uqcrfs1	UCRI	UP	-10.02	0.66
776	Carhsp1	CHSP1	UP	-10.55	0.98

777	Fam136a	F136A	UP	-2.92	1.22
778	Chchd3	MIC19	UP	-6.71	2.45
779	Snw1	SNW1	UP	-4.78	0.43
780	Rprd1b	RPR1B	UP	-6.49	1.01
781	Ranbp3	RANB3	UP	-7.13	0.81
782	Arpc2	ARPC2	UP	-2.91	1.14
783	Smc3	SMC3	UP	-14.93	0.60
784	Tubb2b	TBB2B	UP	-1.92	0.22
785	Atic	PUR9	UP	-8.21	1.51
786	Snx2	SNX2	UP	-3.95	0.13
787	Pfdn1	PFD1	UP	-9.38	0.46
788	Pin4	PIN4	UP	-5.54	0.79
789	Rbm8a	RBM8A	UP	-8.22	1.83
790	Napg	SNAG	UP	-7.21	1.70
791	Sugt1	SGT1	UP	-2.71	1.07
792	Hnrnpa0	ROA0	UP	-1.71	0.47
793	Cacybp	CYBP	UP	-16.53	1.59
794	Rpl11	RL11	UP	-1.90	0.17
795	Mrps28	RT28	UP	-3.76	0.17
796	Gins3	PSF3	UP	-3.84	2.13
797	Zcchc8	ZCHC8	UP	-10.91	1.36
798	Luc7l	LUC7L	UP	-10.82	2.22
799	Spcs2	SPCS2	UP	-2.17	0.30
800	Uqcrc1	QCR1	UP	-5.29	1.92
801	Rpl15	RL15	UP	-3.10	0.15
802	Tsfm	EFTS	UP	-16.23	1.20
803	Cmss1	CMS1	UP	-2.46	1.41
804	Mtrex	MTREX	UP	-1.41	0.59
805	Rps19	RS19	UP	-2.23	0.88
806	Ube2v1	UB2V1	UP	-13.13	0.85
807	Pbdc1	PBDC1	UP	-8.55	0.62
808	Hnrnpm	HNRPM	UP	-1.14	0.39
809	Lman1	LMAN1	UP	-4.95	0.25
810	Cyc1	CY1	UP	-2.83	0.24
811	Tars1	SYTC	UP	-3.76	0.23
812	Ddx56	DDX56	UP	-1.09	0.09
813	Lsm12	LSM12	UP	-1.96	0.55
814	Znf706	ZN706	UP	-10.83	1.90
815	Gatd3	GAL3A	UP	-6.95	1.56
816	Ciao2b	CIA2B	UP	-5.22	1.29
817	Tbcb	TBCB	UP	-1.40	0.76
818	Rab1b	RAB1B	UP	-2.39	0.85
819	Necap2	NECP2	UP	-3.93	0.56
820	Sarnp	SARNP	UP	-5.25	0.94
821	Rpl34	RL34	UP	-1.48	0.12
822	Bcas2	SPF27	UP	-12.12	1.20
823	Dlst	ODO2	UP	-4.91	1.61
824	Sec23b	SC23B	UP	-1.31	0.14
825	Ppil6	PPIL6	UP	-4.32	0.44
826	Nop56	NOP56	UP	-2.60	0.89
827	Trir	TRIR	UP	-5.37	0.28
828	Lhpp	LHPP	UP	-2.68	1.09
829	Serpinb12	SPB12	UP	-3.43	1.43
830	Dusp3	DUS3	UP	-10.00	0.91
831	Arpc5l	ARP5L	UP	-6.57	0.59
832	Chmp4b	CHM4B	UP	-8.98	0.72
833	Eef1g	EF1G	UP	-10.93	0.76
834	Rexo2	ORN	UP	-13.96	0.59
835	Gsdmd	GSDMD	UP	-2.95	0.54
836	Efhd2	EFHD2	UP	-4.00	0.39
837	Cnpy3	CNPY3	UP	-19.92	1.10
838	Atp5po	ATPO	UP	-1.16	0.58
839	Alg5	ALG5	UP	-1.72	0.12
840	Prkar1a	KAP0	UP	-1.95	0.86
841	Ftsj3	SPB1	UP	-8.06	0.95
842	Plin3	PLIN3	UP	-1.27	0.70
843	Lman2	LMAN2	UP	-5.81	0.39
844	Pgam1	PGAM1	UP	-6.36	2.35
845	Xrn2	XRN2	UP	-7.51	0.23
846	Ampd2	AMPD2	UP	-5.00	0.52
847	Eif3k	EIF3K	UP	-4.23	2.15
848	Pycr3	P5CR3	UP	-4.77	0.56
849	Trmt112	TR112	UP	-7.25	1.12

850	Eif3f	EIF3F	UP	-14.51	3.21
851	Ciao2a	CIA2A	UP	-6.74	1.53
852	Ethe1	ETHE1	UP	-11.38	1.80
853	Mecr	MECR	UP	-15.55	1.26
854	Atp5pd	ATP5H	UP	-1.05	0.78
855	Emc7	EMC7	UP	-2.32	0.15
856	Pycard	ASC	UP	-11.33	1.23
857	Upf1	RENT1	UP	-3.60	0.22
858	Ehd4	EHD4	UP	-8.45	1.58
859	Set	SET	UP	-2.31	0.20
860	Stx12	STX12	UP	-9.87	0.62
861	Cars1	SYCC	UP	-3.32	0.27
862	Mesd	MESD	UP	-4.10	0.39
863	Lima1	LIMA1	UP	-1.02	0.24
864	Ranbp2	RBP2	UP	-2.34	1.34
865	Sdf2l1	SDF2L	UP	-1.31	0.37
866	Dkc1	DKC1	UP	-0.92	0.47
867	Rnf114	RN114	UP	-7.64	1.02
868	Jph3	JPH3	UP	-3.55	0.48
869	Tmod3	TMOD3	UP	-1.88	0.64
870	Ide	IDE	UP	-8.23	0.64
871	Stk3	STK3	UP	-1.02	0.60
872	Gtf2ird1	GT2D1	UP	-1.23	0.33
873	Dazap1	DAZP1	UP	-5.58	1.87
874	Rpl38	RL38	UP	-10.20	0.92
875	Sh3glb1	SHLB1	UP	-2.45	0.28
876	Myg1	MYG1	UP	-7.94	2.05
877	Tmod2	TMOD2	UP	-9.98	1.22
878	Hyou1	HYOU1	UP	-5.68	0.54
879	Adrm1	ADRM1	UP	-6.31	0.29
880	Nudt5	NUDT5	UP	-19.10	1.42
881	Sart3	SART3	UP	-9.09	0.82
882	Cd2ap	CD2AP	UP	-11.04	2.03
883	Git2	GIT2	UP	-5.78	1.04
884	Nt5c	NT5C	UP	-8.94	1.94
885	Stap1	STAP1	UP	-5.79	0.46
886	Znf207	ZN207	UP	-3.12	0.19
887	Glrx	GLRX1	UP	-5.28	1.19
888	Rhoa	RHOA	UP	-5.64	0.59
889	Pin1	PIN1	UP	-7.38	1.42
890	Ptk2b	FAK2	UP	-7.23	1.34
891	Lsm4	LSM4	UP	-1.53	0.82
892	Plec	PLEC	UP	-10.27	1.54
893	Cnpy2	CNPY2	UP	-8.79	0.16
894	Ehd1;Ehd3	EHD1 ;EHD3	UP	-6.82	0.48
895	Vapb	VAPB	UP	-4.38	0.81
896	Rdh11	RDH11	UP	-2.40	0.13
897	Qki	QKI	UP	-2.58	1.31
898	Vps29	VPS29	UP	-7.33	0.70
899	Zranb2	ZRAB2	UP	-3.32	1.56
900	Gyg1	GLYG	UP	-5.68	2.47
901	Comp	COMP	UP	-1.87	0.35
902	Esd	ESTD	UP	-1.82	1.44
903	Tmed2	TMED2	UP	-5.80	0.21
904	Ptges3	TEBP	UP	-2.25	0.52
905	Srsf10	SRS10	UP	-5.90	0.37
906	Psma4	PSA4	UP	-4.82	0.92
907	Psmb2	PSB2	UP	-5.52	0.28
908	Psma1	PSA1	UP	-4.16	0.21
909	Tapbp	TPSN	UP	-6.22	0.36
910	Myo1c	MYO1C	UP	-5.18	0.42
911	Ruvbl2	RUVB2	UP	-3.41	0.42
912	Ak2	KAD2	UP	-2.04	0.42
913	Ak3	KAD3	UP	-11.26	0.83
914	Ccs	CCS	UP	-6.71	1.87
915	Farsb	SYFB	UP	-1.34	0.57
916	Eif4h	IF4H	UP	-5.62	0.28
917	Coro1b	COR1B	UP	-12.79	1.45
918	Coro1c	COR1C	UP	-11.50	1.64
919	Suclg1	SUCA	UP	-2.70	0.14
920	Ctsz	CATZ	UP	-6.12	0.60
921	Snx1	SNX1	UP	-10.35	0.33
922	Timm9	TIM9	UP	-3.46	0.61

923	Timm8a1	TIM8A	UP	-7.05	2.23
924	Tagln2	TAGL2	UP	-11.74	1.16
925	Psmd13	PSD13	UP	-8.05	0.21
926	Apip	MTNB	UP	-7.09	0.56
927	Celf2	CELF2	UP	-1.90	0.49
928	Aldh18a1	P5CS	UP	-8.18	1.94
929	Uba2	SAE2	UP	-14.59	1.14
930	Atp6v1c1	VATC1	UP	-7.66	0.53
931	Deaf1	DEAF1	UP	-2.73	0.26
932	Strap	STRAP	UP	-13.94	1.30
933	Suclg2	SUCB2	UP	-4.41	0.31
934	Sucla2	SUCB1	UP	-10.79	0.94
935	Crlf3	CRLF3	UP	-1.39	1.08
936	Unc119	U119A	UP	-7.57	1.77
937	Psma5	PSA5	UP	-1.08	0.30
938	Plpbp	PLPHP	UP	-10.07	0.58
939	Cul4b	CUL4B	UP	-6.55	1.03
940	Tbc1d8b	TBC8B	DOWN	-1.46	-0.74
941	H2ac11	H2A1B	DOWN	-0.92	-0.31
942	Safb;Safb2	SAFB1 ;SAFB2	DOWN	-20.11	-2.79
943	Kif23	KIF23	DOWN	-1.40	-0.25
944	Myo1e	MYO1E	DOWN	-2.23	-0.30
945	Myo1e;Myo1f	MYO1E ;MYO1F	DOWN	-4.12	-1.34
946	Rap1gds1	GDS1	DOWN	-5.77	-0.55
947	Atp2b1	AT2B1	DOWN	-2.38	-0.35
948	Hk1;Hk2	HXK1 ;HXK2	DOWN	-11.73	-1.42
949	Bin1	BIN1	DOWN	-10.24	-0.58
950	Myh11	MYH11	DOWN	-4.61	-0.62
951	Myh10	MYH10	DOWN	-1.21	-0.20
952	Myh11;Myh9	MYH11 ;MYH9	DOWN	-12.41	-0.70
953	Hsd17b10	HCD2	DOWN	-13.47	-0.69
954	Dctn1	DCTN1	DOWN	-15.54	-3.08
955	Eftud2	U5S1	DOWN	-1.60	-0.54
956	Psmb1	PSB1	DOWN	-2.01	-0.15
957	Gsto1	GSTO1	DOWN	-1.36	-0.92
958	Grcc10	C10	DOWN	-2.90	-0.35
959	Exoc7	EXOC7	DOWN	-1.71	-1.04
960	Dhx15	DHX15	DOWN	-1.05	-0.39
961	Kpna3;Kpna4	IMA3 ;IMA4	DOWN	-8.56	-0.24
962	Kpna3	IMA4	DOWN	-1.65	-0.90
963	Anp32a	AN32A	DOWN	-13.00	-0.52
964	Psmb9	PSB9 ;PSB9_MUSMB	DOWN	-3.63	-0.34
965	Psmd14	PSDE	DOWN	-4.00	-0.79
966	Anxa3	ANXA3	DOWN	-1.66	-0.78
967	Ap1b1	AP1B1	DOWN	-4.96	-0.18
968	Ap1b1;Ap2b1	AP1B1 ;AP2B1	DOWN	-9.12	-1.26
969	C1qbp	C1QBP	DOWN	-3.31	-0.55
970	Myadm	MYADM	DOWN	-16.24	-1.63
971	Hnrnph1;Hnrnph2	HNRH1 ;HNRH2	DOWN	-3.59	-0.54
972	Hnrnpf;Hnrnph1	HNRH1 ;HNRPF	DOWN	-11.42	-0.58
973	Timm44	TIM44	DOWN	-7.59	-0.74
974	Hmgb3	HMGB3	DOWN	-5.15	-0.70
975	Banf1	BAF	DOWN	-1.73	-0.69
976	Copb2	COPB2	DOWN	-4.57	-0.42
977	Septin7	45907	DOWN	-9.84	-0.93
978	Atp2a2	AT2A2	DOWN	-8.60	-0.73
979	Atp2a2;Atp2a3	AT2A2 ;AT2A3	DOWN	-6.06	-0.29
980	Pik3c2g	P3C2G	DOWN	-5.56	-0.48
981	Eif3d	EIF3D	DOWN	-19.51	-1.82
982	Nmt1	NMT1	DOWN	-2.21	-0.19
983	Sfn	1433S	DOWN	-3.38	-0.37
984	Sfn	1433B	DOWN	-2.02	-0.26
985	Snx3	SNX3	DOWN	-15.49	-2.51
986	Snx12	SNX12	DOWN	-3.53	-0.20
987	Hsd17b12	DHB12	DOWN	-1.13	-0.09
988	Smpd2	NSMA	DOWN	-3.75	-0.43
989	Dhcr7	DHCR7	DOWN	-13.57	-2.99
990	Capns1	CPNS1	DOWN	-4.50	-1.94
991	Dnmt3a	DNM3A	DOWN	-1.55	-0.57
992	Lin7c	LIN7C	DOWN	-5.47	-0.94
993	Yme1l1	YME1L1	DOWN	-1.30	-1.29
994	Coro1a	COR1A	DOWN	-1.89	-1.10
995	Coro1a;Coro1c	COR1A ;COR1C	DOWN	-17.04	-0.48

996	Dhfr	DYR	DOWN	-1.95	-0.78
997	Hprt1	HPRT	DOWN	-5.88	-0.52
998	H2-D1;H2-L	HA11 ;HA12 ;HA1L	DOWN	-6.46	-0.41
999	H2-K1	HA1D	DOWN	-1.23	-0.10
1000	Hbb-b1;Hbb-b2	HBB1 ;HBB2	DOWN	-11.60	-3.11
1001	H3c2	H3C	DOWN	-1.10	-0.13
1002	Fabp4	FABP4	DOWN	-22.76	-2.19
1003	Got1	AATC	DOWN	-6.23	-1.10
1004	Got2	AATM	DOWN	-10.87	-0.53
1005	Ctsl	CATL1	DOWN	-20.09	-1.49
1006	Ptprc	PTPRC	DOWN	-1.51	-0.38
1007	S100a4	S10A4	DOWN	-8.90	-0.53
1008	Anxa2	ANXA2	DOWN	-14.94	-0.69
1009	Aprt	APT	DOWN	-8.94	-0.23
1010	Fcgr2	FCGR2	DOWN	-15.92	-0.86
1011	S100a10	S10AA	DOWN	-2.53	-0.41
1012	Sod2	SODM	DOWN	-14.46	-0.88
1013	Calm1	CALM1	DOWN	-3.55	-0.15
1014	Anxa1	ANXA1	DOWN	-21.10	-1.96
1015	Slc3a2	4F2	DOWN	-6.34	-0.26
1016	H1-0	H10	DOWN	-7.93	-0.41
1017	Sub1	TCP4	DOWN	-13.50	-0.80
1018	Lamp1	LAMP1	DOWN	-7.96	-0.98
1019	Itgb2	ITB2	DOWN	-1.74	-0.26
1020	Oas1a	OAS1A	DOWN	-3.10	-0.17
1021	Gusb	BGLR	DOWN	-5.02	-0.85
1022	Pfkl;Pfkp	PFKAL ;PFKAP	DOWN	-14.58	-3.10
1023	Rpl7a	RL7A	DOWN	-7.37	-0.52
1024	Gsn	GELS	DOWN	-15.64	-0.76
1025	Dnmt1	DNMT1	DOWN	-2.66	-0.07
1026	S100a6	S10A6	DOWN	-6.96	-1.09
1027	Rpl27a	RL27A	DOWN	-10.81	-1.73
1028	Rpl7	RL7	DOWN	-3.10	-0.35
1029	Mdh1	MDHC	DOWN	-12.92	-0.46
1030	Rpsa	RSSA	DOWN	-7.49	-0.27
1031	Psmd3	PSMD3	DOWN	-1.23	-0.07
1032	Rplp0	RLA0	DOWN	-2.58	-0.16
1033	Spn	LEUK	DOWN	-6.22	-0.20
1034	H1-2	H12	DOWN	-14.39	-2.55
1035	H1-1	H11	DOWN	-6.91	-0.75
1036	Hmga1	HMGA1	DOWN	-1.16	-0.20
1037	Hspa2	HSP72	DOWN	-9.85	-2.81
1038	Hspa2	GRP75	DOWN	-1.45	-1.62
1039	Eno1;Eno2;Eno3	ENOA	DOWN	-7.71	-1.03
1040	Eno2	ENOG	DOWN	-0.99	-0.11
1041	Ptbp1	PTBP1	DOWN	-1.64	-0.68
1042	Cox7c	COX7C	DOWN	-1.42	-0.04
1043	Hk1	HXK1	DOWN	-13.83	-2.69
1044	Mthfd2	MTDC	DOWN	-4.72	-0.37
1045	Rps6ka3	KS6A3	DOWN	-5.79	-0.37
1046	Cfl1	COF1	DOWN	-11.97	-1.27
1047	Cfl1;Dstn	COF1 ;DEST	DOWN	-6.70	-0.20
1048	Fasn	FAS	DOWN	-2.33	-0.63
1049	Cox5b	COX5B	DOWN	-11.41	-0.33
1050	Tmsb4x	TYB4	DOWN	-6.70	-0.85
1051	Tpm3;Tpm4	TPM3 ;TPM4	DOWN	-11.66	-0.39
1052	Akr1b7	ALD1	DOWN	-10.81	-2.77
1053	Akr1b7;Akr1b8	ALD1 ;ALD2	DOWN	-8.64	-2.10
1054	Mfge8	MFGM	DOWN	-10.05	-1.22
1055	Pnp	PNPH	DOWN	-4.59	-1.08
1056	Ppib	PPIB	DOWN	-5.41	-0.82
1057	M6pr	MPRD	DOWN	-10.73	-0.76
1058	Mcm3	MCM3	DOWN	-2.54	-0.13
1059	Ezr	EZRI	DOWN	-2.11	-0.16
1060	Ptma	PTMA	DOWN	-4.07	-0.17
1061	Marcks	MARCS	DOWN	-8.41	-0.38
1062	Map4	MAP4	DOWN	-14.58	-1.30
1063	Plaa	PLAP	DOWN	-11.60	-1.29
1064	Psmb8	PSB8	DOWN	-9.76	-1.92
1065	Adh5	ADHX	DOWN	-3.68	-0.34
1066	Atxn10	ATX10	DOWN	-13.70	-0.80
1067	Marcksl1	MRP	DOWN	-4.14	-0.42
1068	Ptpn6	PTN6	DOWN	-6.69	-0.50

1069	Msr1	MSRE	DOWN	-9.57	-0.35
1070	Dbi	ACBP	DOWN	-1.49	-0.18
1071	Map2k1	MP2K1	DOWN	-3.68	-0.34
1072	Map2k1;Map2k2	MP2K1 ;MP2K2	DOWN	-2.71	-1.40
1073	Ssb	LA	DOWN	-13.72	-1.21
1074	Usp15;Usp4	UBP15 ;UBP4	DOWN	-3.96	-0.19
1075	Rab5c	RAB5C	DOWN	-1.19	-0.48
1076	Pdha1	ODPA	DOWN	-15.93	-1.33
1077	Fbl	FBRL	DOWN	-11.75	-2.24
1078	Canx	CALX	DOWN	-5.32	-0.21
1079	Lig1	DNLI1	DOWN	-7.11	-0.21
1080	Dnm1;Dnm2	DYN1 ;DYN2	DOWN	-1.37	-0.20
1081	Dnm2	DYN2	DOWN	-2.43	-0.23
1082	Cap1	CAP1	DOWN	-5.58	-1.65
1083	Rpl28	RL28	DOWN	-6.78	-0.22
1084	Acsl1	ACSL1	DOWN	-1.81	-0.08
1085	Acsl1;Acsl5	ACSL1 ;ACSL5	DOWN	-4.65	-0.71
1086	Cct8	TCPQ	DOWN	-5.75	-0.99
1087	H1-4	H14	DOWN	-2.34	-0.07
1088	H1-1	H11	DOWN	-9.16	-0.85
1089	H1-3	H13	DOWN	-5.46	-0.62
1090	Acadm	ACADM	DOWN	-3.53	-0.58
1091	Rab11b	RB11B	DOWN	-4.03	-0.44
1092	Pla2g4a	PA24A	DOWN	-3.11	-0.23
1093	Capza1	CAZA1	DOWN	-9.21	-0.66
1094	Gsr	GSHR	DOWN	-7.89	-0.46
1095	Mtx1	MTX1	DOWN	-1.02	-0.13
1096	Mapk14	MK14	DOWN	-8.46	-1.26
1097	Rpl6	RL6	DOWN	-8.54	-1.47
1098	Pcnt	PCNT	DOWN	-7.51	-0.33
1099	Cox7a2	CX7A2	DOWN	-2.96	-0.24
1100	Slc25a4	ADT1	DOWN	-8.09	-0.89
1101	Clec10a	CLC10	DOWN	-10.27	-0.60
1102	Hnrnpa1;Hnrnpa3	ROA1 ;ROA3	DOWN	-1.36	-0.22
1103	Mcm5	MCM5	DOWN	-6.48	-0.45
1104	Impdh1	IMDH1	DOWN	-7.68	-0.57
1105	Ahcy	SAHH	DOWN	-7.71	-2.24
1106	Acadvl	ACADV	DOWN	-2.96	-0.10
1107	Rab7a	RAB7A	DOWN	-12.24	-2.12
1108	Gla	AGAL	DOWN	-6.22	-0.29
1109	Hdgf;Hdgfl2;Psip1	HDGF ;HDGR2 ;PSIP1	DOWN	-3.90	-1.02
1110	Atp6v0d1	VAOD1	DOWN	-10.01	-2.08
1111	Slc25a5	ADT2	DOWN	-9.14	-0.78
1112	Slc1a5	AAAT	DOWN	-5.18	-0.43
1113	Rab2a	RAB2A	DOWN	-4.65	-1.19
1114	Idh2	IDHP	DOWN	-2.59	-0.16
1115	Stom	STOM	DOWN	-6.22	-0.26
1116	Psmc4	PRS6B	DOWN	-1.84	-0.39
1117	Adsl	PUR8	DOWN	-2.17	-0.42
1118	Ddx6	DDX6	DOWN	-10.47	-1.96
1119	Rab8a	RAB8A	DOWN	-2.93	-0.42
1120	Rab1A	RAB1A	DOWN	-1.83	-0.70
1121	Atp5mpl	ATP68	DOWN	-8.71	-1.25
1122	Usp5	UBP5	DOWN	-5.79	-1.56
1123	Actn4	ACTN4	DOWN	-2.69	-0.16
1124	Snrpa1	RU2A	DOWN	-1.30	-0.08
1125	Tm9sf2	TM9S2	DOWN	-17.24	-2.56
1126	Cpne2	CPNE2	DOWN	-4.61	-0.88
1127	Ruvbl1	RUVB1	DOWN	-8.41	-2.28
1128	Pcbp1	PCBP1	DOWN	-5.82	-0.33
1129	Pcbp1;Pcbp2	PCBP1 ;PCBP2	DOWN	-4.05	-0.10
1130	Cdc42	CDC42	DOWN	-3.72	-0.21
1131	Eif4a1	IF4A1	DOWN	-3.29	-0.19
1132	Rab10	RAB10	DOWN	-4.24	-0.14
1133	Ube2d3	UB2D3	DOWN	-2.53	-0.46
1134	Ube2m	UBC12	DOWN	-0.99	-0.26
1135	Ube2n	UBE2N	DOWN	-2.90	-0.40
1136	Arf1;Arf3	ARF1 ;ARF3	DOWN	-1.95	-0.21
1137	Abce1	ABCE1	DOWN	-4.74	-1.24
1138	Rpl26	RL26	DOWN	-3.43	-0.49
1139	Psme3	PSME3	DOWN	-14.60	-0.92
1140	Rpl27	RL27	DOWN	-1.85	-1.11
1141	Sec61a1	S61A1	DOWN	-7.06	-0.60

1142	Sumo2	SUMO2	DOWN	-6.74	-1.20
1143	Hnrnpk	HNRPK	DOWN	-7.74	-0.83
1144	Ppp1ca;Ppp1cc	PP1A ;PP1G	DOWN	-5.13	-0.16
1145	Psmc1	PRS4	DOWN	-3.85	-0.30
1146	Psmc5	PRS8	DOWN	-2.94	-0.21
1147	Rps8	RS8	DOWN	-3.88	-0.45
1148	Ywhae	1433E	DOWN	-9.85	-0.46
1149	Lsm3	LSM3	DOWN	-2.34	-0.15
1150	Snrpd1	SMD1	DOWN	-10.16	-0.86
1151	Snrpd2	SMD2	DOWN	-10.13	-2.14
1152	Psmc6	PRS10	DOWN	-3.67	-0.29
1153	Rpl18a	RL18A	DOWN	-2.70	-0.16
1154	Mtpn	MTPN	DOWN	-6.10	-0.35
1155	H4c1	H4	DOWN	-13.24	-1.32
1156	Rab1A	RAB1A	DOWN	-16.69	-1.49
1157	Ran	RAN	DOWN	-2.35	-0.20
1158	Gnb1;Gnb2	GBB1 ;GBB2	DOWN	-6.75	-0.20
1159	Gnb2	GBB2	DOWN	-7.16	-0.46
1160	Cycs	CYC	DOWN	-5.24	-0.38
1161	Ybx1;Ybx3	YBOX1 ;YBOX3	DOWN	-15.09	-2.32
1162	Rps27a;Uba52	RL40 ;RS27A	DOWN	-2.59	-0.55
1163	Pafah1b1	LIS1	DOWN	-9.95	-0.37
1164	Vamp2;Vamp3	VAMP2 ;VAMP3	DOWN	-3.85	-0.84
1165	Mapk1;Mapk3	MK01 ;MK03	DOWN	-12.63	-3.14
1166	Ppp1cc	PP1G	DOWN	-2.44	-0.90
1167	Hmgb1	HMGB1	DOWN	-6.55	-0.49
1168	Dynll1	DYL1	DOWN	-0.91	-0.06
1169	Rps17	RS17	DOWN	-4.18	-1.00
1170	Ppp2ca	PP2AA	DOWN	-2.11	-0.13
1171	Rpl22	RL22	DOWN	-4.49	-0.45
1172	Ube2l3	UB2L3	DOWN	-1.62	-0.14
1173	Rack1	RACK1	DOWN	-1.49	-0.09
1174	Ywhaq	1433T	DOWN	-1.02	-0.04
1175	Tuba4a	TBA4A	DOWN	-12.25	-0.70
1176	uba4a;Tuba8	TBA4A ;TBA8	DOWN	-2.35	-0.08
1177	Tuba1c	TBA1C	DOWN	-6.19	-0.23
1178	Ywhah	1433F	DOWN	-1.10	-0.06
1179	Cct4	TCPD	DOWN	-6.06	-0.42
1180	Tgfbi	BGH3	DOWN	-9.65	-0.34
1181	Cbx1	CBX1	DOWN	-12.24	-5.69
1182	Arf5	ARF5	DOWN	-5.58	-1.62
1183	Erh	ERH	DOWN	-18.37	-1.51
1184	Ap2m1	AP2M1	DOWN	-3.82	-0.75
1185	Srsf3;Srsf7	SRSF3 ;SRSF7	DOWN	-6.95	-0.58
1186	Mcm2	MCM2	DOWN	-11.44	-0.70
1187	Ncf4	NCF4	DOWN	-4.10	-0.47
1188	Atp1b3	AT1B3	DOWN	-1.33	-0.25
1189	Psme1;Psme2	PSME1 ;PSME2	DOWN	-3.34	-0.62
1190	Psme2	PSME2	DOWN	-2.29	-0.62
1191	G3bp2	G3BP2	DOWN	-5.78	-0.55
1192	Anxa4	ANXA4	DOWN	-5.75	-0.86
1193	Atp5pf	ATP5J	DOWN	-8.51	-0.35
1194	Ctsc	CATC	DOWN	-1.84	-0.35
1195	Anp32e	AN32E	DOWN	-4.94	-0.28
1196	Dab2	DAB2	DOWN	-3.00	-0.18
1197	Rplp2	RLA2	DOWN	-4.66	-0.20
1198	Prdx5	PRDX5	DOWN	-3.80	-0.09
1199	Xdh	XDH	DOWN	-7.48	-0.27
1200	G6pdx	G6PD1	DOWN	-15.45	-2.09
1201	Hnrnpul2	HNRL2	DOWN	-6.98	-0.21
1202	Top2a	TOP2A	DOWN	-4.74	-0.49
1203	Ly9	LY9	DOWN	-10.26	-0.57
1204	Uba1	UBA1	DOWN	-13.16	-4.85
1205	Fabp5	FABP5	DOWN	-9.58	-0.34
1206	Eif5b	IF2P	DOWN	-3.88	-0.31
1207	Anxa7	ANXA7	DOWN	-8.55	-0.63
1208	Ssrp1	SSRP1	DOWN	-5.16	-0.59
1209	Ncf1	NCF1	DOWN	-2.69	-0.99
1210	Zc3h18	ZCH18	DOWN	-4.98	-0.41
1211	Ppp4r2	PP4R2	DOWN	-0.97	-0.40
1212	Mgat3	MGAT3	DOWN	-1.85	-0.56
1213	Osbp	OSBP1	DOWN	-18.03	-3.78
1214	Arhgap45	HMHA1	DOWN	-2.49	-0.98

1215	Abraxas2	ABRX2	DOWN	-5.29	-1.13
1216	Hk3	HXK3	DOWN	-3.90	-0.72
1217	Srsf4;Srsf6	SRSF4 ;SRSF6	DOWN	-8.44	-0.83
1218	Gpsm3	GPSM3	DOWN	-6.14	-1.14
1219	Esyt1	ESYT1	DOWN	-0.91	-0.13
1220	Ttll12	TTL12	DOWN	-4.32	-0.71
1221	Dip2b	DIP2B	DOWN	-2.37	-0.46
1222	Sf3b2	SF3B2	DOWN	-11.88	-1.31
1223	Edc4	EDC4	DOWN	-3.47	-0.42
1224	Ppp1r7	PP1R7	DOWN	-0.97	-0.27
1225	Lrrfip1	LRRF1	DOWN	-1.90	-0.26
1226	Dnah12	DYH12	DOWN	-1.73	-0.17
1227	Ddx17;Ddx5	DDX17 ;DDX5	DOWN	-1.48	-1.11
1228	Srrm1	SRRM1	DOWN	-5.97	-0.39
1229	Spag9	JIP4	DOWN	-8.57	-1.78
1230	Eml6	EMAL6	DOWN	-1.77	-0.25
1231	Luc7l3	LC7L3	DOWN	-2.02	-1.75
1232	Arcn1	COPD	DOWN	-7.86	-2.25
1233	Samhd1	SAMH1	DOWN	-4.08	-0.21
1234	P4ha1	P4HA1	DOWN	-2.89	-0.61
1235	Serpinb6	SPB6	DOWN	-1.93	-0.90
1236	Vdac2	VDAC2	DOWN	-3.23	-0.26
1237	Vdac3	VDAC3	DOWN	-13.16	-0.62
1238	Vdac1	VDAC1	DOWN	-3.94	-1.36
1239	Rbbp7	RBBP7	DOWN	-8.08	-0.44
1240	Tmpo	LAP2B	DOWN	-4.14	-0.77
1241	Tmpo	LAP2A ;LAP2B	DOWN	-9.62	-0.79
1242	Hcfc1	HCFC1	DOWN	-5.69	-0.52
1243	Lcp1	PLSL	DOWN	-3.38	-0.29
1244	Lcp1;Pls3	PLSL ;PLST	DOWN	-11.95	-0.31
1245	Soat1	SOAT1	DOWN	-14.23	-0.76
1246	Hspa4	HSP74	DOWN	-7.01	-0.61
1247	Hadh	HCDH	DOWN	-6.61	-0.16
1248	Glg1	GSLG1	DOWN	-1.07	-0.78
1249	Fxr1	FXR1	DOWN	-7.17	-0.53
1250	Gdi2	GDIB	DOWN	-3.69	-0.38
1251	Hsph1	HS105	DOWN	-2.06	-0.14
1252	Kif5b	KINH	DOWN	-4.28	-0.27
1253	Myh10;Myh9	MYH10 ;MYH9	DOWN	-4.08	-0.36
1254	Pcbp2	PCBP2	DOWN	-12.20	-0.50
1255	Pea15	PEA15	DOWN	-7.21	-0.21
1256	Ddx3x	DDX3X	DOWN	-5.36	-0.45
1257	Snrpa	SNRPA	DOWN	-3.08	-0.15
1258	Tsn	TSN	DOWN	-2.91	-0.80
1259	Eif4g2	IF4G2	DOWN	-1.86	-0.29
1260	Ly6e	LY6E	DOWN	-3.39	-0.48
1261	Lilrb4a	LRB4A	DOWN	-11.83	-3.05
1262	Stxbp2	STXB2	DOWN	-3.45	-0.53
1263	Sqstm1	SQSTM	DOWN	-10.04	-1.66
1264	Atp1a1	AT1A1	DOWN	-1.13	-0.14
1265	Vcl	VINC	DOWN	-6.89	-0.33
1266	Cltc	CLH1	DOWN	-1.13	-0.14
1267	Mars1	SYMC	DOWN	-3.12	-0.07
1268	Swap70	SWP70	DOWN	-3.37	-0.77
1269	FAM120A	F120A	DOWN	-2.16	-0.45
1270	Nomo1	NOMO1	DOWN	-2.90	-0.42
1271	Tpm4	TPM4	DOWN	-6.47	-0.43
1272	Cpsf6	CPSF6	DOWN	-8.77	-0.37
1273	Dnajc8	DNJC8	DOWN	-2.30	-0.41
1274	Sri	SORCN	DOWN	-3.54	-0.65
1275	Xpnpep1	XPP1	DOWN	-1.00	-0.49
1276	Snrnp200	U520	DOWN	-3.56	-0.37
1277	Abcf1	ABCF1	DOWN	-6.50	-0.34
1278	Xpo1	XPO1	DOWN	-8.02	-0.93
1279	Pcnp	PCNP	DOWN	-2.74	-0.60
1280	Snx6	SNX6	DOWN	-6.45	-0.60
1281	Txlna	TXLNA	DOWN	-0.93	-0.32
1282	Lrpprc	LPPRC	DOWN	-2.23	-0.33
1283	Pigs	PIGS	DOWN	-7.64	-0.70
1284	Ecpas	ECM29	DOWN	-5.52	-0.98
1285	Stoml3	STML3	DOWN	-1.46	-1.03
1286	Washc2	WASC2	DOWN	-12.05	-0.72
1287	Atp1a1;Atp1a2	AT1A1 ;AT1A2	DOWN	-2.21	-0.25

1288	Ugt1a7	UD17	DOWN	-3.63	-0.24
1289	Lsm8	LSM8	DOWN	-2.45	-0.22
1290	Rps9	RS9	DOWN	-5.31	-0.48
1291	Rps27	RS27	DOWN	-9.33	-0.40
1292	Rpl35	RL35	DOWN	-1.23	-0.13
1293	Rps27l	RS27L	DOWN	-5.22	-0.23
1294	Atp5mk	ATPMK	DOWN	-4.47	-0.48
1295	Ostc	OSTC	DOWN	-9.72	-2.53
1296	Luc7l2	LC7L2	DOWN	-9.31	-2.26
1297	Eml2	EMAL2	DOWN	-10.97	-0.60
1298	Dek	DEK	DOWN	-1.04	-0.57
1299	Mybbp1a	MBB1A	DOWN	-3.85	-0.39
1300	Otub1	OTUB1	DOWN	-6.96	-0.32
1301	Fnbp1	FNBP1	DOWN	-2.52	-0.73
1302	Septin9	45909	DOWN	-4.29	-1.34
1303	Rraga	RRAGA	DOWN	-0.97	-0.41
1304	Nucks1	NUCKS	DOWN	-1.27	-0.57
1305	Gatd1	GALD1	DOWN	-8.97	-1.69
1306	Psmd11	PSD11	DOWN	-4.22	-1.21
1307	Samm50	SAM50	DOWN	-1.24	-0.08
1308	Aars1	SYAC	DOWN	-4.25	-0.70
1309	Tm9sf4	TM9S4	DOWN	-6.31	-0.85
1310	Slc25a12	S2512	DOWN	-2.41	-1.00
1311	Echs1	ECHM	DOWN	-8.41	-1.79
1312	Clic6	CLIC6	DOWN	-2.67	-0.36
1313	Iars2	SYIM	DOWN	-3.23	-2.33
1314	Nceh1	NCEH1	DOWN	-1.10	-0.29
1315	Slc25a24	SCMC1	DOWN	-8.92	-1.77
1316	Lars1	SYLC	DOWN	-2.81	-0.91
1317	Ckap4	CKAP4	DOWN	-1.82	-0.11
1318	Acbd3	GCP60	DOWN	-4.00	-0.42
1319	Hadha	ECHA	DOWN	-5.58	-2.16
1320	Nars1	SYNC	DOWN	-13.44	-1.20
1321	Hus1	HUS1	DOWN	-6.16	-0.46
1322	Asph	ASPH	DOWN	-1.11	-0.24
1323	Flna;Flnc	FLNA ;FLNC	DOWN	-6.08	-1.40
1324	Sec62	SEC62	DOWN	-8.95	-0.97
1325	Qdpr	DHPR	DOWN	-1.72	-0.23
1326	Rsl1d1	RL1D1	DOWN	-2.24	-1.57
1327	Acaa2	THIM	DOWN	-7.79	-0.65
1328	Pkn2	PKN2	DOWN	-7.79	-1.86
1329	Ift57	IFT57	DOWN	-13.51	-2.73
1330	Taok3	TAOK3	DOWN	-13.57	-2.48
1331	Lpcat2	PCAT2	DOWN	-12.15	-1.61
1332	Agps	ADAS	DOWN	-2.08	-0.21
1333	Ppp4r4	PP4R4	DOWN	-5.73	-0.82
1334	Ncaph	CND2	DOWN	-15.83	-0.87
1335	Cpne1	CPNE1	DOWN	-6.44	-1.44
1336	Septin11	45911	DOWN	-1.48	-0.09
1337	Septin11	45911	DOWN	-5.13	-0.35
1338	Dock2	DOCK2	DOWN	-1.03	-0.44
1339	Rassf4	RASF4	DOWN	-11.52	-1.35
1340	Macroh2a2	H2AW	DOWN	-3.65	-1.51
1341	Pus7l	PUS7L	DOWN	-1.74	-1.96
1342	Nup88	NUP88	DOWN	-1.16	-0.92
1343	Smco1	SMCO1	DOWN	-5.90	-1.21
1344	Gnl3	GNL3	DOWN	-1.76	-0.38
1345	Pygb	PYGB	DOWN	-0.93	-0.53
1346	Acad9	ACAD9	DOWN	-5.10	-1.15
1347	Afg3l2	AFG32	DOWN	-5.78	-1.83
1348	Acsl5	ACSL5	DOWN	-10.61	-1.97
1349	Slc25a1	TXTP	DOWN	-1.07	-0.91
1350	Gfm1	EFGM	DOWN	-4.61	-1.15
1351	Plekho2	PKHO2	DOWN	-1.23	-0.14
1352	Fermt3	URP2	DOWN	-8.45	-0.97
1353	Nckap1l	NCKPL	DOWN	-11.07	-0.87
1354	Sdha	SDHA	DOWN	-4.24	-0.93
1355	Agfg1	AGFG1	DOWN	-6.48	-0.36
1356	Ddx18	DDX18	DOWN	-4.44	-0.50
1357	Eif3l	EIF3L	DOWN	-5.82	-0.74
1358	Blmh	BLMH	DOWN	-3.55	-0.48
1359	Gspt1	ERF3A	DOWN	-3.89	-0.87
1360	Hnrnpl	HNRPL	DOWN	-2.32	-0.22

1361	Sgpl1	SGPL1	DOWN	-1.15	-0.06
1362	Uqcr10	QCR9	DOWN	-0.96	-0.16
1363	Dync1li1	DC1L1	DOWN	-7.63	-1.67
1364	Dnttip2	TDIF2	DOWN	-6.06	-2.18
1365	Ptrh2	PTH2	DOWN	-0.98	-0.32
1366	Tmx1	TMX1	DOWN	-1.01	-0.33
1367	Cops8	CSN8	DOWN	-2.68	-0.92
1368	Mavs	MAVS	DOWN	-2.14	-1.03
1369	Cth	CGL	DOWN	-1.18	-0.38
1370	Rnpep	AMPB	DOWN	-1.60	-0.15
1371	Uhrf1	UHRF1	DOWN	-10.64	-0.92
1372	Hdlbp	VIGLN	DOWN	-2.06	-0.58
1373	Hnrnpul1	HNRL1	DOWN	-2.25	-0.14
1374	Ddx39a	DX39A	DOWN	-8.13	-2.11
1375	Rcc1	RCC1	DOWN	-4.67	-0.32
1376	Rpa1	RFA1	DOWN	-2.26	-0.27
1377	Zng1	ZNG1	DOWN	-1.11	-0.18
1378	Flnc	FLNC	DOWN	-6.30	-1.62
1379	Tram1	TRAM1	DOWN	-3.37	-2.17
1380	Acot7	BACH	DOWN	-3.22	-0.72
1381	Rab14	RAB14	DOWN	-4.83	-0.55
1382	Ck054	CK054	DOWN	-1.14	-0.14
1383	Acly	ACLY	DOWN	-2.34	-0.88
1384	Ndufs1	NDUS1	DOWN	-5.91	-0.39
1385	Rbmxl1	RMXL1	DOWN	-9.49	-0.81
1386	Csde1	CSDE1	DOWN	-12.74	-0.95
1387	Eif3h	EIF3H	DOWN	-4.04	-0.38
1388	Dap	DAP1	DOWN	-2.82	-0.21
1389	Basp1	BASP1	DOWN	-5.81	-0.97
1390	Asl	ARLY	DOWN	-11.58	-0.41
1391	Arrb2	ARRB2	DOWN	-15.97	-2.87
1392	Twf1	TWF1	DOWN	-7.62	-1.02
1393	Ndufv1	NDUV1	DOWN	-4.75	-0.27
1394	Ugp2	UGPA	DOWN	-7.25	-0.93
1395	Snx18	SNX18	DOWN	-3.89	-0.39
1396	Smarca5	SMCA5	DOWN	-5.37	-0.52
1397	Scpep1	RISC	DOWN	-1.39	-0.59
1398	Supt16h	SP16H	DOWN	-3.32	-0.26
1399	Fdps	FPPS	DOWN	-1.30	-0.13
1400	Rab31	RAB31	DOWN	-10.84	-0.48
1401	Lrch4	LRCH4	DOWN	-0.89	-0.61
1402	Etfdh	ETFD	DOWN	-2.52	-0.67
1403	Acaa1a	THIKA	DOWN	-1.02	-0.38
1404	Sf3b3	SF3B3	DOWN	-6.81	-0.74
1405	Mthfd1	C1TC	DOWN	-0.92	-0.08
1406	Far1	FACR1	DOWN	-2.06	-0.19
1407	Nop2	NOP2	DOWN	-1.98	-0.63
1408	Mtarc2	45718	DOWN	-5.31	-1.02
1409	Pycr2	P5CR2	DOWN	-5.24	-0.28
1410	Prkx	PRKX	DOWN	-5.89	-0.38
1411	Pdia6	PDIA6	DOWN	-1.54	-0.64
1412	Stoml2	STML2	DOWN	-1.67	-0.05
1413	Mvd	MVD1	DOWN	-19.84	-2.30
1414	Rap1b	RAP1B	DOWN	-1.70	-1.07
1415	Sfxn1	SFXN1	DOWN	-4.34	-0.68
1416	Lims1	LIMS1	DOWN	-8.77	-0.42
1417	Hadhb	ECHB	DOWN	-1.74	-0.96
1418	Actr3	ARP3	DOWN	-7.63	-0.73
1419	Psat1	SERC	DOWN	-5.89	-0.18
1420	Vwa5a	VMA5A	DOWN	-6.01	-0.22
1421	Tmed9	TMED9	DOWN	-1.99	-0.33
1422	Aco2	ACON	DOWN	-2.30	-0.65
1423	Cmas	NEUA	DOWN	-11.86	-0.25
1424	Dpp3	DPP3	DOWN	-12.99	-2.75
1425	Clint1	EPN4	DOWN	-1.22	-0.50
1426	Prpf19	PRP19	DOWN	-5.34	-0.55
1427	Triobp	TARA	DOWN	-2.66	-0.17
1428	Etfa	ETFA	DOWN	-4.02	-2.60
1429	Klb	KLOTB	DOWN	-9.68	-0.31
1430	Rtn4	RTN4	DOWN	-1.81	-0.80
1431	Atp5mg	ATP5L	DOWN	-2.08	-0.14
1432	Pno1	PNO1	DOWN	-9.59	-1.19
1433	Lamtor1	LTOR1	DOWN	-2.11	-0.79

1434	Ntpcr	NTPCR	DOWN	-4.16	-0.47
1435	Cisd2	CISD2	DOWN	-6.04	-0.64
1436	RTRAF	RTRAF	DOWN	-4.24	-0.48
1437	Nudt21	CPSF5	DOWN	-12.11	-0.67
1438	Glrx3	GLRX3	DOWN	-1.63	-1.00
1439	Ywhab	1433B	DOWN	-5.03	-0.66
1440	Arl8b	ARL8B	DOWN	-7.13	-0.24
1441	Cyb5b	CYB5B	DOWN	-10.08	-0.87
1442	Ndufb3	NDUB3	DOWN	-1.30	-0.26
1443	Slc25a11	M2OM	DOWN	-1.27	-0.49
1444	Raver1	RAVR1	DOWN	-14.73	-1.36
1445	Snx1;Snx2	SNX1 ;SNX2	DOWN	-1.71	-0.80
1446	Manf	MANF	DOWN	-4.11	-1.26
1447	Ndufs4	NDUS4	DOWN	-2.94	-0.26
1448	Ssr1	SSRA	DOWN	-1.21	-0.55
1449	Blvra	BIEA	DOWN	-2.99	-1.41
1450	Gar1	GAR1	DOWN	-6.12	-0.50
1451	Creld2	CREL2	DOWN	-9.53	-2.29
1452	Tpd52l2	TPD54	DOWN	-2.09	-0.74
1453	Ola1	OLA1	DOWN	-9.67	-2.37
1454	Nsfl1c	NSF1C	DOWN	-1.06	-0.66
1455	Gars1	GARS	DOWN	-1.17	-0.08
1456	Ptms	PTMS	DOWN	-9.77	-0.69
1457	Oxct1	SCOT1	DOWN	-7.40	-1.29
1458	Dynll2	DYL2	DOWN	-3.63	-0.14
1459	Snu13	NH2L1	DOWN	-3.14	-1.07
1460	Cndp2	CNDP2	DOWN	-2.87	-0.26
1461	Tmed10	TMEDA	DOWN	-5.74	-0.24
1462	Chchd2	CHCH2	DOWN	-5.33	-0.40
1463	Coro7	CORO7	DOWN	-1.96	-1.32
1464	Agpat3	PLCC	DOWN	-7.48	-0.81
1465	Fam227b	F227B	DOWN	-13.05	-3.87
1466	Sf3a3	SF3A3	DOWN	-14.04	-3.93
1467	Ndufv2	NDUV2	DOWN	-2.11	-0.50
1468	Prps1	PRPS1	DOWN	-5.17	-1.16
1469	Rpl22l1	RL22L	DOWN	-11.30	-0.81
1470	Rpl37	RL37	DOWN	-6.44	-0.37
1471	Itpa	ITPA	DOWN	-1.08	-0.21
1472	Rpl4	RL4	DOWN	-4.87	-1.74
1473	Snx5	SNX5	DOWN	-12.12	-0.53
1474	Psmd12	PSD12	DOWN	-4.38	-0.25
1475	Tnfaip8l2	TP8L2	DOWN	-5.19	-1.52
1476	Gatm	GATM	DOWN	-6.54	-2.52
1477	Mrpl12	RM12	DOWN	-9.75	-0.78
1478	Uqcrc2	QCR2	DOWN	-5.32	-0.27
1479	Ap2b1	AP2B1	DOWN	-17.24	-0.73
1480	Rpn2	RPN2	DOWN	-3.08	-0.52
1481	Srpra	SRPRA	DOWN	-6.61	-0.42
1482	Tmem43	TMM43	DOWN	-0.92	-0.64
1483	Pak1ip1	PK1IP	DOWN	-1.91	-0.27
1484	Ssr3	SSRG	DOWN	-0.99	-0.45
1485	Ndufa8	NDUA8	DOWN	-2.50	-0.99
1486	Cyb5r3	NB5R3	DOWN	-3.72	-1.01
1487	Akr1e2	AKCL2	DOWN	-14.09	-0.82
1488	Ndufs3	NDUS3	DOWN	-9.17	-0.65
1489	Etfb	ETFB	DOWN	-7.23	-2.67
1490	Pik3ap1	BCAP	DOWN	-1.48	-0.09
1491	Vps35	VPS35	DOWN	-4.62	-0.62
1492	Mvp	MVP	DOWN	-8.41	-1.23
1493	Mycbp	MYCBP	DOWN	-6.47	-0.17
1494	Cse1l	XPO2	DOWN	-1.93	-0.84
1495	Inpp5d	SHIP1	DOWN	-2.25	-0.24
1496	Anp32b	AN32B	DOWN	-5.74	-0.41
1497	Tm9sf3	TM9S3	DOWN	-7.69	-0.65
1498	Plek	PLEK	DOWN	-12.14	-2.69
1499	Dync1h1	DYHC1	DOWN	-10.45	-0.81
1500	Isyna1	INO1	DOWN	-5.85	-0.32
1501	Nit2	NIT2	DOWN	-2.24	-1.48
1502	Prmt1	ANM1	DOWN	-4.67	-1.56
1503	Copb1	COPB	DOWN	-2.63	-0.18
1504	Ddx21	DDX21	DOWN	-3.48	-0.46
1505	Ralb	RALB	DOWN	-2.66	-0.18
1506	Flii	FLII	DOWN	-1.13	-0.60

1507	Sh3bgrl	SH3L1	DOWN	-11.65	-0.91
1508	Uchl3	UCHL3	DOWN	-1.42	-0.17
1509	Iqgap1	IQGA1	DOWN	-3.97	-1.30
1510	Mrpl39	RM39	DOWN	-4.18	-0.12
1511	Fmnl1	FMNL1	DOWN	-4.22	-1.04
1512	Scly	SCLY	DOWN	-4.84	-0.24
1513	Arpc3	ARPC3	DOWN	-4.35	-1.15
1514	Txnrd1	TRXR1	DOWN	-10.21	-0.59
1515	Acsl4	ACSL4	DOWN	-0.93	-0.13
1516	Psma6	PSA6	DOWN	-3.14	-0.20
1517	Slc7a8	LAT2	DOWN	-4.35	-0.32
1518	Slc25a13	S2513	DOWN	-1.59	-0.39
1519	Clic4	CLIC4	DOWN	-7.79	-0.55
1520	Dnaja2	DNJA2	DOWN	-4.70	-0.26
1521	Slc25a10	DIC	DOWN	-4.18	-0.38
1522	Eif3i	EIF3I	DOWN	-2.12	-0.95
1523	Macroh2a1	H2AY	DOWN	-2.41	-0.24
1524	Fhl3	FHL3	DOWN	-8.35	-1.44
1525	Dstn	DEST	DOWN	-0.93	-0.15
1526	Sec11a	SC11A	DOWN	-1.26	-0.23
1527	Acot9	ACOT9	DOWN	-5.97	-1.24
1528	Sqor	SQOR	DOWN	-13.18	-3.00
1529	Psmb3	PSB3	DOWN	-13.45	-0.76
1530	Plp2	PLP2	DOWN	-5.59	-1.35
1531	Sae1	SAE1	DOWN	-10.94	-0.94
1532	Skp1	SKP1	DOWN	-8.67	-0.66
1533	Slc37a2	G6PT3	DOWN	-6.67	-1.89
1534	Pfkp	PFKAP	DOWN	-2.34	-0.64
1535	Vapa	VAPA	DOWN	-2.22	-0.13
1536	Bub3	BUB3	DOWN	-3.86	-1.41
1537	Bcl10	BCL10	DOWN	-4.31	-0.31
1538	Lipa	LICH	DOWN	-17.88	-5.86
1539	Eif2s3x	IF2G	DOWN	-2.04	-0.22
1540	Slc7a5	LAT1	DOWN	-9.29	-0.41
1541	Eif3g	EIF3G	DOWN	-6.06	-1.21
1542	Ddx39b	DX39B	DOWN	-10.59	-1.33
1543	Vars1	SYVC	DOWN	-4.01	-0.47
1544	Hnrnpc	HNRPC	DOWN	-3.31	-0.14
1545	Dnpep	DNPEP	DOWN	-7.14	-0.29
1546	Hnrnpf	HNRPF	DOWN	-8.03	-1.28
1547	Ddx39b	DX39B	DOWN	-7.80	-0.37

Chapter 4 - Application of surface plasmon resonance to elucidate the cooperative DNA binding mechanisms of NFATc1 and c-Jun

Text S.1 Running scripts for calculating molecular diameters

```
from pymol import cmd
import numpy as np
from scipy.spatial import ConvexHull
# Function: Calculate the maximum diameter of a molecule (or selection)
def calculate_maximum_diameter(selection="polymer"):
    # Get the atomic coordinates of the selected part
    coords = cmd.get_coords(selection, 1)
    # If no atom is found, return a message
    if coords is None or len(coords) == 0:
        print("No atoms found in the selection.")
        return
    # Computing Convex Packets with ConvexHull
    hull = ConvexHull(coords)
    max_diameter = 0.0
    atom1_index, atom2_index = None, None  # To store indices of the two atoms with max diameter
    # Calculate the maximum distance between two points on the convex packet
    for i in range(len(hull.vertices)):
        for j in range(i + 1, len(hull.vertices)):
            dist = np.linalg.norm(coords[hull.vertices[i]] - coords[hull.vertices[j]])
            if dist > max_diameter:
                max_diameter = dist
                atom1_index, atom2_index = hull.vertices[i], hull.vertices[j]
    print(f"Maximum diameter of the selection: {max_diameter:.2f} Å")
    # Get the coordinates of the two atoms
    atom1_coords = coords[atom1_index]
    atom2_coords = coords[atom2_index]
    atom1_coords=[73.459, 35.4, 35.104]
    atom2_coords=[-6.256, 30.055, 85.697]
    print(atom1_coords+atom2_coords)
    # Create pseudoatoms to mark the two atoms
    cmd.pseudoatom(object="atom1_marker", pos=atom1_coords, color="blue", name="Atom1")
    cmd.pseudoatom(object="atom2_marker", pos=atom2_coords, color="green", name="Atom2")
    # Draw a distance object to connect the two atoms
    cmd.distance("max_diameter_line", "atom1_marker", "atom2_marker")
    # Label the atoms and the distance
    label_text = f"Max Diameter: {max_diameter:.2f} Å"
    cmd.pseudoatom(object="plabel", pos=(atom1_coords + atom2_coords), label=label_text,
name="DiameterLabel")
    #cmd.alter("plabel", "color = 'red'")  # Set label color to red
    #cmd.alter("plabel", "font = 'Arial'")  # Set font to Arial
    #cmd.alter("plabel", "fontsize = 10")  # Set font size to 10
    # Optionally, show labels and markers
#   cmd.show("labels", "label")
#   cmd.show("spheres", "atom1_marker or atom2_marker")
    return max_diameter
# Call function to calculate the maximum diameter of protein and DNA complexes
```

```
calculate_maximum_diameter("polymer")
```

Curriculum Vitae

Curriculum Vitae



Bo Cao was born on February 19, 1990, in China. He received his Bachelor's degree in Clinical Medicine from Xinjiang Medical University in 2015, followed by a Master's degree in Orthopedics in 2018 at the same institution. During his master's studies, he focused on bone tissue engineering, bone infection treatment, and the early application of bioactive materials in orthopedics.

In 2020, he started his PhD research at Maastricht University, the Netherlands, where he joined the M4i in close collaboration with the MERLN institute. His research centers on the development of non-antibiotic strategies for preventing and treating infections related to orthopedic implants. His work integrates biomaterials, protein biochemistry, electron microscopy, surface plasmon resonance, and mass spectrometry to study host–pathogen interactions and infection mechanisms at the molecular level.

Throughout his academic journey, Bo has built a multidisciplinary background spanning orthopedics, analytical chemistry, protein biochemistry, biophysics, and computational biology. His strong foundation in both clinical and molecular sciences allows him to approach biomedical challenges from both translational and mechanistic perspectives. He has participated in multiple national research projects funded by the National Natural Science Foundation of China (NSFC), focusing on vascularization and antibacterial functionality in bone tissue engineering.

With a deep commitment to interdisciplinary science, Bo Cao aims to bridge the gap between clinical needs and laboratory innovation in orthopedic infection treatment. His passion lies in developing practical, biomaterial-based solutions that are effective, safe, and resistant to the growing threat of antimicrobial resistance.

List of publications

This thesis is based on the following publications

1. **Cao B[1].,** Cillero-Pastor B[1*]**.,** Honing M[1]**.** Orthopedic implant infection with emphasis on bacterial biofilm formation, host response, and techniques used in diagnosis, prevention, and treatment. Ready for submission.

2. **Cao B[1].,** Darya Hadavi PhD[1]**.,** Cillero-Pastor B[1*]**.,** Honing M[1]**.** Surface roughness of titanium implants modulates macrophage inflammatory response. Submitted to Bone & Joint Research.

3. **Cao B[1].,** Cillero-Pastor B[1*]**.,** Honing M[1]**.** Effect of titanium surface roughness on macrophage-bacteria interactions. Submitted to Biofilm.

4. **Cao B[1].,** Darya Hadavi PhD[1]**.,** Cillero-Pastor B[1*]**.,** Honing M[1]**.** Application of surface plasmon resonance to elucidate the cooperative DNA binding mechanisms of NFATc1 and c-Jun. Biochimica et Biophysica acta. General Subjects 1870.6 (2026): 130924-130924.

5. **Cao B[1].,** Cillero-Pastor B[1*]**.,** Honing M[1]**.** Structure-guided disruption of NFATc1 rewires macrophage polarization to enhance clearance of *S. aureus* on implant surfaces. In preparation.

Other publications

1. **Cao, B.** Cao, Bo,*; Wei, Renqian PhDa; Ke, Yu MSca; Sandström, Edith PhDb; Cheng, Erlin PhDc; Li, Yi PhDa; Mo, Sizhuan MSca. Comparison of external Orthofix pertrochanteric fixator and internal proximal femoral nail antirotation fixation for intertrochanteric fractures in high-risk elderly patients. International Journal of Surgery Open 62, 681-688 (2024).

2. Wang, J. & **Cao, B.** Spinal teratoma with recurrent epileptic episodes in adults: a case report. Case Reports in Neurology 16, 249-255 (2024).

3. **Cao, B.** & Wang, J. A rare case report of an adult with intraspinal gouty stones and concurrent knee joint involvement. Clinical Case Reports 13, e70573 (2025).

4. **Cao, B. B.,** Wang, J. J. & Ren, Q. Q. A rare case of unexplained recurrent intracerebral haemorrhage. Journal of Surgical Case Reports 2025 (2025).

5. **Cao, Bo,** Cheng, Erlin PhDb; Wang, Guiqing MDa; Wei, Renqian PhDa,*. Mitigating complications in peroneal nerve trophic flaps through superficial venous connections: a case-control study. Annals of Medicine and Surgery 87.11 6945-6953 (2025).

Acknowledgments

Acknowledgements

As I bring this PhD journey to a close, I find myself filled with deep gratitude for the many people who have supported, guided, and inspired me along the way. Completing this thesis has been both an academic and personal journey, and it would not have been possible without the help of many individuals to whom I owe my sincerest thanks.

Maarten, first and foremost, I would like to express my deepest gratitude to you, for your unwavering support, guidance, and encouragement throughout the past five years. Thank you for offering me the opportunity to join your research group and for believing in my potential from the very beginning. When I first arrived, my English was far from fluent, and I knew little about Dutch language or culture. Yet, under your mentorship, I not only grew academically but personally as well. You taught me how to approach problems critically, how to design experiments thoughtfully, how to manage research projects efficiently, and how to communicate ideas clearly—whether in presentations or in writing. You showed me how to identify meaningful research questions, and more importantly, how to challenge them with a critical and open mind. Your passion for life, your perpetual optimism, and your sense of humor have left a lasting impact on me. I have been continually inspired by your dedication—not only to science but also to maintaining a vibrant and active lifestyle. The fact that you still participate in triathlons in your sixties is nothing short of remarkable and has been a true source of motivation for me. Thank you for your constant encouragement during our monthly meetings and for always pushing me to be better, while making the journey enjoyable. It has been an honor to learn from you.

Berta, I would also like to extend my heartfelt thanks to you, for being both a dedicated mentor and a kind friend throughout my PhD journey. Your support has gone far beyond academic guidance—you have truly been a beacon of warmth and encouragement in both my research and personal life. Looking back, I am deeply touched by your tireless effort in helping me revise my first manuscript—more than forty times. Your patience, rigor, and high standards profoundly shaped the way I approach scientific writing. Your dedication has set an example I will always strive to follow. More than that, I will never forget how you extended a helping hand when my family and I went through a very difficult time. Your support was truly a case of "offering help in times of need"—a gesture we will remember with sincere gratitude. In those moments, you were not only my mentor, but also a friend, standing by us when we needed it most. Your sense of responsibility, your compassion, and your integrity have left a deep impression on me. You have inspired me not only as a researcher, but also as a human being. Thank you for being a role model, and for walking with me through both the sunshine and the storm.

Ron, I would also like to express my sincere gratitude to you. Thank you for your outstanding leadership and for creating an exceptional yet warm research environment. Under your guidance, M4I has become a place where scientific excellence and human connection coexist—something I feel privileged to have experienced. You have taught us that true scientific progress is only possible through collaboration and unity—that only by

working together can we climb the “Mount Everest” of science. Your message has always been clear and inspiring: science is not a solitary pursuit, but a collective effort. I am especially grateful for the weekly Tuesday morning meetings, which have been invaluable for my academic development. Through them, I have learned how to formulate meaningful scientific questions, how to analyze them critically, and how to engage in thoughtful scientific discussion. These sessions were more than just meetings—they were training grounds for rigorous thinking and scientific maturity. Thank you for fostering an international, open, and diverse academic atmosphere where ideas are freely exchanged and creativity is encouraged. It has been a privilege to grow as a scientist under your leadership.

Dear members of my PhD assessment committee, I would also like to extend my sincere thanks to you. I truly appreciate the time you take to evaluate my work and the professional feedback you provide. Your thoughtful comments and suggestions are of great value and will help to strengthen the final version of this thesis.

Benjamin, I would like to sincerely thank you for your generous support and technical expertise during my project. Thank you for helping me install the AlphaFold software and for patiently guiding me through the data analysis process. Your deep knowledge and problem-solving skills were truly impressive, and I learned a great deal from you. What I appreciated most was your willingness to help whenever I had questions—no matter how small or complex. Your dependable, solution-oriented approach and friendly attitude made it easy to seek help and move forward with confidence. Your support not only saved me valuable time but also helped me overcome technical challenges that I could not have solved alone. Thank you for being such a skilled and kind colleague, your help meant a lot to me.

Darya, I would like to express my heartfelt thanks to you for your generous and patient support throughout my research. Thank you for training me so carefully and thoroughly in the use of mass spectrometry instruments—your step-by-step guidance gave me the confidence and skills I needed to work independently. I am especially grateful for your help in designing scientific figures and in shaping the structure and clarity of my manuscripts. Your attention to detail and your willingness to offer constructive feedback—even when it meant going through the same figures or sections multiple times—made a real difference. You were always patient, always thoughtful, and always kind. Most of all, I want to thank you for your support during the SPR experiments. That was one of the most technically and mentally challenging parts of my project, and without your help, I simply could not have completed it. Your help came just when I needed it most—truly a case of offering support in a moment of difficulty. Your professionalism, patience, and kindness have left a deep impression on me, and I will always remember the way you supported me—not only as a colleague, but as a generous and dependable friend.

Ronny, I would like to sincerely thank you for all the support and guidance you have given me throughout my PhD. Thank you for helping me with ordering reagents and for

patiently teaching me how to use the Q Exactive for sample monitoring. Your hands-on guidance gave me not only the technical skills but also the confidence to carry out complex experiments independently. I am also grateful for your help in protein data analysis. You were always willing to explain things step by step, no matter how many questions I had. Your clarity, patience, and attention to detail made learning proteomics much less overwhelming, and far more enjoyable. Thank you as well for your advice and feedback during the writing of my first thesis chapter. Your thoughtful comments helped me shape my ideas and express them more clearly. I truly appreciate your generosity with your time and your willingness to help, always with a kind and supportive attitude.

Anjusha, I would like to warmly thank you for your kind support and companionship throughout these five years of PhD life. Thank you for helping me with the use of the UHMR for protein analysis, and for always being willing to assist with experiments whenever I needed help. I am especially grateful for the many weekends we spent working together in the lab—your dedication and team spirit made even the busiest days feel manageable. I truly enjoyed our lunch breaks and the conversations we shared afterwards. Those small moments of laughter and connection brought light to the daily routine and made this long journey so much more enjoyable. It has been a joy to go through this PhD journey with you by my side—as a colleague, a teammate, and a friend.

Yuandi, I would like to sincerely thank you for the patient and thorough training on SPR techniques. Your clear guidance and hands-on support not only helped me understand how to operate the SPR instrument but also gave me the confidence to independently design and perform experiments. Your attention to detail and willingness to answer my many questions made the learning process smooth and enjoyable. Thanks to your generous help, I was able to overcome the initial challenges of using SPR and successfully complete this crucial part of my research. Your support truly made a significant difference, and I am deeply grateful for your kindness and expertise.

Peiliang, I would like to sincerely thank Peiliang for generously sharing your knowledge of chemistry with me. Your clear explanations and patient guidance helped me better understand many complex chemical concepts that were essential for my research. Your willingness to take the time to teach and clarify made a significant difference in my learning journey. I truly appreciate your support and the encouragement you provided along the way. Your expertise not only strengthened my scientific foundation but also inspired me to approach problems with greater confidence.

Mudita, I would like to warmly thank you for the many weekends we spent working hard together. Your consistently positive and optimistic attitude has deeply inspired and motivated me throughout this journey. I truly cherish the moments we shared—not only in the lab but also during our enjoyable conversations about life and beyond. Your cheerful spirit made even the busiest days feel lighter and more rewarding. It has been a pleasure to share this PhD experience with you, both as a colleague and as a friend.

Bryn, I would like to extend my heartfelt thanks to you for your generous help with the analysis of my peptides and polymers. I am truly grateful for your warm and kind support—you were always ready to lend a hand with such enthusiasm and patience. Your gentlemanly grace and calm demeanor left a lasting impression on me. I greatly enjoyed our spontaneous post-lunch conversations, which were always light-hearted and uplifting. Working alongside you on weekends, pushing through challenges together, turned what could have been tiring days into some of my most cherished memories. Thank you for making the journey not only more manageable, but also genuinely meaningful.

Mo, I would like to thank you for generously providing access to the surgical cell culture lab, the protein laboratory, and the gene laboratory. Your support with these essential facilities made it possible for me to carry out key parts of my research. I truly appreciate your help and the resources you made available, which played an important role in the smooth progression of my experimental work.

Annemarie, I would like to sincerely thank Annemarie for your kind support with ordering experimental materials and for the training you provided on ELISA techniques. Your clear guidance helped me quickly become confident and efficient in performing the assays. I am especially grateful for your kindness and warmth throughout our interactions. Your friendly and helpful attitude always made the lab a more welcoming and supportive place. Thank you for being such a thoughtful and dependable colleague.

Ye, I would like to sincerely thank you for providing access to the bacterial laboratory and the Protein Biochemistry Core Lab at M4I, as well as the essential facilities for protein purification. Your support was crucial in enabling this part of my research. I am especially grateful for your valuable advice on protein expression and purification strategies. Your expertise and willingness to share your knowledge helped me improve my experimental design and overcome technical challenges. Thank you for your kind support and for facilitating a smooth and productive workflow.

I would also like to express my sincere thanks to my colleagues **Jinahua, Charles, Isabeau, Sebastian, Alijoscha, Sylvia, Andrej, Rob, Michiel, Philippe, Laura, Mirella, Eva, Kasper, Caroline, Ian, Tim, Christel, and Theodore**. It has been a great pleasure working alongside all of you. Thank you for your help, your support, and the many enjoyable moments we shared throughout these years. Whether it was in the lab, during meetings, or over coffee breaks, your collaboration and friendship made my PhD journey both productive and memorable. I truly appreciated the team spirit and the positive atmosphere we created together.

Finally, I would like to express my deepest gratitude to my family for their unwavering support throughout this journey. To my wife, **Xiaoyun**, thank you for standing by my side through all the challenges of these past five years. Your patience, understanding, and unconditional support have meant everything to me. Without you, I could not have completed this PhD. I am also profoundly grateful to my parents for their lifelong support

and encouragement in my academic journey. Your belief in me gave me the strength to keep going, even during the most difficult times. This achievement is as much yours as it is mine.

Bo Cao

